600545

RADC-TDR-63-415
FINAL REPORT

394-p #5.00

PASSIVE OPTICAL TECHNIQUES INVESTIGATION

TECHNICAL DOCUMENTARY REPORT NO. RADC-TDR-63-415

January 1964

Techniques Branch
Rome Air Development Center
Research and Technology Division
Air Force Systems Command
Griffiss Air Force Base, New York

DDC
JUN 3 1964

Project No.4506, Task No.45060

(Prepared under Contract No. AF30(602)-2886 by A. D. French, B O.R. Bakeman, and others, General Electric Company, Heavy Military Electronics Department, Syracuse, N.Y.)

Best
Available
Copy

DDC AVAILABILITY NOTICE

Qualified requesters may obtain copies from the Defense Documentation Center (TISIR), Cameron Station, Alexandria, Va., 22314. Orders will be expedited if placed through the librarian or other person designated to request documents from DDC.

Releasable to OTS.

LEGAL NOTICE

When US Government drawings, specifications, or other data are used for any purpose other than a definitely related government procurement operation, the government thereby incurs no responsibility nor any obligation whatsoever; and the fact that the government may have formulated, furnished, or in any way supplied the said drawings, specifications, or other data is not to be regarded by implication or otherwise, as in any manner licensing the holder or any other person or corporation, or conveying any rights or permission to manufacture, use, or sell any patented invention that may in any way be related thereto.

DISPOSITION NOTICE

Do not return this copy. Retain or destroy.

Suggested Keywords: Parameters, Celestial Background, Atmospheric Effects
Detection Theory, Sensor Capabilities

ABSTRACT

The parameters and trades involved when using various Passive Optical Te niques to separate earth orbiting objects from the celestial background and the capability of Orbit Prediction from angle only data are presented. In addition b discussions of the celestial background, atmospheric effects, target brightness factors, lens (optical) design, detection theory and sensor capabilities are rep in modified handbook form.

PUBLICATION REVIEW

This report has been reviewed and is approved. For further technical infor mation on this project, contact Mr. Bernard DiTano, EMATS, Ext. 74245.

APPROVED: Bernard DiTano

BERNARD DITANO
Project Engineer
Surveillance & Control Division

APPROVED: Irving J. Gabelman for Lt Colonel USAF

ARTHUR J. FROHLICH
CHIEF, Techniques Branch
Surveillance & Control Division

FOR THE COMMANDER:

Irving J. Gabelman

IRVING J. GABELMAN
Chief, Advanced Studies Group

AIR FORCE, Caro Show Prtg. Co. 5/8/64 - 160

TABLE OF CONTENTS

Section	Title
I	Problem Analysis and Techniques Investigation. . . . .
II	Equipment Parameters and Trades . . . . .
III	Measurement and Evaluation Techniques . . . . .
IV	System Selection Criteria and Trades . . . . .
V	Orbital Prediction Capability for Angle Data. . . . .
VI	Conclusions and Recommendations . . . . .
Appendix I	**Probability of Occultation** . . . . .
Appendix II	**Bi-Static Space Surveillance** . . . . .
	System Calculations . . . . .
Appendix III	**Single Site M. T. I. System Calculations** . . . . .
Appendix IV	**Smoothing for Best Estimates** . . . . .
Appendix V	**Equations for $\Delta\hat{A}$ and $\Delta\hat{\dot{A}}$** . . . . .
Appendix VI	
Appendix VII	**Clear Weather Frequency (Nighttime) for Upstate New York** . . . . .
Glossary of Terms	. . . . .

LIST OF ILLUSTRATIONS

Figure	Title	Page
I-1	Parallax Angle of an Object as Changed by Earth's Rotation	I-3
I-2	Midas Satellite, 1930' 10" E. S. T., 1/10/62 From Cazenovia Test Site	I-5
I-3A	Stereo Photos Showing Several Star Levels	I-8
I-3B	Suggested Method of Viewing Stereo Photos	I-8
I-4	Conversion Chart, Intensity Ratio to Stellar Magnitude Difference	I-10
I-5	Conversion Chart, Intensity Ratio vs Stellar Magnitude Difference	I-11
I-6	Conversion Chart, Intensity Ratio vs Stellar Magnitude Difference	I-12
I-7	Conversion Chart Intensity Ratio vs Stellar Magnitude Difference	I-13
I-8	Eye Response Curves	I-18
I-9	Approximate Values for Average Sky Brightness (Mag/sec^2 vs Elevation Angle Above Horizon, Moonless Night)	I-22
I-10	Star Density Distribution Chart	I-26
I-11	Summary of Star Data Count	I-28
I-12A	Aureole of the Moon	I-35
I-12B	Approximate Sky Brightness Change vs Moon Age	I-36
I-13	Background Light vs Field of View - 1000 Line Scan	I-37
I-14A	North Polar Sequence	I-38
I-14B	This is a carefully measured series of stars near the pole whose magnitudes are used as a standard for measurements, in photovisual and photographic magnitudes	I-39
I-15	Graphic Time Table of the Heavens	I-41
I-16		I-43
I-17	Refraction Correction (subtract) for Observed Elevation Angles, Object at Infinity	I-44
I-18	Angular Error Due to Atmospheric Refraction as a Function of Optical Field of View	I-46

LIST OF ILLUSTRATIONS (CONT)

Figure	Title	Page
I-19	Summary of Variations in Atmospheric Refraction.	I-49
I-20		I-50
I-21	Maximum Angular Error Due to Change in Atmospheric Refraction-Error Across Field of View vs Field of View. (Assuming Bias Correction as a Function of Field of View and Mount Elevation)	I-51
I-22	Increase in Visual Magnitude Due to Atmospheric Attenuation	I-53
I-23	Transmission of Various Kodak Wratten Filters plus S-20 Response Curve	I-54
I-24	Atmospheric Attenuation Factor	I-58
I-25	NASA Wallops Island Balloon, Viewed from Schenectady by GE Electro-Optical System: 6:30 PM 2/27/60; Range 600 Miles; Scan 1/30 Second: Optics 2.8 Inch.	I-59
I-26	Angular Rate of a Circular Orbit at Zenith of an Observer on Earth (Neglecting Earth's Motion)	I-62
I-27	Photo Visual Magnitude vs Distance for a 1 Meter Radius Sphere; Diffuse Reflecting Surface, Sun Illuminated	I-64
I-28	Change of Magnitude with Change of Diameter of Reflecting Body (-m) or with Change of Distance to Body (+m).	I-65
I-29	Relative Luminosity of a Diffuse Sphere as a Function of Phase Angle (Magnitude Difference Scale Included for Each 20°s of Phase Angle, Plus Specular Reflector Reference)	I-67
I-30	Magnitude Change with percent Reflectivity of a Reflecting Object	I-68
I-31A	Illumination of a Satellite, etc., 45°N. (Sunrise and Sunset Times for a Satellite at Various Heights (miles)). .	I-69
I-31B	Illumination of a Satellite, etc., 30°N. (Sunrise and Sunset Times for a Satellite at Various Heights (miles)). .	I-70
II-1	Total Angular Field of View vs Focal Length for Typical Image Sizes	II-9
II-2	Background Brightness, Increase in Magnitudes Over Unintegrated Sky Value (mag/sec^2) vs Resolution Element Size Single Dimension of Square	II-11
II-3	Reduction of Stray Light in a Reflecting Telescope.	II-14
II-4	Newtonian System without Folding.	II-22

LIST OF ILLUSTRATIONS (CONT)

Figure	Title	Page
II-5	Newtonian System, Folded	II-23
II-6	Schwarzchild System	II-25
II-7	Conder System	II-26
II-8	Schmidt System	II-27
II-9	Wright Camera	II-28
II-10	Schmidt System with Flat Mirror	II-29
II-11	Schmidt-Cassegrain System	II-30
II-12	Maksutov System	II-31
II-13	Folded Wynne System	II-31
II-14	Distortionless System	II-32
II-15	Linfoot Meniscus - Schmidt System	II-33
II-16	Baker "Super-Schmidt" System	II-34
II-17	Foci of Axial and Marginal Rays	II-39
II-18	Summary Error Characteristics of Optical Systems for Surveillance Applications	II-41
II-19	Point Object Detection in Flat Field Background	II-46
II-20	Point Object Detection Drawn as Probability Curves	II-47
II-21	Detection Star Magnitude	II-56
II-22	Plot of N_{SD}/CM^2 Second vs M_{SD}	II-59
II-23	Plot of N_{SD} V_S X^2 N_B	II-59
II-24	Plot of D_{SN} VS E_{SN} when a Point Object is just Detectable	II-62
II-25	E_{SN} Required for Detection as Function of Line Pairs Viewed using Square Mask on Monitor	II-64
II-26	Line Resolution Sensitivity for S20 Standard Scan Eye View MgO Target	II-68
II-27	These Pictures Demonstrate Limited Blooming and Recovery Speed of GE Thin Film MgO Image Orthicon when Operated Properly	II-71
II-28	Detail View, GE Thin Film MgO Image Orthicon	II-72
II-29	Available Low Light Level MgO Image Orthicon Tubes	II-74
II-30	Relative Photocathode Response, Amps per Watt	II-76
II-31	Photocathode Responses	II-77
II-32A	Scene Illumination vs Typical Resolution Sensitivity by Type	II-81

LIST OF ILLUSTRATIONS (CONT)

Figure	Title	Page
II-32B	Effects of Contrast Reduction.	II-82
II-33.	An Example of Underscanning of I. O.for Increased Resolution - Jupiter and its Principle Moons, 1029 Line Scan.	II-83
II-33A	Normal Scan, 1029 Line Full Scan	II-83
II-33B	4 to 1 Underscan with 1029 Lines: Moons have Increased in Size, Hence Resolution was Exceeded Earlier; Probably at Approximately 3 to 1 or 3000 Lines.	II-83
II-34	Resolution Element Size and Background Brightness Increase per Resolution Element vs Focal Length for Various Line Resolution (Square Raster)	II-86
II-35	Image Build Up Signal vs Frame Number.	II-88
II-36	Great Orion Nebulae; 1/30 sec Continuous Scan; 1029 Lines; 16-1/2" Reflector; 240" F. L.; Z5396 Tube	II-89
II-37	Great Nebula of Orion; 1/2 sec Integration; 16-1/2" Reflector. 240" F. L. ' Z5396 Tube.	II-90
II-38	Sine Wave Response of Cascaded Electro Optical System . .	II-94
II-39A	Field of View vs Focal Length, Short and Medium Focal Lengths (1 to 100 inches); Max (1.55°) Effective Diagonal on Photocathode; Multiply by .707 for Square Raster; Multiply by .6 and .8 for 3 ×4 Aspect Ratio for 3" MgO Orthicon Normal Scan	II-96
II-39B	Field of View vs Focal Length, Short and Medium Focal Lenths (1 to 100 inches); Max (1.55°) Effective Diagonal on Photocathode; Multiply by .707 for Square Raster; Multiply by .6 and .8 for 3 ×4 Aspect Ratio for 3" MgO Orthicon Normal Scan	II-97
II-40	Basic Storage Tube Electrode Arrangement	II-107
II-41	Typical Secondary Emission Curve.	II-108
II-42	Storage Tube Operating Modes.	II-108
II-43		II-109
II-44	S-Shape Geometric Distortion	II-114
III-1	Target Relative Angular Velocity vs Target Altitude	III-13
III-2	Target Image Parallax Versus Site Separation and Target Height	III-14
III-3	Target Image Parallax	III-16
III-4	Star Magnitude of Sun Illuminated Target.	III-17
III-5		III-18

LIST OF ILLUSTRATIONS (CONT)

Figure	Title	Page
III-6	Detector Irradiance vs Target Variables	III-19
IV-1	Star Density vs Magnitude	IV-5
IV-2	Nonocculation Probability vs Field of View	IV-6
IV-3	Nonocculation Probability for Extreme Star Densities	IV-8
IV-4	Nonocculation Probability vs Image Growth Rate	IV-9
IV-5	Nonocculation Probability vs Threshold Image Size	IV-10
IV-6	Effect of Image Growth Rate vs Minimum Image Diameter for 99 percent Probability	IV-11
IV-7	Effect of Image Growth Rate vs Minimum Image Diameter for 90 percent Probability	IV-12
IV-8	Refraction Error Between Center of Field of View and Edge	IV-15
IV-9	Curvature of Field Error	IV-18
IV-10		IV-21
IV-11	Minimum Parallax for Bodies at 10^{o} Elevation	IV-22
IV-12	Minimum Parallax for Bodies at 20^{o} Elevation	IV-23
IV-13	Minimum Parallax for Bodies at 30^{o} Elevation	IV-24
IV-14	Minimum Parallax for Bodies at 60^{o} Elevation	IV-25
IV-15	Coverage Loss for Range - Angle Mode	IV-27
IV-16	Maximum Parallax for Bodies at 10^{o} Elevation	IV-29
IV-17	Maximum Parallax for Bodies at 30^{o} Elevation	IV-30
IV-18	Maximum Parallax for Bodies at 60^{o} Elevation	IV-31
IV-19	Maximum Parallax for Bodies at 90^{o} Elevation	IV-32
IV-20A		IV-36
IV-20B	Site Displacement Due to Earth Rotation	IV-37
IV-21	Angular Velocity Due to Earth Rotation Alone (Maximum)	IV-38
IV-22	Maximum and Minimum Angular Velocity Relative to Site on Stationary Earth	IV-39
IV-23	Maximum and Minimum Total Angular Velocity Relative to Site on Earth	IV-40
IV-24	Minimum Time Lapse to Detect all Satellites Below a Given Altitude	IV-41
IV-25	Maximum Time Lapse to Detect all Sattelites Above a Given Altitude	IV-42
IV-26	Basic MTI System	IV-45

LIST OF ILLUSTRATIONS (CONT)

Figure	Title	Page
IV-27		IV-46
IV-28A		IV-48
IV-28B		IV-49
IV-29		IV-57
IV-30		IV-61
IV-31	Accuracy in Establishing Local North	IV-62
IV-32	Accuracy in Establishing Local Latitude and Longitude	IV-63
IV-33	Accuracy in Establishing Local Elevation	IV-64
IV-34	Encoder Angular Accuracy as a Function of the Number of Encoder Bits	IV-66
IV-35A	Examples of Resolution Possible with 16-1/2", f/5 Reflector ~240" focal length RCAA Telescope and 1029 Line Scan; 1/30 sec Rate, Continuous Scan of Moon; Hazy Night, No Filter	IV-71
IV-35B	Examples of Resolution Possible with 16-1/2", f/5 Reflector ~240" focal length RCAA Telescope and 1029 Line Scan; 1/30 sec Rate, Continuous Scan of Moon, Hazy Night, No Filter	IV-71
V-1	Flow Chart-Orbit Prediction from Optical Data	V-2
V-2	Range Error at Reference Position as a Function of Measurement Errors	V-6
V-3	Range Error at Reference Position as a Function of Tracking Time and Time Lapse Between Independent Observations	V-7
V-4	Prediction Ahead - 90% Confidence Tube Radius as a Function of Angular Distance from the Reference Position	V-8
V-5	Prediction Ahead - 90% Confidence Tube Length as a Function of Angular Distance from the Reference Position	V-9
V-6	Tube Radius at Reference Time as a Function of Tracking Time and Time Lapse Between Observations	V-10
V-7	Prediction Ahead - Tube Radius 1/4 of a Period After Reference Time	V-11
V-8	Tube Length at Reference Time and 1/4 of a Period After Reference Time as a Function of Tracking Time	V-12
V-9	Orbit Prediction from Three Observations - Range Error Corresponding to the Second Observation as a Function of Time Lapse Between Observations	V-13
V-10	Prediction Ahead - 90% Confidence Tube Radius as a Function of Angular Distance from the Reference Position	V-14

LIST OF ILLUSTRATIONS (CONT)

Figure	Title	Page
V-11	Prediction Ahead - 90% Confidence Tube Length as a Function of Angular Distance from the Reference Position	V-15
V-12	Flow Chart - Monte Carlo for More than Three Sets of Observations	V-19
V-13	Flow Chart - Monte Carlo Study for Three Sets of Observations	V-23
V-14	Flow Chart - Orbit Estimation from Three, Equally Spaced, Sets of Optical Data	V-24
AI-1	Detector Relative Response	AI-3
AI-2	Relative Distribution of Star Classes vs Wavelength of Maximum Radiation	AI-4
AI-3	Partial Probability F_1 0° Galactic Latitude	AI-9
AI-4	Partial Probability F_2 0° Galactic Latitude	AI-10
AI-5	Partial Probability F_3 0° Galactic Latitude	AI-11
AI-6	Partial Probability F_1 0° to 90° Average	AI-12
AI-7	Partial Probability F_2 0° to 90° Average	AI-13
AI-8	Partial Probability F_3 0° to 90° Average	AI-14
AI-9	Partial Probability F_1 90° Galactic Latitude	AI-15
AI-10	Partial Probability F_2 90° Galactic Latitude	AI-16
AI-11	Partial Probability F_3 90° Galactic Latitude	AI-17
AI-12	Representative Density - Log Exposure Curve	AI-19
AI-13	Image Growth Characteristic for an Image Orthicon Used with an Image Cancelling Mask	AI-21
AII-1	Bistatic System Geometry	AII-2
AII-2	Calculated Parallax Variation with Azimuth and Elevation	AII-4
AII-3	Bistatic Coordinate Geometry	AII-5
AII-4	Bistatic Coordinate Geometry	AII-6
AIII-1	Site Displacement Geometry	AIII-1
AIII-2	Angular Velocity Relative to Center of Earth at Perigee	AIII-4
AIII-3	Angular Velocity Relative to Center of Earth at Apogee	AIII-5
AIII-4	Earth-Satellite Geometry	AIII-6
AVII-1	Equivalent "dark hours" 10 Year Average, Syracuse, N. Y.	AVII-4

LIST OF ILLUSTRATIONS (CONT)

Figure	Title	Page
AVII-2	Equivalent "dark" Hours 10 Year Average, Albany, N. Y.	AVII-5
G-1	Coordinates on the Earth.	G5
G-2	The Celestial Sphere	G6
G-3	Celestial Equator and Ecliptic	G7
G-4	Coordinates on the Celestial Sphere	G7

PROJECT ENGINEER'S EVALUATION

The final draft report for "Passive Optical Techniques Investigation," has been reviewed by the Project Engineer and is found to be acceptable for publication. The investigation was sponsored under RADC Contract AF30(602)-2886.

The purpose of this study and investigation is concerned with the night-time space surveillance problem of separating orbiting objects in a celestial environment and the capability of orbital prediction when using ground based passive equipments.

The investigation covered:

a. The factors effecting detection and trades essential in the utilization of a candidate system. Since the conditions of the celestial background and targets cannot be controlled they must be established and trade-offs made between (1) Lens diameter, (2) Field of view, and (3) Image time for obtaining the required capability.

b. Separation techniques and combinations (Hybrid Systems) of which best applies to the threat present for solution (height, brightness, velocity of targets, etc.). The evaluation of these techniques is based on the ability to cancel stars (background) for the range of intensities involved and the retention of the targets versus its complexity.

c. Orbital prediction capability from angle only data.

d. The factors effecting false alarm rate, and detection probability.

e. Some limited measurements of various separation factors.

f. The detection of a target versus orbit height.

The results of this investigation are of great value to the Air Force in the field of passive optical processing. The complete problem of space surveillance has been investigated, with primary emphasis on techniques, system trade-offs, and parameters vital for passive detection. These results are essential in the utilization of a system capable of performing the passive night-time space surveillance task.

Bernard Ditano

BERNARD DITANO
Project Engineer

INTRODUCTION

The principle purpose of this study and investigation is concerned with the nighttime space surveillance problem of separating orbiting objects in a celestial environment and the capability of Orbital Prediction when using ground based (ea passive equipments. The content of the celestial environment, the equipment parameters, detection theory, separation techniques, and system trades applica! are emphasized. Information is included to illustrate the effects of some of the factors when considering other problem areas (discrimination and identification, high resolution and/or precision position information, etc.).

This report is written in several sections corresponding to the contract st items. The theme of each section is noted below.

SECTION	THEME
I.	Problem Analysis and Techniques Discussions.
II.	Equipment Parameters and Trades.
III.	Measurements and Evaluation (Part II).
IV.	System Analysis and Trades.
V.	Overall Orbit Prediction Capability (from angle only data).
VI.	Overall Conclusions (Part II).

Section I includes discussions of problem areas and brief descriptions of the techniques applicable to space surveillance system tasks. Section II includes equipment aspects, detection theory, operational theory and linearity and registr problems, etc. Section IV includes a few approaches to system aspects of the separation problems for baseline separation and single station catalog separation Section V discusses the Orbit Prediction problem. Since no actual system requir ments were specified, the report material is presented in a modified handbook format together with several postulated system configurations, to illustrate appli cation of its content to this and other electro-optical requirements. Part II of th report will present general conclusions and recommendations in addition to perfo mance measurement and evaluation criterion. A glossary of terms and definitio is included in Part I following the text material.

SECTION I. PROBLEM ANALYSIS AND TECHNIQUES INVESTIGATION

A. GENERAL PROBLEM DISCUSSION AND BOUNDARIES

The separation, discrimination, and identification of a specific object in an environment with other objects in a night sky background is an extensive field The Electro-Optical Space Surveillance Task is concerned with detection and separation of the objects from the night environment by passive means; that is utilizing reflected celestial illumination, primarily the sun. The altitude of objects detected may be quite large depending on location and the amount of the reflected illumination and therefore angular rates may vary from 2 or 3° per sec, to sidereal rate and even retrograde, with inclinations from polar to equatorial.

Since low altitude objects (orbiting satellites and ballistic trajectory targets less than 2000 miles above earth surface) are illuminated only a few hours of the day, they are assumed to be under 24 hr. surveillance by the active radar network. They are not considered targets for the electro-optical system surveillance task but are of concern since they will be detected and would otherwise cause false alarms. In fact, their appearance rates may account for 80 to 98% of the alarms until their orbits are established.

In this report we will touch primarily on techniques where separation is detected using one or more specific object or target characteristic. Discrimination and identification may also be obtained thru use of electro-optical techniques and systems but they are not specifically reported here. The separation techniques applicable fall into one or more of the following four categories, namely:

1. **Object or Target Signature**
   - a. **Spectral Identification**
   - b. **Scintillation, tumbling, etc.**
   - c. **Variation of Illumination during orbit**
2. **Catalogue**
3. **Location of Object**
   - a. **Depth of Focus**
   - b. **Rate Maneuver**
   - c. **Celestial Displacement**
4. Motion of the Object to Background
   - a. **Monocular Systems (time displaced change with respect to background)**
   - b. **Binocular Systems (position displaced simultaneous; 3D displacement with respect to background)**

1. OBJECT OR TARGET SIGNATURE

Object detection and separation by signature also involves discrimination and identification by virtue of specific spectral response, scintillation-tumbling, or variation of illumination, etc., in that it also distinguishes it from others as well as the background. For spectral identification, the alternate use of band filters to measure response at specific spectrum bands is the principle technique. Various photocathode surface responses can be used to extend capability of the method S-10, S-16, S-20, S-1, and middle and far infrared tubes and/or detectors with band filters can also be used, however, energy differences are small (therefore, little use is considered) except for re-entry.

For scintillation-tumbling, etc., the variation of returned and collected energy is analyzed to resolve identifying characteristics and so classify the objects or targets involved.

For a vehicle which moves with respect to observer, the amount of illumination and thus reflected energy reaching observer changes according to its motion. The illumination and phase of illumination are involved in setting the object brightness and are representative of its motion. The reflected and collected energy by the detection system additionally varies with the vehicle motion and the phase (angle position) with respect to the detector. Thus, the extent and rates of change of returned energy will define an object from others and its background. This change is difficult to measure with sufficient precision (it is also affected heavily by atmospheric conditions, see Section I-C) in practice and hence has little favor as a single technique. However, a discussion on the general subject is hardly complete without this much written.

2. CATALOGUE

A fundamental method of recognizing a new target or object is simply to count and keep track of every object and celestial body, etc. Except when classifying only larger close-by objects (which can be practical because of small numbers), the numbers get fantastic to say the least. Total stars to 6th magnitude number approximately 1-1/2 per degree^2 but total stars to 16th magnitude number approximately 2500 per degree^2. Thus, until real micro-storage catalogue capacities at fantastic access speeds are available, this technique will not be considered practical using computer techniques. It is on the other hand quite practical to use a film or picture of the field of view and then reference it for a catalogue to find new targets by (1) using the film to cancel existing stellar objects before being registered on the sensor or (2) by scanning the picture and video comparing it to the electronically scanned sensor present view.

3. LOCATION OF OBJECT

An object can be "depth" separated from a background of other objects by measuring the focus plane change between object and infinity even though there is no relative motion during the measuring period. Here we are using the basic principles of lens object and image distances as a function of focal length: — the focal length does not have to be exceptionally long either. For instance, at 1500 inch focal length there is an easily recognized change of focus plane for the moon (at 240,000 miles) and the stars (at infinity).

Practical ranging systems based on this principle have been built and proven by the GE Company's Advanced Electronics Laboratory at Ithaca (using point detectors).

An object with little or no relative motion during the processing time period involved can also be "depth" separated by use of maneuvers of the observer or observing station. The maneuver has to be scheduled accurately or known accurately for the processing system to distinguish the object with respect to others and/or the background of objects. The maneuver can be aircraft maneuvers, space vehicle maneuvers in case of an air or space borne detection system, in addition to programmed maneuvers if a ground based system is used. The simplest form of a ground-based maneuver system is a fixed earth position system; the earth's rotation providing the maneuver. In this case, the constant earth rotation of the observer produces a displacement that generates a parallax change of the air or space borne object to background. When at or near the equator the displacement due to rotation rate is greatest, but above 70° latitude the relative displacement decreases rapidly and, of course, is zero at 90° (earth's pole) even though the earth's rotation rate is unchanged. This method is particularly appropriate for space probe vehicles traveling in celestial space and is one of the simplest to implement in practice. It is described here by an example:

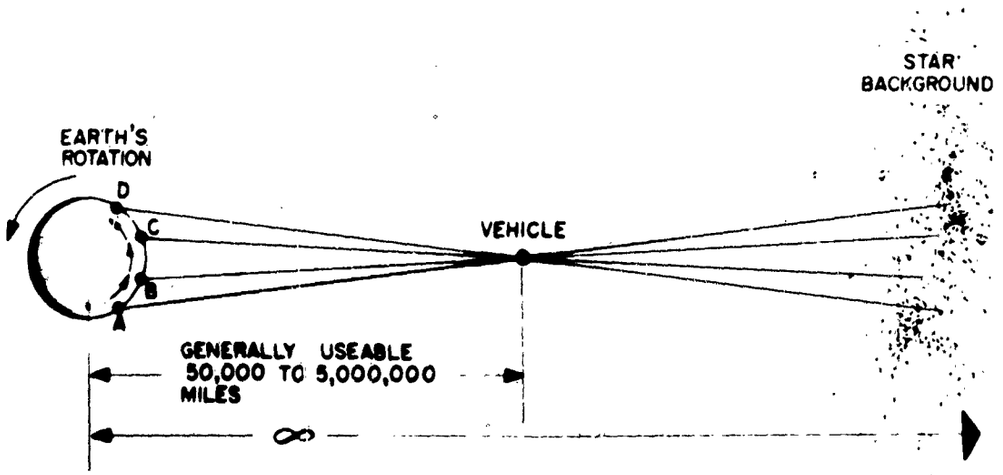


Figure I-1. Parallax Angle of an Object as Changed by Earth's Rotation

Referring to Figure I-1, as our position on earth moves from A to B with earth's rotation, the parallax angle of an object (generally appropriate for 50,000 to 500,000 miles) changes. For one hour, the lateral vector varies from approximately 500 miles to 1000 miles (B-C area) back to 500 miles. Using 600 miles/hour as a mean, this is 10 miles/minute of time. Since 1 sec of arc is 1.1 miles at moon distance; then 10 miles will be 9 sec of arc change in 1 min of time at 240,000 miles.

Using a 16" F/15 telescope at cassegrain focus (240" focal length) the field of view is approx. 20 min or 20 × 60 sec/600 lines = 2 secs/resolution element.

Since the minimum occupation of a faint target is 2 or 3 resolution elements and a space is desired between successive exposures of a double or triple exposed photograph, a minimum of 6 elements must be traversed. 6 × 2 sec = 12 sec.

Thus a minimum of 12 sec/9 sec/min. of time or 1-1/3 mins. f time between exposures.

Allowing some error for the telescope clock track error (R. A.) (though this usually proves to be almost negligible) and some error due to vibration and system instability, exposures taken approximately 2 to 3 mins. of time apart will permit detection and discrimination of a space probe (at lunar distance) from stars, planets, asteroids. This spacing will also eliminate fast moving objects (satellites or airplanes) which will traverse beyond the near vicinity in any min. of time as well as be in a different direction to earth axis rotation.

4. MOTION OF OBJECT TO BACKGROUND

When the motion of object is at or near stellar rates (celestial background) the method described in the previous paragraphs is best suited, however, as the motion difference to stellar background increases, several other techniques will give us motion detection in shorter times. The simplest of all is motion defined "looks" when the exposure is long enough to produce blurring; a stretching in the motion direction and/or trailing effects from the moving target. Figure I-2 illustrates this in case of a photograph of the monitor during a pass of the Midas satellite. Here the signal on the monitor was not blurred, but by taking a long exposure of the monitor the film record readily distinguishes the moving object.

The more sophisticated techniques for moving target identification (M T I) fall into two basic categories:

a. **Monocular systems, where detection of a change in position with respect to background pattern is dependent on a time interval between two or more separated looks, and requires image storage.**

b. **Binocular or stereo systems, where detection of position difference with respect to background pattern is dependent on time synchronized "looks" from two or more equipments separated by a reasonable baseline (3D).**

   The binocular or stereo is sometimes described as a simultaneous 3D MTI system, though it should be noted that processing time is still involved and thus does not necessarily have any distinct advantage over the simpler and less expensive monocular systems.

   To adapt monocular or binocular systems for successful spatial separation between object and background, positive position separation is required, either through time or baseline separation, for passive systems. The extent of separation needed to obtain a given false alarm or detection probability depends on:

   1) **Tolerances and stability of all components and equipments in the system link.**

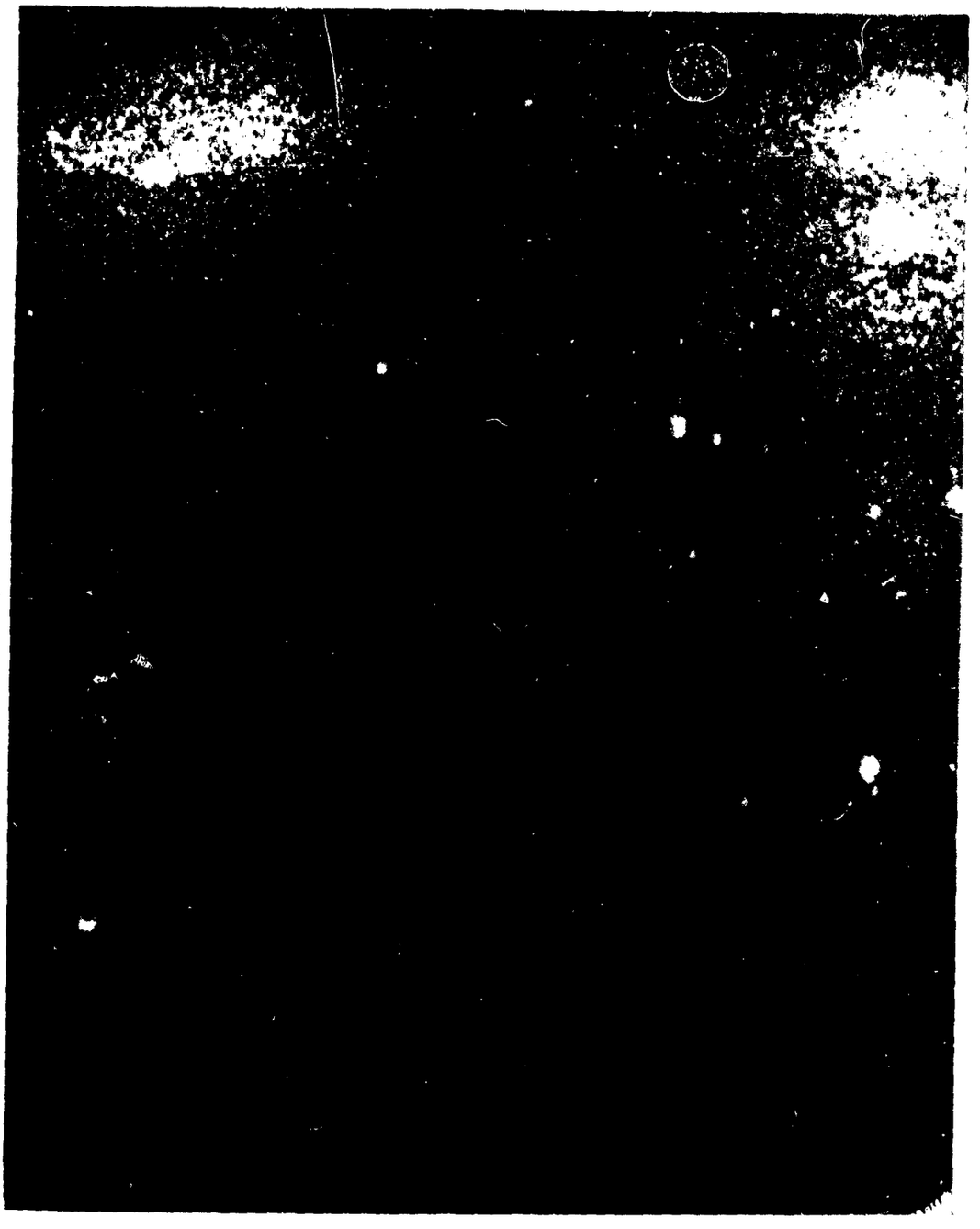


Figure I-2. Midas Satellite, 1930' 10" E.S.T., 1/10/62, From Cazenovia Test Site Near Syracuse; 1029 Line Scan; TT&H 5" f/4 Remote Control Zoom Lens Set for Approximately 12" Focal Length; Approximate Mount Angles (Az 27°, El 68°), 1/2 sec f/4.7 Polaroid Film Exposure of Monitor

2) Relative target velocities and the stability, and motion of objects in the background (planets, asteroids, comets and meteors) as read through the "seeing" conditions of the local atmosphere or atmospheres.

Range measurements in a single sensor system can be obtained by measuring target look angle versus time (assuming the target is orbiting the earth).

A multiple station (stereo) system can be used just for separation (star cancellation), with the only available information being target look angle versus time. However, if the target is present in both fields of view, the additional information of relative target angle between the two stations can be used to find range directly from one time image by triangulation.

a. Monocular Systems

In case of monocular systems two fundamental approaches are generally considered:

The first involves making a film catalog (exposed negative) of the sky at the same scale as the electro-optical system by using same optics. After developing the negative it is programmed in front of the sensing device and serves to cancel the background of stars catalogued. Any object that has moved significantly from the time of exposure or was not at the location of a previous image, will not be cancelled and thus is detected.

Due to celestial changes from day to day, week to week including proper motions of stars (the stars move too if considered over longer periods of time), new negatives will be needed. All moving celestial bodies, comets, planets, asteroids, etc., will show as moving targets depending on up-dating of negatives and, of course, meteors and new satellites will continually need to be accounted for to reduce the possibilities of panic. Because of the actual large reduction of processing capacity possible in the approach over one not including cancellation of "fixed" objects and stars, studies of potentials and limitations of the methods were initiated some time ago on a GE-funded program and pertinent phases have been implemented to evaluate the method by actual experiments. To date some successes have been achieved in addition to uncovering new problems with this technique. The light loss due to film transmission and the extra relay lens needed reduce systems performance; preliminary data indicates this may be 2 or 3 star magnitudes. The film loss itself can be reduced or nearly eliminated by special negatives and development procedures.

The second approach registers all objects and celestial objects and transfers the entire field of view at a particular instant to a storage media (storage tube. delay line, drum, film, etc., tape, could be used but B W capacity might limit in case of a high performance system). A few seconds (for faster moving objects) or a few minutes (for slower moving objects) later, a second view of the same field of celestial sky is compared with the earlier stored picture and the non-cancelled objects displayed and information fed on for processing. This is thus a temporary cataloguing system using a delay interval suited to the relative motion of object and observer.

A complete operating MTI delay interval Electro-optical system using a storage tube and comparison logic has been built and tested on a GE-funded program. It has proven quite satisfactory and is being used to determine component tolerances and stability requirement needed for a production prototype. This MTI system has

pointed up some shortcomings, some of which can be completely or nearly completely corrected by design changes.

A variation of the above approach uses two similar (matched) image orthicon cameras using the same optics through a beam splitter or optical switch so that one I.O. is exposed but not readout until (t) seconds later when the second I.O. is exposed and both are readout simultaneously and the videos compared.

Further details and variations of the two I.O. systems are covered in Section I-E & F.

b. Binocular System

A brief study of separation (baseline) distances needed for various altitude satellites and the probable equipment tolerance needed for adequate recognition is reported in Section IV. One of the bigger factors is the atmospheric stability, as exemplified by the photographs in Figure I-3.

Unless some of the system and equipment tolerances can be reduced, the practicality and advantages of a binocular system over a monocular system will not necessarily be achieved.

Several attempts to take simultaneous stereo photographs of the ECHO satellite from Syracuse and Schenectady encountered weather problems. Since the sites involved were roughly 95 miles apart and the satellite only 1000 miles high, we hoped to get pictures looking over each other's shoulders to effectively reduce the differential pointing angle. Due to the broken cloud weather at both locations, only a few simultaneous frames were obtained and these with the satellite nearly overhead. Consequently, entirely separate star backgrounds were photographed. Lack of targets in the 30,000 to 300,000 mile range will make observational work difficult for simultaneous 3D experiments on targets at these ranges. This is the most likely range for practical use of separated sites, whereas time-lapse single station 3D requires only a few seconds separation for ranges below 30,000 miles; this is of course less stringent on equipment requirements.

The transfer of information between baseline separated sites does not appear to be too difficult. The complete image is required for stereo separation. With modern TV microwave links the full or nearly full bandwidth information can be sent quite economically where security will not restrict its use.

Problems in the film cancellation method (monocular or binocular) include refraction errors, extent of cancellation needed (density), optical system linearities, alignment, electronic stability, motion and changes in motion needed for orbit prediction, target spreading, storage media versus sensor equipment linearities and registration stability, etc., in addition to the ever present data output format.

Combinations of binocular and monocular systems can provide many features of both and increase performance limits for certain applications. Here, however, careful analysis of application requirements and equipment tolerances must be made carefully to delineate the specific conditions for improved performance; otherwise, the expenses of the more complicated system may not be justified. See Section I-E & F.

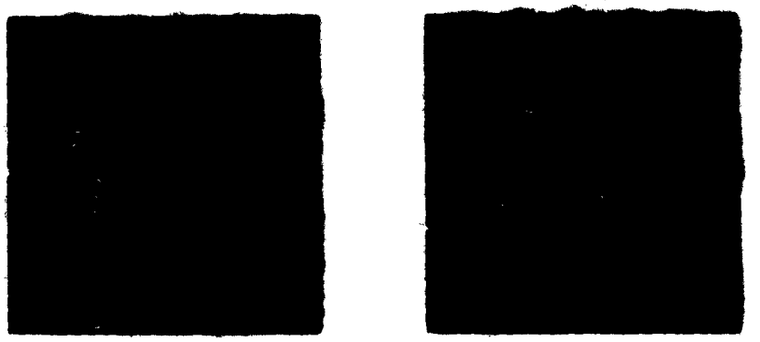


Figure I-3A. Stereo Photos Showing Several Star Levels

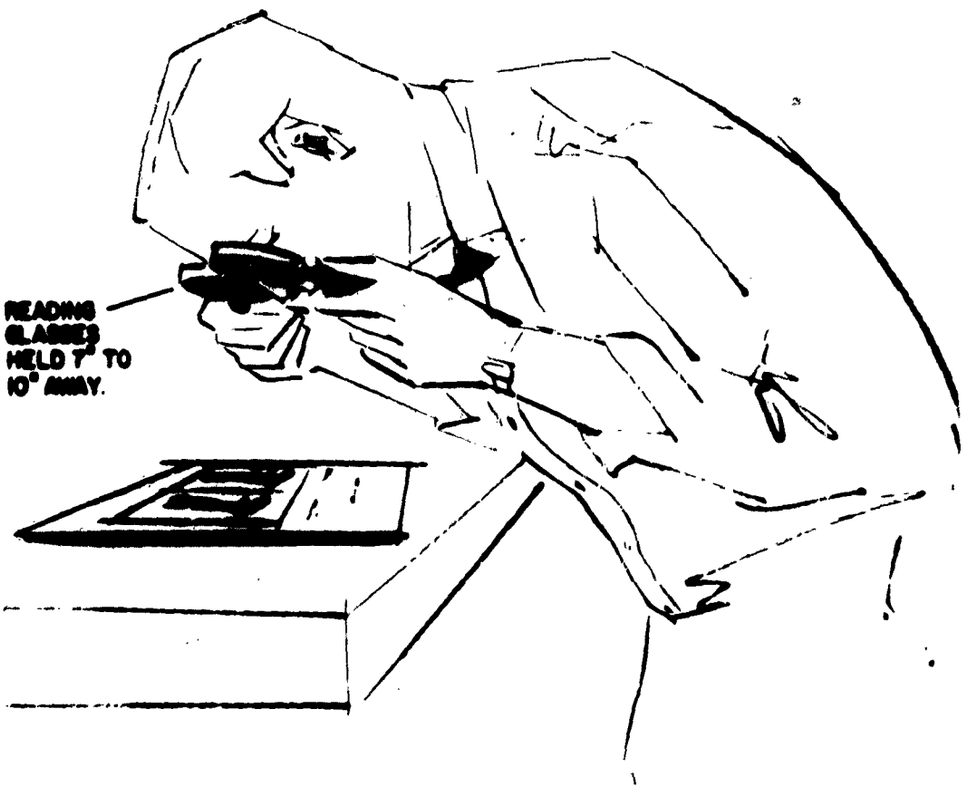


Figure I-3B. Suggested Method of Viewing Stereo Photos

B. THE CELESTIAL ENVIRONMENT

In aero-space surveillance tasks the celestial environment is the background (content and variations) against which the target or object is to be detected, separated, confirmed and/or tracked and in some cases resolved. It, in most cases, furnishes the illumination of the object (usually the sun), see Section I-D, and the isolation provided by the shadow of the earth and celestial position.

The electro-optical equipment performance for detection and separation of an object will be limited by the background, primarily equipment noise and sky brightness. We are concerned with both day and night conditions when observing from earth mounted stations, but since this study is concerned only with nighttime operation we will limit reporting accordingly. From earth orbiting or space stations many other factors must be considered but this is likewise beyond the scope of this study and report.

Since much of the published work akin to the celestial environment is in astronomical and/or photometric literature, special note is included here on basic definitions and conversion tables before continuing with the detail discussions of the celestial environment.

1. ASTRONOMICAL AND PHOTOMETRIC TERMS, LIGHT SOURCES, AND VISION FACTORS

a. Astronomical Terms

1) Stellar Magnitude (difference) Δm.

Most astronomical data and calculations are based on use of stellar magnitudes differences. These are similar to the decibel scale (db) commonly used by the engineer. To the engineer the stellar magnitude difference $\Delta m = (m_y - m_x) = 2.5 \log I_x/I_y$. I_x and I_y are the respective intensities of two sources being compared. In another form $I_x/I_y = 10^{0.4m}$. Thus, the stellar magnitude scale is seen to be a compressed db scale. To the astronomer this equation is used in the form $(5\sqrt{100})^m = I_x/I_y$. Thus, the stellar magnitude difference Δm is the exponent of the $5\sqrt{100}$ needed to equal the ratio of two intensity sources with positive increasing values indicating fainter sources.

Stellar Magnitude Difference (Δm)		Intensity Ratio $\left(\frac{I_x}{I_y}\right)$	Decibel Scale (db)
1.0	=	2.512 ≈ 2-1/2 ratio	4
2.0	=	6.31 ≈ 6-1/3 ratio	8
3.0	=	15.85 ≈ 16 ratio	12
4.0	=	39.81 ≈ 40 ratio	16
5.0	=	100 = 100 ratio	20

The symbol for stellar magnitude difference = m. The subscript v is added to designate visual magnitude (m_v), the subscript p designates photographic. To simplify conversion of Intensity Ratio to Stellar Magnitude differences and vice versa, refer to Figures I-4 through I-7.

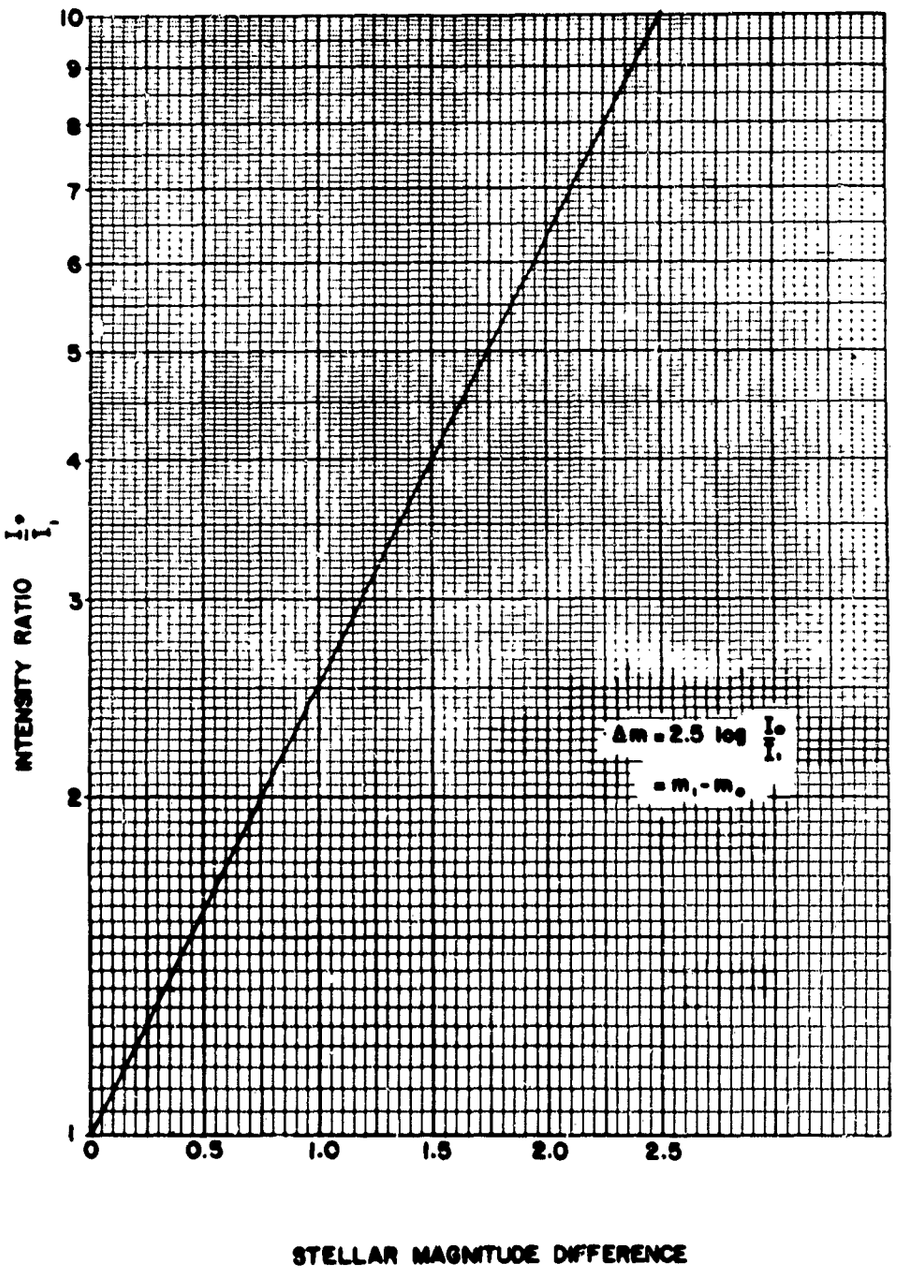


Figure I-4. Conversion Chart, Intensity Ratio to Stellar Magnitude Difference

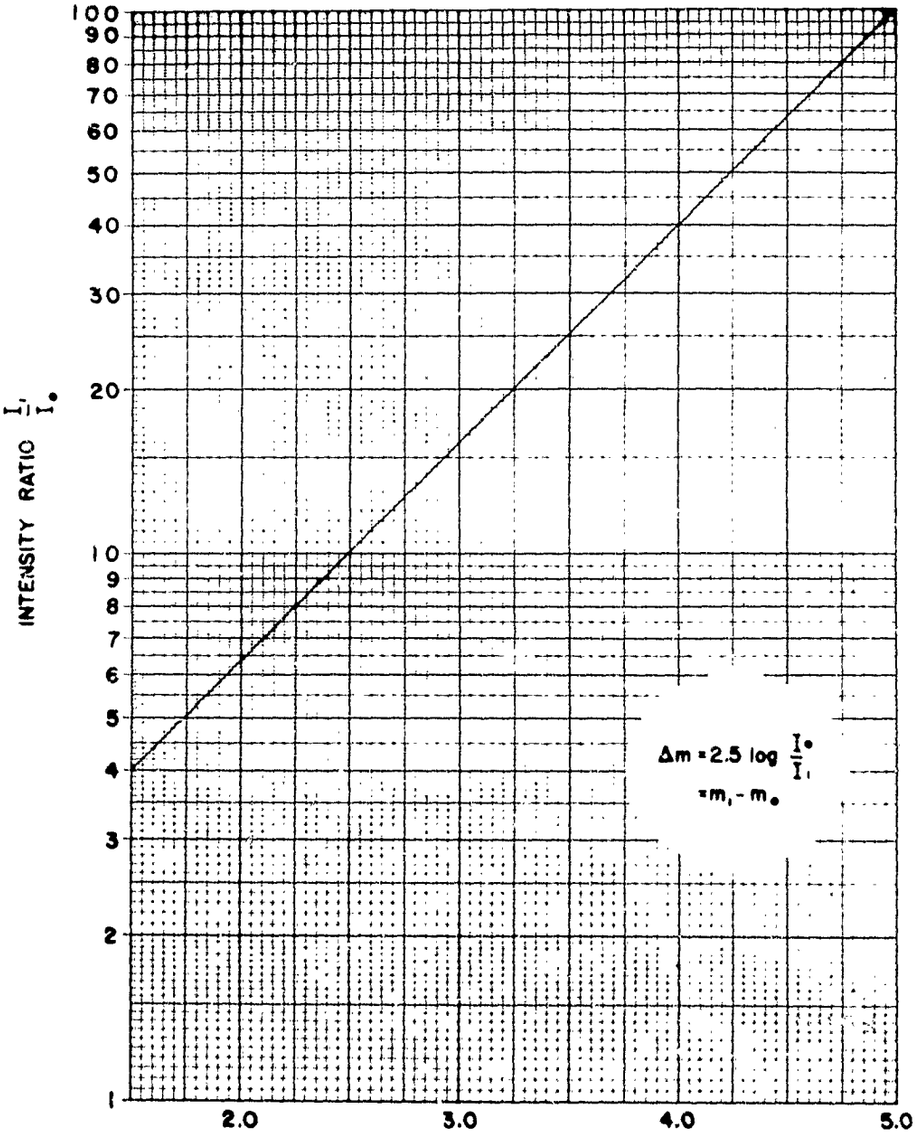


Figure I-5. Conversion Chart, Intensity Ratio vs Stellar Magnitude Difference

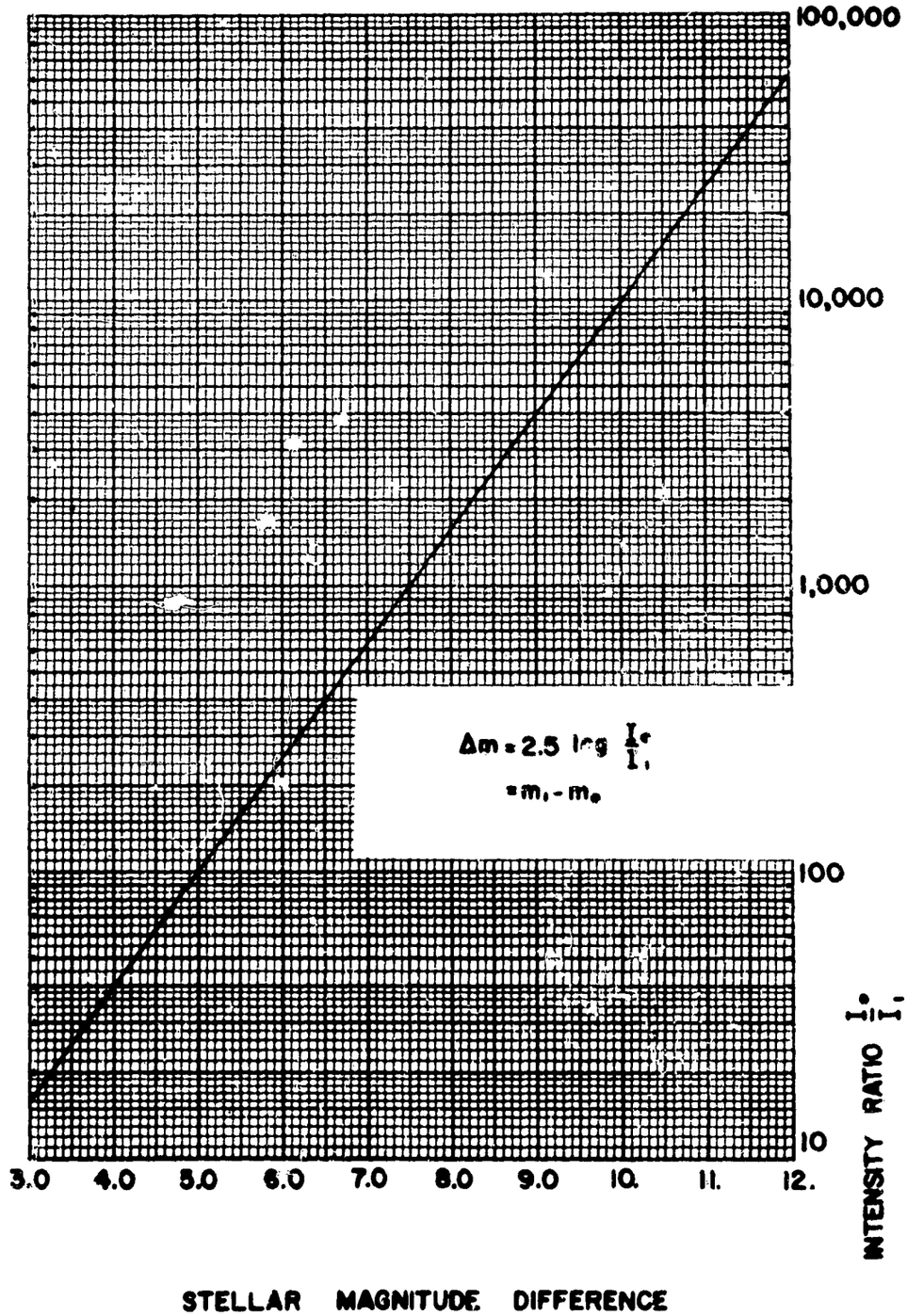


Figure I-6. Conversion Chart, Intensity Ratio vs Stellar Magnitude Difference

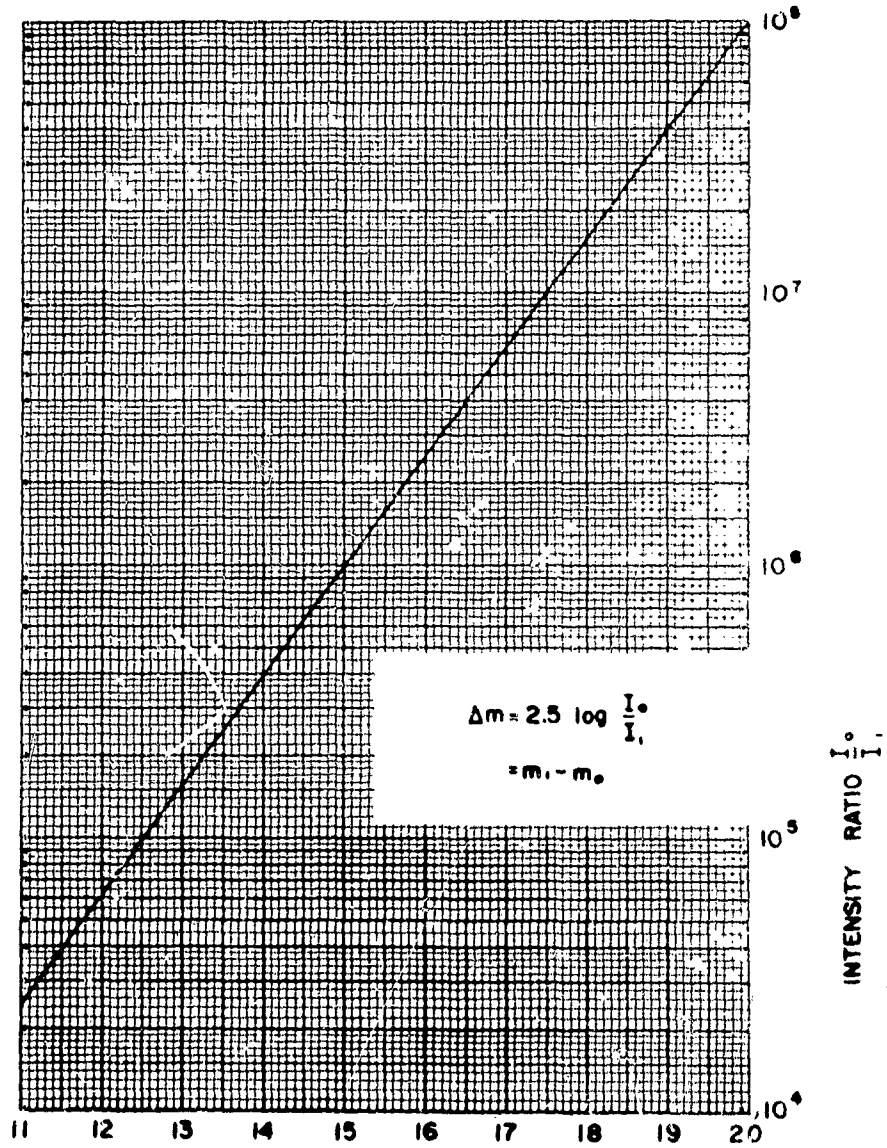


Figure I-7. Conversion Chart, Intensity Ratio vs Stellar Magnitude Difference

Magnitude measurements are made by visual observation, photographic measurement, and photometric measurement; m_v refers to magnitude measured visually, wavelength peaked at 5500Å; m_p refers to magnitude measured photographically; m_{pg} are peaked in the blue region (4500 - 4700Å); while m_{pv} are peaked in the visual region but measured photographically. Photometric magnitudes are measured in any of 6 or more wavelength peaks, depending on the photometer.

2) Stellar Magnitude, apparent (h) m

In addition to stellar magnitude differences, the specific brightness value of a particular object can be measured in terms of the stellar magnitude scale (as 5th magnitude star = $5m_{pv}$ or $m_{pv} = 5$). This is simply the numerical magnitude difference referenced to a zero magnitude source. To provide for the variation of brightness with distance, the designation of apparent or absolute is added. Thus, the apparent stellar magnitude (x) m is the measure of the brightness as observed in terms of the value of $m_x = 2.5 \log (I_o/I_x)$ with respect to a zero stellar magnitude source, i.e., $(m_x - m_o)$; positive increasing numbers indicate decreasing brightness.

3) Stellar Magnitude, absolute (h) M

The absolute stellar magnitude (h) M is the apparent stellar magnitude (m) of a given star referenced to a standard distance of 10 parsecs (pc). A parsec is 3.0857×10^{18} cm or 3.262 light years or 206,265 Astronomical Units (an AU being the mean earth to sun distance).

The value of brightness or stellar magnitude may be in terms of photovisual spectrum response (m_{pv}), Photographic (m_{pg}) which is astronomical film Type 103 a-O response, bolometric (m_{bol}) which is the black body spectrum response curve, infrared (m_{ir}), etc.

The specific value of brightness of an object or source of zero magnitude visual spectrum ($0m_v$) is defined as a source of brightness equal to 2.43×10^{-10} lumen/cm^2. If we use a visual pass band filter in front of a photon counter we would collect 10^6 photons per square cm of receiving aperture per second of time from a $0m_v$ source. Thus, $0m_v = 10^6$ photons/cm^2/sec and 15 $m_v = 1$ photon/cm^2/sec with the subscript used according to the photon collecting element and filter response band used (visual, photographic, bolometric, etc.).

Star brightness values are often referenced as measured "outside" the earth's atmosphere or "inside" the atmosphere. The difference is the absorption of the atmosphere for the spectral response of sensor used and, of course, the black body source temperature. The values vary from author to author as well as including sensor response, and average around 85% transmission for the visual spectrum (see Section I-C for more detailed values for other responses). An apparent visual magnitude of $0m_v$ is the same whether looked at on the earth or above earth's atmosphere but the irradiance does change, thus $0m_v = 10^6$ photons/ cm^2/ sec above atmosphere but is only 85 percent as bright ($.85 \times 10^6$ photons/cm^2/sec at earth's surface looking straight up).

Unless otherwise noted: (1) the stellar magnitude values are generally assumed to be apparent stellar magnitudes, (2) the word magnitude refers to stellar magnitude unless otherwise noted, (3) the abbreviation sec. or min. is used for second(s) or minute(s) of time whereas $\overset{\frown}{\text{sec.}}$ or $\overset{\frown}{\text{min.}}$ is used for second(s) or minute(s) of arc or angle.

b. Photometric Terms

Luminous Flux (F) is proportional to the rate of flow of radiant energy and to a luminosity factor which depends on the spectral distribution of that energy, and is thus determined by the response of the human eye. The luminosity factor for radiation of a particular wavelength is the ratio of the luminous flux to the radiant power producing it. The unit of luminous flux is the lumen (lm) or the luminous flux emitted by one international candle through one steradian. Thus a 1 candle power source gives off 4π lumens of flux, or one lumen on a one foot square area at one foot radius from the source. One lumen of maximum visibility radiation (5550Å) = 1.47×10^{-3} watts.

Luminous Intensity (I) or candlepower of a point source of light is the solid-angular density of the luminous flux emitted in the direction considered: it is the flux per steradian in that direction, $I = dF/dw$. The unit is the new candle (cd) or candela or the lumens per steradian.

International Candle has been the standard of luminous intensity for light sources (especially incandescent lamps) and the conventional unit (candle). One international candle = 1.019 cd (candela or new candle). One Hefner candle = .903 cd.

Note: In the past the lumen was defined in terms of the flux from a candle. The present day standard is a brightness or luminence of a black body at freezing temperature of platinum (2042°K) with a standard value of 600,000 new candles/meter^2.

Luminance (B) of an element of a luminous surface, from a given position, is the luminous intensity per unit area of the surface projected on a plane perpendicular to the line of sight, and including only a surface of dimensions small in comparison with the distance from the observer, $B = dI/dA \cos \theta$; θ = angle between plane and line of sight. The conventional units are the candle/cm^2 (or stilb), candle/in^2, candle/ft^2.

The luminance of any surface, in a specified direction, can also be expressed in terms of the lumens per unit area from a perfectly diffusing surface of equal brightness. Brightness expressed in the Lambert System is obtained by multiplying by π; $B = \pi dI/dA \cos \theta$. Thus, units are now Lambert's ($1/\pi$ candles/cm^2) and Foot-Lambert's ($1/\pi$ candles/ft^2).

Lambert's law surface $\Delta I_\theta = \Delta I_n \cos \theta$ candle/cm^2, so $B = \Delta I/\Delta A$ = a constant, independent of θ.

Brightness Units and Conversion Factors:

Stilb (sb) (c/cm^2)	c/in^2	c/ft^2	Lamberts (L)	Millilambert (ml)	Foot-Lambert (ft-L)
1.0	6.45	929.0	3.142	3142.0	2919.0
0.155	1.0	144.0	0.48695	487.0	452.0
0.00108	0.00694	1.0	0.0034	3.381	3.142
3183.0	2.054	295.7	1.0	1000.0	929.0
0.00032	0.00205	0.2957	0.001	1.0	0.929
0.0003426	0.00221	0.3183	0.001076	1.0764	1.0

1 $0m_v$ star per sq. degree outside atmosphere = 0.82×10^{-6} sb; 1 $0m_v$ star per sq. degree inside clear unit air mass = 0.68×10^{-6} sb (star at zenith)

Illumination of a surface (Illuminance) (E) is the luminous fluxdensity ove the surface or the flux per unit area of intercepting area $E = dF/dA$. The practical units of illumination are the lumen/ft^2 (foot candle), lumen/cm^2 (phot) and lumen/r (lux) (meter candle).

Illuminance produced by a point; $E = I \cos \theta / r^2$, where r = distance; θ = angle between normal to surface and direction of source.

Illuminance produced by an extended source of brightness B (such as sun, moon); $E = BA/a^2 + b^2$, where A = area of disc; a = radius of disc; b = distance of disc.

Illumination Units and Conversion Factors:

Lux (lx) (meter-candle)	Phot (ph) (lumens/cm^2)	Milliphot	Footcandles (ft-c) (lumen/ft^2)
1.0	0.0001	0.1	0.0929
10000.0	1.0	1000.0	929.0
10.0	0.001	1.0	0.929
10.764	0.0010764	1.076	1.0

Quantity of light or luminous energy (Q) is the integration of the luminous flux (F) per time period or unit of time; $Q = \int F\, dt$. The unit is the lumerg (cgs), Talbot (mks), or lumen-seconds or lumen-hours. Where small quantities of light are involved the units are expressed in photons for the area units involved as photons/cm^2. One star ($m_V = 0$) = 10^6 photons/cm^2 of lens aperture, for every second of image time.

The relationship of Illumination (I) incident on a surface and Surface Brightness (or luminance) (B) is dependent on the reflectivity factors of the surface or object areas involved and the background surface. A surface having one lumen/cm^2 of Illumination and 100% reflectivity, has an apparent brightness, of one lambert (radiating over a hemisphere).

Thus Scene Brightness (B) or luminance equals Scene Illumination (E) times the scene Reflectance (R), i.e., $B = ER$. The ratio of the reflectivity factors throughout the scene (objects to background of scene) is defined as the contrast ratio and thus sets the ability to distinguish or resolve features of the surface or object. The higher the Illumination source and the greater the contrast ratios involved, the better the resolution capability (sharper) to distinguish features. By geometric optics the photocathode illumination E, in foot candles, is related to the scene brightness B, in candles/ft^2, and for object distance large with respect to focal length, $E = \pi B/4 (f^2)$ where f is the f/number of the optic system. (If B is in foot lamberts, eliminate the π.)

c. Light Sources

1) The Sun

Mean brightness of sun's disk outside atmosphere 2.08×10^5 stilbs = 6.53×10^5 lambert.

Apparent brightness 1.4 to 1.6 $\times 10^5$ stilbs (c/cm^2) = 1.3 to 1.486 $\times 10^8$ candles/ft^2

Candle power of sun = 3.17 $\times 10^{27}$ cd

Light flux outside earth atmosphere at mean solar dist. E = 14.14 phot

Solar Luminosity 3.86 $\times 10^{26}$ watts

Solar radiation emittance at surface F = 6.35 $\times 10^{10}$ erg cm^{-2} sec^{-1}

Solar magnitude, (apparent) m_{pg} = -26.41, (absolute) M_{pg} = 5.16

m_{pv} = -26.86 M_{pv} = 4.71

m_{bol} = -26.95 M_{bol} = 4.62

color index = $M_{pg} - M_{pv} = m_{pg} - m_{pv}$ = 0.45

Spectral type G-2 = dwarf star with 6000°K (10,000°F surface temperature) (internal temperature~15 million° K)

Total solar radiation:

solar constant (flux of total radiation received outside of earth's atmosphere per unit area at mean sun-earth distance) =

1.97 (cal/cm^2)/min = 1.374 $\times 10^6$ (erg/cm^2)/sec

mean radiation intensity of sun's disk (F) = 2.02 $\times 10^{10}$ erg/cm^2/sec/sterad.

Size (mean) 30 mins.

2) The Moon

Apparent brightness 2.54 $\times 10^{-1}$ stilbs = 2.36 $\times 10^2$ candles/ft^2

Lunar Magnitude full moon $-12.2m_{pg}$

quarter moon $-11.4m_{pg}$

earth illuminated $-2.0m_{pg}$

size (mean) 30 mins.

Moonlight (clear night) brightness = 1.61 $\times 10^{-7}$ stilbs = 1.5 $\times 10^{-4}$ candles/ft^2

Moon Aureole brightness (see also Figure I-12A and 12B) up to 2 $\times 10^{-5}$ stilbs

Normal sky brightness (total sky average) (see also Figure I-9) 5 $\times 10^{-4}$ stilbs (Allen)

d. Human Vision Factors

The human eye, plus the associated portion of the brain, provides the means for seeing.

Human vision and interpretation affect electro-optical equipment and/or system performance when eye viewing monitors or using vision as a comparison or evaluation measure. The spectral response of the human eye is basic to the definitions of many photometric terms (Section I-1-b).

In addition to its ability to accommodate a large variation in brightness, the pupil size of the human eye can be adjusted from about 8mm opening to 2 mm thereby further extending its range. For daytime or cone vision its range varies from 10^{+3} (max scene brightness readily accommodated) to 10^{-3} ft lamberts.

In addition, if allowed to adapt itself to dark scenes, low ambient light levels; visual purple regenerates in about 1/2 hour, and the detection limit is extended by a factor of about 1000 to 10^{-6} ft lamberts for rod or night vision. In addition to increased sensitivity, there is also a shift toward blue of the spectral response of the "dark adapted" eye. See Figure I-8.[1]

Response Curves of Human Eye, Normal and Low Light Level (Dark Adapted)

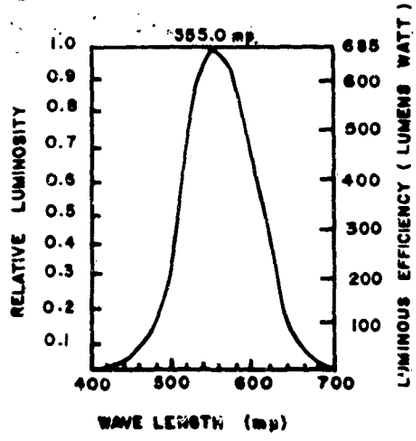


Figure I-8A: Relative Luminosity Curve for the Standard Observer; Scale at Left, Relative Luminosity; Scale at Right, Luminous Efficiency

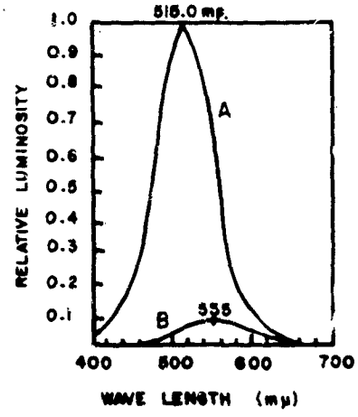


Figure I-8B: Relative Luminosity Curves Under Conditions of (a) subdued lighting (dark adapted) (b) good lighting (daytime vision)

Figure I-8. Eye Response Curves

The "grey level" of any portion of the field of view of the eye is set by the scene brightness in that area. The eye measures grey scale or variations of brightness by scanning or vibrating to detect a variation of light intensity on adjacent rods or cones. This is much like the function of a chopper and/or reference source in a point detector system. The amplitude of this vibration varies depending on the extent of the image or edge being read. The frequency has been determined experimentally to be approximately 130 cy/sec.

(1) F. W. Sears, Optics Addison-Wesley Publishing Co., Inc., Reading, Mass. 5th printing, 1958.

If the eye is subjected to total darkness and allowed to become dark adapted, it begins to see "grey" and sometimes other weird effects. What is actually happening is the gain is turned up until the system "noise" is read in the output, then readjusted and tried again always looking for the faintest recognition of some incoming photons.

The luminance limit of color perception, with daylight (cone) vision associated with the fovea region, is 10^{-3} ft. lamberts. Night (rod) vision, associated with the parafovea region, has no color perception.

Scene Brightness or Luminance needed for various conditions of human vision:

10^{3} foot lamberts - max acceptable scene brightness

10^{-1} foot lamberts - needed for color contrast recognition

10^{-2} foot lamberts - needed for color perception

10^{-3} foot lamberts - daylight vision minimum

10^{-6} foot lamberts - lower scene brightness threshold of dark-adapted eye

Range of scene brightness accepted by eye is one billion (10^{-6} to 10^{3}) foot lamberts.

The resolving power of the eye is its ability to produce separate images of close objects. The retina of the eye consists of a large number of light sensitive elements, the rods and cones, each having a spacing between centers of 0.001 to 0.003 mm. Each rod and cone produces a separate visual sensation in the brain. Thus, two image points reaching a single rod or cone will be judged as one by the brain. Since the image of the two points are two different disks, they must be separated by a distance equal to the width of a rod or cone in order to be distinguished as two separate points.

Thus the resolving power = 1 $\widehat{\text{min}}$.

Storage time or exposure time of the eye = 0.2 seconds

Normal pupil diameter = 6-8 mm dark adapted, 2-4 mm day vision

Diameter of the eye = 25 mm filled with fluid of n = 1.33

Quantum efficiency of the eye = 10% max-dark adapted

Visibility (spectral) bandwidth about 1068Å peaked at 5550Å for day vision and at 5150Å for night vision.

Relative visibility factor (Kλ) for Normal (visual) Brightness (5×10^{-4} stilb or greater) photopic vision.

The Photopic Curve (International) (for Cone vision at fovea) See Figure I-8A (day vision).

Kλ

(Å) → / ↓	0	100	200	300	400	500	600	700	800	900
3000									.00004	.00012
4000	.0004	.0012	.0040	.0116	.023	.038	.060	.091	.139	.208
5000	.323	.503	.710	.862	.954	.995	.995	.952	.870	.757
6000	.631	.503	.381	.265	.175	.107	.061	.032	.017	.0082
7000	.0041	.0021	.00105	.00052	.00025	.00012	.00006	.00003		

Equivalent width of Kλ curve = $\int K\lambda \, d\lambda$ = 1068Å

Kλ lumens = .00147 watts = mechanical equivalent of light

Luminous Energy in Lumergs = 680 $\int K\lambda \, e\lambda \, d\lambda$ when $e\lambda \, d\lambda$ is element of energy in Joules

Relative visibility for dark adapted eye (10^{-7} stilb or less) scotopic curve (Rod vision) See Figure I-8B (night vision)

λ(Å) → / ↓	0	100	200	300	400	500	600	700	800	900
4000	.0185	.040	.076	.132	.212	.302	.406	.520	.650	.770
5000	.900	.985	.960	.840	.680	.500	.350	.228	.140	.083
6000	.0490	.0300	.0175	.0100	.0058	.0032	.0017	.00087	.00044	.00021
7000	.00010									

2. SKY BRIGHTNESS, MOONLESS NIGHT

The "night" includes the period of the night between the twilight hours (defined as the period from sunset to time sun is 18° below Horizon and again from 18° below Horizon to sunrise). The standard sky brightness figure for an "astronomically clear" moonless night usually quoted in astrophysical literature is equivalent to one 22.5 visual magnitude star per square second of arc as observed at Mt. Wilson, or simply 22.5 $m_V/\widehat{sec}^2$. Since Mt. Wilson is approximately 5,900 ft. above sea level and often has particularly clear and stable sky conditions, this value will not normally be attained for other locations.

Different astronomers, observers, and researchers express the sky brightness in different manners. For instance, Allen[2] gives total brightness, zenith mean sky as 400 tenth magnitude stars per square degree (visual). This is equivalent to 21.27 $m_V/\widehat{sec}^2$.

$$400 = -6.51 \text{ m}$$
$$10\text{th mag} = +10 \cdot \text{ m}$$
$$\widehat{\text{degrees}}^2 \text{ to } \widehat{\text{sec}}^2 = \underline{+17.78 \text{ m}}$$
$$21.27 \text{ m}_V/\widehat{\text{sec}}^2$$

Mitra[3] gives a figure of 0.045 first mag. stars/$\widehat{sec}^2$ which is 22.15 mag/$\widehat{sec}^2$ but from the context of his discussion, it would seem reasonable that he meant

[2]C. W. Allen, Astrophysical Quantities, Oxford University Press, 1955.

[3]S. K. Mitra, The Upper Atmosphere, Asiatic Society, Calcutta, 1952.

zero magnitude stars, which is the more normal expected reference. This then would give 21.15 mag/$\widehat{\text{sec}^2}$.

$$.045 = +3.37 \text{ m}$$
$$\widehat{\text{degrees}^2} \text{ to } \widehat{\text{sec}^2} = \underline{+17.78} \text{ m}$$
$$21.15 \text{ m}_V/\widehat{\text{sec}^2}$$

Dole[4] quotes an average brightness of the clear moonless night sky as 2×10^{-8} candles/cm^2. This is approximately 21.6 $m_V/\widehat{sec^2}$. He does not mention his source.

From the foregoing, for calculation purposes, the sky viewed from a low altitude (near sea level) point can be assumed to be about 21 to 21-1/4 $m_V/\widehat{sec^2}$ and up to 22-1/2 $m_V/\widehat{sec^2}$, if higher elevations are to be selected. See also reference[5].

Caution: If the lens and sensor combined resolution (see Section II-A) does not resolve one square second of arc but rather a larger value, then the brightness must be increased by the ratio of the larger area to one square second. Values smaller than one square second of arc should not be used where earth's atmosphere is involved. (See Section i-C on atmospheric effects.)

Of course, any contemplated sites should be surveyed carefully and actual background values measured, since the condition and reflectance of the surrounding terrain (topographical conditions, existence of nearby hills, mountains, plains, deserts, type of vegetation, season of year, etc.) local weather conditions, as well as nearby communities and cities, will affect the brightness and sky glow conditions.

3. SKY BRIGHTNESS GRADIENT (MOONLESS NIGHT)

Since we will be working at angles other than zenith, we need to derive some representative figures for other elevation angles or as the astronomers say, "altitude". Referring to the astronomical references and reducing the values, less the resolved stars, and drawing a smooth curve thru the results, we have Figure I-9 for the plot of the means (the values are fainter for the celestial pose areas and brighter if at the celestial equator).

$30^o = 21.13 \text{ m}_V/\widehat{\text{sec}^2}$

$25^o = 21.03 \text{ m}_V/\widehat{\text{sec}^2}$

$20^o = 20.91 \text{ m}_V/\widehat{\text{sec}^2}$

$15^o = 20.78 \text{ m}_V/\widehat{\text{sec}^2}$

$10^o = 20.6 \text{ m}_V/\widehat{\text{sec}^2}$

NOTE: Elevations below 15^o should not be considered unless sufficiently away from inhabited areas so that local sky glow is insignificant.

---

[4]Dole, Visual Detection of Light Sources Near the Moon, RM 1900 ASTIA #AD133032.

[5]D. J. LaCombe, The Brightness of the Clear Sky, G. E. Co. Report #TIS R63EMH1.

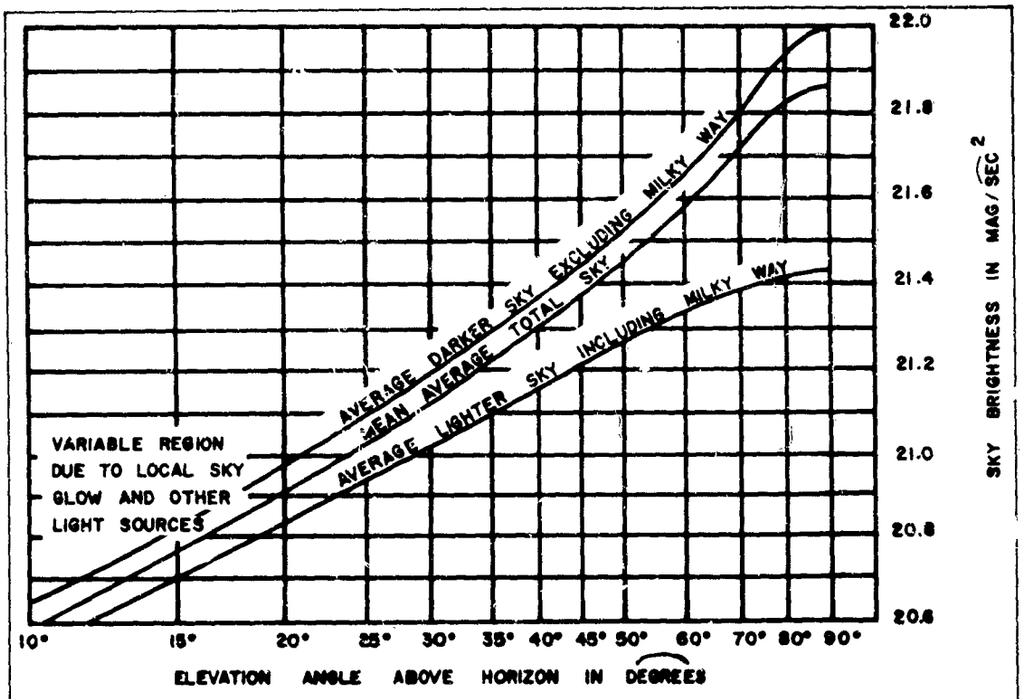


Figure I-9: Approximate Values for Average Sky Brightness (Mag/$\widehat{sec}^2$ vs. Elevation Angle Above Horizon, Moonless Night)

Figure I-9. Approximate Values for Average Sky Brightness (Mag/$\widehat{sec}^2$ vs Elevation Angle Above Horizon, Moonless Night)

4. SKY BRIGHTNESS COMPOSITION (MOONLESS NIGHT)[3]

The sky brightness includes:

Starlight and scattered starlight	30%
Galactic light	5%
Zodiacal light	15%
Air glow	40%
Scattered light from the last three sources	10%

The above table shows that about 60% to 50% of the total light is from parts of the sky where a star is not being seen by a single or adjacent resolution element. The other 40% to 50% is from brighter resolved stars or celestial formations. (The values vary depending on proportion of stars being resolved. The more stars resolved, the less light left in the unresolved sky.)

[3]S. K. Mitra, The Upper Atmosphere, Asiatic Society, Calcutta, 1952.

NIGHT SKY	Photographic (10th Mag. stars/degree^2)	Visual	Photometry stilbs
Zodiacal light	20	30	2×10^{-9}
Faint Stars m<6th Galactic pole	16	30	2.5×10^{-9}
Faint Stars m<6th Mean Sky	48	95	7×10^{-9}
Faint Stars m<6th Galactic Equator	140	320	22×10^{-9}
Total brightness Zenith Mean sky	200	400	30×10^{-9}
Total brightness at 15° altitude	300	700	50×10^{-9}

Aurora brightness = 20×10^{-6} stilb (max)

Spectral distribution mean sky intensity is 10^{-7} cm^2 sec^{-1} sterad^{-1} Å^{-1}

Å →	3200	3600	4000	4500	5000	5500	6000	6500
	1.4	1.1	1.3	2.0	2.0	3.0	5	6

Color index of night sky $M_{pg} - M_{pv} = +0.5$

Zodiacal light is the cone of faint light elongated in the direction of the ecliptic (sun's path); the base and strongest light covers about 20° at the horizon and fades away at 60 to 80° from base. Best seen on the western horizon after sunset and on the eastern horizon before sunrise, it is caused by small particles and inter-stellar dust reflecting sunlight. About 15 percent of the zodiacal light is polarized whereas only 2 to 4 percent of the night sky is, and the planes of polarization of both pass through the sun. This fact is the basis for polarization filters. However, unless the filter efficiency is high (low absorption), little if any, improvement results. 15 percent of 15 percent = 2-1/4 percent of sky light which constitutes the polarized light portion. This could be 15 percent if looking directly at zodiacal light.

Zodiacal light in terms of 10th magnitude stars/degree^2 for various elevations:

10°	20°	30°	40°	50°	60°	70°	90°	110°	130°	150°	170°	180°
20K	4K	1.5K	900	600	450	330	210	150	130	140	170	200

Galactic light is the light from the Milky Way scattered by inter-stellar dust. It varies from a maximum value of 57 10th mag stars/degree^2 at the galactic equator to about 8 at 32° galactic latitude. The total contribution to night sky is about 5 percent.

Air Glow causes the largest non-resolved area light. This consists primarily of lines and bands; primarily atomic lines at 5577Å, 6300, 6363, 5890 and 5896Å, and bands 4-5000Å and 7-9000Å (Na) and 10440Å (OH) and 3-400Å (O_2).

Under conditions of extensive air glow and haze, filters might be used ahead of the sensing element to reduce the sky brightness saturation and to recover a portion of the lost performance. When the air glow is primarily in the 5577 and 6300Å lines, interference filters will be very effective in reducing its brightness, but the improvement is limited as the objects or targets, having the sun as an illuminator, will be filtered as well. (See Section I-C)

Total starlight from whole sky = 490 $m_{pv} = O_m$ stars = 9.2×10^{-5} ft candles

candles ≈ 21 m_v/sec^2 = 250 $m_{pg} = O_m$ stars

Typical values for Night Sky Brightness in terms of number of 10th magnitude stars/$\widehat{\text{degree}}^2$ are shown in the following Table:

Star light in each magnitude interval m+1/2 to m-1/2 in equivalent numbers of mean 10th m_v stars/$\widehat{\text{deg}}^2$.

m_{pv}	Galactic Equator b-0°	Galactic Pole b-90°	$mean_{pg}$	$mean_{pv}$
0	.7	.3	.5	.8
1	1.3	.6	.8	1.3
2	2.0	.8	1.3	2.2
3	3.0	1.0	1.7	3.0
4	4.0	1.2	2.1	4.5
5	5.2	1.5	2.5	5.0
6	6.1	1.7	3.2	5.6
7	6.7	1.9	3.4	6.3
8	7.9	2.0	3.5	6.8
9	9.6	2.1	3.9	7.4
10	11.0	1.9	4.1	8.7
11	12.6	1.7	4.6	8.7
12	13.8	1.5	4.6	9.3
13	14.1	1.2	4.6	8.9
14	14.4	.9	4.4	8.5
15	14.1	.6	3.9	8.1
16	11.5	.5	3.5	6.9
17	11.0	.3	2.9	5.5
18	7.9	.2	2.1	4.4
19	5.0	.1	1.3	2.6
20	3.1	.1	1.0	1.8
21	5.0	.6	4.5	1.2
21.5		.8		1.5
TOTAL	180	22	61	119

5. STAR TYPES AND COLOR INDEX

Star type is a method of classification of stars by their spectra. Originally there were 4 types, I through IV, and then V and VI were added. The spectral classes (temperature) now universally adopted is the "Harvard" (Draper) classification. It classes stars O, B, A, F, G, K, M, plus types R, N, branching off at G, and S at K5 or Mo. The region between any two letters is divided in tenths: thus B3A is a star type 3/10ths of the way from B toward A, etc.

A and K stars are most common in the Milky Way. Early and Late type stars denote Types B-A and K-M, respectively, following the assumptions that Type I was the youngest and Types III and IV the oldest before Giants and Dwarf stars (in the M region or late K) were discovered. Early stars have few absorption lines, mostly ionized Hydrogen. Late stars have many lines (iron and other metals).

Color index is the difference in stellar magnitudes between photographic (m_{pg}) and the photometric or photovisual (m_{pv}) magnitude. The visual index is usually the greater. Color index of the night sky = $m_{pg} - m_{py} = +0.5$. By definition, the color index of Ao stars = O (white) so blue stars are - and red stars are +.

Types B2-B3 are white; AO pure yellow, K2 orange yellow; MO orange; R orange red; Nc deep orange red. Of the 225,000 stars to about 10th mag, 20,000 are similar to our sun. 95% of these are within 3000 light years of us.

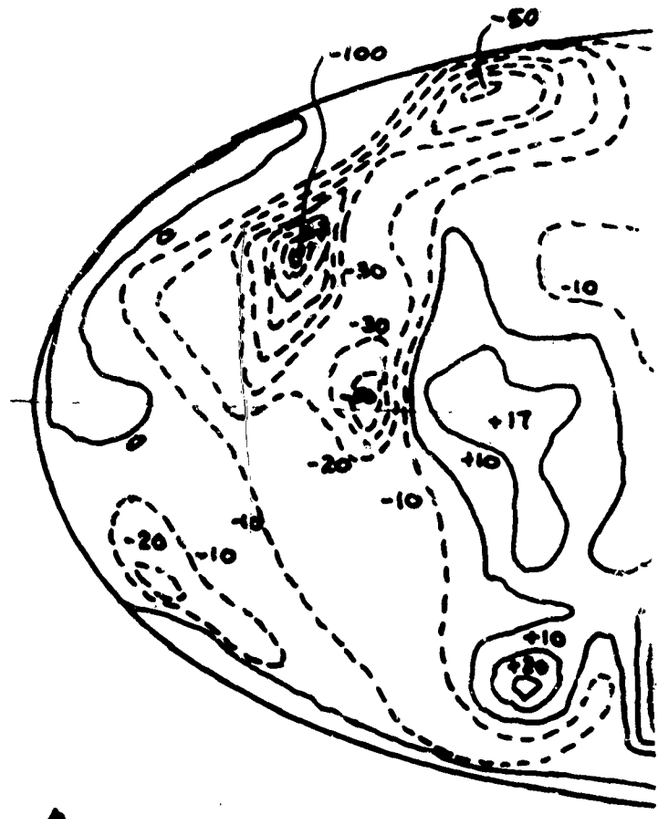
Our sun is a dwarf G2 star.

6. STAR DENSITIES AND DISTRIBUTION

The stars are distributed very heavily along the galactic equator due to the Milky Way and sparsely at the poles with a fairly random fluctuation of densities between. See Figure I-10.

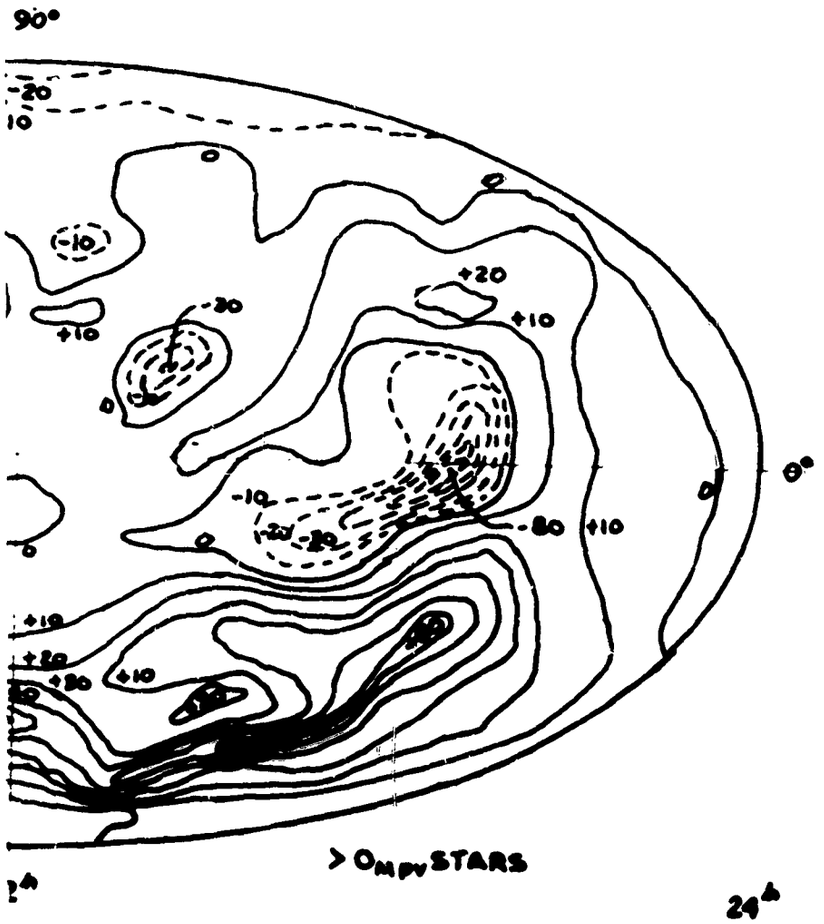
Star counts seen by Electro-Optical equipment are, of course, dependent on the response of the sensing surface or film and filter used as well as color of the stars. Since the S-10, S-20, and S-1 photocathode responses extend into the near infrared region (S-10 to .78 micron, S-20 to .85 microns, S-1 going to 1.1 + microns) the count of stars in these regions will be higher. But since these photocathodes do not in general cover below 3100Å where astronomical film type 103a-O is still sensitive, the star counts here will be lower than with film. Also since the larger counts involve stars of higher temperature (blue) the star counts when using Image Orthicons will, in general, be lower than astro counts by a factor of 2 or 3, even considering the higher counts of the Red and IR stars (older stars). Another factor, the fainter stars, individually do not take up as many resolution elements, so the total field occupancy in practice, will be less than expected from astrophysical data.

Stars are always point sources: however, due to atmospheric perturbations, they always appear to be one $\widehat{sec}^2$ or more. For the same reason two stars must be separated by more than one $\widehat{sec}$ to be resolved.



Numbers Represent Variat
As Log of Multiplier - T

Figure I-



Averages in Terms of Hundredths
+ 30 = .30 log N ∴ N = 2 = Multiplier
Density Distribution Chart

Star Numbers

Nm - number of stars per $\widehat{\text{degree}^2}$ brighter than magnitude m for mean galactic latitude 0-90°

m	Photographic	Visual
0		.00005012
1		.0002512
2	.0009120	.0009772
3	.002512	.003548
4	.007762	.01288
5	.02344	.05981
6	.07244	.1175
7	.2042	.3467
8	.5623	1.000
9	1.549	2.818
10	4.169	8.138
11	11.22	21.88
12	28.84	58.88
13	74.13	147.9
14	182.0	363.1
15	416.9	891.3
16	955.0	1995
17	2138	4365
18	4365	9120
19	7943	15,850
20	14,790	28,180
21	25,120	

Total stars to 6th magnitude (approx 1 1/2 per $\widehat{\text{degree}^2}$)

Total stars to 16th magnitude (approx 2500 per $\widehat{\text{degree}^2}$)

Figure I-11[6] summarizes star-count data.

one (m_{bol} = O) star = 2.27×10^{-5} erg/cm^2 sec outside earth's atmosphere

one (m_V = O) star = 2.43×10^{-10} phot. = 2.43×10^{-6} lux outside earth's atmosphere

one (m_V = O) star/degree^2 = 0.81×10^{-6} stilb = 2.55×10^{-6} lambert outside atmosphere

0.68×10^{-6} stilb = 2.17×10^{-6} lamberts inside clear unit air mass

---

[6] Trumpler & Weaver, Statistical Astronomy.

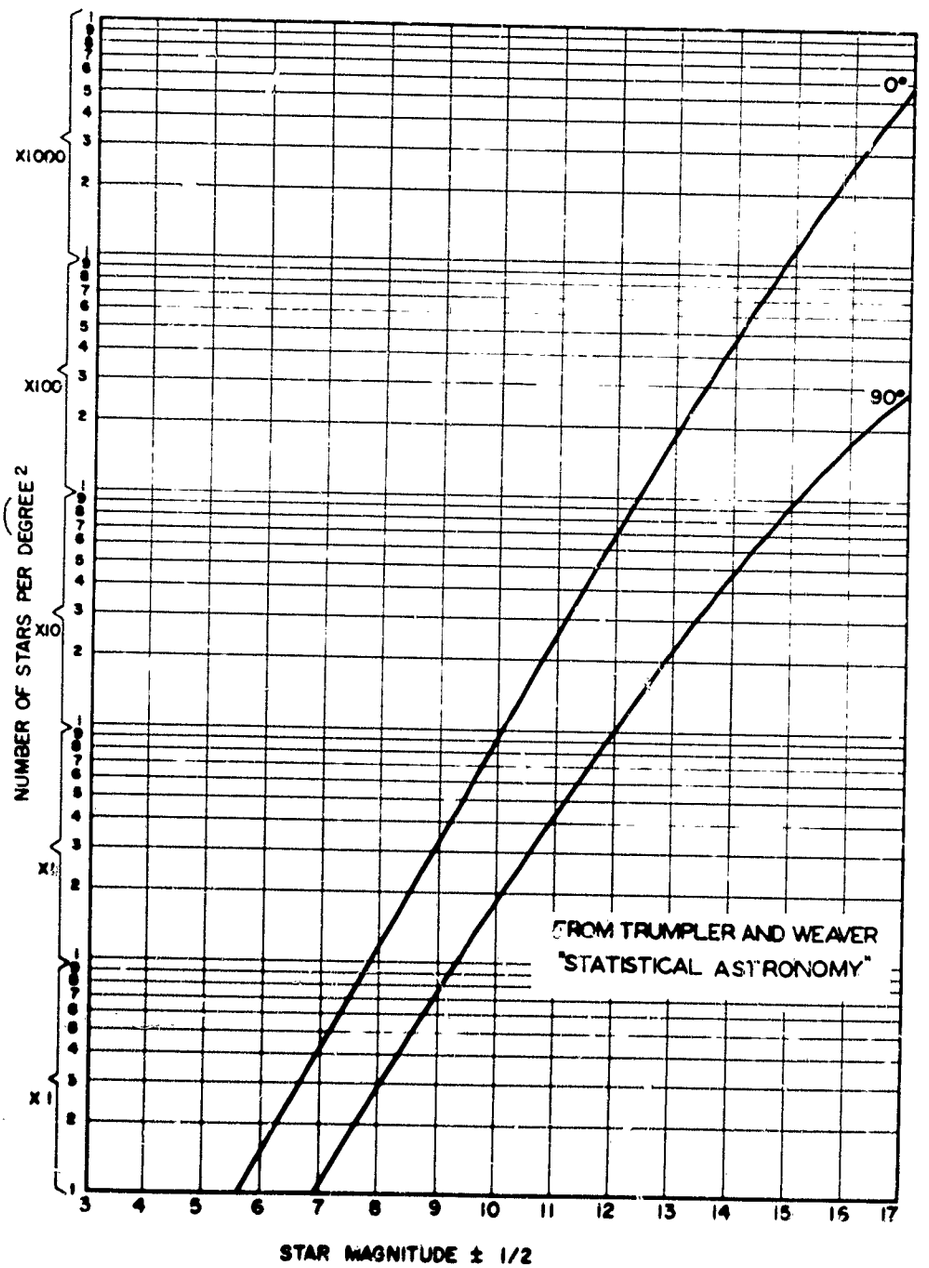


Figure I-11. Summary of Star Data Count

Variation from observer to observer runs 2 to 1, with the larger variations primarily in the southern hemisphere. Thus, for southern installations, special note should be taken if the performance expected is to be guaranteed. Star counts from astro-physical literature can be considered too large when considering the MgO Image Orthicon with S-10 or S-20 photocathode as a sensor. Because of this the total resolved stars and total field occupancy factors will be amazingly low for long focal length optics in relation to published data.

Of course, star clusters, nebulae, etc., will make observations impossible in certain areas of the sky; i.e., M31, the great nebulae in Andromeda, covers an area of almost two square degrees and is 4.8 mag. total. The Milky Way will severely limit highly sensitive systems in that portion of the sky. To keep the saturation levels manageable, special precautions should be taken and the systems should be examined for lost performance with backgrounds as bright as 18th mag/$\widehat{\text{sec}}^2$ of arc — (attained also on full moon night even though at considerable distance from moon and Milky Way) if Milky Way is to be worked.

7. MOVING CELESTIAL OBJECTS

The celestial environment consists of many objects; (planets, asteroids, comets, meteors, etc.), which move with respect to the more generally "fixed" stars. No stars are really fixed. All change (have "proper motion") over the years. This must be recognized and treated accordingly especially when using techniques involving Moving Target Identification (MTI) methods. Since the MTI techniques may be selected to resolve objects with very small differential motions with respect to the general stellar background, the extent of "infinite" distance (3D) background will vary with the application. Even medium focal length optics (60" or more) will resolve the closer planets and comets for even relatively short time intervals.

A priori knowledge will help account for the more prominent objects (solar planets, the brighter catalogued comets); but, since even the brighter repeating comets (6th Mag. or brighter) are not catalogued completely, comets can represent undesired targets and cause false alarms. A like situation occurs with asteroids. Meteors are only catalogued as "showers", so they will always be with us as unidentified targets!

a. Stars - Proper Motion

Some stars have apparent angular motion on the star sphere at right angles to the line of sight. It is found by comparing the star's present position with its position many years (centuries) earlier; precession, nutation, parallax and aberration being allowed for. Normally, proper motions are a few seconds of arc per century but some have proper motion of several $\widehat{\text{secs}}$. per year. For example: m 9.4, Barnard's Star in Ophiuchus, moves 10 $\widehat{\text{sec}}$/yr. (Location [1950.0] 17^h 55^m α; $+4^o$ 33' γ) See glossary for celestial coordinate discussion.

b. Variable Stars

The variable stars will effect performance if brightness variation is part of an MTI method. However, the time constant of star brightness variation is usually long with respect to the detection system and is thus of little concern. Position variation of certain variable stars likewise must be considered with certain MTI methods. Thus a star catalogue or film taken today may not be entirely useful next week. For example, the time constant of Cepheid variables are as low as 1 day or less.

c. Comets

There are about 40 comets per year brighter than 9-lth Mag, with no estimate available for fainter ones, and several are generally in the sky at the same time. Their angular rates vary, but are usually low for most of their traverse. However, at their higher rates they will be detectable by longer focal length system even in relatively short time-lapse periods. It is estimated that between one comet per day and one per week would be detectable in the entire sky.

d. Asteroids

There are approximately 10^6 asteroids of 16th magnitude or brighter. Their motion will average 1/3 to 1/5 degree per day, although some at times move 10 times this figure. Mean appearance and disappearance rates will be 100 per day, with the number in the sky visible to a 16th magnitude detector at any one time being 10^3 to 10^4. For a 30 · 30 field this is about one per hour. The majority of the known asteroids are in the region between Mars and Jupiter.

e. Meteors

In the 3 to 10th magnitude range, there are approximately 1.4 to 3.5 per degree^2 per hour during non-shower periods. (Fainter meteors would be moving too fast to alarm for all ordinary variations of aperture and field of view tradeoffs that we expect to use.) On meteor shower nights, the numbers increase from 10 to 100 times. The following tabulation lists the common re-occurring showers and rates.

Meteor Showers

Name	Max. Date	Normal Duration Dates	Hourly Rates	Associated Comet
Quadrantids	Jan 3	2-4	30	
Lyrids	Apr 21	20-22	10	1861
Eta Aquarids	May 5	3-10	12	Halley
Delta Aquarids	July 28	24-6	20	
Piscid Australids	July 29	26-5		
Perseids	Aug 12	1-20	50	1862 III
Giacobinids	Oct 9	9		1933 III
Orionids	Oct 20	15-26	16	Halley
Taurids	Nov 7	025-25	6	Encke
Leonids	Nov 15	11-20	10	1866 I
Andromedids (Bielids)	Nov 23	18-26	1	Biela
Geminids	Dec 12	9-14	50	
Dec Ursids (Bec Var)	Dec 22	21-22	12	
Arietics	June 7	M30-J14	60	
Zeta Perseids	June 7	2-13	40	
Beta Taurids	July 1	20-10	24	

Meteor Rates

Magnitude (m± .5)	Log N	N (Whole Earth)	Single Observer	10^{o} Field (24^{h})	10^{o} Field (Per Hour)
-5	3.65	4.4×10^{3}	4.4×10^{-2}	4.4×10^{-4}	1.8×10^{-5}
-4	4.05	1.1×10^{4}	1.1×10^{-1}	1.1×10^{-3}	4.6×10^{-5}
-3	4.45	3.6×10^{4}	3.6×10^{-1}	3.6×10^{-3}	1.5×10^{-4}
-2	4.85	7.2×10^{4}	7.2×10^{-1}	7.2×10^{-3}	3.0×10^{-4}
-1	5.25	1.8×10^{5}	1.8	1.8×10^{-2}	7.5×10^{-4}
0	5.65	5.1×10^{5}	5.1	5.1×10^{-2}	2.1×10^{-3}
+1	6.05	1.34×10^{6}	1.3×10	1.3×10^{-1}	5.6×10^{-3}
+2	6.45	3.55×10^{6}	3.6×10	3.6×10^{-1}	1.5×10^{-2}
+3	6.85	9.4×10^{6}	9.4×10	9.4×10^{-1}	3.9×10^{-2}
+4	7.25	1.8×10^{7}	1.8×10^{2}	1.8	7.5×10^{-2}
+5	7.65	5.1×10^{7}	5.1×10^{2}	5.1	2.1×10^{-1}
+6	8.05	1.34×10^{8}	1.3×10^{3}	1.3×10	5.6×10^{-1}
+7	8.45	3.55×10^{8}	3.6×10^{3}	3.6×10	1.5×10^{0}
+8	8.85	9.40×10^{8}	9.4×10^{3}	9.4×10	3.9×10^{0}
+9	9.25	1.8×10^{9}	1.8×10^{4}	1.8×10^{2}	7.5×10^{0}
+10	9.65	5.1×10^{9}	5.1×10^{4}	5.1×10^{2}	2.1×10^{1}
+11	10.05	1.3×10^{10}	1.3×10^{5}	1.3×10^{3}	5.6×10^{1}
+12	10.45	3.55×10^{10}	3.6×10^{5}	3.6×10^{3}	1.48×10^{2}
+13	10.85	9.4×10^{10}	9.4×10^{5}	9.4×10^{3}	3.9×10^{2}
+14	11.25	1.8×10^{11}	1.8×10^{6}	1.8×10^{4}	7.5×10^{3}
+15	11.65	5.1×10^{11}	5.1×10^{6}	5.1×10^{4}	2.1×10^{3}

Note: These data should be regarded as being good to only one significant figure, and could differ even more in absolute value, though not in relative value.

8. CELESTIAL FORMATIONS (BODIES, CLUSTERS, ETC.)

Pertinent information on celestial formations (bodies, clusters, nebulae, etc.) is included here for convenience (note magnitude for Mercury and Venus are given at their greatest altitude or elongation from the sun, whereas all others are given at quadrature (90°) from sun: Mercury 18°-28°; Venus 47°-48°).

	m_{pv}		m_{pv}
Mercury	-0.2	Pallas	7.9
Venus	-4.08	Juno	8.65
Earth — seen from sun	-3.80	Vesta	6.2
Mars	-1.94	Eros	9.9
Jupiter	-2.4	Moon	-12.7
Saturn	+0.8	Io	5.52
Uranus	+5.8	Europa	5.65
Neptune	+7.6	Ganymede	5.10
Pluto	14.7	Callisto	6.25
Ceres	7.1		

Periodic Comets		Period in Years
Encke	1951 Mar 16	3.3
Grigg Skj	1947 April 18	4.9
Tempel 2	1946 July 2	5.2
Pons-Winnecke	1945 July 10	6.1
Forbes	1948 Sept 16	6.4
Kopff	1945 Aug 11	6.5
Schwassman W2	1948 Aug 23	6.5
Giacobini — Z	1946 Sept 18	6.6
d'Arrest	1950 June 6	6.7
Daniel	1950 Aug 24	6.8
Brooks 2	1946 Aug 25	6.95
Reinmuth	1950 July 23	7.4
Whipple	1948 June 25	7.41
Faye	1947 Sept 28	7.4
Oterma	1950 July 15	7.88
Schaumusse	1943 Nov 25	8.1
Wolf 1	1950 Oct 23	8.3
Comas-Sola	1944 Apr 11	8.52
Vaisala 1	1949 Nov 10	10.55
Neujmin 3	1951 May 27	10.9
Tuttle 1	1939 Nov 10	13.6
Schwass W1	1941 June 9	16.2
Neujmin 1	1948 Dec 15	17.8
Crommelin	1928 Nov 4	27.9
Pons-Brooks	1884 Jan 26	71.6
Olbers	1887 Oct 8	72.5
Halley	1910 Apr 19	76.0

Globular Clusters

Designation (Messier #, etc.)	NGC #	l	b	Diam. (min)	M_{pc}
47 Tuc	104	272°	-45°	54'	5
	2149	148	26	6	11.5
Δ 445	3201	244	9	29	8.6
M68	4590	269	36	9	9.1
M53	5024	305	79	16	8.6
ω Cen	5139	277	15	65	4.7
M3	5272	8	78	20	7.2
M5	5904	332	46	22	6.9
M4	6121	319	16	21	7.1
M13	6205	27	40	21	6.7
M12	6218	344	25	15	7.9
M62	6266	322	7	10	8.1
M19	6273	324	9	10	8.1
Δ 366	6397	304	-12	30	7.
M22	6656	337	-9	26	6.2
Δ 295	6752	303	-26	42	7.1
M55	6809	336	-25	22	7.1
	7006	32	-21	2	11.5
M15	7078	33	-28	15	7.3

Selected Dark Nebula

	l	b
52 Cyg.	40°	-8°
Cygnus	43	-4
North America	53	0
Cygnus	60	3
Cephus	70	2
Auriga	136	-6
Taurus	139	-14
S Monoceros	170	3
Orion	175	-20
η Carina	254	0
Coal Sack	272	0
θ Ophiuchi	329	4
Scutum	356	-3

Interstellar Space

Radiation Density 12×10^{-13} ergs/cm^3

Equivalent Black Body temperature 3.5°K

= .1μ	25000°K
= .2μ	15000°K
visible + UV	10000°K
IR	3000°K

Selected Bright Diffuse Nebulae

	Messier No.	NGC IC	m_V	surface brightness mag/$\widehat{min}^2$	10th Diam. ($\widehat{min.}$)	Stars (m_V)	Galactic long l	Galactic lat. b
Near γ Cass		159			15'	2.3	91°	-2°
Pleiades	M45				120'	3.0	134	-22
Great Orion	M42	1976	4	20	50'	5.4	177	-18
	M43	1982	9	1		6.8	177	-17
		1977				4.6	176	-18
Near Ori (horsehead)		1434			50		174	-16
30 Doradus (L Magg. Cl)		2070			7		246	-31
	M78	2068	8.3	0.4		10.4	173	-13
Rosette NGC	2237-8	2246			80	7.4	173	-1
η Carinae	3372				150	7.	255	-1
Trifid	M20	6514	8.5		25	6.9	334	-1
Lagoon	M-8	6523	5.8		40	6.1	333	-2
	M-16	6611	6.4		15	8.3	344	0
Ω Swan, horse-shoe	M-17	6618	7	2	25		342	-2
Cygnus Loop		6960			50		41	-8
Cygnus Network		6992-5			50		43	-10
North America		7000			120	6.0	53	1
		7023			18	7.2	71	13

Open Clusters

Designation	NGC #	l	b	Diam ($\widehat{min.}$)	No. of Stars	Magnitude range m_V	Total m_V
M-103	581	96°	-1°	6'	30	9-14	6.9
h Persei	869	102	-3	30	300	7-14	4.3
x Persei	884	103	-3	30	200	8-14	4.6
M-34	1039	112	-15	30	70	8-14	5.7
Perseus		115	-6	210	50	3-7	2.0
Pleiades		134	-22	110	120	3-12	1.2
Hyades		147	-21	360	100	0-9	0.5
M-38	1912	140	2	19	100	8-12	6.6
M-36	1960	143	2	17	50	8-13	6.3
M-37	2099	145	4	25	200	11-12	6.2
	2477	221	-5	6	200	10-	5.7
Praesepe	2632	174	34	90	100	6-11	3.7
o Vel	I2391	238	-8	40	12		2.4
M67	2682	184	33	16	80	10-14	7.3
θ Carinae	I2602	257	-5	70	25		1.4
	3532	257	+1	45	130		3.3
Sco-Cen		290	10	2000	110	1-7	-1.0
Coma		196	85	300	40	5-10	2.8
Urs Maj		90	60	1000	100	2-7	-0.2
K Cru	4755	271	2	11	30	6	5.0
M-21	6531	335	-2	12	40	7-13	6.6
M-16	6611	345	-1	19	40	8-13	6.1
M-11	6705	355	-4	12	80	11-14	6.5
	6885	34	-5	10	30	6-14	8.7

9. SKY BRIGHTNESS (MOON IN SKY)

The brightness of the sky with the moon varies with the phase of the moon and the angular distance from the moon. The brightness of the total sky at full zenith moon is about 17-1/2 mag/$\widehat{sec}^2$; however, since we look at specific parts, the brightness versus the angular distance from the moon is of more importance. Figure I-12A gives the aureole of the moon which should be used with Figure I-13 to determine variation in specific areas of sky under moonlight conditions. Figure I-12B gives sky brightness versus moon phase.

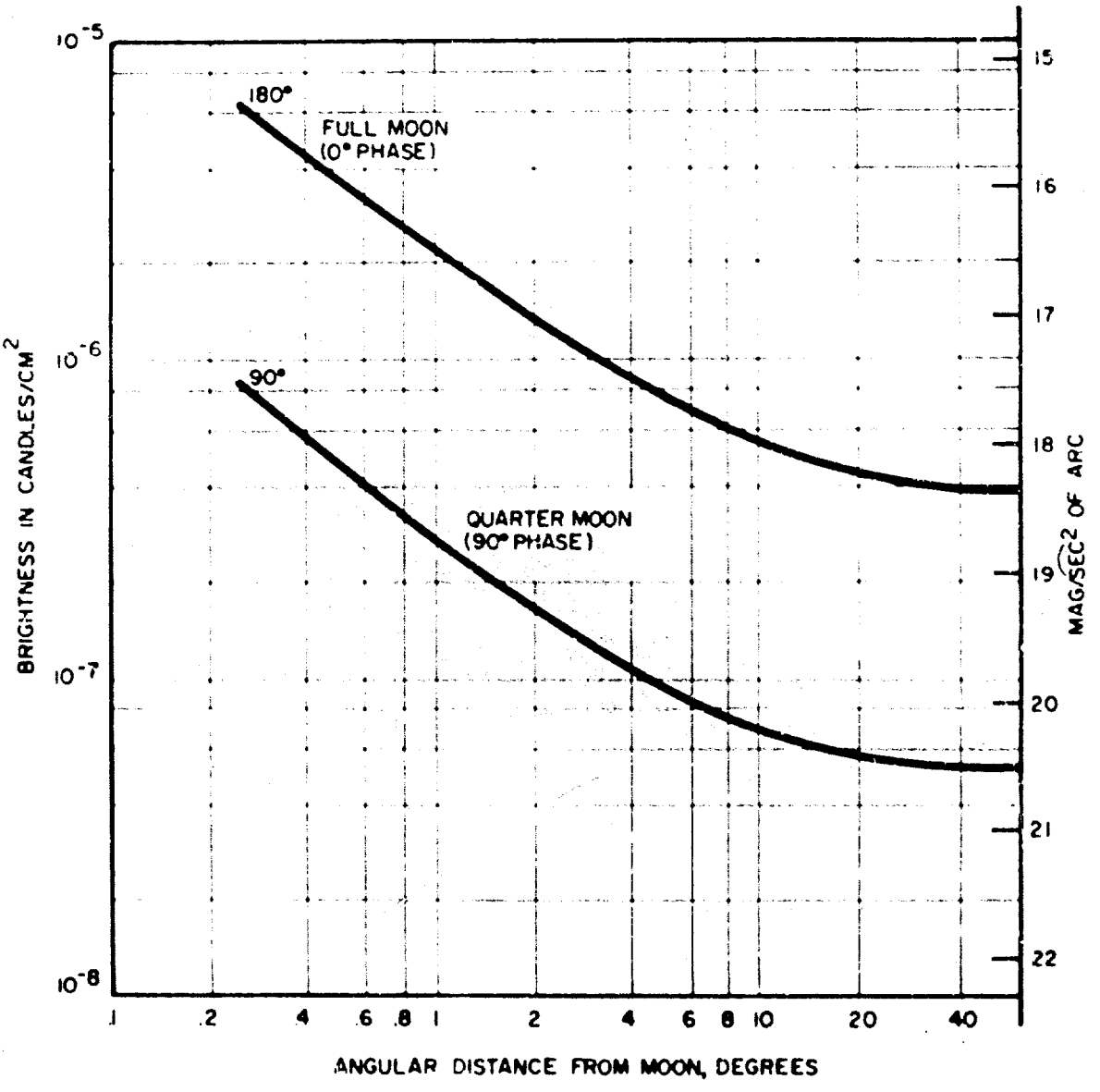


Figure I-12A. Aureole of the Moon

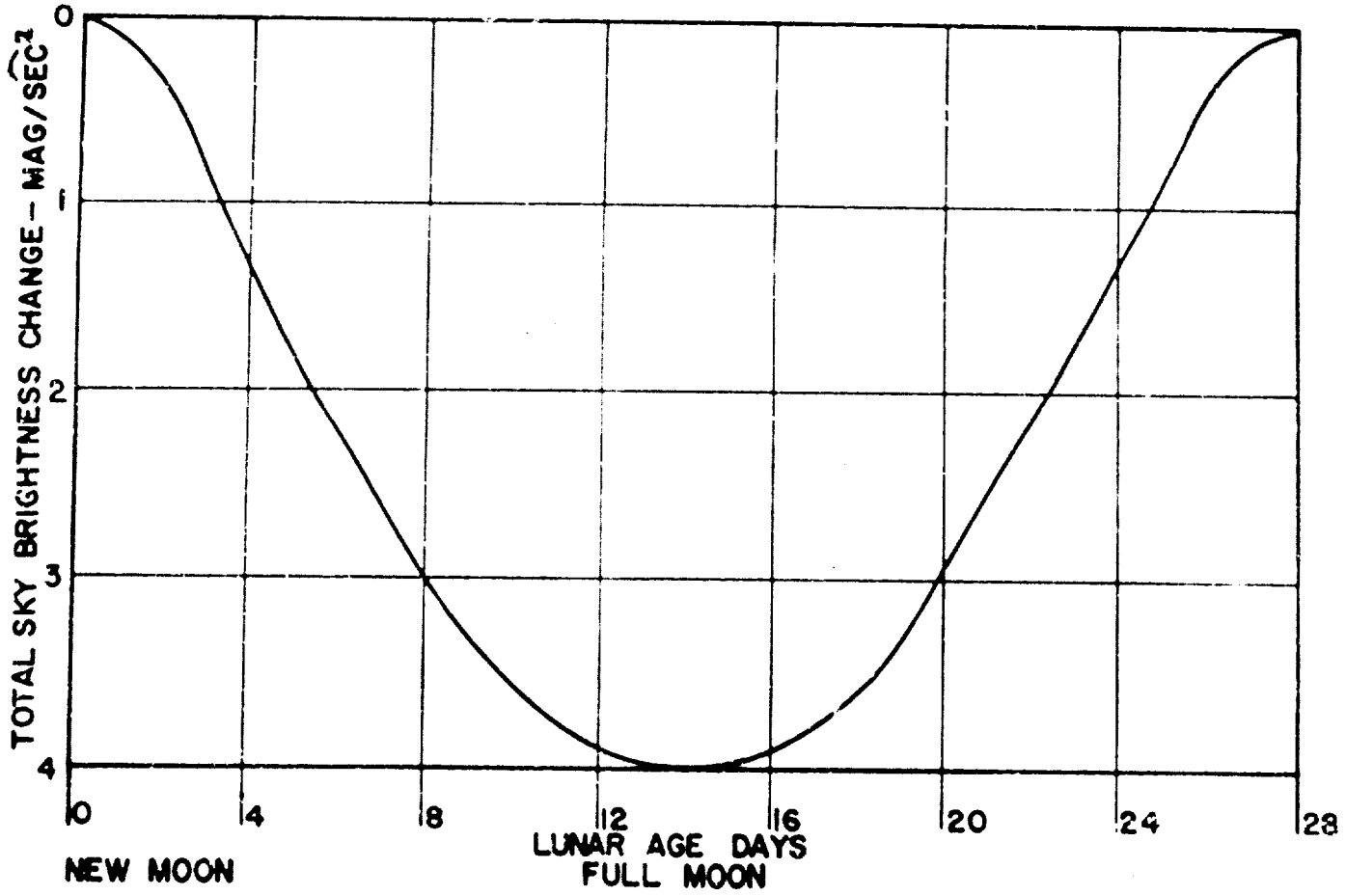


Figure I-12B. Approximate Sky Brightness Change vs Moon Age

The summary of all these light sources and the total effect on sky brightness is perhaps best illustrated by the composite graph of Figure I-13.

10. CELESTIAL CATALOGUES, ETC.

a. Calibration Using Stars

Many selected areas of the heavens are well calibrated because different observers study different areas of the heavy constellations. Typical of these is the Polar Sequence or the star area near the celestial pole (star Polaris). Figures I-14A and 14B illustrate the chart and corresponding calibration.

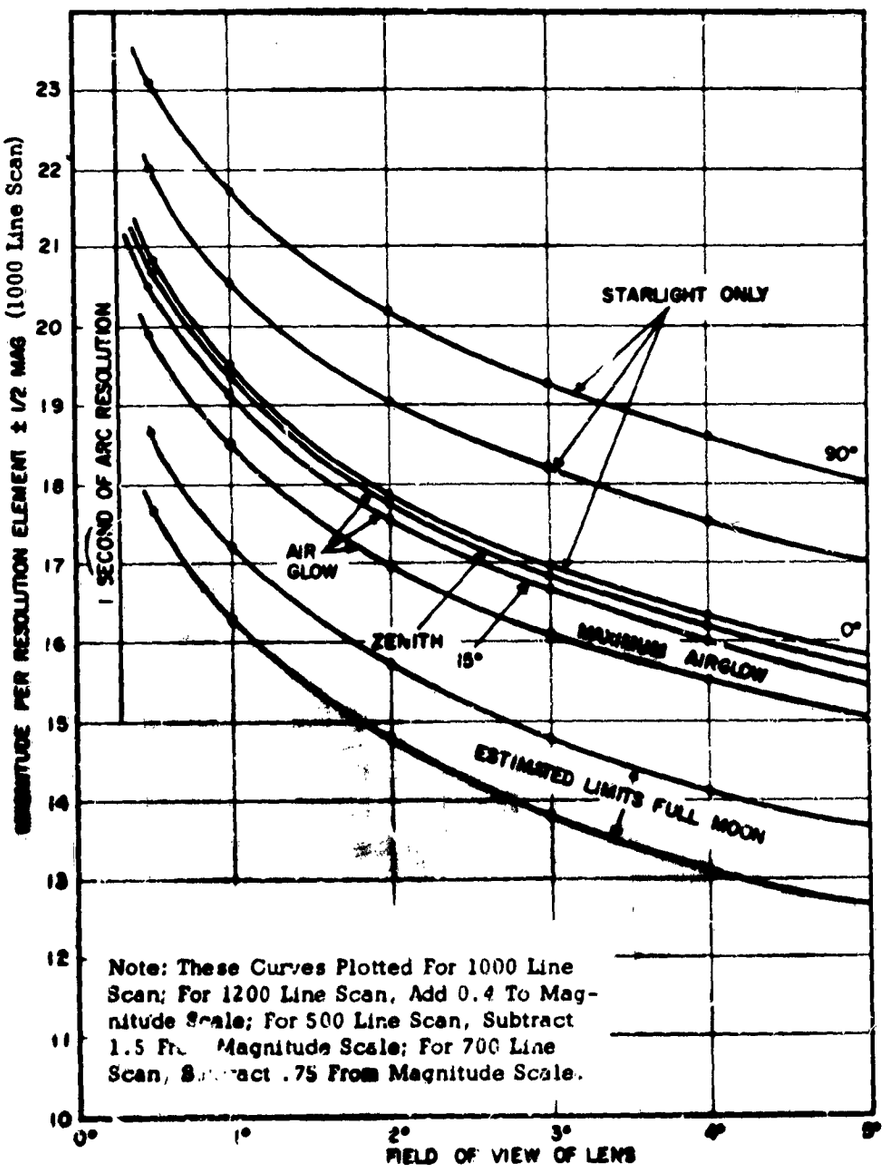


Figure I-13. Background Light vs Field of View -- 1000 Line Scan



Figure I-14A. North Polar Sequence

North Polar Sequence

W Ps	HD or BD		SP	mpg	mpv	C
1s	8	890	F8	2.6	2.1	+.0.40
1	166	205	AO	4.27	4.30	-0.12
2	212	710	AO	5.15	5.31	-0.16
3	221	525	FO	5.75	5.62	+0.13
4	166	926	A3	5.89	5.81	+0.08
5	5	914	A2	6.46	6.49	-0.03
2s	107	192	FO	6.48	6.31	+0.17
3s	107	113	F2	6.65	6.39	+0.26
1r	51	802	M	6.69	5.09	+1.60
6*	66	368	AO	7.13	7.07	+0.06
7	96	870	B8	7.38	7.54	-0.15
2r*	103	030	M	7.91	6.34	+1.57
8	14	369	FO	8.33	8.10	+0.23
9	17	376	A	8.94	8.80	+0.14
3r	114	282	K2	8.96	7.54	+1.41
10*	21	070	A5	9.15	9.03	+0.12
4r	187	138	KO	9.23	8.21	+1.02
11	89°	18	A	9.77	9.57	+0.20
12	89°	25	A	10.08	9.77	+0.31
5r	112	428	KO	10.15	8.65	+1.50
4s	89°	12	G	10.31	9.84	+0.47
13*	89°	29	A	10.55	10.33	+0.22
6r	89°	9	G5	10.51	9.28	+1.23
14	89°	1	A?	10.93	10.53	+0.40
7r	89°	35	G2	10.96	9.85	+1.11
5s	89°	37	G5	11.09	10.02	+1.07
15			A	11.27	10.90	+0.37
6s	89°	26		11.37	10.65	+0.68
8r*	89°	31	G5	11.43	10.44	+0.99
16			A?	11.57	11.23	+0.34
17	--	--	--	11.88	11.31	+0.57
9r				11.95	10.95	+1.00
18				12.28	11.88	.40
10r				12.60	12.06	.54
7s	--	--	--	12.61	12.06	.55
19*				12.68	12.24	.44
20				12.99	12.50	.49
11r				13.22	12.05	+1.17
21	--	--	--	13.34	12.51	+0.83
22				13.46	12.85	+0.61
23				13.59	13.01	+0.58
12r*				13.78	12.48	+1.30
24	--	--	--	13.92	13.29	+0.63
25				14.13	13.57	+0.56
8S				14.51	13.70	+0.81
26				14.65	13.65	+1.00
9s				14.74	13.71	+1.03
27				14.90	14.23	+0.67
10s				15.30	14.47	+0.83
11s				15.30	14.34	+0.96
28				15.33	14.48	+0.85
12s				15.36	14.64	+0.72
13s				15.53	14.48	+1.05
29				15.88	15.17	+0.71
14s				16.03	15.02	+1.01
30				16.20	15.41	+0.79
31				16.41	15.59	+0.82
15s				16.58	15.68	+0.90
32				16.76	15.55	+1.21
16s				16.87	15.47	+1.40

HD = Henry Draper Catlogue No.

BD = Bonn Durch musterung No.

SP = Spectral Classification

m_{pg} = Photographic Magnitude

m_{pv} = Photo visual Magnitude

c/i = Color Index = $m_{pg} = m$

Figure I-14B. This is a carefully measured series of stars near the pole whose magnitudes are used as a standard for measurements, in photovisual and photographic magnitudes.

b. Sky Charts

For general sky charts and atlases:		Approximate Cost
Norton's Star Atlas	stars, clusters, etc. to 6-1/3 mag	$ 5.25
Atlas Coeli (1950.0)	thru 7-1/2 magnitude	$ 17.50
Bonner Durchmusterung	thru 10th magnitude	$ 100.00
The Astronomical Catalogue	thru 21st magnitude	$ 2500.00

The Maryland Academy of Sciences, Baltimore, Maryland, issues yearly a "Graphic Time Table of the Heavens" (published in January issue of Sky and Telescope for each new year) which provides general information on astronomical events during the year. Figure I-15 is a sample for the year 1963. Wall chart size 40 × 27 is available at $1.50 a copy. Those involved in applications involving celestial environment are referred to their local astronomical association or society and its official magazine "Sky and Telescope" for up to date information on astronomical observations, etc.

11. SURFACE ENVIRONMENT

Operation of Electro-Optical equipment and/or systems for surveillance, detection, tracking resolution, identification or discrimination of objects and terrain against surface background and environment will depend primarily on variation of reflectivity (contrast) of the objects' surface and background features.

The brightness of an object (distributed or point sources) to be observed vs the makeup of the surface background environment is dependent on the illumination reaching the scene and object, and the reflectance of the scene and object surface in the direction of the observer (sensor). The table below gives the illumination on earth's surface under various conditions. This is a composite table of many sources; variances of 2 to 1 are common (in some cases as much as 4 to 1) depending on source and measurement technique used. Since the illumination of interest is the total illumination from the whole sky (1/2 the complete celestial sphere or 2π steradians) this is the value tabulated below.

Direct Sunlight – clear summer day at noon	1.0×10^4 ft candles = lumens/ft^2
Sky-light-clear summer day at noon (20% of Sunlight)	$.2 \times 10^4$ ft candles
Total Flux Direct Sunlight and Skylight at noon	1.2×10^4 ft candles
Sun on Horizon	275 ft candles
Daylight – cloudy	100 ft candles
Very dark day and sunset	10 ft candles
Twilight	1 ft candle
Late Twilight	10^{-1} ft candles
Full moonlight, clear bright night, (moon at zenith)	3×10^{-2} ft candles
Full moonlight clear night 1 hour after twilight	2×10^{-2} ft candles

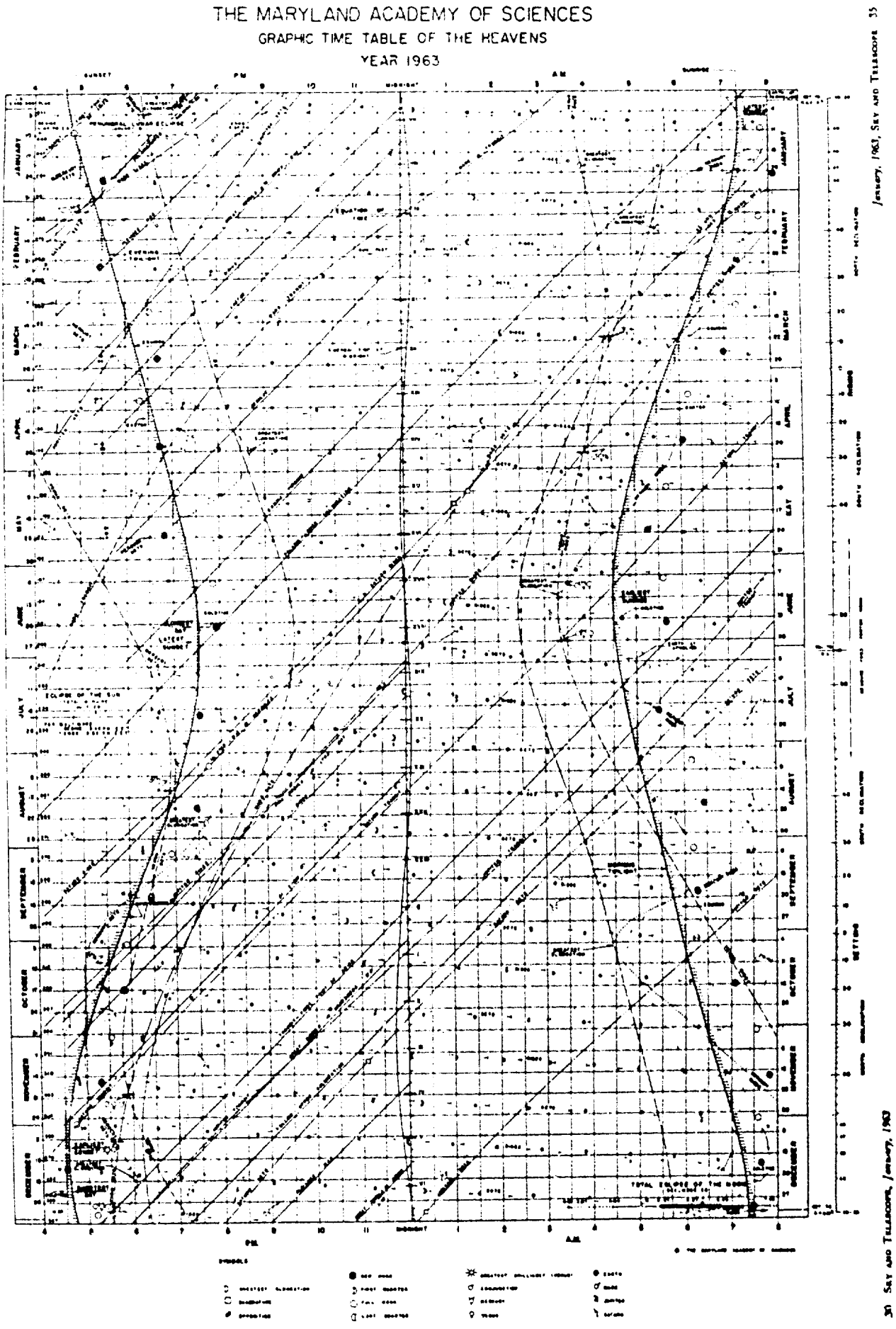


Figure I-15. Graphic Time Table of the Heavens

Best Available Copy

Full moonlight moderately cloudy night	4.5×10^{-3} ft candles
Quarter moon, clear night	10^{-3} ft candles
Clear moonless night Starlight only	10^{-4} ft candles
Moonless -- Heavily Clouded night	10^{-5} ft candles
Interior – typical normal for daylight	20 ft candles
Interior – typical normal for artificial light	10 ft candles

The variation of sky illumination for total sky versus the moon phase and position effect the total sky brightness and is illustrated by Figure I-12B.

C. ATMOSPHERIC EFFECTS

The earth's atmosphere greatly effects the quality and extent of "seeing" possible with ultra violet, visual and infrared photographic and electro-optical equipments. It causes limits beyond which it will be very difficult or impossible to "see". It is this atmospheric "seeing" which causes the tremendous interest and need for an Orbiting Astronomical Observatory. The advent of the G. E. low light level thin film MgO Image Orthicon, because of its tremendous "high speed" in relation to film, offers new possibilities for reducing the problem. It will be covered in detail later in Section II-C, suffice it to say, we have a new research and measuring tool here that will help us cut the atmospheric effects and alter some of the limits accordingly.

The atmospheric effects and their limitations as covered in this section are:

1. Refraction
2. Absorption
3. Scattering of Light and Haze Background
4. Dancing
5. Scintillation
6. Pulsation
7. Defocusing
8. Inversion Layer
9. Dust and Smoke Content
10. Weather

For aero-space surveillance systems these effects place certain restrictions on equipment performance. For moderately short focal lengths (under 50") as would be expected to be used for surveillance, the dancing and pulsation effects will be negligible on normally "good" nights.

1. REFRACTION

a. General Description

The effect of atmospheric refraction upon the propagation of light rays from a satellite is an effective bending of the path of each ray. As a result the satellite is observed at a higher elevation angle than that of its true position.

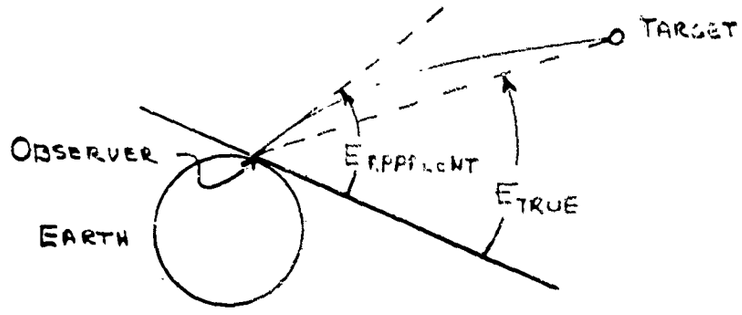


Figure I-16.

Refraction follows a definite pattern although there are day-to-day and hour-to-hour variations due primarily to temperature and pressure. These are usually small and often will be within equipment and/or systems tolerances. Refraction varies with elevation angle.

The magnitude of the refraction error ($E_A - E_T$) depends upon the position of the satellite with respect to the earth and the index of refraction along the path of observation. Since the magnitude of the index of refraction is a function of such parameters as observer's location on the earth, weather, time of day, and season of the year, it becomes an overwhelming task to conduct a complete analysis. Therefore, to simplify the analytical problem, atmospheric models which are representative of average conditions are employed.

Different atmospheric models show similar results.

Norton's Star Atlas [7] gives the mean refraction for 50°F (10°C) and 29.6" (752 mm) Barometer, when looking from earth to objects at infinity; also see Figure I-17.

For other temperatures, add 1% per 5°F if cooler (subtract if hotter).

For other pressures add 3 1/2% per inch if higher.

---

[7] A. P. Norton, Norton's Star Atlas, Gall and Inglis, London and Edinburgh, 1940.

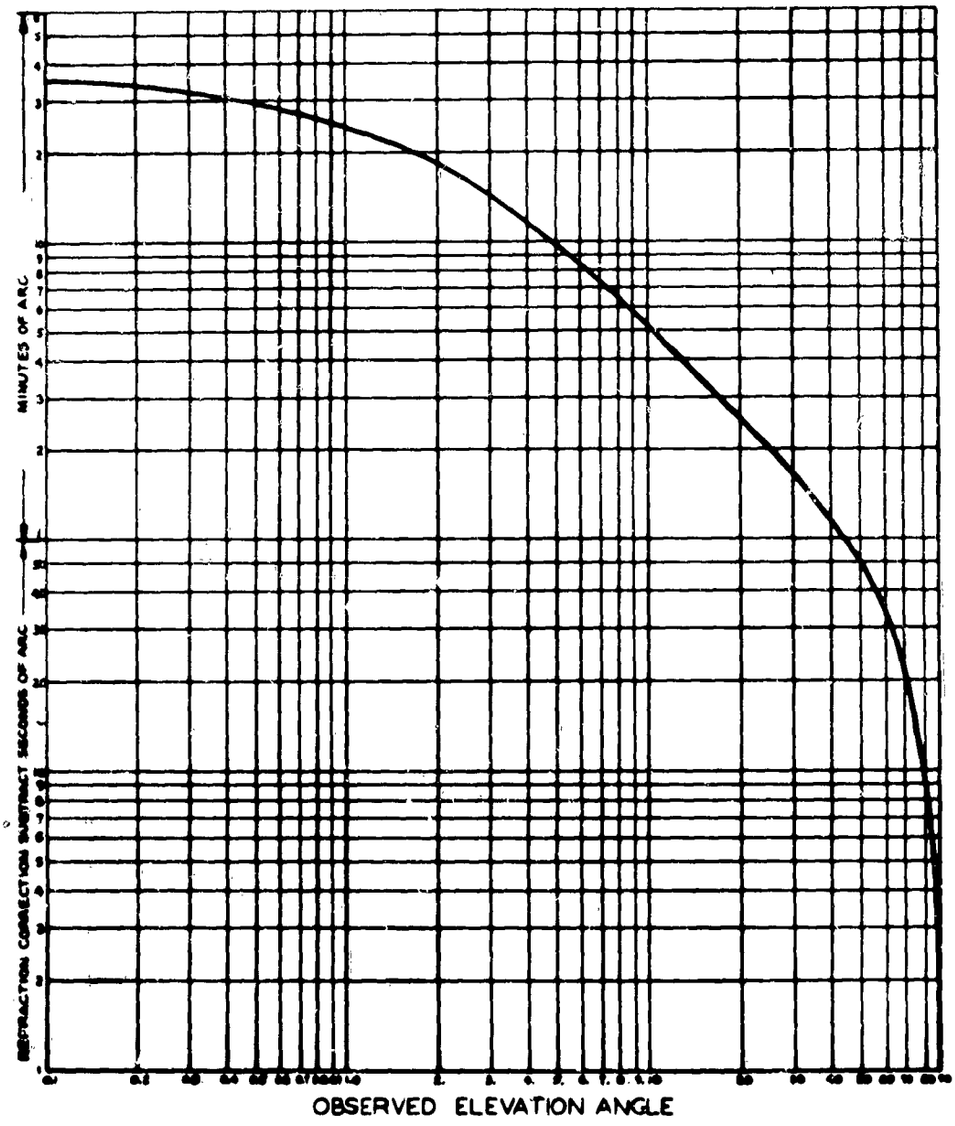


Figure I-17. Refraction Correction (subtract) for Observed Elevation Angles, Object at Infinity

Observed Elevation Angle	Subtract Refraction	Observed Elevation Angle	Subtract Refraction	Observed Elevation Angle	Subtract Refraction
0°	34'54"	5°	9'47"	25°	2'3"
1/4°	31'30"	6°	8'23"	30°	1'40"
1/2°	29'3"	7°	7'20"	35°	1'22"
3/4°	26'35"	8°	6'30"	40°	1'09"
1°	24'25"	10°	5'19"	45°	58"
2°	18'9"	12°	4'25"	50°	48"
3°	14'15"	15°	3'32"	65°	27"
4°	11'39"	20°	2'37"	80°	10"

The results of two other atmospheric models under standard conditions (760 mm and 0°C) are shown in the Table below:

Apparent Elevation	Plane Parallel Layer Model	Concentric Spherical Shell Model
20°	166.06 $\widehat{\sec}$	164.50 $\widehat{\sec}$
25	129.55	128.82
30	104.12	104.16
45	60.38	60.32
60	34.86	34.85
75	16.18	16.18
90	0.00	0.00

The theories leading to the data of the above table have been verified experimentally by McCruady, Pawsey and Payne-Scott, and Marner and Ringen. The data for the concentric spherical shell model is plotted in Figure I-18.

The major variations in this data are due to changes in weather, satellite position, etc. These variations will now be considered in detail.

The refractive index (m) used in the atmospheric model can be written as:

$$m = 1 + a\frac{P}{T} + b\frac{e}{T^2} \qquad \text{Eq. I-1}$$

where:

a, b = constants

P = partial pressure of dry air

e = partial pressure of water vapor

T = temperature of air

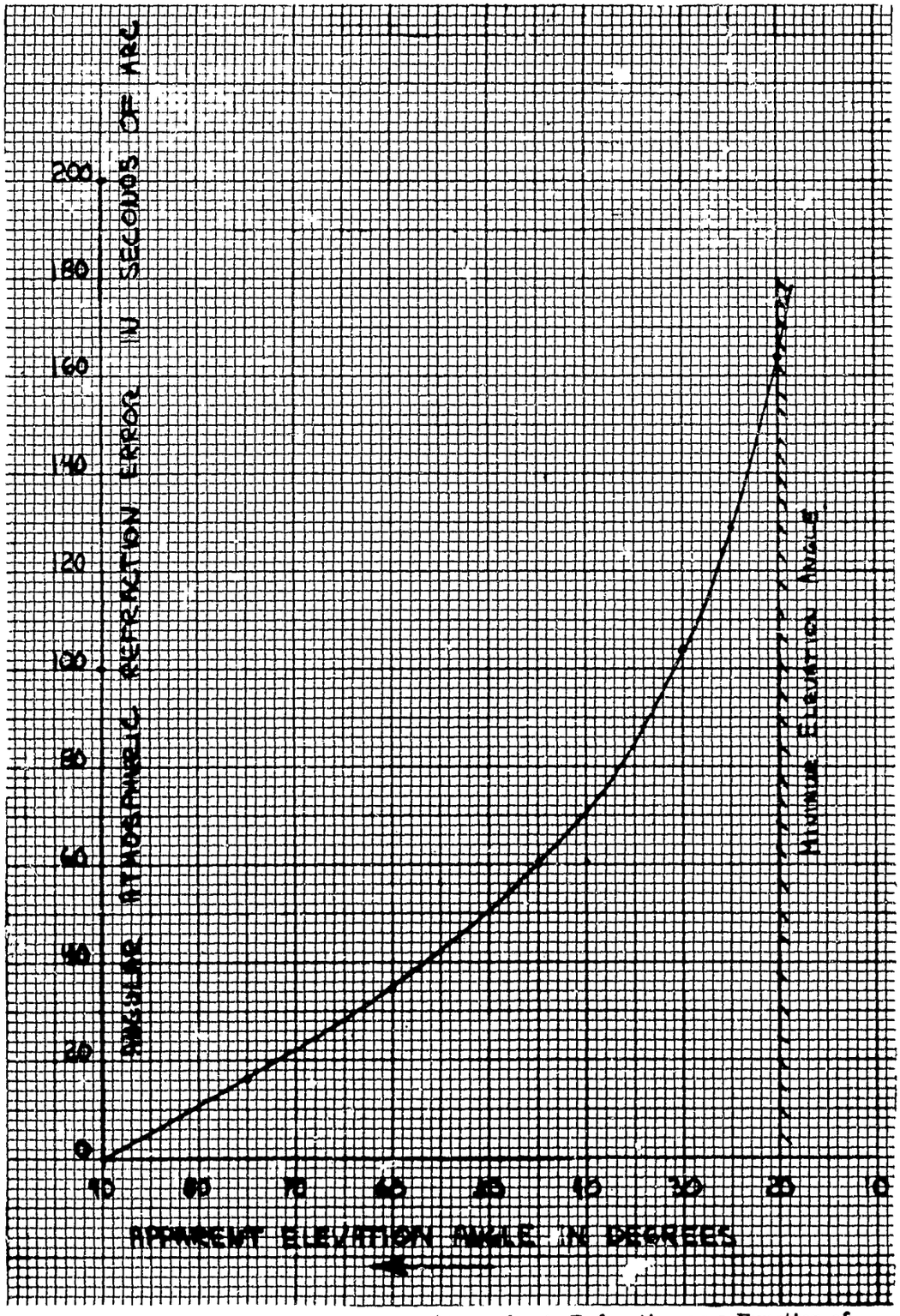


Figure I-18. Angular Error Due to Atmospheric Refraction as a Function of Optical Field of View

The first two terms (1 = a P/T) apply to both optical and radio frequencies while the third term (b e/T^2) is an explicit water vapor relationship required only at radio frequencies. The variation with T and P for optical wavelengths has been tabulated in reference #16 and is discussed below. Several other miscellaneous factors affect the atmospheric model and will also be considered.

b. Variation with Surface Air Temperature

The data of the following table is based upon a surface air temperature of 0°C (32°F). At other temperatures the refraction differs, becoming greater at lower temperatures and less at higher temperatures. Using tabulated corrections in reference #16 the following table has been prepared to illustrate the variation with surface air temperature, assuming a target at infinity (worst case).

Apparent Elevation	Standard Refraction	Standard (+32°F)		-0°F		+100°F	
		Error	% Error	Error	Error	Error	% Error
20°	164 sec	0	0	-32 sec	-18%	18 sec	+11%
30°	104	0	0	-18	-17	18	+17
50°	50	0	0	-12	-24	6	+12
90°	0	0	0	-0	0	0	0

c. Variation with Atmospheric Pressure

The data of the table above is based upon an atmospheric pressure of 760 mm (29.83 inches or 1010 millibars) at sea level. At other pressures the refraction differs, becoming greater as pressure increases, and smaller as it decreases. A study of the tabulated corrections in reference (8) reveals that the maximum change in the data of the table for a barometric pressure variation of 28.2 - 32.2 inches of mercury is approximately ±5%. This corresponds to a target at infinity with an apparent elevation angle of 20° or more.

d. Variation with Humidity

Humidity has a relatively slight effect on atmospheric refraction at optical frequencies. (This is not true for radio frequencies.) The variation at the horizon from completely dry air to very moist air is less than ±1%. See Reference #8.

e. Variation with Wind

Wind is believed to have some effect upon refraction, the change apparently increasing as the square of the wind velocity. However, at 30 knots the change on the horizon is believed to be less than ±1%.

f. Variation with Latitude

Latitude has a slight effect upon refraction because of the decrease in the radius of the earth and the increase of gravity as latitude increases. The variation at the horizon is about ±1%.

---

(8)N. Bowditch, American Practical Navigator, US Navy Hydrographic Office Publication #9, 1958.

g. Variation with Wavelength

The various wavelengths present in the sensor spectrum (3000-7000Å for the I.O.) are refracted through slightly different amounts. The total dispersion at the horizon for the I.O. is approximately ±1%.

h. Variation with Range

The classical astronomy references are concerned only with heavenly bodies which are considered to be at a slant range of infinity. Thus the data in the refraction tables are based upon a range of infinity. However, for satellites this is not necessarily true. G. H. Millman (reference #9) has investigated this variation in atmospheric refraction for radio waves using the water vapor term in equation I-1 for the refractive index. It was found that the variation for slant ranges other than infinity is very small. For example the variation with a change in range from 1000 nm to infinity is one percent or less. Likewise the variation with a change in range from 100 nm to infinity is three percent or less.

i. Summary of Variations

It should be noted that all values given above represent the maximum percentage variations expected. Since the atmospheric refraction error itself decreases as the elevation increases, the resulting variation also decreases with elevation. The expected variation is also reduced by the fact that the atmospheric model assumes some value of each parameter near the mean of the extreme limits discussed above.

Thus it can be concluded that the maximum variation in atmospheric refraction error due to weather conditions, range, etc., would be less than ±30%. If continuous ground temperature and parametric pressure information was factored into the atmospheric refraction error calculation, a variation of not more than ±10% would be expected. See Figure I-19.

j. Effect on Field of View

The differential change of refraction across the field of view of a selected lens is generally negligible, however, the size change should be checked since a change of elevation will, in effect, change the size of the field of view and cause apparent star motions. This must be taken into account in an MTI equipment as the size change amounts to many resolution elements when at the lower angles even for small (3°) fields of view. In addition, if star field pictures are taken at one elevation angle and compared to the same field taken later at a different elevation angle the size change due to refraction could be the largest error causing non-cancellation. Fortunately, this error is fairly consistent and thus can be program-corrected either by hand or automatically.

k. Effect on Angle Measurement

The combined effect of the variations summarized in Figure I-19 and the error across the field of view (assuming a bias correction) given by Figure I-21 is analyzed in Section IV.

(9) J. H. Millman, Atmospheric and Extraterrestial Effects on Radio Wave Propagation, GE Co. Report #TIS R61EMH29.

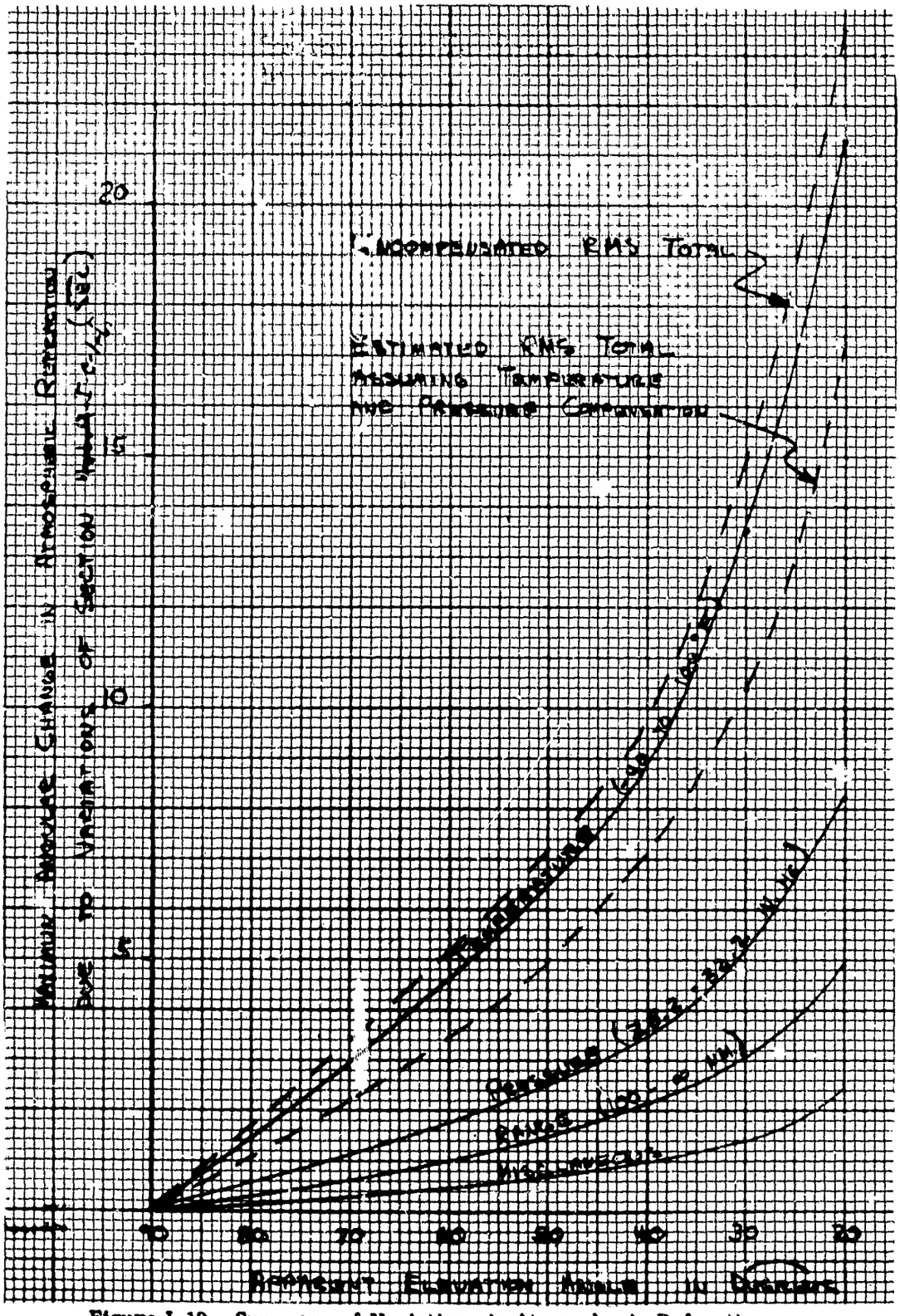


Figure I-19. Summary of Variations in Atmospheric Refraction

The above bias error can be compensated for by adding a correction which is a function of the mount elevation angle and the field of view. If this is done the error in angular measurement is reduced to that arising from the difference in refraction across the field of view. The magnitude of the remaining error can be obtained from Figure I-18 as shown in Figure I-20.

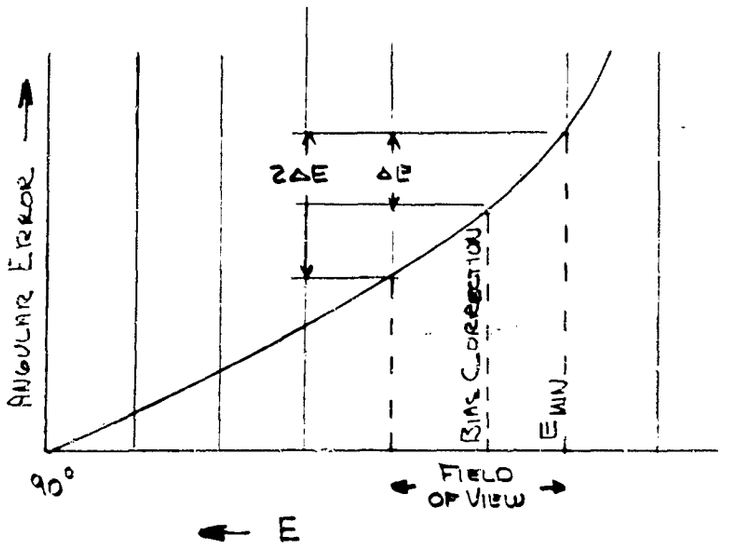


Figure I-20.

The maximum error due to the change in atmospheric refraction across the field of view is then given by ΔE which is plotted in Figure I-21 for minimum elevation angles of 20, 30 and 50 degrees.

2. ABSORPTION

The generally accepted values of clear weather atmospheric absorption at the zenith are about 15% or +0.21 mag absorption/air mass for visual response and 30% or +0.44 mag/air mass at photographic (103a-O) response. For S-20 photocathode response this value would be 0.15 to 0.17 mag/air mass for low temperature sources (<2000°K) and the visual values or more for high temperature sources (>4000°K). For other Elevations:

Elevation Angle or "Altitude"	Absorption Distance in Air Masses	Additional Mag Loss	Total Attenuation Loss: Photographic (pg)	Photovisual (pv) & S20	S-20 (<2000°K Targets)
90 & 80°	1.0	.00	.44 mag	.21 mag	.16 mag
70	1.1	.0103	.45	.22	.17
60	1.2	.096	.54	.30	.25
50	1.3	.283	.72	.49	.44
40	1.6	.57	1.01	.78	.73
30	2.0	.75	1.19	.96	.91
20	2.9	1.15	1.59	1.36	1.31
10	5.6	1.96	2.3	2.07	2.02

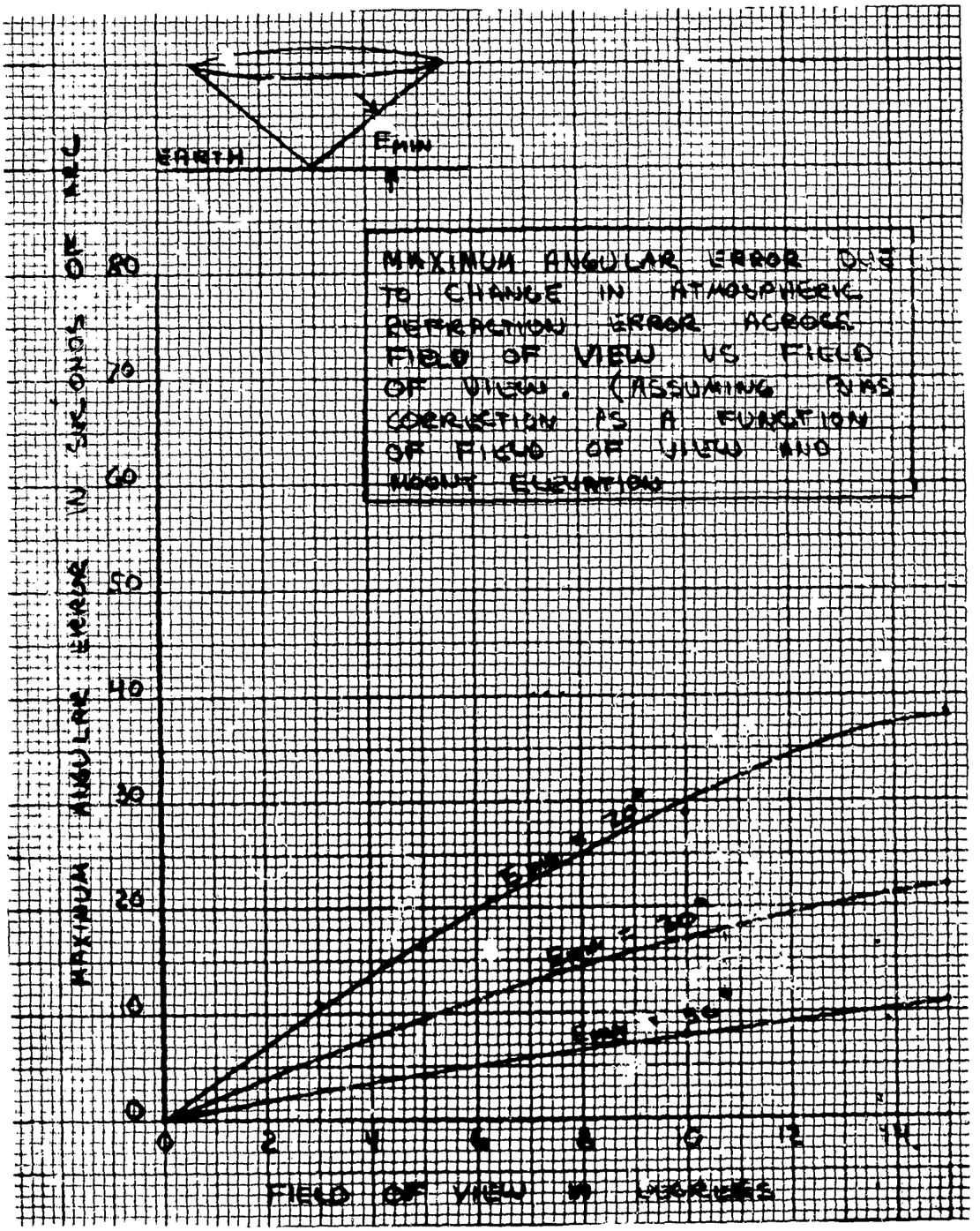


Figure I-21. Maximum Angular Error Due to Change in Atmospheric Refraction Error Across Field of View vs Field of View. (Assuming Bias Correction as a Function of Field of View and Mount Elevation)

Norton's Star Atlas [6] gives absorption for different angles as follows: (these are less than above)

Zenith distance (Angle from Zenith)													
47°	58°	64°	69°	71°	73°	75°	77°	79°	80°	84°	86°	88°	89°
No. of Mags Diminished													
0.1	.2	.3	.4	.5	.6	.7	.8	.9	1	1.5	2	2.5	3

The following brief data is taken from Allen [2]. For further detail his referenced work is advised.

Fractional Atmospheric Transmission to total solar radiation in clear air for various water vapor content and elevation is presented below:

	Water Vapor in cm of precipitable water per unit air mass					
Air Mass	0.0	.5	1.0	2.0	3.0	4.0
.5	.902	.852	.837	.821	.812	.805
1.0 (90° El)	.859	.794	.778	.762	.752	.745
2.0 (30° El)	.796	.715	.699	.682	.671	.644
3.0 (19-1/2° El)	.743	.652	.636	.618	.609	.604
4.0 (14-1/2° El)	.704	.607	.590	.572	.565	.560

Figure I-22 represents the summary effect of various atmospheric conditions as given in Allen (2).

3. SCATTERING OF LIGHT AND HAZE (NIGHT-TIME AND DAYLIGHT)

Scattering of light is caused primarily by the water vapor content and dust in the atmosphere. When the water vapor content approaches saturation, haze increases and finally thickens to the point of fog conditions. The primary effect of scattering under normally clear conditions (low water vapor content) is loss of contrast in addition to a normal amount of attenuation.

In the case of haze some improvement with filtering is possible, depending on its extent. No. 3, 8, 15, 21, 23A, 25, 29, 92, and 79 Wratten cut off filters (progressively light yellow into red) are useful in improving contrast. (See Figure I-23.) Since the response of the S-20 photocathode surface extends to 8000 + Å, the 92, 89B, and 87C are effective in extending daylight seeing ability. For instance, an 89B filter with a 40' focal length lens and a S-20 photocathode Image Orthicon, will permit tracking of 1st mag. stars throughout a bright clear daylight sky. Without filters, several magnitudes brighter will be required. In daytime exercises with I.O.'s, the less sensitive S-10 tubes with a 23A, 25, or 29 Wratten cut off filter are generally best for building up contrast against a clear blue or hazy blue sky. A red filter (#29) will help sharpen distant scenes over nearby vegetation or a valley.

Note: A single gelatin filter will attenuate about density 3 maximum.

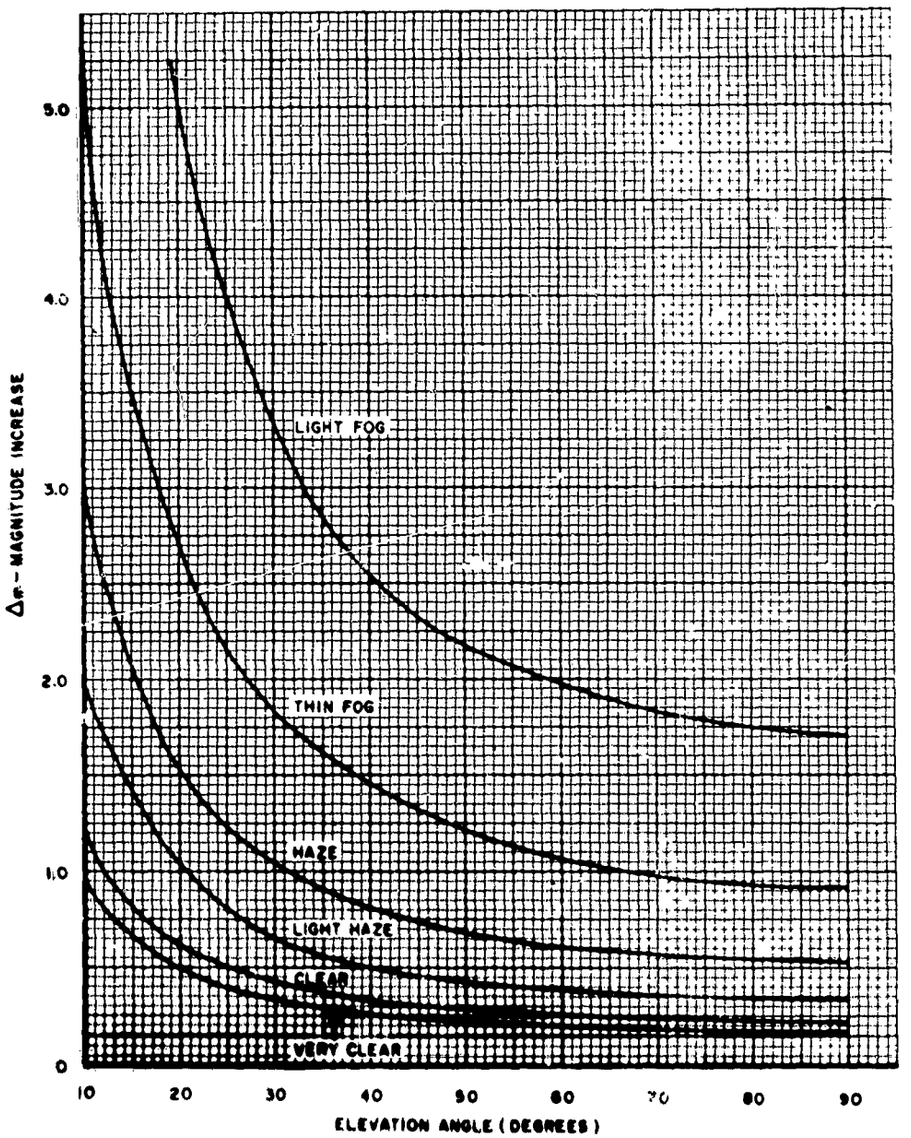


Figure I-22. Increase in Visual Magnitude Due to Atmospheric Attenuation

The signal-to-noise improvement is due to the difference of the scattering coefficient of haze from all other sources, vs the direct spectral illumination from the object diffused by the haze, which improves with longer wavelengths. For more details on air glow, see the discussion in Section I-B.

Monochromatic filters can be used to cut down the refractive components caused by atmospheric disturbances that produce distortions and limit high resolution ability. However, since any single look angle may actually see through several layers of disturbance, then a single filter would no longer be helpful. Therefore,

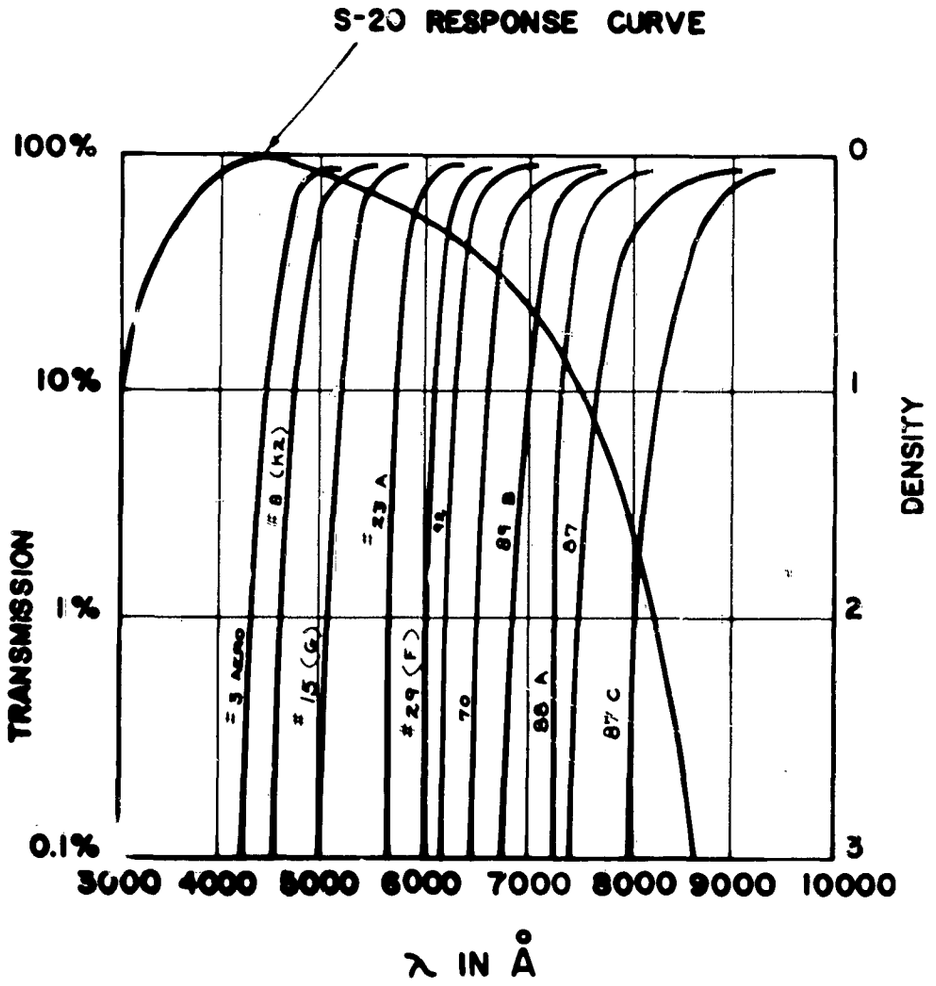


Figure I-23. Transmission of Various Kodak Wratten Filters Plus S-20 Response Curve

the improvement may only be partial and then only on "good" seeing conditions. More tests are needed to define the areas and conditions of use and extent of improvement possible, and will be reported accordingly.

For the higher northern latitudes (also southern) the cold upper air water content more generally will be in the form of ice crystals, which in addition to scattering also act as reflectors; and since there may be many reflectors, some are always glinting; thus, the sky will be apparently much brighter than one would otherwise expect from calculations. This is particularly true under moonlight conditions where in essence we can have two bright sources of light (the sun not necessarily being just below the horizon) as the scatter and glint effect carries sun glint as well as moonlight through the atmosphere with much less than normal isolation.

Scattered light is partially polarized (15%) approximately in the plane of the sun's path but for only that light due to the sun (approximately 15%); so polarization

filtering will not be very effective, (15% of 15%), especially when filter losses are considered. Filtering in general, will offer only a partial improvement of signal to noise ratio as the sun and most nearby stars have, in general, the same spectrum. However, in cases of air glow or light haze, some recovery of otherwise lost performance is possible. A red filter is helpful in "thinning" the Milky Way (because of predominance of "blue" stars) but again this recovers only a portion of the lost performance since it cuts down the signal too!

4. DANCING (POSITION VARIATION)

This effect describes the phenomenon of change of observing angle across the picture with time. These changes are readily apparent with long focal length optics (450 + inches). The frequency and extent of this dancing varies with the stability and "seeing" conditions of the sky. It is primarily caused by temperature differentials and moving layers.

Dancing is defined as the motion of an image about some mean position in a random manner. This motion is highly correlated over a field of view of several degrees of arc. For this reason it is associated with atmospheric disturbances nearer the surface of the earth as a result of formation of warm air cells at the surface of the earth, which periodically break loose and rise into the atmosphere.

The spectrum of the dancing frequency contains several peak regions. The first often occurs around 0.05 cps. The second peak may occur around 1 cps and is also associated with turbulence near the observer.

The larger and obvious motions are low in frequency (.05 to 5 cy/sec), though motion may extend into the kilocycle range for smaller amplitudes. Thus on a "good" night, dancing amounts to 1 to 2 seconds of arc; on a poor night it is 6 to 10 sec and even in the 10 to 15 sec region quite often; the large values are lower in frequency. No work involving "seeing" would be conducted on hot humid days as the results can have fluctuations in the degree range.

The dancing effect severely limits simultaneous comparison of base-line separated photos even for a few feet separation due to the different atmospheric paths. Figure I-3A illustrates this problem. When the photos are viewed in stereo, several levels of star backgrounds are apparent and these were taken only a few seconds of time apart! These photos were taken with the same equipment from the same mount so linearity and equipment distortions should have cancelled from picture-to-picture. The field was large and 1/5th sec. eye integration was used so that the usual scintillation effects should have been small, if any.

Since the thin film Image Orthicon can be exposed for short periods by controlling the photocathode bias, it is a new means to explore this phenomenon and (hopefully) partially conquer it.

For short exposures (less than 30 millisecs) dancing will materially effect position and thus affect cancellation in MTI but if integrated over long periods, it averages out and thus does not affect stellar position data obtained over reasonable periods (10 seconds or more).

5. SCINTILLATION (VARIATION OF INTENSITY)

Scintillation (intensity modulation due to instantaneous reflection and absorption of particles in atmosphere, primarily water vapor) can be quite extreme; even bright stars twinkle! However, for all normal continuous looks, integration over a moderate time (1/5 sec. or so) will reduce or eliminate this as a problem. With short exposures, as is possible with the MgO I.O.'s, the period and frequency will be important since as the scintillation period is approached, stars and targets may be completely lost (when the signal comes through similar or nearly similar paths) in some fast short exposures.

The frequency of scintillation is primarily in the 0.1 to 20 cy/sec. range and may cause a 100% modulation of received intensity. Scintillation in the lower frequency range has been studied quite extensively and is generally correlated to the wind conditions at or near the tropopause. The extent occurs over several seconds of arc, but tends to cancel out after 20 seconds of arc. This explains the reduction of scintillation with planets as compared to stars. Figure I-3A and B illustrates how this, the dancing and refractive effects combine to vary star positions within a field of view to such extent as to effect cancellation if stereo methods are being considered.

The source of this phenomenon is attributed to the winds near the tropopause (25-55 kilofeet) depending on latitude and time of year.

Since scintillation varies inversely as a function of the transmit-receive cone size, scintillation will be reduced by using larger apertures. That is, the resultant scintillation over a large aperture approaches zero. At the same time the detail content attainable in the image may not be improved by the larger aperture, as it may appear to be defocused (see discussion on Pulsation in following paragraphs).

6. PULSATION (CHANGE OF SIZE OF IMAGE)

This phenomenon is closely aligned to diffusion and change of focus, but since it is readily apparent, even with small optical telescope systems, and is of higher frequency, it is generally classed separately. Pulsation is generally attributed to intermediate layers of disturbance; however, this is still open to discussion.

Pulsation defines the change of point source image size with time and is random in nature. The smaller size apertures give sharper images, the large size, fuzzy images. At higher powers the image looks like a pinwheel moving first in one direction and then the other with the rays receding and extending randomly.

Change of point source size with time (pulsation) will cause incomplete cancellation in comparison circuitry. It will cause increased element occupancy when integrated over longer time periods in an attempt to get lower cancellation false alarm rates.

The effect is readily studied by the variation size of stars (point sources) imaged on a film plate or focal plane. The smallest possible image, of course, will be limited by the circle of confusion of the optics involved and is not to be confused with the pulsing effect itself.

It is generally believed that the sharpest or smallest image is also the true image. As the image of a larger object (other than point source) is resolved, the

exact shape comes under question since both pulsation effects and dancing effects are apparent. Analysis of the effect to date points to validity in the assumption that the smallest, sharpest is probably the more exact - but there is still some question.

7. DEFOCUSING

There is very little literature on the defocusing phenomenon and less on the defocusing gradients. Astronomers have long noted that longer focal length photographs of the moon and planets move in and out of focus over a period (generally on a 1/2 to 2-1/2 min. cycle). Since it is relatively slow, techniques are more easily adapted (most involve manual control) to vary the focus to obtain good focus over long exposure times, or simply shutter exposure to those periods of good focus.

The extent of area or angle within a given field of view that will be in focus at any one time is probably more a function of aperture than field of view. That is, this problem is more pronounced with larger apertures (20" or more) than with small (less than 10 inches) apertures. Even short exposures, 5 milliseconds or so, exhibit this effect.

More studies are necessary before this phenomenon and its causes are better understood. Defocusing is not of serious concern except in high resolution work.

8. INVERSION LAYER

When working with larger apertures, 12" (to a small degree) and especially over 24", the inversion layer introduces distortions. The atmosphere, due to this phenomenon, acts to refract various parts of a plane wave by different amounts.

9. DUST AND SMOKE CONTENT

Dust in the atmosphere can be a serious limitation on "good seeing" but since it is primarily a matter of site location, due to local wind and air conditions, it should be treated as an important factor influencing site selection and thus hopefully eliminated or at least minimized as a factor.

Smoke effects predominantly the photographic (blue) and visual wavelengths with little or no effect as the near and infrared wavelengths are used. For instance, even the S-1 photocathode surface will see through all but the very dense smokes, provided, of course, visual cut off filters are used to limit saturation from nearside light reflected from the smoke itself.

10. WEATHER

Except for light haze and smoke, visual and near infrared equipments are, for all practical purposes, limited to clear weather operation. However, even the S-20 response, which extends to .85 microns, permits penetration of haze and very light fogs provided red cutoff filters are used to cut down saturation from nearside reflected and scattered light. See Figure I-24. Figure I-25 shows that even without filters the improvement to .85 microns permits viewing through light overcast even though not possible with eye.

Light and moderate fogs can be penetrated to a degree by use of infrared; the further into the infrared, the better the penetration. The S-1, with an 87C Wratten

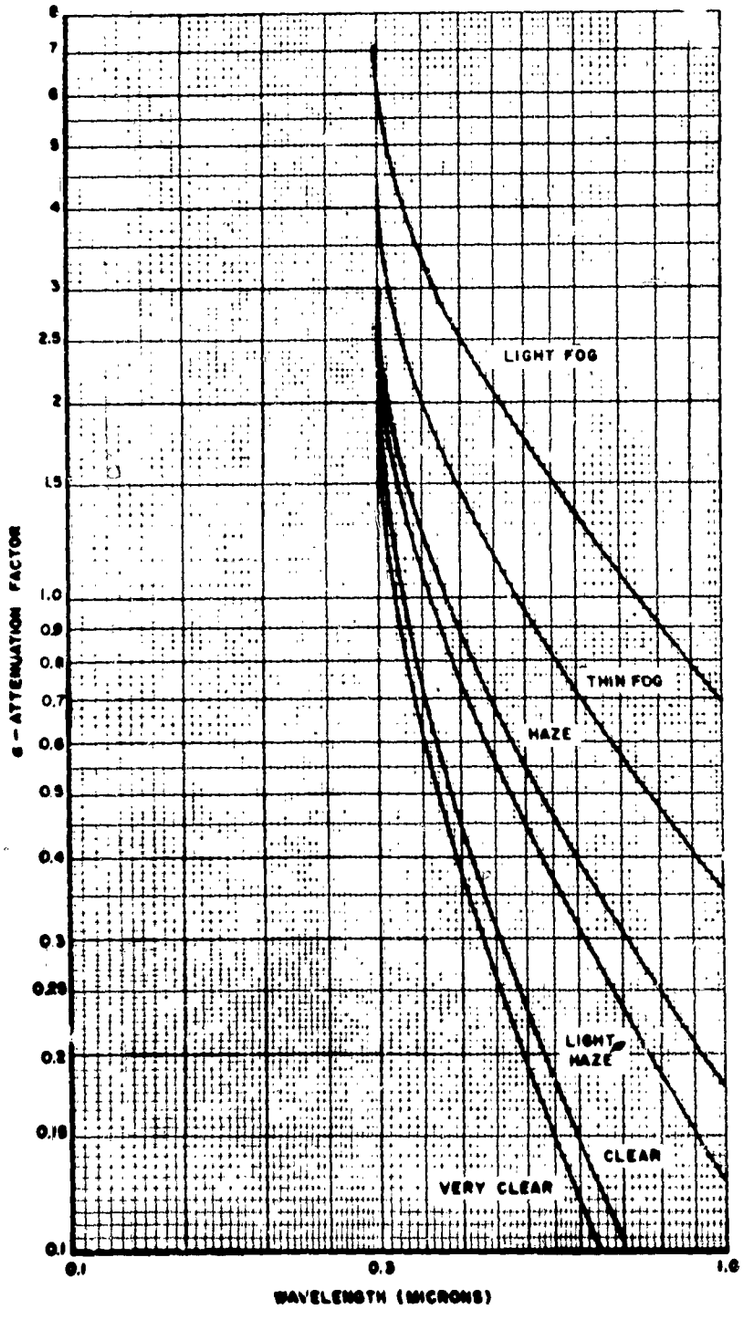


Figure I-24. Atmospheric Attenuation Factor

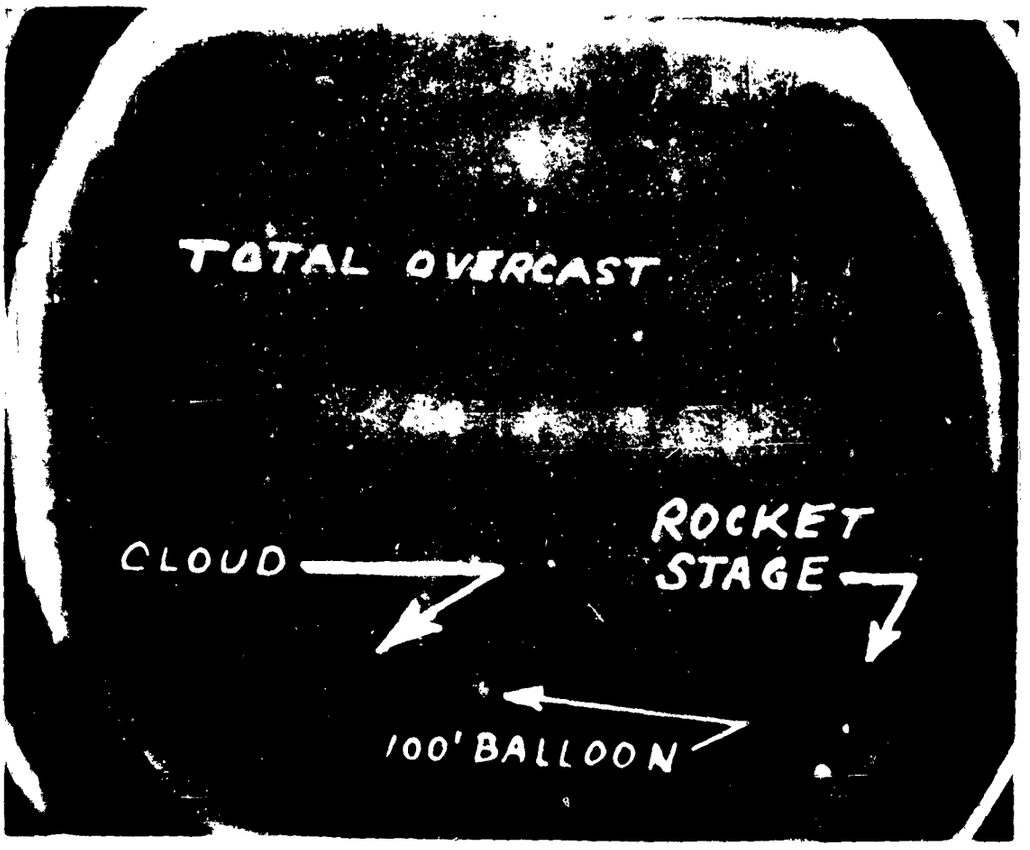


Figure I-25. NASA Wallops Istand Balloon, Viewed from Schenectady by GE Electro-Optical System: 6:30 PM 2/27/60; Range 600 Miles; Scan 1/30 Second: Optics 2.8 Inch

filter to cutoff nearside reflected light to reduce saturation of the tube, will penetrate reasonable distances in light and medium fogs. See Figure I-22 in addition to Figure I-23.

Where missile launch monitoring is desired, the flame energy can be seen using near infrared, though visually it will not be observable. Here it is a matter of getting the sensing equipment nearby and then following the missile up through the fog. The success here is due to the fact that though the fog penetration is impossible for only relatively short horizontal distances, the vertical or altitude thickness of fog is relatively small. The denser fogs generally being more compact in thickness are thus penetrated as are the lighter fogs; 1500 to 3500 ft. thickness being reasonable estimates from weather bureau data.

For more detail discussion, see G. E. TIS Reports on this subject.

Rain is more readily penetrated using near infrared than would normally be expected. In fact, heavy rain is often less of a problem than light rain especially in scene surveillance. Snow, as particle size increases, is more heavily attenuated; however, again penetration is better than with fogs. Red and deep red filtering

helps to cut down nearside reflection and light from saturating sensing element and thus improves penetration ability.

11. SUMMING UP THE EFFECTS

The common important factor is the frequency or time dependence of the "Seeing" problems. If short exposures are made (approximately 5 msec or shorter) dancing is stopped, as is defocusing in portions of the field, thus leading to sharp images. For an appreciable fraction of the time, a pulsating image will also remain sharp, if the exposure is made at the time of smallest image. In "excellent" seeing the stable condition may last from 10 to 20 msec. Inversion layer spectra shows similar effects but much more needs to be done to document and thoroughly explain the effects which for the most part are random with time, though they may have some periodicity.

Thus little can be done with direct processing until more knowledge is available. The I.O.'s sensitivity coupled with its ability to be exposed at varying controlled times offers hope for some breakthroughs; in the meantime, we will have to design around many "Seeing" errors. G.E. Photo-electric Observatory Report[10] treats "seeing" problems in more detail.

D. TARGET BRIGHTNESS FACTORS

The targets or objects to be detected, separated, confirmed, resolved, tracked, etc., must have one or more characteristics distinct enough for detection with respect to background. Thus, besides being bright enough for detection, at least one other characteristic (most commonly, motion) must also be present to confirm separation. The factors include the following:

1. Velocity and Location
2. Illumination and/or Brightness
3. Reflectivity
4. Illumination period
5. Spectral Response
6. Attitude
7. A priori Information

The rates and brightnesses[11] of medium and high altitude satellites and space probe targets dictate different parameters and trades in the system synthesis and thus represent important considerations for establishing performance.

NOTE 1. It is usually the relative target velocity that sets performance limit and affects other criteria; hence it should be established early in the system analysis procedure.

---

[10]J. F. Spalding. Photo-Electric Observatory Report #3. G.E. Co. #61GL146, 1961.

[11]D. J. LaCombe, The Prediction of the Brightness of a Body in Space, GE Co. Report #TIS R62EMH60.

NOTE 2. In addition to the data given in this section, the Volunteer Satellite Tracking Program – Phototrack Bulletin has been included in Appendix VI for reference.

1. TARGET VELOCITIES (RELATIVE TO BACKGROUND)

The targets and objects that are to be detected, etc., against the sky noise background include such a wide range of velocities, altitudes, locations, and directions that no one method will cover all possibilities.

A satellite will have a zenith (maximum) angular rate set by its period, which is proportional to the 3/2 power of its distance from the center of the earth.

The angular velocities involved range from retrograde velocities (backwards to earth's rotation) through zero, relative to celestial rate (earth rotation 15°/hr), to 3°/sec for a 100 mile altitude satellite.

At 3000 miles the zenith angular rate is 3.5° per minute of time.

At moon distances the rate will resemble that of the moon or approximately one $\widehat{hr}$/day; 15° per 24 hrs., 0.6 $\widehat{min}$/min. of time.

For other values refer to Figure I-26.

The targets can usually be grouped into four categories involving their velocity:

(a) Low altitude targets (orbiting satellites and ballistic trajectory targets) 100 to 2000 miles. (3° to 0.1°/second)

(b) Medium altitude targets (orbiting satellites, high lob missiles, etc.) 1200 to 30,000 miles. (15° to 1°/minute) (15 $\widehat{sec}$/sec to 1 $\widehat{sec}$/sec.)

(c) High altitude targets (orbiting satellites, including synchronous satellites, moon orbits, etc.), 15,000 to 300,000 miles. (1°/min. to sidereal rate or even retrograde)

(d) Space probes 100,000 miles or greater. (At or near sidereal rates).

Low altitude satellites are illuminated for only a few hours of the day and can be catalogued by the active radar network and thus are not considered targets for Electro-Optical surveillance, except as they would affect false alarm rate unless considered. Medium and high altitude satellites and space probes provide a field of application for electro-optical requirements/systems, and are also generally well beyond the capabilities of the most powerful radars. Figure I-26 illustrates the range of velocities of orbiting vehicles and space probes.

2. ILLUMINATION FACTORS

a. Illumination Sources and Object Size and Location

A target or object in orbit or on a ballistic trajectory (unless carrying a brighter self-contained light or energy source) normally will be illuminated by one or more of the following: the sun, the moon albedo, the earth albedo, or a directed

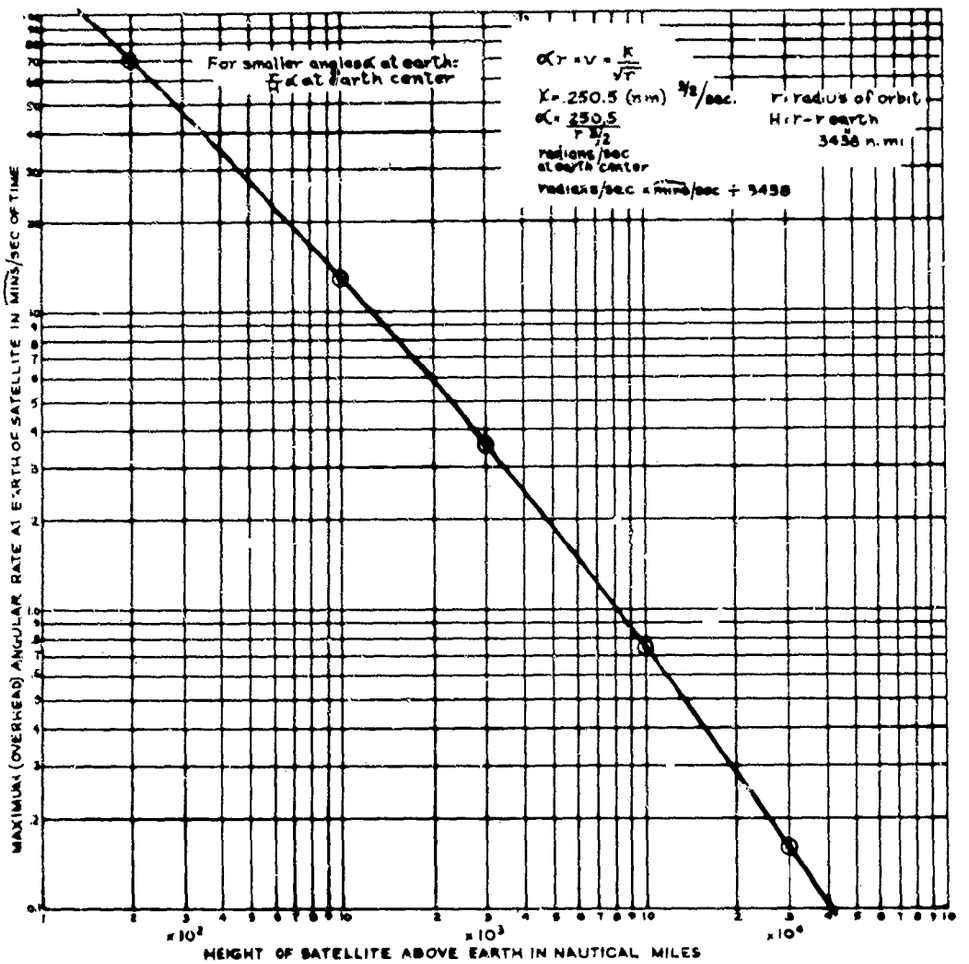


Figure I-26. Angular Rate of a Circular Orbit at Zenith of an Observer on Earth (Neglecting Earth's Motion)

light beam or other energy source (such as a laser). Since we are considering only passive systems, the latter possibilities will not be discussed.

If the target is not in the shadow of the earth (or moon) the primary source of illumination (for objects within the solar system boundaries) will be the sun, with much less from the moon or earth albedo.

The sun's total brightness is	-26.8 magnitudes
The full moon is	-12.2 magnitudes
The earth illuminated (new moon) is	-2.0 magnitudes

The luminous intensity of a specularly reflecting sphere is

(1) $I = a\,FR^2/4$ where a) is the reflectance efficiency

F) is the Incident Radiation (14,200 ft. candles from the sun at earth distance)

or 1.42×10^4 lumens/ft^2

R) is the object radius

The luminous intensity of a diffuse sphere with full phase (0^o) illumination is

(2) $I = 2/3\ a\ F\ R^2\ K$ where K is the phase function and is equal to 1 at full phase $K = \frac{(\pi - \phi)\cos\phi + \sin\phi}{\pi}$

The resulting illumination to the observer is inversely proportional to the square of its distance from the observer; i.e., $E = 1/D^2$ when D is $<<$ than the sun-earth distance.

The following table gives the photo-visual magnitudes of a one meter radius, 100% reflecting diffuse, full phase sphere at various ranges when illuminated by the sun and viewed through one standard atmosphere for absorption (xenith). For other elevation angles and conditions, see Figure I-22.

d Miles	m Photo-visual	d Miles	m Photo-visual
100	-0.3	700	3.9
150	+0.6	800	4.2
200	+1.2	900	4.5
250	+1.7	1000	4.7
300	+2.1	1200	5.1
350	+2.4	1500	5.6
400	2.7	2000	6.2
450	3.0	3000	7.1
500	3.2	4000	7.7
600	3.6	5000	8.2

See Figure I-27 for other values.

The specular sphere is dimmer than a full phase diffuse sphere by the ratio of the constants 2/3 and 1/4 for formulas 1 and 2 and thus is 3/8ths (this corresponds to 83.7^o phase of a diffuse sphere) and is constant regardless of phase. Thus to convert from a full phase diffuse to a specular reflector add 1.05 mag. and do not correct for ϕ angle.

For greater ranges add 5 mag. for every 10 times of range. See Figure I-28.

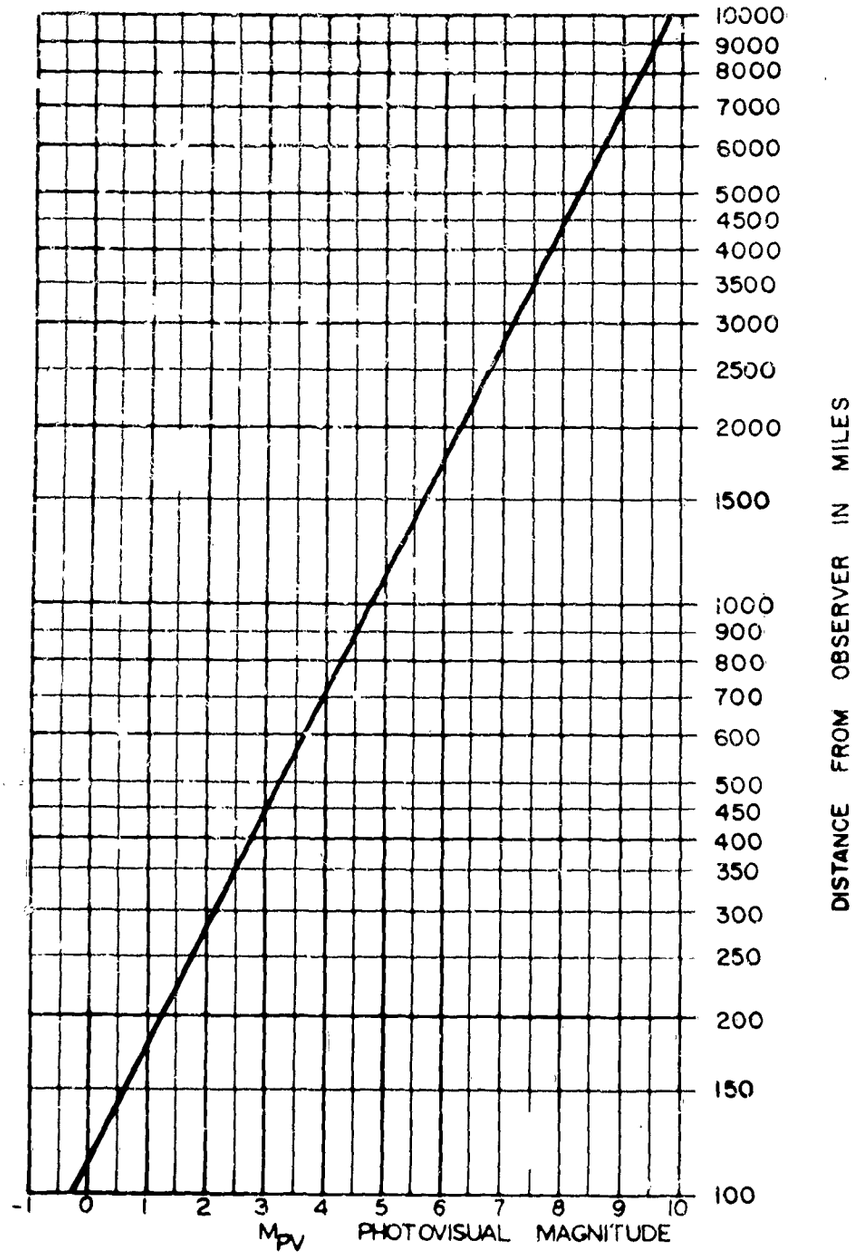


Figure I-27. Photo Visual Magnitude vs Distance for a 1 Meter Radius Sphere; Diffuse Reflecting Surface, Sun Illuminated

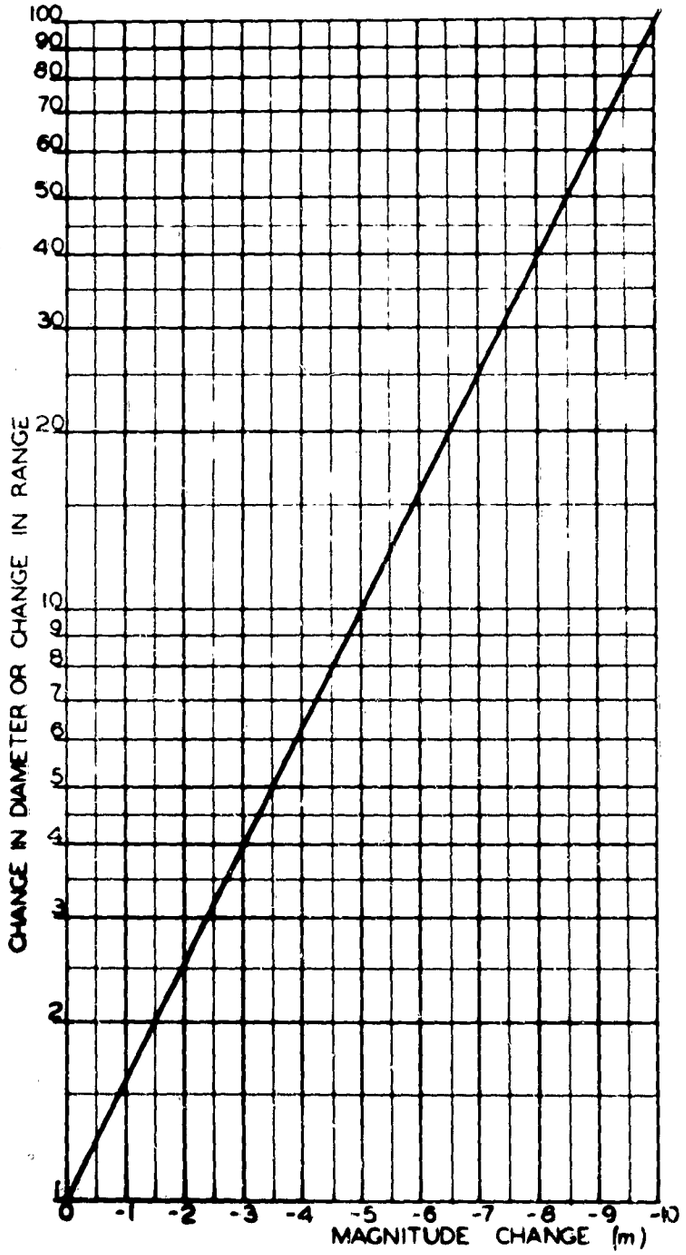


Figure I-28. Change of Magnitude with Change of Diameter of Reflecting Body (-m) or with Change of Distance to Body (+m)

For other sizes:

a change of (+) 1.58 in diameter, change (-) 1 mag.

a change of (+) 3.17 in diameter, change (-) 2-1/2 mag.

a change of (+) 10 in diameter, change (-) 5 mag.

For other values, see Figure I-28.

b. Phase Angle of Illumination (similar to moon phases), Diffuse Sphere Only

The intensity of reflection illumination of a diffuse sphere is proportional to the amount of illuminated area reflecting toward the detector, i.e., the illumination varies with the phase angle (angle of illumination source to object to observer).

The following table lists typical values of the phase function (K) and the corresponding magnitude differences for various phase angles. For other values refer to Figure I-29.

Phase Angle (ϕ)	Phase Function (K)	Add Magnitude (m)
20°	.955	.06
40°	.805	.25
60°	.605	.55
83.7°	.375	1.05
120°	.11	2.4
140°	.035	3.6
160°	.005	5.8

Illumination or Brightness change rate can help identify an elliptical orbit condition by the rate of change of brightness. However, reflectivity and target attitude may overshadow this effect; consequently, it can not normally be used.

3. REFLECTIVITY FACTORS

The energy reflected (radiated or re-radiated) depends on the surface reflectivity (from shining metal to dull black absorption type paint). The following table illustrates corrections for various reflectivities: See Figure I-30.

90%	Add	.16 mag
60%	Add	.66 mag
40%	Add	1.0 mag
16%	Add	2.0 mag
6.3%	Add	3.0 mag
2.5%	Add	4.0 mag
1%	Add	5.0 mag
0.1%	Add	7.5 mag
.01%	Add	10.0 mag

4. ILLUMINATION PERIOD

The period of day that a low altitude satellite is illuminated depends on its altitude, the calendar day and the latitude of the observer. Figures I-31A and I-31B are typical of 45° and 30° latitudes.

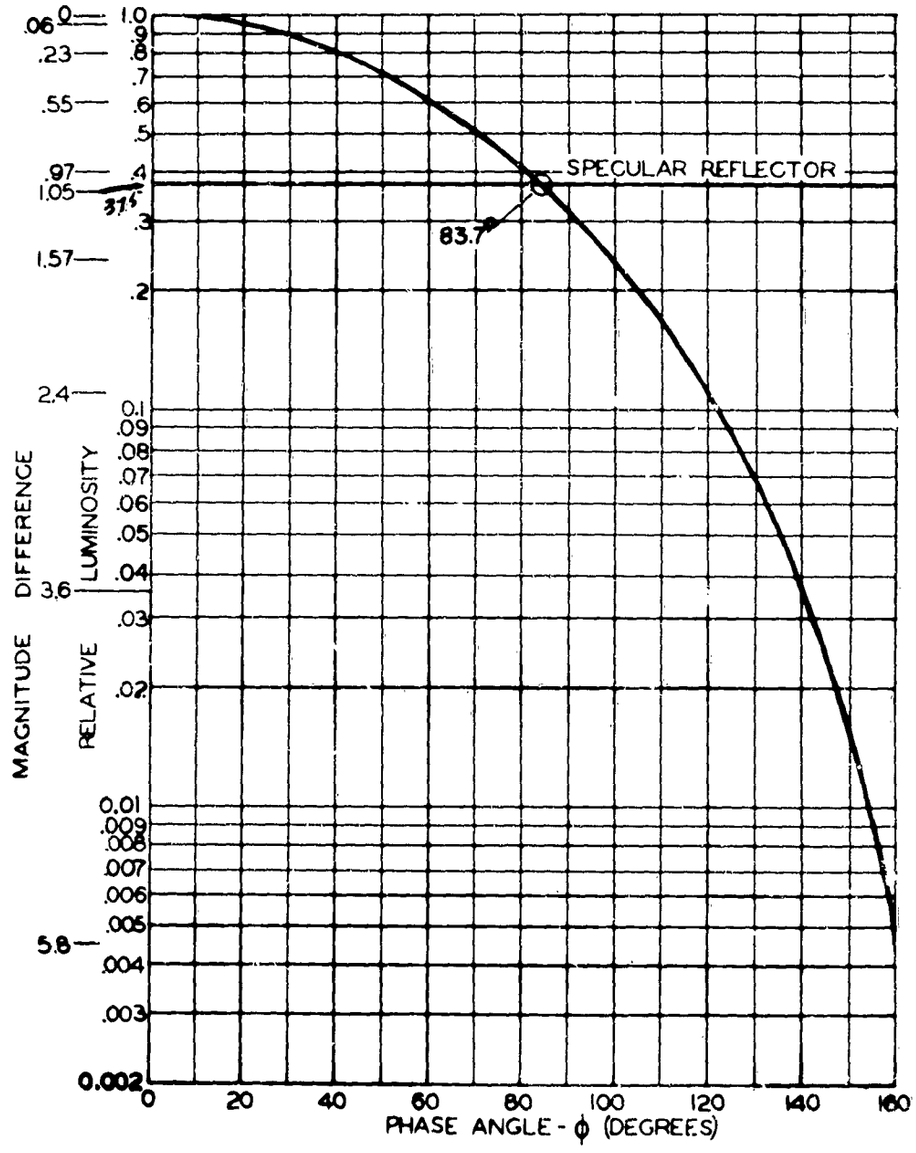


Figure I-29. Relative Luminosity of a Diffuse Sphere as a Function of Phase Angle (Magnitude Difference Scale Included for Each 20°s of Phase Angle, Plus Specular Reflector Reference)

Higher altitudes than shown are illuminated nearly or wholly throughout the night hours.

5. SPECTRAL RESPONSE

The spectral response depends, of course, on the illumination source and the body itself. For the most part we are concerned only with sun illuminated objects.

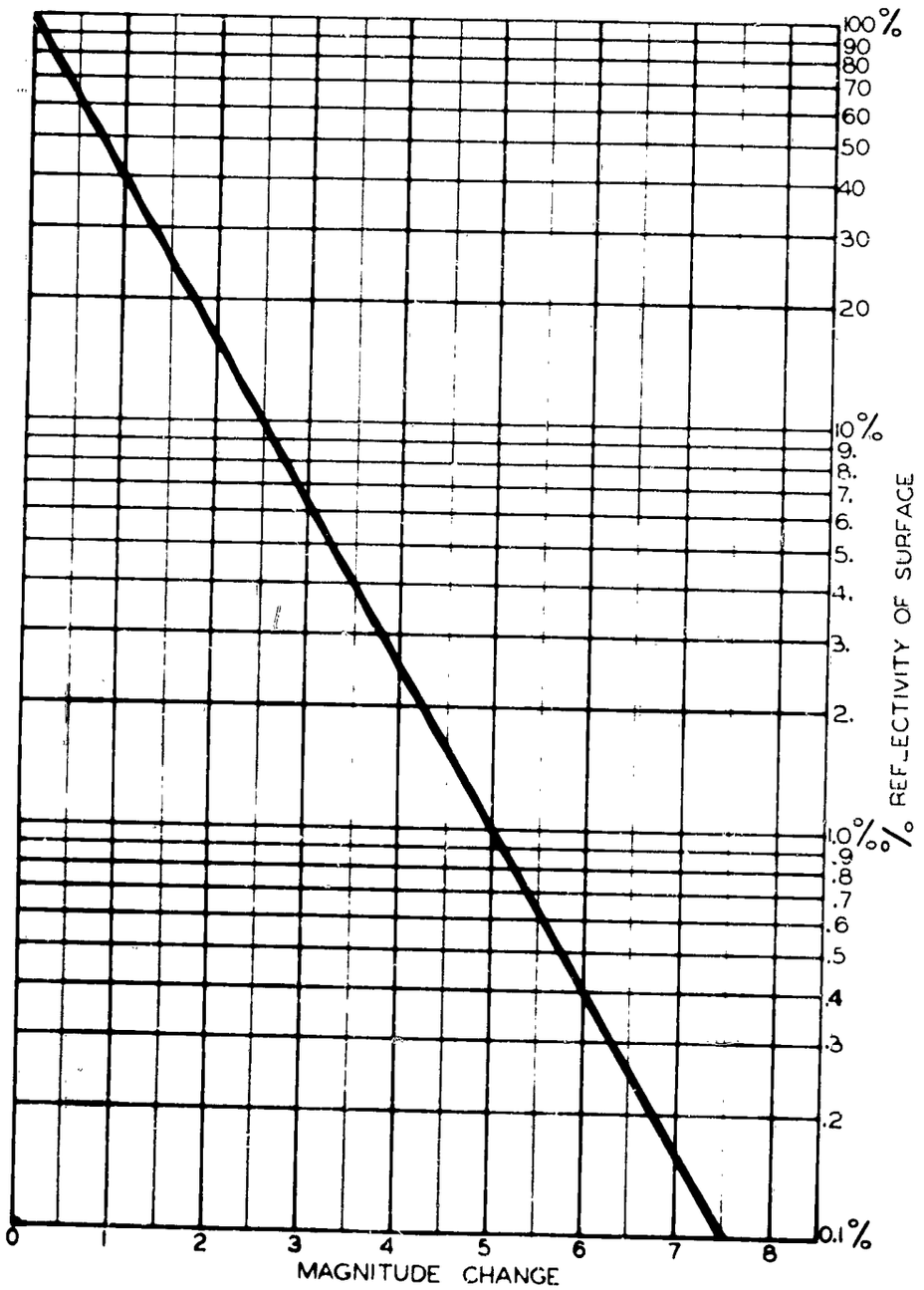


Figure I-30. Magnitude Change with Percent Reflectivity of a Reflecting Object

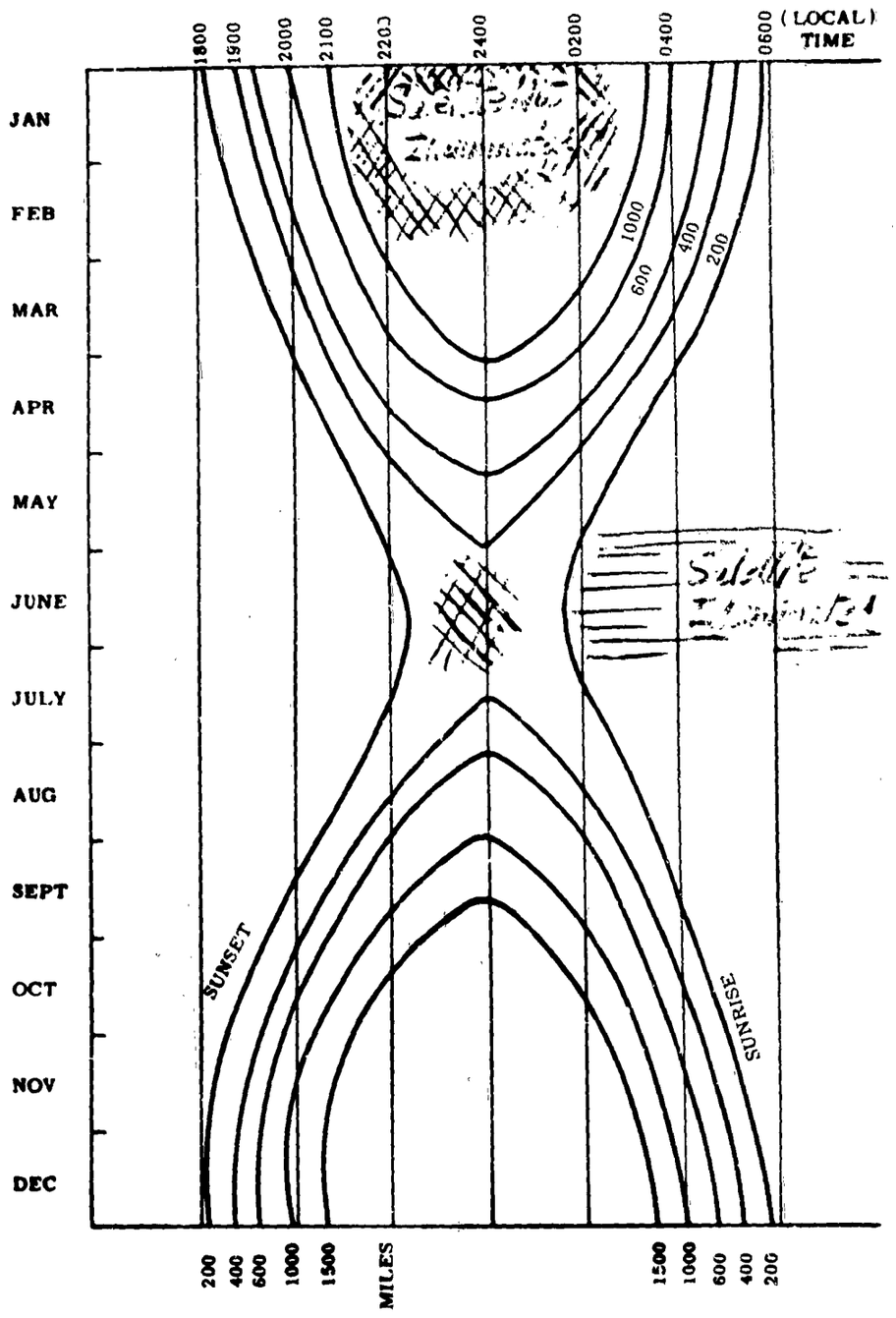


Figure I-31A. Illumination of a Satellite, etc., 45° N. (Sunrise and Sunset Times for a Satellite at Various Heights (miles)

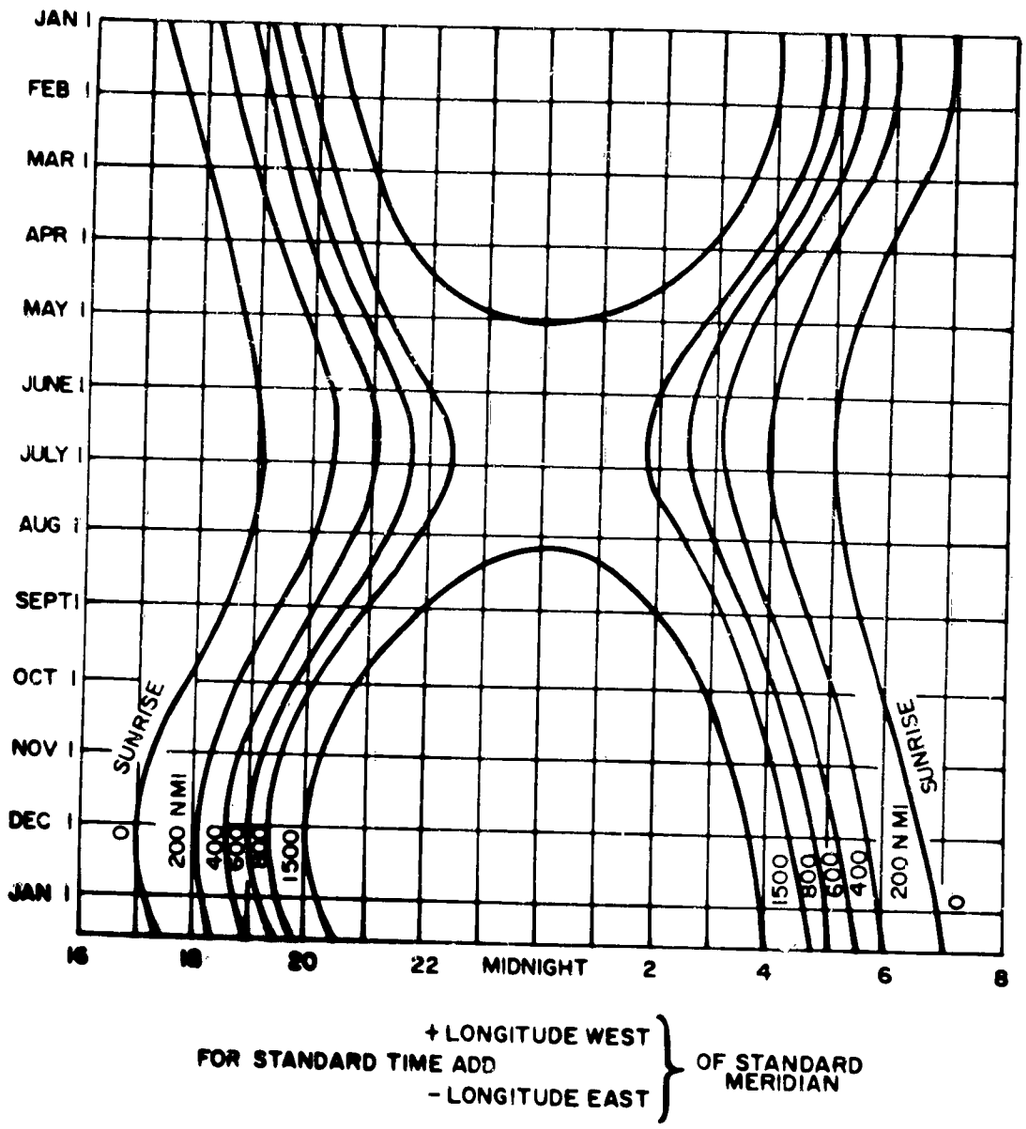


Figure I-31B. Illumination of a Satellite, etc., 30° N. (Sunrise and Sunset Times for a Satellite at Various Heights (miles)

However, with infrared electro-optical equipment, the target's temperature will establish the value of luminosity. Thus, each case should be checked carefully if not specifically defined in the requirements. The matching of object vs background to sensing element spectral response can be of great use in confirming specific objects, though normally the differences from the sun spectrum will be small. However, we might be concerned with differences in spectra of stars to object, as many stars differ in the infrared regions though normally the energy values are too low for satisfactory results.

6. ATTITUDE

The attitude of the target may be used as a separation method but it is more important as an identification feature, i.e., tumbling, spinning or other motion setting up periodic variations of reflectivity can help provide identification and purpose of the object. The presence of "Paddle Wheels" etc., are a factor especially in size and glint conditions in considering separations as well as identification.

7. A PRIORI INFORMATION -- ORBITAL PARAMETERS

Knowledge of type, sizes, drag ratio, orbital parameters, etc., of expected and possible configurations of vehicles will often aid in separation of object as well as identification and classing of various objects, and thus this becomes important to the art.

E. PASSIVE OPTICAL TECHNIQUES FOR SEPARATING OBJECTS

An introductory discussion of techniques for separating objects from a celestial background was given in Section I-A. The various passive techniques specifically suited to the aerospace surveillance task are outlined in this and subsection F. In Section IV, systems applications of these techniques are reviewed and analyzed for probable performance.

The two basic separation methods are the Binocular (stereo) baseline (two or more simultaneous looks to stereo (3D) separate an object located between observer and the stellar background), and the monocular (single station) using catalog comparison methods; that is: the separation of a new object from the celestial environment is by comparison of the present with that of some interval catalogued in the past. The advantages, disadvantages and system conditions are discussed in Section IV.

1. BASELINE (MULTI SENSOR) SEPARATION TECHNIQUES

Where immediate recognition of an object not at infinity is desired or if the catalogue reference of a single site may not be sufficiently up-to-date, then two baseline separated sensors can be used to "triangulate" and separate objects from the stellar background (infinity): 3D or Stereo Effect.

The two sensors or sites are separated on the earth's surface by some baseline distance and operated so as to view simultaneously the same celestial position. If an object is not in the stellar background plane but is at some finite location (altitude) between the background and the observing stations it will be observed in slightly different positions relative to the stellar background. In the multi-station, baseline separated, Site (stereo) system this apparent angular displacement (parallax) is used as a basis for separating the object from the celestial background.

2. MONOCULAR (SINGLE SENSOR) SEPARATION TECHNIQUES

The monocular or single sensor separation techniques utilize catalog comparison methods; i.e., the separation of a new object from the celestial environment is by comparison of the present environment with that of some interval cataloged in the past. The interval may be a temporary or short time catalog, for the delay interval (M.T.I.) technique, or a long time or nearly permanent catalog for the reference techniques.

In actual equipment functions the comparisons are made by; (1) using a delay interval of a present electronic picture image or frame with a similar earlier picture or frame temporarily stored (catalogued) on a storage tube, magnetic (video) tape, thermoplastic tape, or a second delayed scanned image orthicon, etc.; (2) recording the photon output transmitted thru a special film negative (taken earlier - permanent catalog) registered to cancel the known environment at the image plane ahead of the sensor; or (3) reference to a catalogue of the known environment such as scanning a film picture and comparing with the video of the image orthicon sensor.

Note that methods 2 and 3 give instantaneous results much like the Binocular or multisensor baseline separated method in its stereo analysis for separation. Note also that the stereo analysis is complicated electronically though simple for the human eye and brain.

a. Delay Interval-Temporary Catalog (MTI) Technique

One of the most direct techniques for separating objects is the comparison of a present condition or view with that of an interval cataloged in the past, the interval delay being selected according to the relative velocity of motion of object and observer with respect to the field of view being covered. This technique, commonly termed a Moving Target Indication (MTI) Technique, will thus distinguish or separate an orbiting object from a stellar background.

In the M.T.I. system, the two views are compared on an element by element basis and if the image signal of a source occurs in nearly the same position in both views it is considered to be a star and is rejected. If, however, a signal does not occur in nearly the same position in both views it is considered to be a target and is accepted for further processing. The basic technique used to detect the apparent motion is to store an image of the video signal output from the 1.0 sensor electronics (camera) and then, while keeping the "look" position fixed on the same celestial field, electronically compare successive video images with the one stored and process the difference.

The picture is read into a storage tube and then at the time of comparison is read out and compared. In this way the storage tube linearity and image orthicon linearity is of no concern. Errors would occur if the write-in-read-out registration of the storage tube differs, this is generally small. See Section IV for further discussion.

b. Film Catalog (Image Plane Cancellation) Separation Technique

Object separation by reference to an earlier recorded (catalog) reference can be accomplished (1) by using the reference catalog in the form of a film negative introduced between the collecting element (optics) and the sensor (I.O. Tube) to cancel non-moving or previously present celestial objects or (2) by using the reference catalog in the form of a picture, scanned electronically and compared with the video from the observing I.O. equipment for cancellation of the non-moving or previously present celestial objects electronically. Note: both catalogs can be up-dated by adding or removing or moving known objects such as planets, etc.

Note: In method 1 the cancellation is at the image plane before the Sensor whereas in method 2 the cancellation is at the video output of the sensor.

Film catalog image plane cancellation technique consists of a film negative placed between the optics or collector and the image orthicon or sensor. The object of the negative is to prevent the light from the stars and other celestial bodies from striking the sensor and at the same time to allow any light from satellites or other space vehicles to pass through and be detected by the sensor.

The negative is prepared by placing an unexposed photographic plate in position which is later to be occupied by the negative and exposing it to radiation from the collecting optics. Upon development, the areas of the plate exposed to star light will be darkened while the other areas will remain clear or nearly so. This exposed plate when placed between the collector and the sensor where it was exposed will attenuate the starlight and transmit the light from any source that was not in the background when the plate was exposed. See Section IV for further discussion.

c. Film Catalog (Video Cancellation) Separation Technique

Cancellation of the previously recorded celestial environment can be accomplished by scanning a catalog reference photograph with a flying spot scanner and then comparing this electronic picture with that video from the image sensor (I.O. camera) when looking at a similar field of view. Any new or different position of objects from the referenced photograph would immediately be apparent.

The technique is similar in many respects to that of image plane cancellation and the same problems are experienced, such as (1) obtaining a good and complete reference catalog, (2) keeping it up-to-date and (3) registration required for adequate performance.

In the case of registration, the image plane cancellation problem is primarily electro-mechanical adjustment for alignment whereas the video comparison scheme allows for electronic servoed alignment. The error signal source is the same of course, and is quite complicated since translation and rotation are involved.

The performance of the video comparison is quite similar (possibly better) since the relay lens loss (and film attenuation if any) is eliminated.

F. SUPPLEMENTARY TECHNIQUES

The prime purposes of aero-space surveillance systems are to (1) provide an alarm for new objects and (2) provide orbital prediction data. Of course, the sooner and more accurate the positional data is, the better and more useful the predictions. The production of accurate positional data from a surveillance equipment is compromised in favor of improving alarming and detection probability. That is, the field of view is made larger so as to cover more sky in less time, this sacrifices positional data accuracy. For low appearance rates a supplemental system involving tracking of designated or suspicious alarms for accurate orbit or trajectory prediction may be appropriate and a most practical overall system network. Further discussions are included in Section IV.

SECTION II. EQUIPMENT PARAMETERS AND TRADES

A. OPTIC PARAMETERS AND MOUNT REQUIREMENTS

The optics portion (the lens system) of any equipment involving electro-optics or optics imaging techniques is the energy collecting and transfer device between the object (including environment) and sensor. The sensor and electronics (or film) is the detection and/or reading device.

The performance of the combination depends on the number of photons collected from the target and background for each resolution element in the total picture or imaging area and is primarily a function of:

a. Lens effective area (aperture diameter squared minus any aperture blocking)

b. Lens effective focal length and the f/number

c. Quality and type of lens

d. Imaged area or sensor type and collecting area

e. Time per picture (exposure time or scan time)

f. Resolution ability and time per resolution element (TV lines and bandwidth)

g. Relative angular velocity of object to lens axis

The primary performance limitation of a space surveillance system is set by the selection and capability of the optical lens system and the brightness of the night sky background. The lens "speed" is maximized to get a large collecting aperture together with a wide field of view. However, the focal length cannot be made too large otherwise the integrated energy per sensor resolution element area of the faster moving small objects will not be sufficient for detection for the allowable time; that is, the sky must be covered tonight; economically!

The aperture size, focal length and lens optical quality needed also depends on the detector type, size and sensitivity (speed) and the flux density of the target to be detected or resolved in a given background and field of view. The flux density of target may be (1) concentrated in a point source, (2) spread over an area due to its being resolved, or (3) spread over a length due to target motion. Thus we have three distinct conditions or cases to analyze in selecting a lens. Before taking up these cases in detail a few paragraphs on optical fundamentals seem in order.

1. RESOLVING POWER OF A LENS

Two equal intensity points can be distinguished as separate when their diffraction disk images formed on the retina (or sensor) do not overlap more than the half power radius of one of the disks. Hence the theoretical limit of resolution is the half power diameter of a single disk image at the lens image plane, for images of about the same intensity.

θ = Angular limit of resolution in radians = $\frac{1.22\lambda}{D}$

λ = Wavelength of light D = diameter of the lens

For 5500Å and D in inches this becomes $\frac{4.56}{D}$ = θ in $\widehat{\text{secs}}$

No matter how perfectly the aberrations of a lens (lens system) are corrected, the image of a point object can never be a point, but rather a small diffraction disk (Airy disk). To minimize the physical size of the disk, the lens diameter (aperture) must be maximized and the focal length minimized. In addition to lens optical design factors the size of the disk is a function of wavelength and the wave character of the incoming light.

In making larger lenses, it is increasingly difficult to grind them precisely and thus this diffraction limit is less likely to be approached in practice. For instance, a good 5" lens can reach the diffraction limit of 0.9 $\widehat{\text{sec}}$ in separating two similar brightness point sources. However, a 24" lens will be more nearly 0.33 to 0.4 $\widehat{\text{sec}}$ rather than the 0.2 $\widehat{\text{sec}}$ diffraction limit. The single edge of a spread resolved object will, of course, be 1/2 of this angle and if the contrast at the edge is sharp (around 100%) and the signal to background is high, then the edge will be defined to about 1/3 or 1/4 of the arc limit for separating two similar brightness point sources. Thus, for a high performance high resolution system, resolution element size (grain size, no. of TV lines, etc.) should be selected at 1/3 to 1/4 the lens resolution limit for 2 point sources. Also, there is no point in going any smaller as the lens limit will diffuse edges and points to these values.

The above paragraphs assumed a lens of such optical quality that all other lens errors were less than the diffraction limit, which is not always possible in practice. The following discussion of aberrations of lens or lens system, treats some of these errors. The optical systems engineer and/or designer compromises and trades one factor for another of the separate aberration conditions and chromatic variations in meeting the requirements of particular applications. The aberrations are interdependent and correction of one may aggravate or even reduce another. As long as he has a sufficient number of variables to work with (kind of glass, type of lens, system configuration, f/number, focal length, aperture, stops, etc.) he can attain a reasonably good lens for a given requirement.

Thus, lens specifications should be written more in terms of requirements at the focal plane or, better yet, the sensor surface and then if the designer chooses, for example, to stop down a larger diameter to meet other requirements he will have such freedom. Obviously, such complete freedom is not always practical, so the optical designer and equipment engineer will need to cooperate for making the best trades for successful and economical application.

The following discussion of aberration of lenses is condensed from the discussion in the G.E. Optical Engineering Handbook (1) Section I.

(1) J.A. Mauro, G.E. Optical Engineering Handbook, G.E. Publication, Ordnance Dept., Scranton, Pa., 1962.

2. ABERRATION OF LENSES

There are seven classical aberrations defined for an optical system plus chromatism and achromatism. The monochromatic aberrations are:

1. Spherical aberration
2. Coma
3. Astigmatism
4. Curvature of field
5. Distortion chromatic aberration
6. Longitudinal
7. Lateral

a. Chromatism

Most optical materials have an index of refraction that changes with wavelength. Since the index of refraction determines the focal length of a refracting surface, the focus point varies for different wavelengths (color) of light. This action is demonstrated by a prism in separating a beam of light into its spectrum.

This effect permits analyzing a light source but it is a very undesirable aberration in an optical system. Thus, in a single refracting lens, unless the source is monochromatic, the image of a point source cannot be a point but rather a composite of blurred circles of different magnifications forming a halo of colors about the image point, depending on the wavelengths of light from the source.

b. Achromatism

To correct chromatism a combination of two or more kinds of glass (Flint and Crown) with different refractive indices and dispersions are selected. By selecting different curvatures and thickness with the difference indices a lens system with the right focal length can be calculated so the individual dispersions will "cancel".

Chromatic aberrations do not exist in optic systems employing mirror surfaces since mirror optics do not use the index of refraction to form an image.

c. Spherical Aberrations

Light rays from a spore point source will come to the focal point if they are close to the principal axis (paraxial region). However, as the distance off axis is increased, the more the rays are refracted in passing through. These marginal rays cross the principal axis closer to the lens than the ideal focal point. The difference in focus point of the marginal rays to the paraxial rays is the spherical aberration. It is positive for a converging lens and negative for a diverging lens and increases as the square of the aperture. By combining lens of different refracting power, spherical aberration can be corrected.

It is also possible to eliminate spherical aberration in an achromatic lens while still retaining the ratio of total curvatures of the two elements required for chromatic correction. Although the condition for achromatism and the required

focal length completely define the total curvature of the two glasses that make up the achromat, they put no restrictions upon the distribution of these curvatures over the two surfaces of each element. Thus an infinite number of lenses are possible with a given pair of glasses, and among them are those curvatures that are required for the correction of spherical aberration. The process of changing or redistributing the curvature of a lens without changing its focal length is known as "bending" a lens.

d. Lens Bending

By changing the radii of the two surfaces of a lens the spherical aberration can be reduced to a minimum, but cannot be made to disappear entirely. This is shown by drawing a graph using the shape factor "q" which is defined as:

$$q = \frac{r_2 + r_1}{r_2 - r_1}$$

where r_1 and r_2 = radii of the lens surfaces.

e. Aspherizing

Aspherizing is the process of modifying one or more spherical surfaces in an optical system to compensate for spherical aberration.

f. Extra-Axial Points

For objects points off the principal axis, called extra-axial, additional aberrations become troublesome in the formation of optical imagery and steps must be taken to correct them, as was shown for chromatic and spherical aberrations. When defining these aberrations let us consider monochromatic light, as in the case of spherical aberration. Since white light is made up of the wavelengths of all colors, an image of an ordinary point source would contain a summation of individual aberrations for every wavelength emanating from the source. Hence, monochromatic light is chosen for simplicity.

g. Astigmatism

A monochromatic extra-axial point source sends off radiation that strikes a lens obliquely. After refraction such a point forms either a line or a blurred ellipse as an image instead of a point, a phenomenon that is known as astigmatism. If a fan of rays emanating from an object strikes the lens vertically, in the so-called primary or tangential plane, it comes to a focus at one point. If the fan of rays strikes the lens horizontally, however, in the so-called secondary or sagittal plane, it comes to a focus at another point. (The primary and secondary planes are taken perpendicular to each other.) Each possible fan of rays emanating from the same source and striking the lens between these two defining planes, thus, will find corresponding positions between these points.

If a screen is placed at the first point it will show a short horizontal line as the image of the point. If the screen is moved toward the second point, this image line changes first into an ellipse and then into a circle. As the screen is moved further toward the second point, the circle changes into a vertical ellipse whose major axis increases and minor axis decreases until finally a straight

vertical line is formed at the second point. Hence, the object is not represented by an image point anywhere in the image space. The difference between the image points is called the astigmatic difference and the round disk or circle formed between the points is called the circle of least confusion.

Unless astigmatism is corrected in an optical design, the definition of the image will be reduced. Note that there is no astigmatism for images formed on the principal axis. Also, while astigmatism is independent of the aperture of the lens system, it varies with the image height from the principal axis.

h. Curvature of Field

The positions of the tangential and sagittal foci may be plotted for object-point rays striking the lens at varying angles. The plot of these focal points will form curved surfaces. The tangential surface will almost always have the greatest curvature. If there was no astigmatism the tangential and sagittal foci would coincide, and the image-points would lie on a curved surface called the Petzval surface. The Petzval surface is also commonly known as the curvature of field, and uncorrected is a cubic function of the angle off axis. The Petzval curvature is present even after astigmatism has been corrected. Hence, if a flat screen were placed at the axis focal point the image would appear sharp only in the center of the field and would be out of focus toward the edges. Petzval curvature may be positive or negative. With the proper combination of positive and negative lenses a flat anastigmatic field can be obtained.

i. Distortion

Common forms of image distortion produced by lenses, after all other aberrations are reduced almost to zero, are pin cushioning and barrelling. If the image point makes an anglular change greater than the corresponding object point for each position away from the principal axis, a distorted image of a square grid will be formed. The lens is then said to have negative or pincushion distortion. On the other hand, if the image point makes an angular change smaller than the corresponding object point for each position away from the principal axis, the image of the square wire grid would be distorted, and said to have positive or barrel distortion. It is to be noted that distortion is a cubic function of the image height, but is independent of the aperture size.

The difference between the ideal position of the image point and its actual position with respect to the axis is taken as a measure of the distortion. It specifically refers to the circular ring or zone around the principal axis and in the plane of the image. Distortion is measured in percentage and defined by the following equation:

$$\text{Percent Distortion} = \frac{h' - h}{h} \times 100$$

where

h' = Magnification of actual image

h = Magnification of ideal image

Image distortion affects only the relative locations of the various image points with respect to the principal axis. Since all these points lie in the same plane perpendicular to the principal axis, image distortion does not affect sharpness.

j. Coma

Coma is the irregular shape of the image area for point objects located just off the principal axis and is the most objectionable of the oblique aberrations. While an astigmatic image is blurred, it is nevertheless symmetrical about its axis or principal ray. In the case of coma, however, there is no indication where the image center should be.

A comatic image will be obtained, when the principal ray strikes the image plane either above (positive coma) or below (negative coma) the focus of the edge rays.

The cone of rays through each zone of the lens comes to a focus as a circle rather than a point. The largest circle (at the bottom) contains the foci of all rays passing through the outer most zone. The smaller circles (near the top) are formed by rays passing through successively smaller zones of the lens. The smallest (top) circle is actually a point at the vertex of the figure and contains the principal ray through the center of the lens. When a comatic image is viewed it appears as a varying intensity cone because more light is concentrated toward the vertex of the figure than toward the lower end.

It is evident that image points on the principal axis have no coma. As the field is increased, however, by selecting image points farther off, the axis coma increases quite rapidly. The comet-shaped image grows as the square of the aperture and directly with the distance between the object point and the principal axis. Since coma is a function of the shape of the lens, it can usually be reduced by correcting the lens curvature, i.e., by bending.

k. Transverse Chromatic Aberration

Another oblique aberration, known as transverse chromatic aberration or lateral color, is the result of a variation of the magnification with the wavelength of light. This aberration exists even when a system has been chromatically corrected for axial points. Its effect is to produce tiny spectra arranged radially around the principal axis. Transverse aberration is measured in terms of the difference in image sizes. It does not exist at all for axial image points and does not vary with aperture. All the wavelengths meet at the focus point after correction, nevertheless, the magnification of images varies with wavelength, thus a tiny spectral array will be imaged for each object point.

l. Lens Correction

Since oblique (extra-axial) aberrations vary with the distance of the object point from the principal axis and with the aperture, they become troublesome in the case of systems with a wide field of view or large apertures. These conditions are particularly prevalent in camera lenses, and the difficulty in correcting the aberrations readily explains why they are so expensive. Most telescopic systems have a rather small field of view and a fairly small aperture, and, therefore are not greatly troubled by aberrations due to extra-axial image points.

It is impossible to correct an optical system for all aberrations for more than one specified object point. Apparently this would eliminate the possibility for any appreciable depth of field (range of object distances for which sharp definition can be obtained). It should be remembered, however, that it is unnecessary to remove all aberrations completely. Aberrations need only be reduced to the magnitudes tolerable in the required usage of the instrument.

3. CAMERA LENS SYSTEMS

Camera lens systems differ from other types in the requirement for producing relatively large images on flat surfaces, that is, they must deliver a flat, as well as a large, image field. Consequently, camera lenses must be highly corrected for curvature of field, astigmatism, coma, distortion, and transverse chromatic aberration. A small amount of spherical aberration can be tolerated, however, inasmuch as the grain of the photographic emulsion or resolution element size of the sensor, itself limits resolution of the finest detail. In order to obtain accurate reproduction of the image adjustable focusing must be used.

Other factors determining the quality of image reproduction are the brightness of the object, the amount of light that is allowed to pass through the lens, and the sensitivity of the photographic film, or sensor.

a. Focal Ratio or f/Number

The amount of light in lumens/cm^2 that a lens objective delivers to the image plane is determined by its focal ratio or f/number (symbolized f/). It may be expressed simply as

$$\text{focal ratio or f/number (f/)} = \frac{\text{focal length of objective}}{\text{diameter of entrance pupil}}$$

Thus, a focal ratio of f/1.5 means that the focal length is 1.5 times the size of the entrance pupil. (The amount of light is also proportional to the exposure time.)

If the focal length is constant, the focal ratio (or f/number) increases as the entrance pupil is decreased, or conversely, the focal ratio decreases as the entrance pupil is increased. An adjustable diaphragm, of course, permits changing the f/number as desired. However, the rating given to a lens always refers to the largest available opening of the diaphragm.

Speed. The focal ratio of a lens is commonly called its speed, although the relation between them is actually inverse. The relationship between focal ratio and speed arises from the fact that increasing the size of the entrance pupil (that is, decreasing the f/number) increases the brightness of the image and, consequently, cuts down the time required to record the image on the plate. The smaller the f/number, therefore, the greater is the speed of the lens. Hence, an f/1.5 lens is fast compared with an f/8 lens. For an infinitely distant object, the amount of light falling on the film (and hence the speed) is inversely proportional to the square of the f/number. The stopping device in a lens takes the form of an adjustable iris diaphragm between the lens elements which can be set to the desired f/number marked on a scale. The scale in common use is marked f/2, f/2.8, f/4, f/5.6, f/8, f/11.3, etc. Since these numbers increase by $\sqrt{2}$ for each step, stopping down to the next number entails doubling the exposure time, to collect the same number of photons.

b. Depth of Focus

Another effect of stopping down a lens is to increase the depth of focus. It can be shown that with a sufficiently small aperture, the depth of focus can be increased to such an extent that all objects at a distance from the lens between a few feet and infinity would appear equally sharp on the negative and a focusing device would not be necessary. Such conditions actually hold for box cameras. However, the depth of focus increases not only with increasing f/numbers, but also with increasing object-to-lens distance and decreasing focal length of the lens. Hence, to make a suitable compromise between depth of focus and speed, the majority of lens-sensor equipment designed for serious work must be provided with focusing device provision.

c. Total Angular Field of View

The total angular field for a lens with a given focal length is limited by the required corrections of lens aberrations, and determines the useful frame size of a lens. Conversely, the frame size employed by a particular sensor or photographic plate area limits the total angular field of view for a lens of a given focal length. Consequently, aberrations and poor definition are introduced beyond these boundaries if the lens is used with a larger frame size. Usually this angle, θ, is calculated from the diagonal, D, of the frame and focal length (FL).

The total angular field for any lens, noting the focal length and the frame size can be obtained from Figure II-1. Curves showing focal length versus total angular field of view have been plotted for diagonals of various film or sensor sizes. By using the diagonal curve for the film size desired, the total angular field of view can be determined for a lens of known focal length.

4. THE POINT SOURCE TARGET CASE (NON-MOVING) (CASE 1)

In the case of stars, and other targets, which can be considered point objects; the amount of energy concentrated at the image plane of a lens system is proportional to the collecting area or aperture (the square of the aperture diameter $(D)^2$).

The field of view of the lens system is set by the focal length and the size of image plane utilized (sensor size). For a given sensor size, the field of view varies inversely with the focal length, i.e., the longer the focal length the smaller the field of view.

The smallest portion of a given field of view that can be resolved (resolution element angular size) depends on the lens optical quality and sensor ability. In the case of film, it is a function of grain size; in the case of an electronically scanned detector, it depends on the resolution capability of the image section, spot size of the beam and the number of scan lines. As we go to smaller fields of view with the same detector size, a single detector resolution element sees a smaller look angle, up to a limit; the absolute limit is the Rayleigh or diffraction limit for that size of aperture. See Section II-A-1. The practical limit is a larger angle depending on the lens optical quality, or the atmosphere, whichever limits first. For all cases where the resolution element is more than 1 $\widehat{sec}^2$, the celestial background brightness values selected must be increased accordingly. Thus, if the smallest resolvable element is 10 $\widehat{sec}$ × 10 $\widehat{sec}$ or 100 $\widehat{sec}^2$ of arc, the background light on each resolution element amounts to 100 times or -5 magnitudes. Thus, if we are using 21 1/2m/$\widehat{sec}^2$ for a clear sky location, this would increase to 16 1/2 m per

resolution element for our equipment. See Figure II-2 for apparent background brightness increase vs resolution element area for other values. Also see Figure II-34, showing brightness increase and resolution element size vs focal length. A resolution element can be defined or limited by incoming object angle size at focal plane (atmospheric perturbations diffraction, etc.) or limited or defined by image physical size, capability of sensor (film grain size, number of scan lines, beam diameter, etc.).

Since the resolvable element angular view area varies inversely with the square of the focal length, the amount of background energy competing with the target signal can be reduced by increasing focal length ($1/F^2$); that is, the background energy is spread out by changing focal length (looking at a smaller portion of sky area), whereas the target energy remains as a point source and is not spread out. Thus the longer the focal length, the smaller the background energy per resolution element and the better the signal to background until the point source image starts to spread either (1) because it starts to be resolved, or (2) because of lens minimum optical resolution limit is reached (diffraction limit or aberration correction limit) or (3) due to the atmospheric spreading of the point target being imaged.

The exposure needed for a given threshold level for a point source is not dependent on focal length, but is proportional to the collecting aperture area $(D)^2$ of the lens, as long as the focal length is long enough so that the background energy per resolution unit is small compared to the signal energy. Thus, the point source flux is proportional to $(D)^2$ and the background flux density varies with $(D/F)^2$.

Similar to the control of signal energy vs background by focal length is control by changing the size of the resolution element by use of a higher resolution sensor, as long as the resolution element size is still larger than the point source optical image.

There is a point, in the other direction, where a single resolution element gets so large that the background energy begins to restrict the performance. (f/number is defined as ratio of F/D.) Therefore, as the f/number is decreased, a point is reached where the background light will become so large that the sensor elements are saturated with background. In this case, if the sensor resolution can be increased the background light would no longer be saturating because it is spread out more and thus the system detection performance would be improved. For example, with a fast lens $<$ f/2 such as f/0.9, on a bright night, or in the Milky Way, a 1200 line system will out-perform a 500 or 200 line system.

5. THE DISTRIBUTED TARGET CASE (CASE 2)

The extent (field of view) of a scene of distributed target imaged by a lens system is inversely proportional to the focal length (similar to background in the first case). But the amount of energy in a given scene is constant; therefore if we look at less area of the scene (or spread a resolved target out further) by increasing focal length, each resolution element area will receive (see) proportionally less energy by $(1/F^2)$. If we increase the area of aperture, the available flux at the image plane will increase proportionally as before. Thus for extended sources, the available flux density at the sensor resolution elements (exposure) is a function of D^2/F^2 or the inverse square of the f/number. It is constant as long as the f/number (F/D) is constant (the case of photography). Also a faster lens (smaller f/number) allows darker scenes to be viewed or photographed with a given sensitivity (speed) of the sensor.

b. Depth of Focus

Another effect of stopping down a lens is to increase the depth of focus. It can be shown that with a sufficiently small aperture, the depth of focus can be increased to such an extent that all objects at a distance from the lens between a few feet and infinity would appear equally sharp on the negative and a focusing device would not be necessary. Such conditions actually hold for box cameras. However, the depth of focus increases not only with increasing f/numbers, but also with increasing object-to-lens distance and decreasing focal length of the lens. Hence, to make a suitable compromise between depth of focus and speed, the majority of lens-sensor equipment designed for serious work must be provided with focusing device provision.

c. Total Angular Field of View

The total angular field for a lens with a given focal length is limited by the required corrections of lens aberrations, and determines the useful frame size of a lens. Conversely, the frame size employed by a particular sensor or photographic plate area limits the total angular field of view for a lens of a given focal length. Consequently, aberrations and poor definition are introduced beyond these boundaries if the lens is used with a larger frame size. Usually this angle, θ, is calculated from the diagonal, D, of the frame and focal length (FL).

The total angular field for any lens, noting the focal length and the frame size can be obtained from Figure II-1. Curves showing focal length versus total angular field of view have been plotted for diagonals of various film or sensor sizes. By using the diagonal curve for the film size desired, the total angular field of view can be determined for a lens of known focal length.

4. THE POINT SOURCE TARGET CASE (NON-MOVING) (CASE 1)

In the case of stars, and other targets, which can be considered point objects; the amount of energy concentrated at the image plane of a lens system is proportional to the collecting area or aperture (the square of the aperture diameter $(D)^2$).

The field of view of the lens system is set by the focal length and the size of image plane utilized (sensor size). For a given sensor size, the field of view varies inversely with the focal length, i.e., the longer the focal length the smaller the field of view.

The smallest portion of a given field of view that can be resolved (resolution element angular size) depends on the lens optical quality and sensor ability. In the case of film, it is a function of grain size; in the case of an electronically scanned detector, it depends on the resolution capability of the image section, spot size of the beam and the number of scan lines. As we go to smaller fields of view with the same detector size, a single detector resolution element sees a smaller look angle, up to a limit; the absolute limit is the Rayleigh or diffraction limit for that size of aperture. See Section II-A-1. The practical limit is a larger angle depending on the lens optical quality, or the atmosphere, whichever limits first. For all cases where the resolution element is more than 1 $\widehat{sec}^2$, the celestial background brightness values selected must be increased accordingly. Thus, if the smallest resolvable element is 10 $\widehat{sec}$ × 10 $\widehat{sec}$ or 100 $\widehat{sec}^2$ of arc, the background light of each resolution element amounts to 100 times or -5 magnitudes. Thus, if we are using 21 1/2m/$\widehat{sec}^2$ for a clear sky location, this would increase to 16 1/2 m per

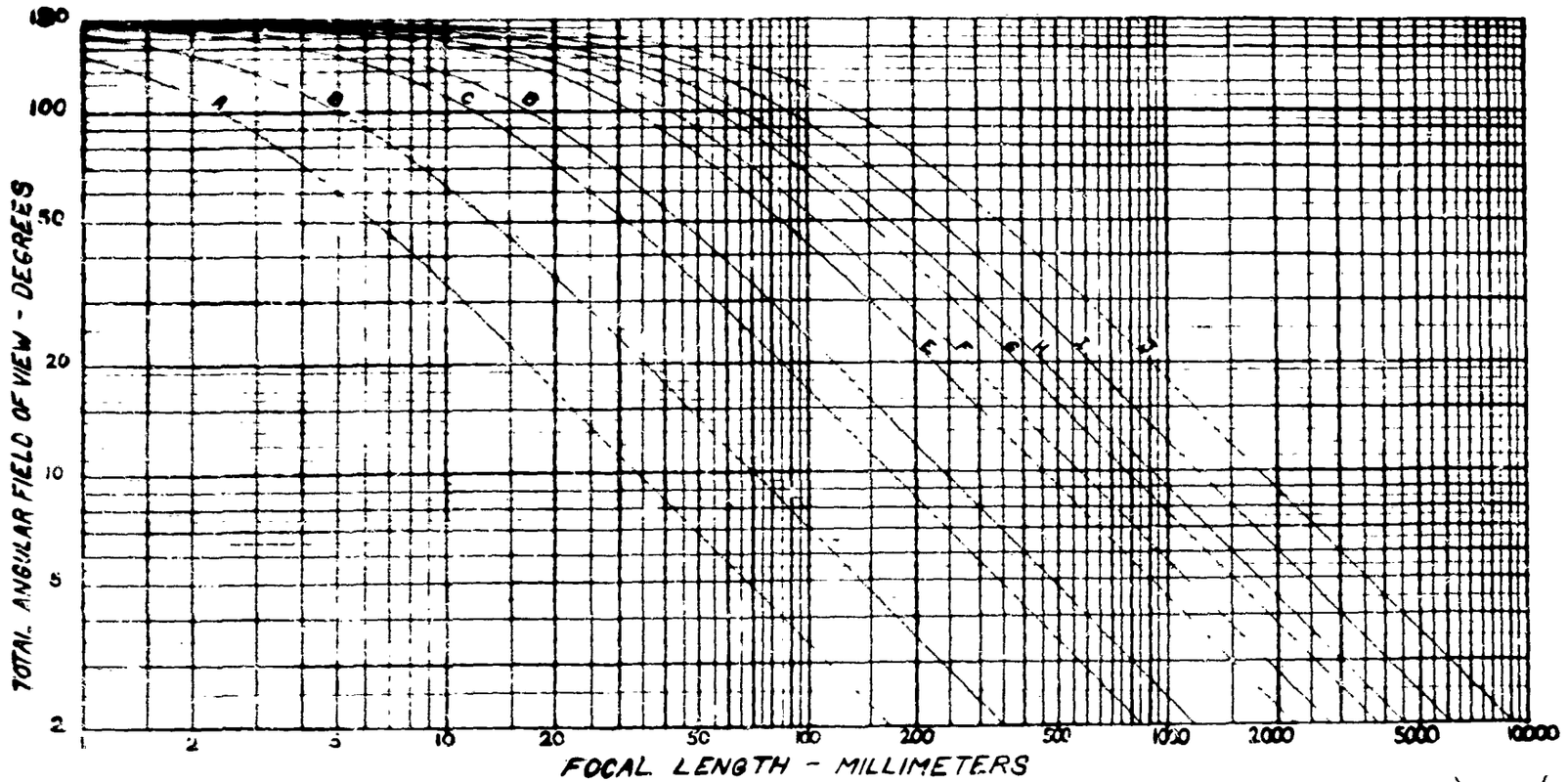


Figure II-1. Total Angular Field of View vs Focal Length for Typical Image

resolution element for our equipment. See Figure II-2 for apparent background brightness increase vs resolution element area for other values. Also see Figure II-31, showing brightness increase and resolution element size vs focal length. A resolution element can be defined or limited by incoming object angle size at focal plane (atmospheric perturbations diffraction, etc.) or limited or defined by image physical size, capability of sensor (film grain size, number of scan lines, beam diameter, etc.).

Since the resolvable element angular view area varies inversely with the square of the focal length, the amount of background energy competing with the target signal can be reduced by increasing focal length ($1/F^2$); that is, the background energy is spread out by changing focal length (looking at a smaller portion of sky area), whereas the target energy remains as a point source and is not spread out. Thus the longer the focal length, the smaller the background energy per resolution element and the better the signal to background until the point source image starts to spread either (1) because it starts to be resolved, or (2) because of lens minimum optical resolution limit is reached (diffraction limit or aberration correction limit) or (3) due to the atmospheric spreading of the point target being imaged.

The exposure needed for a given threshold level for a point source is not dependent on focal length, but is proportional to the collecting aperture area $(D)^2$ of the lens, as long as the focal length is long enough so that the background energy per resolution unit is small compared to the signal energy. Thus, the point source flux is proportional to $(D)^2$ and the background flux density varies with $(D/F)^2$.

Similar to the control of signal energy vs background by focal length is control by changing the size of the resolution element by use of a higher resolution sensor, as long as the resolution element size is still larger than the point source optical image.

There is a point, in the other direction, where a single resolution element gets so large that the background energy begins to restrict the performance. (f/number is defined as ratio of F/D.) Therefore, as the f/number is decreased, a point is reached where the background light will become so large that the sensor elements are saturated with background. In this case, if the sensor resolution can be increased the background light would no longer be saturating because it is spread out more and thus the system detection performance would be improved. For example, with a fast lens < f/2 such as f/0.9, on a bright night, or in the Milky Way, a 1200 line system will out-perform a 500 or 200 line system.

5. THE DISTRIBUTED TARGET CASE (CASE 2)

The extent (field of view) of a scene of distributed target imaged by a lens system is inversely proportional to the focal length (similar to background in the first case). But the amount of energy in a given scene is constant; therefore if we look at less area of the scene (or spread a resolved target out further) by increasing focal length, each resolution element area will receive (see) proportionally less energy by $(1/F^2)$. If we increase the area of aperture, the available flux at the image plane will increase proportionally as before. Thus for extended sources, the available flux density at the sensor resolution elements (exposure) is a function of D^2/F^2 or the inverse square of the f/number. It is constant as long as the f/number (F/D) is constant (the case of photography). Also a faster lens (smaller f/number) allows darker scenes to be viewed or photographed with a given sensitivity (speed) of the sensor.

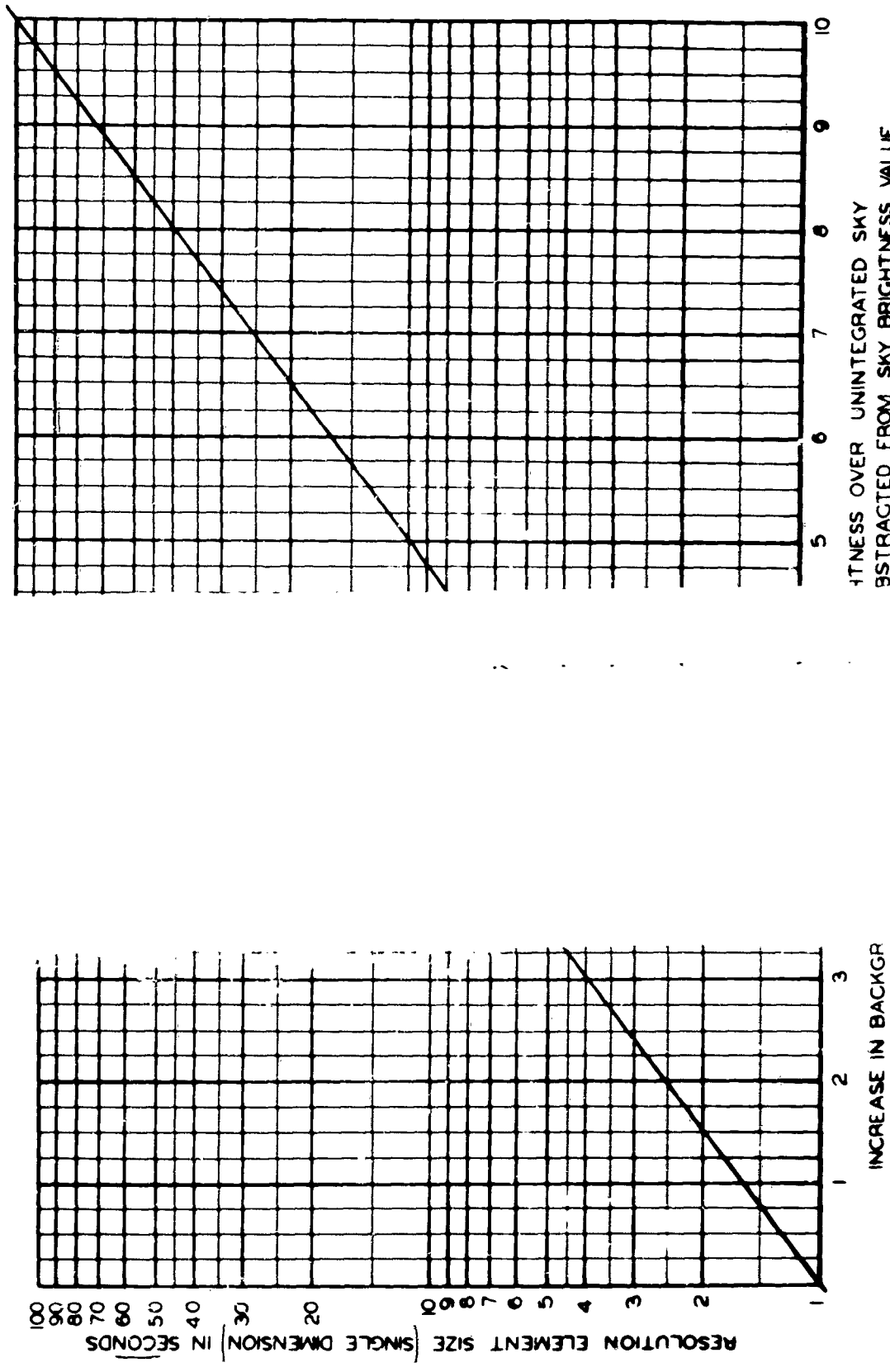


Figure II-2. Background Brightness, Increase in Magnitudes Over Unintegrated Sky Value (mag/sec^2) vs Resolution Element Size Single Dimension of Square

Several interesting situations occur in the aerospace environment as a result. Since the sun is the illuminator in most cases (for the moon, satellites, etc.) and is constant for similar distances from sun, then on resolved objects the brightness per unit angular area is set and is constant (except for reflecting efficiencies). Thus, if the focal length is long enough to resolve the object, say the "Echo" balloon, or any real large satellite, into many resolution elements, the brightness of the image and contrast (maximum signal to background) available to the system will depend only on the f/number, not the diameter or focal length, as long as the focal length and diameter are large enough to resolve the object (and the optics are not diffraction limited and atmosphere permitting).

Similarly in scene viewing, the faster the lens, the more energy density at the detector. In this case, if the lens is fast enough to reach saturation levels of the sensor in portions of a given scene, better results and more details can be resolved with smaller resolution elements (more scan lines, finer grain film, etc.).

6. THE MOVING TARGET CONDITION (CASE 3)

The moving target may either be a point or distributed source. For any source the signal is a direct function of flux density, and flux density is directly related to aperture area (D^2), and inversely proportional to total image area. A spread object has an image spread in two dimensions, and if it has or does not have relative movement during the exposure the spread in either dimension is proportional to the focal length (F). So a spread object image area is always proportional to (F^2), and the signal is proportional to (D^2/F^2).

For a point target with relative movement during the exposure, the total flux collected is still proportional to aperture area (D^2). A point object with exposure movement is spread only in the dimension of relative movement, and this dimension is proportional to (F). Therefore, the image area is proportional to (F), and the signal is proportional to (D^2/F).

Thus, the first point is to determine the object or target angular velocity, then calculate the amount of energy arriving on a single resolution in the unit of time (dwell time) or conversely the number of resolution elements sharing the energy in the unit of time (scan time). This will determine detectivity performance neglecting any sensor time constant loss. If we express this in terms of aperture, focal length, etc., we will see that the exposure for a trailed or moving object is proportional to D^2/F for a given unit of time.

If we are to improve seeing ability of an object of a given angular velocity and size against a given background (to overcome sensor time constant loss and reduced dwell time) we must (1) increase aperture or (2) increase field of view of decreasing focal length. This latter technique makes the single resolution element cover more of the sky at a time and thus allows more time for the target to be in a single resolution element. Since these two factors are somewhat incompatible (we want a large aperture, small f/number system) we must consider many trades to obtain high performance on small, fast moving targets. A thorough analysis of energy available from target and from the background will define which dimension is being "trailed" and which is a point source. For diagonal motion the rates will only be $\sqrt{2}$ of the actual rate, but we have the rate in both dimensions.

7. LENS EFFICIENCY AND STRAY LIGHT

The lens discussion thus far covers refractive optic systems. For reflective optics, cassegrain, catadioptic, Schmidt, Bowers, etc., special precautions must be taken in addition to using effective aperture (actual aperture minus aperture blocking due to secondary mirror and supports, etc.).

a. Lens Efficiency - Transmission Loss

A surface that separates two media is called an interface. When light passes through an interface its direction changes abruptly, part of the light is reflected back into the first medium, while the rest proceeds into the second medium, but in a changed direction. The portion that proceeds into the second medium is said to be refracted. At each surface separating the two media there will be reflections and refractions. As a result, the amount of light transmitted through the second medium is less than the incident light. The amount of light transmitted in an optical system is further reduced because of the absorption of light in the glass medium and the cutting down of light bundles by the diaphragms.

In the case of a lens (refraction index - 1.5) surrounded by air, 4% of the light incident upon each surface is reflected. Consequently, a lens or glass plate in air loses 8% of the incident light by reflection. In photographic objectives and military instruments, such as periscopes, range-finders, and gunsights, which have many glass surfaces, a considerable amount of light is thus lost. Reflection losses can be cut down considerably by coating the air to glass surfaces with anti-reflection coatings.

Lens efficiency factors can thus be determined from the medium transmission losses and number of surfaces involved in a refractive lens system and used in the equations outlined; see Section II-A-8 and 9.

The small percentage of surface reflection from each lens surface in a refractive system must be checked (even if baffled) especially if more than one lens assembly is involved, since the range and sensitivity of the image orthicon will see even the smallest amount of reflection as another diffuse object if it comes within the limits of the photocathode surface. Even though this light may not appear as an image, it may contribute to the background light level in the lens system even when baffled and supposedly absorbed in the "optically black" lens tube. All background and "stray" light not absorbed adds to the sky background light level and thus causes the overall lens-sensor system to appear background limited sooner than would be predicted solely from sky background and lens resolution calculations.

In a refractor lens system this effect is generally small (less than 3/4th Mag/Sec^2 except in extreme cases).

b. Stray Light

In a reflector telescope system, light (sky light, side light, etc.,) can get to the image focus plane (sensor) without going through the normal optical paths.

To reduce this "stray" light, the telescope if not encased should be wrapped with heavy black felt or velvet cloth for a temporary measure until a more permanent case can be made. If possible extend the case to reduce total angular open area. See Figure II-3.

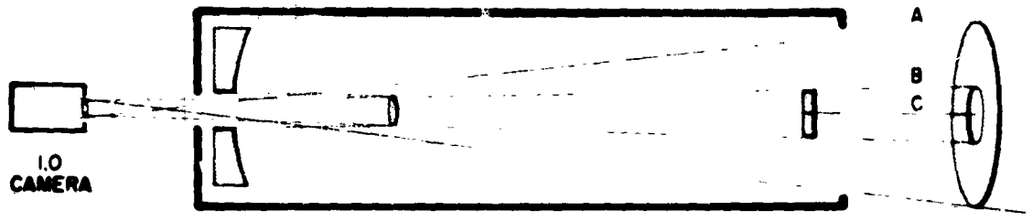


Figure II-3. Reduction of Stray Light in a Reflecting Telescope

The following discussion outlines a procedure for closely approximating the background contribution for "stray light" in reflecting and catadioptic lens configurations. If careful attention is given, the lens-sensor system will consistently perform very closely to calculated performance as experienced in our various experiments with different optics systems.

Using the dimensions of the telescope, determine the ratio of the light from dotted region (angular area × background light/unit area including unresolved + resolved stars, milky way, moon, etc., for area to be surveyed) vs the angular area of the main beam and its relative optical gain (effective aperture area vs the sensor area). The background light in this case is normally at least twice the background light used in other calculations since resolved stars are now present.

A typical reflecting telescope may have 3-1/2 times as much background light reaching the sensor from the stray light (dotted region) than through the optical path, thus the background is increased to 4-1/2 times or a decrease of about 1-1/2 stellar Magnitudes.

$$\text{Effective Aperture} = \frac{\pi}{4} \quad (D^2 - d^2)$$

Stray Light Area = area of cone AC - cone BC

Background Light including stars, etc. = $2 \times M_{B/R}$ (at least)

$$\text{Main Optical Beam Area} = \frac{\pi}{4} \times (\text{field of view})^2$$

$$\text{Main Optical Gain} = \frac{\text{Area of Collector}}{\text{Area of Sensor}} \quad \text{(effective aperture used)}$$

$$\frac{\text{Ratio of Stray light angular area} \times 2 \times \text{Background light}}{\text{Main beam angular area} \times \text{Optical gain}}$$

NOTE: To reduce this value a carefully designed cone shape shield can be installed from the reflecting mirror hole forward tapering to intersection of the 1st and 2nd reflection beam outlines.

8. SIGNAL DETECTION -- LENS SYSTEMS-POINT TARGET CASE

When lens-sensor equipments are used at or near thresholds of noise background conditions, then a systematic analysis for lens and sensor parameters

is needed. A brief discussion is given here; for more detail refer to Section II-B, C and D as well as the referenced reports.

The lens system is basically an energy collecting and transfer device. The sensor, be it the human eye, film, or photocathode of an intensifier, or image orthicon with scanning beam and electronics, is the detection and imaging device. If we point the lens to the sky and move it at celestial rates so that there is no relative angular motion of a single resolved target point source (star or object) with respect to the lens axis, then we have a signal plus sky background on one resolution element and background on all nearby elements:

N_B	N_B	N_B
N_B	$N_B + NS$	N_B
N_B	N_B	N_B

If we look, or expose film or expose a photocathode at the image focus plane of this lens for a finite time, we hope to detect the presence of a signal in a background of noise. This means the signal area has to be significantly different from other background areas of equal size, so that the probability of the background being the signal value is very small. Since the number of background photons collected by an area equal to the signal area in size (used to form the image) has a Poisson distribution, there will be background image noise due to the non-uniformity of transmission or brightness variation of these individual background areas. The sigma of these background areas (same area size as the signal size) is the square root of the background mean number of photons in the areas used to form the background image, with a Poisson distribution. The difference between the mean background image photons and the mean of image signal photons is defined as the signal. Thus

$$S/N = \frac{\text{Peak}}{\text{r.m.s.}} = \frac{\text{No. of signal photons } (N_S)}{\sqrt{\text{Noise Background } (N_B)}}$$

for good detection (approximately 90%) and a low false alarm rate (approximately 10^{-4}) the signal should be 5 times the rms noise (sigma) of the background. This constant of 5 was first used by Albert Rose of RCA, in 1948.

$$S/N \text{ Detection} = 5 = \frac{N_S}{\sqrt{N_B}}$$

A normal image system has additional noise which has to be included to explain system operation. For an image orthicon the equipment background N_E has to consider added beam scanning noise, and preamplifier noise. For a film image the equipment background N_E has to consider developed particles due to fogging.

$$\frac{S}{N} = \frac{N_S}{\sqrt{X^2 N_B + N_E}}$$

$$N_S = N_O \times 10^{-.4 m_S} \times \frac{\pi}{4} D_I^{\,2} \times t \qquad (2)$$

$$N_B = N_O \times 10^{-.4 m_B} \times \frac{\pi}{4} D_L^{\,2} \times t$$

m_S = stellar mag of Object in mag/$\widehat{\text{sec}}^2$

m_B = background mag/$\widehat{\text{sec}}^2$ sky

X is signal spread in sky $\widehat{\text{sec}}$/sig width

If $X^2 N_B \ll N_E$ then $\frac{S}{N} = K D_L^{\,2} \times \text{Eff. of Lens} \times t \qquad (3)$

This will be true for a long focal length, small diameter lens and short exposure times. This is also the condition in a laboratory test where the background noise is made to approach zero.

Thus $S/N = \frac{N_S}{\sqrt{X^2 N_B + N_E}}$ as $N_B \rightarrow O$

becomes

$$S/N = \frac{N_S}{\sqrt{N_E}}$$ or limited by equipment noise.

If $X^2 N_B > N_E$ then $\frac{S}{N} = K \frac{D_L \sqrt{t}}{X} \sqrt{\text{Eff of Lens}} \qquad (4)$

$$X = \frac{\text{Total Image Width}}{\text{Lens Focal Length}} \times 57.3^{O} \times \frac{3600}{\text{Active TV Lines}} \times \frac{\text{TV Spread Lines}}{\text{Signal}} \qquad (5)$$

Since

$$S/N = \frac{K \cdot D^2 \cdot \text{Eff} \cdot t\, N_S}{\sqrt{X^2 K \cdot D^2 \quad \text{Eff} \cdot t \cdot N_B + N_E}}$$

$$= \frac{K \cdot D^2 \cdot \text{Eff} \cdot t \cdot N_S}{X \sqrt{K \cdot \text{Eff} \cdot D \cdot \sqrt{t} \cdot \sqrt{N_B}}} = \frac{K \sqrt{\text{Eff}} \cdot D \cdot \sqrt{t} \cdot N_S}{X \sqrt{N_B}}$$

Summarizing, we note for point sources when the background noise is smaller than the equipment noise (the condition for a long focal length lens with short exposure times) equation (3) shows S/N increase with square of lens diameter (D_L^2) and directly with exposure time (t) Thus performance curves have a slope of 1-1/2 magnitudes for each doubling of diameter or $\sqrt{t}$. When the equipment noise is less than the background noise (X^2 N_B) then equation (4) shows S/N increases only directly with the Lens diameter and square root of exposure time and inversely with the signal spread factor (X).

Thus, as sky background noise begins to become a factor, the slope decreases to 3/4th mag. for each doubling of lens diameter and then performance quickly limits as the sky background noise gets larger than the signal.

9. SIGNAL DETECTION - DISTRIBUTED TARGET CASE

A distributed target may be an extended target within a general scene being viewed, the level of which is above minimum detectable levels, or it may be an extended (resolved) target in an otherwise noise limited background.

In this case our $S/N = N_S/\sqrt{N_B + N_E}$ relationship involves the size of both $N_S + N_B$ which varies with resolution element size and f/number of optics.

If the background term (N_B) is small with respect to equipment noise N_E such as with large f/number Lens, then S/N varies inversely with the square of lens f/number ($1/f^2$) and inversely with size of the resolution elements and directly with exposure or integration time (6). As the f/number of lens is reduced near f/1 8 or below and/or resolution element size is larger, the background term increases until performance is limited by it. Note reducing resolution element size will allow use of smaller f/number optics and thus better resolution performance at same scene brightness level provided target image was not spreading due to lens or atmospheric limits.

10. LENS AND OPTIC SYSTEMS

Lens and Optic systems frequently used with electro-optical equipment are shown below by type (2).

The Galilean and Keplerian refractor telescopes are noted for their simplicity. The Galilean is shorter for the same magnification and has a narrower field of view since the eye piece becomes a field stop. It presents, however, an erect image, which is, in some cases, an advantage.

Among reflecting telescopes (which do not suffer from chromatic errors), the Newtonian is preferred for small telescopes, since only one aspheric element needs to be made (the primary paraboloid). The secondary mirror is a flat.

The Cassegrain and Gregorian both require a hole drilled in the primary, and an aspheric secondary (elliptical for Gregorian, hyperboloid for Cassegrain). Both have the advantage that the primary tube length is about 1/2 of the focal length, while the Newtonian requires a full length tube.

---

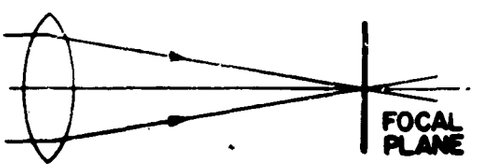
(2) Strong, John, Concepts of Classical Optics, W.H. Freeman & Co. 1958.

Certain optical systems are notable for freedom from one or more of the monochromatic defects: spherical aberration, coma, astigmatism, field curvature, and distortion.

The Schmidt system, using spherical primaries, is free of off axis aberrations (coma and astigmatism). Curvature and spherical aberrations remain, but the corrector plate cancels spherical aberration. The Bouwers, Hayward and Maksutov systems are variations to accomplish a similar result.

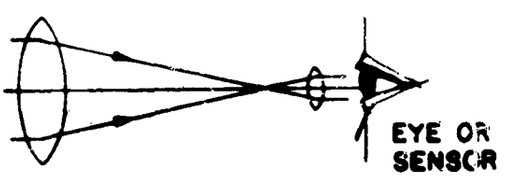
a. Refractor Systems (Lens optical systems involving only the refractive properties of lens materials)

1. Simple and multiple lens systems such as conventional camera lens, zoom lens etc.,including those employing many elements for aberration corrections, etc.

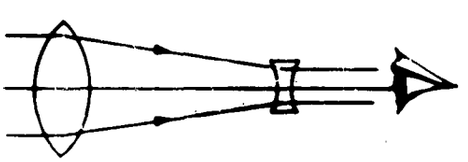


2. Telescope systems.
Note: Eye pieces added for eye viewing. Magnification, etc.

a. Keplerian



b. Galilean



Note: Galilean often used in front of a camera lens to make a telephoto lens.

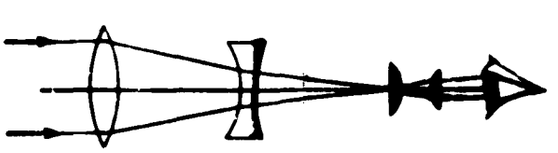
c. Refractor with eyepiece Huygenian.



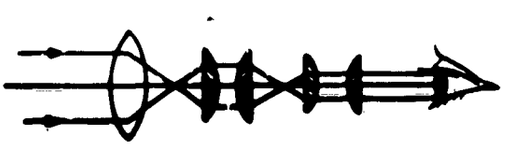
d. Refractor with Ramsden eyepiece.



e. Refractor with Barlow

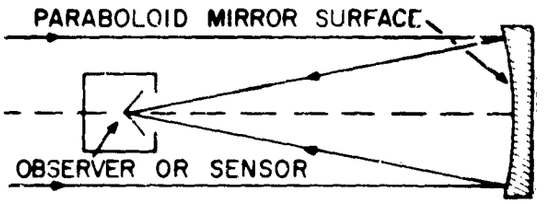


f. Refractor with erecting lens.



b. **Reflector Systems** (Optic systems involving a curved mirror surface as the primary collecting optical surface)

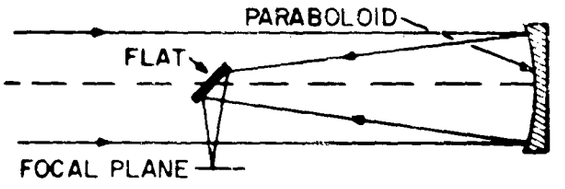
1. Hale



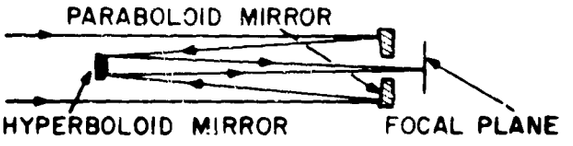
2. Herschelian



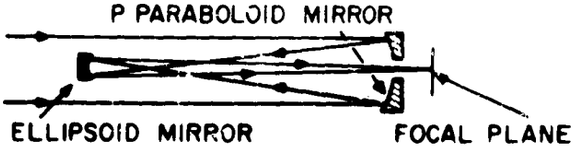
3. Newtonian



4. Cassegrain



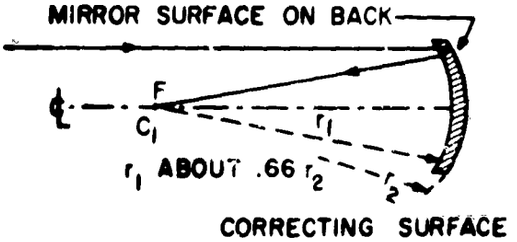
5. Gregorian



c. Catadioptic **Systems** (Optic systems employing a negative corrector plate diverging rays to a spherical mirror with short focal length)

In catadioptic systems the resulting focal plane is a curved surface, thus field flatteners or special provisions are generally needed for its use. Advantage is in ability to have short focal lengths for large apertures (small f/numbers) (0.5 to 2.0 common range, less than 1 often used).

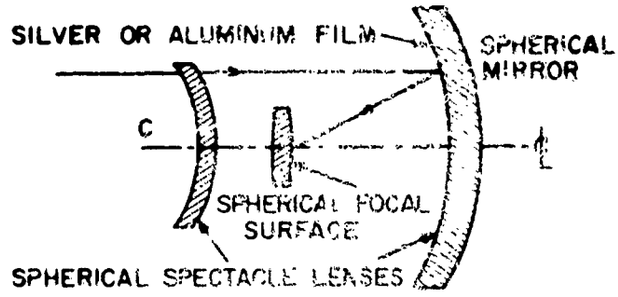
1. **Mangin Mirror**



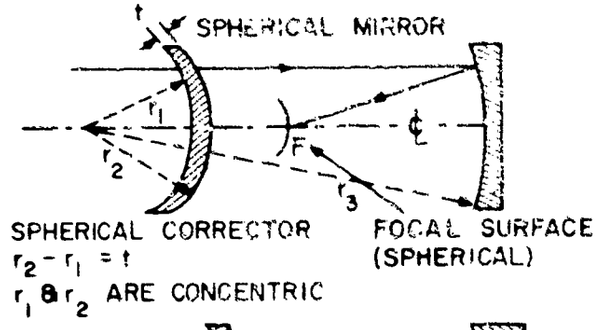
R about .66 R_2

Not strictly a catadioptic system but similar in principle.

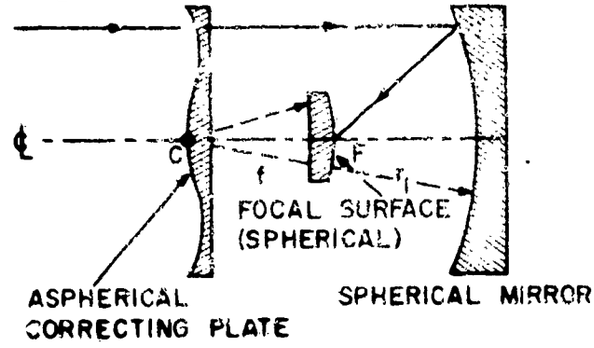
2. Bouwers



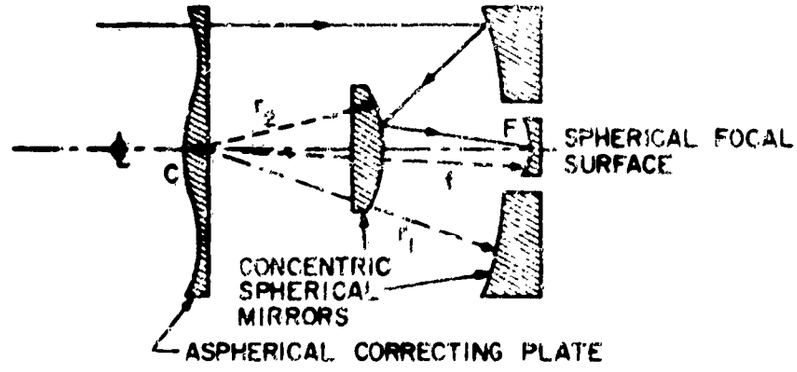
3. Maksutov



4. Schmidt



5. Hayward



11. OPTIC SYSTEMS FOR SATELLITE DETECTION AND SEPARATION

Preliminary design studies indicate typical apertures, taking into account the sky background, air scatter and image tube properties, of 25 to 35 inches with aperture ratios from f/0.7 to 1.8 (focal lengths of 24 to 42"). For discussion purposes an aperture of 27" and f/1.5 giving a focal length of 40" is selected.

The other requirements are that the resolution of the optics should take full advantage of the image tube resolution. For these calculations it is assumed that

TV resolution may be eventually increased to a 2000 line scan and that three n lines will be required to cover a point image. If the sensitive area of the ıera tube is one inch high this will require an optical circle of least confusion ıc image of a point source) of about .0015 inch or a resolution of 60 line pairs millimeter (60/Lp/mm). This resolution should be maintained over the entire 1-1/2" sensitive area or a circle of 1.65". The image at the photocathode uld be flat within its depth of focus, which for an f/1.5 system is about .006 ıes.

The optical distortion should ideally be negligible, or less than one-tenth of percent. If this is not feasible it should be as low as practical and predictable.

a. Refractor Lens System

A refractor lens system appears completely impractical at present. An 5, 40 inch focal length lens would require at least five transparent glass ele- ıts 27 inches in aperture. The total glass thickness in the lens would be about nches. Not only would such elements be difficult to obtain in high-quality glass, the weight of them would be at least 1700 pounds and the loss due to absorption siderable. From a purely optical point of view, it is very difficult, if not im- sible to design a lens of this focal length which would not show objectionable ›matism over a wavelength range of 3500 to 8000 Angstroms. The chromatism ›mpound lenses is chiefly a function of their focal length, and when the focal th approaches one meter it becomes impossible to control. Recent independent ıarches by Nippon Kogaku, producer of Nikon Camera, and Carl Zeiss Incorpor- , have shown that for focal lengths in excess of one meter mirror systems of- .he only solution to the cnromatism problem even over the normal photographic elength range 3800-6500 A.

b. Newtonian System

The Newtonian telescope consists of a paraboloidal mirror with the de- ›r at the primary focus, or by use of a diagonal mirror the focus is turned out e side at right angles to the axis. This system works well for f/ratios f/8 or e. However, if the system is drawn to scale at f/1.5 as shown in Figure II-4 ll be seen that there are several objections.

1. The camera tube is pointed downward when the telescope is aimed upward. This is not recommended.

2. The focusing coil assembly around the camera tube has a diameter about .3 as great as the mirror. When the central obscuration of an optical system exceeds 20 percent there is serious loss of energy concentration in the central diffraction images. In general terms this results in low contrast fine detail and "mushy" image. The light loss due to the obstruction is about 11 percent.

3. The image formed by a paraboloidal mirror does not lie on a flat surface but has a radius of curvature exactly equal to the mirror or 60 inches. Over a 1.6 inch picture this radius will result in a sagitta or variation from a plane of .021 inches which is considerably greater than the depth of focus previously calculated to be .006 inches at the most. It might be possible to flatten this image with a field lens.

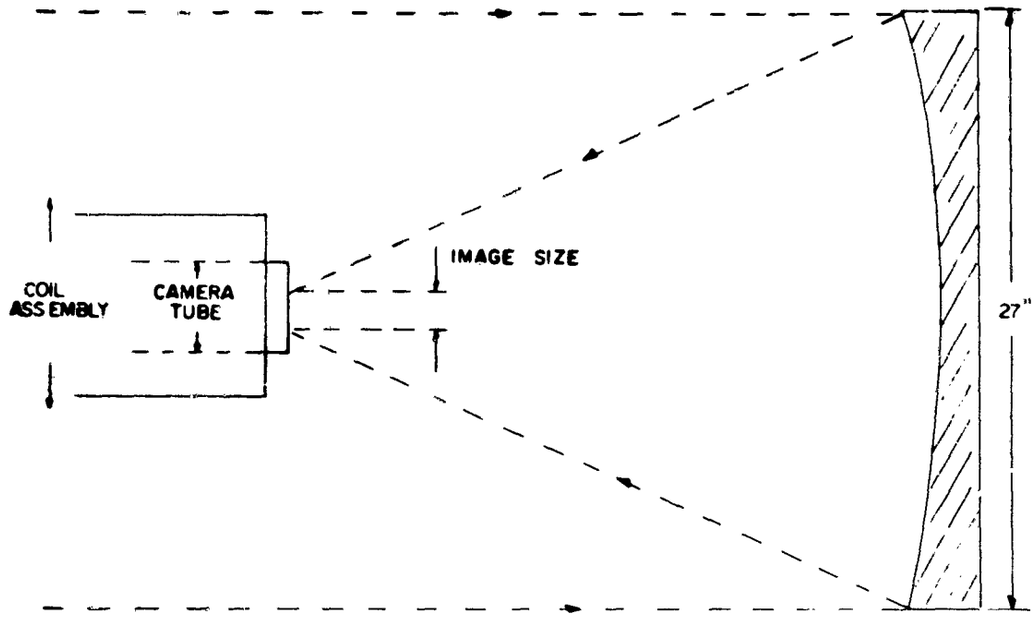


Figure II-4. Newtonian System without Folding

The folded Newtonian system drawn to scale in Figure II-5 shows the problem of trying to place a mirror in a large aperture beam. In order to bring the image outside the edge of the entrance pupil it is necessary to use a flat mirror having a projected length of 15 inches which forms a major obstruction in the light path. This is totally impractical. When the aperture ratio is f/8 or less the reflected cone of light is long and narrow and can be folded with a relatively small mirror.

Conclusions on the Newtonian System

Beside the mechanical difficulties mentioned, it must be realized that the paraboloidal mirror forms a perfect image only on the optical axis (i.e., at the center of the image) and that off-axis rays form images with amounts of coma and astigmatism that increase with the angle. The amount of these two chief aberrations has been calculated by K. Schwarzschild and his figures are reported in Baker's "Telescopes and Accessories" and elsewhere. Unfortunately, these tables were not computed for aperture ratios larger than f/3.0. Several years ago we had to extend these tables and the values were calculated from theory and also checked by actual measurement of aberration on a precision test bench. The agreement was as good as could be expected when it is realized that the aberrations have to be separated by eye and each is compounded by several higher orders of aberration of the same type.

To take examples; Schwarzchild's table shows that an f/10 paraboloid with 40 inches focal length would show at the edge of a three degree total field a coma of ten seconds of arc. This would amount to an image of point source about .002 inch diameter which is satisfactory. For an f/3 paraboloid the coma at the edge

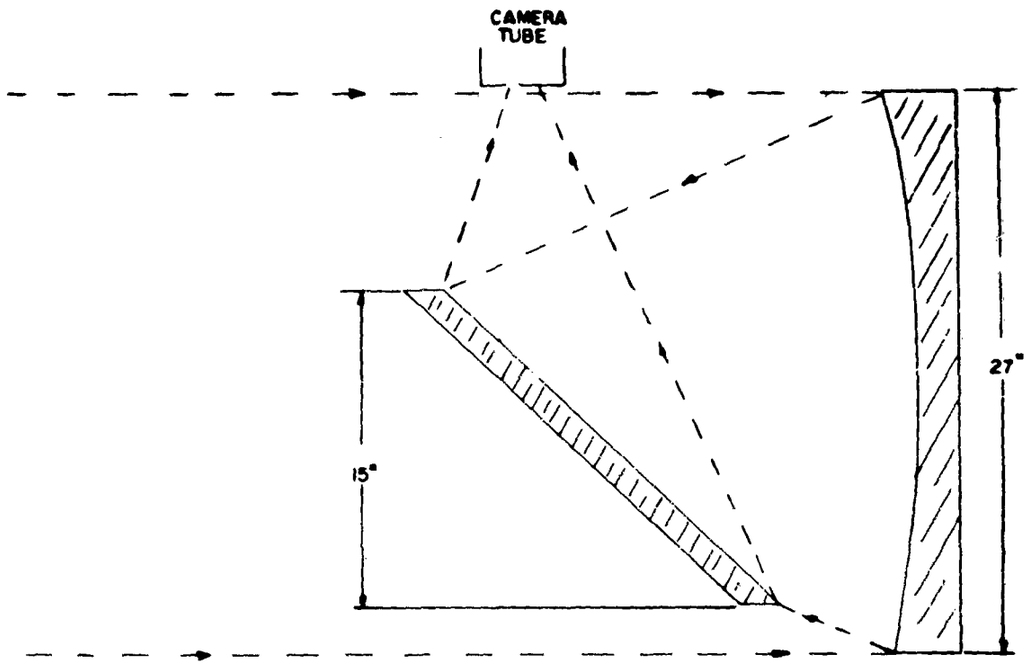


Figure II-5. Newtonian System, Folded

of the field amounts to 116 seconds of arc and for a 40 inch focal length this amounts to an image aberration of .224 inches which is quite poor.

Our calculations show that for an f/1.5 paraboloid the coma would amount to seven minutes 44 seconds of arc or an aberration of .896 inches which is absolutlely intolerable.

The comparable figures for astigmatism are as follows:

f/Ratio	Astigmatism (Seconds of Arc)	Aberration (Inches)
f/10	13.5	.0024
f/3	48.0	.0081
f/1.5	96.0	.0172

The Combination of the two aberrations we have calculated as follows:

f/Ratio	Astigmatism & Coma (Seconds of Arc)	Aberration (Inches)
f/10	17.0	.003
f/3	132.0	.240
f/1.5	750.0	.900

We believe these figures show that the off-axis aberrations of the paraboloid make it unfit for the proposed use. In addition the above shows that there are severe problems to folding the beam and that the aberration of coma at the edge of a three degree field would be absolutely intolerable.

c. Schwarzchild Telescope

After K. Schwarzchild had completed his analysis of the errors of the paraboloid he developed the only physically possible design of a two-mirror telescope free of spherical aberration and coma. There are many variations on the design; it is possible to have a flat or curved image, but all the systems have astigmatism. Reference to the table in paragraph (b) will show that this is the smaller defect in large aperture telescopes.

An f/1.5 Schwarzchild system is drawn to scale in Figure II-6. Normally the design is not recommended for an f/ratio less than f/3 because of the great difficulty of figuring the aspheric mirrors. The parameters of this system are:

f/ratio of system	f/1.5
Equivalent focal length	40 inches
Diameter of primary mirror	27 inches
Focal length of primary	100 inches
f/ratio primary	f/3.7
Separation of mirrors	50 inches
Diameter of secondary mirror	13.36 inches
Focal length of secondary	33.4 inches
f/ratio secondary	f/2.6
Distance of focus from secondary	20 inches
Tube length	96 inches

The good features of this design are that the camera tube could be installed at the first focus. The bulky coils around the tube would not be as large as the central shadowed area and would not cause any additional light loss. Both mirrors have f/ratios greater than f/1.5. It becomes increasingly difficult to manufacture aspheric surfaces at a low f/ratio. It is not possible to quote definite figures, but the following are typical:

Difficulty to Produce Aspheric Surface

f/11	Usually very easy
f/8	Requires only short time
f/3.5	Usually considered the practical maximum
f/1.5	Extremely time consuming and requires great ability

In our opinion it would be far easier to make the two larger f/ratio Schwarzchild mirrors than to make one f/1.5 paraboloid.

The bad features of the design are the large obscuration ratio. The secondary mirror cuts off about one-quarter of the light and the reflection losses total about 18 percent so that the "transmission value" of this design is about 61 percent compared to an ideal f/1.5 system with no losses. The long tube length is normally required to prevent the camera tube seeing around the secondary. If a bright object such as the moon were outside of the image field and the telescope tube did not extend beyond the secondary mirror, then direct light from the moor could fall on the camera tube face.

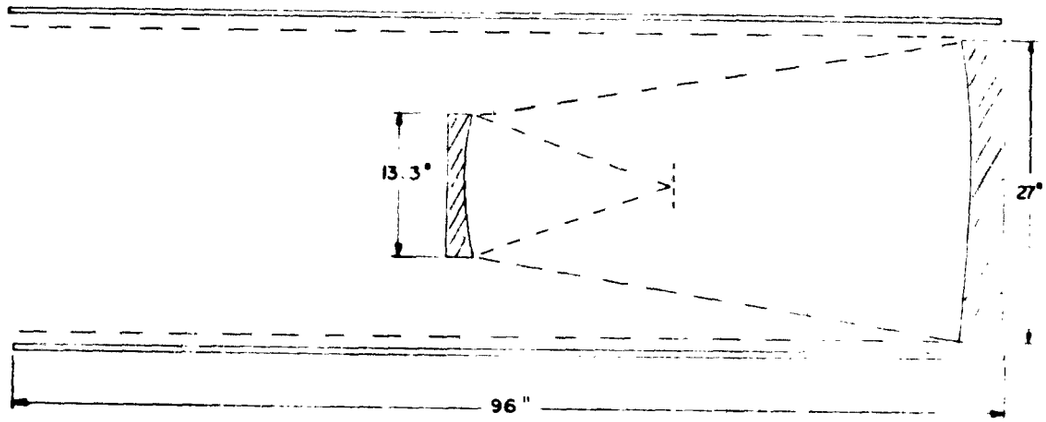


Figure II-6. Schwarzchild System

It is expected that the image quality would be good, the only aberrations being astigmatism and distortion. These have not been calculated, but until they are, it is believed that they would be satisfactory.

d. Couder Telescope

The Couder telescope uses two aspheric mirrors and is corrected for spherical aberration, coma and astigmatism, but has a curved image. An f/1.5 Couder telescope is drawn to scale in Figure II-7. The dimensions of this system are:

f/ratio of system	f/1.5
Equivalent focal length	40 inches
Diameter of primary mirror	27 inches
Focal length of primary	130 inches
Aperture ratio of primary	f/4.9
Separation of mirrors	80 inches
Diameter of secondary	13.0 inches

Focal length of secondary	22.2 inches
Aperture ratio secondary	f/1.7
Distance of focus from secondary	15.4 inches
Tube length	100 inches

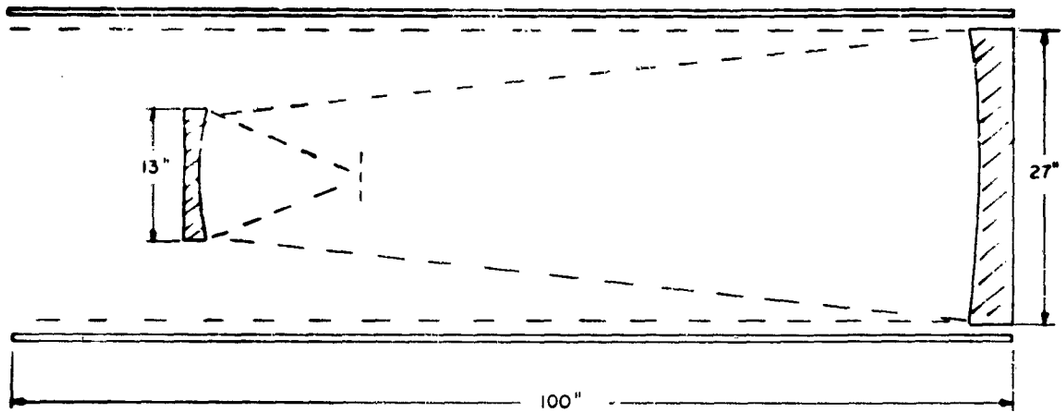


Figure II-7. Couder System

The good features of this design are correction of all the aberrations except distortion and image curvature. The radius of curvature of the image is half the focal length or 20 inches and the sagitta (depth of curvature)across a 1.6" image is about .016 inches. This value is only about .010 inch more than the calculated depth of focus and could easily be removed by the use of a field-flattener lens.

The transmission efficiency is only slightly greater than the Schwarzchild system, about 65 percent. Because the camera tube is closer to the secondary the stray light problem is less bad, but the total tube length is about the same.

As regards the difficulty of manufacture, the large f/4.9 primary would be less difficult than the Schwarzchild f/3.7, but the small secondary now has the high aperture ratio of f/1.7. As far as can be estimated at present, the manufacturing problems of the two systems are about equal.

e. The Schmidt System

In the previous designs the chief optical problem has been the off-axis aberrations of the aspheric primary mirror. As was shown in the case of the paraboloid, the off-axis aberrations at f/1.5 were intolerable, but they can be corrected to usable value by a second aspheric mirror. The manufacture of any large aspheric mirror to high accuracy is a major undertaking. The Schmidt system avoids the problem by using a spherical mirror which is easy to make and a thin lens or "corrector plate" which usually has one aspheric side. In this design the diameter of the corrector plate becomes the limiting aperture and the mirror has to be somewhat larger.

The layout of an f/1.5 Schmidt system is shown in Figure II-8. The dimensions are as follows:

f/ratio system	f/1.5
Focal length	40 inches
Diameter of primary mirror	33 inches
Focal length of primary	40 inches
Diameter of correcting plate	29 inches
Separation corrector and mirror	80 inches
Tube length	84 inches

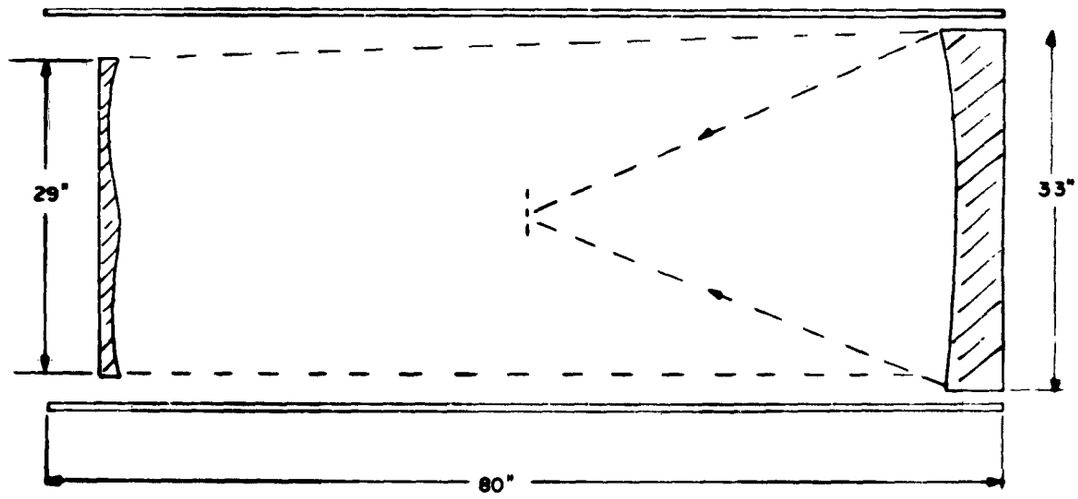


Figure II-8. Schmidt System

The advantages of this system are that the image is fully corrected except for distortion and image curvature over the entire field. The large primary mirror is a sphere which can be machine made. The corrector plate requires a large piece of relatively thin optical glass of high quality and while it has an odd aspheric surface which must be handmade, the actual curvatures are not steep (the drawing is exaggerated) and the accuracy requirement on this surface is only about one-quarter that of an aspheric mirror. The reason for this is that a mirror is a reflecting surface and any error in the surface slope doubles the deviation of a reflected ray, while in the case of a refracting element made of a material with an index about 1.5, an error in the slope of the surface results in a deviation of the refracted ray only about half as great.

Bad features of the Schmidt design shown in Figure II-8 are that the camera tube face is pointed downward when the telescope is aimed at the sky. This light path could be folded by a flat mirror so that the light was brought back through a hole in the center of the mirror, but this involves the problem of folding a high aperture beam, requires a large flat mirror and results in considerable light loss due to obscuration.

The radius of curvature of the image surface in a Schmidt system is equal to the focal length or 40 inches in this case. The sagitta over the 1.6 inch image area would amount to .003 inch which is only slightly greater than the .006 inch depth of focus and easily corrected with a field lens or may even be ignored. The chromatism of the extremely weak corrector plate is not enough to give trouble at f/1.5.

The Optic systems above involve one or more large aspheric surfaces. Another well known design is the Cassegrain.

f. Cassegrain System

Primarily, this system is designed for a long focal length in a compact space and is not satisfactory for aperture ratio higher than f/8. This is due to the fact that the secondary mirror becomes very large and the off-axis aberrations, especially coma is even worse than the Newtonian or paraboloidal mirror.

g. Wright Camera

The Schmidt principle of using a corrector plate has been applied to several variations, one of these is the Wright camera shown in Figure II-9. This arrangement uses a primary mirror that is an oblate spheroid which differs from a sphere by the same amount as a paraboloid, but in the opposite direction. The chief purpose is to produce a flat image and a shorter instrument. With this arrangement the corrector plate is moved in from two focal lengths of the primary to one focal length reducing the tube length to one-half. The corrector plate now has to be twice as strong because it is "parabolizing" an oblate spheroid. This position of the corrector introduces astigmatism and the high power of the plate acting as a lens introduces chromatism. The maximum recommended aperture is about f/3 due to the difficulty of making the two aspheric surfaces.

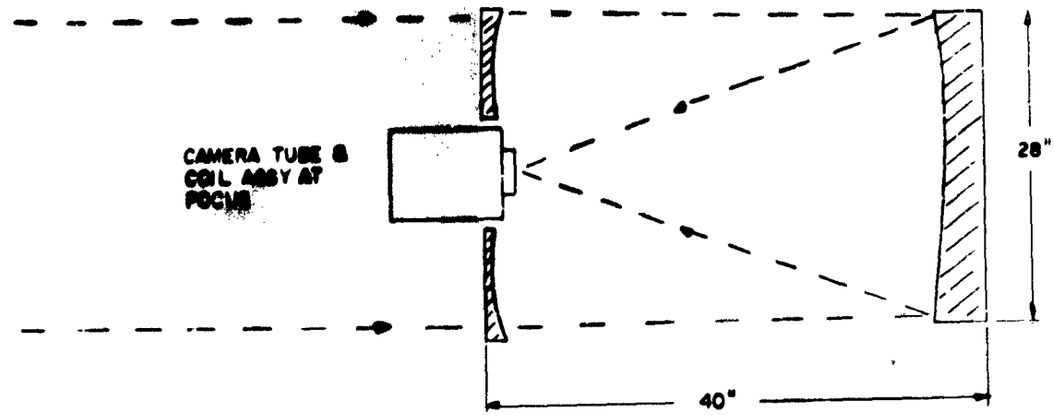


Figure II-9. Wright Camera

h. Schmidt-Cassegrain System

This name has been given to a system developed during this study using the Schmidt principle, presumably with a spherical mirror, and a convex folding mirror to flatten the field and reverse the position of the image surface. As was mentioned earlier, the Schmidt system can be folded with a flat mirror, but at f/1.5 the aperture angle is so large that the mirror offers a major obstruction. As shown in Figure II-10, if the focal length is 40 inches, a flat folding mirror has to be at half this distance or 20 inches from the mirror and this leads to a mirror 14 inches in diameter.

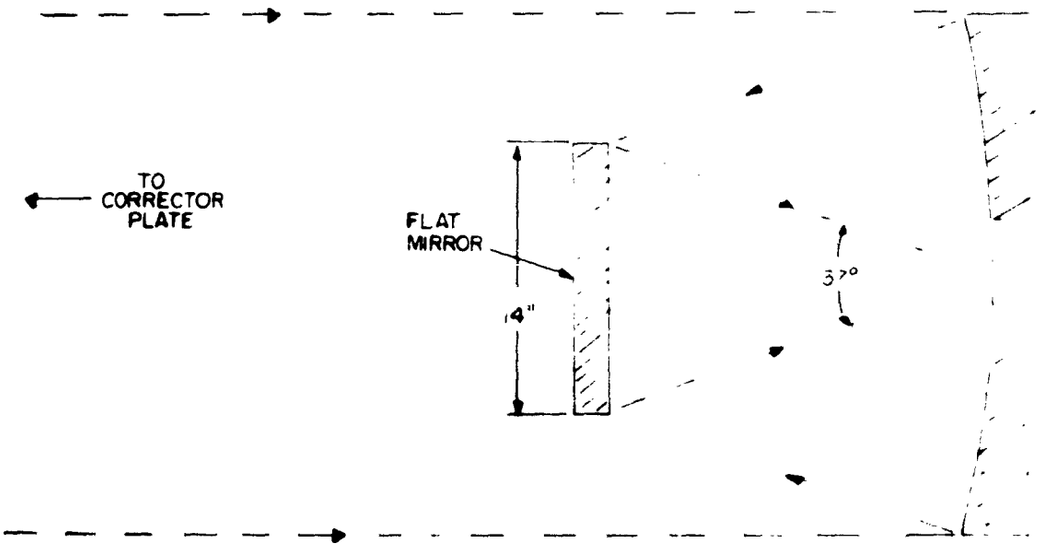


Figure II-10. Schmidt System with Flat Mirror

The situation can be somewhat improved by the use of a convex mirror which decreases the aperture angle of the rays. Of course, the aperture angle falling on the camera tube cannot be reduced below 37 degrees or the system will not have an f/1.5 aperture ratio. Since a convex mirror must necessarily decrease the aperture angle this means that the aperture ratio of the primary must be increased. In Figure II-11 the primary mirror has a speed of f/1.0, though the entire system has a speed of f/1.5. The diameter of the folding mirror has been reduced from 14 required for a flat mirror to 11 inches. The aperture ratio of the secondary is not f/1.5 but only about f/7. This convex mirror should be a hyperboloid which is not too difficult to make at this aperture ratio.

If the obscuration is further reduced the aperture ratio of both the corrector plate and the secondary become very high and they are consequently difficult to make. The effective "transmission" of the system shown in Figure II-11 compared to an ideal of f/1.5 system with no obscuration or reflection losses is about 70 percent.

The optical quality is satisfactory, providing a resolution of at least a 35 micron spot over the entire nearly flat field. The exact amount of distortion has not been calculated, but it will probably be least for a flat mirror and increase

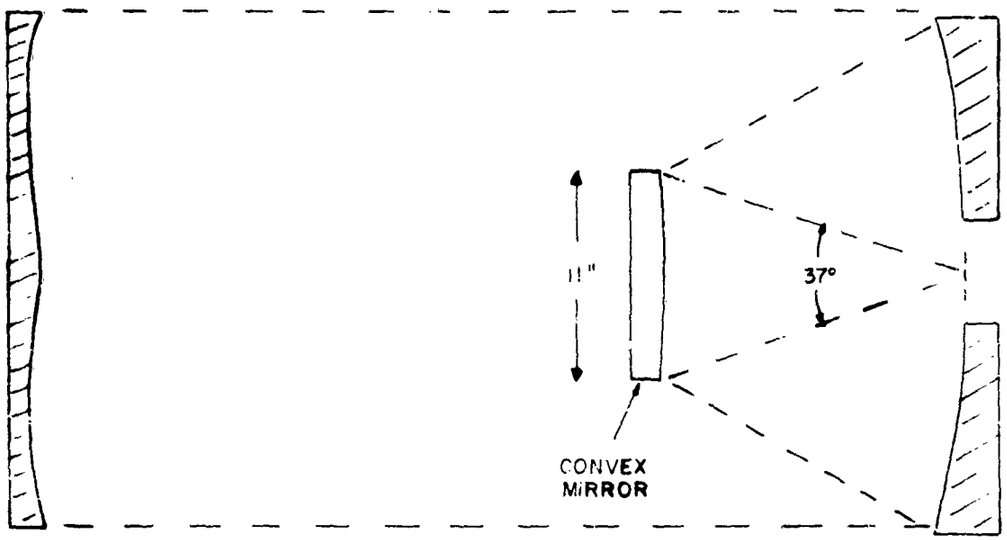


Figure II-11. Schmidt-Cassegrain System

with the power of the secondary. In some cases it has been necessary to achromatize the corrector plate by making it of two pieces of glass.

i. Maksutov or Bouwers Camera

All of the designs discussed to this point require at least one aspheric surface which has to be hand-made and the cost of which increases tremendously with decreasing f/ratio. The design invented simultaneously by Maksutov and Bouwers uses the principle of the Schmidt system but instead of an aspheric corrector uses a plate with two spherical curves which approximates the action of the Schmidt plate. Most authorities have come to the conclusion that this system works well up to f/2.5 and can be made faster with some loss of image quality. An f/1.5 Maksutov system is shown in Figure II-12 where it can be seen that the length of the system is only about half that of the Schmidt. The Maksutov corrector with its spherical surfaces is easier to make than the aspheric Schmidt, but it requires a thicker piece of glass.

The image surface in this design is turned the wrong way for a camera tube. If we attempt to fold this system we find the same difficulty as in the folded Schmidt, the secondary mirror becomes a major obstruction. A possible solution is the same as that suggested in the case of the Schmidt, to increase the speed of the primary and use a convex secondary. If the speed of the primary mirror in the Maksutov system is increased above f/1.5, it is found that the power of the corrector lens becomes impractical. A common solution to this problem of a strong lens is to "split" it into two equal components. In this case the two halves have equal power and are spaced symmetrically about the radius of curvature of the primary. The first such system was constructed by Wynne and is essentially a two-corrector Maksutov that can be made as fast as f/0.8. Figure II-13 shows an

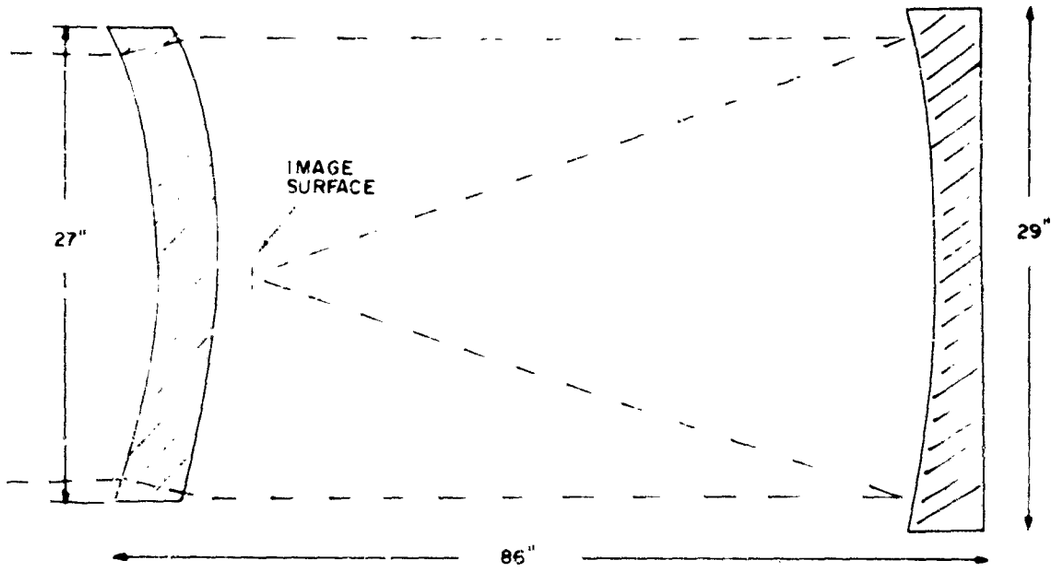


Figure II-12. Maksutov System

f/1.5 folded Wynne system. The curvature of the correctors is now much less than a single lens because the power is divided between the two. Actually, the system could be made more compact than shown. The total length could be reduced to about 70 inches and the obscuration to less than ten percent.

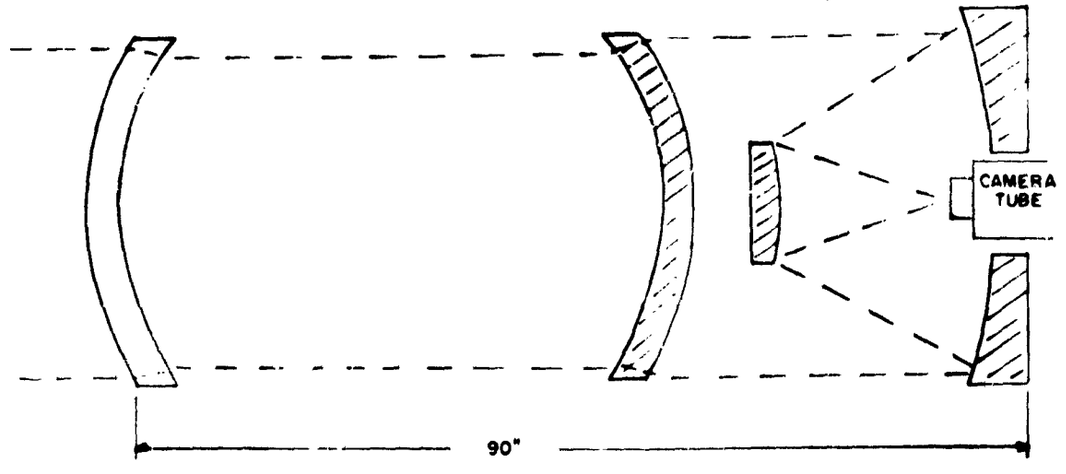


Figure II-13. Folded Wynne System

j. Variations on the Schmidt Principle

The design of the Schmidt system calls for a spherical primary mirror and a thin oddly-contoured corrector at a distance of twice the focal length of the primary. This system produces perfect (diffraction limited) images with a slight amount of distortion and image curvature. For use with a camera tube the image is facing the wrong direction and it would be desirable to fold the light path. It has been shown that at f/1.5 a flat folding mirror results in a major light loss and of course does nothing to improve the distortion or field curvature. A convex folding mirror can be made to correct both these aberrations and at the same time shorten the telescope. The most promising of these is shown in Figure II-14. In this arrangement which has been calculated by J.G. Baker and others, the primary is spherical, the secondary which is considerably smaller is only slightly aspheric. It is a sphere from which about .4 micron of glass has been removed at the edges, the corrector is of the usual Schmidt type. This telescope is considerably shorter than the classical Schmidt (about .6 the length) and is completely free of distortion as well as all the usual aberrations and has a flat field. The only difficult part to make is the corrector plate and it is quite possible to develop a similar Maksutov design. The system shown in Figure II-13 could be made distortionless also, but it would probably require two lenses as shown and would have a much greater tube length than Figure II-14.

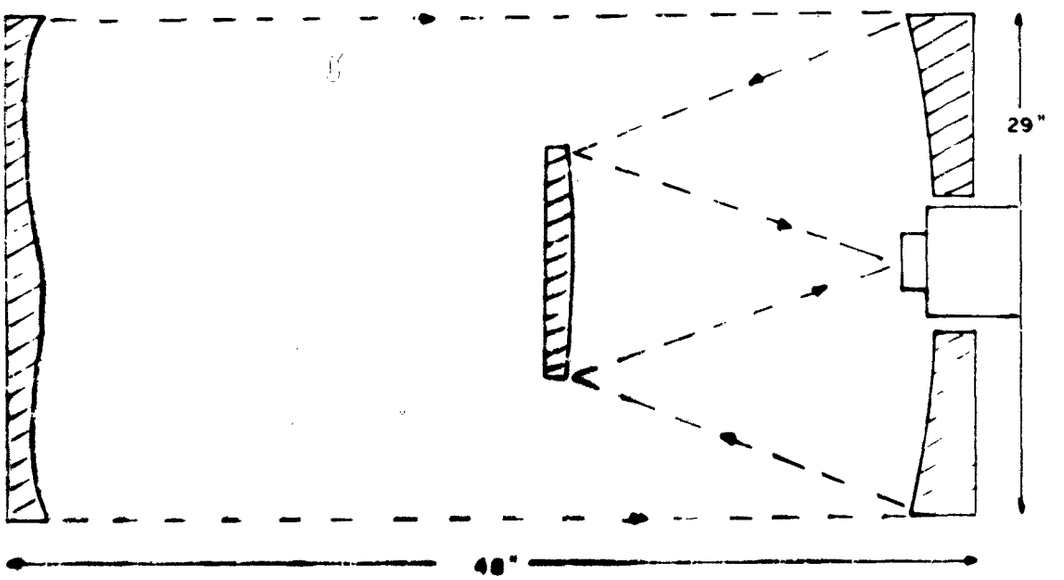


Figure II-14. Distortionless System

k. Comparison of Schmidt and Maksutov Correctors

Essentially, the aspheric Schmidt plate and the Maksutov meniscus lens perform the same function; they "parabolize" a spherical mirror not only for axial, but also off-axis rays. They are two different means of accomplishing the same thing, but they are not equal. The following differences are tabulated:

1. The Schmidt plate can be made from a thin piece of glass. The Maksutov lens is made from a fairly thick piece of glass.
2. The actual curvatures on the Schmidt plate are extremely slight, but they are aspheric. The curvatures of the meniscus lens are steep, but they are spherical. While it is simple to make these surfaces on a machine the two must be perfectly centered, a not too simple operation.
3. The Schmidt plate at high aperture ratios introduces chromatic aberration, the meniscus lens, oddly enough does not.
4. The meniscus lens in high apertures introduces coma and astigmatism, the Schmidt plate does not.

Because of these differing properties several persons notably Baker and Linfoot have proposed and designed systems using both kinds of correctors to obtain still better results. One of these is the Linfoot Meniscus-Schmidt which has been built as fast as f/1.2 with nearly perfect imagery. Since the correction is divided between two optical elements neither one has to be as strong as a single f/1.2 corrector and hence they are fairly simple to make. This is shown in Figure II-15. Of course, a system at f/1.5 could be folded as in Figure II-14 and made distortionless. In this design the aberrations are less than either the Schmidt or Maksutov.

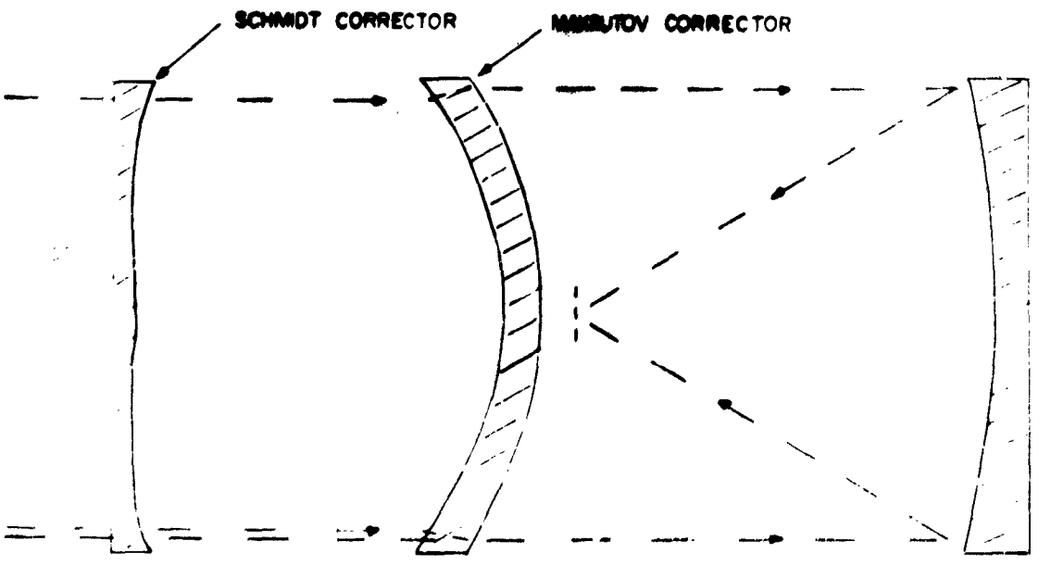


Figure II-15. Linfoot Meniscus - Schmidt System

The final development of these ideas is the Baker "Super-Schmidt" in which two aspheric corrector plates are sandwiched between a split Maksutov lens as in the Wynne camera. This design is capable of nearly perfect imagery up to about f/0.8 and is shown diagramatically in Figure II-16.

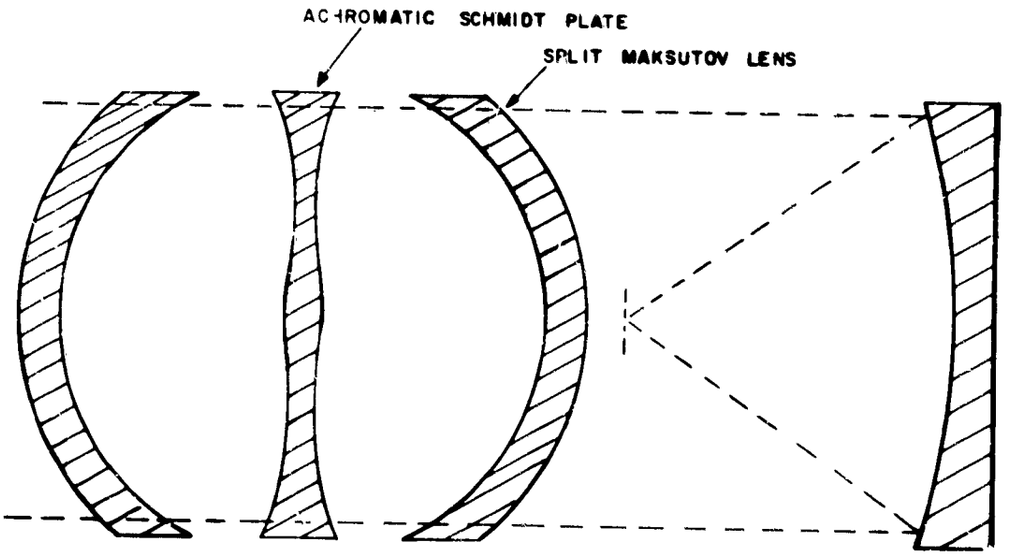


Figure II-16. Baker "Super-Schmidt" System

There are several possible designs that meet the optical requirements. The one that appears to be the simplest to construct and has the least mechanical problems is that shown in Figures II-11 and II-14 which may be described as a Schmidt-Cassegrain. These systems are known to be distortionless and to show image quality surpassing the requirements. The most compact is that shown in Figure II-14 which uses a Schmidt corrector. It is also possible to have a similar system with a meniscus lens corrector, but if a split meniscus corrector is required the system will be at least 80 inches long. So far as can be seen at present, the two are optically equal. The meniscus system will show less chromatism over a long spectral range. The cost of the optics appears to be about equal, the thin aspheric corrector or the thick meniscus are equally difficult to make. The rigidity of alignment of these systems cannot be overemphasized. Bending of the tube must be less than .002 inch in any position and the separation of the primary and corrector must not change more than about .006 inch with temperature. This requires an extremely stiff or compensated structure made of Invar or compensated by bimetallic construction. The mounting for these optics is a large part of the expense. For mechanical reasons, the distortionless Schmidt-Cassegrain shown in Figure II-14, or alternatively the equivalent Maksutov design if it can be made with a single corrector is recommended for the aerospace surveillance task.

Possible Field

Either of these systems (Schmidt or Maksutov) will produce a good field of about 20 degrees. The only difference between a Schmidt-Cassegrain designed for

3 degrees and one designed for 20 degrees is that the larger field requires a slightly larger primary mirror and secondary and will therefore show somewhat greater obscuration. The difference in cost is negligible.

1. Chromatic Aberration of the Schmidt Corrector

The Schmidt corrector plate acts like a weak lens and therefore possesses chromatic aberration which cannot be corrected by the associated mirrors. As in any lens, the amount of chromatism is a function of:

1. Focal length. Actually this corrector has no focus and this factor is the distance of the corrector from the image. The magnitude varies directly with this distance.
2. Spectral range of detector. Photographic film has a range of about 3000-7000Å, the range of the camera tube may be even greater. The magnitude of the effect varies with the variation in dispersion of the glass. All known glasses show high dispersions for short wavelengths so that it is really the amount of ultraviolet that determines the dispersion.

Below is shown the spectral range which will show the same amount of dispersion in different parts of the spectrum:

Spectral Region	Spectral Range
1.0 micron	1800 Å
.75	1000
.70	800
.65	600
.57	500
.50	400
.45	300
.43	250
.41	200
.39	180
.37	150
.36	100

This table shows that if the allowable dispersion was say six units, then if this were at the red end of the spectrum it could cover the spectral range from .5 micron to 1.0 micron, while if it were at the blue end it would cover only the range from .36 to .45 microns.

These figures indicate that it may be more economical to eliminate the ultraviolet, if the total energy loss is small, than to achromatize the corrector plate. There is an excellent set of sharp cut-off filters available which remove the ultraviolet or blue at any desired wavelength and transmit the remainder of the radiation nearly completely.

3. The aperture ratio of the primary. It is difficult to place an exact figure on the point where achromatization becomes necessary without actually calculating the case. It can be said that a 96 inch focus f/2 system does not show objectionable color, nor does a 30 inch f/1.5. However, for the distortionless system shown in Figure II-14, where the corrector plate has been moved in from twice the focal length of the primary to about 1.1 focal lengths and the aperture ratio of the primary has been increased to about f/1.0 to compensate for the reduction of aperture angle by the convex secondary and for the obstruction loss; the power of the corrector plate also has to be increased. The general recommendation is that for this system and a focal length in the region of 40 inches the chromatism of the corrector plate may become objectionable depending on the required short wavelength spectral range.

At this point, it appears that we have a borderline case where no definite decision can be made, but there are several alternatives:

a. Limit the blue end of the spectrum with a filter.

b. Use the Meniscus-Schmidt system as shown in Figure II-15, and folded if desired.

c. Achromatize the Schmidt plate.

Any of these alternatives appears to be less expensive than the long tube of the conventional Schmidt or the Wynne system.

m. Conclusion

There appear to be several systems that meet the optical requirements. All of them are modifications of the Schmidt or Maksutov camera. Considering the cost of both the optics and the mounting, the system shown in Figure II-14 is favored. Its merits are:

1. Shortest length.
2. Completely free of distortion and all major aberrations except possibly chromatism. Means for combating the chromatism, if final analysis shows it to be troublesome, have been discussed.
3. Flat field.
4. Good image quality out to at least 20 degrees field, more if required.
5. Folded design allows placing the camera tube or tubes outside the telescope, and if fiber optics are used to segment the field, the length of the optics will be less than a non-folded system.
6. The convex secondary mirror is not a difficult part to make. It is almost a sphere slightly figured around its edge.
7. The spherical primary is easily made.
8. The resolution could be made to exceed the present requirements if needed. For the lowest cost the specifications should call for no more resolution than can be used to advantage.

1. Chromatic Aberration of the Schmidt Corrector

It is not possible to decide on whether or not the chromatic aberration of the corrector plate will prove troublesome. There are several alternative designs for the corrector plate; in fact an entire family of curves all of which correct the spherical aberration of the primary and have various advantages. For example, there is the corrector plate curve that requires removing the least material and is therefore easiest to make and there is the corrector plate that shows minimum chromatism. With this second design which is the one Schmidt himself preferred, the system can be made as fast as f/1.0 without showing chromatism. The principle is as follows:

The curvature of the plate is such that it corrects all rays to a given zone of the mirror having a radius. .707 times the full aperture. The plate then treats all light inside this zone as overcorrected and outside as undercorrected for spherical aberration, with the resulting effect that this zone of the plate has a null effect for both spherical and chromatic aberrations. It follows that the residual chromatism introduced by such a plate consists of two portions, one overcorrected outside the zone and the other undercorrected inside the zone, and these two portions tend to nullify each other.

Or in other words; by proper design it is possible to reduce the chromatism to about one-quarter of the amount indicated by simple theory of correction for the marginal rays.

2. Distortion of the Schmidt

The basic principle of the Schmidt camera, which is the use of a spherical mirror with an aperture stop at its radius of curvature, leads to a system in which angular magnification is independent of field angle, and therefore is constant. Basically the system has no distortion.

The two factors which introduce minor amounts of distortion are attempts to flatten the naturally curved image surface and "cosine magnification" of the corrector plate.

The normal Schmidt system has a focal surface whose radius of curvature is exactly equal to the focal length of the primary. If a large portion of this image is used its depth will exceed the depth of focus when this image is placed on a flat detector. It is common therefore to use a plano-convex lens, flat side toward the detector to shorten the focus of the axial rays. Such a lens is called a field-flattener. One way to look at the operation of such a lens is shown in Figure II-17a where curved wavefronts are shown entering a plano-convex lens. Since light travels slower in glass than in air the center of the wavefront is retarded most by the thickest part of the lens and if the lens is designed properly the wavefront emerges practically flat.

Another way to look at the matter is to draw the ray paths. Figure II-17 shows the foci of axial and marginal rays falling on a curved surface Figure II-17c shows what happens when the field-flattener is used. The curved surface of the lens not only changes the focus but also the lateral position of the focus because for rays in intermediate zones it acts as deviating wedge as well as a lens. This kind of distortion can be calculated by finding the zone of the field-flattening lens where

the maximum distortion occurs and then finding the prism deviation from the lens power. Knowing the required lens thickness the lateral deviation or distortion can be found.

In this case the most sensitive zone for a 1.6 inch diameter field-flattener is at .586 inches from its center. The radius of curvature of the image surface in a 40 inch focal length Schmidt is 40 inches. The sag or depth to the focal surface across a 1.6 inch diameter is .008 inches. To flatten out a wavefront with this curvature requires a lens that has a variation in thickness calculated from the formula:

$$T = \frac{nV}{(n-1)}$$

where

T is variation in thickness

n is the refractive index of the glass

V is the sag in the wavefront

If a glass with an index of 1.5 is used T becomes .024 inches and the radius of the lens is 13.3 inches. The slope angle of the convex surface at a zone .586 inches from center is 2-1/2 degrees and the optical deviation angle is 75 minutes of arc. The thickness of the lens at this point is about .0096 inches. Where a ray travels .0096 inches and is deviated from its true course by 75 minutes its position will be deviated .0002 inches from the true position and this is the maximum distortion due to this cause. Even with a focal length as short as 30 inches the maximum displacement of any point in the image will be .00032 inches. Both of these dimensions are less than a resolution element of the optical or TV system and therefore probably not worth considering. For the record, this type of distortion is not the normal cubic variety, but is positive or pincushion zonal distortion.

The second source of distortion is the corrector plate. It is designed to have zero power for paraxial rays, but which can have any one of several shapes described by a family of curves. Normally, the corrector plate is installed flat side toward the incoming light so that paraxial rays are all normal to this surface and are not demoted until they strike the aspheric surface. Off-axis rays strike the flat surface of the corrector at an angle and are refracted so that they are displaced from their true paths by an amount determined by the thickness of the plate and the difference between the angles of incidence and refraction.

It is normal to make a corrector with a thickness one-twentieth to one-fortieth its diameter so that it is a relatively thin lens. A full treatment of this kind of distortion has been given in an astronomical paper which is not presently available. It is believed the distortion is quite small and thus unimportant for the field angles considered in this study.

There is a full discussion of all of the errors of the Schmidt to the fifth order, with and without field-flatteners in the book "Recent Advances in Optics".[3] According to the formulas, distortion due to the corrector plate is more or less of the

---

[3]Linfoot. Recent Advances in Optics, Oxford University Press, 1955.

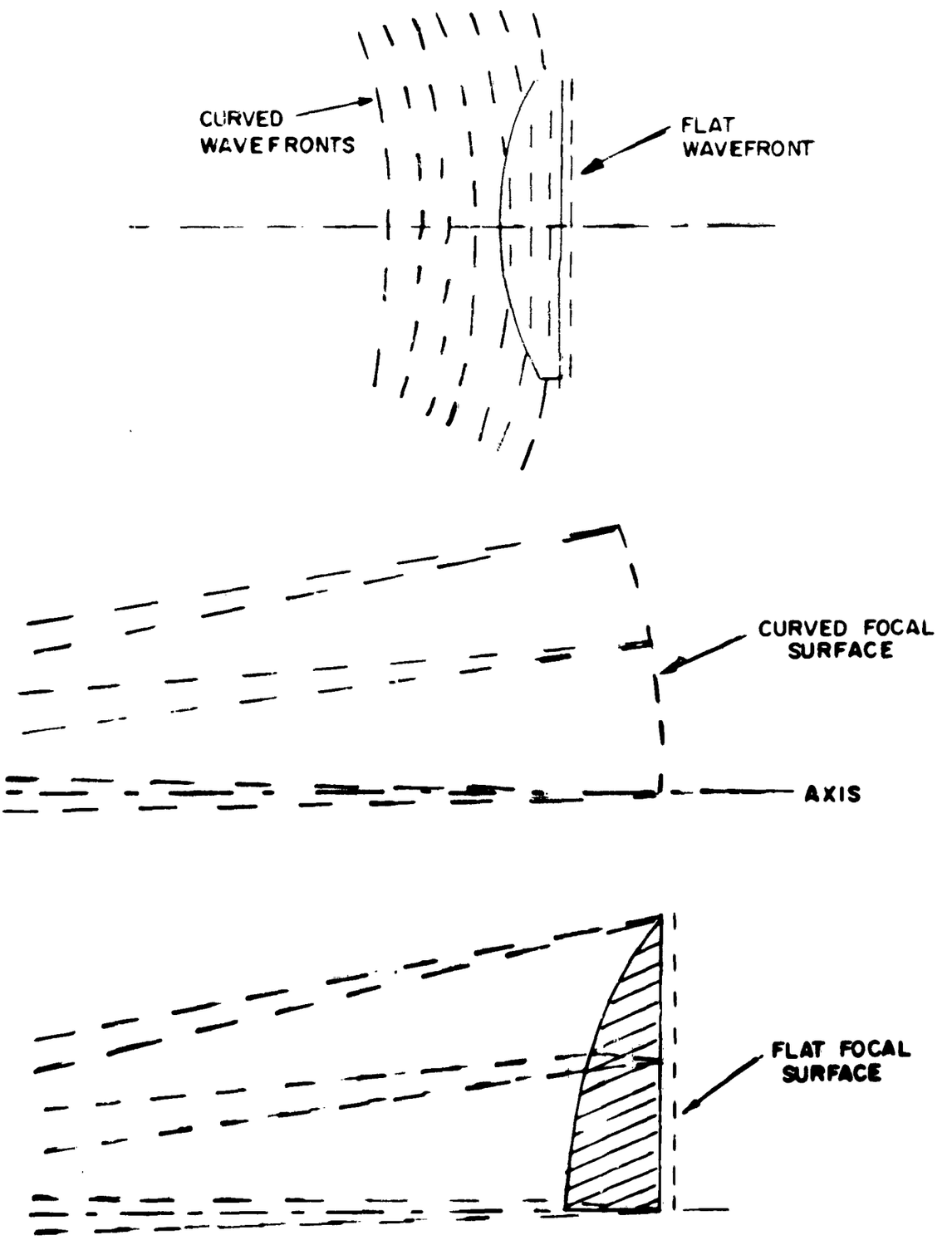


Figure II-17. Foci of Axial and Marginal Rays

normal type, reaching a maximum at the edge of the image, and for the proposed system would amount to only .00005 inches at the edge of a central field the size of one image tube and even if six image tubes were used the distortion would be only .0005 inches or less than a resolution element.

Thus for the size fields we have considered, the normal Schmidt system distortion with or without a field-flattener is negligible in that it is less than a resolution element.

12. FIBER OPTICS

The optics generally offer a larger image plane area without serious distortion than a single image orthicon or other electrical sensors can serve. Fiber optics offer the possibility of coupling more than one I.O. to this image plane. They also can be used to couple a rectangular area to a square area or vice versa.

From about 1956 to 1961 there was a great deal of work done in the field of fiber optics. The Journal of the Optical Society of America published papers on the subject in pretty rapid fire order from 1957 to 1961. A notable series of papers by N.S. Kapany and others covers the subject very thoroughly. The first paper in the series was in 1957, V47, page 413. The concluding paper (No. 9) was published in 1961, V51, page 1067. Other good papers by Hicks, Snitzer, Sigmund, and others appear. One by Snitzer on waveguide modes in 1961, V51, page 499 is useful. There was also a general article in the Scientific American about a year ago and a front cover illustration showing waveguide effects.

In general the fiber systems used to couple a lens image plane to an I.O. can be treated as a geometrical element. Waveguide effects do not appear in fibers over ten wavelengths in size. General Electric developed a fiber transmission system using four micron diameter fibers. Waveguide propagation was evident if looked for closely, but did not have any effect on output resolution. Skew rays behave peculiarly, for example, a single fiber illuminated at an angle by a single pencil of light will distribute light in an annulus at its exit end. For this reason it is not strictly correct to assign a numerical aperture to a fiber system although this is frequently done. Bends generate skew rays and may result in light entrapment inside the fiber. These effects are minor in most applications, resulting in a slight loss of efficiency. The absorption coefficient of a typical fiber is 10^{-4}/cm which is about 1% absorption per meter: - Very low.

The following data (about two years old) from Mosaic Fabrications, Inc.; 205 Chapin Street; Southbridge, Massachusetts; serves to illustrate the availability and versatility of fiber optics.

LIMITATIONS OF THE PRESENT STATE OF THE ART

The following are a few devices that may be of interest. The limits are in some cases dependent on each other and in some cases dependent on less obvious parameters so that in each case of real interest, someone familiar with the art should be consulted for a more exact opinion. This is only a rough guide.

CRT FACE PLATES

Size: up to 10"

Fiber size: down to 5 microns

Optical Type	Monochromatic	
	S ' rical	Coma
Schmidt	0	0
Maksutov (Bouwers)	0	Neg.
Cassegrain	0	0
Newtonian	0	0

ıs			Chromatic Aberrations	
ım	Curvature of Field	Distortion	Lateral	Longitudinal
	Subst.	Neg.	Neg.	Neg.
	Subst.	Neg.	0	0
	Subst.	Neg.	---	---
	0	Neg.	---	---

Subst - Substantial

Neg. - Negligible

0 - None

Figure II-18. Summary Error Char

of Optical Systems for Surveillance Applications

Numerical aperture: up to .95

Distortion: up to 1% (but the distortion is not correctable by standard optics)

Inner curvature: probably no restrictions

STRIP FACE PLATES (FOR READING OUT A SINGLE LINE OR TYPE OR THE LIKE)

Size: up to 1/2" by 10"

Fiber Size: down to 5 microns

Maximum number of fibers: up to 50,000

Numerical aperture: up to .95

Distortion: less than .005" absolute

FIELD FLATTENERS (TWO DIMENSIONAL)

Same as face plates, plus:

Field angle correction: Should not operate out of or into an optical system slower than F/4. O.K. for contact work.

FIELD FLATTENERS (ONE DIMENSIONAL)

This area is unexplored, but the total number of lines across the width is probably not limited. The minimum fiber size is probably around 10 microns. Field angle correction is the unknown quantity here.

IMAGE DISSECTORS (FOR CONVERTING A SINGLE OPTICAL LINE TO SEVERAL LINES ON AN IMAGE TUBE)

Size: up to 20"

Fiber Size: down to 5 microns

Maximum number of fibers: 10,000

Numerical aperture: up to .7

Distortion: up to 5%

Field angle correction: Unknown, but don't count on working into an optical system slower than F/3.

FLEXIBLE PERISCOPES (CURRENTLY UNAVAILABLE)

Size: up to 1/2" diameter

Length: up to 25 feet

Maximum number of fibers: up to 1,000 across diameter

Fiber size: down to 10 microns (down to 2 microns for very short runs and special applications)

Numerical aperture: up to .6 (.85 for contact work)

Flexibility: less than you would imagine

OPTICAL MILLEFIORI

Cross sections: square, rectangular, round hexagonal

Fiber size: down to 3 microns

No. of fibers across diameter: up to 50

Numerical aperture: up to .7

Diameter: up to 1/2"

IMAGE CONDUIT

Cross section: round

Fiber size: down to 3 microns

No. of fibers across diameters: 500

Numerical aperture: up to .7

All of the above devices can be used to give magnification or demagnification. In some cases this makes the job harder, in other cases easier. When magnification or demagnification is used, the minimum fiber size at the small end can be as low as sacrifice transmission efficiency.

Spectral transmission range at least .4200 to 1 micron in all cases. For a length of 2" or less .3800 to 2 microns. For a length of 1/2" or less .3600 to 2.5 microns. For critical applications special glasses may be used which go out to .3200 microns. This will generally result in a low numerical aperture (around .3).

"Optical mosaics" refers to fused blocks such as CRT face plates, field flatteners, etc.

"Millefiori" are single strands of fairly arbitrary cross section (circular, square, etc.) composed of 2,000 or less elements fused together. They are reasonably flexible up to .030" diameter and can in any case be hot bent to any desired path.

"Image conduit" is the same but composed of more elements -- up to 100,000. These will carry a reasonably good picture.

Single fiber refers to clad optical grade fiber. We don't encourage the sale of this as a raw material, but where the customer wants to experiment with fancy configurations or where the single fiber is the end product -- it can be bought.

13. MOUNT REQUIREMENTS

Mount precision (smoothness)and angular accuracy is only moderately critical in the actual surveillance system in that it need only be held within one resolution element size or approximately 8 to 12 secs (.002° to .003°) depending on system field of view for the exposure time of the sensor. The type of mount (axis arrangement) most generally will be equatorial that is rotation in declination and hour angle to follow star movement. Since this rate is slow (≈ 1 revolution/day) special care is needed to obtain the smoothness required.

When obtaining a catalog with photographic film or plates, etc., the precision and smoothness must be about twice as great as indicated above and over the longer period of time required for the film exposure.

For other supplementary applications where high resolution viewing or precision tracking is required more precise mounts are needed. Here the practical limits vary depending on system requirements. For instance, if the track is only the sidereal axis motion smooth worm drives, weight or spring loaded, are adequate and inexpensive; however, if the track motion varies then an expensive precise mount is needed plus special provision for handling jitter and non-uniformity (Precision) in motion. In this case, torque motor drives, air or hydraulic bearings etc., are usually needed plus special tracking techniques.

14. OPTICS-SENSOR TRADES

Before completing the optics selection and equipment design calculation techniques, we must examine potential sensors and their characteristics and specifications and possible processing techniques, as these will affect:

a) Limits of resolution.
   1. Optical quality of image for the full spectrum of the sensor.
   2. Photocathode resolution and charge spreading.
   3. Scanning beam diameter.
   4. Electronic circuitry.

b) Energy required per picture and per resolution element vs single and groups of scanning lines.

c) Sensitivity and detectability limits.
   1. Background level (sky or scene illumination level).
   2. Beam noise (shot noise).
   3. Circuit noise.
   4. Integration capability of sensor.

d) Extent of baffling permitted to reduce background noise buildup and reflection losses in reflecting optics systems, optical losses and transmission efficiencies in refractive elements, etc. Use of spun or cast aluminum coated mirrors instead of glass, etc.

In addition to detection parameters and processing techniques, the system requirements should be analyzed to be sure of a compatible system. For instance; large optics are only needed for applications involving Fast Moving Object Surveillance and Detection. For other requirements use smaller optics with integration time set for detection limit desired. Also, detection is not limited to an object (star or satellite) the same magnitude as the background magnitudes per square second of arc. When a short focal length lens is used, a single resolution element looks at a background sky area of many $\widehat{\text{secs}}^2$ and thus the background is increased accordingly, and depending on its value can limit performance. For long focal lengths the background might be fainter than the equipment noise limit and thus would not be reached.

Though optics systems are generally used for a diametrical view (round field) or a square or nearly square (3 × 4 raster) they are by no means so limited.

One pertinent variation applicable to the space surveillance task is the "strip view". That is the field of view is small in the vertical axis (elevation or declination) and extensive in the horizontal axis (azimuth or hour angle). This technique permits a ring fence or fans to be established thru which objects of interest must pass. Much like the "fans" of the early warning radars.

The Maksutov optics adapts well to this technique in that it can be made to have a long narrow-image plane area. By making it narrow the light obstruction due to the collecting image plane surface minimizes this otherwise disadvantage. The image is collected from its curved focal plane thru use of filter optics and fed to a series of I.O.'s to the extent of resolution and horizontal angle coverage desired. (60^{o} or more is practical from a single optics system).

The economics of the optics - fiber system - number and type of sensors, and mount package will vary with ingenuity of the manufacturing techniques available to the contractor involved, and thus will determine the choice.

These paragraphs illustrate the possibilities available to the system design group as long as equipment is not specified but rather only the task to be accomplished.

B. DETECTION ANALYSIS

This subsection will define and analyse detection, and will calculate detection loss and performance limits of an image orthicon.

a. Introduction

For most image devices the eye is used as the final detector. Such devices include image amplifiers with a continuous non-scanned output, and image orthicons and vidicons that use a scanned electron beam readout with a cathode ray tube scanned image presentation.

When the eye is used as the final detector, the problem of detecting a point object is a function of the viewing conditions. The eye has a finite integration time (usually considered 0.2 seconds) and a viewing angle approximately 5 arc minutes in diameter for this integration time. The smallest object the eye can resolve is about 1 arc minute in diameter; and the resolution sensitivity of the eye is a function of the illumination level. This discussion will assume that the overall brightness and gain of the image display system (monitor) can be adjusted for best viewing conditions, including an optimum viewing distance from the monitor.

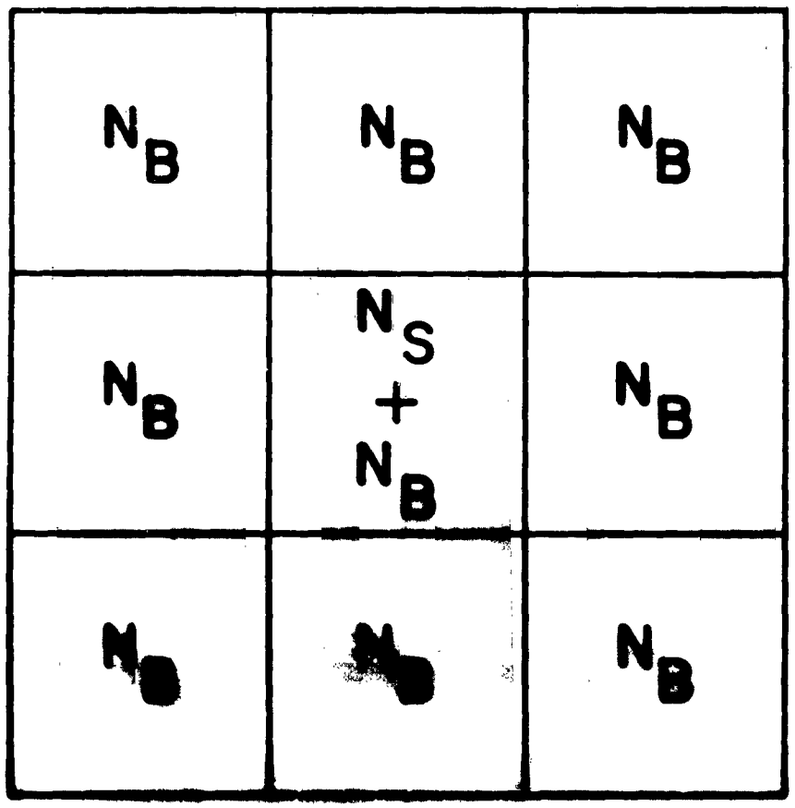
In 1948, Albert Rose of RCA[4] found that a signal-to-noise ratio of 5 was necessary for detection of a point object with a "flat field" background. The signal is defined as the mean number of differential flashes or quanta in the object area, compared to the flashes in any object-sized area of the adjacent background. The signal originally was negative, or less than the average background, but for small contrast the theory holds for signals greater or less than the average background. The noise is defined as the sigma or fluctuation of the flashes in all object-sized background areas, which for a Poisson process is the square root of the mean

[4]Rose, Albert, Journal of Optical Society of America Vol. 38,p. 196; 1948.

number of flashes in each object-sized area. The signal mean and background mean flashes are the time integration of the total flashes in the eye integration time of 0.2 seconds, if the image is viewed directly. Figure II-19 shows the analytical image.

For Detection: (From Rose)

$$\frac{N_s}{N_B} \geq \sqrt{5} \qquad (1)$$



N IS A NUMBER OF LIGHT FLASHES IN THE AMPLIFIED OUTPUT, OR THE IMAGE LIGHT PHOTONS OR PHOTOELECTRONS.

Figure II-19. Point Object Detection in Flat Field Background

What does this signal-to-noise ratio of 5 (or greater) mean in terms of percent detection and false alarm rate? It is assumed that both signal and background have Poisson distributions of time variation between successive images, and the background has a spacial/Poisson distribution for each image. The following brief analysis of detection and false alarm considers just one image, and defines the probability that the signal area with a mean of $N_B + N_s$ has a specific value (x) or greater to be the detection probability, with a comparable false alarm rate defined as the

probability that one of the background elements with a mean of (N_B) can be (x) or greater. The assumption has been made that N_B is large enough so the Poisson distribution is Gaussian even in the tail areas of small probability. The sigma equal to the square root of the mean relation of a Poisson distribution has been kept, but the analysis would be unmanageable if the actual Poisson distribution were used to analyze false alarm rates of 10^{-3} to 10^{-7}.

Even with the assumption of a Gaussian curve, the false alarm rates are a function of the assumed background mean N_B, unless a detection probability of 0.5 is required. The detection probability and false alarm rate for two values of N_B (100 and ∞) and two ratios of peak signal to rms noise (5 and 6) follows. Figure II-20 shows point object detection drawn as two probability curves.

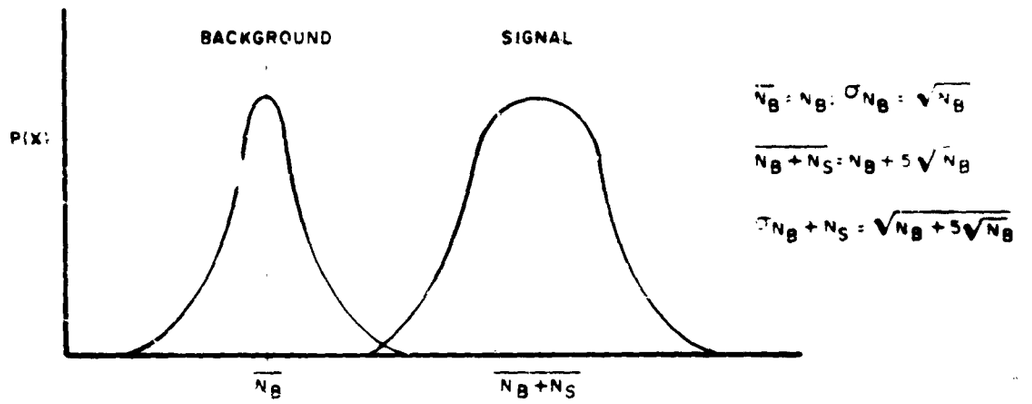


Figure II-20. Point Object Detection Drawn as Probability Curves

Now to define various signal-to-noise ratios: the image signal-to-noise ratio is defined by the number relations of image photons collected by a lens.

$$I_{SN} = \frac{N_{s\ photons}}{\sqrt{N_{B\ photons}}} \qquad (2)$$

So the image signal-to-noise ratio I_{SN} can be changed by a change of the lens used to make the image, or the image integration time, but is not a function of subsequent quantum efficiency, etc.

The detection signal-to-noise ratio is defined by the number relations of the final particles used to form the image viewed by the eye: for an image orthicon the particles are photo electrons, and the background has to consider the additional electrons not caused by the background photons. For a film image the particles are developed silver crystals, and the background has to consider the additional background developed particles due to fogging and not caused by background photons. Since there is some image spreading, the background particle number has to be counted in an area equal to the spread area.

DETECTION PROBABILITY AND FALSE ALARM RATE

CONDITION	DETECTION PROBABILITY	FALSE ALARM RATE
$N_B = \infty$	.50	$.28 \times 10^{-6}$
$\frac{S}{N} = 5$	.90	$.108 \times 10^{-3}$
	.99	3.79×10^{-3}
$N_B = 100$	.50	$.28 \times 10^{-6}$
$\frac{S}{N} = 5$	.90	$.3 \times 10^{-3}$
	.99	1.62×10^{-2}
$N_B = \infty$	.50	$.987 \times 10^{-9}$
$\frac{S}{N} = 6$	.90	1×10^{-6}
	.99	$.125 \times 10^{-3}$
$N_B = 100$	.50	$.987 \times 10^{-9}$
	.90	$.6 \times 10^{-5}$
[illegible]	.99	1.15×10^{-3}

$$D_{SN} = \frac{n_{s\ (electrons)}}{\sqrt{X^2 n_{B\ (electrons)}}} \qquad X^2 \text{ is the image spread in terms of resolution elements} \qquad (3)$$

The detection signal-to noise-ratio is a function of the image quantum efficiency, amplifier and scanning beam noise, thermal background electrons from the photocathode, and other system variables. The detection signal-to-noise ratio D_{SN} is always equal to or less than the image signal-to-noise ratio I_{SN}. And a detection signal-to-noise ratio of 5 is required for good probability of detection. The performance of any given device can be expressed by the ratio D_{SN}/I_{SN}, where the best performance gives the largest ratio.

b. Point Image Detection

1) Star Detection and Image Signal-to-Noise Ratios

The theoretical limit of star magnitude or intensity that can be detected depends upon the finite background illumination of the night sky. Therefore, a calculation will be made of the image signal-to-noise I_{SN} as a function of the lens, exposure time, and background intensity.

A report by John Spalding[5] gives the background intensity in terms of star magnitude per angular area, and the sky resolution limit of 1 square arc second of angular area as the spread of any point source due to atmospheric turbulence. Thus, the background number should be calculated from a 1 square arc second of angular area.

Star magnitudes are a method of compressing the intensity ratios, similar to a db scale. The origin of star magnitudes was based on the ability of the unaided eye to see a range of intensities called 5 steps or magnitudes. Measurements showed that this range of 5 magnitudes had an intensity ratio of 100. This can be expressed mathematically, with each subscript referring to a specific or generalized star magnitude:

$$\frac{I_o}{I_5} = 100: \log_{10} \frac{I_o}{I_5} = \log_{10} 100 = 2 \qquad (4)$$

In general:

$$(K) \log_{10} \frac{I_o}{I_5} = K \times 2 = 5: K = 2.5 \qquad (5)$$

$$\log_{10} \frac{I_o}{I_x} = \frac{2}{5} M_x = 0.4\, M_x: \frac{I_o}{I_x} = 10^{0.4 M_x} \qquad (6)$$

So, the larger the star magnitude M_x, the smaller the intensity I_x. Negative star magnitudes imply an intensity greater than the reference I_o. This I_o intensity is due to a point, and its units are flux (in lumens, photons persecond, or watts) per unit area perpendicular to the flux, in square centimeters usually.

[5]Spalding, J., "Photoelectric Observatory Report #1", GEL TIS 60 GL 186.

The flux density of the zero magnitude intensity can be given in the following terms:

$$I_o = 2.43 \times 10^{-10} \frac{\text{lumens}}{\text{cm}^2} \qquad \text{Outside Atmosphere} \qquad (7)$$

$$I_o = 2.07 \times 10^{-10} \frac{\text{lumens}}{\text{cm}^2} \qquad \text{Inside Atmosphere}$$

Atmosphere Transmission at Zenith: = .85

$$N_o = 10^6 \frac{\text{photons}}{\text{cm}^2 \text{ second}} \quad \text{x (t exposure cm}^2 \text{ lens)} \qquad \text{Outside Atmosphere} \qquad (8)$$

If the background is given or calculated in terms of star magnitude M_B per night sky square second of arc:

$$\frac{N_o}{N_B} = 10^{0.4M_B} : \frac{N_B}{N_o} = 10^{-0.4M_B}: \quad N_B = N_o \times 10^{-0.4M_B} \times t \times \text{cm}^2$$

Now, for any image system the minimum background angular area, whatever the system resolution, is 1 square second of arc due to the atmosphere. Therefore, this will be the assumed resolution limit of film. But a scanned image has a resolution image area equal to the total image area divided by the square of the number of scan lines (for a square raster), and this resolution image area will be equivalent to X^2 square seconds of arc, where X is a function of the number of TV scan lines and the lens focal length.

The general expression for the image I_{SN} assuming photon noise only is:

$$I_{SN} = \frac{N_S}{\sqrt{X^2 N_B}} \qquad A\text{-}1$$

where X^2 is the number of square seconds of sky per image resolution element (X is always 1 or greater) N_S is the number of photons per picture of a star, and N_B is the number of photons per square second of sky per picture due to background.

For a scanned image system,

$$X = \frac{\text{Image Width}}{\text{Lens Focal Length}} \times 57.3 \times \frac{3600}{\text{TV Lines Active}} \qquad A\text{-}2$$

After a photocathode conversion from photons to photoelectrons, or a film conversion from photons to developable grains of silver, a quantum efficiency is defined as:

$$e = \frac{\text{converted particles}}{\text{photons}} = \frac{n}{N} \qquad A\text{-}3$$

$$D_{SN} = \frac{n_S}{\sqrt{X^2 n_B}} = \frac{N_S \times e}{X^2 N_B e} = \frac{N_S \times \sqrt{e}}{\sqrt{X^2 N_B}} \qquad \text{A-4}$$

$$N_S = N_o \times 10^{-0.4M_s} \times t\left(\begin{matrix}\text{exposure}\\ \text{seconds}\end{matrix}\right) \times \frac{\pi}{4} \times D_{Lens}^{\ 2}\ (cm^2)$$

$$N_B = N_o \times 10^{-0.4M_B} \times t\left(\begin{matrix}\text{exposure}\\ \text{seconds}\end{matrix}\right) \times \frac{\pi}{4} \times D_{Lens}^{\ 2}\ (cm^2)$$

$$D_{SN} = \frac{N_o \times 10^{-0.4M_S} \times \frac{\pi}{4} \times D_{Lens}^{\ 2} \sqrt{e\,t}}{X\sqrt{N_o \times 10^{-0.4M_B} \times \frac{\pi}{4} \times D_{Lens}^{\ 2} \times t}} \qquad \text{A-5}$$

For good detection, $D_{SN} = 5$:

$$5 = \frac{10^{-0.4M_{SD}}}{10^{-0.2M_B}} \times \frac{D_L}{X} \times \sqrt{N_o \times t \times e \times \frac{\pi}{4}} \qquad \text{A-6}$$

$$\frac{10^{0.4M_{SD}}}{10^{0.2M_B}} = \frac{D_L}{5X}\sqrt{N_o \times t \times e \frac{\pi}{4}}$$

$$0.4M_{SD} = 0.2M_B + \log_{10}\left(\frac{D_L}{5X}\sqrt{N_o \times t \times e \times \frac{\pi}{4}}\right) \qquad \text{A-7}$$

$$M_{SD} = 0.5M_B + 2.5\log_{10}\frac{\sqrt{N_o \times \pi/4}}{5} + 2.5\log_{10}\frac{D_L\sqrt{e \times t}}{X} \qquad \text{A-8}$$

Now, if equation 8A is evaluated for the best conditions of Mount Palomar:

t = 10 hours = 36000 seconds: X = 1 arc $\widehat{sec}^2$ / resolution element

D_L = 200 inches = 508 cm: M_B = 21.5 mag/arc $\widehat{sec}^2$ sky

$N_o = 0.85 \times 10^6 \frac{\text{photons}}{cm^2\,sec}$ (Inside Atmosphere)

$$M_{SD} = 10.75 + 2.5\log_{10} 163 + 2.5\log_{10} 508\sqrt{36000}\ \sqrt{e}$$

M_{SD} = 28.75 magnitude for $e = 1.0$

M_{SD} = 26.25 magnitude for $e = 10^{-2}$

M_{SD} = 25.0 magnitude for $e = 10^{-3}$

2) Star Detection Loss Due to Image Orthicon

The visual photon image is changed by the image orthicon into a photoelectron charge image that is read by a scanning beam, amplified by an electron multiplier, amplified and processed (level clamped and sync added) external to the image orthicon, and displayed on a monitor. The following analysis will find the resultant monitor detection ratio for visual evaluation, and will also consider the electronic signal to noise ratio for electronic evaluation. These assumptions are made:

a. The photocathode quantum efficiency e, the mesh transmission target photocathode secondary emission S_t, and dynode (1) secondary emission S_1 are all uniform, so there is a "flat field" output with a "flat field" illumination input. There is no grain, mottling, spots, shading, etc.

b. The monitor detection is not limited by the eye angular acuity. The brightness, gain, and viewing distance can be adjusted for optimum viewing.

c. The electrical signal-to-noise ratio is not affected by an amplifier external to the image orthicon.

d. A perfect eye integration of 0.2 seconds.

e. Linear beam landing characteristics.

To emphasize assumption c, the camera preamp is assumed to be perfect with no noise. This cannot be, but the analysis will then show a theoretical limit of detection determined by various constants of the image orthicon. And if enough image orthicons constants are accurately known, the comparison of analysis with performance will show the detection loss that can be assigned to the external amplifier.

The analysis will calculate the detection loss of the image orthicon by expressing the detection signal-to-noise ratio in terms of the original signal-to-noise (at the photocathode) as the signal passes through the image orthicon. The D_{SN} will be found before the photo electrons from a charge image on the target, the D_{SN} of the target charge pattern, the D_{SN} of the return scanning beam, and the D_{SN} after amplification by the electron multiplier stages, where:

N = Average or mean number of visible photons per picture exposure, in a given area.

I_{SN} = Image signal to noise ratio.

D_{SN} = Detection signal to noise ratio as an image is processed for eye display.

E_{SN} = Electrical signal to noise ratio of a scanned image.

e = Average photocathode quantum efficiency =

$$\frac{\text{Output Photo electrons}}{\text{Input Visible photons}}$$

α = Target mesh transparency

S_t = Average target secondary emission ratio for photocathode photo-electrons

S_1 to S_n = Average secondary emission of the nth stage of electron secondary emission.

The image signal to noise ratio of photons at the image plane of a lens is:

$$I_{sn} = \frac{N_S}{\sqrt{N_B}} \qquad (1)$$

After a conversion to photoelectrons and transmission through the target mesh

$$D_s = \frac{N_S \epsilon \alpha}{\sqrt{\epsilon \alpha (N_B + N_T)}} \qquad (2)$$

N_T are the thermal electrons emitted by the photocathode; for a S20 with 10^{-15} amps/cm^2 at 25°C, in 0.2 seconds exposure time approximately .1 thermal electrons are emitted per resolution element, so the thermal "noise" electrons will be disregarded. This assumption could not be made if an S1 photocathode or elevated temperature operation was considered.

The D_{SN} of the target charge pattern will now be calculated. It is assumed that all of the secondary electrons from the target are collected by the target mesh.

$N_t = N_{pe} (S_t - 1)$ (3) N_t positive target charge

N_{pe} photocathode electrons

so the signal is $N_S \epsilon \alpha (S_t - 1)$ (4).

The total variance of the background charge is calculated using the results of exercise 3, page 74, Probability and Statistics by Arley and Bach.[6] This exercise shows the relation of mean and sigma for a primary electron stream, a secondary emission surface, and a secondary electron stream:

PRIMARY ELECTRONS	→	SECONDARY EMISSIONS	→	SECONDARY ELECTRONS
Mean $\bar{Z}_o$		Mean $\bar{y}_1$		Mean $\bar{Z}_1$
Sigma σZ_o		Sigma σy_1		Sigma σZ_1

(5)

$$\bar{Z}_1 = \bar{Z}_o \bar{y}_1 \; ; \; \sigma Z_1^2 = \sigma Z_o^2 (\bar{y}_1)^2 + \sigma y_1^2 (\bar{Z}_o)$$

(6) Arley & Bach, Probability and Statistics

Now assuming that both the primary electron stream and the secondary emission have Poisson Distributions:

$$\bar{Z}_o = N_B \epsilon \alpha \; : \; \sigma Z_o^2 = N_B \epsilon \alpha \text{ (If Poisson)} \tag{6}$$

$$\bar{y}_1 = S_t \; : \; \sigma y_1^2 = S_t \text{ (If Poisson)}$$

$$\sigma_t^2 = \sigma Z_1^2 = N_B \epsilon \alpha \, S_t^2 + S_t \, (N_B \epsilon \alpha) \tag{7}$$

$$D_{SN} = \frac{N_S \epsilon \alpha \, (S_t - 1)}{\sqrt{N_B \epsilon \alpha \, (S_t^2 + S_t)}} = \frac{N_S}{\sqrt{N_B}} \cdot \frac{\sqrt{\epsilon \alpha \, (S_t - 1)}}{\sqrt{S_t^2 + S_t}} \tag{8}$$

(Target Charge)

It is now necessary to calculate the readout beam detection ratio. The readout beam scans the gun side of the target and leaves "negative charge" electrons in areas where the image light intensity has built up a positive charge since the last sweep or scan. The part of the scanning beam which doesn't land on the target and cancel positive image charge is called the return beam. The return beam is directed back to the scanning gun, where it strikes the first anode in a series of secondary emission electron multipliers. The output current from the last electron multiplier is the signal current of the image orthicon. When there are target areas of no net positive charge the output current is maximum. When the area being scanned has the maximum target charge due to image light intensity, there is a maximum signal with a minimum output current.

The depth of beam modulation (the percentage of the scanning beam that can be used to discharge the target) is somewhat dependent on the charge spread of the signal. If the beam current is increased there is less modulation of the beam, less spread of the target signal point charge, and more beam noise.

There is some question about the amplitude of beam noise. If the amplitude of beam current can be controlled by a control grid voltage there has to be some space charge between control grid and cathode. Therefore the beam current released by the control grid is not as random as a temperature limited emission electron beam, and does not have the Poisson Distribution associated with temperature limited emission. But the beam goes through a limiting aperture of 1.5 mil diameter (0.0015 inch) which might make the beam more random and give it a Poisson Distribution.

This analysis assumes there is some space charge limit of scanning beam sigma:

$$\sigma^2 \text{ Beam} = \Gamma^2 \qquad \sigma^2 \text{ Poisson} \; : \; (\Gamma^2 \leq 1) \tag{9}$$

The total scanning beam electrons in the signal area of X^2 resolution elements would have to be at least equal to the signal plus background target charge $(N_S + X^2 N_B) \epsilon \alpha \, (S_t - 1)$ in the X^2 resolution element area. How many more beam electrons are required is dependent on the beam modulation assumed:

$$\text{Beam Modulation} = \frac{1}{K} \tag{10}$$

$$\eta \text{ Beam} = (N_S + X^2 N_B)\, \epsilon\, \alpha\, (S_t - 1)K \tag{11}$$

$$\sigma^2 \text{Beam} = (N_S + X^2 N_B)\, \epsilon\alpha\, (S_t - 1)K\, \Gamma^2 \tag{12}$$

The return beam will be the difference between the number of scanning beam electrons and the target positive charge (in electrons). The return beam sigma squared will be the sum of beam and target variances, however.

$$\begin{bmatrix}\text{Signal}\\ \text{Area}\end{bmatrix} \eta \text{ return} = \eta \text{ beam} - \eta \text{ target} = N_S \epsilon\, \alpha\, (S_t - 1) \tag{13}$$

$$\begin{bmatrix}\text{Background}\\ \text{Area}\end{bmatrix} \sigma^2 \text{ return} = \sigma^2 \text{ beam} + \sigma^2 \text{ target} \tag{14}$$

$$D_{SN}\ (\text{Return Beam}) = \frac{N_S\, \epsilon\, \alpha\, (S_t - 1)}{\sqrt{(N_X + X^2 N_B)\, \epsilon\, \alpha\, (S_t - 1)\, K\, \Gamma^2 + X^2 N_B\, \epsilon\, \alpha\, (S_t^2 + S_t)}} \tag{15}$$

The equation for the return beam detection signal to noise ratio is no longer in the form $N_S/\sqrt{X^2 N_B}$ that can be related to the original image I_{SN}. This is nearly the final image orthicon D_{SN}, if a noiseless electron multiplication is assumed.

Without showing the details, and using the previous secondary emission analysis of Arley and Bach the output detection signal to noise ratio is:

$$D_{SN}\ \text{Output} = \frac{N_S \sqrt{\epsilon\alpha}\ (S_t - 1)}{\sqrt{N_B(S_t - 1)K\Gamma^2 + \frac{1}{S_1}) + X^2 N_B [K\Gamma^2 (S_t - 1) + S_t^2 + S_t + \frac{(K-1)(S_t-1)}{S_1}]}} \tag{16}$$

Inserting typical values for an S20 magnesium oxide target image orthicon:

$\epsilon = .25$
$\alpha = .75$
$S_t = 11$
$K = 1.5$
$\Gamma^2 = 0.8$
$S_1 = 3$

(a) 184 $\frac{\mu \text{amps}}{\text{Lumen}}$ for an S20
(b) 5000°K Black Body
(c) 0.85×10^6 $\frac{\text{photons}}{\text{cm}^2 \text{ second}}$ for a (o) magnitude star

(17)

For image detection D_{SN} is required to be 5 or greater:

$$N_{SD}^2 - 22.5\, N_{SD} - 195\, x^2 N_B = 0 \tag{18}$$

$$N_{SD} = 11.2 + \sqrt{11.2^2 + 195 X^2 N_B} \qquad (19)$$

TABLE 1

N_{SD}	$X^2 N_B$	Plot in Figure II-23
22.5	0	
29		
56.8	10	
151	100	
453	1000	

To compare the analysis with experimental data, calculations were made using four different focal length lenses, with a 1029 line TV system. The image spread area was assumed to be 2 TV lines, so X^2 was 4. The eye-monitor viewing integration time of 0.2 seconds was assumed, and was used for the exposure or picture time. A square raster with a 1.25 inch square image on the photocathode was assumed. The plot of analysis with measured performance is shown in Figure II-21.

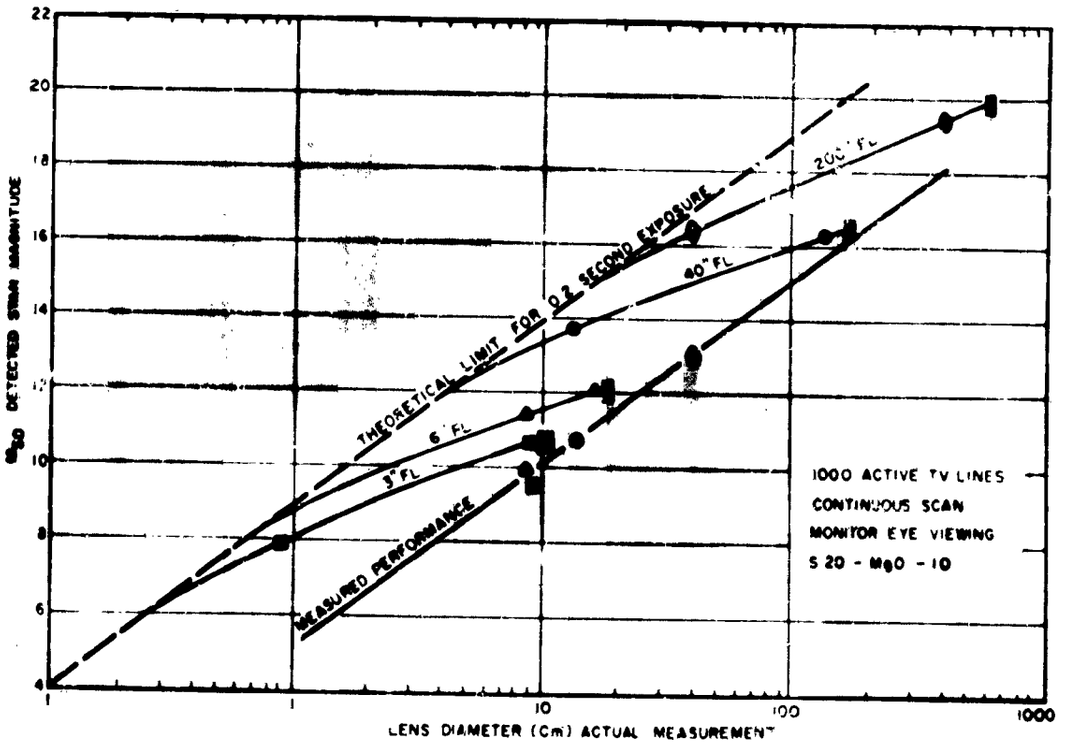


Figure II-21. Detection Star Magnitude

ANALYSIS VS MEASUREMENT

Constant	Case 1 RCAS 200" F L 15"D 38cm	Case II TT Hobson 40" F L 5"D 12.7cm	Case III Astro Berling 6" F L 3.3"D 8.3cm	Case IV Super Feran 3" F L 3.45"D 8.75cm
θ-square field	0.363^{o}	1.82^{o}	12^{o}	24^{o}
$\frac{\text{Arc Sec}^2 \text{ Sky}}{\text{Res Elem}}$	1.7	42.8	1870	7480
$\frac{N_B}{\text{Cm}^2 \text{ Res El Sec}}$	$1.7 \times \frac{.21}{100}$	$42.8 \times \frac{.21}{100}$	$1870 \times \frac{.21}{100}$	$7480 \times \frac{.21}{100}$
A Lens (cm^2) Includes losses	775	78.6	35.3	35.8
$\frac{N_B}{\text{Res El}}$ (0.1 sec)	.276	.705	13.8	56.2
$\frac{X^2 N_B}{(0.2 \text{ sec})}$	2.2	5.64	110	450
N_{SD} (D_{SN} = 5)	35	45	160	325
$\frac{N_{SD}}{cm^2 \text{ sec}}$	.225	2.86	22.5	45.4
$\frac{N_o}{N_{SD}}$	3.77×10^{6}	2.97×10^{6}	3.77×10^{4}	1.67×10^{4}
M_{SD} Analysis	16.4	13.7	11.4	10.7
M_{SD} Measured	13	11	10	9.5

NTV Active = 1000
Lens Transmission = 60% to 80%
No = $.85 \times 10^{6}$ photons/cm^2 sec
Background 21.5th Mag/sec^2 arc
Eye Integration Time 0.2 sec
Photocathode Scanned Area 1.25" × 1.25"

ANALYSIS VS MEASUREMENT

(1) $$\frac{\text{Sky Arc Sec}^2}{\text{Resolution Element}} = \frac{1.26'' \times 57.3 \times \text{Lens Focal Length (inches)}}{3600 \text{ (TVL) active}}^2$$

(2) Lens Area $= \frac{\pi}{4}$ (D inches $\times$ 2.54)$^2 \times$ T lens

For the refractive lenses, a transmission T of 60% was assumed.

For the refractive lens, a transmission T of 80% was assumed.

(3) X^2N_B was calculated for 0.2 second integration time assuming any detectable spread 2 lines high and wide.

(4) N_{SD} was calculated from the graph of N_{SD} vx X^2N_B assuming 0.2 seconds image time.

(5) M_{SD} considers the N_O flux density of zero mag point object after atmospheric attenuation.

Some of the measured data agrees with the results of the analysis. In all cases the analysis predicts better performance than the measured performance. Some of the increased performance predicted by analysis might be due to the assumption of a 21.5 magnitude star per square arc second of sky background, which would rarely be found in the Syracuse-Schenectady area where most of the performance results were measured.

One result of the analysis is the dependence of the required star photons for detection on the number of background photons. This means the detection star magnitude is a function of lens focal length as well as the lens collection area.

The analysis assumes linear beam landing characteristics, or equal increments of target current for equal increments of target charge. This condition is equivalent to assuming a monochromatic scanning beam in terms of thermal velocities. John Spalding has reported a longer time constant for faint stars: when viewing a new star field it is noticeable that faint stars take seconds of integration before they become detectable. So, the detectability of faint stars is improved with continuous operation, using the eye integration time of 0.2 seconds compared to a monitor photo of a single scan of the charge pattern on the target after a photocathode integration of the same 0.2 seconds. The better continuous performance is a function of the beam landing characteristics. A discussion of the velocity distribution of an image orthicon scanning beam was given by Hans Heil of the Electronics Lab., Syracuse, at an Image Intensifier Symposium October 6-7, 1958, Fort Belvoir, Virginia.

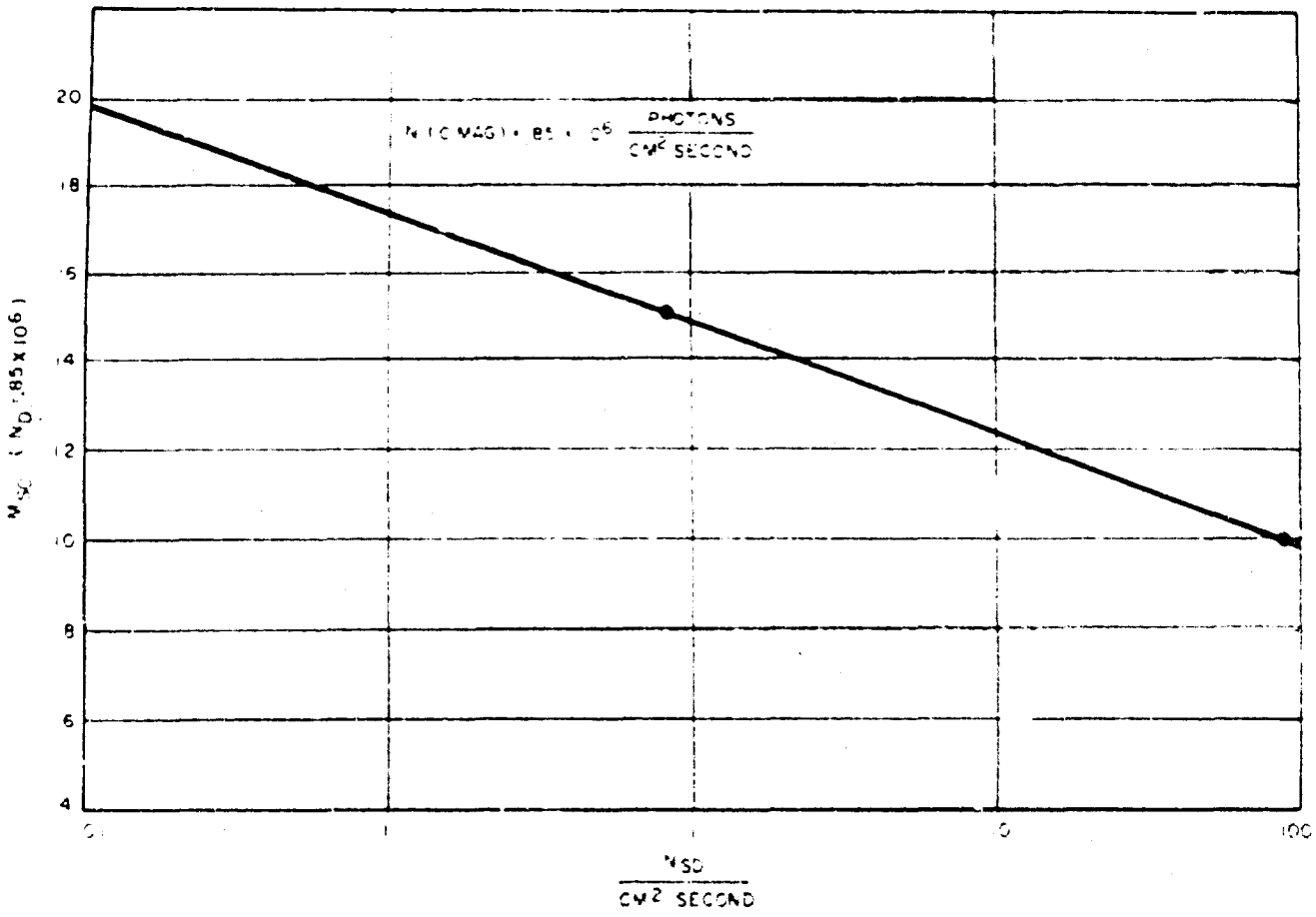


Figure II-22. Plot of $\frac{N_{SD}}{CM^2 \text{ Second}}$ vs M_{SD}

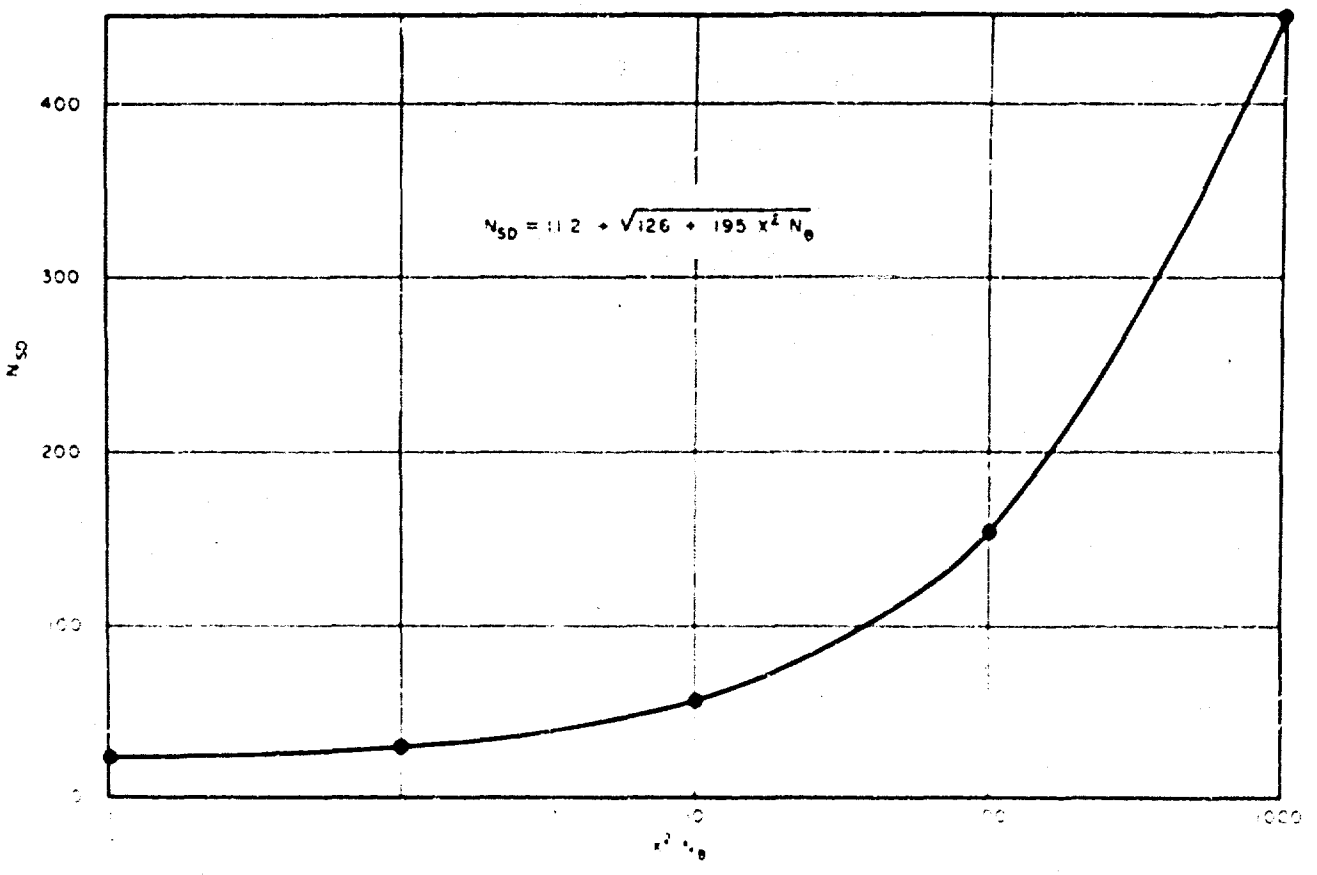


Figure II-23. Plot of N_{SD} Vs $X^2 N_B$

Figure II-21 shows the calculated performance using four different focal length lenses. The major questions that result from the analysis are:

1. Is the scanning beam an emission limited with a Poisson distribution, or does it have an equivalent space charge?
2. Because of the beam landing characteristics of a non-monochromatic scanning beam, what is the actual time of photocathode integration for a single image to give the same detection ability as continuous operation, when scaling lens diameters and focal lengths?

The conclusions to be drawn from the analysis are:

1. $D_{SN} = K\sqrt{\epsilon\ \alpha}$
2. The secondary emission ratios S_t and S_1 should be large to maximize D_{SN}, but the typical values of present I. O. Tubes are not the performance limiting variables.
3. Most of the I.O. performance loss is due to a quantum efficiency less than one, and the noise added by the scanning beam and preamplifier.
4. The analytical results show that the star magnitude that can be detected is a function of lens diameter, lens focal length, exposure time. and number of active TV scan lines, for a given image orthicon.
5. It appears the preamplifier noise is more important when using a long focal length lens, with the smaller required beam current due to a smaller field of view. The difference between analysis and measured performance is greatest for the longest focal length lens, with the largest f/ratio.
6. The final detection equation (16) has two regions of interest. When long focal length lenses with large f/ratios are used, the background can be neglected and the required N_{SD} photons for detection is a constant. In this region (defined as I) a doubling of lens diameter will result in 1.5 magnitude increase in detection; doubling the integration time will result in a 0.75 magnitude increase in detection. If a small f/ratio larger diameter lens is used, the background is larger, and the required N_{SD} photons for detection is proportional to the square root of the background photons. In this (region II), a doubling of lens diameter will result in a 0.75 magnitude increase in detection, and doubling the integration time will result in a 0.375 magnitude increase in detection. As the f/ratio approaches 1, the theoretical detection magnitude approaches the measured performance, because the preamp noise is no longer large in respect to the beam noise.
7. If the photons per cm^2 second from a 0 magnitude (visual) star are counted after passing through at "normalized" visual passband, the photons counted are much smaller than the photons that could be counted after passing through the much broader "normalized" passband of an S20 photocathode. A rough analysis of a 5000°K black body radiation gives 0.25×10^6 photo-electrons per cm^2 second for a (0) magnitude star that contains 1×10^6 "visual passband" photons per cm^2 second. And this value is used in the analysis of star detection, when the photons per cm^2 second outside the atmosphere are assumed to be 1.0×10^6 for a 0 magnitude point source.

3) Star Detection Signal to Noise Compared to Electrical Signal to Noise

There is a difference between the eye signal-to-noise ratio (D_{SN}) defined earlier in terms of photoelectrons or monitor photons, and the electrical signal-to-noise ratio of the scanned signal used to produce the visual image.

For a single line "electronic look" at an image, the peak signal is proportional to the flux per resolution element (n_s/X^2), assuming the signal is spread over X^2 resolution elements, with an arbitrary resolution element width equal to the TV scanning line width. The peak signal voltage, as previously stated, is proportional to the average number of signal electrons per resolution element per scan, and the rms noise voltage of the background is proportional (with the same proportionality constant as the signal voltage) to the square root of the number of background electrons per resolution element per scan.

n_s Signal electrons/resolution element

n_B Background electrons/resolution element

$$E_{SN} = \frac{\text{peak signal}}{\text{rms noise}} = \frac{n_s/X^2}{\sqrt{n_B}} \tag{9}$$

By adding x lines electrically (by circulation or delay line) the electrical signal would increase by x and the electrical noise (Poisson) would increase by the $\sqrt{X}$. The E_{SN} after x lines have been added, would be

$$E_{SN}[\text{X lines added}] = \frac{n_s}{\sqrt{n_B}} \frac{1}{X^2} \frac{X}{\sqrt{X}} \tag{10}$$

This improvement in E_{SN} would vary with the line scan number, and the full improvement would only appear on the last line scan used to write the image. (This scheme would not work with an interlaced scan.) Therefore, the best E_{SN} would be displaced from the center of the spread point object to the last scan line of the object.

Now, if a sampling technique could be used to add up the amplitudes of X resolution elements, the E_{SN} would again be improved by $\sqrt{X}$:

$$E_{SN}\begin{bmatrix}\text{X lines added} \\ \text{X elements added}\end{bmatrix} = \frac{n_s}{\sqrt{n_B}} \frac{1}{X^2} \sqrt{X}\sqrt{X} = \frac{n_s}{\sqrt{X^2 n_B}} \tag{11}$$

This improvement would also result in the best detection at the final element position of the scan line; thus, if successive scan lines moved from top to bottom, and each scan line moved from left to right, the best E_{SN} would occur at the time corresponding to the lower right hand element of the spread point object.

The sampling technique of adding elements sounds complicated, but is easy to achieve by decreasing the bandwidth by a factor of X, which would not

change the peak amplitude of the signal (at the time corresponding to the last resolution element), but would decrease the rms noise by a factor of $\sqrt{X}$.

The final detection D_{SN} is a function of the total signal electrons and total background electrons:

$$D_{SN} = \frac{n_{St}}{\sqrt{X^2 n_{Bt}}} \tag{12}$$

Now, if there K_s scans during the eye integration time t (eye):

$$D_{SN} = \frac{n_s \cdot K_s}{\sqrt{n_B \cdot K_s}} = E_{SN}\begin{bmatrix}\text{Full}\\ \text{Processing}\end{bmatrix}\sqrt{K_s} = E_{SN}\begin{bmatrix}\text{No}\\ \text{Processing}\end{bmatrix} X\sqrt{K_s} \tag{13}$$

Therefore, if it were possible to add electronically the K scans that occur during the eye integration period, the electrical E_{SN} could be made equal to the detection D_{SN}. This K scan addition can be approximated by using a photocathode integration period of t(eye) before the target charge pattern is scanned. Thus, electronic processing can achieve an E_{SN} nearly equal to the eye view D_{SN}.

If an image has a 2 line spread, and the eye is integrating 6 TV scans, the ratio between the visual signal-to-noise ratio and the electrical signal-to-noise ratio would be $2\sqrt{6}$, or 4.9 to 1. Therefore, a point object barely detectable visually, with a $n_{ST}/\sqrt{n_{BT} X^2}$ of 5, would have an electrical peak signal to rms noise ratio of one (approximately). As shown by Figure II-24, an E_{SN} of 1.0 is difficult to detect.

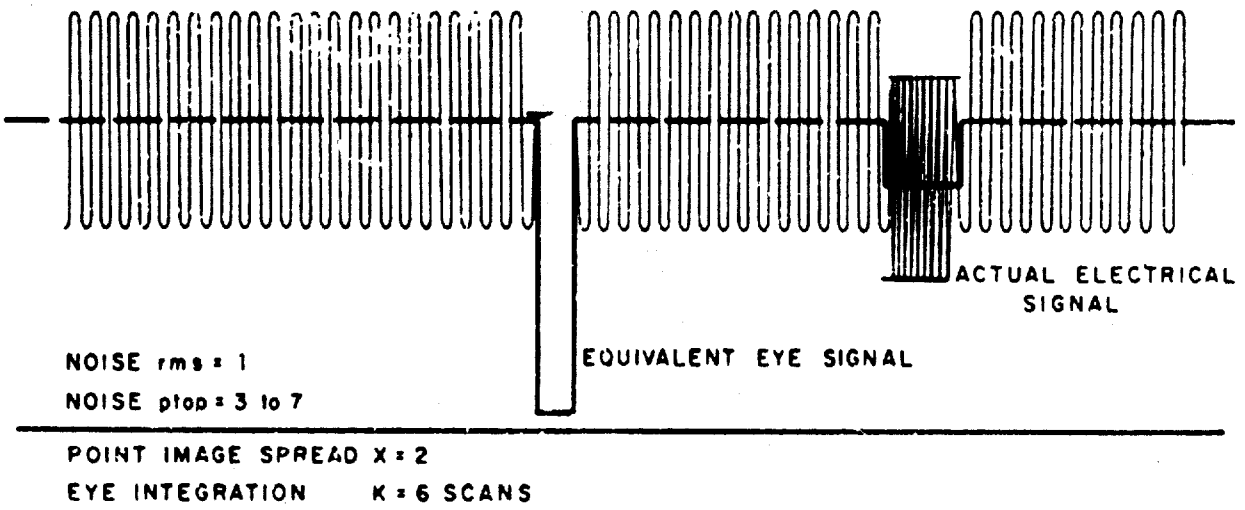


Figure II-24. Plot of D_{SN} vs E_{SN} When a Point Object is Just Detectable

If it is assumed that the image is not spread more than two image lines for a 5 times greater than the just detectable star intensity, then this 5 times intensity increase (a star magnitude decrease of 1.75) would give the just-electronically detectable star magnitude. Or the electronic detection would be 1.75 star magnitudes less than the continuous 0.2 second monitor eye detection. But, if the image line spread increases from 2 lines to 3 lines for a point source intensity 5 to 10 times the eye detectable minimum intensity, it would take 7.5 times the minimum eye detectable intensity to give the same electronic detectability. Or, with a 3 line spread with increased intensity, the electronic detection would be 2.2 star magnitudes less than the continuous 0.2 second monitor detection. This assumes 1/30 second per complete scan, or 6 TV pictures in every eye integration period.

4) Spread Object Detection

a. Detection Theory of Picket Fence Spread Objects

The differences between a point source with a random orientation in an image scene, and the repetitive pattern "picket fence" of TV resolution charts, are many. For one thing, the detection criteria of theory is difficult to relate to actual images. And the tube has to be operated with more beam current to limit image spreading, since an image spread will give an information loss.

When viewing the TV image, the viewing distance is varied so that the area of interest is approximately 5 arc minutes by 5 arc minutes of angular viewing area. This is the most effective area for integration and detection, as reported by Mertz[7] in 1950. Mertz also discussed the bandwidth of measured noise as a function of noise perception. He concluded that with a flat noise spectrum the "spectrum level" (rms noise voltage per unit bandwidth) necessary to just perceive noise is independent of the noise bandwidth used to display the noise. If the probability of detecting noise is equivalent to the signal masking effectiveness of the noise, then the noise rms voltage (proportional to the square root of the bandwidth used to measure the noise) is not an effective measure of detection probability. The important variable with flat spectrum noise is spectrum level, or rms noise voltage divided by the square root of the measurement bandwidth.

To review this conclusion, when viewing a medium spacial frequency (line pairs per inch) picket fence pattern, only the noise in the same spacial frequency region is effective in masking the signal; you can look at the pattern at the appropriate viewing distance and disregard or omit the low and high spacial frequency noise. And for any given TV scan system there is a definite relation between spacial and time frequencies. Thus, for flat spectrum noise, the important variable is "spectrum level" or noise rms voltage or current per unit bandwidth. The viewing eye is then considered a "bandpass" device.

There are two extremes of operating conditions: where noise is independent of the image intensity, which might be approached by high illumination conditions; and where the system has been designed and adjusted for best performance so part of the noise is photon noise. This analysis considers the limiting condition of detection due to image photon signal and noise, with an image loss due to the quantum efficiency only. The video amplifier noise is not considered in finding the maximum performance limit set by the image orthicon photocathode.

[7] Mertz, P., "Perception of Television Random Noise", Journal Society Motion Picture and TV Engineers, Vol. 54, pp. 8-32; January 1950.

[redacted]

b. Calculation of TV Line Resolution Sensitivity

This analysis calculates the detection D_{SN} of one square black bar in a grey or white background, then multiplies this D_{SN} by a factor of 2 to convert (using Coltman's measurements, Figure II-25)[8] from one line pair to 4 line pairs. It is assumed, with a standard wedge type TV resolution chart, that there is no difference between one TV line and one TV line pair (since there is no signal more white than the background). And it is assumed the standard wedge resolution of 4 black lines and 4 white spaces is equivalent to 4 line pairs.

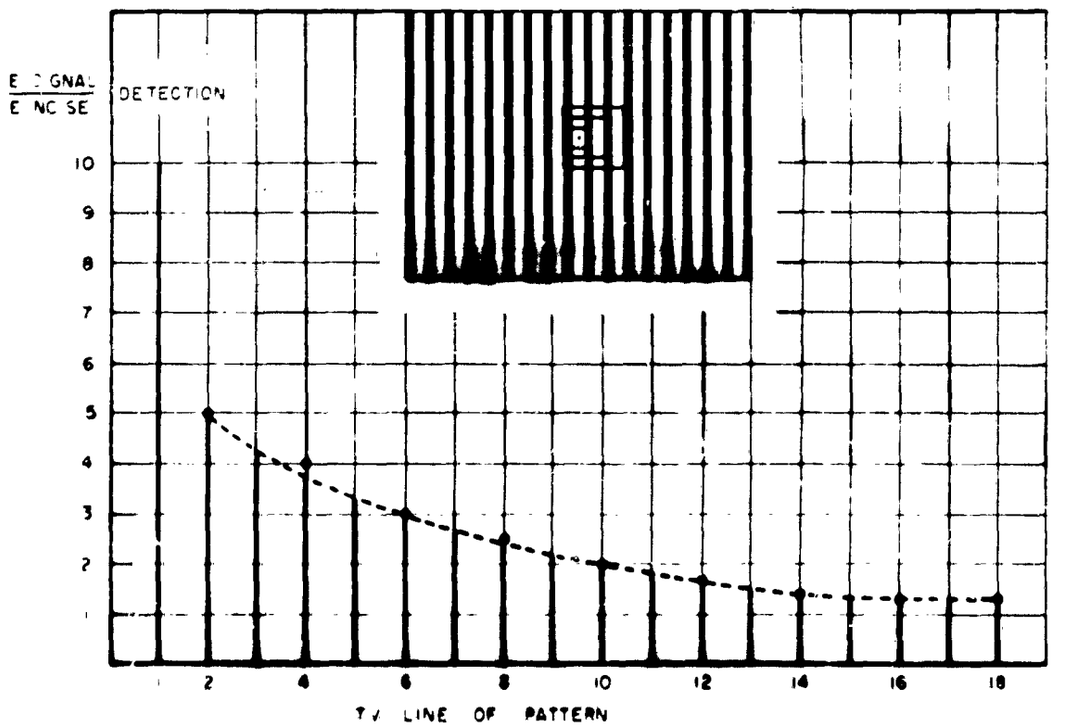


Figure II-25. E_{SN} Required for Detection as Function of Line Pairs Viewed Using Square Mask on Monitor

If X is the number of resolution element widths equivalent to the signal width:

$$X = \frac{\text{TVL active}}{\text{N signal}} \quad \frac{f_B}{f_s} \tag{31}$$

[8] Coltman and Anderson, "Noise Limitations to Resolving Power in Electronic Imaging," IRE, Vol. 48, pp 858; May 1960.

If the signal contrast is defined as the ratio of signal intensity to kground intensity (a background reflectance greater than any signal reflectance) i signal areas always having less intensity than the background intensity:

$$C = \text{Signal Contrast} = \frac{n_S/A}{n_B/A} = \frac{R_{Back} - R_{Sig}}{R_{Back}} = \frac{e\,max - e\,min}{e\,max} \qquad (32)$$

$n_{S/A}$ Signal photo electrons per unit area (one resolution element)

$n_{B/A}$ Background photo electrons per unit area (one resolution element)

R_B Background reflectance

R_S Signal reflectance

With this analysis there is no possibility of a contrast g eater than one.

$$n_S = C \cdot n_B : n_B \frac{\text{photo electrons}}{\text{resolution element}} \qquad (33)$$

$$D_{SN} = \frac{n_S X^2}{\sqrt{n_B X^2}} = \frac{n_S \cdot X}{\sqrt{n_B}} = C\sqrt{n_B}\, X \qquad (34)$$

So here the resolution element is one active scan line wide, and one ive scan line high.

And if the background density is calculated for the number of TV scan s, then the lines that are finally resolved will be in terms of image height.

$$n_B = \frac{n_{\text{Total Photocathode Photoelectrons in the Raster Area}}}{TVL_{active} \times \frac{4}{3} TVl_{active}}$$

$$n_B = \frac{n_{PT}}{TVL}\, 2\, \frac{3}{4} \qquad (35)$$

$$D_{SN} = \sqrt{n_B} \cdot C \cdot X = \sqrt{\frac{3}{4} \frac{n_{PT}}{TVL} 2} \cdot C \cdot \frac{TVL}{N\,signal} \qquad (36)$$

If $D_{SN} = 5$, N signal becomes the number of lines per picture height can be resolved if the signal has only one TV line:

$$N_{resolved} = \frac{1}{5}\sqrt{\frac{3}{4} n_{PT}} \cdot C$$

Adding the factor of 2.0 to include the increase of detection due to 4 line pairs:

$$N_{resolved} = \frac{2}{5}\sqrt{\frac{3}{4}\, n_{PT}} \cdot C \tag{37}$$

$$N_{resolved} = 0.346\sqrt{n_{PT}} \cdot C \tag{38}$$

Equation (38) gives the resolution in terms of total raster area photoelectrons from the photocathode that would be required per picture to give the resolution lines $N_{resolved}$. This number of photoelectrons is gathered in the total eye or monitor photograph integration time, and would be the amount collected from a flat field of average transmission or reflectance not considering any signal areas. So, to convert from photoelectrons to incident photocathode photons:

$$N_{Resolved} = 0.346\sqrt{N_{PT} \cdot \epsilon} \cdot C \tag{39}$$

From the results of numerical analysis using 2800°K black body radiation with a S20 response, the resultant sensitivity is approximately 150 microamperes per lumen. This is equivalent to approximately 9.4 to 10^{+14} photo-electrons per lumen second. It is easier to evaluate the photoelectrons per lumen second, than to choose a rather arbitrary photon total, with its associated average quantum efficiency. This value of photoelectrons per lumen second has to be multiplied by the target-mesh transmission of 70%.

$$\frac{\text{Photoelectrons}}{\text{Lumen Second}} = 9.4 \times 10^{14} \times \alpha = 6.6 \times 10^{14} \text{ (S20)} \tag{40}$$

Solving for total photocathode photons per picture, with a 1.8 inch diagonal and 0.2 seconds to include the eye integration time:

$$n_{PT} = FC_p \times 6.6 \times 10^{14} \times \left(\frac{12}{25}\right)\left(\frac{1.8}{12}\right)^2 \times 0.2$$

$$n_{PT} = 1.4 \times 10^{12}\, FC_p \tag{41}$$

This analysis assumes no noise from the target secondary emission, beam, electron multiplier, or preamplifier. (With high beam currents the preamp noise can be neglected).

And finally, for white light and S20 photocathode

$$N_{Resolved} = 0.346 \times C \times \sqrt{1.4 \times 10^{12}\, FC_p} \tag{42}$$

Now to solve for the required FC (footcandles) photocathode illumination to give 100 TV lines resolution (vertical) with 100% contrast, 4 line pairs, white light and a S20 photocathode:

$$100^2 = (.346)^2 \times 1.4 \times 10^{12}\ FC_p : FC_p = 4.9 \times 10^{-8}$$

The following table shows the footcandles of illumination required (from analysis and from measurement) to give various TV line resolution capabilities. A calculation is also made of the photons required per line resolved resolution element.

TABLE 2
S20 RESOLUTION SENSITIVITY

$N_{resolved}$	Footcandles at Photocathode		Photons/Resolved Res Elem	
	Analysis	Measured	Analysis	Measured
100	4.9×10^{-8}	1.2×10^{-7}	102	252
200	2.0×10^{-7}	4×10^{-7}	102	210
300	1.4×10^{-7}	9.5×10^{-7}	102	222
400	7.9×10^{-7}	1.9×10^{-6}	102	250
500	1.2×10^{-6}	4.0×10^{-6}	102	336
600	1.8×10^{-6}	8.0×10^{-6}	102	466

The measured and analysis data for resolution sensitivity are plotted in Figure II-26. The analysis results are better than the measurement results.

Coltman, in his 1960 IRE Article (reference 8), gives a requirement of 2.6×10^5 photoelectrons per second for a theoretical resolution limit of 100 line pairs per picture. It is assumed that this resolution is equivalent to 200 TV lines per picture width, with the minimum electrical E_{SN} required for detection of 8 line pairs or more. To convert photoelectrons per second to number of footcandles: From the previous analysis

$$\frac{n_{photoelectrons}}{picture} = 1.3 \times 10^{16} \times F.C. \times 0.05 \times \frac{12}{25} \left(\frac{1.8}{12}\right)^2 0.2 \frac{seconds}{picture}$$

$$\frac{n_{photoelectrons}}{picture} = 1.4 \times 10^{12} \times F.C. = 2.6 \times 10^5 \times 0.2 \frac{second}{picture}$$

$$FC = \frac{.52 \times 10^5}{1.4 \times 10^{12}} = 3.7 \times 10^{-8} \text{ foot candles}$$

Coltman

$N_{resolved}$ = 200 TV lines (width) = 150 TV lines (height)

This value for Coltman is plotted in Figure II-25.

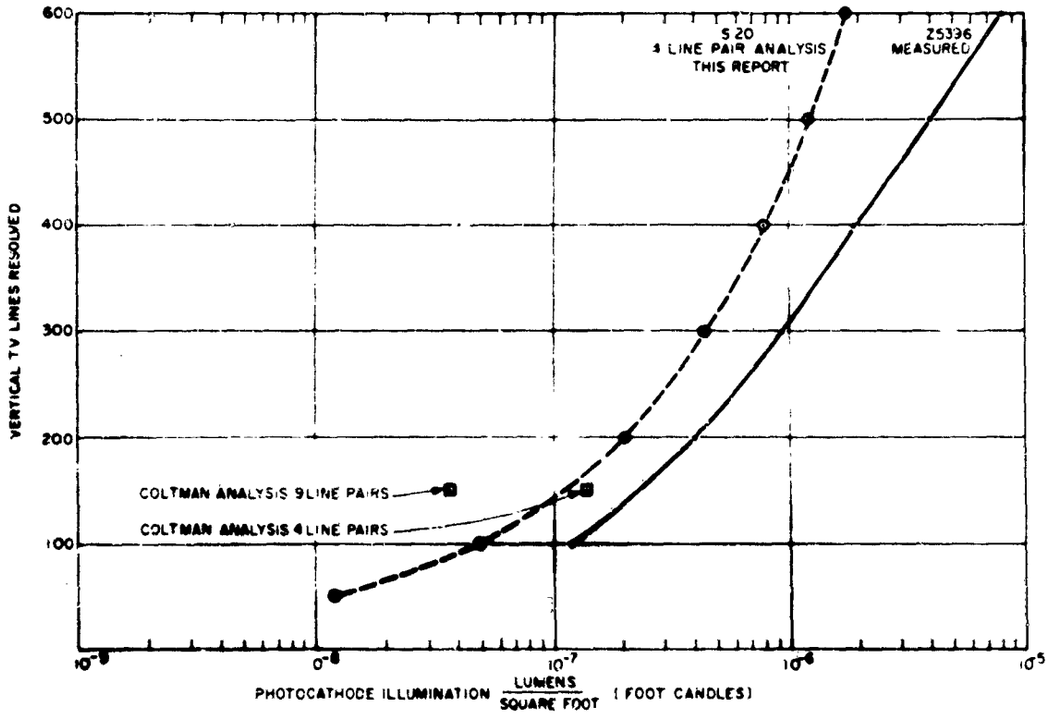


Figure II-26. Line Resolution Sensitivity for S20 Standard Scan Eye View MgO Target

A check with Coltman's Figure II-25 shows an E_{SN} improvement from .25 for 4 line pairs (our analysis) to .13 for 9 line pairs (Coltman analysis). This would be equivalent to an illumination improvement of $(2.5/1.3)^2$, or would mean that $(2.5/1.3)^2 \times 3.7 \times 10^{-8}$ foot candles would be required for a 4 line pair pattern, using Coltmans analysis. It appears the analysis of this report agrees with Coltman at the 150 TV line per picture height point.

At lower line resolutions Coltman's more complete analysis considers the detection loss due to additional noise background of thermal photoelectrons and amplifier noise, plus the detection loss due to finite screen size, and the associated loss due to less than 9 or 10 line pairs on the TV monitor.

At a higher number of lines resolved, Coltman considers the detection loss due to the spacial frequency loss in contrast of the image orthicon. The contrast loss at higher spacial frequencies is equivalent to a decrease of beam modulation at higher spacial frequencies.

The changes in curve shape between the report analysis and the measured results can also be explained in terms of additional amplifier and thermal

noise at the low number of resolved lines, and a spacial frequency contrast loss for the higher number of resolved lines.

C. COMPONENT OPERATING THEORY

This subsection will discuss details of operation, and limitations of performance of various specialized image components. Part II-C-1 will discuss scanned image tubes, concentrating on the thin film (MgO target) image orthicon. Part II-C-2 will discuss scanned image storage for temporary catalog or integration for improved signal-to-noise ratio improvement, concentrating on secondary emission non-destructive readout storage tubes.

1. SCANNED IMAGE SENSORS

Imaging sensors in this discussion are limited to electronically scanned devices and direct view devices, thus excluding the mechanically scanning thermograph sensors and similar image recorders.

Imaging sensors are available in various sizes, sensitivities, resolution, spectral response, time constants, etc. They range from small vidicons to large image orthicons.

The principles used in vidicons and orthicons differ in that the common vidicon measures the variation of resistance of the sensing layer "target" material as established by the scene energy; whereas, in the orthicon, the variation of electical charge on the sensing layer is measured. In the vidicon the sensing surface is scanned with an electronic beam, with the resistance variation of the "target" changing the beam current, for "target" modulation. This "Target" modulation causes a change in voltage across the load resistor which is then amplified externally. In the orthicon the electrical charge is imaged on the "target" or sensing layer by photo electrons emitted by the photocathode of the image section. The image is focused electro-statically and magnetically from the photocathode to the "target." The electron beam as it scans the "target" discharges it, in so doing the amount of reflected or "return" beam charges by the extent of "target" charge. The modulated return beam is amplified by an internal electron multiplier before being applied to external video amplifiers.

Vidicons and orthicons generally have external magnetic deflection systems, though electro-static deflection is just now coming into being. A variety of sensing layer or "target" materials are used depending on type. The image orthicon image section is available with one of several photocathode surfaces (S-1, S-10, S-20, etc.). Because of its many features (speed, sensitivity, resolution, etc.) the GE thin film low light level MgO image orthicons will now be discussed in detail together with application notes.

a. The Thin Film MgO Image Orthicon

1. General Operation

The image orthicon development has been primarily concerned with broadcast studio work, where controlled lighting is possible, to permit operation with a signal well above the tube and circuit background noise. In color camera work, the color filters needed added severely to the light requirements; hence, development was initiated to produce a low light level image orthicon. This GE

development features a high gain, thin-film magnesium oxide (MgO) "target" (or sensing layer) with a sensitivity of twenty to fifty times that of the glass "target" tubes (such as the 5820). Sensitivity in this case is the amount of photocathode illumination required for a specific resolution.

Besides sensitivity, this target has several other specific advantages. Its extreme thinness and anisotropic property virtually eliminate sideways leakage, thus increasing resolution capability over the standard glass target of the type 5820 Tubes. Resolution upwards of 2000 lines per inch have been easily obtained.

The thin film MgO image orthicon may be used to store for long periods before being read off, which permits additional sensitivity by use of low frame rates or beam pulsing with long integration times.

Another feature is that it is nearly void of any stickiness and burn-in, since operation depends on electron conduction, which is not a depletion process, rather than on ion conduction as in the glass "target" tubes. Thus, the tubes can be under-scanned for long periods without permanent deterioration.

The recovery from light saturation or blinding is nearly immediate, with no after effects; see Figure II-27 where when operating at maximum low light level, a Navy 24" signal search light was blinked directly at the camera from 3 miles distance. Only a 1-1/4 inch diameter area of a 17" monitor was bloomed and this recovered within 2 scan periods (1/15 sec) whereas our own (human eye) sight was still obscured!

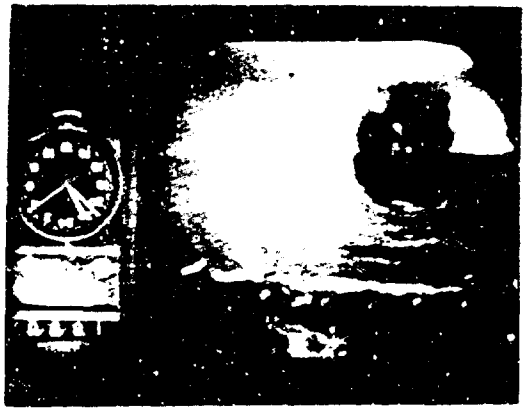
2. Operational Detail

The image orthicon basically is divided into 3 sections. The image section consists of a photocathode sensing surface which releases photoelectrons when subjected to incoming photons. The photo-electrons are electrostatically and magnetically focused on the "target" or sensing layer thus creating a charge pattern representative of the scene energy striking the photocathode. See Figure II-28.

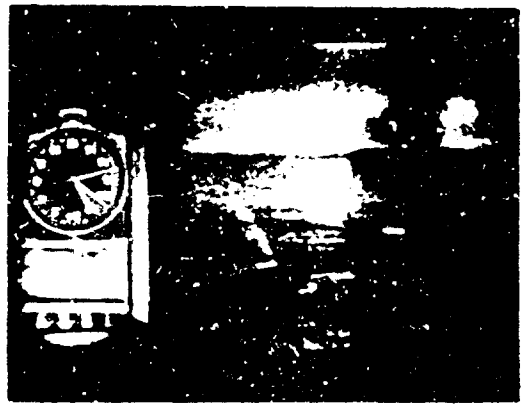
The photo-electron charge pattern is one of maximum positive charge in areas of greatest primary electron density, due to the secondary emission (approximately 10 for electrons having a photocathode to target mesh velocity of 500 ev). The target mesh collects all of the target secondaries from the photocathode side, unless the primary beam intensity from the photocathode is great enough to raise the target surface positive in respect to the target mesh potential.

The electron gun provides a controllable electron beam directed toward the target which is caused to scan the target according to a pattern established by the electro-magnetic deflection coil system and associated driving electronics. The beam current is set to neutralize the charge pattern on the target and in so doing is modulated by the extent of the charge and the beam current level used. The reflected (and modulated) beam returns through the same deflection field, and is amplified by the electron multiplier (essentially "noise free" gain so that sensitivity is limited to the "shot noise" of the scanning beam) to a level appropriate for further external amplification.

Since the beam noise may be limiting sensitivity (with a good preamp) we wish to use the lowest value of beam current commensurate with the scene illumination to get the best signal-to-noise viewing.



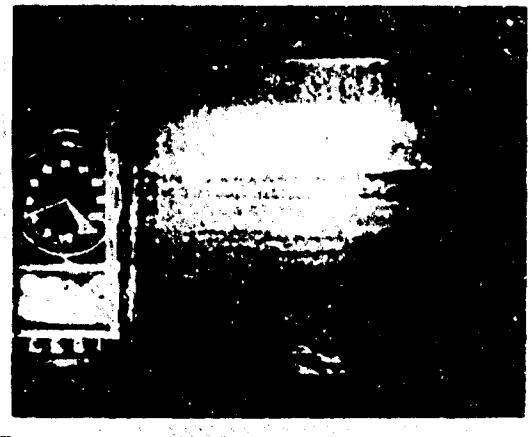
A. Starlight Night. Horizon Not Visible to Dark Adapted Eye with 7 x 50 Night Binoculars (Submarine Officer); 24" Navy Searchlight Directed at Camera from Distance of 2 miles; Note Minimum Bloom



B. One scan 1/30 sec After Extinguishing Searchlight



C. Two scans 1/15 sec After Extinguishing Searchlight



D. Three Scans 1/10 sec After Extinguishing Searchlight; Chart Room Light on Tug Visible (Though All Lights Supposed to Be Extinguished); Other Lights on Horizon Are Navigation Aids

Figure II-27. These Pictures Demonstrate Limited Blooming and Recovery Speed of GE Thin Film MgO Image Orthicon When Operated Properly

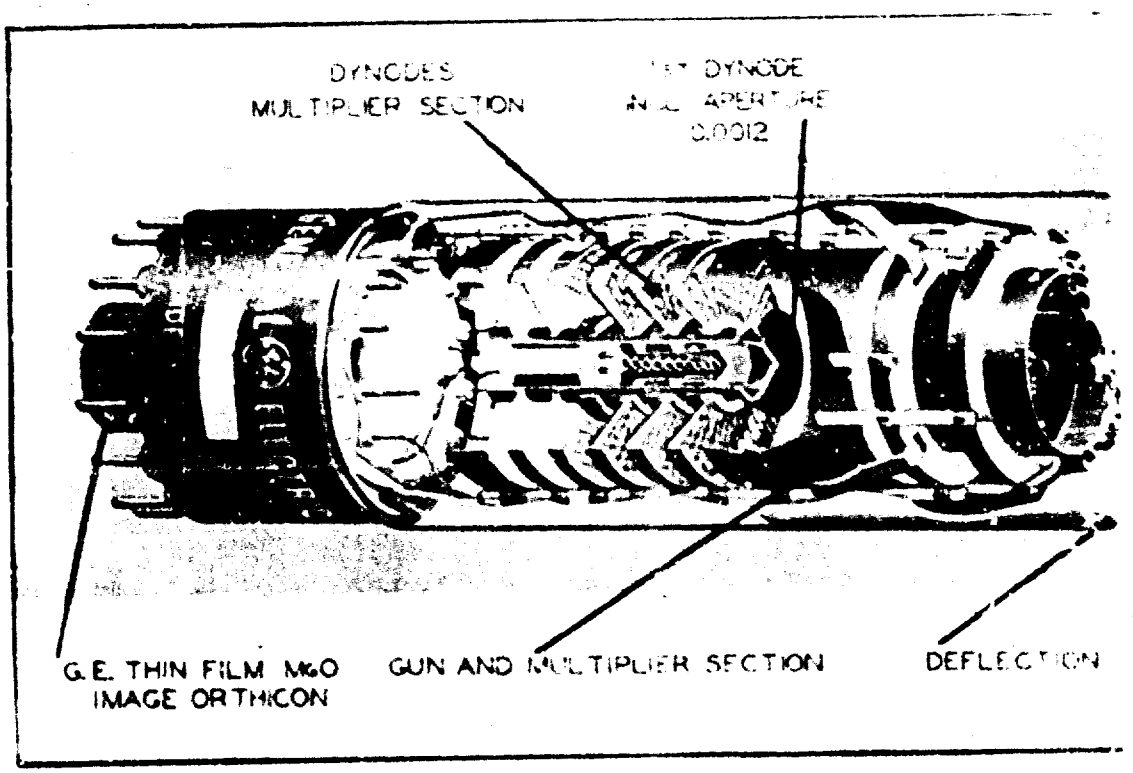
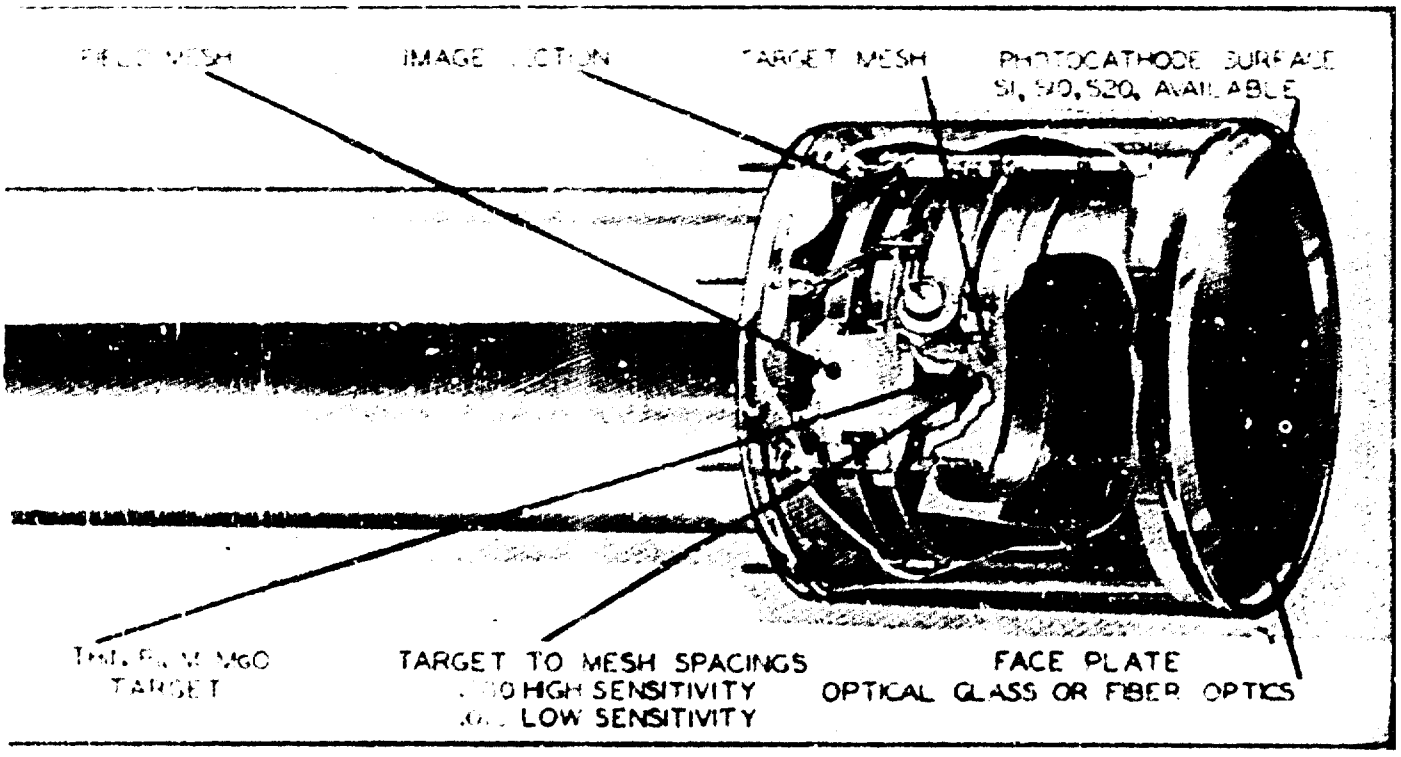


Figure II-28. Detail



E Thin Film MgO Image Orthicon

For highlighted areas we need more current, thus more beam noise, hence the lower illuminated areas or intensity sources will be compromised when setting the beam current to prevent saturation of the higher intensity areas. Techniques are being investigated for beam control within a scene, but until they are developed we must set the beam current higher for the overall desired results.

The target (sensing layer) current is the difference between the beam current and the return current. The signal current is the target current amplified by the electron multiplier and since the target current represents the charge established on the target by the image section photo electrons, it is proportional to incoming signal or photons. For each single resolution element the beam landing current-voltage relationship applies when, and only when, the beam is on that element. The radiation intensity (incoming signal) builds up the single element target-cathode voltage while the beam is not scanning the element and it is discharged by the beam when it covers the element. The voltage after scan is determined by the amount of charge supplied by the beam which is a function of beam current.

The operation of a scanned image tube is affected by the beam landing characteristics. The beam landing characteristics are non-linear and therefore the transfer characteristics are non-linear in the low and high radiation regions comparable to low and high target voltage changes. The beam current has to be greater than the target current just necessary for discharge, otherwise abnormal image spreading will occur because the charge is not fully discharged and thus will spread to adjacent elements until the beam current supplied over the element and nearby elements will discharge the total charge.

For viewing star fields (varying intensity point sources against a background) a compromise setting of beam current is made between minimizing spreading and that needed for detection of the lower intensity star images near or at background light (noise) level.

When viewing a scene (distributed objects) etc., the beam is set to obtain desired resolution of the brighter areas. Even in this case some spreading may be allowed in order to better view low intensity areas of the scene.

For studio TV operation the beam current would be increased until there is no apparent spreading in maximum intensity areas and the illumination would be controlled so that no areas would be detection limited by the shot noise of the high beam current used in order that no objectionable noise (snow or grainness) would appear in the picture. Further details (the operating levels, characteristics, and techniques of signal modulation, the effects of varying point source targets such as stars versus distributed scenes as in studio work, different conditions of scanning period, number of lines, and comparison resolution-sensitivity) are covered in the following technical notes on the use of these tubes. Much of the notes here treat operation for other than studio use which is adequately advisable in commercial TV literature.

3. Tube Characteristics

The GE low light level MgO image Orthicon tubes are available with various photocathode surfaces, target to mesh spacing, standard or militarized and ruggedized versions. The following table plus Figure II-29 summarizes those presently available. Some are standard available tubes while others are still in the special purposes category.

General Electric offers a wide and diversified line of image orthicons which incorporate significant breakthroughs in the state of the art . . . for unlimited television applications in fields of . . . COMMERCIAL BROADCASTING . . . SCIENTIFIC . . . INDUSTRIAL . . . MILITARY . . . such as RESOLUTION improved as much as 50% . . . SENSITIVITY improved 50:1 . . . LIFE extended 3 to 5 times . . . SUPER-RUGGEDIZED to exceed 600 lines at 1000 cycles, 44 g's . . . and dc acceleration of 90g's.

SPECIAL PURPOSE • SCIENTIFIC • INDUSTRIAL • MILITARY

TYPE	FEATURES	SPECTRAL RESPONSE	†RESOLUTION SENSITIVITY	APPLICATIONS—USER PROVEN*
GL-7538	magnesium oxide target 10 to 20 times more sensitive than 5820	3200–6950 Å peak blue S-10	500 @ 1.4 x 10^{-6} 200 @ 1.5 x 10^{-6}	*low light level surveillance space navigation *electro optical telescope systems
GL-7409	same as GL-7538 plus: super-ruggedized	same as GL-7538		*airborne fire control *missile and satellite-borne systems drone guidance *tank fire control
GL-7967 (a)	magnesium oxide target 50 times more sensitive than 5820 due to photo cathode.	3200–7400 Å high red sensitivity S-20	500 @ 4.8 x 10^{-9} 200 @ 5.0 x 10^{-7}	*extreme low light level surveillance *orthicon intensifier studies *underwater observation *astronomical studies
GL-7969 (b)	magnesium oxide target ultra-violet sensitive	2500–7000 Å peak UV	500 @ 1.4 x 10^{-6} 200 @ 1.5 x 10^{-6}	*missile detection spectrographic detectors *underwater observation medical biological studies
GL-7629	same as GL-7538 plus: higher signal noise ratio above 10^{-4} ft-c illumination on photocathode	3200–6950 Å peak blue S-10	‡equivalent ASA rating 32,000—64,000	*medical X-Ray intensifier studies *closed circuit training *simulated aircraft training *stereo X-Ray studies

DEVELOPMENTAL • SCIENTIFIC • INDUSTRIAL • MILITARY

Z-5395 (c)	magnesium oxide target infra-red sensitive	3200–10,800 Å peak infra-red S-1	500 @ 7.6 x 10^{-6} 200 @ 1.0 x 10^{-5}	*infra-red detection: passive and active daylight star tracking *aerial mapping spectrographic detectors
Z-7809	same as GL-7538 plus: fibre-optics faceplate	same as GL-7538		medical television *fibre-optics systems photographic printing high speed information scanning
Z-7810	same as GL-7967 plus: fibre-optics faceplate	same as GL-7967		*fibre-optics systems *radiation scintillator studies photographic printing high speed information scanning
Z-7814	same as GL-7967 plus: field mesh flatter fields improved corner resolution	same as GL-7967		electro-optical telescope systems extreme low light level surveillance underwater observation orthicon intensifier studies

COMMERCIAL BROADCAST • NETWORK • EDUCATIONAL

G-7629	high reliability very long life low light level sensitivity semiconductor target	3200–6950 Å S-10	equivalent ASA rating 32,000–64,000	remote black/white as low as 1 ft-c scene illumination remote color—as low as 5 ft-c scene illumination long life studio service
GL-8092	same as GL-7629 plus: field mesh flatter fields improved corner resolution		32,000–64,000	studio color 40 to 100 ft-c illumination remote color
GL-5820	good gray scale glass target stable performance		8000–16,000 (new tube)	studio black/white 100 ft-c scene illumination educational TV
GL-7293	same as GL-5820 plus: field mesh flatter fields improved corner resolution		8000–16,000 (new tube)	studio black/white high quality monochrome educational TV
GL-8093	same as GL-7293 plus: very high signal noise ratio for video tape recording and color		8000–16,000 (new tube)	high quality video tape recording high quality color educational TV

*Super-ruggedized version (a) ZL-7806 (b) ZL-7807 (c) ZL-7804
†Resolution sensitivity is defined as television lines per target inch at specified photocathode illumination in foot-candles.
‡Equivalent ASA ratings based on exposure at knee of transfer characteristic curve and frame time of 1/30 sec.

Figure II-29. Available Low Light Level MgO Image Orthicon Tubes

Old No.	Type No.	Photocathode Surface	Mesh-Target Spacing	Field Mesh	Ruggedized
	GL-7629	S10	10 mil	No	No
	GL-8092	S10	10 mil	Yes	No
	GL-7821	S20	10 mil	Yes	No
Z-5294	GL-7538	S10	80 mil	No	No
Z-5358	GL-7409	S10	80 mil	No	Yes
Z-5396	GL-7967	S20	80 mil	No	No
	Z-7806	S20	80 mil	No	Yes
Z-5453	GL-7969	S10 (UV face plate)	80 mil	No	No
	Z-7807	S10 (UV face plate)	80 mil	No	Yes
	G-7814	S20	80 mil	Yes	No
	Z-7809	S10 (Fiber Optic Face Plate)	80 mil	No	No
	Z-7810	S20 (Fiber Optic Face plate)	80 mil	No	No
Z-5395		S1	80 mil	No	No
	Z-7805	S1	80 mil	No	Yes

The S-20 Tubes are 3 to 4 times more sensitive than the S-10 versions. The spacing of the target affects the sensitivity and the noise content for a given ambient light level. The close spaced tubes are not as sensitive nor as "noisy," but when extreme sensitivity is desired the wider spaced S-20 tubes are needed. In military, low light level (night) applications the wider spaced tubes are almost always used whereas for daytime operation the closer spaced S-10 versions should be used.

The spectral response of the photocathode surfaces normally available are shown in Figure II-30. For other photocathode surfaces refer to Figure II-31. For those applications involving response in the ultra-violet (UV), tubes with special UV face plates should be used since it is the glass face plate that cuts off the UV response of most of the suitable photocathode surface materials.

The increased sensitivity of the S20 photocathode compared to the S10 photocathode is shown by the photocathode spectral response curves. The ratio of 3 to 4 times sensitivity for the S20 assumes a wide spectral input from 2800°K to 5000°K black body; in some narrow spectral bands the S20 response is only 2.5 times the S10 response, but the S20 response is wider. One problem of the S20 is the non-uniformity of the photocathode quantum efficiency. The S20 is much less uniform in quantum efficiency, or sensitivity, across its surface than the S10

The GL-7967 is the most widely used of the special tubes; it is a wide spaced S-20 tube and therefore most sensitive for night use. For daytime use the

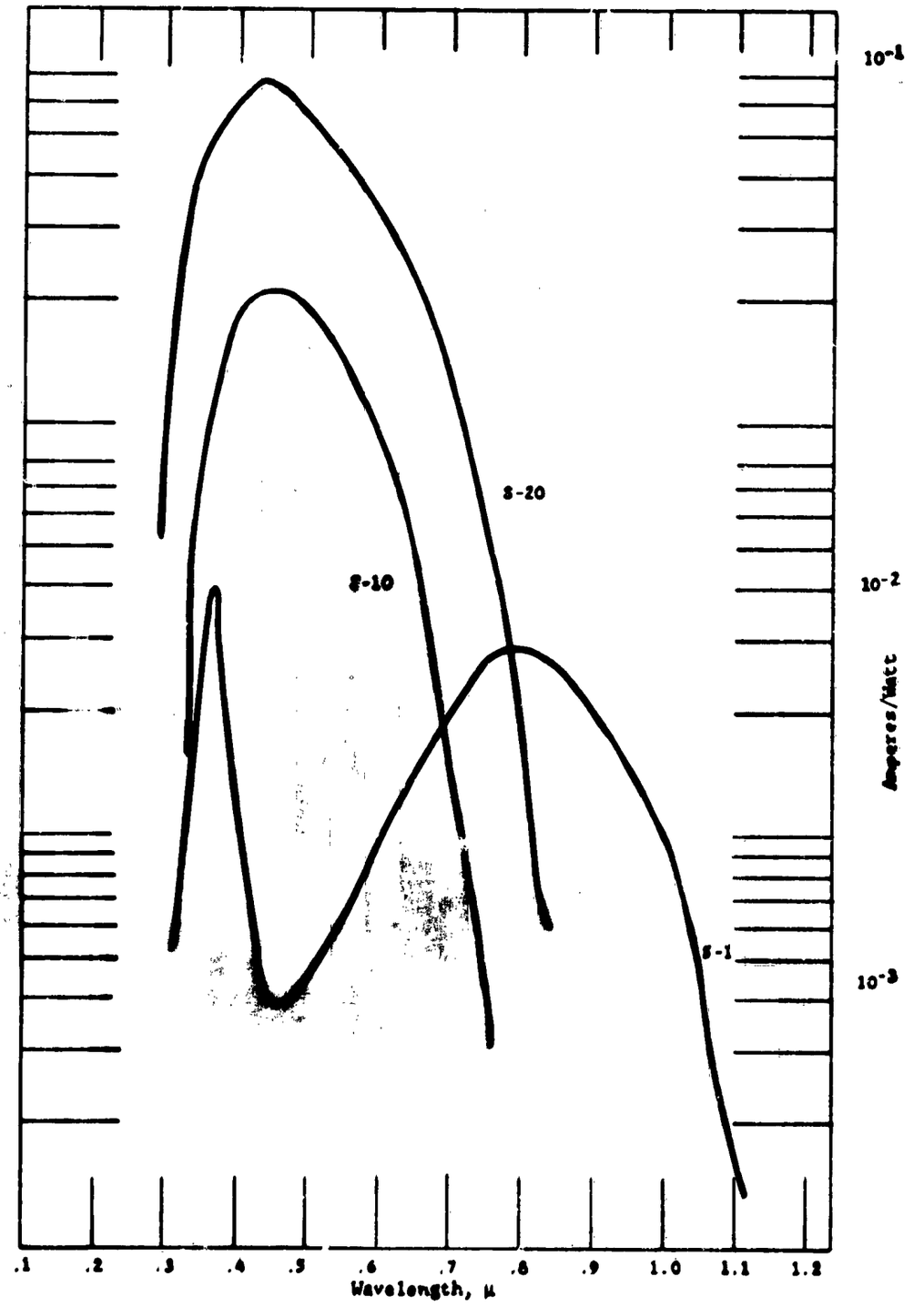
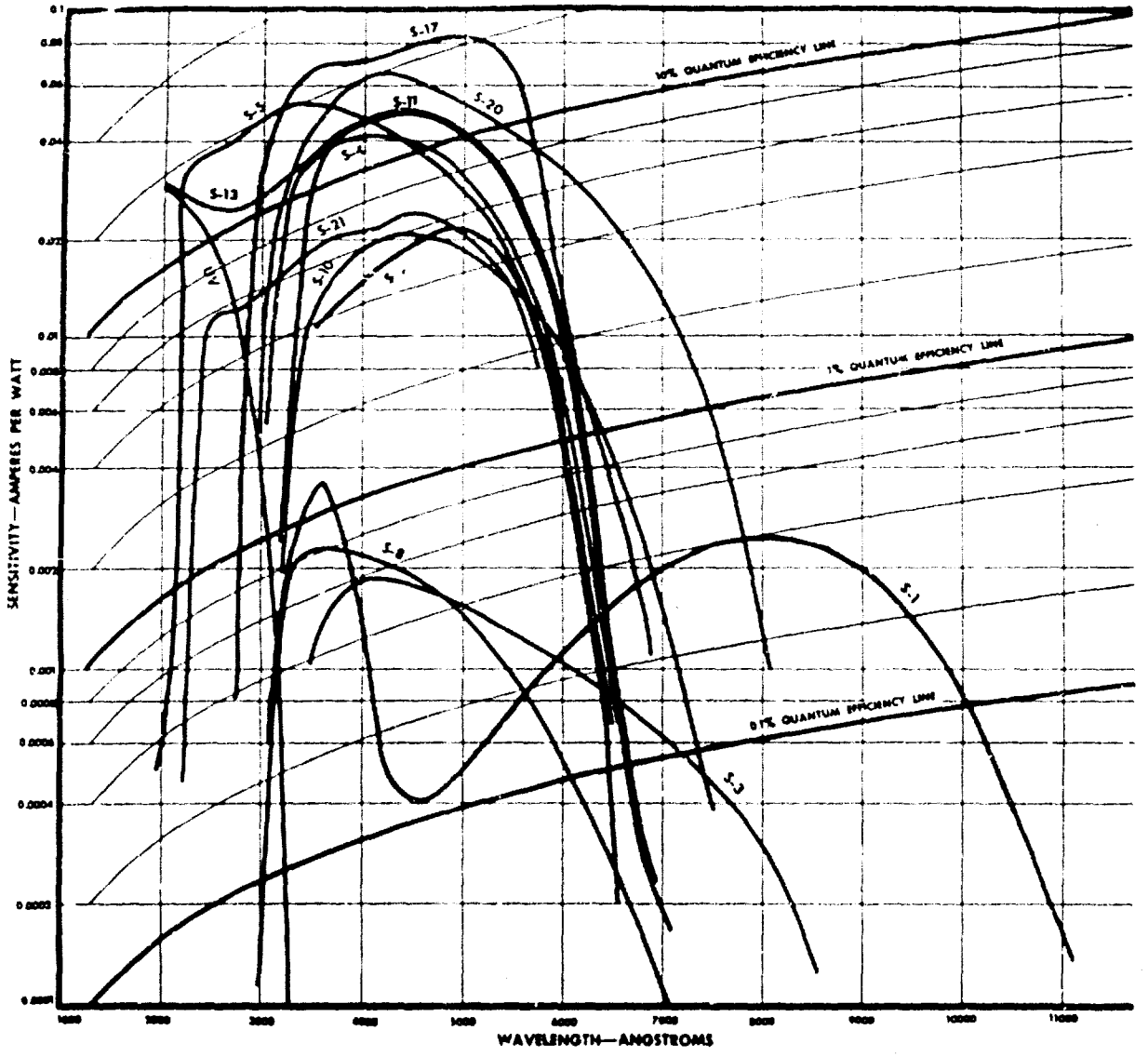


Figure II-30. Relative Photocathode Response, Amps per Watt



Device S Number[1]	Principal Photocathode Components[2]	Entrance Window Material	Photocathode Supporting Substrate[7]	Luminous Sensitivity[4] (μa/lumen)	Typical Photocathode Dark Current[5] @ 25°C (amps/cm²)
S-1	Ag O Cs	Visible light transmitting glass[6]	Entrance window or opaque material[7]	25	10^{-11} - 10^{-13}
S-3	Ag O Rb	Visible light transmitting glass[6]	Opaque material[7]	6.5	10^{-13}
S-4	Cs Sb	Visible light transmitting glass[6]	Opaque material[7]	40	10^{-14}
S-8	Cs Sb	U.V. transmitting glass[6]	Opaque material[7]	40	10^{-14}
S-8	Cs Bi	Visible light transmitting glass[6]	Opaque material[7]	3	10^{-14} - 10^{-15}
S-9	Cs Sb	Visible light transmitting glass[6]	Entrance window	30	10^{-14}
S-10	Ag Bi O Cs	Visible light transmitting glass[6]	Entrance window	40	10^{-13} - 10^{-14}
S-11	Cs Sb	Visible light transmitting glass[6]	Entrance window	60	10^{-13} - 10^{-15}
S-13	Cs Sb	Fused silica	Entrance window	60	10^{-13} - 10^{-15}
S-17	Cs Sb	Visible light transmitting glass[6]	Opaque reflecting material[7]	135	10^{-13} - 10^{-15}
S-19	Cs Sb	Fused silica	Opaque material[7]	60	10^{-13}
S-20	Sb K Na Cs	Visible light transmitting glass[6]	Entrance window	150	10^{-13} - 10^{-14}
S-21	Cs Sb	U.V. transmitting glass	Entrance window	30	10^{-14}
UV[8]	Cs Te	Sapphire	Opaque material[7]	0	

NOTES

1. The S number is the designation of the spectral response characteristic of the device and includes the transmission of the device window material.
2. Principal components of the photocathode are listed without regard to order of processing or relative proportions.
3. When the supporting substrate is the entrance window, an intermediate semitransparent electrically conductive layer may be used.
4. Corresponding to the specific absolute response curves shown in the figure using a 2870°K color temperature tungsten lamp test source.
5. Specific dark current excludes DC leakage.
6. Lime glass and Kovar sealing borosilicate glass are commonly used for visible light transmitting glass.
7. The opaque material used as the supporting substrate for photocathodes in which the input radiation is incident on the same side as the emitted photoelectrons is usually metallic in nature.
8. An S number designation has not yet been assigned to this experimental "solar blind" photoemissive surface.

Figure II-31. Photocathode Responses

GL-7629a is highly recommended; it is an S-10 close spaced commercial broadcast MgO tube. It has excellent uniformity with minimum noise in addition to the other advantages of MgO tubes.

4. Ruggedized Image Orthicon

Complete printed specifications are not available at this time; however, each tube is identical to the non-ruggedized tube listed below, except that it has been designed to meet the following ruggedization specifications.

Ruggedized Tube		Equivalent Non-Ruggedized Tube		Photocathode
G-E Development Number	E1A Type Number	G-E Development Number	E1A Type Number	
ZL-7805	-	Z-5395	-	S-1
ZL-7806	-	Z-5396	GL-7967	S-20
ZL-7807	-	Z-5453	GL-7969	UV
ZL-5358	GL-7409	Z-5294	GL-7538	S-10

Shock - 100G's

Per specification MIL-E-5272C (ASG) Paragraph 4.1.5.5 with the following differences:

a) 12 impact shocks of 30 G.

b) The shock shall be applied in the following directions:

1) Vertically perpendicular to longitudinal axis, 3 shocks in each direction.

2) Parallel to the minor horizontal axis, 3 shocks in each direction.

c) The shock pulse width is defined by the use of a 0.2 to 250-cycle-per-second filter.

Vibration - 10 G's

Under the conditions specified in MIL-E-5272C (ASG) Paragraph 4.7.12 Procedure XII except at operating temperature only. Center horizontal resolution at 3×10^{-5} maximum foot-candles, photocathode illumination will be at least 350 lines with 5G applied acceleration in the frequency range from 50 to 500 cycles per second and a double amplitude of 0.036 inch from 5 to 50 cycles per second.

Humidity

Under the conditions specified in MIL-E-5272C (ASG) Paragraph 4.4.1 Procedure I. Following this test, the interelectrode insulation of the end pins 5, 6, 7, 8, 9, and 10 each with respect to all other and base pins grounded and with 350 volts (minimum) applied is greater than 500 ohms.

Acceleration - 70 G's

Constant acceleration when applied perpendicular to the longitudinal axis of the tube for 10 minutes.

5. Technical Notes for MgO Image Orthicon Application

The success of applications using the GE low light level (MgO) Image Orthicon is dependent on the proper selection of the variable parameters of the environment, the tube as a sensor, the optical system, the scanning pattern, the video processing, and the readout system. Lack of proper consideration in any one of these areas may cause much dissatisfaction. It is the purpose of this section to discuss the relative factors and trades available to the equipment/system engineer in the use of the MgO Image Orthicon tubes for special purpose applications.

a. Resolution/Sensitivity Continuous Scan - Distributed Targets (Scenes)

Continuous scanning of the I.O. target is the normal mode of operation, together with eye viewing of the monitor to observe the scene. The normal television use for which much of the published data is written involves scenes of distributed targets (extended sources and resolved target scenes); that is, a studio scene, an outdoor sports event or such. Here the ambient light level is usually sufficiently above the noise level of the tube and a reasonable rendition of the scene contrast is reproduced. Typical performance curves for this studio type of operation are shown in Figures II-32A and B.

Note 1: The curves are plotted for output resolution vs scene illumination. Thus for low light levels the resolution is dependent on the tube sensitivity and scene illumination. At the higher light levels better resolution is available if more scan lines are used. To get higher resolution, sufficient light and proper number of scan lines and bandwidth must be used in the camera electronics and in the monitor used for viewing. The reverse is also true, that is, for low light levels where the ambient light and tube sensitivity show a low resolution picture the number of scan lines can be reduced to approach the limited resolution, and bandwidth lowered accordingly; meaning a less critical (more economical) video amplifier and processor.

Note 2: Scene Brightness or Luminance (B) equals Scene Illumination (E) times the scene and/or Object Reflectance (R), i.e., $B = E \cdot R$.

Note 3: By Geometric Optics the photocathode Illumination $(E)_{pc}$ in ft. candles is related to the Scene Brightness B in candles/ft^2

$$E_{pc}\ (\text{ft candles}) = \frac{\pi B\ \text{candles/ft}^2}{4\ (\text{f/no})^2}$$

If B in footlamberts eliminate π

The theoretical analysis of detection performance at lowest light levels on distributed scenes as read by eye-viewing a monitor, however, shows no improvement by using fewer scan lines, if the scan pattern sweeps the same target area of

the image orthicon in the same time. (Assuming beam current was adjusted at lowest value for detection and thus would be the same as long as the same scan area and time is used irrespective of number of lines.) The energy from the scene hasn't changed, therefore, the average beam current does not change for same performance level. The theory holds for noisy and noiseless (theoretically perfect) video preamplifiers. Bandwidth is usually not a factor since the eye is the ultimate signal recognition detector.

The condition, is, in general, the same for the case where over-scanning is employed (to decrease number of equivalent scan lines) and thus detectability of a specific object in a scene does not change, assuming preamplifier is noiseless and is not causing a loss of resolution sensitivity. The assumption of a "noiseless" amplifier is also valid when the light level is high enough to require a large image orthicon beam scanning current, since the beam current for best performance is large (higher light level). Thus the I.O. noise voltage at the preamplifier input is much greater than the equivalent preamplifier noise at the preamplifier input.

Overscanning will give a detection improvement (will require less light to see the same object) with a practical "noisy" amplifier at very low light levels, since the best performance beam current for overscan is larger than the best performance beam current for standard scan for the same photocathode image. Thus a high performance I.O.system with a low noise figure video preamplifier will show less detection improvement when overscanned, than a system that has a higher noise figure video preamplifier. Some test results have shown a detection improvement at low light levels (equivalent to 100 to 200 vertical TV lines of resolution at 100% contrast) if the I.O. is overscanned. There is a potential problem of large video signals when the beam strikes the metal ring that holds the target. Overscanning, since it covers the complete "target" area or more, will display on the monitor a larger beam scanned area, equivalent to a larger field of view; thus an object will appear smaller (a decrease of object magnification).

Underscanning, of course, will give an object magnification with corresponding decreasing of the field of view displayed on monitor.

Regarding object magnification, a similar viewing effect is noted when using larger or smaller monitors to display the same scene or to view the same monitor at further or closer distances. There is a fall-off due to frequency response when viewing scenes with 200 TV lines or more as noted in Figure II-32A which should be recognized when evaluating performance for higher resolution, but since we are talking here of minimum detection (low resolution seeing) we have disregarded this effect.

The above discussion is further effected, and improvement will be less under condition of less than 100% contrast at low light levels as a quick reference to the % contrast curves Figure II-32B will reveal. The low light level limit is set by the sensitivity (quantum efficiency) of the photocathode (S-20 being the best to date) and the noise in the scanning beam used to read the target charge.

The high limit of resolution possible with the G.E. thin film MgO Image Orthicon is well over 2000 lines per "target" inch. The maximum resolution of a system is limited by the optics or the photocathode resolution, provided there is sufficient light and contrast and that beam current, scan pattern, bandwidth and electronic circuitry is not limiting first, as is often the case. See Figure II-33 A and B The ultimate resolution is, of course, limited by the average intensity

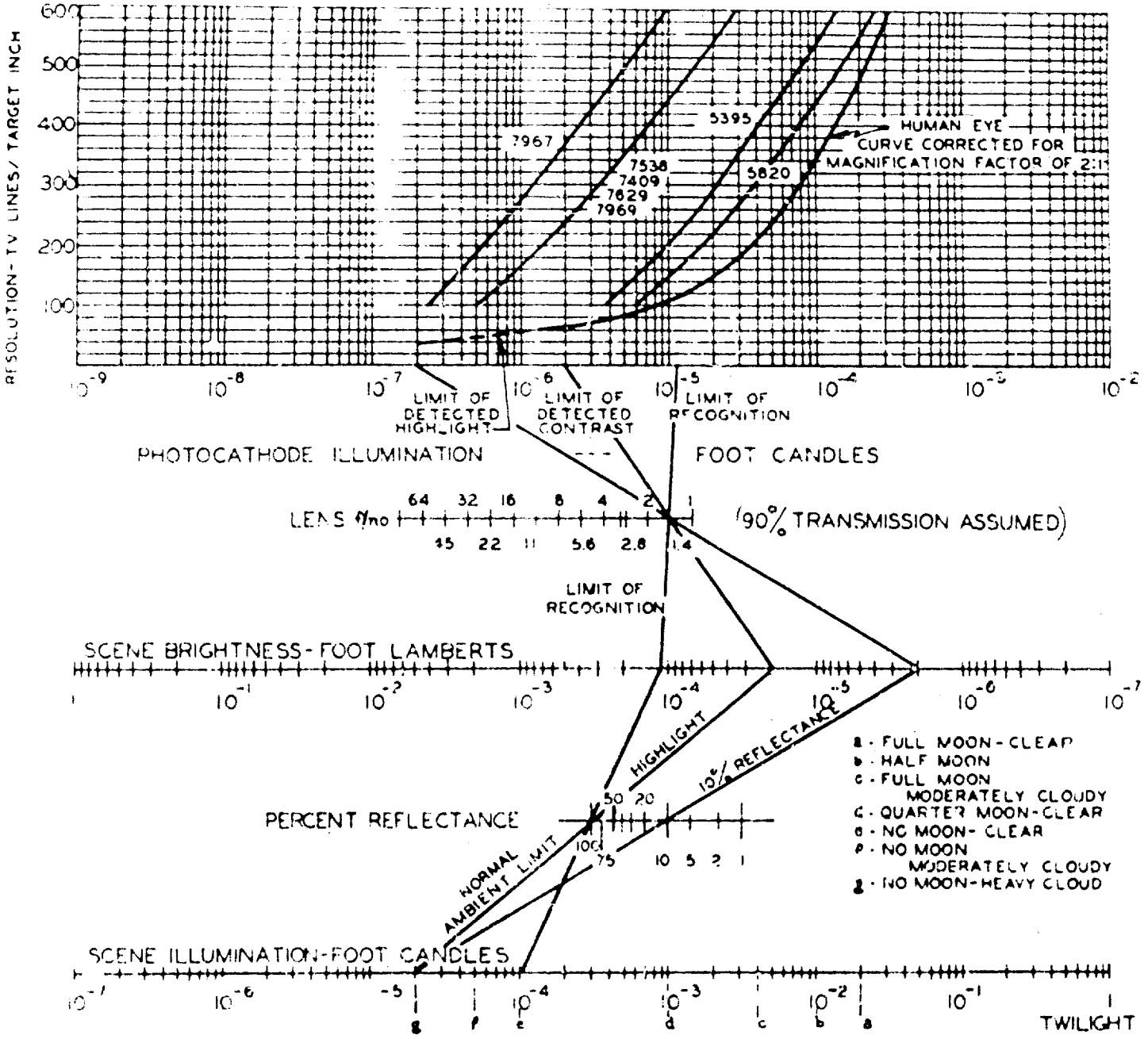


Figure II-22A. Scene Illumination vs Typical Resolution Sensitivity by Type

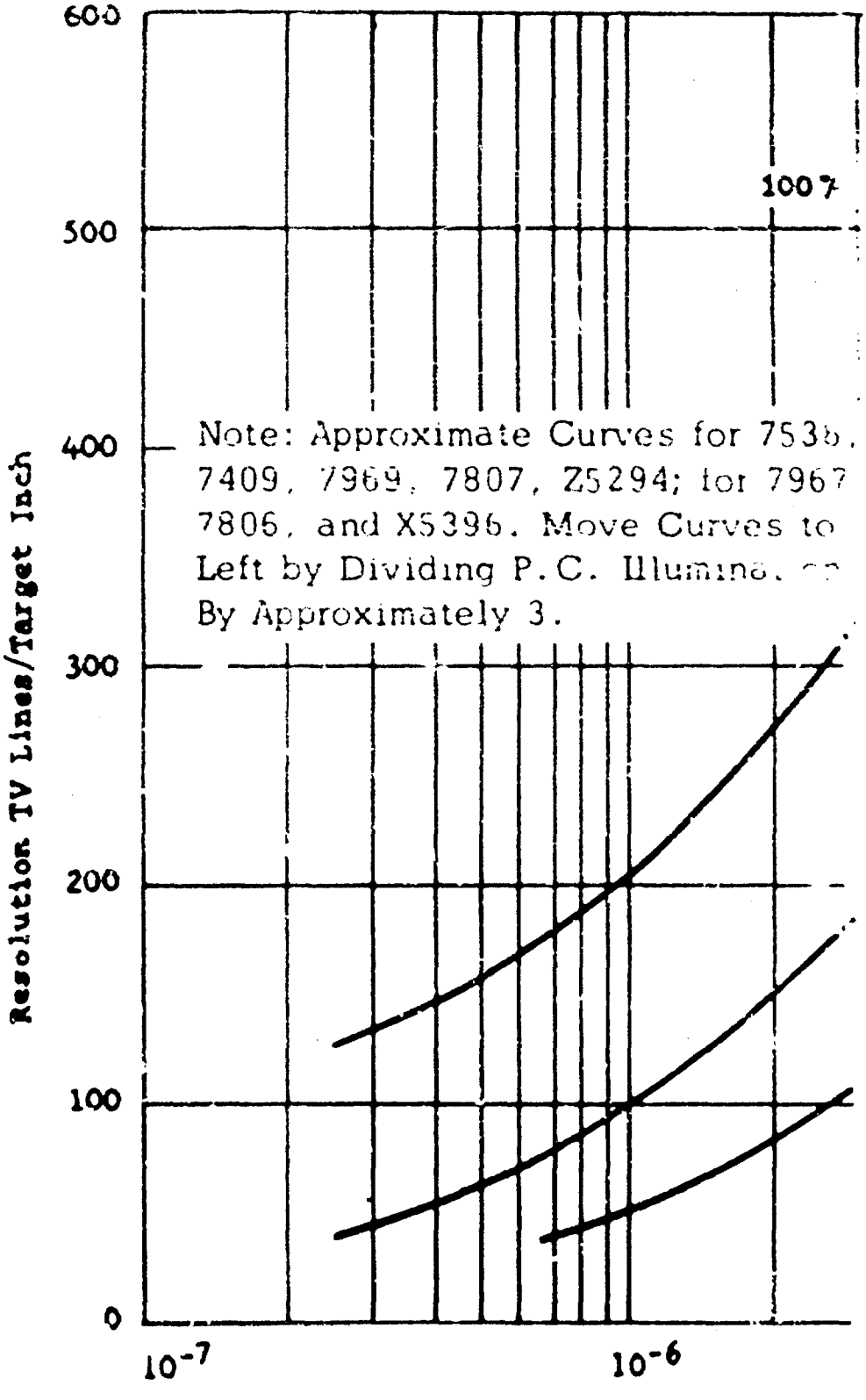
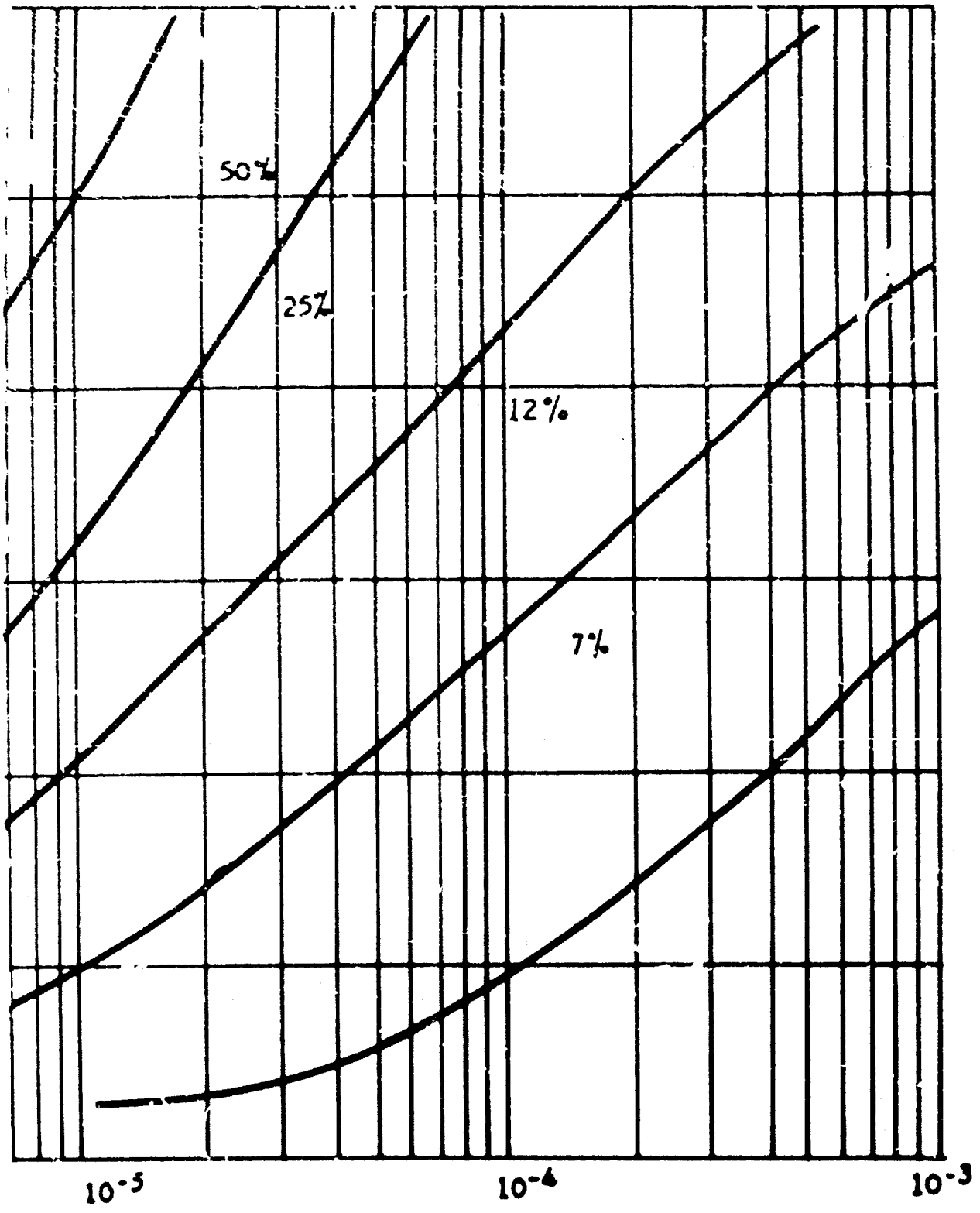

600
500
400
300
200
100
0
Resolution TV Lines/Target Inch
1007
Note: Approximate Curves for 7536, 7409, 7969, 7807, Z5294; for 7967 7806, and X5396. Move Curves to Left by Dividing P.C. Illumina. By Approximately 3.
10^{-7}
10^{-6}

Figure II



cts of Contrast Reduction



Figure II-33A. Normal Scan 1029 Line Full Scan

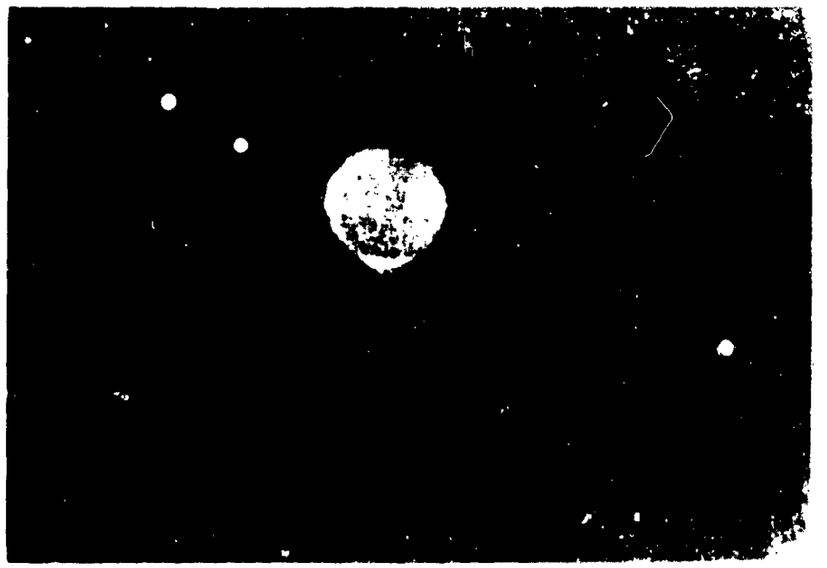


Figure II-33B. 4 to 1 Underscan with 1029 Lines: Moons have Increased in Size, Hence Resolution was Exceeded Earlier; Probably at Approximately 3 to 1 or 3000 Lines

Figure II-33. An Example of Underscanning of I.O. for Increased Resolution — Jupiter and its Principal Moons, 1029 Line Scan

(flux) per line and the contrast between line and background. However, special techniques are needed to demonstrate and/or utilize this resolution as there are no available kinescopes (monitor picture tubes) that will display much over 1200 lines per inch equivalent. The 5" oscilloscope CR tubes such as the 4915 are the only possibility, unless the resolution is used over only a portion (underscanning the I.O. and then displayed across the full monitor) of the field of view.

b. Illumination Range - Continuous Scan - Distributed Object or Area (Scenes)

The range of scene brightness that can be handled depends on operational settings. It is possible to adjust for very close to maximum low light level sensitivity and, without change of settings, view distributed scenes with illuminations increased approximately 10^5 times (if the amplifier is properly designed) without streaking or appreciable loss of resolution (400 lines), primarily lost because of image spreading. More data are needed here to plot a complete resolution versus scene illumination curve, being careful that lens response is not limiting.

c. Resolution/Sensitivity Unresolved Object (Point Source) Scenes (non-moving sources)

Very little data has been heretofore published except for the G.E Photo Electric Observatory Reports by J.F. Spalding on the performance of the G.E thin film MgO Image Orthicon applied to light level scenes having unresolved (point source) star objects. The treatment of various brightness point sources and resolution/sensitivity for various background (sky noise) levels versus number of scan lines, scan period, bandwidth, integration times, etc., is quite complicated. Basic to the discussion is an understanding of the environment and target conditions (see Section I) and the lens or optical parameters involved (discussed in detail in Section II-A.

Important to the understanding of the image orthicon are the conditions of steady state, beam noise, reciprocity, and the effect of integration within the image orthicon and external to it (eye integration of the monitor display).

The resolution sensitivity vs scan lines relationship for extended objects in general holds for point source scenes. However, since point sources may be smaller than the scene line resolution, the celestial scene has a high required resolution and two close sources will be separated below what might be predicted. The difference is small and the sensitivity improvement with fewer scan lines holds as with the distributed scenes, provided (1) the hypersensitization condition does not exist and (2) that sky background level per resolution element is not setting the detection level.

Detection of point sources is a matter of signal to background noise per resolution element as explained by detection analysis. Since the resolution element size is a function of numbers of lines of scan and bandwidth used, then we have a trade between this and the resolution/sensitivity of the tube itself. The limit to be gained is set by the noise in the resolution element, since the lens diameter and focal length can usually be selected so that the desired performance is attained. In the aerospace situation, the background light may be the limiting condition rather than the tube resolution/sensitivity performance, and thus, increasing the number of lines (smaller resolution elements) and larger bandwidth

usually means a gain in overall system performance. For longer focal lengths and large f/numbers, as in high resolution narrow field astronomy however, this might be reversed since the tube and/or electronic noise might be limiting. Each case, therefore, must be analyzed according to its own requirement if a satisfactory application is to result. Of course, we could compromise, if target rates permit, by using more scan lines together with slower frame rates to avoid increasing bandwidth and thus obtain maximum increase in performance.

For normal continuous scan operation, and a given scene contrast level, intensity varies with integration time. However, for the celestial background and pulse operation this can not be extrapolated directly without considering other effects that may introduce a bias in performance data.

Many curves can be drawn to show the trade of resolution element size and background vs focal length, sensitivity vs aperture, limiting magnitude vs aperture for different integration periods. For a sample, see Figure II-34 showing resolution element size and background brightness increases vs focal length. Since each application generally requires a complete set of calculations and/or experimental checks, we have included only the more frequently used curves. From the discussions, the remaining necessary conditions can be calculated.

d. Pulsed Mode

The characteristics of the MgO Image Orthicon tubes permit increased sensitivity by longer integration times, thus large optics are not necessarily needed. As previously discussed, the ability for storage and integration reciprocity leads to special applications and studies where stationary or nearly stationary scenes are involved. (Moving targets detection is limited to the energy received per resolution element size integrated only for dwell time within the element and the time response of the I. O. target.) Data taken during the past four years at Schenectady and Syracuse has established that reciprocity will exist under the conditions defined. Thus, it is only necessary to determine what performance (star magnitude) can be obtained with a given exposure or integration time and trade time for intensity or lens diameter to scale to other values. The following table gives typical gains when using 2 frame readout. See Figures II-36 & 37 for pictures illustrating actual performance using Orion Nebula.

In determining reciprocity and performance it is important to realize, when eye viewing a monitor, that the eye is integrating for 1/5th of a second. Thus, the integration period is not the scan frame period (1/60, 1/30, or 1/15 sec as commonly used) but rather the 1/5th sec eye integration time, since it effectively is integrating 6 scans on monitor in the case of 1/30 sec frame time. If a photograph of the monitor is taken, the number of frames registered on the monitor during the film exposure, times the frame period, should be used for the integration time. Here several frames are often used to get the sufficient light time for adequate film exposure; remembering kinescope resolution is better at low intensities (less image spreading or monitor phosphor)

There is a linearity limit of integration time which cannot be exceeded without clipping. This clipping occurs when the positive charge in any target area exceeds the positive voltage of the target mesh (the target voltage control is actually the target - mesh voltage control). If the target voltage (proportional to intensity times integration time does exceed the target mesh voltage, the secondary electrons due to photocathode current are not collected by the target mesh and are returned to the target to mask the image charge. Another way of viewing this problem is to

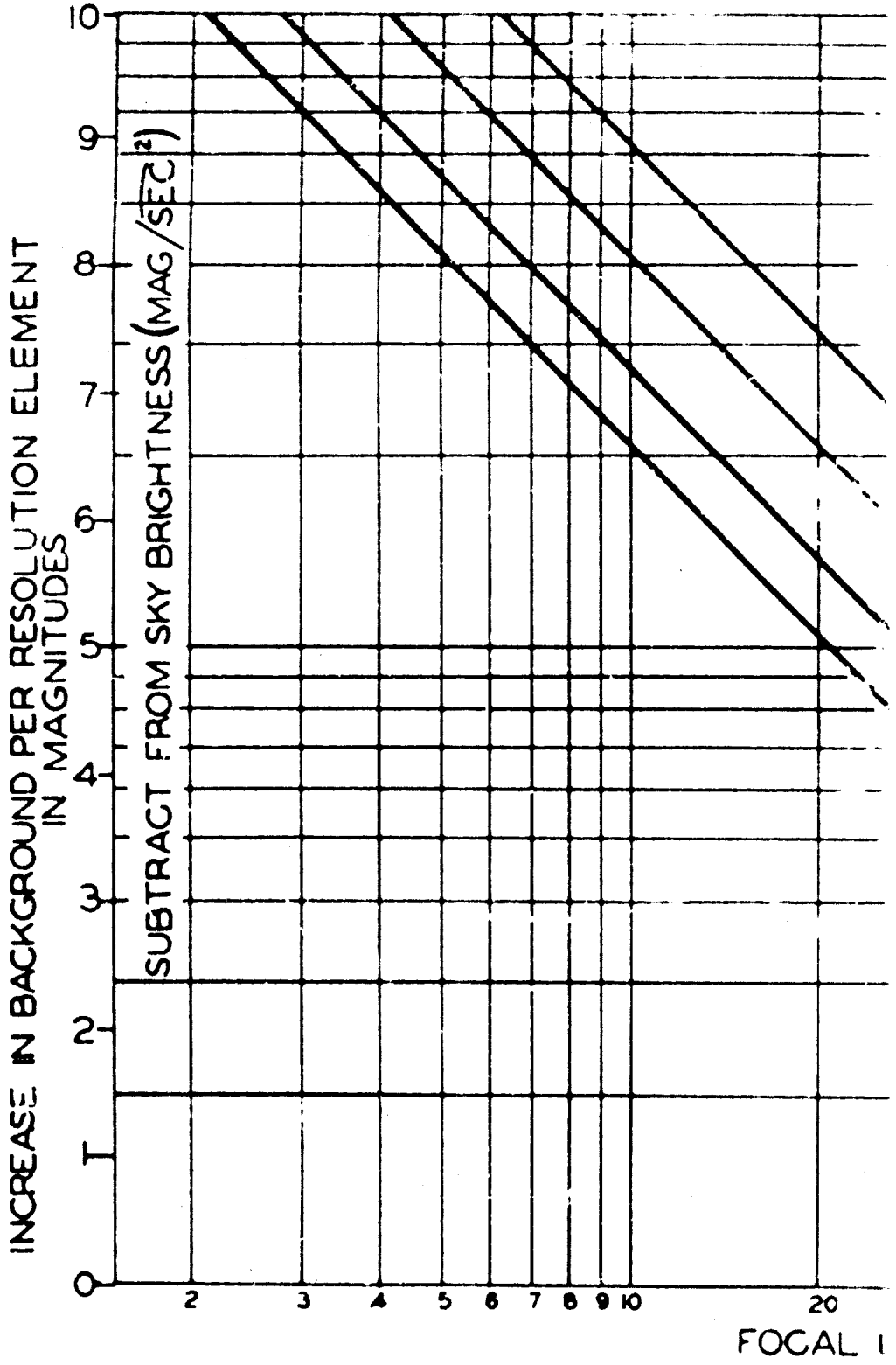
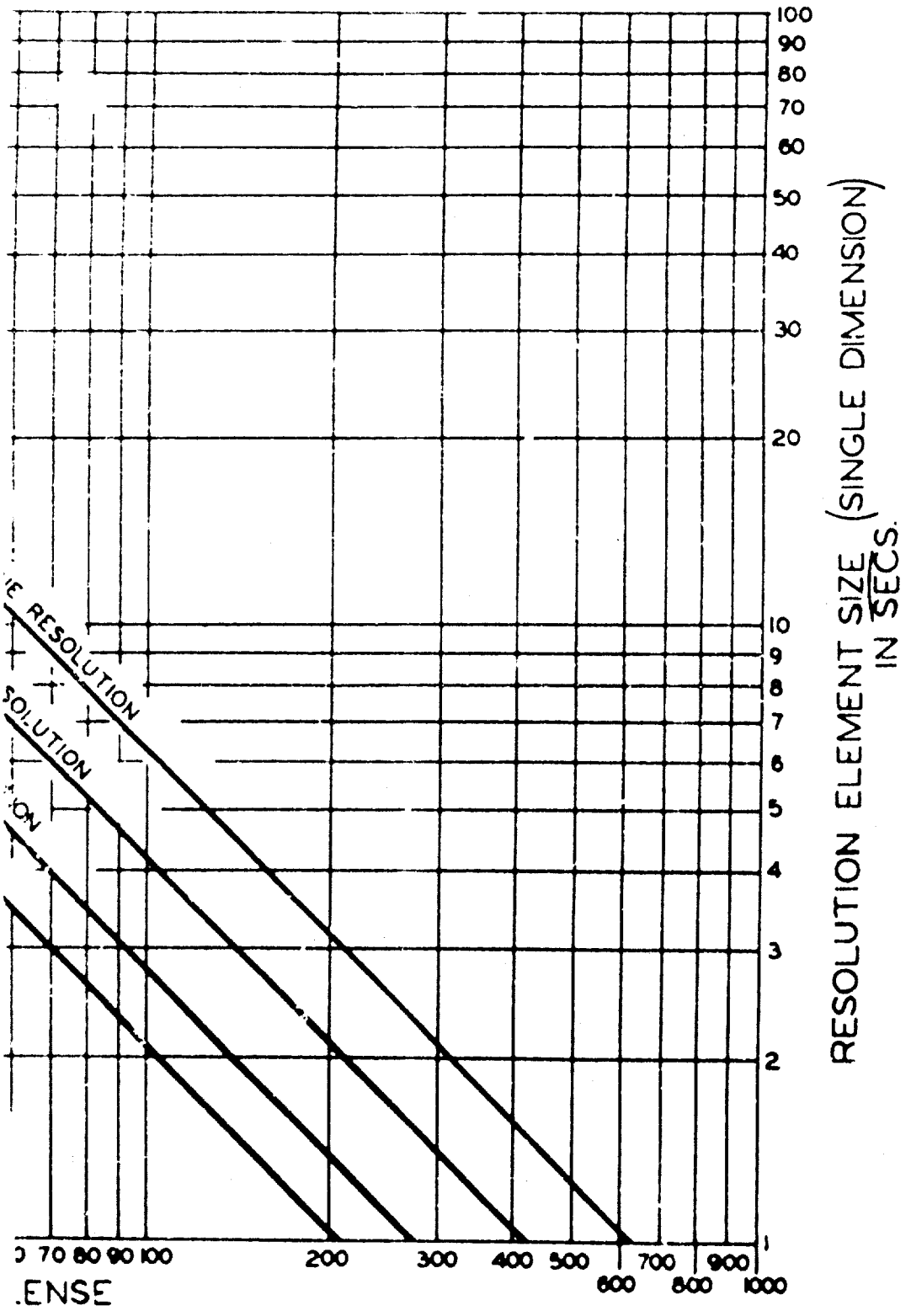
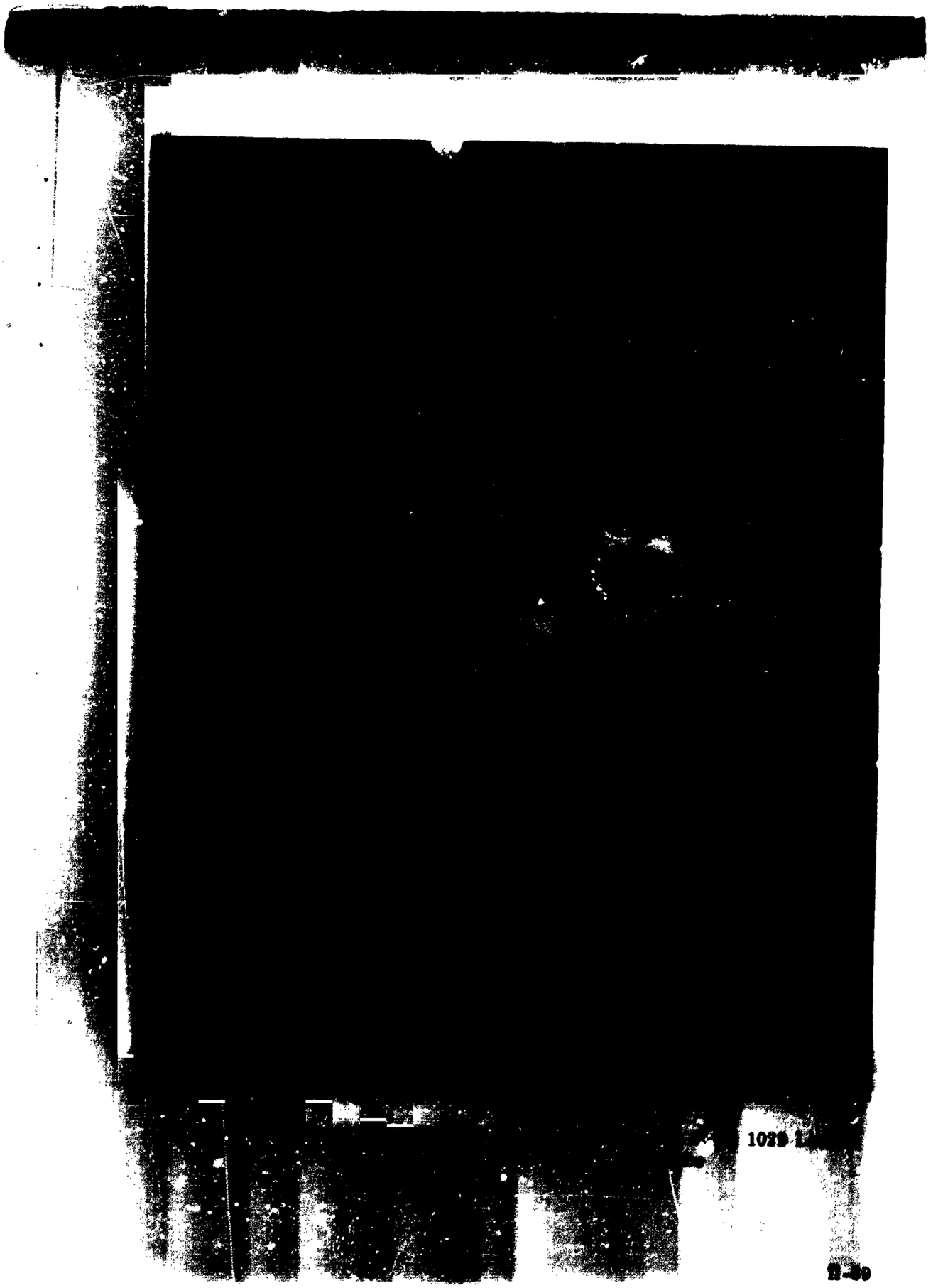


Figure II-34. Resolution Element Size and
vs Focal Length for Va



Brightness Increased per Resolution Element
e solution (Square Raster)



f. Readout Techniques (I.O. Tube)

When pulsing (using integration or short exposure) the choice of number of readout scans is also considered. Here scanning with a low beam current (low shot noise) can be used many times, or one scan of higher beam current could be used. The choice is a matter of the application. For instance, if good intensity (magnitude) calibration were desired on a single still scene, one could use very low beam current and take many scan readouts over a period of time, taking a film record of the monitor for each scan. This way at first all stars including the faintest would show, then next faintest would disappear and so on, until the total beam current used would have discharged the brightest image. This technique provides an accurate calibration of brightness and avoids the laborious film reading techniques of the past.

It is of little use in an aerospace surveillance system since a relatively long time is spent in reading out and getting the I. O. target image discharged; thus, moving objects would be missed completely. For the latter case, one simply uses more beam current and thus accomplishes the target image discharge in one or two scan cycles set by the requirements of object movement. Every object is still read out, but the intensity gradient is less and thus the relative brightness is not easily measured; the beam current is higher so the weaker targets are harder to distinguish due to the higher beam (shot) noise. For most aerospace problems, the trade will probably be between one, two, three or four scan readout cycles, depending on the application.

The trade of one vs two or more scan readouts per exposure of photocathode may be set by the film being used to photograph the monitor. Two scans of lower beam have, in theory, the same performance of one scan of high beam as far as signal detection is concerned (the lower shot beam noise of two scans equals the higher noise of one scan), but two scans will give more monitor integrated light energy for the recording film. (For pulsing, the eye would not be expected to be used, especially for integration periods longer than 1/5th sec) because the time [illegible] readouts accentuates the flashing readouts to the eye viewer.

g. Sensitivity o Moving Point Targets

Sensitivity to moving point targets creates a problem, in that sensitivity seems to have been lost. Actually no sensitivity has been lost at all ! This depends on how sensitivity is defined. The performance is set by the integrated effect of source energy (its strength and the length of time the source energy can charge a single or adjacent resolution element) coupled with the I.O. target response time at that light level plus monitor and eye or film integration time. Thus, for very slow or stationary sources, the performance is set by the accumulated integration time within the system (1/5th second eye integration or readout system integration time if not a human eye). With faster moving targets, the composite integration time (charge accumulated per I. O. scan cycle × number of scans integrated) is progressively less until little or no accumulated charge exists for integration. The response times for the I.O. "Target" (sensing surface) to reach steady state readout are about .050 sec for moderate light levels to about 0.3 or 0.4 seconds for the low light detection limit sensitivity.

When using large f/ratio optics, continuous operation viewing a star field with no photocathode integration sometimes gives erroneous conclusions. The

f. Readout Techniques (I.O. Tube)

When pulsing (using integration or short exposure) the choice of number of readout scans is also considered. Here scanning with a low beam current (low shot noise) can be used many times, or one scan of higher beam current could be used. The choice is a matter of the application. For instance, if good intensity (magnitude) calibration were desired on a single still scene, one could use very low beam current and take many scan readouts over a period of time, taking a film record of the monitor for each scan. This way at first all stars including the faintest would show, then next faintest would disappear and so on, until the total beam current used would have discharged the brightest image. This technique provides an accurate calibration of brightness and avoids the laborious film reading techniques of the past.

It is of little use in an aerospace surveillance system since a relatively long time is spent in reading out and getting the I. O. target image discharged; thus, moving objects would be missed completely. For the latter case, one simply uses more beam current and thus accomplishes the target image discharge in one or two scan cycles set by the requirements of object movement. Every object is still read out, but the intensity gradient is less and thus the relative brightness is not easily measured; the beam current is higher so the weaker targets are harder to distinguish due to the higher beam (shot) noise. For most aerospace problems, the trade will probably be between one, two, three or four scan readout cycles, depending on the application.

The trade of one vs two or more scan readouts per exposure of photocathode may be set by the film being used to photograph the monitor. Two scans of lower beam have, in theory, the same performance of one scan of high beam as far as signal detection is concerned (the lower shot beam noise of two scans equals the higher noise of one scan), but two scans will give more monitor integrated light energy for the recording film. (For pulsing, the eye would not be expected to be used, especially for integration periods longer than 1/5th sec) because the time between readouts accentuates the flashing readouts to the eye viewer.

g. Sensitivity to Moving Point Targets

Sensitivity to moving point targets creates a problem, in that sensitivity seems to have been lost. Actually no sensitivity has been lost at all! This depends on how sensitivity is defined. The performance is set by the integrated effect of source energy (its strength and the length of time the source energy can charge a single or adjacent resolution element) coupled with the I.O. target response time at that light level plus monitor and eye or film integration time. Thus, for very slow or stationary sources, the performance is set by the accumulated integration time within the system (1/5th second eye integration or readout system integration time if not a human eye). With faster moving targets, the composite integration time (charge accumulated per I. O. scan cycle × number of scans integrated) is progressively less until little or no accumulated charge exists for integration. The response times for the I.O. "Target" (sensing surface) to reach steady state readout are about .050 sec for moderate light levels to about 0.3 or 0.4 seconds for the low light detection limit sensitivity.

When using large f/ratio optics, continuous operation viewing a star field with no photocathode integration sometimes gives erroneous conclusions. The

faintest star that can be detected with the eye integration time of 0.2 seconds sometimes takes more than 0.2 seconds to appear on the monitor when the lens is uncapped or the optics is moved to a new field of view. This means the effective integration time for minimum detection intensity can be greater than the eye integration time and the sensitivity for this low intensity is decreased, due to the increased integration time required for detection. The cause of this increased integration is the non-linear beam landing characteristic; if the photocathode intensity in one area is low, with an associated slightly positive target voltage, not much beam current will land and this area will have a larger target voltage for the second scan, which will cause more target "landing" current, and this "bootstrapping" increase of target voltage char in the "dark" area will increase for a non-moving target until an equilibrium exists between the photocathode current positive charge (due to secondary emission) and the negative charge left by the scanning beam. This time to reach equilibrium, the "time constant" of beam landing, has to be considered with low intensity moving objects. The only way to decrease this effect is to add a uniform photocathode illumination (use a faster optics to collect more sky background) or make the scanning beam monochromatic. Unless the sky background is very dark, experience has shown that an f/1.0 optics will collect enough background to make the "time constant" of eye detectable objects 0.2 seconds or less.

Accumulated charge - integration time curves or loss of sensitivity vs rate can be drawn for various conditions with different ordinates. But since each case should be checked specifically, we have avoided general curves with their numerous exceptions and variances from system to system.

h. Image Size (Point Source) - Target Spreading

The size of an image of point source reproduced by an I.O. tube and equipment depends on the intensity of the source. The minimum size of an image is generally two or three scan lines; though occasionally, if excellent lens quality and best focus of the lens and I.O. tube are combined with stable conditions of atmospheric seeing, a detected image size of 1 line can be achieved.

Except for the faintest (or nearly faintest) images, the beam will supply maximum target change as it crosses an image; therefore, the image grows or spreads until it is large enough for the maximum beam landing current, integrated over this size, to discharge it and maintain a steady state condition. Thus, except in the case of the faintest image, there is little recognizable beam intensity modulation (as was the case of distributed scenes defining grey levels) but rather simply pulse width modulation. This leads to use of various noise reduction schemes, such as pulse width discriminators, reduction of bandwidth, and line to line correlation schemes.

The extent of the image size versus intensity varies with the settings of the I.O. target bias voltage and beam current determining the actual slope. Typical values of image size in terms of number of scan lines are 2 lines plus 1 to 1-1/2 lines per stellar magnitude less than the minimum detectable magnitude. (The 1 to 1-1/2 variation can be controlled by beam and target settings as noted.) The extent of field occupancy is set by totaling the number of stars of each magnitude times the spreading at that magnitude, from the detection limit magnitude and all smaller magnitudes. For a 16th magnitude detection limit about 5 to 20% of a $3^{o} \times 3^{o}$ field of view will be unavailable for target detection, because of image spread. The 5% to 20% variation depends on the portion of the sky that is viewed.

Typical capability for handling a wide range of intensities by variation of target and beam settings is clearly illustrated in Figure II-37 when 15th-16th Magnitude Nebula light is clearly evident and the 4th magnitude stars are not overly large (in fact as displayed with less spreading than in Figure II-36 where only 13th mag sensitivity is being attained but with different target and beam setting).

i. Image Orthicon Focus Requirements

It can be shown from the detection analysis of star images that good focus is required for best detection. This is easily seen when adjusting an image orthicon chain: nothing can be seen until optical focus, image focus (photocathode to target), and scanning beam focus (magnetic external and electrostatic internal) are very close to their correct values.

Most of the measurement work on the variation of detection with focus has used spread object test charts, where detection has been evaluated by plotting the change of aperture response with focus. Aperture response is the relative spacial frequency transfer characteristic of an image tube electrical output using a variable spacial frequency, constant light intensity, repetitive pattern optical input. It shows how the equivalent beam modulation is changed (decreased) by a decrease of image size (increase of spacial frequency), which makes detection more difficult. A 10% loss of aperture response will result in a 10% loss of spread object detection. A 10% loss of aperture response will result in some loss of point object detection; but the exact loss is not a direct function of aperture response. A typical Sine Wave image response is shown in Figure II-38.

To achieve good optical focus the image orthicon and optics have to be rigidly mounted so there is no relative movement between them. Table 5 shows the voltage and current regulation required to guarantee a maximum aperture loss of 10%, using a standard TV scan and evaluating the aperture response at an equivalent frequency of 5 Mc (400 TV lines).

Table 5. Required Focus Regulation.

Variable	% Regulation for 10% Loss of Aperture Response at 400 TV Lines
$\frac{\text{Photocathode}}{\text{Image}}\left(\frac{V_{PC}}{V_{G6}}\right)$ Ratio	1%
Magnetic Beam Focus Current	0.1%
Electrostatic Beam Focus (V_{G4})	0.2%

One other focus detection loss is due to the interaction of the time varying magnetic fields, used to deflect the scanning beam, with the stream of photoelectrons that makes the target image. This interaction causes image defocusing. The improved magnetic shielding of new "color TV" image orthicon yokes give an aperture response improvement of 40% at 400 TV lines frequency (5 Mc).

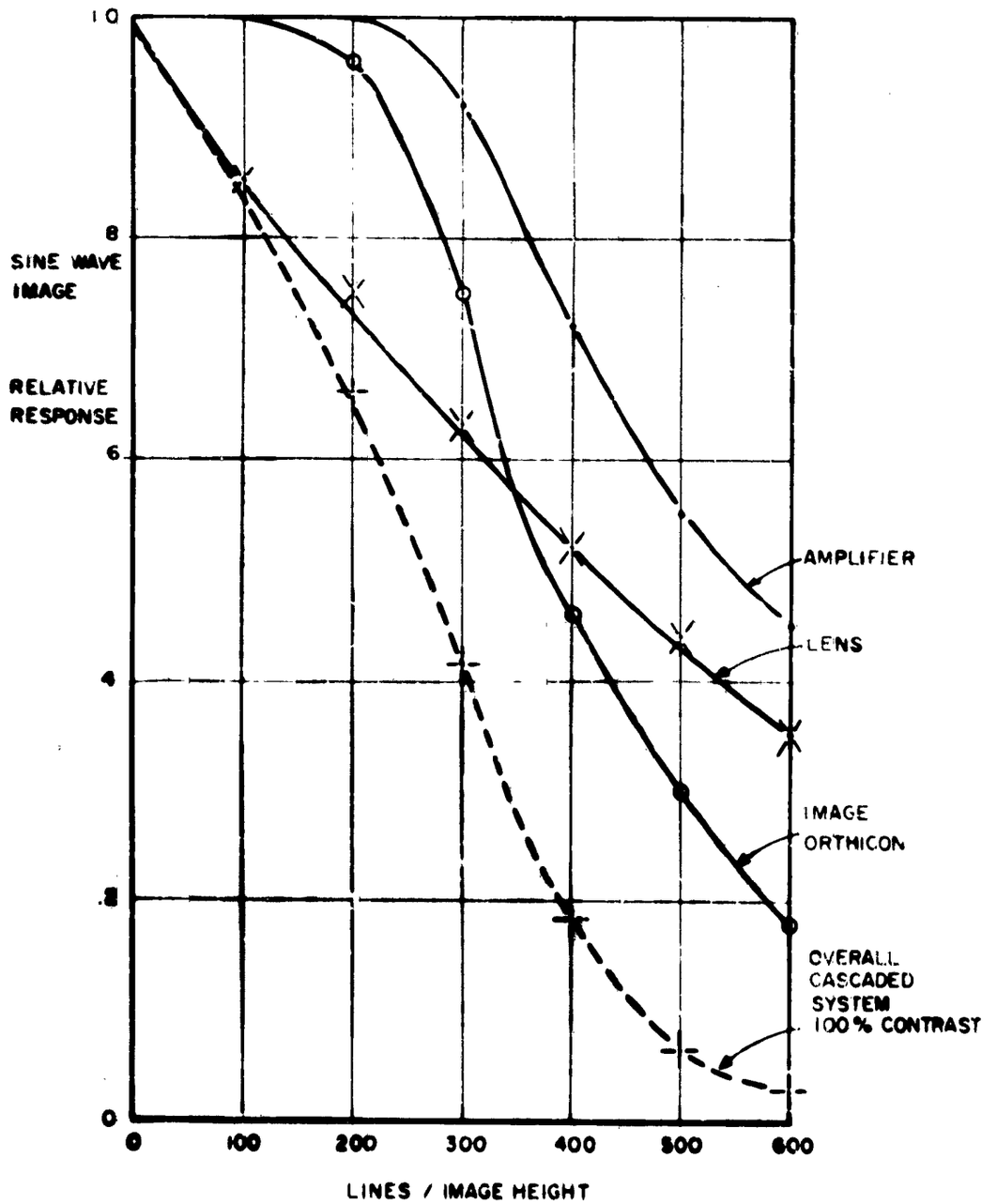


Figure II-38. Sine Wave Response of Cascaded Electro Optical System

j. Interlaced Versus Non-Interlaced Scanning

The question of interlaced versus non-interlaced equipment scanning involves several choices. Both, in theory, will perform equally as to sensitivity, resolution, etc. However, due to spreading, stability, and circuit linearity, non-interlaced scanning will be more satisfactory and practical for research and experimental work -- especially, if image cancellation and similar techniques, where linearity is to be a factor, are to be studied. Some flicker will be apparent if using a P-4 phospor monitor tube. However, from experience at the Schenectady Observatory, it is not objectionable and is offset by its advantages in selecting film recording equipment. Practically the only reason to use an interlaced scan is to tie in with a commercial TV network or to use unmodified commercial monitors!

k. Under Scan - Electronic Zooming

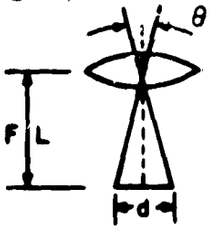
Underscanning is a form of electronic zooming; i.e., we can scan less than the usable area of the I.O. target and display area scanned on the full monitor view. By varying the amount of area actually scanned, we have electronic zooming. Underscanning, for long periods, will not harm thin film MgO I.O tubes (this is not true for glass target I.O.'s). The resolution/sensitivity, of course, changes as explained in earlier paragraphs, but normally with sufficiently lighted scenes, the full advantage of 2 to 1, or even 3 to 1, zooming, can be realized provided light level or exposure time is properly adjusted. Figures II-33A & B illustrates 4 to 1 underscan while looking at Jupiter and its four principal moons.

l. Field of View (angular)

The total angular field of view of a lens system with a given focal length is limited by the required corrections of the lens aberrations, which thus determines the useful sensor element size (frame size in case of camera film detector surface or photocathode size, in case of electrical sensors). Thus aberrations and poor definition are introduced if larger fields than the designer planned are attempted with the same lens.

The calculation of field of view is based on focal length and dimensions of the sensor size, with the assumption that the lens is corrected for the size selected (less than maximum size specified by the designer).

$$\theta = 2 \tan^{-1} \frac{d}{2FL}$$



If we avoid large fields of view (where the arc tangent varies from linear conversions) we can use the simplified expression: the angular field of view in radians per unit length of sensor surface is equal to the inverse of the focal length. Converting to degrees this becomes

$$\theta \text{ (degrees)} = \frac{57.3xd \text{ (inches)}}{\text{focal length (inches)}}$$

For 1.55" diagonal photocathode surface of the 3" Image Orthicon this becomes

$$\theta = \frac{57.3 \times 1.55}{FL} = \frac{89}{FL} \text{ (inches)} \quad \text{diagonal degrees}$$

This is plotted in Figures II-39A and B.

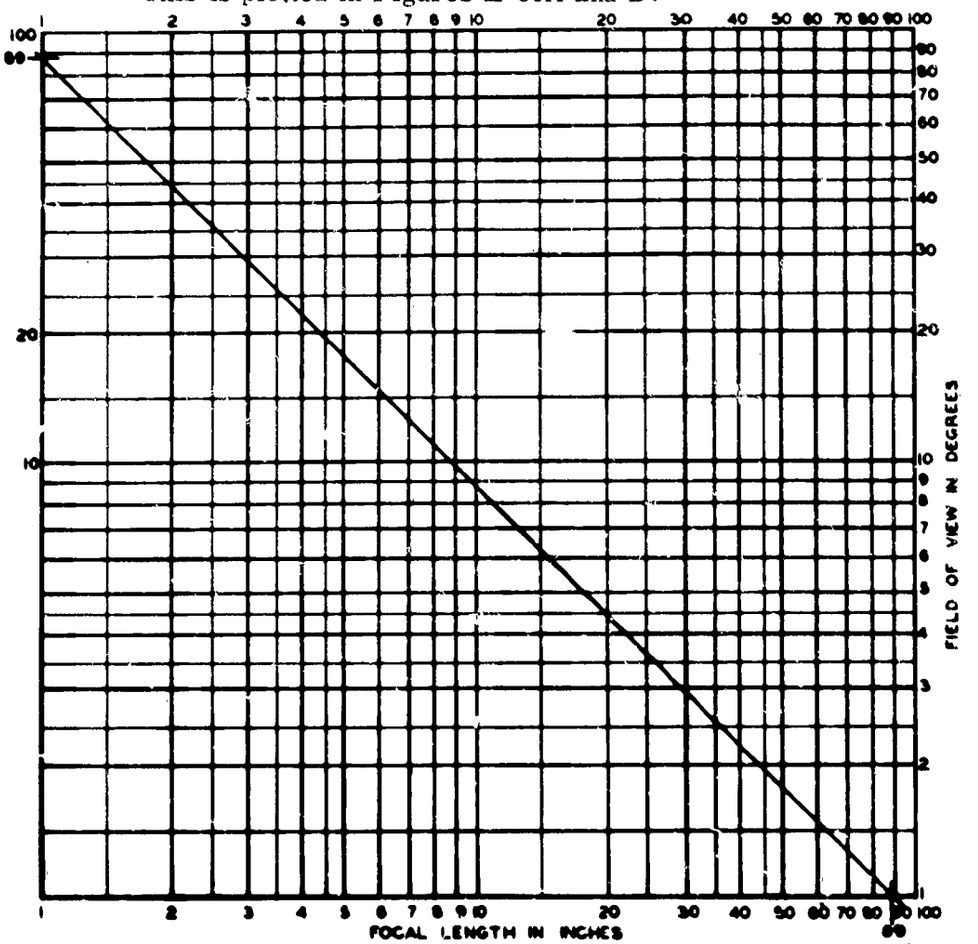


Figure II-39A. Field of View vs Focal Length, Short and Medium Focal Lengths (1 to 100 inches); Max (1.55°) Effective Diagonal On Photocathode; Multiply by .707 for Square Raster; Multiply by .6 and .8 for 3 ×4 Aspect Ratio for 3" MgO Orthicon Normal Scan

m. Fiber Optics Faceplate Tubes

G.E. has a group of Fiber Optics faceplate tubes for those applications requiring the focus plane at the external surface. The fiber bundle limits resolution to approximately 870 TV lines per inch of photocathode, and limits the input area to 1.5 inch diameter.

Use of a Fiber Optic coupling system avoids some of the losses inherent in conventional Optical Lens coupling and provides a new flexibility with the optics. Whenever a camera tube can be closely coupled with the object to be viewed, a fiber optic faceplate tube should be considered as the optics may be simplified or

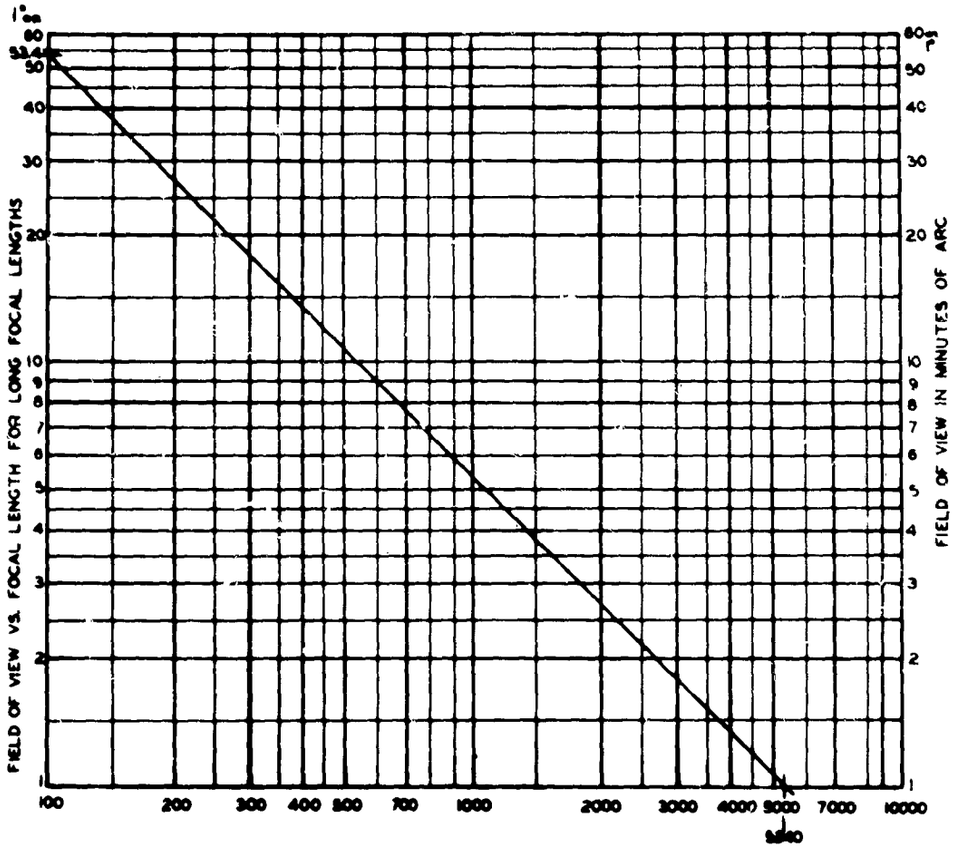


Figure II-39B. Field of View vs Focal Length, Short and Medium Focal Lengths (1 to 100 inches); Max (1.55°) Effective Diagonal On Photocathode; Multiply by .707 for Square Raster; Multiply by .6 and .8 for 3 × 4 Aspect Ratio for 3" MgO Orthicon Normal Scan

even eliminated in some cases. Applications include devices with fiber optic type outputs, such as flexible fiberscopes, intensifier tube coupling, radiation scintillators, and complex fused fiber optic shapes. Other applications include front surface reading such as photograph film or printing in close contact to the faceplate without any lens system.

n. Scanning Period - Bandwidth

The choice of scanning period varies with application. If viewing a monitor is of utmost concern then the time honored 1/30 sec interlaced scan of commercial TV is hard to beat. In military applications, viewing is generally only a "monitoring" procedure and can be provided by special means, in order that the scanning period and format can be tailored to the system integration time requirements. For instance; if the integration period is 1/2 sec a non-interlaced raster (even with a large number of lines) will still keep bandwidth requirements low. Additionally slower scanning means less target spreading (physical area) hence higher resolution for separating objects, and less total field occupancy, therefore, a higher probability of detection since more time and space is available to find the target of interest.

Bandwidth is generally selected so that horizontal resolution is equal or more than the vertical line resolution.

Resolution is not always a function of bandwidth. It may be, as mentioned earlier, limited by the I. O. photocathode resolution, the I.O. target, the I.O. beam diameter, or the monitoring tube (beam or phosphor size) if this is the readout, or input-limited by the atmosphere or lens resolution.

b. Video Processing Techniques

The primary concern of video processing is to extract useful information by a combination of equipment and techniques and present it for viewing or data processing.

The output of the sensing device is generally amplified with circuits designed especially for emphasizing and/or extracting various features and detail information. The type and extent of video processing applied depends largely on the application.

Ordinary TV and industrial TV distributed scene viewing usually needs: good grey scale, low noise, high and low frequency peaking, gamma correction, aperture correction, horizontal and vertical shading, in addition to the usual brightness and contrast control.

Detection of objects in a celestial environment does not need grey scale but rather high sensitivity (low noise - high gain), high and low frequency peaking "contrast enhancement" techniques, especially when using higher f/number reflecting optics. Horizontal and vertical shading is generally not needed as tube uniformity is generally good and thus can be illuminated to keep circuit noise and pick up problems to a minimum. Some cloud discrimination is possible with proper video processing.

High resolution of objects, lunar scene viewing and mapping, missile launch monitoring, etc., requires higher resolution, more TV lines and slower scanning to minimize bandwidth requirements, high sensitivity (low noise - high gain), adjustable high and low frequency peaking and in some cases extensive use of "contrast enhancement" techniques.

Moving target identification involves a combination of many processing techniques to cover the host of conditions imposed by varying target rates and sky background conditions. Monitoring for eye viewing requires reasonable scan frame rates (similar to commercial TV but not necessarily as fast). Non-interlace does give flicker, but this is not objectionable for monitoring only purposes. When slower frame rates are used the longer persistant phosphors such as P-7 should be used to ease the strain on the operator's eyes; for very slow rate use memory display tubes or film read out.

The P-7 does not, as commonly believed, limit the resolution attainable for viewing. We have been operating a P-4 and P-7 monitor side by side for over a year (including photographing) with similar (800 line) resolution attained on both.

1. Monitor Recording

Film recording of information displayed on a CRT Oscilloscope or TV type monitor are much the same except of the size of viewing tube. Where serious recording is intended the 5" CRT and scope camera should be used, as higher resolution tubes and greater precision is generally available as well as more phosphors. Besides matching tube and film, the rates and periods as well as other details of the application are important if satisfactory results are to be expected.

The characteristics of tube and application include

1. Sweep or writing rates, recycling period, no of scans to be filmed, per film picture.
2. Spot size of the writing trace.
3. The decay rate of the CRT phosphor.
4. Brightness and contrast in CRT picture (beam current and voltage of CR Tube).
5. Spectral emittance of the phosphor used in the CRT screen.

The film characteristics include:

1. Film spectral sensitivity.
2. Film speed.
3. Reciprocity and other exposure characteristics.
4. Graininess and transfer characteristics.
5. Contrast and density range (grey scale).
6. Developing and printing procedures.

The final selection should be checked with actual tests for practical and satisfying results.

Table I summarizes the most common phosphors used for photographic recording and Tables II and III show the relative speeds of different phosphor-film combinations, with different developing times. From the above note that a P-11 CRT with Photoflure (green) Cineflure or Linagraph ortho are very good for fast work; Tri X for ormal work and Photoflure (blue) for very fast. For more details refer to Kodak Data Book #P-37 on films for CRT Recording (available thru Kodak dealers).

2. Standard and Non-Standard I.O. Chain Processing

For the purposes of this section some of the various processing techniques are defined and briefly outlined. It is not the intention here to develop design details but rather to serve as an introduction to the possibilities of processing. The application section deals with some of the combinations of features needed for specific requirements and the trades to be made.

Tab

Screen Type	Persist-ence	Decay Time* (In Micro-Seconds)	Fluore-cence
P4	Medium or medium-short	112 14,000	White
P11	Short	30	Blue
P15	Extremely short	1.7	Blue-g and ne ultravi
P16	Extremely short	0.1	Violet near-u violet
P24	Extremely short	2.5	Light g

*Decay time of a cathode-ray tube phosph full value to 1/e (36.8 percent) of the full intensity to fall to 10 percent of the full

hosphor Characteristics

Phospho-rescence	Wave-Length of Peak Radiant Energy	Applications	Remarks
White or blue-white	4500 Å 5800 Å	Television picture tubes	Some P4 fluorescent powders are available with a silica coating for burn resistance.
Blue	4550 Å	Special oscilloscope for photographic recording	Produces a brilliant actinic spot. Widely used for photographic recording.
Blue-green and near-ultraviolet	5100 Å	Flying-spot scanners or special oscilloscopes	Helpful for high-resolution, high-frequency, continuous-motion recording. Not as actinic as P11.
Violet and near-ultraviolet	3800 Å	Flying-spot scanners	Has stable exponential decay.
Light green	4900 Å	Color flying-spot scanners	

ually measured as the time it takes for t e light intensity to fall from its
Sometimes, however, it is measured a the time required for the light
The decay times given in this table are t 1/e of the full value.

Table II. Relative CRT Speeds* of Kodak Films

Normal Development: 4 minutes in Kodak Developer D-19 at 68 F (20 C)

Phosphor	P11	P4	P15	P16	P24
Photoflure, Blue Sensitive	2400	180	60	200	83
Photoflure, Green Sensitive	1800	500	250	130	240
Cineflure	1800	500	250	130	240
Linagraph Ortho	1800	500	250	130	240
Royal Ortho (sheet)	1000	250	130	80	130
Linagraph Pan	900	320	120	82	120
Tri-X Negative	900	320	120	82	120
Linagraph Shellburst	500	180	60	48	73
Eastman High Speed Positive, Type 5305	360	51	25	45	28
Royal-X Pan Recording**	320	150	65	23	47
Eastman Television Recording, Type 5374 and Type 7374	100	11	5.2	7.5	5.2
Eastman Fine Grain Release Positive, Type 5302 and Type 7302	35	4	2	6	2
Kodalith Ortho, Type 3	32	5	[illegible]	5	8
High Contrast Copy	20	12	6	4	5

*Measured at a density of 1.0 (net) and relative to the speed of 100 assigned to Eastman Television Recording Film, Type 5374, when exposed to a P-11 phosphor and developed in Kodak Developer D-19 for 4 minutes at 68 F (20 C).

**A greater speed advantage will be realized if Kodak Developer DK-50 is used.

Table III. Relative CRT Speeds* of Kodak Films

Extended Development: 15 minutes in Kodak Developer D-19 at 68 F)

Phosphor	P11	P16	P24
Royal-X Pan Recording	6300	600	1200
Photoflure, Blue Sensitive	5400	500	220
Cineflure	4100	250	360
Linagraph Ortho	4100	250	360
Royal Ortho (sheet)	3900	220	400
Tri-X Negative	2600	200	370
Linagraph Pan	2600	200	370
Linagraph Shellburst	2400	190	260
Eastman High Speed Positive	630	82	25
Eastman Television Recording, Type 5374 and Type 7374	250	19	14

*Measured at a density of 1.0 (net) and relative to the speed of 100 assigned to Eastman Television Recording Film, Type 5374, when exposed to a P-11 phosphor and developed in Kodak Developer D-19 for 4 minutes at 68 F.

a. Aperture Correction

Aperture correction is used to accentuate rapid transitions from black to white or white to black. It helps to sharpen the picture. It is accomplished by providing an increase in gain with increase in frequency (usually 0.3 db or 0.6 db/mc).

b. High and Low Frequency Peaking

Low frequency - high frequency peaking is used to obtain a video amplifier with a flat response over wider frequency range than would be obtained in a straight video amplifier.

Often the peaking is adjustable to permit variations such as over peaking the lows and/or highs (usually the high as the latter accomplishes in part a modified form of aperture correction).

c. Gamma Correction

Gamma correction is used to correct black compression in the monitor picture tube (monitor). It is used where scene viewing (studio and outdoor sports) displayed on a picture tube is the prime concern as in commercial TV and industrial TV. It is of questionable value in low light level military scene application and is not needed for applications involving point sources (celestial background, etc.).

d. Shading

Horizontal and Vertical - is primarily needed where non-uniform image orthicons are useful. It is useful only if the non-uniformity increases (or decreases) linearly from left-to-right, up-to-down when only sawtooth shading is available. Scene non-uniformity or tube non-uniformity not varying nearly linearly or on a simple sawtooth curve would require too many versions of circuitry to be practical and is thus not used. The uniformity of the G. E. thin film MgO I. O. tubes is generally excellent and thus good electronics are used shading circuitry can be eliminated for nearly all applications. (For studio work it is also used to correct for non-uniform lighting.) Elimination means much less chance of unnecessary pick up and noise being added in the video circuits.

e. Scene A. G. C.

Automatic Gain Control feedback in the video amplifier can be used for two purposes. The first is to control video gain to reduce chance of video saturation on larger signals. The second allows correction for poor (variable) shading where signal level is involved. The choice of filtering in the feedback or control function is optimized to the type and extent of correction desired. Generally slow in relation to bandwidth but faster than a single line of scan (perhaps 1/10 to 1/3 of scanning frequency).

f. Iris Control

Thin film MgO Image Orthicons can handle (without adjustment) from 10,000 to 100,000 light intensity range without serious effects, provided the

electronic chain is not limiting the performance. Where light ranges greater than this are to be encountered then some form of iris control of the lens or optical portion of the system should be provided. This can be manually set or automatically controlled. In the latter case the automatic control signal may be developed from separate detection sources (light meter type operation) or by monitoring the image section of the I.O. and using this as a means of iris control. Iris control can also be accomplished by short pulsing the I.O. photocathode and thus eliminating the lens iris and associated control. See Section II-C-1-a-5-e.

g. Underscanning

Underscanning the I.O. target has been discussed in Section II-C-1-a-5-k on I.O. operation. In summary it provides a form of zooming, that is, only a portion of the total scene is scanned and displayed on the full monitor viewing area, thus presenting a "close-up" of that portion of the scene. Since the G.E. thin film MgO I.O. tubes have a high resolution capability (2000 lines or more) a three or four to 1 underscan is possible with an apparent gain of resolution, using 525 to 1029 line scanning. (This of course is only true if the optics, scene, brightness and/or the atmosphere or environment, has the extended resolution capability.) The MgO tubes can be underscanned for reasonably long periods without damage or permanent "picture framing" (though sometimes it will take a few minutes before the effect disappears depending on the extent of the after image effect on the particular tube in use). With underscanning in a celestial background the beam current should be reset to maintain maximum performance.

h. Overscanning

Overscanning the I.O. tube is generally done for one of two reasons - The first, as an aid in equipment set up, adjustment, etc. The second; to have fewer scan lines which may result in improved resolution sensitivity with very low light levels.

3) Video Processing of Point Objects

The analysis of detection or image signal to noise ratio compared to electrical signal-to-noise ratio shows that an electrical signal to noise ratio equal to the detection signal to noise ratio can be achieved if:

1. X lines of point image spread are added by RF or video delay lines.
2. X resolution elements are added by a suitable decrease of video bandwidth.
3. K scans equal to the image integration time are added with perfect registration between individual scan images.

It is difficult to add X lines of video information without some bandwidth loss and variable delay misregistration. The signal processing techniques of radar (VICI, etc.) can be used with increased system complexity, including a frequency transfer of video to some video modulated RF frequency and a determination of horizontal scan frequency from the RF circulation line delay. The value of X (number of circulations or number of video delay lines) is usually determined by the line spread of the minimum detectable signal. And this line spread is a function of the beam current adjustment and the background intensity of the specific field of view. Usually X is assumed to be 2 or 3 for the minimum detectable signal.

The technique of resolution element addition by decreasing bandwidth can be easily accomplished, and has been proven effective when using a storage tube temporary catalog of a star field.

The integration of K scans can be accomplished, in theory, by target charge integration or pulsing. In other words, a single scan readoff at the target charge pattern after a non-scanned photocathode-on interval of 0.2 seconds (K of 6 for 1/30 second scan) should result in the same image detection as continuous operation of the image orthicon with eye detection using monitor viewing. There are limits of integration time, sky intensity, and optics diameters and focal lengths that cannot be exceeded because of excessive target charge "clipping".

One method of overcoming the scan integration problem is to add successive scans on a storage tube in the "write" mode, and "readoff" the integrated total of a number of scans.

An equipment problem that the eye automatically solves is "stationary" noise, or flat field nonuniformities of electrical output. Since these nonuniformities are stationary or repeat from scan to scan, one method of getting rid of them is to write the electrical scanned output of a uniform illumination input on a storage tube, and subtract the storage tube readoff signal from succeeding scanned outputs of an image, on a point by point basis. This results in an increased system complexity.

Another method of cancelling stationary noise is indirect in theory but does not result in increased system complexity: most stationary noise is equivalent to a large image size with low equivalent video frequencies, and surveillance systems require electronic detection using peak detectors, so a peak detector designed to work on bandpass video could accomplish most of the "stationary noise" processing the eye does. This peak detector would look at video that has already passed through a bandpass filter, or it would have a detection threshold that would follow low frequency variations.

4) Noise Spectrum

An image orthicon is usually considered a very high output impedance current generator, with a 10pf to 20pf capacity to ground output impedance. The two methods used for achieving an overall flat frequency response both use a large 100K load resistor as the preamplifier load resistance, followed by (1) peaking circuits that give a rising voltage gain versus frequency past the input RC cutoff frequency, or (2) to use feedback to effectively decrease the equivalent resistance of the 100K input resistor. In either method, the amplifier noise spectrum with zero beam current, at a point where the overall signal frequency response is flat, will not be flat Gaussian noise. The rms noise per cycle will be greater at the high end of the overall video bandwidth, than at the low frequency end. If the image orthicon beam current is increased until the complete video bandwidth noise is due to beam current, the noise spectrum will be flat. A fairly good method of evaluating a specific image orthicon premaplifier is to find the output annode DC beam current required to increase the preamp noise by 50%. The better the preamp, the lower the required output annode current for beam noise equal to amplifier noise. Unfortunately, the beam noise versus DC output current, and output capacity, etc., of image orthi cons vary enough so the same I.O. tube has to be used to evaluate preamps.

To restate the effect of noise on eye image detection: when viewing a "medium" spacial frequency repetitive pattern or point object, only the noise in

the same spacial frequency region is effective in masking the signal. So for flat spectrum noise, the important variable is rms noise per unit bandwidth, and the viewing eye is then considered a "bandpass" device. So the amplifier noise level in the spacial frequency region of interest is more important than the overall video bandwidth amplifier noise. And just as the eye adjusts to view objects of a specific desired size, the electronic processing before peak detection can use a bandpass filter to look for objects of a specific desired bandwidth.

5) Image Intensifier Orthicon.

The image intensifier orthicon (I^2O) incorporates an image intensifier section ahead of the conventional image orthicon. The intention is to get the sensitivity of the image converter with the advantages of image orthicon - electrical (scanned) output!

The published curves of low light level performance of the presently available I^2O S-20 tubes show that the best tubes require about 1/4th (300 line resolution) to 1/10th (100 line resolution) of the scene illumination necessary for equivalent performance of the thin film I.O.'s. Thus, for low light level surface scene surveillance not requiring more than 400 line resolution, the I^2O has a definite sensitivity advantage, though the circuitry is more extensive.

In its presently available form, the I^2O is limited to 400 lines resolution. Thus, it may be background limited because of increased resolution element size. Also, the resolution ability to separate point sources is limited to this 400 line resolution. For these reasons the I^2O requires a large focal length optics

Summing the differences:

1. Photocathode area is greater for I^2O (requires more glass for same f/ratio)
2. Less beam landing problems (has more pre-"target" light amplification).
3. I^2O has more scatter; therefore, less contrast.
4. From Parton[10]: measurements for less than 400 resolution lines/picture width -
   a. No object movement: scene intensity needed for I^2O is approx. 1/10th intensity needed by I.O. for given line resolution.
   b. With object movement: intensity I^2O approx. 1/10 to 1/100 intensity I.O. for given line resolution (this due to 2 above).
5. I^2O limited to 400 line resolution plus an additional reduction in the corners.
6. Requires long focal length lens (with associated small field of view) to limit the celestial background per resolution element.
7. The I^2O is subject to blooming and therefore further loses its appeal.

2. CATALOG IMAGE STORAGE

All separation techniques that use single site relative movement between a target and the celestial background require some method of image storage. Some operating problems and theory of operation are discussed; for electronic scanned storage tubes, astronomical film, and electronic tape recording.

a. Electrostatic Storage Tube

This general description of operation of an electrostatic image storage tube with direct electronic readout uses the Raytheon QK-685 as a model. The theory of operation would apply in general to other manufacturers electrostatic storage tubes. A more detailed reference is Raytheon Technical Information Bulletin Number 142-I, "A Survey of Recording Storage Tube Types" by Alvin S. Luftman.

Figure II-40 shows, schematically, the arrangement of the storage screen and collector electrodes of the storage tube. The storage screen is a fine metal mesh of about 1000 lines per inch. The side of the mesh facing away from the collector plate, and toward which the electron beam is directed, is coated with a dielectric material having a maximum secondary emission ratio considerably greater than unity. Figure II-41 is the secondary emission curve of a typical material of this nature.

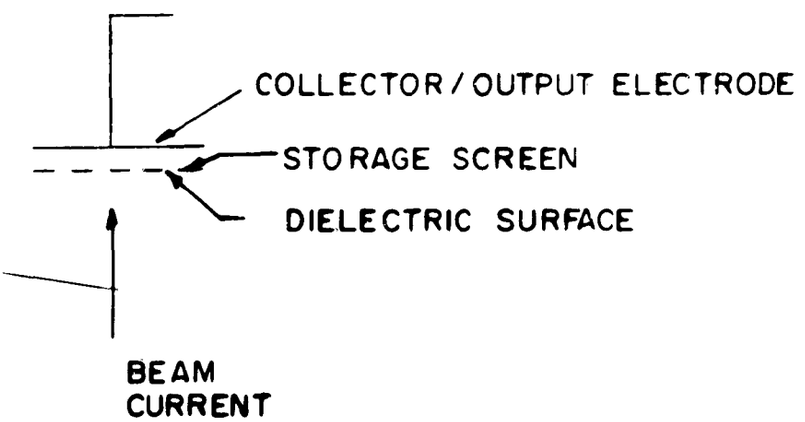


Figure II-40. Basic Storage Tube Electrode Arrangement

Now if the electron beam is allowed to strike the dielectric surface at a potential less than the critical value V_c, the secondary emission ratio will be less than unity; that is, the rate at which secondary electrons leave the dielectric surface is less than the arrival rate of those in the primary electron beam. This charges the surface of the dielectric in a negative direction, approaching cathode potential as a limit. As long as the dielectric surface is maintained at a potential higher than V_c, however, secondaries are emitted at a higher rate than the primaries arrive, so the surface charges in a positive direction. On this basis, we can explain the various operating modes of the tube; see Figure II-42.

In the "prime" mode of operation, the storage screen is connected to a potential of about 20 volts, positive with respect to cathode. This is below the critical potential, so the dielectric surface charges in the negative direction until it

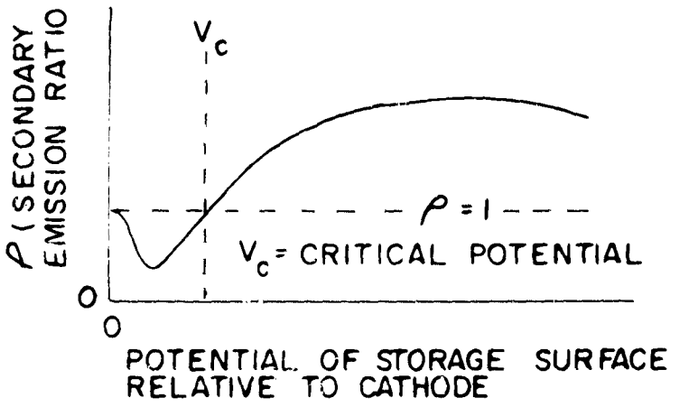


Figure II-41. Typical Secondary Emission Curve

reaches zero volts, i.e., cathode potential. A relatively large beam current (50 μa) is used to minimize the time required to reach equilibrium. Note that the dielectric surface is now 20 volts negative with respect to the storage screen mesh.

BEAM CURRENT	MODE	STORAGE SCREEN	DIELECTRIC SURFACE
50 μa	PRIME	20 V	20 V ↓ 0 V
1.5 μa	WRITE	300 V	280 V ↓ 285 V
10 μa	READ	15 V	-5 V ↓ 0 V

Figure II-42. Storage Tube Operating Modes

Switching the storage screen mesh potential to +300 volts with respect to cathode places the tube in the "write" mode. The dielectric surface is now at +280 volts with respect to cathode, which is near the maximum of the secondary emission curve. The electron gun bias is switched nearly to cutoff and the video input signal is adjusted to provide an average current of a few microamperes in the writing beam. The surface of the dielectric is charged in the positive direction, more or less, depending upon the video signal amplitude. The maximum highlight areas correspond to about a five-volt increase in storage surface potential. After writing,

then, the highlight areas of the surface are at a maximum of +285 volts while the black areas remain at +280 volts.

To read out the stored information, the storage screen mesh potential is dropped to about 15 volts. This puts the maximum highlight areas at zero volts and the black areas at -5 volts. The apertures in the storage screen mesh now serve to modulate the readout beam (about 10 μa) as it swept by; that is, in regions of zero storage surface potential, maximum beam current passes through to the collector while beam current is cut off in regions of -5 volt potential. It is seen then that video output signal current is produced in the collector circuit; maximum current corresponding to white, zero current to black.

Of course, in order for the operation to take place as just described, there must always be maintained on the beam side of the storage screen an accelerating field for the emitted secondary electrons, so that they will be drawn away from the storage surface. If, as shown in Figure 1, no other electrode is present between the electron gun and the storage screen, such an accelerating field would be provided by the electron gun anode which operates at +3500 V. The QK-685, however, is provided with an electrostatic lens system following deflection and preceding the storage screen. (See Figure II-43 for detail drawing). The purpose of this system, consisting of two cylindrical Aquadag bands (L1 & L2) inside the large diameter portion of the glass tube envelope and a mesh electrode (decelerator) preceding the storage screen, is to bend the electron paths subsequent to deflection so they are normal to the storage screen. This results in more uniform storage screen operation at the expense of some deflection-defocusing of the beam. The decelerator electrode is normally operated at +760 V. Since this is higher than the storage screen potential during prime, write or read, the necessary secondary electron accelerating field is always present during these modes.

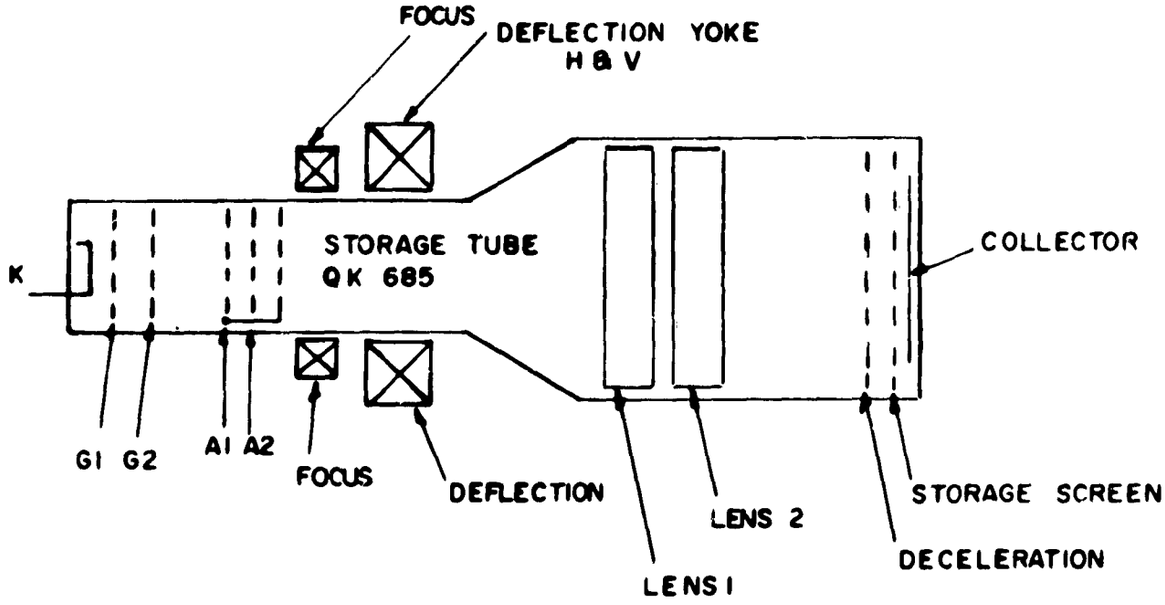


Figure II-43.

The inclusion of the decelerator electrode, in addition, makes possible a fourth operating mode (called the "erase" mode) following the read mode and preceding prime. In this case, the storage screen mesh is connected to the decelerator potential and beam current is the same as for the prime mode. Since the primary electron energy (+760V) is still above critical potential, all areas of the dielectric surface are rapidly brought to equilibrium with the decelerator and the storage screen mesh; that is, the storage screen surface potential is brought to zero with respect to the mesh. Complete and rapid erasure is thus attained, and the time required to reprime the storage surface is minimized.

One operating parameter that is very important when evaluating storage tubes is the time required for erasing and priming. For instance, the minimum time between the last non-destructive electronic readout of the stored image "a" and the start of writing image "b" is approximately one second for the QK-685.

One use of the storage tube, other than time storage of an image for separation due to relative movement of target and star background, is image integration of a number of scans to give a signal to noise ratio improvement. This integration can be accomplished with either analog (gray scale) or digital (on-off) video, writing-on a number of scans, before reading-off the integrated sum of scans. It is necessary to make sure that the dynamic range of the storage screen mesh is not exceeded; if the maximum highlight "white" area of the screen is limited to plus 5 volts in respect to the "black" screen charge, and 5 scans are to be integrated, then the average cathode current and PG1 modulating voltage have to be limited so no area of the screen is charged positive more than 1 volt per scan. This limiting is more easily accomplished with digital on-off video.

b. Astronomical Film

The following discussion of astronomical film is brief; for a more detailed discussion Kodak has a handbook P-9 " Kodak Plates And Films For Science And Industry."

For celestial work, Astronomical Plate Film Type 103a- ( ) is used almost exclusively. It is relatively slow (faster than Type 103) but offers good "reciprocity"; that is, a linear trade of exposure (intensity) for time and vice versa is possible over a wide range.

A summary of the characteristics of Astronomical Film and other photographic constants follow:

Kodak Astronomical Film 103a-( ) is available in the following:

Spectroscopic Sensitizing Classes

103a-O 2500 to 5000Å;	Especially Valuable and nearly flat	from 2500 to 4600Å
103a-J 2500 to 5500Å;	Especially Valuable and nearly flat	from 4500 to 5500Å
103a-G 2500 to 6000Å;	Especially Valuable and nearly flat	from 4500 to 5700Å

Spectroscopic Sensitizing Classes

103a-D 2500 to 6500Å;	Especially Valuable and nearly flat	from 4500 to 6200Å
103a-E 2500 to 6900Å;	Especially Valuable and nearly flat	from 5500 to 6600Å
103a-F 2500 to 6900Å;	Especially Valuable and nearly flat	from 4500 to 6800Å
103a-U 2500 to 5000 & 6500-7600Å;	Especially Valuable and nearly flat	from 6700 to 7400Å

Further data Type 103a-O (fast Blue Sensitive Plates)

Illumination flux per unit photographic density at 4300Å Radiation for 1 sec exposure = 2/10 ergs/cm^2, flux in ergs/cm^2, for other wavelengths (λ):

λ in Å	3000	3500	4000	4500	5000	5500	6000	6500	7000
103a-O Plates .2ergs/cm^2	.15	.18	.2	.6	60				
Pan Chromatic Plates	.4	.2	.3	.4	1.0	5	8	8	50

Photon flux per unit density-Blue Sensitive plates, and 4300Å Radiation = 4×10^{10} photons/cm^2

Mass of silver deposited for unit photographic density P = 1.1×10^{-4} g/cm^2

Photographic Grains: diameter = 1×10^{-4} cm
area = 10^{-8} cm^2
mass = 4×10^{-13} g

Number of grains for unit photographic density = 2×10^8 grains/cm^2

Photographic Resolution in resolvable lines/mm

Fast emulsion	= 65 lines/mm (Tri-X)
Process emulsions	= 100 lines/mm (micro-film)
Special very slow emulsions	= 500 lines/mm

Density of star image - 1 hour exposure on 103a-O (fast Blue Plate)

$\log D = 2 \log d - 2 \log w - 0.4\, m_{pg} - 0.7$, **where,**

d = telescope objective dia. (inches)
w = image dia (cm) on plate
D = photographic density (assumed <1)

Energy depth of Electron traps for latent image

E = 0.77 electron volts

Atmospheric Absorption

Absorption at visual response for a fairly clear atmosphere = 0.21 mag/air mass

Absorption at photographic (103a-O) response for a fairly clear atmosphere = 0.44 mag/air mass

Absorption for S-20 photocathode response for a fairly clear atmosphere = 0.15 to .017 mag/air mass for low temp targets.

The atmospheric transmission for S-20 for sun temperature targets is 75% or 0.32 mag/air mass.

Faster films give poorer resolution (grain size), poorer grey scale, and early reciprocity failure, and therefore are not suited to accurate calibration and measurement work.

It should always be remembered, however, that good film can never improve performance that is limited by the optics involved though pretty pictures will be obtained. Thus, the diffraction limit, circle of confusion, aberrations and color correction errors in the optics coupled with the existing atmospheric conditions are usually the limits of performance, and the pretty pictures may not be as good as short exposures with noisy electronic scanning (line) readout.

c. Electronic Recording on Plastic Tape

Recording units are available or are being developed using plastic tape. These tapes can be grouped by the sensitive surface "film" used to write on the information:

a) Magnetic film with magnetic write and magnetic read-off.

b) Thermoplastic film with modulated electron scan beam write, and optic read-off either as a visual image or a flying spot electronic output.

c) Photographic film surface exposed by a modulated electron scan beam or a Cathode Ray Tube image (Kinescope), and optic read-off either as a visual image or a flying spot electronic output.

Each of these recording units is a complex device with advantages and disadvantages of operation, bandwidth, cost, processing time, playback registration, and linearity, etc. Recording is a separate study area, with many books and articles available.

D. LINEARITY AND REGISTRATION

The separation of target from background due to relative movement require both the storage of images for some time period, and the ability to register the present image element by element with the stored past image. The separation of target from background due to relative position (stereo) requires the ability to

register the station A image element by element with the station B image. So linearity and registration of image orthicons and storage tubes are important considerations, when evaluating the separation performance of hypothetical systems.

1. IMAGE ORTHICON

When comparing the images from two image orthicons, the registration problem is one of matching linearities of the video time versus image position. It is assumed that synchronizing and image transfer problems give no error and there are no lens linearity problems, when evaluating image orthicon linearity. There are time invariant linearity problems which will be called linearity problems; there are also slowly time varying changes of overall size and linearity which will be called stability problems.

Most of the development effort for image orthicon multiple tube "registration" has been in the area of studio color TV pickup cameras. These color TV cameras use three orthicons, and the present "one location" 3 orthicon registration precision should be obtainable with a 2 locations, 2 orthicon system. With the standard 3 high 4 wide aspect ratio: within a center diameter 8/9 of the total height, the registration precision can be held to 1 part in 2400 or 0.042% of the vertical height; outside the 8/9 of total height diameter, the registration precision decreases to 1 part in 500 or 0.2% of the vertical height.

Improvements in registration performance are continuously being made. At present, it is felt that the most serious problem is the mechanical tolerances of the image orthicons. Another cause of misregistration now being studied is caused by the target charge bending the beam. Since the beam velocity near the target is almost zero, it can be deflected by the charge on the target (non-uniformly from tube to tube). This phenomena is not fully understood.

The linearity problems of the image orthicon include the transfer of a visual photocathode image to target charge pattern (Image Linearity), and time versus target position of scanning beam (Scan Linearity).

Image linearity is primarily a function of the amplitude and end field direction of the solenoid magnetic field used for beam focus, and the electrostatic lens used to accelerate and focus photoelectrons on the target "film". The major effect of the magnetic field on image focus is a DC size bias, or change of the average photocathode to target size decrease. The major non-linearity of the image electrostatic lens is S-shape geometric distortion The G6/PC (grid six/photocathode) voltage ratio for minimum S-distortion is a function of the magnetic focus field shaping in the image section. This ratio E_{G6}/E_{PC} for minimum distortion is approximately 0.8, with the normal focus magnetic field strength at photocathode divided by field strength at target ratio of 0.5. A 1% variation of E_{G6}/E_{PC} results in an S distortion peak to peak of 0.5% of the picture height. See Figure II-44. An excellent description of aperture response losses due to loss of focus, and registration linearity problems, as a function of current and voltage regulation is found in an article by K. Sadashige in the June 1962 issue of the Journal of the SMPTE, "Stability Criteria for Television Camera Tubes".

The scan linearity of an image orthicon is effected by the magnetic field versus time relation of scan, beam bending due to target charge, beam bending due to metal target mounting ring, and flatface distortion which results in pincushioning if the magnetic scan field is a linear ramp function.

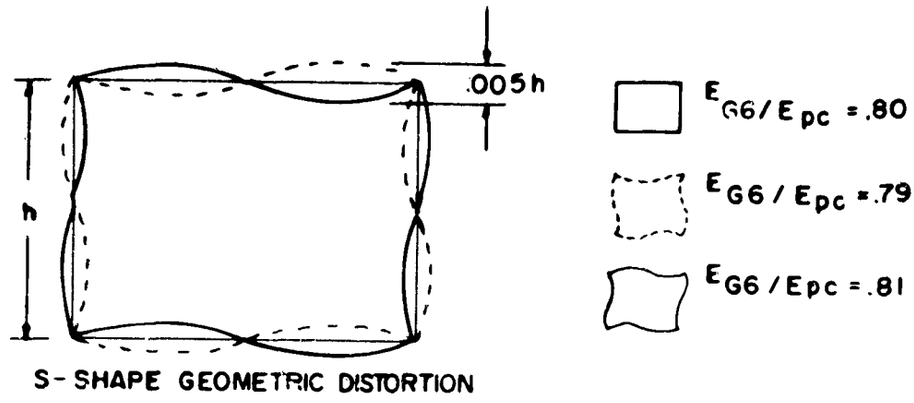


Figure II-44. S-Shape Geometric Distortion

For all of the above effects, the important consideration for target separation is not the total deviation from true time-space linearity, but the lack of uniformity between two individual image orthicons, or the misregistration. The registration precision of color TV cameras has already been reported.

When using the time of target video during sweep to get target position in the field of optical view, the time-space linearity does limit the accuracy of target location. Thus linearity of sweep time versus photocathode image location does limit orbital prediction accuracy, if the spacial coordinates are determined by measuring target video time in respect to sweep time. The target mounting ring assembly is made of magnetic material, which distorts the focus and sweep magnetic fields. So for better time-space linearity it is desirable to limit scan sweep size, so the beam comes no closer to the target ring than 10% of the target diameter at the corners of the scan.

2. STORAGE TUBES

When using a storage tube as an MTI unit, the registration problem is one of matching the stored image element by element with the present image. Assuming no image orthicon time stability problems, registration is then a question of write-on to read-off registration of the storage tube. Will the write-on scan trace the same path across the storage mesh as the read-off scan? With a single gun storage tube using a continuous magnetic sweep, the linearity problems of both image orthicon and storage tube sweeps should be cancelled.

Development work with one single gun storage tube has shown there is a registration problem between write-on and read-off scans. It is a repeatable misregistration, as the following explanation will show, and it can be cancelled by programming DC bias corrections in the scan systems, during the readout scan.

The electron optical system of QK-685 incorporates an electrostatic collimating lens system following deflection and preceding the image storage section of the tube. The collimating lens system consists of the decelerator electrode and two cylindrical aquadag bands (L1 & L2) coated inside the large diameter portion of the glass envelope. The collimating lens system functions in conjunction with the high-voltage accelerating anode to maintain beam focus as the beam is decelerated from the 3500 V anode potential, while also causing the deflected beam to be bent such that the electrons approach the storage screen at (ideally) normal incidence. Since the

storage screen is effectively shielded from the collimating lens region of the tube, switching of storage screen potential between the various storage cycle anodes does not affect focus, deflection sensitivity or linearity. However, if the electron paths, as they enter the region between the decelerator and the storage screen are not exactly aligned with the electric field in this region (i.e., perpendicular to storage screen) there will be a lateral displacement of the electron paths which is proportional to the potential difference between the storage screen and the decelerator. This lateral shift is analogous to that experienced by a light beam obliquely incident upon a plane parallel surfaced glass plate. Since the potential between the storage screen and the decelerator is shifted from -460 volts during write to -740 volts for the readout mode, it can be seen that the amount of lateral shift of the raster can indeed be quite different for the two modes. Of course, if a QK-685 tube could be assembled with perfect alignment, especially as regards the storage screen and decelerator being exactly perpendicular to the electron optical axis of the tube, no misregistration would occur. Raytheon now places a specification of 1% on the maximum allowable misregistration for production tubes. This would amount to about five scan lines vertically for a 525 lines raster, which is of the same order of magnitude we observed with our particular tube.

So the main problems to be solved when using a storage tube as an MTI system to cancel a star background are:

1. The problem of electronic detection with minimum loss.
2. The non-uniform sensitivity of an image orthicon across the field of view.
3. The number of storage tubes required: (a) For short time (seconds) image storage, to separate with larger relative target velocities. (b) For long time (minutes) image storage, to separate star backgrounds with small relative target velocities.

SECTION III. METHODS TO MEASURE AND EVALUATE SEPARATION TECHNIQUES

A. FACTORS OF SURVEILLANCE

This section outlines some of the methods for measurement and evaluation of separation techniques to determine performance capability using modest equipment. Some limited test results are included.

The major factors for a successful surveillance system are: 1) initial detection capability, 2) an adequate separation technique, and 3) processing of target information and data for orbital prediction or other system requirement(s).

The earlier sections of this report have covered the factors effecting detection and the trades open to the designer in producing a candidate system. Since the conditions of the celestial background and the targets (size, orientation and velocity) are not under the control of the designer, he must establish what these are (unless given in the systems requirement), and then trade between: 1) Lens Diameter, 2) Field of View and, 3) Image Time for attaining the required capability.

Having established the detection requirement, the designer is now concerned with which of the separation techniques or combination (Hybrid Systems) best applies to the threat presented for solution (height and brightness of targets to be separated, etc.). Typical separation techniques are covered in Section IV.

The evaluation of a separation technique is based on its ability to cancel stars for the range of intensities involved, and its retention of the targets vs its complexity and economic value. How well this is done is measured in terms of the False Alarm Rate and the Probability of Target Detection required by the specification or threat.

Factors effecting the False Alarm Rate and Probability of Target Detection are:

1) Registration Errors
2) Direct Video and Stored Video Target Image Spread
3) Cancellation Range (Intensity ratio of stars that are cancelled)
4) Detection Loss - number of targets lost (not retained for processing), or increase of image time to assure star cancellation.
5) Complexity of the Storage Technique or Comparison Technique Used
6) Length of Delay Time(s) used
7) Use of processing for additional target information and alarm analysis of retained signals.

The output requirement and ultimate purpose is next approached. In the case of predictions, the compromise of high volume accurate data for orbit prediction versus time to survey the sky for direct surveillance output, versus the minimal

data needed for acquisition information for a higher accuracy (limited quantity of tracks) precision track unit for better orbit prediction should be checked. Also an analysis of degree of needed track data accuracy versus orbital mechanics (mathematical equations, etc.) should be considered in the complete system synthesis.

Typical data requirement for orbital predictions are briefly covered in Section V and the suggestions for future study outlined in Section VI.

The remainder of this section covers in more detail:

1) the factors effecting False Alarm Rate, Detection Probability, and Complexity
2) measurement and test programs, using modest equipments
3) some limited measurements of various separation factors
4) hybrid separation system and
5) the detection of a target vs orbit height

B. EVALUATION OF SEPARATION TECHNIQUES

The fundamental criteria of a separation technique are: does it cancel all stars (False Alarm Rate), does it retain all pertinent targets (Detection Probability), and does it do it economically, that is within reasonable complexity? In applying these criteria to the possible separation techniques, the contributing factors are measured and compared against the results desired. The principle factors involved are briefly outlined here.

1. FALSE ALARM RATE (% STARS NOT CANCELLED)

a. Film Catalog or "Permanent Storage" Image Cancellation Techniques

The factors effecting the ability to cancel when using a film negative at the image plane for direct cancellation, or a flying-spot scan of film with video cancellation, include:

1. the differential atmospheric refraction across the field of view, and the "D.C." refractive pointing error as a function of the elevation angle being viewed (and the elevation angle when the film was originally exposed).
2. the short and longtime stability of the film and film mount in repeating, within stringent tolerances, the complete field image each time a particular film negative is recalled for use, including wear, tension, and temperature effects.
3. the flexibility to adjust, update, or otherwise account for moving celestial objects such as planets, asteroids, variable stars
4. dirt (or dust) on the film
5. maximum density cancellation ratio for stars (point sources) and nebulae, etc. (extended sources), (the few very bright planets and stars might be handled in the alarm processing)
6. image spreading

7. the problem presented by differential tube sensitivity across the imaging surface (no sensor device will be ideal).

b. Delay Interval - Temporary Storage Catalog (M.T.I.) Techniques

The factors concerned here are mostly short term changes. That is, changes near or within delay interval or system cycle plus those introduced by the equipment mounts, or methods involved such as:

1. writein - readout registration including image spread
2. integration required for setting level of peak detector to maintain reasonable false alarm rates to handle scintillation (background) and system noise
3. type of separation, that is, by direction as well as distance of image motion (for alarm processing function if used).

c. Stereo or Baseline Separation Techniques

The factors here include:

1. weather differences at the two sites
2. differences in refraction due to differences in atmospheric conditions at the separated sites as well as difference (D.C. bias) due to look angle difference with respect to horizon for same star fields (this can be minimized by non-level mounting - mutually level) and programming D.C. bias
3. slaving accuracy and precision as effects mount registration
4. differences in tube (image surface) sensitivity for two tubes as well as individual field variation
5. two I.O. registration (sweep)
6. synchronization including storage tube equipment.

Common to all the above are effects of atmospheric dancing, weather, clouds, including especially wisps of haze, high cirrus and ice crystal conditions, meteors and passing aircraft lights.

2. DETECTION LOSS (% TARGETS LOSS)

a. Film or "Permanent" Storage Techniques

The factors effecting the detection loss in film catalogue techniques are:

1. fog level (attenuation added in light path) or scanning noise level if separate film is read and compared at video if that version of "permanent" storage is used
2. reduction of "open" sky area available due to image spread required for cancellation (see false alarm discussion)
3. weather (catalogue need not include fainter stars when sky is less clear or moon is out, etc.)

b. Temporary Storage (M.T.I.) Techniques

The factors effecting the detection loss here are:

1. integration time to obtain necessary peak detection over noise background (electronic signal to noise) for transfer of signal to storage tube (use of Schmidt trigger for digitized video, etc.)
2. loss of digitized video versus losses in analog video cancellation
3. direct video target spread "open" sky available
4. total delay interval cycle time necessary for motion detection (cycle time for repeated sky coverage) (fast moving targets getting through undetected).

c. Stereo Techniques

The factors effecting detection loss here are:

1. site and weather (primarily cloud) differences at the separated sites
2. transfer of information for all or partial processing.

3. SYSTEM COMPLEXITY (ECONOMIC FACTORS)

The film catalog systems require mechanical precision in various forms in addition to the electronic detection and alarm functions.

The temporary storage tube technique (M.T.I.) minimizes mechanical requirements but requires unduly large numbers for higher altitude target separation due to the longer storage time needed. Thus single site systems require more complexity in equipment if the higher altitude targets are to be separated. They are logistically simpler with less administration needed, etc. Due to weather and lack of redundancy, a single site is less reliable than a multiple site system possessing single site processing for low altitude separation. It is, of course, more reliable than the multi-system if both sites must be functioning for stereo separation of the higher altitude targets.

Multiple site (stereo) systems require more logistic support and administration expense; however, they offer redundancy if equipped for single site low altitude target processing (temporary storage). For higher altitude target separation, the stereo technique should be less complex than single site processing.

C. EQUIPMENT ASPECTS IN EVALUATION OF SEPARATION TECHNIQUES

Our primary objective in measurement and evaluation of separation techniques is to do adequate testing with modest equipments (small lens diameter - limited function equipment) to provide necessary confidence that system goals and requirements can be met.

To meet this challenging objective the functions of separation are evaluated in various phases, but in realistic environment. In accomplishing this measurement task we are especially concerned with:

1) getting the same number of stars in the field of view as with a final system (star density)

2) determining the ratio of intensities of stars and targets that can be processed by various functions of a system

3) an integrated image orthicon and storage tube equipment for assessing the functions of a short term delay (M. T. I.)

4) a suitable presentation method for evaluating performance - monitor and camera, etc.

5) ancillary equipment needed and precautions with it and finally

6) site selection and construction factors.

The following paragraphs discuss these items in greater detail as functional parts of equipment.

1. OPTICS COLLECTOR

Typical satellite surveillance systems will require 25 to 36" diameter optics of 25 to 40" focal length (f/no. of .7 to 2.0). These lead to fields of view of 2^{o} to $3\text{-}1/2^{o}$. Such optics are expensive and unwieldy to handle in anything short of a full system setup. To simulate capability for testing the separation functions of a typical system, we are primarily concerned with:

a. obtaining a similar detected star density at the sensor

b. obtaining images for relative quality and

c. maintaining a reasonable field of view

We do not need the overall system aperture or field of view. To get the same number of detected stars in the field of view as a 15 to 16th Stellar magnitude detection system having a 27" f.l. optics ($2\text{-}3/4^{o}$ field of view), we merely select optics such that the field of view is larger to make up for the lesser detection ability, or the detection ability is greater for a smaller field of view.

If we use more than a $10^{o} \times 10^{o}$ field of view, we will have too large a variance of star density in a single field of view, i.e., we would cover more than the width of the Milky Way average if we were checking in it, or we would be getting into denser areas when wishing to test only the sparser sections of the sky. Thus we do not wish to use less than 6 in. (150 mm) focal lengths if using a 3" image orthicon for sensor.

As for aperture, this needs to be selected as large as practical to minimize integration time needed. Refractive optics should be used to avoid the stray light problems inherent in reflective optic system which would raise the background light to levels that would limit star densities obtainable. Thus a 6" f/0.9 to 1.0 (6 to 7" aperture), is a good choice and a 6" f/1.8 (3-1/3" aperture) lens is a close practical second choice (and more economical). The f/1.8 lens require the integration time to be increased modestly to account for the smaller aperture.

Farrand Optical Company offers a 6" f/.87 lens and Astro Berlin offers a 6" f/1.8 of excellent quality at reasonable cost.

To illustrate the above selection: Refer to Figure I-11 for star densities and Figure II-21 for detection star magnitudes (in POTI report).

We wish to make the number of stars seen by the testing system equal to the number seen by the larger surveillance system optics:

Thus, N_{SD} for $^{30\text{" Dia.}}_{27\text{" f.l.}}$ optics = $N_{SD}\ ^{6\text{" Dia.}}_{6\text{" f.l.}}$

but from Figure I-11 at 0°

$$N_{SD}\ ^{30"}_{27"} \text{ at 15-1/4 mag. detection} = 1200 \text{ stars/degree}^2 \left(\frac{K}{27"}\right)^2$$

and $N_{SD}\ ^{6"}_{6"} = X \left(\frac{K}{6"}\right)^2$

$$X = 1200 \times \left(\frac{6}{27}\right)^2 \quad 1200 \times .05 = 60 \text{ stars/degree}^2$$

from I-11 at 0° 60 stars/degree^2 = 11-3/4 mag.

from Figure II-21 a 6 to 7" dia. lens = 11th mag. at 0.2 sec integration (eye)

Thus, this lens will require 0.4 sec integration to get the 11-3/4 mag. needed for these densities.

From Figure I-11 at 90° and 15-1/4 mag. $N_S\ ^{30"}_{27"} = 100$ stars/degree^2 $\left(\frac{K}{27}\right)^2$

$$X = 100 \times \left(\frac{6}{27}\right)^2 = 5 \text{ stars/degree}^2$$

from I-11 at 90°

5 star/degree^2 = 11th mag., thus the 0.2 sec. eye observations is the only integration needed for the sparser sky densities.

If a 6" f.l. f/1.8 lens is used then an integration time of approximately 3/4 sec or 1-1/2 sec respectively will be needed to account for the lens diameter decrease. (1:1 dia. = 4 to 1 integration time change)

If one tried to use a 12" f/6.0 telescope system then

$$N_S\ ^{12"\ D}_{72"\ f.l.} = X \left(\frac{K}{72}\right)^2 = N_S\ ^{30"\ D}_{27"\ f.l.} = 1200 \left(\frac{K}{27}\right)^2$$

and $X = 1200 \left(\frac{72}{12}\right)^2 = 1200 \times (7.1) = 8500$ star/deg^2

from I-11 this is about 17-1/2 mag!

For 12" diameter optics, detection of 12-1/2 mag is possible for .2 sec. integration, therefore 5 mag. additional gain thru integration or approximately 17 sec integration time (not counting aperture loss due to secondary mirror, etc.) is needed. This is impractical. Also a 12" f/6.0 would be background light limited before 17-1/2 mag. is reached for normal sky backgrounds and normal scanning (see Figure II-34) even excluding stray light (see Section II-A-7).

2. ELECTRONICS

The electronics (TV chain) for evaluating equipment should have special low noise pre-amplifiers with minimum sensitivity to pick up, throughout the electronics functions. A minimum of two pre-amps are suggested; one having 18 to 20 Mc bandwidth, the other a special 4 to 5 Mc low noise, high gain unit.

In addition, approximately 1000 or 1200 line scanning capability is desirable, in addition to usual 525 line scanning. This is especially necessary (1000 line and 20 Mc) when using fast lenses (f/no. <2.0) in Milky Way areas or when the early or late moon is in the sky (full moon will nearly always limit performance).

Non-interlace scanning format is preferred though not absolutely necessary. (one frame, one field.)

The electronics should include provisions for integration to at least 4 secs with trigger output for recording camera synchronization. (Short pulsing as an added feature allows additional capability for measuring atmosphere perturbations.)

3. RECORDING CAMERA

A speed graphic with Polaroid film pack and synchronized (BC) shutter is most handy (and inexpensive) for day to day test analysis.

4. VIDEO PROCESSING EQUIPMENT

If separation techniques are to be evaluated, a minimal equipment using a storage tube with readin-readout and erase electronics plus comparison (cancellation) logic is suggested. Since video processing electronics are dependent on signals from the camera electronics, it is questionable whether these can be separated (purchased separately and married at later dates) without a sacrifice of performance. Stereo (two sensor) equipment should be considered.

5. MONITORING

A two color registered display, using either color TV or 2 color registered black and white would provide a practical monitoring and recording means for separation system performance analysis for detection, registration, motion separation, and target spread evaluation.

6. ANCILLARY EQUIPMENT

a. Mount

A mount with sidereal drive is needed where celestial work is performed. This can be attained at minimum expense, using a good az.-el. unit mounted on a slow rate (sidereal) turntable, tilted to the celestial pole elevation (latitude of observer) to provide right ascension and declination axis motion, (or the az.-el. unit can be equipped with a special low speed reduction unit for sidereal drive with an overriding feature for moving quickly to selected right ascension positions).

b. Star Catalogues, etc.

Star catalogues will be needed to measure the detection performance: with use of small optics, star catalogues for calibration will not need to go to the fainter magnitudes thus less vigorous, less tedious, quicker analysis! (10th mag. is practical.)

Astronomical Tables for star positions - sidereal time, etc., will also be useful.

c. Time

Means for receiving WWV or CHU observatory times signals should be provided and clocks for UT as well as local time are handy.

d. Communications

Intercom to mount, etc., is desirable in addition to standard phone facilitie

e. Satellite Prediction

If much satellite observation is contemplated, arrangements for receiving orbital elements and computing local look angles will be useful in identifying which satellite has been detected. (There are quite a few up there now so that cataloguing is increasingly important.)

7. SITE SELECTION AND CONSTRUCTION

Site selection, preparation and construction must be made to minimize local atmospheric conditions and local thermals as is practiced for astronomical observatories. Particular attention should be given the consideration of convection wall construction - insulation - air flow and conditioning in and around dome - white external painting - location of discharge of heat exchanger, surrounding foliage, etc.

Weather analysis for contemplated location can be made in various ways, remembering that in general there are more clear hours at night than during the day. For a typical analysis see Appendix A-VII.

Facilities needed vary with intended use and should include unless available the following:

a. Operations

Office area

Conference area

Snack area

Recording room

Records area (storage and analysis)

b. Shop - Service

Mechanical

Electronic

[redacted]

c. Air Conditioning

Equipment requirements

Personnel areas

Dome area

Outside wall convection

Supply (if used)

D. SEPARATION MEASUREMENTS TO DATE

1. ACHIEVABLE EXPOSURE DENSITY USING FILM PLATE

In order to have a practical film catalog cancellation system the film mask should ideally be a transparent plate with opaque spots in the positions corresponding to the stars. The density of opaqueness will set the intensity performance ratio of the system. To be practical for a surveillance system, this should be as high as possible (Density 6, 1,000,000:1, or 15 Mag. desired) otherwise several film layers will need to be stacked with ensuing problems. Since published, Kodak data covers only to density 3 (1000:1 intensity - 7-1/2 Mag), a G.E. funded program was initiated to measure densities achievable.

The program was undertaken to determine a combination of astronomical plate material and processing technique to achieve the highest possible density of an exposed area, combined with the lowest possible density of an unexposed area. Since each of these achieved separately are in opposition, it requires special processing techniques to optimize them both together. Various special developers were used and special techniques were also used to reduce unwanted density. The first part of the program considered area exposures and is reported here, the second part considers exposures to point sources and is underway at the G. E. Schenectady Observatory.

The final results for exposured area indicates that type IIa astronomical plates would be the optimum material to use for the process, together with development at 68° for two minutes in D-8 developer to which has been added a restrainer consisting of 1.80 grains per quart of developer of Benzotriazole, (also designated as Kodak anti-fog #1). Processing is for 2 minutes, followed by a rinse in running water and then 5 minute fixation in a rapid fix.

Tests were run on 6 Astronomical Type Plates along with Plus X film; 103a-O; 103a-F; IIa-O; IIa-F; III-O; IV-O. Developers tested were Duktol, full strength; Dektol Diluted 1:1; D-8; D-9; and Kodalith Developer. Each of these was used normally and in combination with anti-fog #1 (Benzotriazole). D-8 was also tested with two concentrations of Benzotriazole. The accompanying table gives the maximum density achieved with each developer-film-anti-fog combination, and also the fog level with that combination.

Three emulsions had satisfactory D max levels: II, III and IV, but the higher speed inherent in IIa made it a logical choice for the process. The choice of IIa-O over IIa-F was prompted by the lower fog level of IIa-O, giving a final dynamic range of 5.70 or 1 to 501,200. This half million to one range was accompanied by a fog level of .20 in a D-8 normal process. Addition of anti-fog gave a .13 fog level and a dynamic range of 467,700 to 1.

The second highest range was achieved by a IV-O emulsion developed in D-19 with anti-fog 1.8 grains Benzotriazole per quart of developer, developed for 5 minutes. A range of 891,300 to 1 resulted, with a fog level of .05. The highest range was 933,300 to 1 with a type IV plate, developed in Kodalith for 3 minutes with 1.8 grain, Benzotriazole added, giving a fog level of .03 and a maximum density of 6.0. Densitometry of values over 5.5 are subject to some error, since pinholes and scratches give lower than actual readings, as does stray light. These figures are, then, on the conservative side, and may give actual dynamic ranges up to 20% higher than read.

Since adequate results were achieved directly with controlled development it was not necessary to investigate the results of intensification; reduction; or second generation duplication on extreme contract materials such as Kodalith.

Exposures were made in an intensity scale sensitometer using neutral density filters to reduce the exposure level to 1/2, 1/10, 1/100, 1/1000 and 1/10,000 of the original level. The initial illumination level, measured with a Spectra photometer was 7.0 foot candles, consisting of a #212 enlarging lamp without reflector at 48-1/2 inches from the sample. Exposure time was 15 seconds giving a basic exposure of 105 foot candle seconds. Elimination of the stray light problem was done by measuring the fog level on an unexposed plate processed along with the exposed plates.

2. TEMPORARY CATALOG SEPARATION - STORAGE TUBE M.T.I. (see also Section IV-D)

For the past two years an internal G.E. program has been conducted in the use of storage tube M.T.I. with I.O. camera equipment for star cancellation. The results of the program emphasize the importance of operational experience with this type of equipment and necessity of carefully designing all electronic functions to be compatible. (A well integrated equipment, no compromise adaptions.)

To minimize detection loss and false alarm rate we need to have:

a. A specially designed Schmidt trigger plus quantized video, so that the trigger can be set to operate near noise level and yet obtain a sufficiently small False Alarm Rate by integrating 3 or 4 units on the storage tube.

b. The Schmidt trigger designed to balance an optimum bandwidth that has determined from analysis of what frequency response is needed to get the best electronic signal to noise. (The full video bandwidth, as set by the scanning pattern parameters, is not the optimum for electronic signal to noise detection where the image is spread over several resolution elements. A spread of several resolution elements is normal for the faintest stars or targets that we can expect to process.)

c. Excellent linearity and position for write in and readout of the storage tube.

The poor results in False Alarm Rate (leading to need for integration of many frames before writein to reduce False Alarm Rate to acceptable values) were traced to non-linearity in the vertical sweep circuits used to drive the storage tube. The non-linearity resulted in excessive line spacing at top of tube such that the space exceeded the line width thus if readout differed by 1/2 line the information could be absent.

Very limited tests were made using analog video but here the uniformity and circuit control of the storage tube is very critical leading us to the digital or quantized writein.

E. HYBRID SYSTEM

A hybrid separation system using both stereo for high altitude target separation, and temporary storage (storage tube MTI) for low altitude target separation has been investigated. The low altitude MTI separation would use one short term storage, and the stereo separation would find the targets in altitudes from the maximum MTI altitude to the maximum stereo altitude.

To review the individual separation system problems: Temporary storage separation with one finite delay time has a maximum target altitude (higher altitude targets have a lower relative angular velocity) that will allow separation. At greater target altitudes the relative movement of the target is not great enough and the target is cancelled along with the stars.

Stereo separation has a maximum target altitude for any given dual site spacing that will not cancel the target. At this maximum target altitude the stereo angular target separation will approximately equal the expected dual image registration error. The minimum target altitude for a stereo system can be set at the point where the angular separation is greater than half of the view field, or at a lower target altitude where the target can be "underneath" the combined view field volume.

To define a hybrid system for separation these variables have to be determined:

1) Dual Site Spacing Distance
2) Temporary Storage Time
3) Image Time (Integration Time)

To solve for these separation variables decisions are made on the basis of the following relationships:

1) Star magnitude detection sensitivity, with lens diameter and image time.
2) Variation of target orbital relative velocity with target altitude.
3) Stereo site spacing versus stereo angular target separation versus target altitude versus target elevation angle.

Table III-1 shows the lens diameter and image time required for a specific star magnitude detection capability. Figure III-1 shows the target relative angular velocity as a function of target altitude, for a 90° elevation overhead view of a circular orbit. Figure III-2 shows the minimum image parallax (stereo angular target separation) as a function of target altitude, for the minimum system elevation angle of 20°. The minimum parallax is approximately 1/3 the maximum parallax (sin 20°/ sin 90°).

TABLE III-1

DETECTION MAGNITUDE	LENS DIAMETER S20 IO	IMAGE TIME APPROXIMATE
16	47 Inch	0.2 second
	25 Inch	0.8 second
14	23.6 Inch	0.2 second
	12 Inch	0.8 second
12	10 Inch	0.2 second
	3.94 Inch	0.8 second

A sample calculation of hybrid system variables will now be made. Assume:

1) 12 magnitude detection using 12 inch diameter lens and 0.2 second image time.
2) MTI minimum separation for target detection is 25 $\widehat{\text{sec}}$.
3) Stereo minimum separation for target detection is 50 $\widehat{\text{sec}}$.

Now make an arbitrary 2 second storage time for temporary catalog.

A. From Figure III-1 and assumption 2 the minimum

$$\frac{\theta}{t} = 12.5 \frac{\widehat{\text{sec}}}{\text{sec}} \text{ for } 25\ \widehat{\text{sec}}$$

separation in 2 seconds gives a maximum target altitude of 20,000 nautical miles.

Now make an arbitrary site spacing distance of 50 n. miles.

B. From Figure III-2 the maximum target altitude that can be separated at 20^{o} elevation angle is 70,000 miles, and the 90^{o} elevation angle maximum target altitude is 200,000 nautical miles.

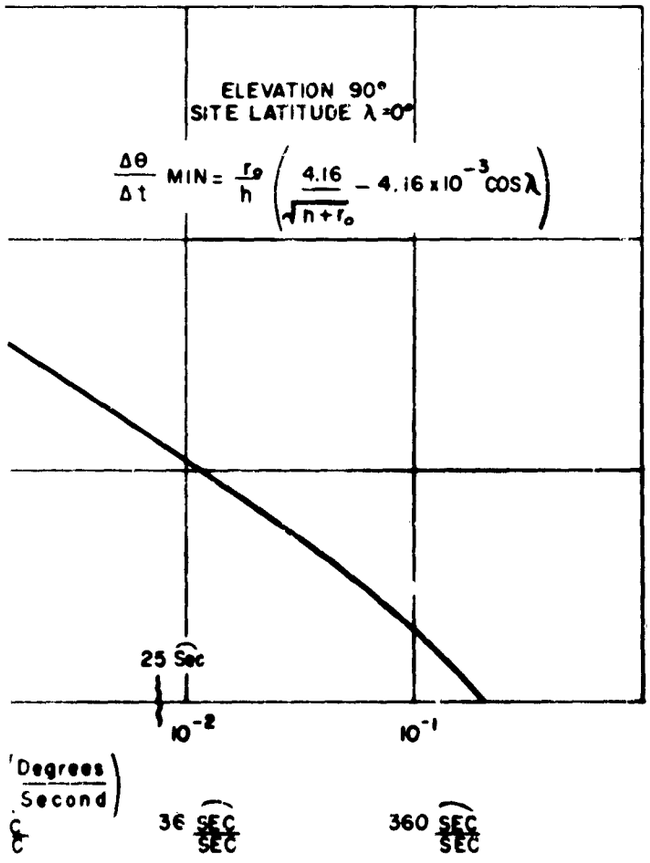
The hybrid system of stereo MTI separation might have advantages of both units, and avoid some of the disadvantages. MTI should work well for low altitude targets (at both sites if desired), and stereo should be able to detect high altitude targets so that long time storage and many storage tubes will not be required. And MTI should allow partial operation when variable weather makes stereo operation difficult.

F. DETECTION OF GIVEN TARGET AS FUNCTION OF ORBIT HEIGHT

It is possible to calculate the range of missile sizes, reflectances, and orbit heights that are equivalent to a given star magnitude. Then by including the circular orbit relative angular velocity it is possible to evaluate the relative detection requirement.

As an example, assume two orbiting targets have the same star magnitude, but one has a larger radius and/or reflection, and is at a greater altitude. Although both targets have the same magnitude, the greater altitude target would be easier to detect because its relative movement during the image time would be smaller. With a smaller relative movement, the energy per resolution element during the

Figure III-1. Ta



ative Angular Velocity vs Target Altitude

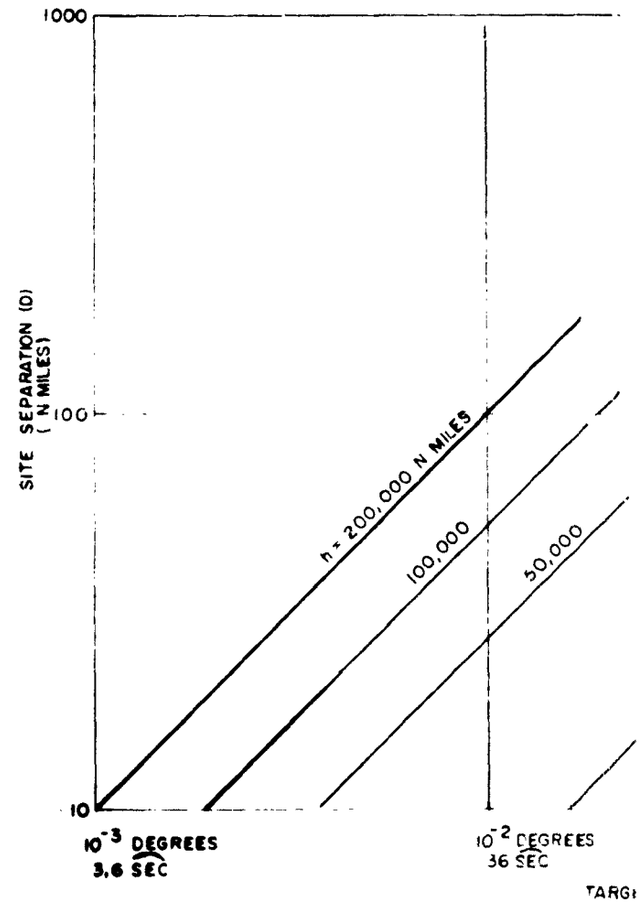
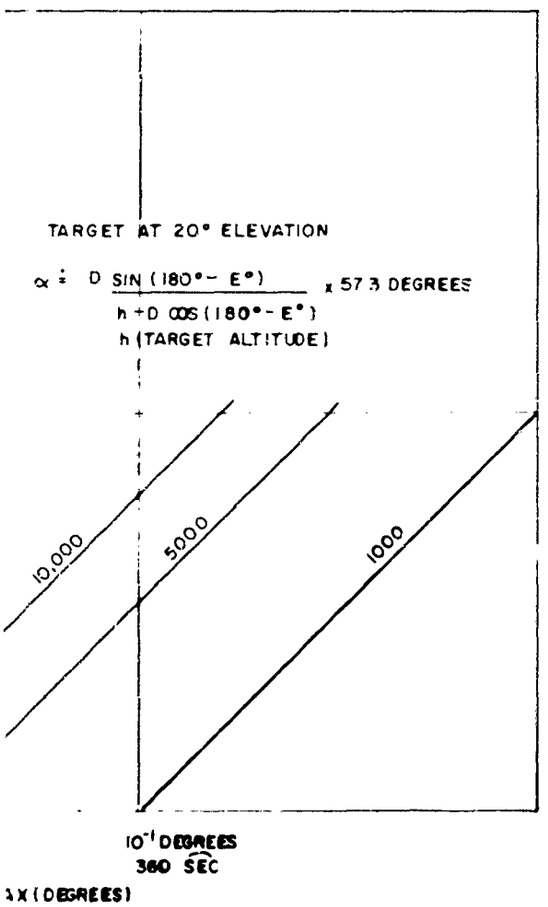


Figure III-2. T



age Parallax vs Site Separation and Target Height

image time would be greater, and this is a major detection criteria. If a more intense (smaller magnitude) target moves 100 resolution elements during the image time, it has to have at least 100 times the intensity of a "stationary" target to have the same detection probability as the stationary target.

The following brief analysis will show the relation between intensity, relative angular velocity, image time, and intensity per resolution element per picture.

$$\text{Intensity I } \left(\frac{\text{watts}}{\text{meter}^2}\right) = \frac{K_1}{h^2}$$

$$\text{Detection Criteria } D_c \quad \left(\frac{\text{watt . seconds}}{\text{meter}^2 \cdot \text{Resol. Element}}\right)$$

$$\text{Relative Angular Velocity w } \left(\frac{\text{degrees}}{\text{second}}\right) = \left(\frac{K_2}{K_3+h}\right)^{3/2} \quad \frac{\Delta^\circ}{\text{second}}$$

$$\theta_{RE} = \frac{\text{Degrees}}{\text{Resol Elem}} = \frac{\text{Field of View}}{\text{TV } \frac{\text{Scan Lines}}{2 \text{ or } 3}}$$

If the relative movement during one image time is less than one resolution element, then the energy per resolution element is the total energy.

$$D_c = I \times t(\text{image}) \qquad (1.$$

No image Movement

If the relative movement during one image time is more than one resolution element, then the energy per resolution element is independent of the image time.

$$D_c = \frac{I \times t(\text{image})}{\frac{\text{Resolution Elements}}{\text{Image}}} = \frac{I}{w} \times \theta_{RE} \qquad (2)$$

$$\frac{\text{Resol Elements}}{\text{Image Time}} = \frac{w \times t(\text{image})}{\theta_{RE}} \quad \left(\frac{\text{Degrees Per Image Time}}{\text{Degrees Per Resol Elem}}\right)$$

Another way of writing the "no image movement" detection criteria when the relative movement is less than one resolution element is:

$$D_c = \frac{I}{w} \times \theta_{RE} \left(\% \text{ of } \frac{\text{one Resolution Element}}{\text{Image Time}}\right) \qquad (3)$$

No Image Movement

Figure III-4 shows a plot of target size, reflectivity, and height that result in a constant star magnitude. As an example, the minimum target radius that can be detected with a 16 magnitude sensitivity, at a height of 166,000 n miles, is approximately 5.3 meters.

By combining the data of Figure III-4 (star magnitude I, apparent size $\sqrt{r}$ a, and height h) with the relative angular velocity w of Figure III-1, and the visual star magnitude to visual photons per cm square second of Figure III-5, it is possible to plot the detection criteria in terms of photons per meter squared degree in Figure III-6.

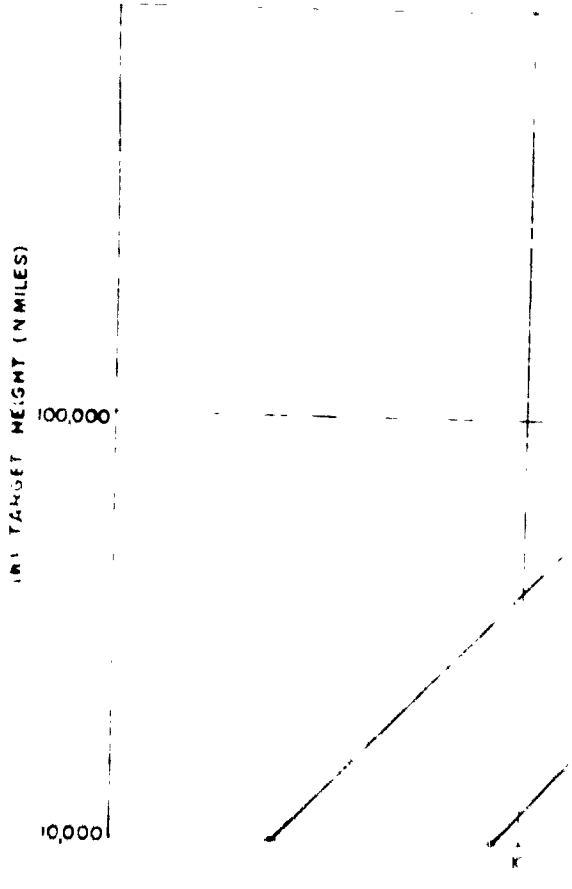
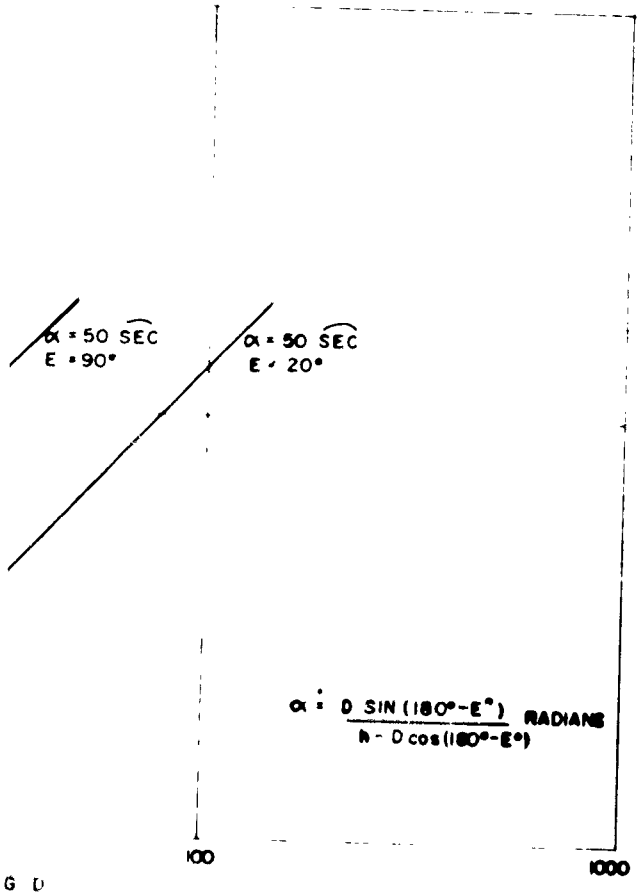


Figure III-3. Tar



arallax

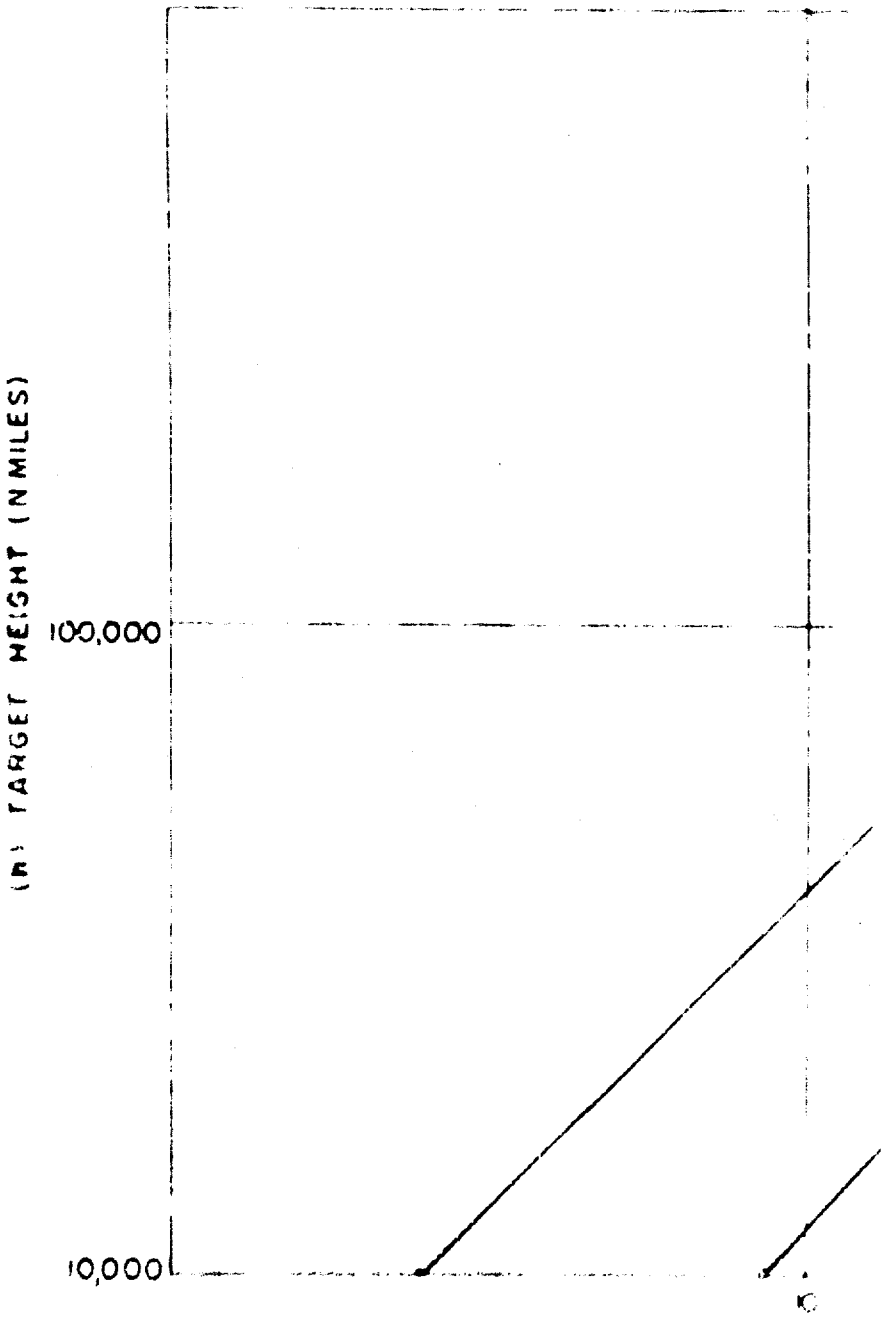


Figure III-3. Tar

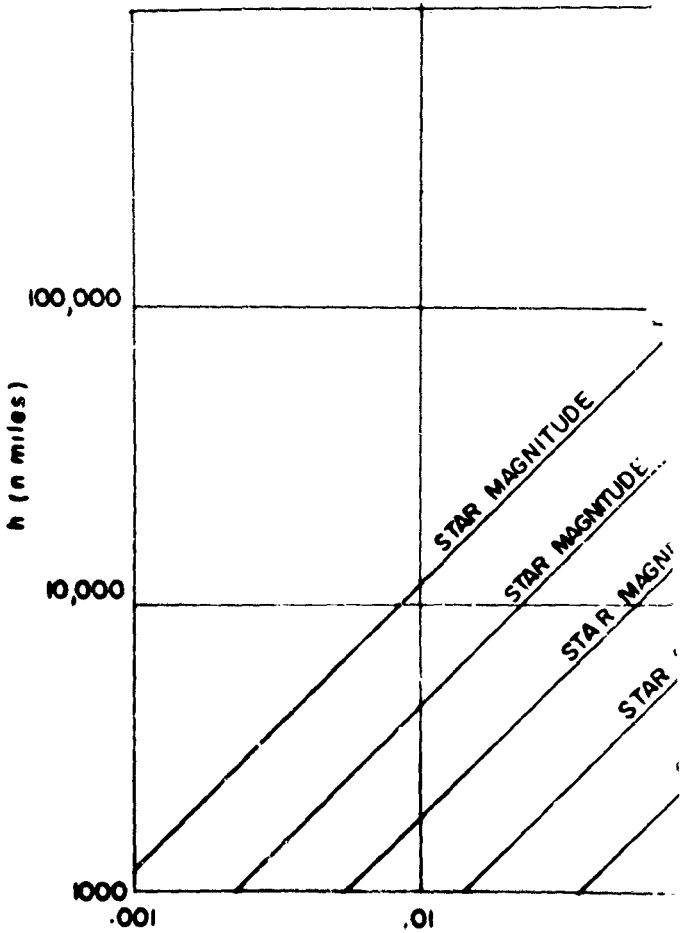
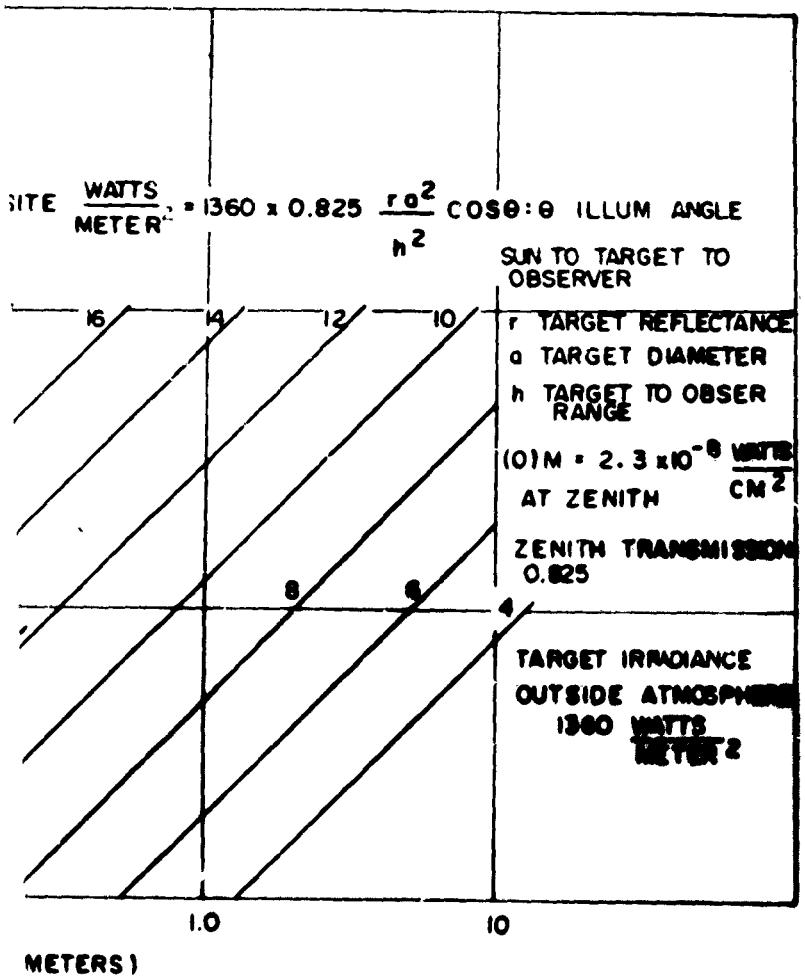


Figure III-4.



ude of Sun Illuminated Target

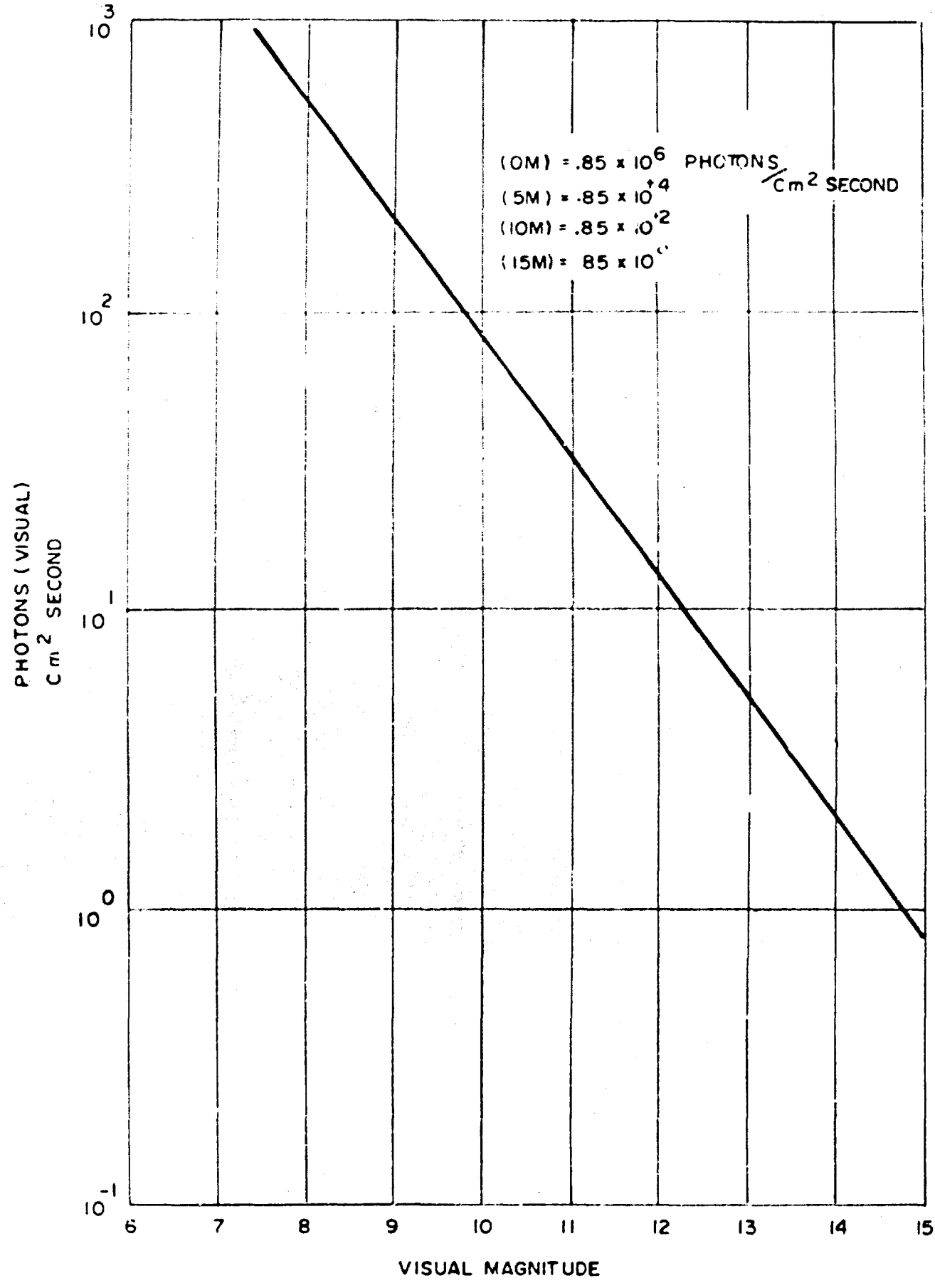

(0M) = .85 x 10^6 PHOTONS/Cm^2 SECOND
(5M) = .85 x 10^+4
(10M) = .85 x 10^+2
(15M) = .85 x 10^
PHOTONS (VISUAL) Cm^2 SECOND
10^3
10^2
10^1
10^0
10^-1
6
7
8
9
10
11
12
13
14
15
VISUAL MAGNITUDE

Figure III-5

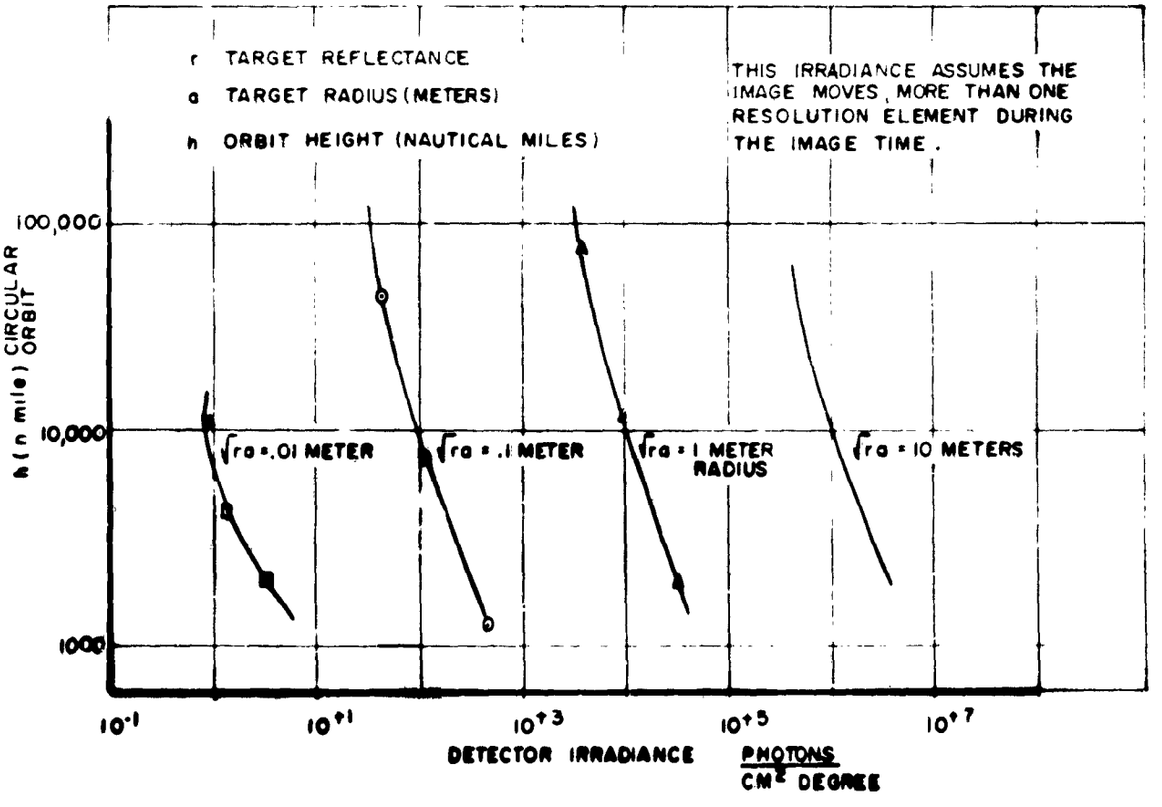


Figure III-6. Detector Irradiance vs Target Variables

Figure III-6 gives the detector irradiance in photons per meter squared degree, for several apparent size targets, as a function of orbit height h. Figure III-6 shows that for any apparent size, detection is more easily accomplished at lower altitude, since intensity increases faster than the relative angular velocity increase, as the orbit height is decreased.

Figure III-6 shows that an analysis of the threat could be used to determine both the detection and separation requirements of a system. The threat can be expressed in terms of apparent target size $\sqrt{r}$ a, and orbital height h. And both the detection requirement and the separation requirement can also be evaluated in terms of apparent target size and target orbital height.

To use Figure III-6 the number of photons required for detection, and the degrees per resolution element must be known. A good number for detection photons is 1000, when an S20 is used. A square 3 degree field of view using a 1000 scanning lines results in 3/500 degrees per resolution element. The data of Figure III-6 says that for an apparent size of 0.1 meter radius, with an orbit height of 10,000 n. miles, the detector irradiation is approximately 10^{-2} photon/cm^2 degree.

$$1000 \frac{\text{photons}}{\text{Res Elem}} = 10^{-2} \frac{\text{photon}}{\text{cm}^2 \text{ degree}} \cdot \frac{3}{500} \frac{\text{degrees}}{\text{Res Elem}} \cdot X(\text{cm}^2 \text{ lens})$$

$$\text{Res Elem} = .6 \times 10^{-2} \text{ degrees: } w = 1.1 \times 10^{-2} \frac{\text{degrees}}{\text{second}}$$

Solving for the required lens area in cm squared:

$$X = \frac{1000}{100} \frac{500}{3} = \frac{5000}{3} = \frac{\pi}{4} D_L^2$$

$$D_L(\text{cm})^2 = \frac{4 \times 5000}{3\pi} = 2120 = 21.2 \times 10^2$$

$$D_L(\text{cm}) = 4.6 \times 10^1 = 46 \text{ cm} = 18 \text{ inches}$$

To check this result, a 10,000 n. mile altitude target with an apparent size of 0.1 meters radius would have a magnitude of (9.75 + 5) or 14.75 magnitude. This would require an 80 cm diameter lens to detect the object in 0.2 seconds, or 51 cm diameter lens to detect the object in 0.5 seconds, where 0.5 seconds is the image time that would give an image movement equal to one resolution element. So the resultant 46 cm required diameter lens is in the right ball park, for any image time equal or greater than 0.5 seconds.

SECTION IV. SYSTEM SELECTION CRITERIA AND TRADES

(Effects of environment, atmospheric, target factors, equipment tolerances, and separation techniques on system selection).

In Sections I and II the characteristics of the celestial environment, atmospheric perturbations, target factors, detection and equipment parameters and separation techniques have been discussed in detail. In this section criteria for accomplishing system synthesis and tradeoffs to minimize limiting effects are discussed.

To facilitate the discussion, a sample system of each category is postulated and analyzed in those areas where special considerations seem in order. No attempt is made here to select the best system for a particular task but rather the discussions are organized to illustrate the trades and typical factors involved. Since System Detection and Atmospheric Effects are common to all systems these are discussed first.

A. DETECTION AREA LOSSES

1. INTRODUCTION

There are many factors that influence the probability of detecting a space vehicle with an imaging optical sensor. This discussion, however, will consider only those factors that are also connected with the problem of separating space vehicles from stars. A good separation technique should have a very low false alarm rate due to imperfect rejection of star images. The system should be designed to accommodate the normal atmospheric and equipment variations that will occur. In addition, the detection probability of the system should not be adversely affected by the constraints of the separation technique. The requirements for high detection probability and low false alarm rate are usually incompatible so that some degree of compromise is usually necessary. Separation techniques will vary somewhat in the amount of detection loss that is necessary to maintain a satisfactory false alarm rate.

Most star separation techniques are basically the same in that they involve the following steps.

a. An exposure of the sky is compared with another exposure of the same region taken either from a different location or at a different time. The other exposure may be the real-time output of another sensor, a temporarily stored analog or digital image, or it may be an analog or digital star catalog.

b. All images common to both exposures are rejected. This may be accomplished by electronic subtraction, by gating, or by mechanical masking.

Two difficulties arise in these systems. First, the characteristics of the sensors produce images that spread beyond their strictly geometric size thus occupying

more of the field of view. Secondly, atmospheric effects and equipment variations cause problems in the alignment of the exposures for complete cancellation making it necessary to cancel a slightly larger image area. The result is that a target image close to a star image may be completely masked out or occulted and thus rendered undetectable. The likelihood of a target being occulted in this manner may be related to the detection probability through the following equation.

$$P_d = P(B)\ P(A/B) \qquad (1)$$

Where: P_d = Probability of detection

$P(B)$ = Probability that the target is not occulted by a by a star image.

$P(A/B)$ = Probability that the target signal is sufficiently above the noise level to exceed a preset threshold, provided the target is not occulted by a star image.

Also,

$$Q(B) = 1 - P(B) \qquad (2)$$

Where: $Q(B)$ = Probability that the target is occulted by a star image.

The probability of the target signal being above noise is determined primarily by the detection characteristics of the sensor and is only secondarily influenced by the separation process.

Because of the image spreading characteristics of most sensors, there will be a certain detection loss due to target occultation even though separation techniques are not used. A relation describing this loss is derived first and used as a standard for comparison. The effect of various atmospheric and equipment variations on the non-occultation probability is then discussed.

2. PROBABILITY OF NON-OCCULTATION

In addition to the image spreading characteristics of the sensor, the number of stars in the field of view will also strongly influence the probability of target occultation. The number of stars in the field of view increases with the angular size of the field of view and with the detector sensitivity. The particular region of sky observed has a significant effect. The average star density to the 16th magnitude, for example, differs by a factor of 13:1 between the galactic pole and the galactic equator. The spectral sensitivity of the sensor will also affect the number of stars seen.

The geometrical size of the star images is an important factor in that it sets the minimum value of occupancy attainable. The minimum geometric image size may be set by the resolution limit of the optical system; however, in ground based surveillance systems it would probably be set by the seeing conditions of the atmosphere. The size of the target image is also important in that larger images would not be so easily occulted. The minimum target image may be set by the size of the target and its range. Small long range targets, however, will have their image sizes limited by seeing conditions.

The probability of occultation is basically the ratio of the total solid angle occupied by star images to the solid angle of the field of view. In deriving this probability the following assumptions were made.

a. The total solid angle occupied by stars is equal to the sum of the solid angles of each star image. The validity of this assumption will depend on the type of sensor used. When the number of stars in the field of view is large, their spread images tend to overlap. A photographic detector would probably produce a combined image smaller than the sum of the individual images. An image orthicon would more likely produce a combined image equal to the sum of the individual images. In any case, this assumption should be valid for occultation probabilities as large as 20 percent.

b. The image spreading characteristics are assumed to be linear to about 4th magnitude. Experiments with the image orthicon indicate a capability of linear operation over a 12 magnitude range. Photographic images show a tendency to depart from linear operation and spread more rapidly at the higher intensity levels. There are fewer bright stars so this departure from linearity is not as important as it would be at the lower intensities.

c. It was assumed that the available star densities compiled according to photographic magnitudes would apply approximately to the spectral response of the image orthicon used. This is discussed further in Appendix I.

d. Images were assumed to be circular. If other image shapes are used, the occultation probability must be corrected. If, for example, electronic blanking gates are used to blank out the star images, the blanked area will be square. The occultation probability would then be multiplied by $4/\pi$.

e. Only stars have been considered. Such sources as the sun, moon, planets, asteroids, etc. have not been included in the analysis. Stars brighter than 4th magnitude, because of their low numbers, have been considered as a single group of magnitude 3.75.

f. The targets to be detected were assumed to be near the threshold level. The probability of a bright target being occulted by star images would be much lower than calculated here. It is also assumed that the targets subtend arcs smaller than the limits imposed by seeing conditions.

A relation for the probability of occultation $\underline{Q(B)}$ has been derived in Appendix I according to the preceeding assumptions. If the image diameter is represented by

$$d = a + b\,(M_t - m) \qquad m \leq M_t \qquad (3)$$

Where: M_t = Threshold magnitude of the detector or the magnitude of a just detectable source.

m = Magnitude of the source

d = Angular size of the image in seconds of arc

a = Minimum angular size of the image or the size of a just detectable image in seconds of arc

b = Rate of image growth in seconds of arc per magnitude

then the probability of occultation $\underline{Q(B)}$ is given by

$$Q(B) = b^2 H_1 + ab H_2 + a^2 H_3 \qquad \text{Percent} \qquad (4)$$

Where: $H_1 = \frac{100\pi}{4(3600)^2} \sum_{m=M_t} N_m (M_t - m)^2$

$$H_2 = \frac{100\pi}{2(3600)^2} \sum_{m=M_t} N_m (M_t - m)$$

$$H_3 = \frac{100\pi}{4(3600)^2} \sum_{m=M_t} N_m$$

N_m = Number of stars per square degree with a brightness within the range m to m + Δ magnitudes.

Figure IV-1 shows the star distributions used for 0° galactic latitude, 90° galactic latitude, and a 0° to 90° average. These distributions were derived from International Critical Tables, Vol. II (McGraw-Hill). Using these star distributions, values of H_1, H_2, and H_3 were computed for threshold magnitudes from 9 to 20. These values are tabulated in Appendix I, Table 3. To aid in the solution of equation 4, the following partial probabilities are defined.

$$F_1 = b^2 H_1$$
$$F_2 = ab H_2$$
$$F_3 = a^2 H_3$$

These partial probabilities may be obtained from the charts in Appendix I, Figures 3 through 11 when a and b are known

The occultation probability is related to the field of view and the number of lines per scan of an image orthicon by

$$P(B) = (3600)^2 \frac{\phi^2}{N^2} (b_n^2 H_1 + n\, b_n H_2 + n^2 H_3) \quad \text{percent} \qquad (5)$$

Where: ϕ = Field of view in degrees

N = Number of lines per scan

b_n = Rate of image growth in lines/magnitude

n = Minimum image size in lines.

The occultation probability is seen to increase as the square of the field of view. Because of this, large fields of view may present a serious limitation to the detection probability. Figure IV-2 shows the variation in non-occultation probability as a function of field of view for an image orthicon operating under average conditions of 1200 lines per scan, 1.0 line per magnitude growth rate, and 2 line minimum image size. The 0° to 90° average star distribution is assumed.

Note that the non-occultation probability for a 3 degree field of view is about 98 percent for a 15th magnitude threshold. When the field of view is increased to

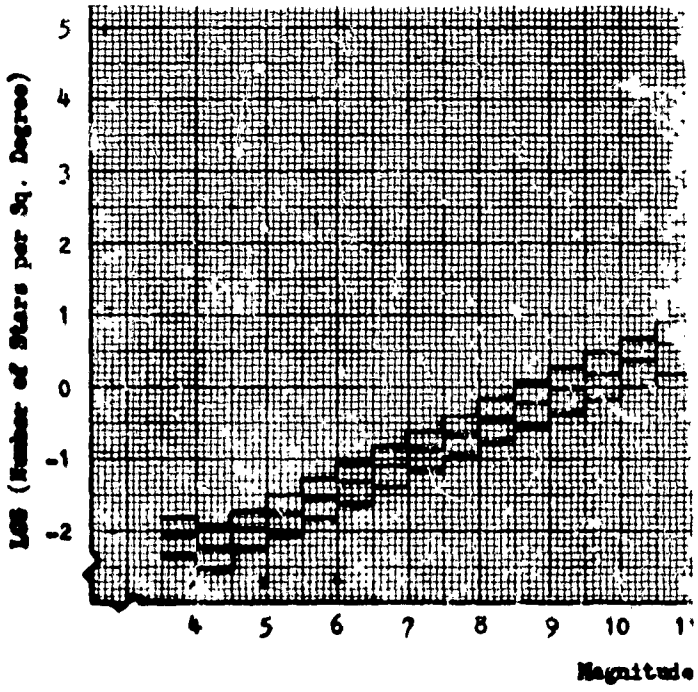
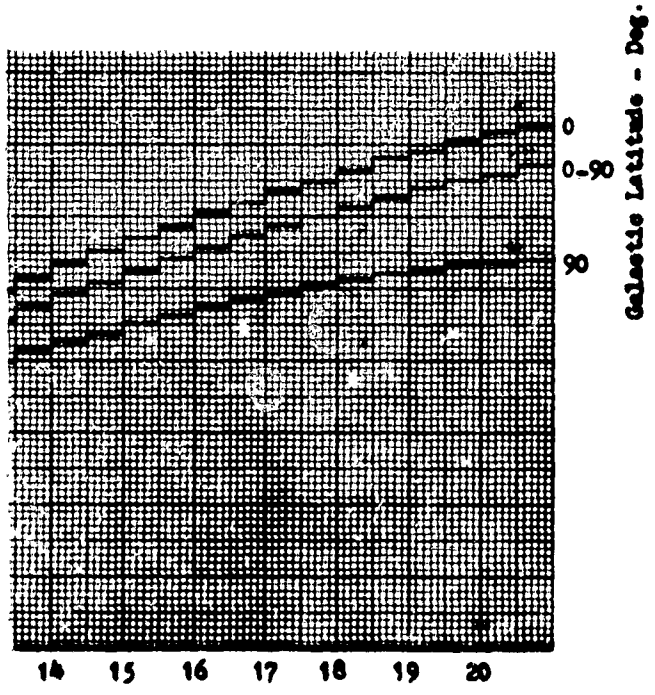


Figure IV-



ity vs Magnitude

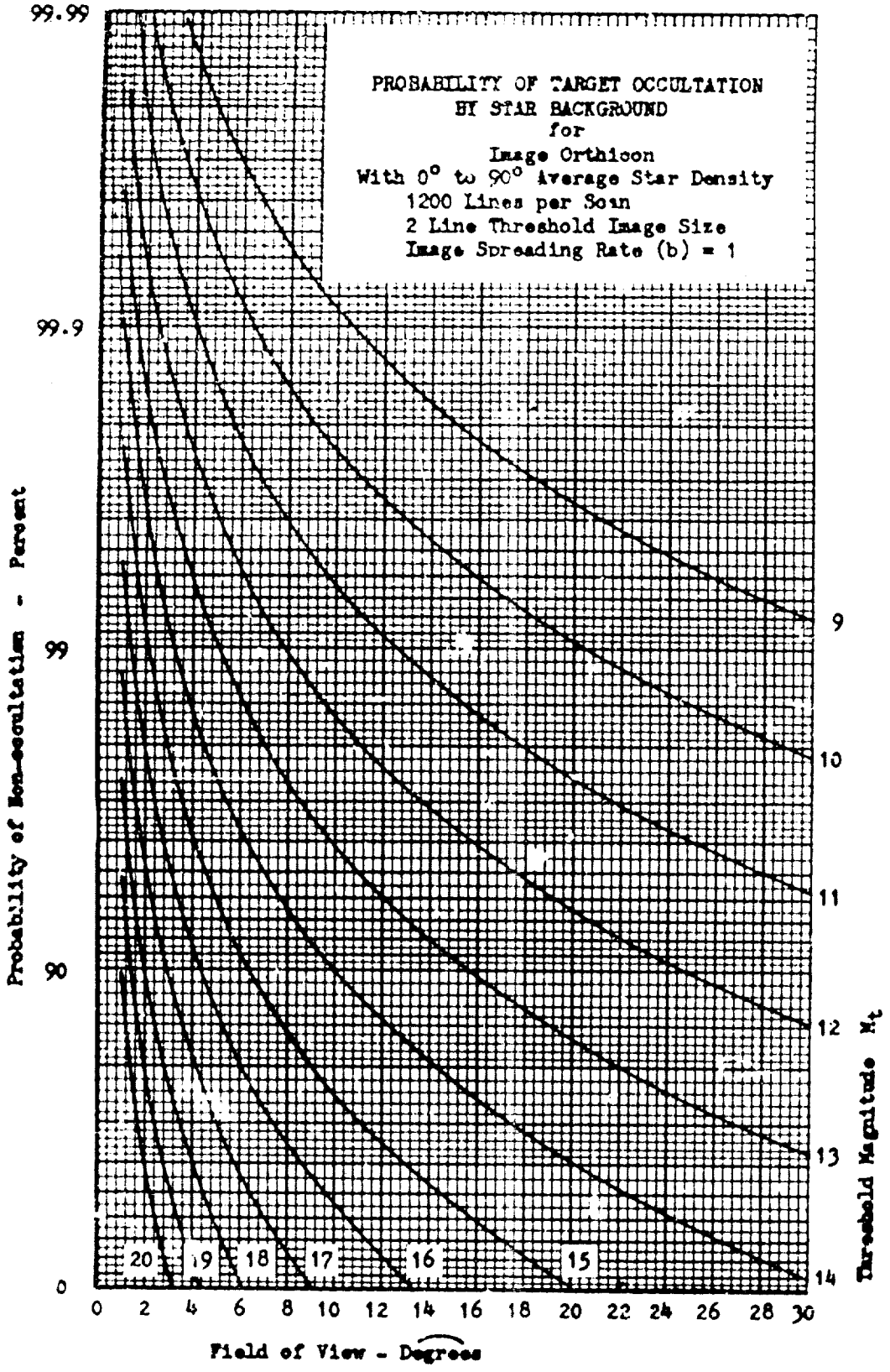


Figure IV-2. Nonocculation Probability vs Field of View

10 degrees, the probability drops to about 76 percent. The reason for this drastic change is related to the minimum image size attainable in the system. Because of seeing conditions, stars usually appear as extended sources. If the angular size of the source is greater than the minimum image size of the sensor, an increase of the field of view will increase the total number of stars in view but will decrease the image size in the same ratio thus preserving the same occultation probability. If either the lens system or the detector system limits the minimum image size to something greater than the angular size of the source, an increase of the field of view will not change the image size. The increased star density will then decrease the non-occultation probability. For most field sizes suitable for surveillance systems the image orthicon line width is a limiting factor. Since most photographic materials are capable of a smaller minimum image, there is a possibility that the use of a photographic image cancelling mask ahead of the image orthicon could make a larger field of view feasible.

Figures IV-3, IV-4, and IV-5 show the calculated probability of non-occultation for an image orthicon with a 3 degree field of view and 1200 lines per scan. Figure IV-3 shows the relative effect of the difference in star density at the galactic pole and the galactic equator. This variation is greater than the variation due to the normal range of image orthicon spreading which is 1.0 to 1.5 lines/magnitude. Figures IV-4 and IV-5 show respectively the effect of variation of the spreading rate b and the effect of different minimum image sizes a.

In order to evaluate the relative importance of the spreading rate with respect to the minimum image size the curves in Figures IV-6 and IV-7 were made. Figure IV-6 shows the combinations of spreading rate and image size required to produce a 99 percent non-occultation probability for a given threshold magnitude. Figure IV-7 provides the same information except for a probability of 90 percent. It will be seen that for a probability of 99 percent the spreading rate will have about the same effect on threshold magnitude as the image size when a = 1.5b. For a probability of 90 percent the same relation holds when a = 2b. When either the growth rate or the minimum image size is much greater than the other, then the largest will have the most effect. The value of the growth rate is usually less than the value of the minimum image size for most sensors and often does not exceed half the maximum image size. An image size of 2 lines is about the minimum for good detection in an image orthicon. The usual growth rate is between 1.0 and 1.5 lines per magnitude for continuous operation; but would be lower for pulsed operation. When allowances are made for errors in cancellation, the minimum image size will usually be the more important factor.

If the target motion is great enough to produce a trailed image during a single exposure, the target will be less likely to be hidden by star images. Generally, star images smaller than the length of the trailed image will not affect the non-occultation probability. Assuming this to be true the results of the previous analysis may be applied to trailed image detection. Given a detection system with

Threshold magnitude = M_t

Minimum image size = a

Image growth rate = b

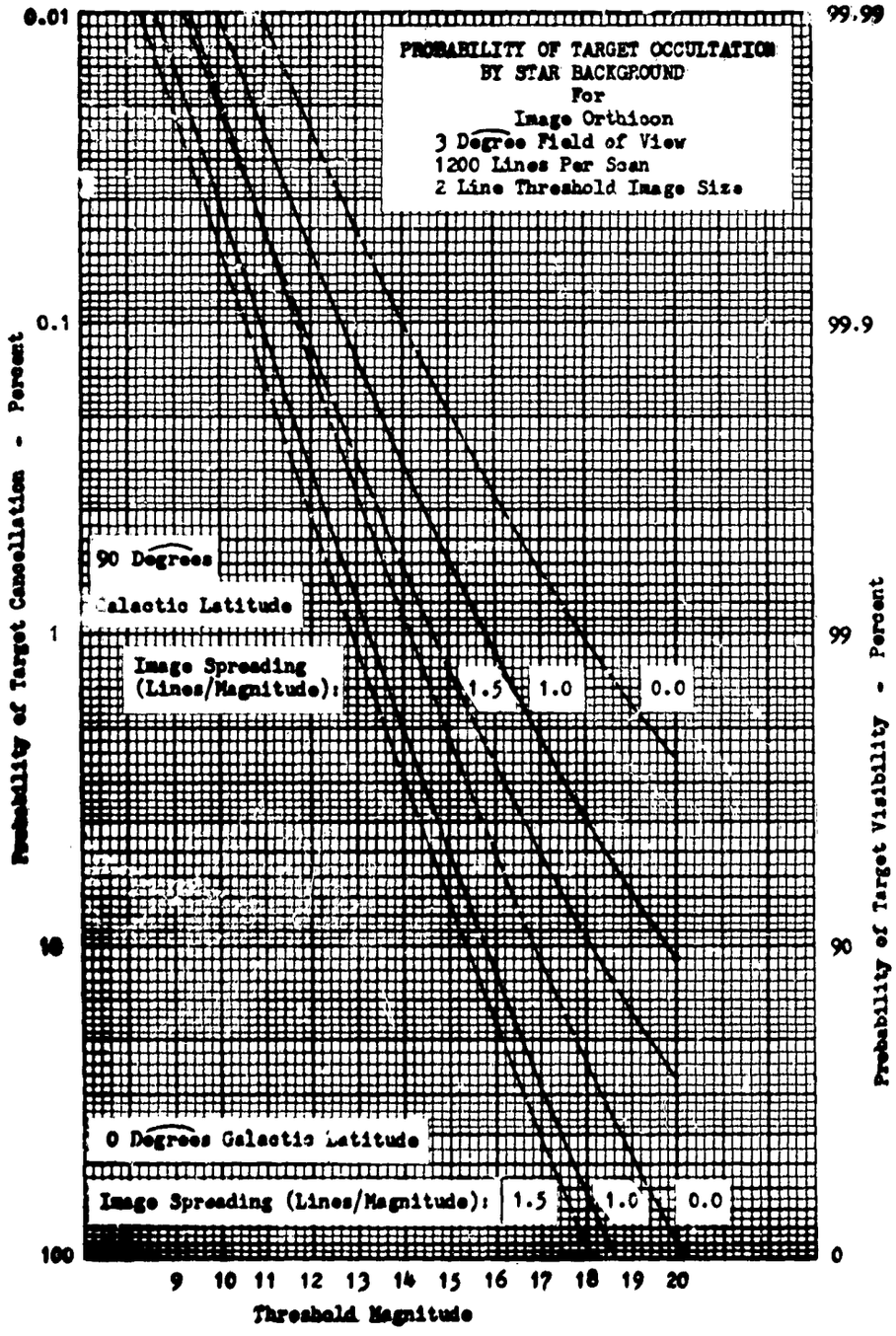


Figure IV-3. Nonocculation Probability for Extreme Star Densities

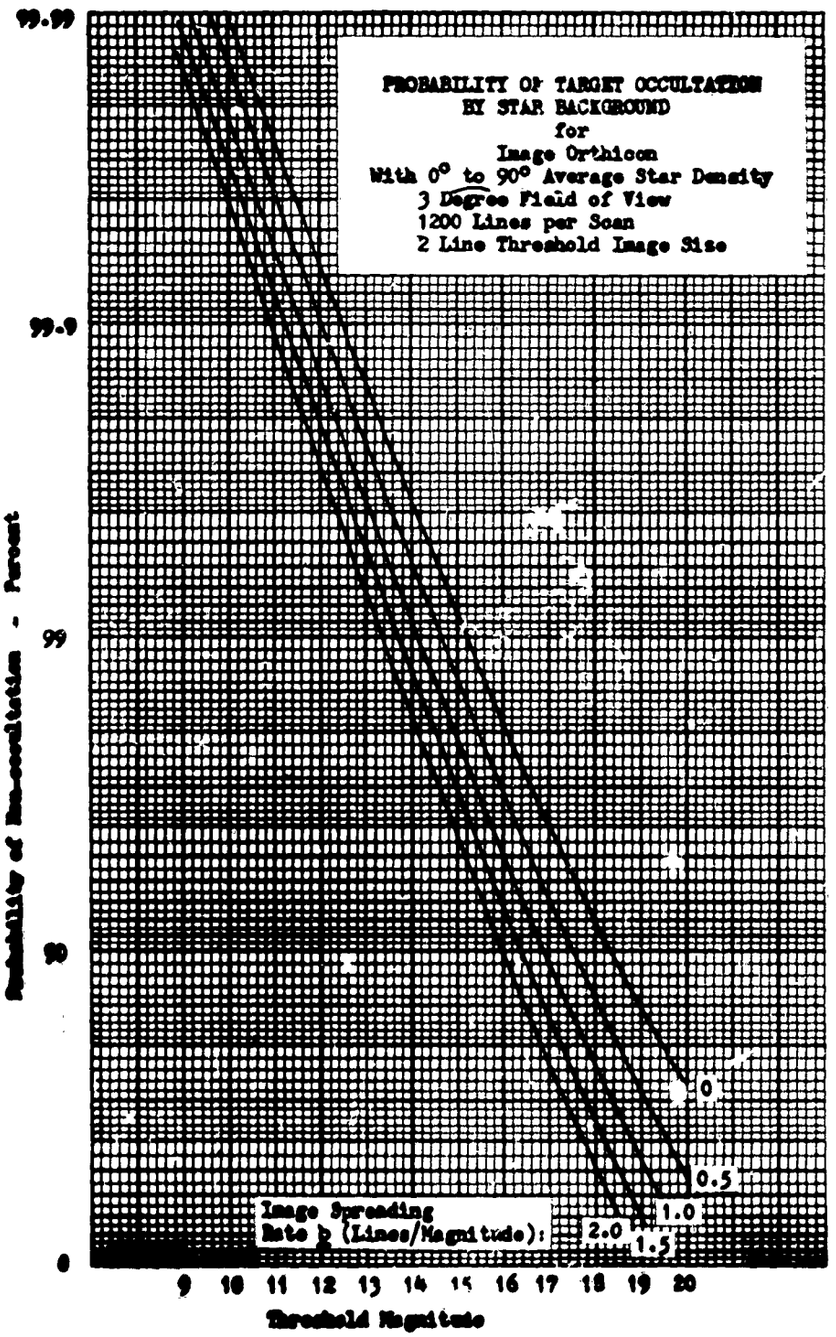


Figure IV-4. Nonocculation Probability vs Image Growth Rate

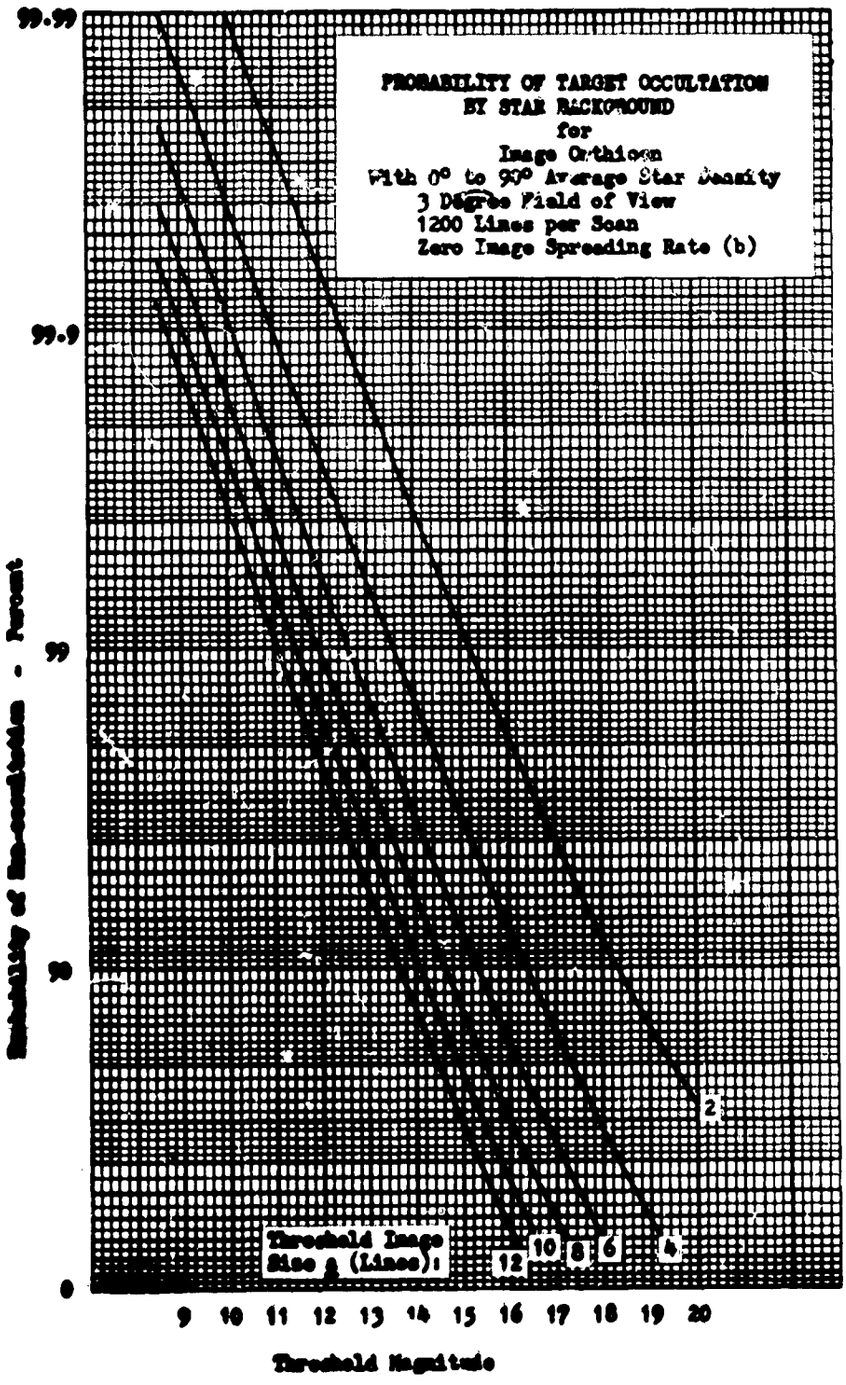


Figure IV-5. Nonocculation Probability vs Threshold Image Size

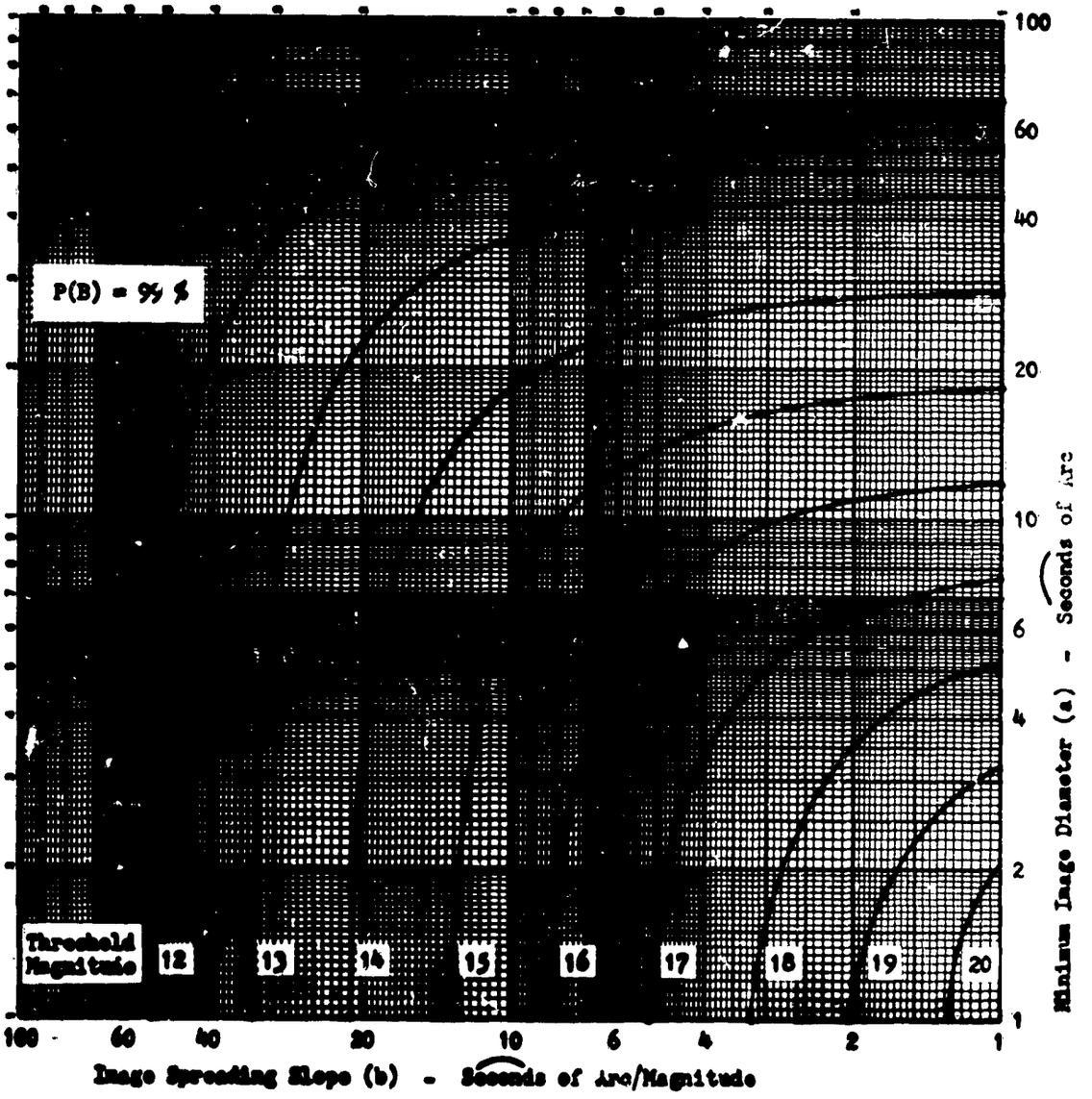


Figure IV-6. Effect of Image Growth Rate vs Minimum Image Diameter for 99 percent Probability

Then the response to a trailed image may be found by using:

$$M_t' = M_t - \frac{(g - a)}{b} \qquad b > 0$$

$$a' = g$$

Where: g = Length of the trailed image

M_t' = Modified threshold magnitude

a' = Modified minimum image size.

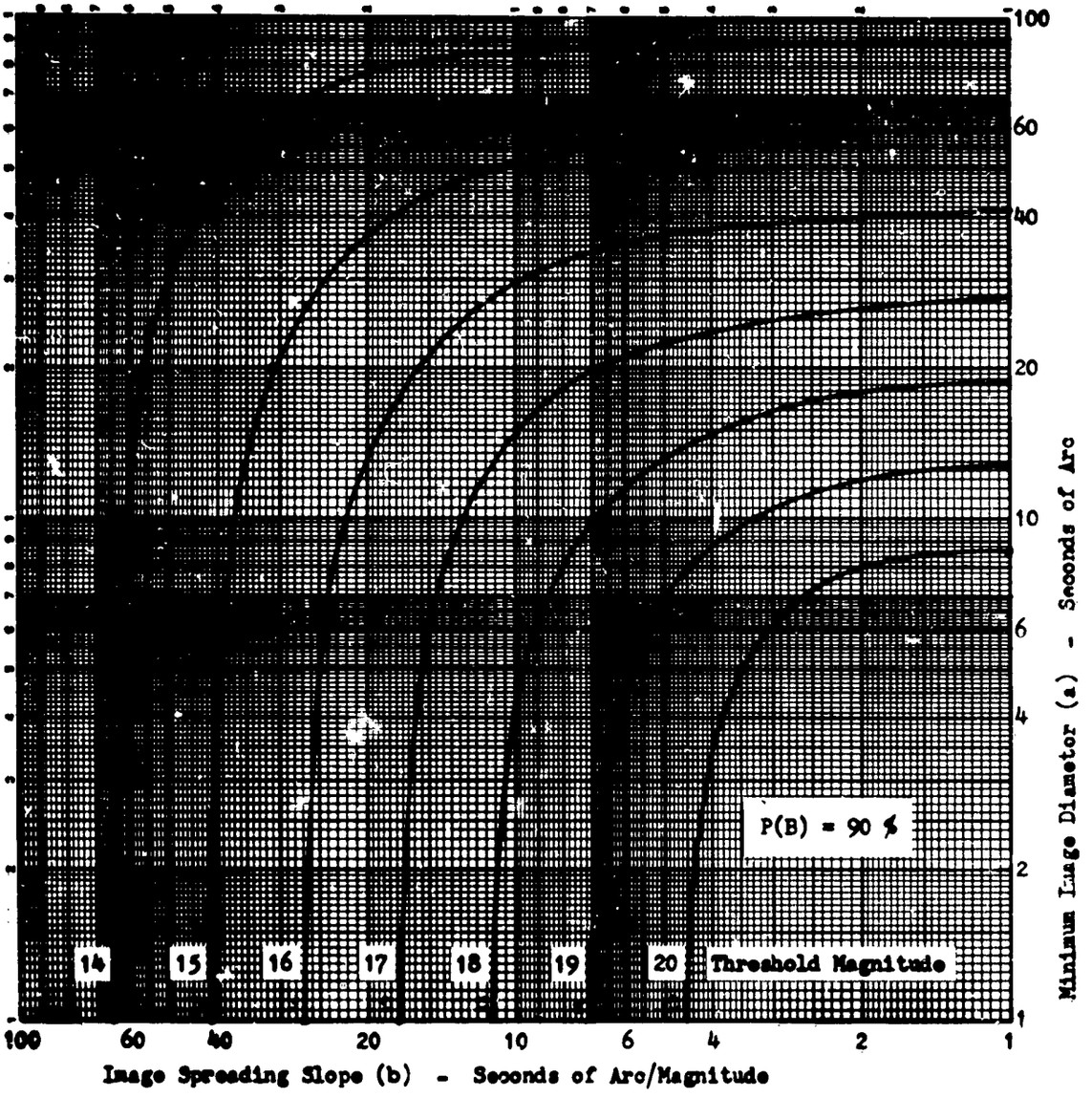


Figure IV-7. Effect of Image Growth Rate vs Minimum Image Diameter for 90 percent Probability

The values of $\underline{M}_b'$ and $\underline{a}'$ would then be used in place of $\underline{M}_b$ and $\underline{a}$ to find the non-occultation probability.

If an image orthicon detector is used with an image cancelling photographic mask, the non-occultation probability may be set by the mask rather than by the detector. Some of the conditions required to achieve this are discussed in Appendix I. Generally, the density-log exposure slope or Gamma of the mask should be greater than unity over the range of operation. The gross fog level should be as low as possible. The mask should also be capable of producing a maximum density of at least two-fifths of the range of magnitudes to be observed. Thus for cancellation over a 15 magnitude range a maximum density of 6 would be required.

B. EFFECTS OF ATMOSPHERIC AND EQUIPMENT VARIATION ON CANCELLATION PERFORMANCE

1. INTRODUCTION

The principal effect of atmospheric and equipment variations on cancellation performance is to cause the images to be misaligned so that they will not cancel completely. In order to insure a low false alarm rate it will usually be necessary to make some provision to accommodate the normal fluctuations and misregistrations that will occur. Some types of errors such as certain systematic errors, bias errors, and long term drift may be corrected by manual or automatic adjustment. Other errors such as random fluctuations, small systematic errors, and short term bounded drift errors are either impractical or impossible to correct. They would probably have to be accommodated by cancelling over an area large enough to include all uncorrected errors. This process has the disadvantage of reducing the useful observation area in the field of view and increasing the probability of target occultation. Cancellation systems may possibly be graded on the basis of the size of the cancelling area required to accommodate the errors inherent in the particular systems. The following analysis is intended to identify some of the major sources of error and to estimate their magnitude.

2. REFRACTION ERRORS

One of the major sources of misregistration error is atmospheric refraction. Although this contributes a systematic error that can largely be corrected, there will remain a smaller differential error over the field of view that will depend on the size of the field of view as well as the elevation angle of observation.

To estimate the magnitude of the error contributed by refraction, it is assumed that the atmosphere is horizontally stratified and that the error occurs in elevation only. It is also assumed that the minimum elevation angle of interest is 20 degrees. Within these limits the total error may be represented by:

$$e = A \cot \theta \qquad \theta \geq 20^{o} \qquad (6)$$

Where: e - Total refraction error measured angle less the true angle

A - Refraction error at 45 degrees

θ Elevation angle

A common value for A is 58.2 seconds at 50°F and 30" pressure. Using this value, the error at 20 degrees elevation would be about 159 seconds. Systems using fixed catalogs of charts for comparison would have to include a means for correcting this error. A method using equation 6 for compensation to the center of the field of view would probably be used. This would remove the major part of the error leaving the differential error between the center of the field and the edges.

An estimate of the differential error between the top or bottom of the field of view and the center of the field of view may be obtained by taking half of the difference between the total error at the top and the total error at the bottom.

Using equation 6,

$$\delta = \frac{e_{bottom} - e_{top}}{2} = \frac{A}{2}\left[\text{Cot}\left(\theta - \frac{\Phi}{2}\right) - \text{Cot}\left(\theta + \frac{\Phi}{2}\right)\right] \qquad (7)$$

Where: δ = Average error between the center of the field of view and the upper and lower edges

Φ = Field of view

Equation 7 may be reduced by trigonometric identity to:

$$= A\left[\frac{\text{Tan}\frac{\Phi}{2}}{\text{Sin}^2\theta}\right]\left[\frac{1}{1 - \text{Tan}^2\frac{\Phi}{2}\ \text{Cot}^2\theta}\right] \qquad (8)$$

This relation, using $A = 58.2$ seconds, is plotted in Figure IV-8 as a function of elevation angle and field of view. It has been assumed that the comparison chart has been corrected for the gross refraction error by shifting the whole chart by the amount given by equation 6 for the elevation angle of the center of the field of view. There would then be no registration error at the center, and the maximum error would be at the maximum and minimum elevation positions. Figure IV-8 gives this maximum error which is the displacement between the observed image and the corresponding image on the comparison chart. Actually there is a small difference between the maximum error at the top of the field and the maximum error at the bottom when the error at the center is zero. This is a result of the nonlinear nature of the refraction error but it is insignificant for fields of view less than 15 or 20 degrees and for elevation angles greater than 20 degrees.

The refraction error occurs largely in elevation, but caution must be observed in applying corrections to surveillance systems using an equatorial coordinate system. The orientation of the axes of the field of view will be constantly changing with respect to azimuth-elevation coordinates. The direction or sense of the refraction error with respect to the axes of the field of view will then depend on the declination of the region being observed, the time of observation, and the latitude of the site. The angle between the direction of the refraction error and the meridian of the field of view may change by as much as 180 degrees. In general, the error given in Figure IV-8 represents a radius of the additional cancelling area required.

A mask system or a system using a permanently stored exposure of the sky for comparison may require either more or less cancelling area than the system using a star chart. The principal difference is that the exposure includes the refraction correction for the elevation angle at which it was made. If it is necessary to increase the cancellation area, the increased area would be centered on the image of the exposure whereas in a star chart system the increased area would be centered on the true position. If the orientation does not change appreciably, the amount of accommodation required would likely be less than would be required with a star chart. The magnitude of the error could be approximated from Figure IV-8 by taking the difference between the errors indicated for the extremes of elevation angles encountered. It is possible, however, for the orientation to change by as much as 180 degrees. When this happens it is possible for the radius of the required cancellation area to be as great or greater than that required for a star chart. Figure IV-8 can be used along with the orientation angle to estimate the amount of error to

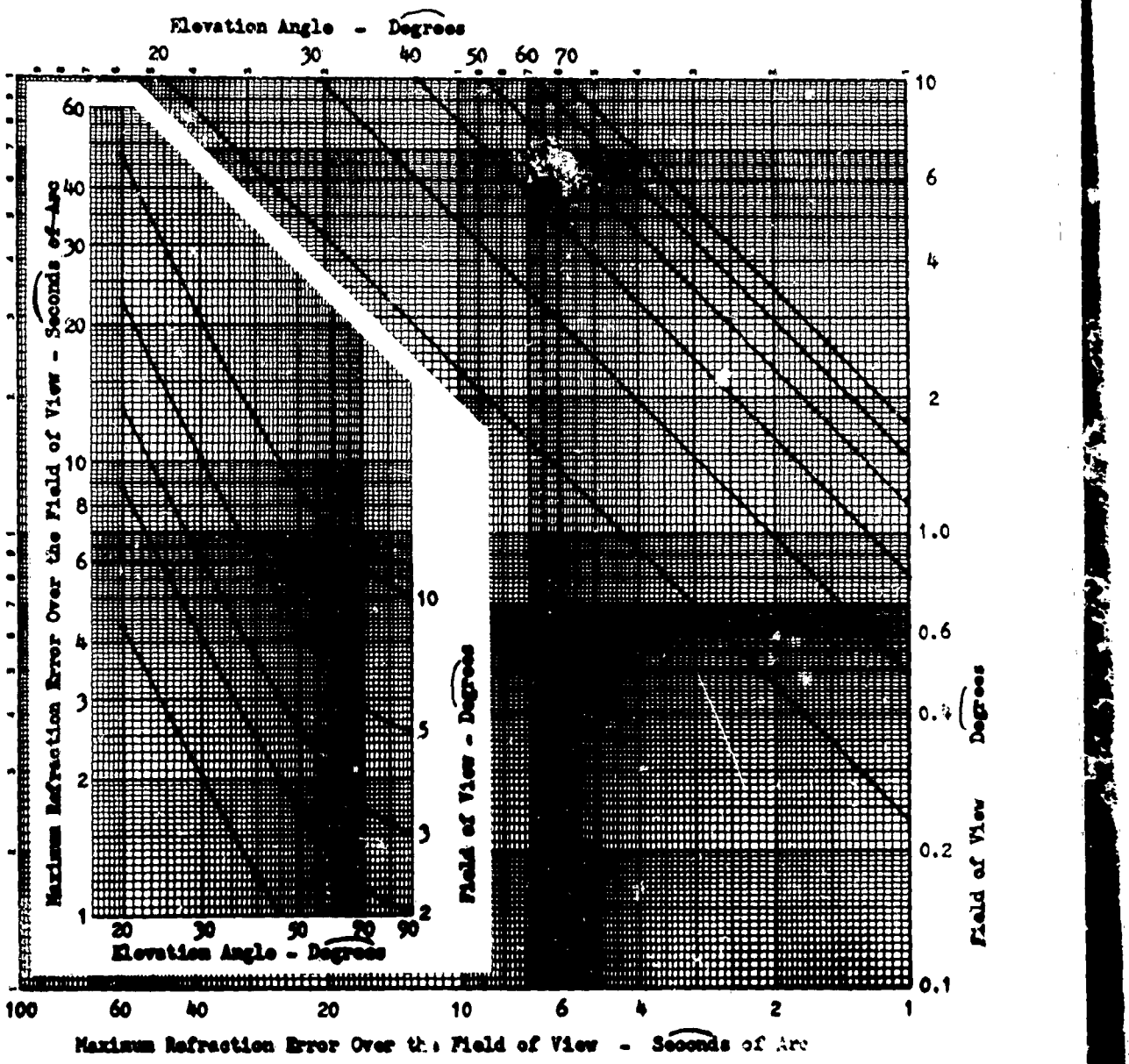


Figure IV-8. Refraction Error Between Center of Field of View and Edge

be cancelled. A polar plot of orientation angle vs. differential refraction error should be prepared centered on the true image position. This can then be used to determine the cancellation area required.

A temporary storage comparison system would exhibit the least refraction error because new exposures are frequently made, each including the total correction for its particular elevation angle. In this way the orientation angle variation is kept to a minimum as well as the change in elevation angle. An estimate of the amount of the error can be made by assuming a maximum elevation rate of 0.25 degrees per minute and reading the error difference from Figure IV-8 for the change of elevation angle between exposures.

A dual station comparison system can also have low cancellation errors due to refraction. The difference in elevation angles of the two stations observing the same region of sky is on the order of:

$$\theta' = \frac{180\ S}{\pi r} = (0.01666)\ S \qquad (9)$$

Where: θ' = Difference in elevation angle of the center of the field of view of the two stations

S = Distance between stations in N. Miles

r = Radius of earth = 3440 nmi.

For separation distances up to 200 nmi. the difference in elevation angles should be less than 3.5 degrees. From Figure IV-8, this would contribute about 3 seconds error at 23 degrees elevation with a 3 degree field of view. The amount of orientation angle difference should be about the same as the elevation angle difference; however, the two factors will not reach their maximum values at the same time. Further investigation of the geometric problems involved in the effect of refraction error on cancellation systems would be desirable.

3. DANCING

Another source of error contributed by atmospheric variations is described as dancing. This is a random fluctuation of the angular position of an image about some mean value. The fluctuation is correlated over short distances, but probably not over a distance long enough for the correlation to have any value in a two station system. Good experimental data is lacking in this area. The few reports available indicate that fluctuations up to 8 seconds of arc are possible.

4. OPTICS

The major source of cancellation error contributed by the optical system is likely to be the field curvature. The source of this error is the coupling of the curved focal surface of the lens system to the flat photocathode of the image orthicon. The effect of the field curvature is to produce a nonlinear correspondence between angular position and distance along the photocathode. An approximation of the magnitude of this error may be obtained as follows. Let:

x = The ratio of the distance to the image from the center of the photocathode to the distance to the edge of the photocathode,

β = The angular displacement of the source from the optical boresite.

Then the angle measured by linearly scaling the distance of the image from the center of the photocathode is given by:

$$\beta_m \quad \frac{\Phi}{2}\ x \qquad (10)$$

Whereas the actual angle is:

$$\beta_a = \mathrm{Tan}^{-1}\left[x\ \mathrm{Tan}\ \frac{\Phi}{2}\right] \qquad (11)$$

Where: β_m = Measured angle

β_a = Actual angle

Φ = Field of view

The angular error may then be defined as:

$$e' = \beta_a - \beta_m = \mathrm{Tan}^{-1}\left[x \,\mathrm{Tan}\,\frac{\Phi}{2}\right] - \frac{\Phi}{2}\,x \tag{12}$$

After making the following approximations,

$$\mathrm{Tan}\,\frac{\Phi}{2} = \frac{\Phi}{2} + \frac{1}{3}\left(\frac{\Phi}{2}\right)^3$$

$$\mathrm{Tan}^{-1}Z \quad Z - \frac{Z^3}{3}$$

and neglecting higher powers of Φ than the third for fields of view less than 10 degrees, the error is:

$$e' = x(1 - x^2)\,\frac{\Phi^3}{24} \tag{13}$$

The maximum error is:

$$e'_{max} = \frac{\Phi^3}{36\sqrt{3}} \qquad \text{at } x = 0.577 \tag{14}$$

The maximum error of equation 14 is plotted in Figure IV-9. Also plotted is the relative error across the photocathode. This error is relatively unimportant for small fields of view but increases rapidly. It would not be a factor in systems that use exposures for comparison that have been taken through the same lens. This would include the mask systems as well as the temporary storage systems. It would not be a factor in two station systems if the optical designs were the same. This error would have to be compensated in a star chart system if the field of view were more than 6 or 8 degrees. This error will add directly to the refraction error at the corresponding elevation angles.

5. SYNCHRONIZING AND TIMING ERROR

In a star cancellation system that requires the comparison of scanned fields such as a permanent storage technique using a flying spot scanner, or a temporary storage technique using a storage tube, or a two station system, a potential source of misregistration is the jitter in the synchronizing of the line sweeps of the two fields. A difference in sweep start times can cause a differential shift of the two images in the direction of the scanning lines. An estimate of the error introduced for a given time error is given by:

$$e_s = 0.0036\,\frac{\Phi N}{kT}\,t \qquad \text{seconds of arc} \tag{15}$$

$$n = \frac{N^2}{kT}\,t \qquad \text{lines} \tag{16}$$

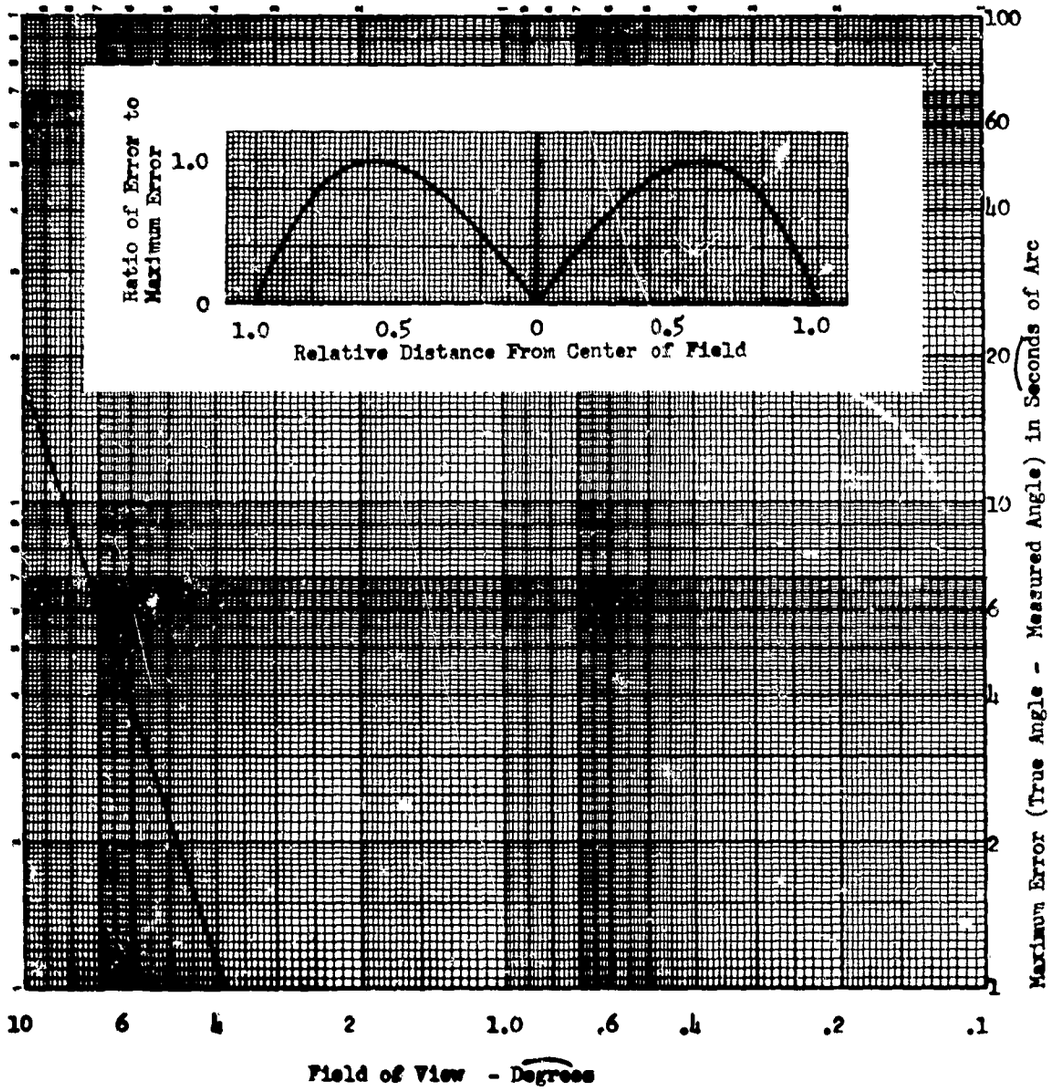


Figure IV-9. Curvature of Field Error

Where: e_s = Angular error in seconds of arc

n = Angular error in lines

N = Number of active lines per scan

T = Time of field scan in seconds

k = Ratio of active horizontal sweep time to total horizontal sweep time

Φ = Field of view in degrees

t = Time error in microseconds

For a field of view of 3 degrees, 1200 lines per scan, 1/30 second scan time, and a horizontal sweep ratio of 0.85,

$$e_s = 457\ t \tag{17}$$

A timing stability better than 22 nanoseconds would be required to hold the angular error within 10 seconds. Synchronizing systems have, however, been built with jitter held to less than 1/2 nanosecond which would correspond to an error less than 0.25 seconds. Synchronization within a single station should not be a problem. Adjustable delays would have to be provided to compensate for the various fixed time delays that would be present.

Synchronization between stations may present more of a problem because of the data transmission circuit characteristics. All transmission systems have a certain amount of delay, but those systems having a variable delay such as HF links should be avoided unless they have been thoroughly tested for this application. Microwave links would probably be the best. Even though synchronization of sweep starts may be held within tolerable limits by means of circuit techniques, a variable transmission delay between synchronization pulses can cause displacement of the image. This is most serious, of course, for threshold images. Again, good data on propagation delay is lacking; however, it would seem that the delay fluctuation of a microwave link would be at least as small as the synchronization jitter and probably smaller.

6. LINEARITY

In scanning circuits using linear sweeps, a departure of the sweep waveform from linear will cause a displacement of the image. The degree of nonlinearity is usually specified by the displacement of the image as a percentage of the total sweep length. The equivalent angular error will be a function of the field of view as indicated by the following equation.

$$e_1 = 3600\Phi u \quad \text{seconds of arc} \tag{18}$$

Where: e_1 = Angular error in seconds of arc

Φ = Field of view in degrees

u = Linearity of sweep expressed as ratio of image displacement to sweep length

For a three degree field of view, a linearity of 1 percent would produce an error of 108 seconds. A sweep linearity of 0.1 percent should be possible, reducing the error to 11 seconds. Fortunately, this source of error is not so important in systems where the same sweep is used for both fields being compared. In this case the important factor is stability, which should be at least 10 times better than the linearity itself. Sweep linearity could well be the major source of error in a two station system.

7. IMAGE ORTHICON RESPONSE UNIFORMITY

The intensity response of the image orthicon as a function of the position of the image on the photocathode will not directly affect the cancellation registration especially in systems using the same tube to produce both fields being compared. When different tubes are used such as in a two station system, the variation in

response can upset the cancellation process by making some stars undetectable at one sensor but detectable at the other. A loss in detection probability would result from the necessity to reduce the sensitivity of the system to the level of the least sensitive area of the image orthicon.

C. THE BASELINE (STEREO) SEPARATION SPACE SURVEILLANCE SYSTEM

The baseline separation technique is based on the registration or the celestial background at infinity vs. an object not at infinity.

The ability to detect or separate is determined by the geometry of the network: The baseline separation and the precision measuring threshold limit. This threshold is set by the stability of the atmosphere, (including refraction), the spot (image) size, the registration ability of two separate but time synchronized sensors and associated electronic stability, and the exchange or transfer of information to a common point for processing.

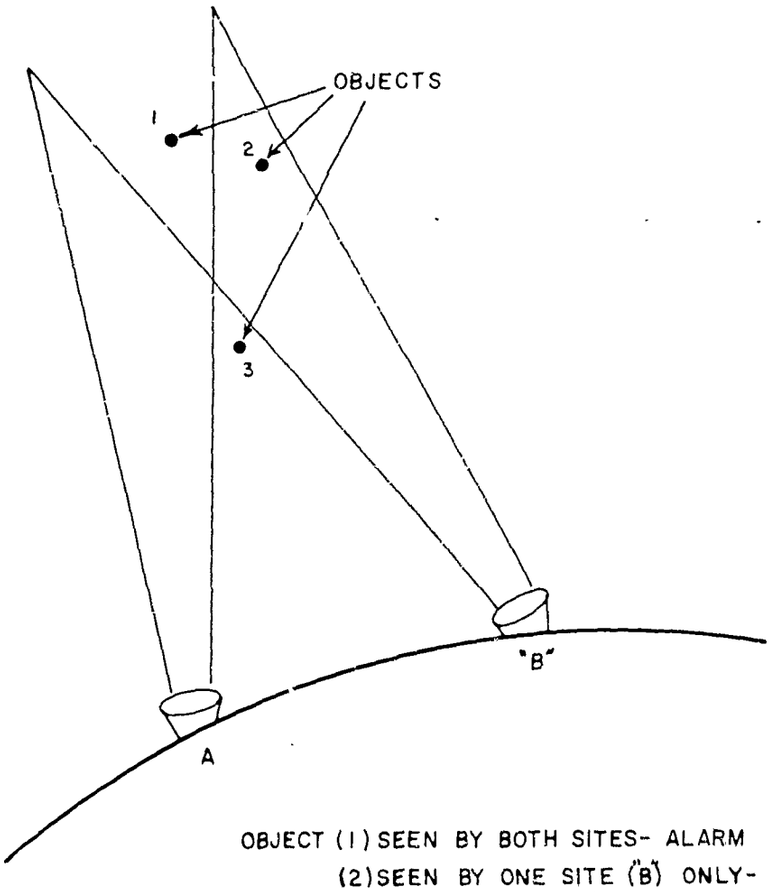
1. GEOMETRY

Two sensors separated on the earth's surface by a distance d, viewing an object in space at a finite altitude will observe it at slightly different positions relative to the star background. In the baseline separated bi-static system this apparent angular displacement (parallax) is used as a basis for separating the object and the star background. The geometrical constraints which limit the performance of this system are discussed below.

It is assumed that sensors at both sites view the exact same star background simultaneously. The view of the sky taken at one site is relayed to the other site where it is compared on a resolution element by resolution element basis with the view taken at that site. The comparison is accomplished in such a way that if the same source of light occurs in both views in nearly the same position it is considered to be a star and is ignored. If, however, a source does not occur near the same position in both views it is considered to be a target and accepted for further processing. The amount of displacement necessary before a source is considered to be a target is referred to as the threshold parallax and is determined by the accuracy with which the two views may be registered in the comparison. This accuracy in turn is determined by the errors accumulated throughout the system including refraction, differences between the two sensors and optics, distortions introduced by the communications, and the degree to which the two sites can be synchronized. This threshold parallax is determined by a separate study which considers these factors and any others which contribute to the registration problem.

An object seen by one site but not the other is immediately accepted for processing as it represents positive separation. See Figure IV-10 case 2.

The amount of parallax displacement between the apparent positions of a body as seen by two separate sites is a function of the altitude of the body, the separation between the sites, and the angular position of the body relative to the two sites. The equations defining the parallax in terms of these quantities are derived in Appendix II, where it is demonstrated that for a given height and site separation the parallax is minimum at the lowest elevation angle in respect to the vertical plane containing the sites. (See Figure IV-10). In order to determine whether all of the space vehicles at a given altitude within a coverage volume will be detected it is necessary to determine whether or not this minimum parallax exceeds the threshold value.



OBJECT (1) SEEN BY BOTH SITES- ALARM

(2) SEEN BY ONE SITE ("B") ONLY- MAY BE CONFUSED WITH OBJECT (1) BY SITE "B" WHEN PROCESSING- ALARM

(3) NOT SEEN BY EITHER SITE

Figure IV-10.

In Figures IV-11, 12, 13, and 14 the minimum parallax is plotted as a function of the site separation for various altitudes, for elevation angles of 10^{o}, 20^{o}, 30^{o}, and 60^{o} respectively. The elevation angle is relative to either one of the two sites. These curves are obtained from the equations derived in Appendix II.

As indicated by Figures IV-11, 12, 13 and 14, the minimum parallax increases with decreasing target altitude and with increasing site separation. Therefore, the site separation necessary to insure that the parallax of all bodies exceeds the threshold value will be determined by the parallax at the maximum altitude to be covered. Therefore, if the coverage volume is bounded by a maximum altitude of 100,000 n. miles and a lower elevation of 20^{o}, and if the threshold parallax is 20 sec. (.0055 degrees), Figure IV- indicates that a site separation of 29 n. miles is required to insure coverage.

Figures IV-11, 12, 13 and 14 are adequate to determine the minimum site separation necessary to insure that the threshold parallax is exceeded throughout a coverage volume.

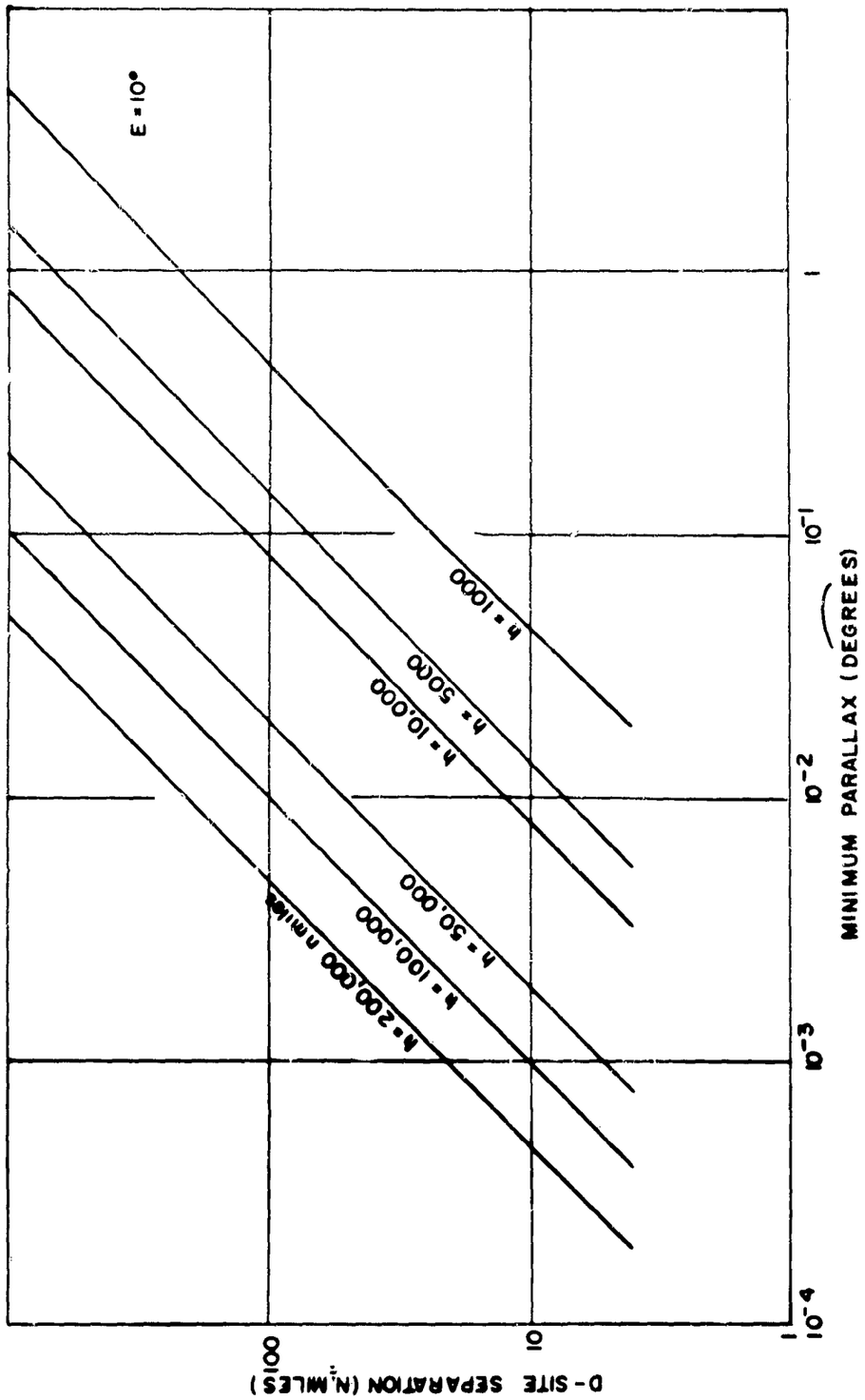


Figure IV-11. Minimum Parallax for Bodies at 10^{o} Elevation

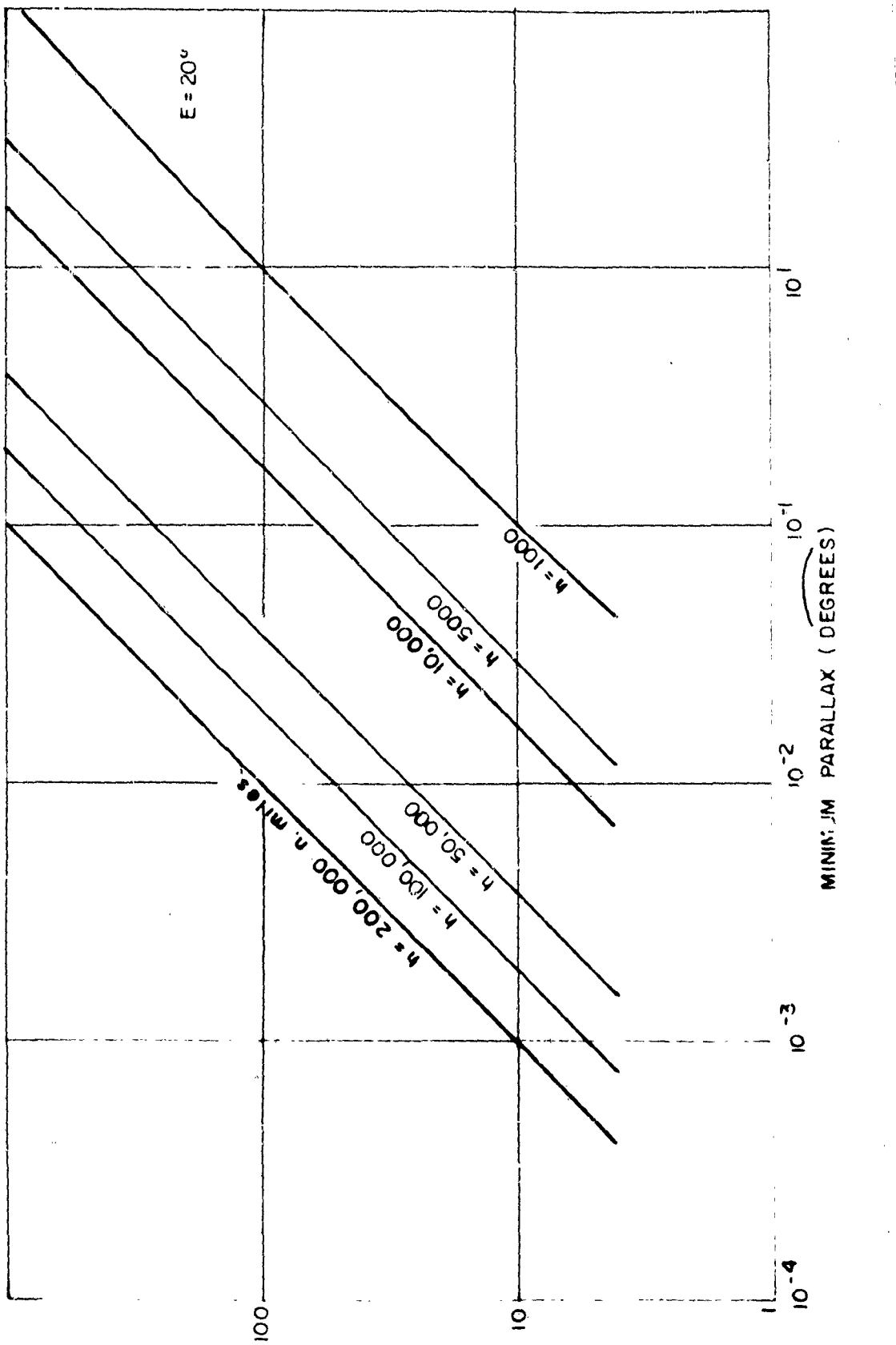


Figure IV-12. Minimum Parallax for Bodies at 20° Elevation

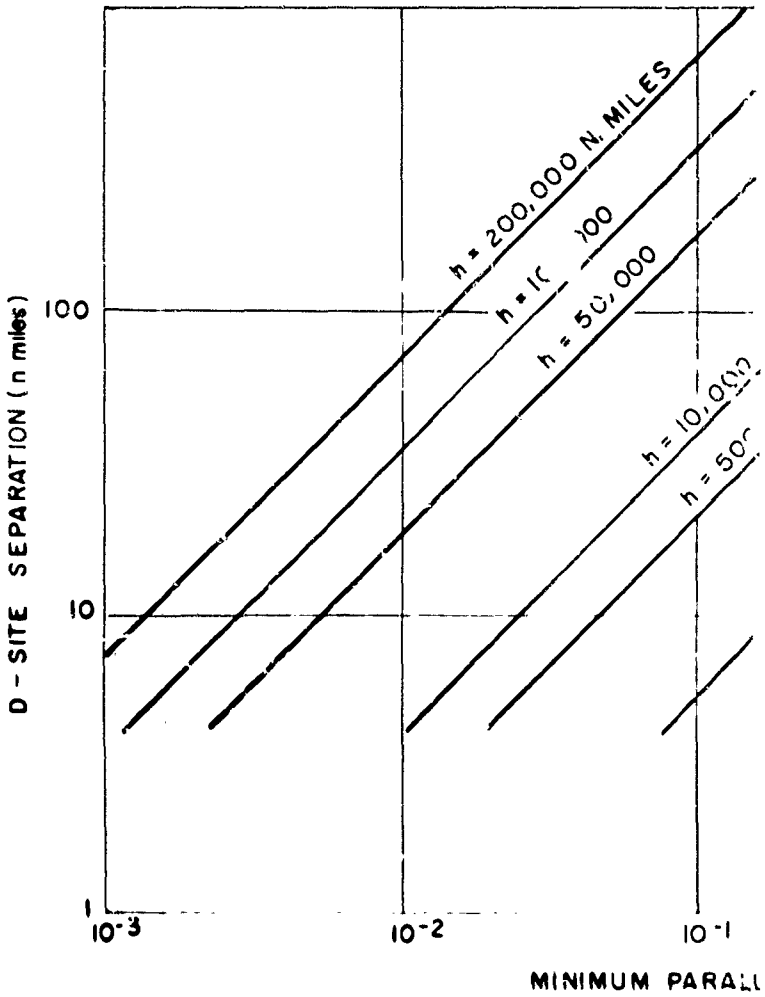
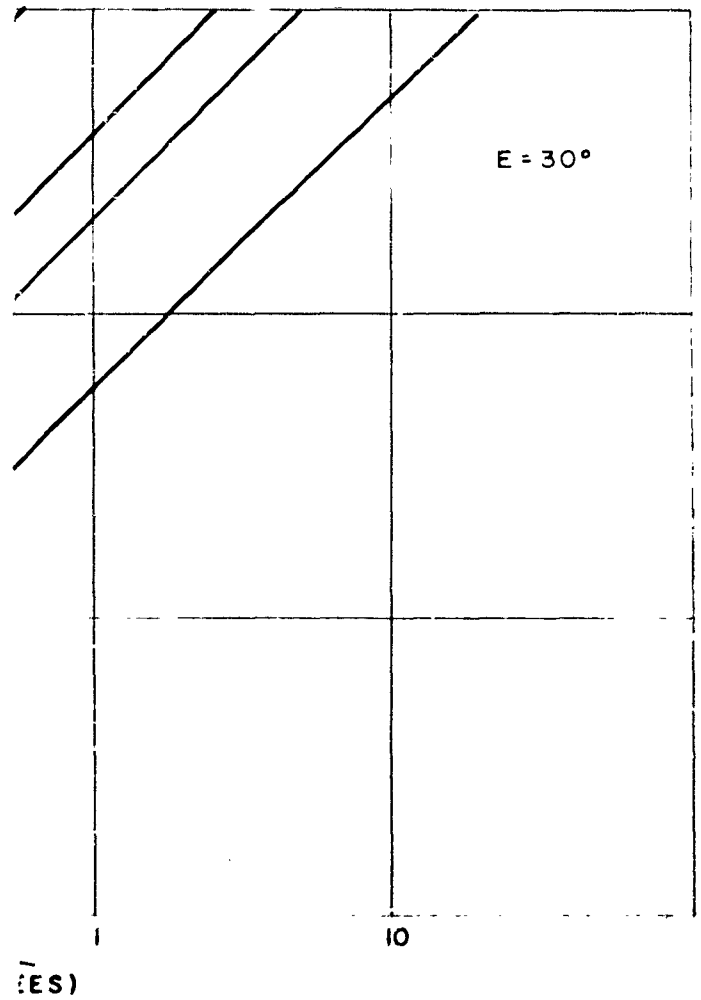


Figure IV-13. Minimum



Bodies at 30° Elevation

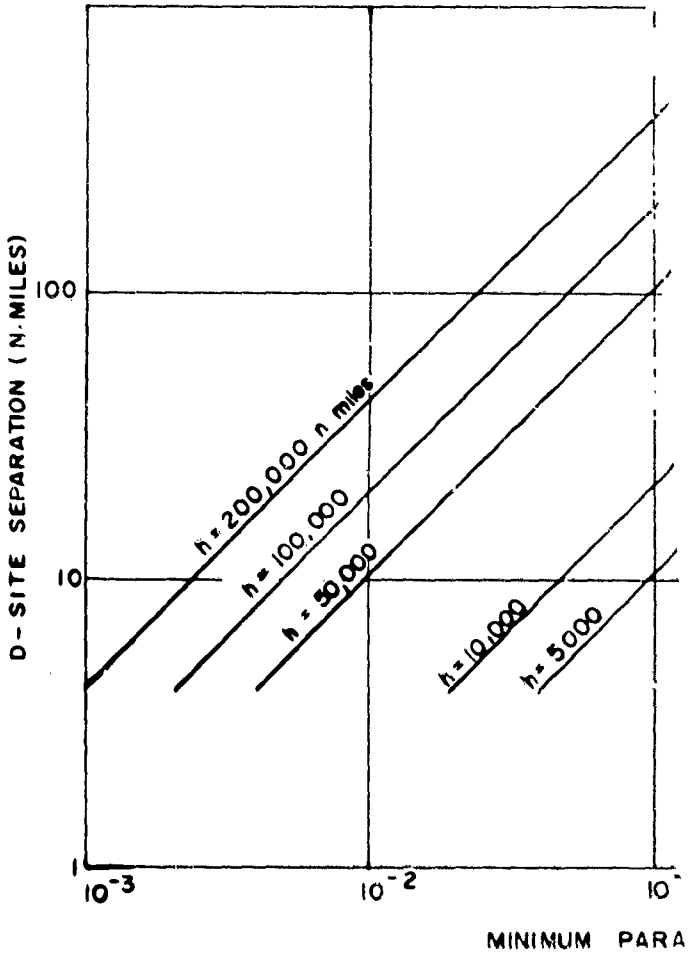
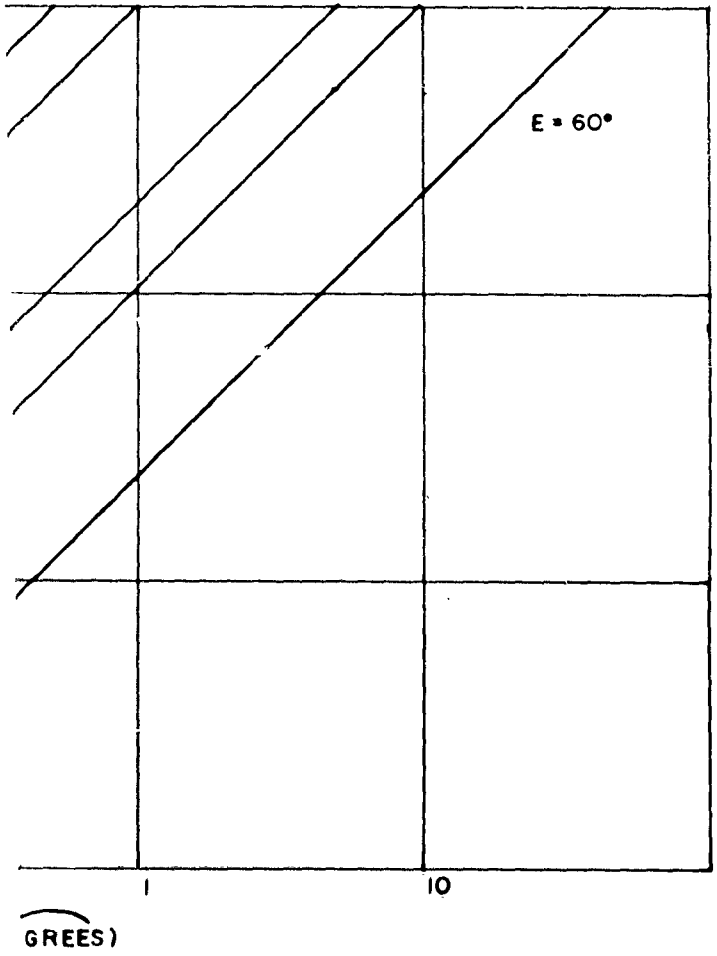


Figure IV-14. Minimu



x for Bodies at 60° Elevation

There are several considerations which make it desirable to keep the site separation as near as possible to the minimum value described above. The problem of communications between the sites is increased as site separation increases. Also, the problem of time synchronization of the two sites becomes more difficult the greater the site separation because the propagation time lapse between sites and its short term variation increase with increasing path length. The problem of registration between the two views of the same star fields is also made more difficult because of the greater change in atmospheric conditions and elevation angle of the star field made possible by increased site separation.

In addition, a more definite limit on the maximum site separation may exist, depending on the nature of the data required from the system and the use to which it is put. These considerations are discussed below.

The objective of a space surveillance system is to detect the presence of satellites or other space vehicles and to determine their trajectories. Detection by the bistatic (absence of cancellation) system requires that the parallax displacement exceed the threshold as described above. The trajectory determination may be accomplished in two ways, each of which represents a possible mode of operation for the bi-static system. One approach would utilize the angular coordinates of the space vehicle as measured at one of the sites in an "angle-only" procedure which is described elsewhere in this report. In this procedure three angular position measurements spaced in time are used to predict the trajectory of a body in space. If angular information is available from both sites simultaneously, it may be considered as redundant data and the prediction accuracy thereby improved. This system, however, only requires that one of the sites be able to see the space vehicle at a given time.

The other approach to trajectory determination would utilize, not only the angular position measurement, but also the angular displacement between the positions. The magnitude of this displacement may be directly related to the range between the site-complex and the space vehicle and, therefore, with the bi-static system it is possible to obtain instantaneous angle and range information about a space vehicle. Using this approach only two readings separated in time are required to determine a trajectory. In order to measure the parallax displacement or range it is necessary that the space vehicle appear within the field of view of the two sites simultaneously, which introduces an additional constraint on the system.

The requirement that the target appear in the fields of view of both sites simultaneously limits the maximum value of the parallax which can be accepted. If the parallax becomes too large the target will be displaced completely out of the field of view of one site when it appears in that of the other. If the parallax displacement is greater than the angular diameter of the field of view, any target appearing in the field of view of one site will not appear in the field of view of the other site. Therefore, the effective field of view of the pair of sites will be zero. If the parallax is less than the diameter of the field of view the effective field of view of the pair of sites will not be zero but will be equal to that portion of the single site field of view which is common to both sites. In Figure IV-15 the ratio of the solid angle contained in the effective field of view of the pair of sites to that contained in the single site field of view is plotted as a function of the parallax, expressed as a fraction of the single site beamwidth. This plot is based on equations derived in Appendix II.

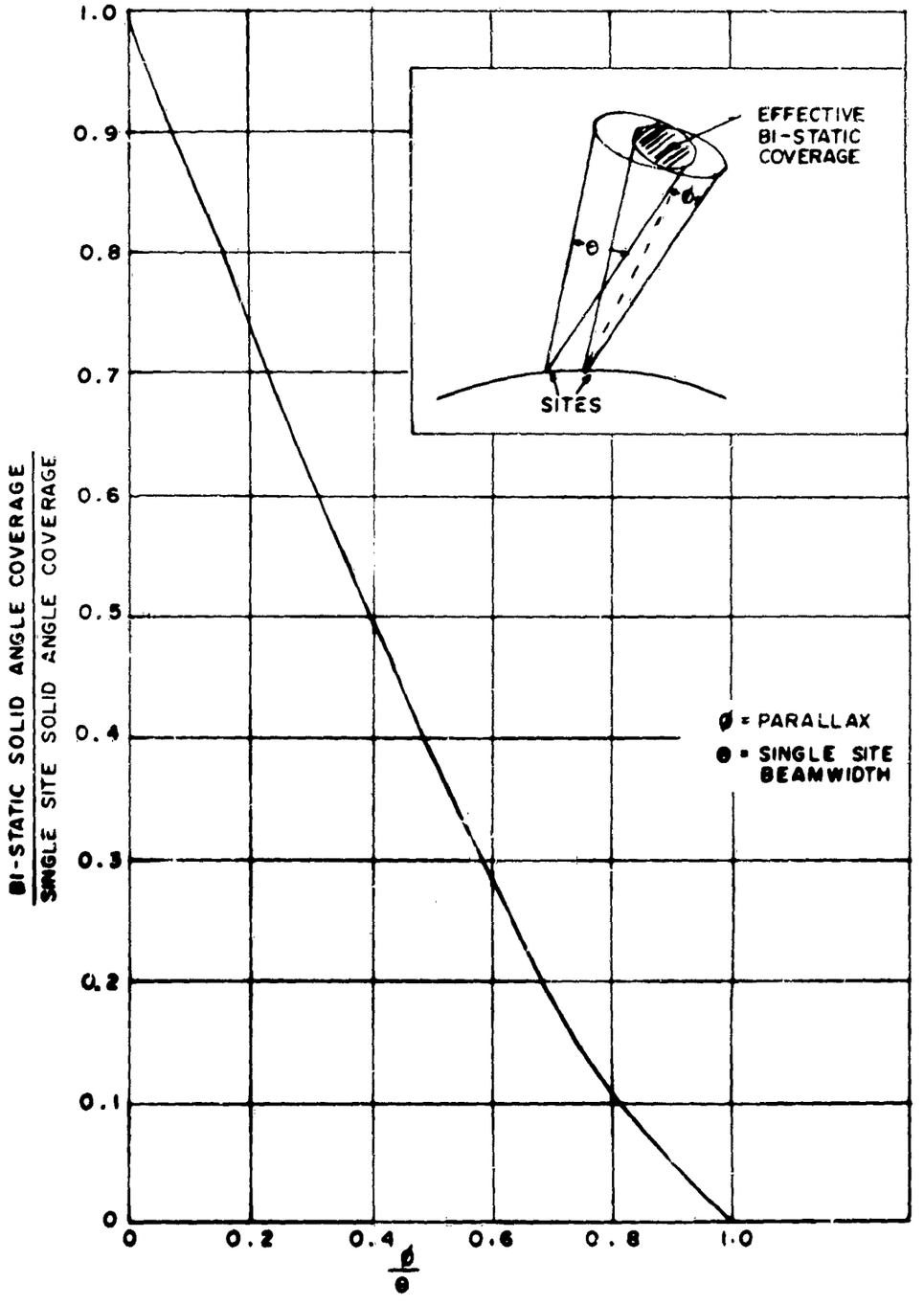


Figure IV-15. Coverage Loss for Range - Angle Mode

Since the parallax is a function of the altitude of the target, the reduction in the field of view will also be a function of the altitude. For a given altitude the reduction in the effective field of view increases with the parallax, and therefore, in order to determine the minimum effective field of view for a given altitude it is necessary to know the maximum parallax which a target at that altitude can have.

In Appendix II it is demonstrated that the parallax of a body at an altitude, h, is maximum when it is at the maximum elevation and when its azimuth relative to the great circle connecting the sites is either $\pi/2$ or $3\pi/2$. In Figures IV-16, 17, 18, and 19, the maximum parallax is plotted as a function of the site separation for elevations of 10^{o}, 30^{o}, 60^{o}, and 90^{o}, and for altitudes between 1000 n. miles and 200,000 n. miles. These curves were obtained from equations derived in Appendix II.

Figures IV-15 to 19 make it possible to estimate for a given altitude the reduction in the effective field of view of the pair of sites imposed by the requirement that the target appear simultaneously in the fields of view of both sites.

As an illustration of the application of these results, a typical system requirement will be considered. Assume it is desired to detect satellites at altitudes between 1000 n. miles and 100,000 n. miles at all elevations greater than 20^{o}, and that the threshold parallax is 20 seconds and the single site field of view is 3^{o} in diameter. The minimum site separation necessary to detect targets at 100,000 n. miles altitude with a threshold parallax of 20 seconds was shown earlier to be 29 n. miles. The maximum elevation to be covered by the system is 90^{o} and therefore Figure IV-19 must be used to estimate the maximum parallax. This figure indicates that for a site separation of 29 n. miles and an altitude of 1000 n. miles a maximum parallax of approximately 1.7 degrees would exist, which is 0.565 times the single site beamwidth. From Figure IV-15, this parallax results in a reduction in the effective coverage of 0.35.

Therefore, for the system considered, the requirement that both range and angle data be obtained by the surveillance system results in a reduction by a factor of about three in the coverage obtained with a pair of sensors. This reduction refers specifically to the lower altitude targets. As the altitude increases the coverage approaches the single site coverage.

The above discussion assumes that in order to be able to measure the target displacement, and therefore the range to the target, it is only necessary that the target appear simultaneously in both fields of view. This may be considered as only an ultimate limit since, for many cases, more stringent conditions must be required. Besides appearing in both fields of view simultaneously it must be possible to associate the image of the target in one view with that in the other. If there is only one image in each field of view this correlation requirement is trivial and reduces to the case considered above. If, however, there are more than one image appearing in one or both of the fields of view it is possible that an image of one target in one field of view may be associated with the image of another target or a false alarm in the other field of view. In this case, an erroneous range measurement would result. The probability of this mis-correlation occurring will be a function of the size of the field of view, the target population density, the false alarm rate, etc. Depending on the magnitude of these factors, it may be necessary to limit the maximum parallax to a value less than that indicated by the requirement that the target appears in both fields of view simultaneously. The maximum parallax applicable in a given case must be determined for a specific system taking into consideration the system parameters, and the required system performance. Assuming that this maximum

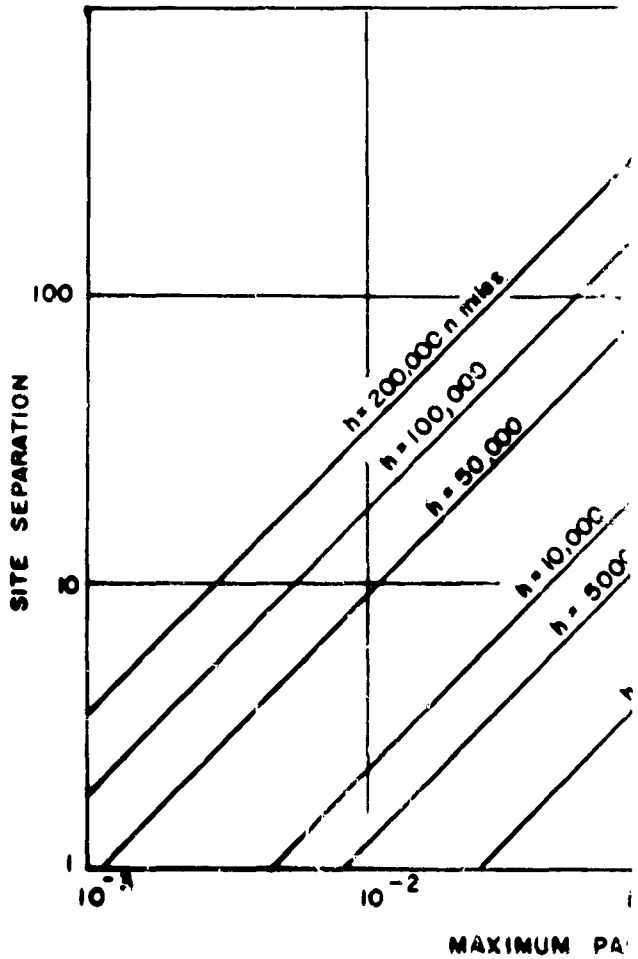
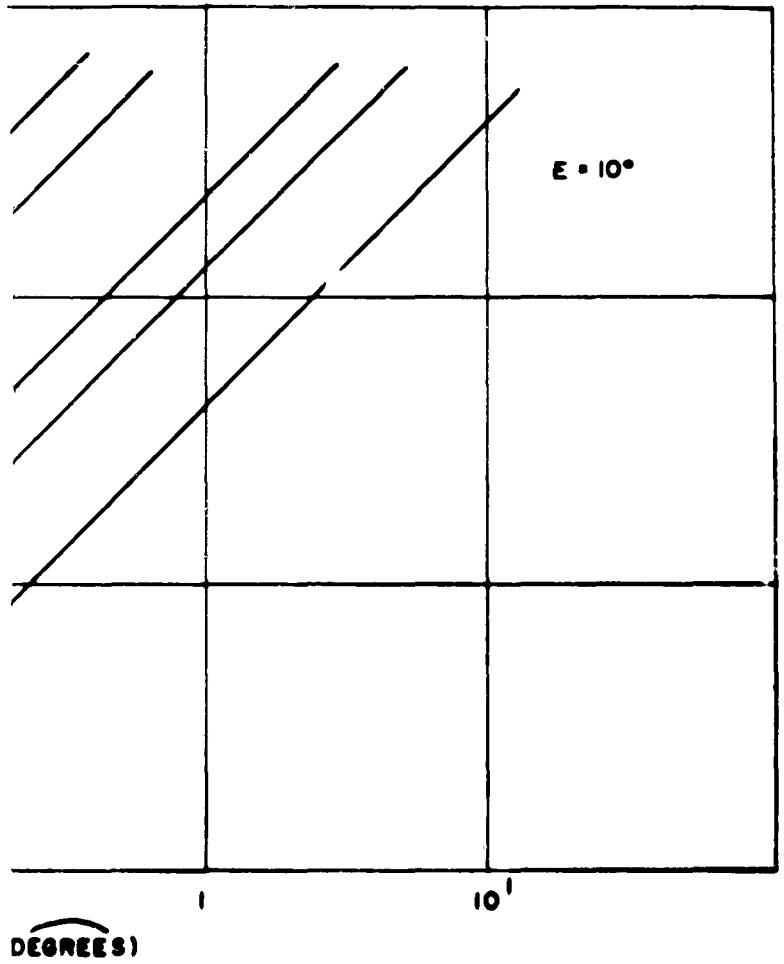


Figure IV-16. Max



arallax for Bodies at 10^0 Elevation

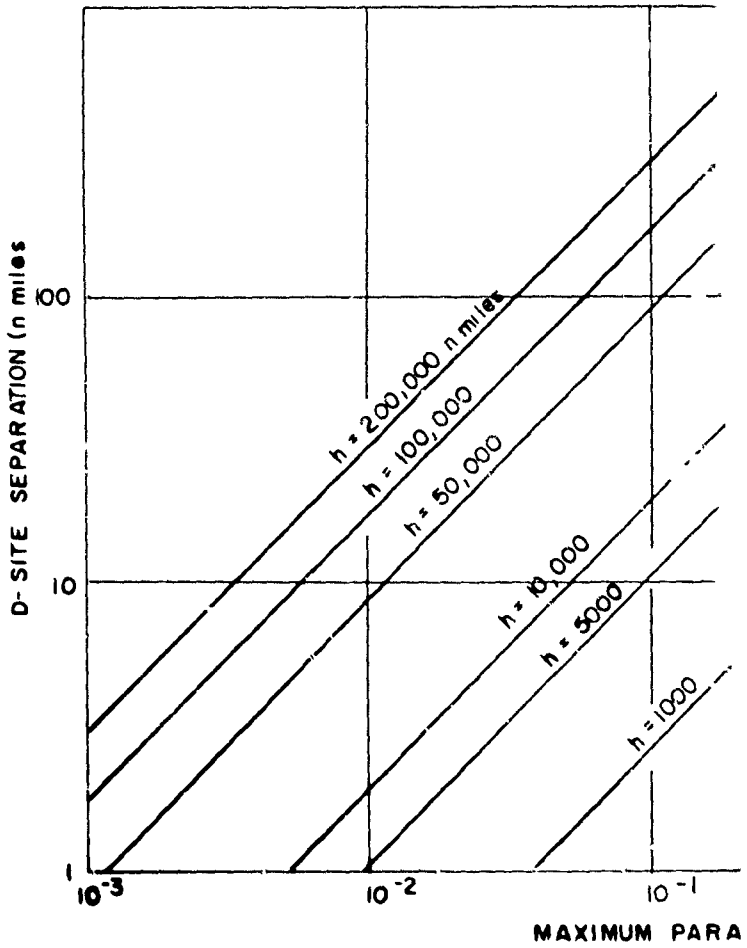
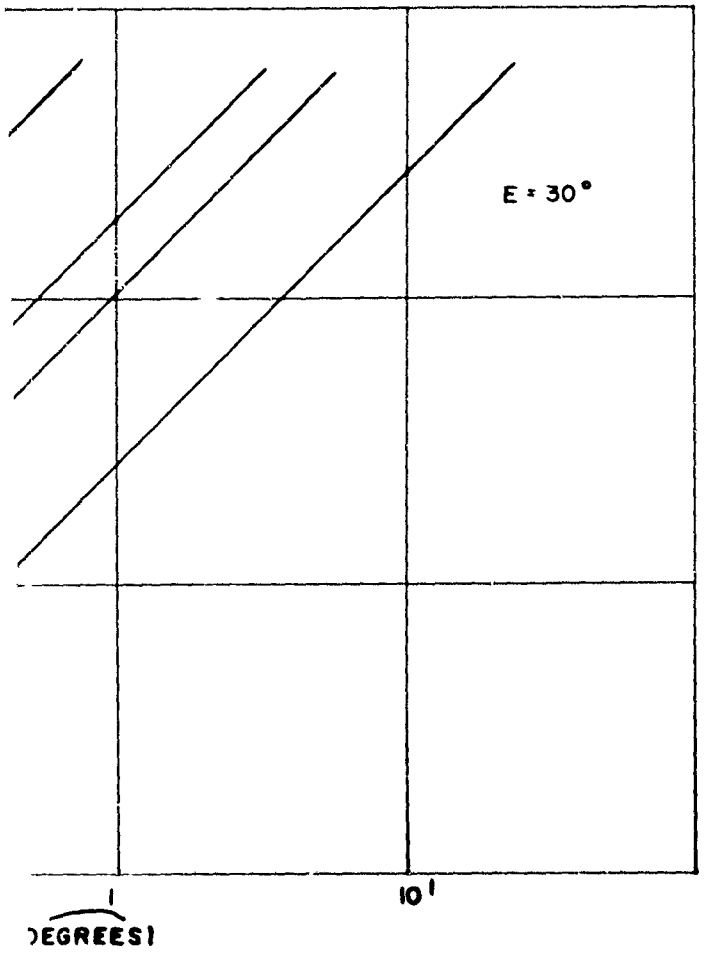


Figure IV-17. Maximum Paral



Bodies at 30° Elevation

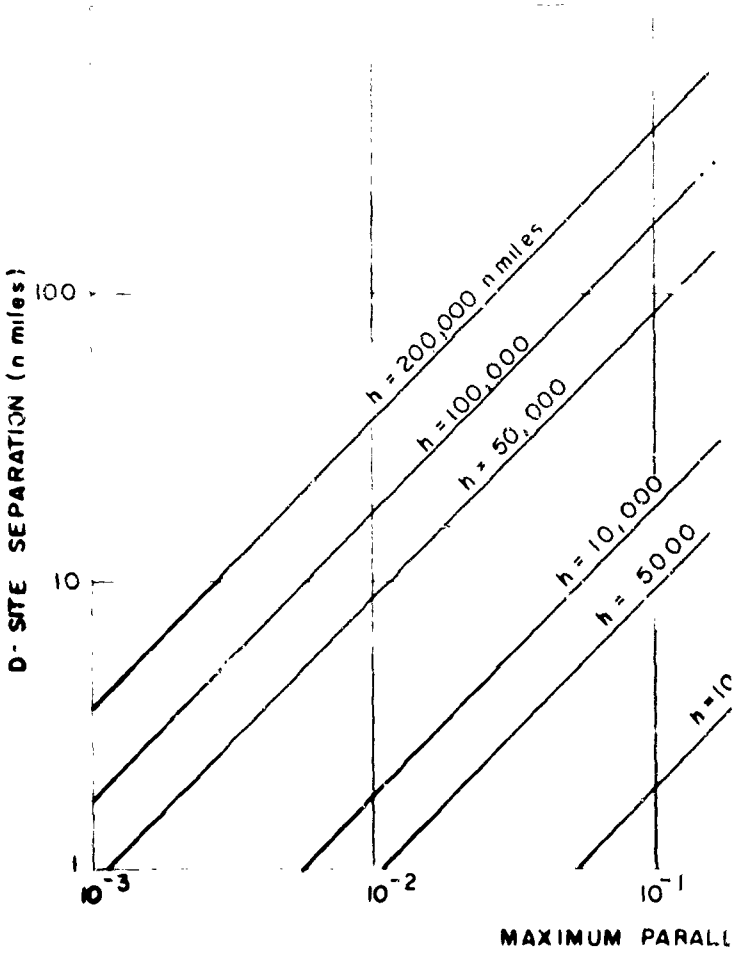
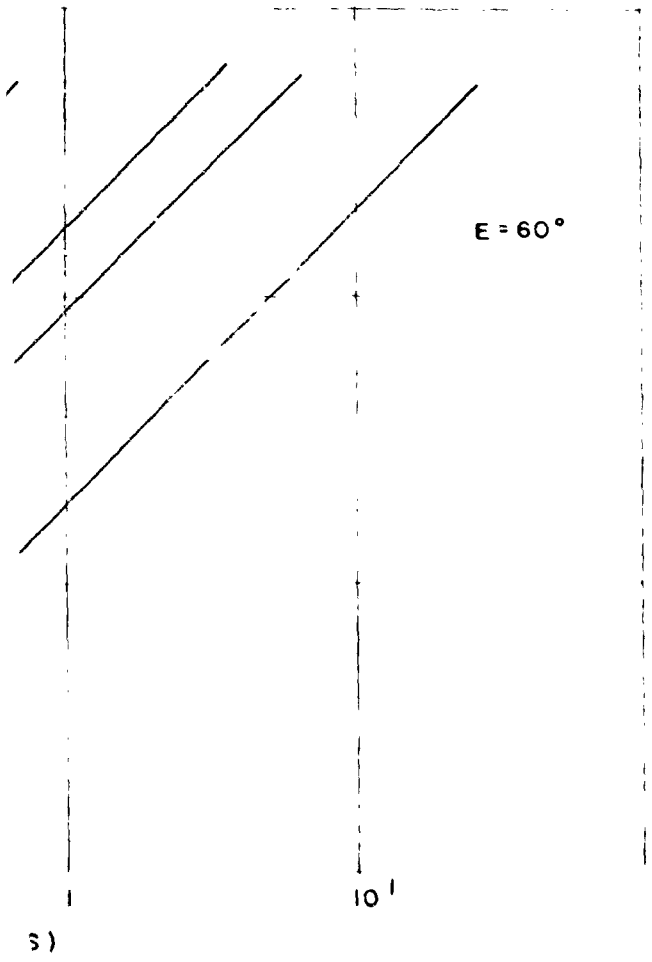


Figure IV-18. Maxim



x for Bodies at 60° Elevation

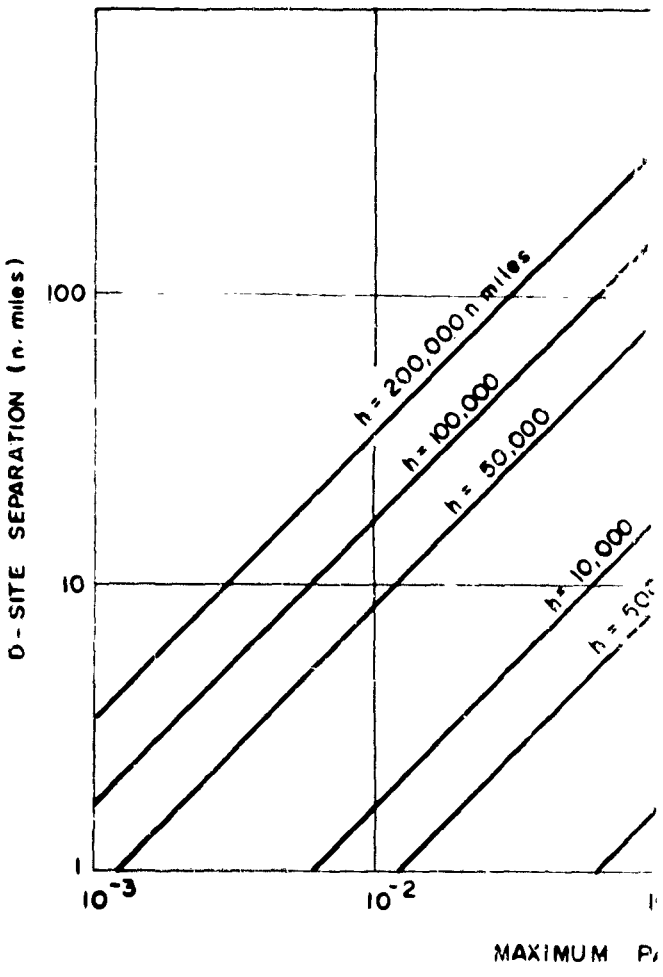
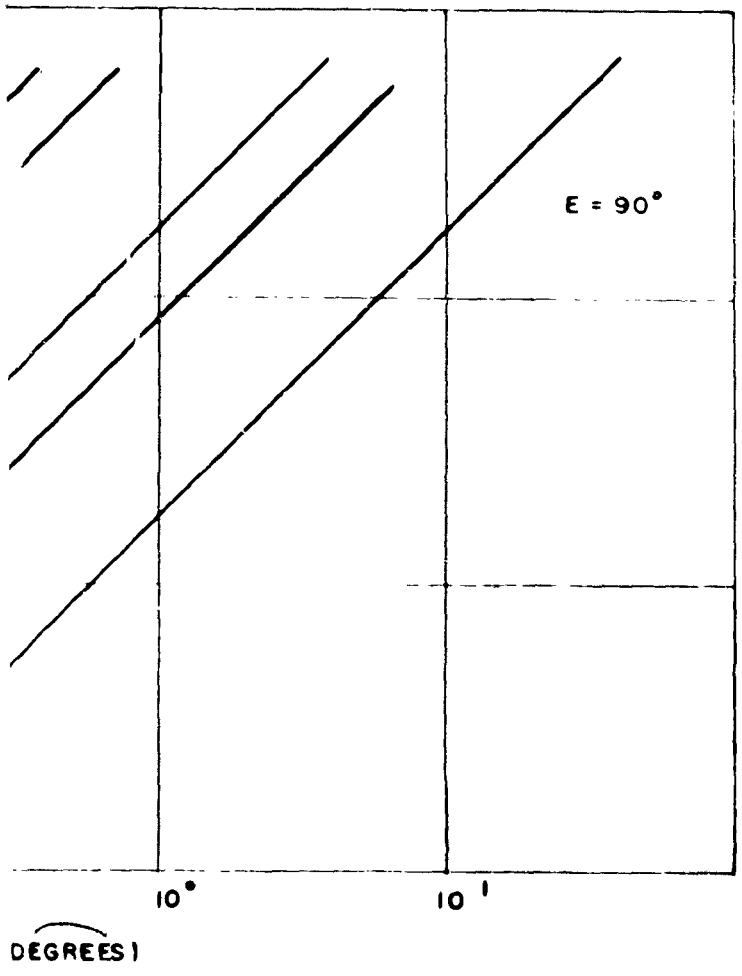


Figure IV-19. Max



allax for Bodies at 90° Elevation

parallax is known for a particular system, the resulting constraint imposed on the altitude coverage may be determined from Figures IV-16 to 19.

For example, for the system considered above, if the maximum parallax is assumed to be 1000 $\widehat{\text{sec}}$ of arc (0.288 degrees), Figure IV-19 indicates that the minimum altitude for which all targets would fulfill this requirement is approximately 6000 n. miles. In order to cover the 1000-6000 n. mile altitude interval the site separation must be reduced below 29 n. miles, however, this would result in a loss of coverage at the high altitudes. In order to cover the whole altitude interval a third site would be necessary which would be separated from one of the other two sites by a distance somewhat less than 29 n. miles. In this way one pair of sites would cover the high altitude targets while the other pair would cover the low altitude targets.

The above discussion indicates that the range-angle mode of operation for the bi-static system imposes additional requirements on the system configuration which, in certain cases may make this mode of operation undesirable. In general, the coverage obtained in the range-angle mode is less than that of a comparable system operating in the angle only mode. This is particularly true when coverage over large altitude intervals is required. The curves presented above may be used to estimate the coverage loss as a function of the system configuration and performance requirements. In order to determine the desirability of operating a particular system in one mode or the other, this coverage loss should be balanced against whatever advantages the range-angle mode might have from the standpoint of trajectory estimation.

2. THRESHOLD MOVEMENT FOR STEREO SYSTEM

Stereo detection (lack of cancellation which can be considered a target) requires a relative position displacement, between the two site images, which is significantly larger than the average misregistration of star positions. If the misregistration is random, and its sigma can be determined, a detection misregistration limit of 3 sigma would give a false alarm rate of approximately 10^{-3}. So 1 out of every 1000 stars detected would be called a target, which would result in too many false alarms.

Therefore, it is assumed that the minimum "detection" misregistration should be at least 4 times the average misregistration sigma. Unfortunately, most of the misregistration errors which have been tabulated are "maximum" errors, and these "maxima" all occur at the edges of the image area. Assuming the worst case near the edges, and also assuming that these edge errors are approximately 3 sigma, the overall 3 sigma stereo registration error is:

Image Dancing: 6 $\widehat{\text{sec}}$

Sweep Registration: 20 $\widehat{\text{sec}}$

$0.2\% \times 1000 \text{ lines} \times 10 \frac{\widehat{\text{sec}}}{\text{line}}$

Refraction Differential Error: 6 $\widehat{\text{sec}}$

Due to different pointing angles $\Delta\theta$ due to non-flat earth.

$\Delta\theta = \frac{360^{\circ}}{21700 \text{ nm}} \times 50 \text{ nm} = .83^{\circ}$

Synchronization Jitter (60×10^{-9} sec): 10 $\widehat{\text{sec}}$

Two Mount Pointing Registration Error: 30 $\widehat{\text{sec}}$

A programmed $\Delta\theta$ bias is assumed.

Total 3σ of Misregistration ($\sqrt{\epsilon\,\sigma^2}$): 38.4 $\widehat{\text{sec}}$

Position Displacement for Detection Threshold (4σ): 51 $\widehat{\text{sec}}$

This "detection" threshold does not consider image size spread. If a suitable method of measuring image centers is employed, image spread due to intensity above detection threshold can be neglected. The problem of measuring the image center due to relative image motion during exposure is different, because the image spread is not symmetrical in both dimensions. The "detection" threshold is approximately 5 scan lines of movement, and most detected images are 2 or more scan lines in diameter. A system which requires a detection displacement large enough so there is no common area between the two target images, would require about 1.5 times the displacement as a system which measured the position of image centers.

3. STEREO ADVANTAGES AND DISADVANTAGES

This list is brief and is not inclusive.

Advantages:

1) Immediate recognition (detection) of targets.
2) Additional information from the displacement angle of a target image, at the two or more sites. This information (if available) can be used to calculate approximate target range.
3) No image storage requirement.

Disadvantages:

1) Operation time is weather limited. Both sites require clear weather, with any moving or stationary clouds causing false alarms.
2) Requires duplicate systems with at least 2 mounts, 2 telescopes, and 2 cameras.
3) The mounts have to be ultra-precise and programmed for the non-flat earth bias pointing error. The alternative is a mount pointing servo to minimize non-cancelled video, with a loss of viewing time required to servo the mount before an image can be taken.
4) The requirement of a communication link with enough bandwidth to transmit the complete scanned image, in real time.

4. SYSTEM ARRANGEMENTS

Multiple site stereo systems can be considered in hybrid configurations:

1) Stereo used only for long range (small relative velocity) separation, in conjunction with a storage tube MTI using only one short range (small time) image storage at the main site.
2) Stereo used to collect additional displacement angle information only, with the stereo site remotely operated from the main site.
3) Other hybrid systems.

The choice of a complete system should consider hybrid configurations. In general the problem of separation lends itself to hybrid systems. Another problem that might be best solved by a "multiple" system is the determination of target orbits, or the measurement of separated (detected) target angle versus time data points. A system designed for target-star separation might operate more efficiently, if any "detected" target could be handed over to an auxiliary tracker optic system. This tracker could give accurate angle versus time information, for longer measurement times and better orbit predictions.

D. THE M. T. I. DELAY INTERVAL-TEMPORARY CATALOG SPACE SURVEILLANCE SYSTEM

In the M. T. I. system two time separated images are compared on an element by element basis. If an image occurs in nearly the same position in both views it is considered to be a star and is cancelled. If, however, a source does not occur in nearly the same position in both images, it is considered to be a target and accepted for further processing.

This comparison procedure may be the same as that employed in the baseline system, and, as in the baseline system, a threshold displacement will exist which a source must have to be considered a target. This threshold displacement must be greater than the maximum displacement which a star image will encounter due to mis-registration. The maximum star displacement will be determined by all the errors throughout the system which contribute to mis-registration of the two views.

The apparent motion of a satellite relative to the star background as seen by an observer on earth is due to two effects: first, the orbital motion of the satellite will in general contribute to the apparent motion and second, the rotation of the earth with the resulting displacement of the observer causes an apparent shift of the satellite due to parallax.

1. DISPLACEMENT DUE TO EARTH ROTATION

In considering the effect of the earth's rotation on the apparent position of a body in space, the body is considered to be stationary in space and all the apparent motion is considered to be due to the motion of the observer. Since the observer is on the rotating earth, if he looks at the body at two different times he will be looking at it from two different positions in space and the body will appear to shift relative to the star background. See Figure IV-20A. This is essentially a parallax effect and the amount of apparent displacement will be a function of the altitude of the body and the distance the observer has moved between looks. Therefore, if the site displacement is known, Figures IV-11 to 14 and 16 to 19 may be used to determine the minimum and maximum displacement of a stationary body as seen from a rotating earth.

The site displacement due to earth rotation for a given time lapse will vary with the latitude of the observation site. The site displacement is plotted in Figure IV-20B from equations derived in Appendix III.

Using the site displacements obtained from Figure IV-20B in conjunction with Figures IV-16 to 19 the maximum angular displacement of the body due to earth rotation may be determined as a function of time, for a given altitude, elevation and site latitude. A more useful quantity which can be determined from the same curves is the apparent maximum angular velocity of the body due to earth rotation.

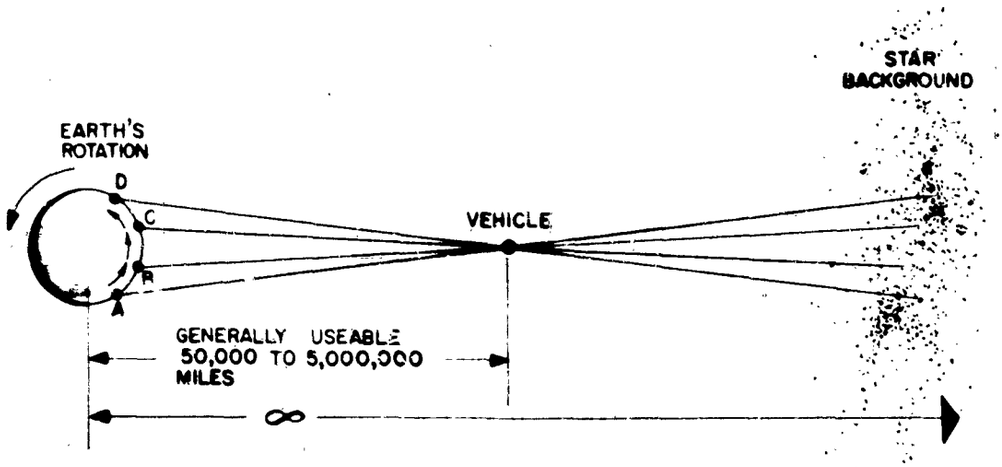


Figure IV-20A.

When this is done it is found that the apparent angular velocity is nearly constant over a wide range of time lapses. This angular velocity is plotted in Figure IV-21 as a function of the altitude of the body and the latitude of the observer, assuming that the body is directly above the site (E = 90°). Since the largest parallax will occur for E = 90°, Figure IV-21 represents the maximum angular velocity due to earth rotation alone which can be observed at any elevation.

2. DISPLACEMENT DUE TO ORBITAL MOTION

The effect of the orbital motion of a body in space on the apparent displacement of the body as seen by an observer on earth may be evaluated by considering the earth as non-rotating with the body in orbit about it.

The maximum and minimum angular velocities of a body relative to an observer on a stationary earth are plotted in Figure IV-22 as a function of the altitude and the elevation of the body as seen by the observer. The calculations resulting in these curves are presented in Appendix III. In these calculations it is assumed that the maximum angular velocity at a given altitude would correspond to that of a body in an orbit with an eccentricity of 1.0 and with a perigee at that height. The minimum angular velocity was assumed to correspond to the apogee angular velocity of a body in an orbit with an eccentricity of 0.8.

Comparing Figures IV-21 and 22 it is evident that the maximum angular velocity due to orbital motion is much larger than that due to earth rotation so that when considering the maximum angular velocity which will be observed the effect due to earth rotation may be neglected.

The minimum angular velocity which will be observed will occur when the angular velocity due to orbital motion and that due to earth rotation are in opposite directions and as nearly equal as possible. The minimum total angular velocity will be approximately equal to the difference between the angular velocity due to orbital motion and that due to earth rotation.

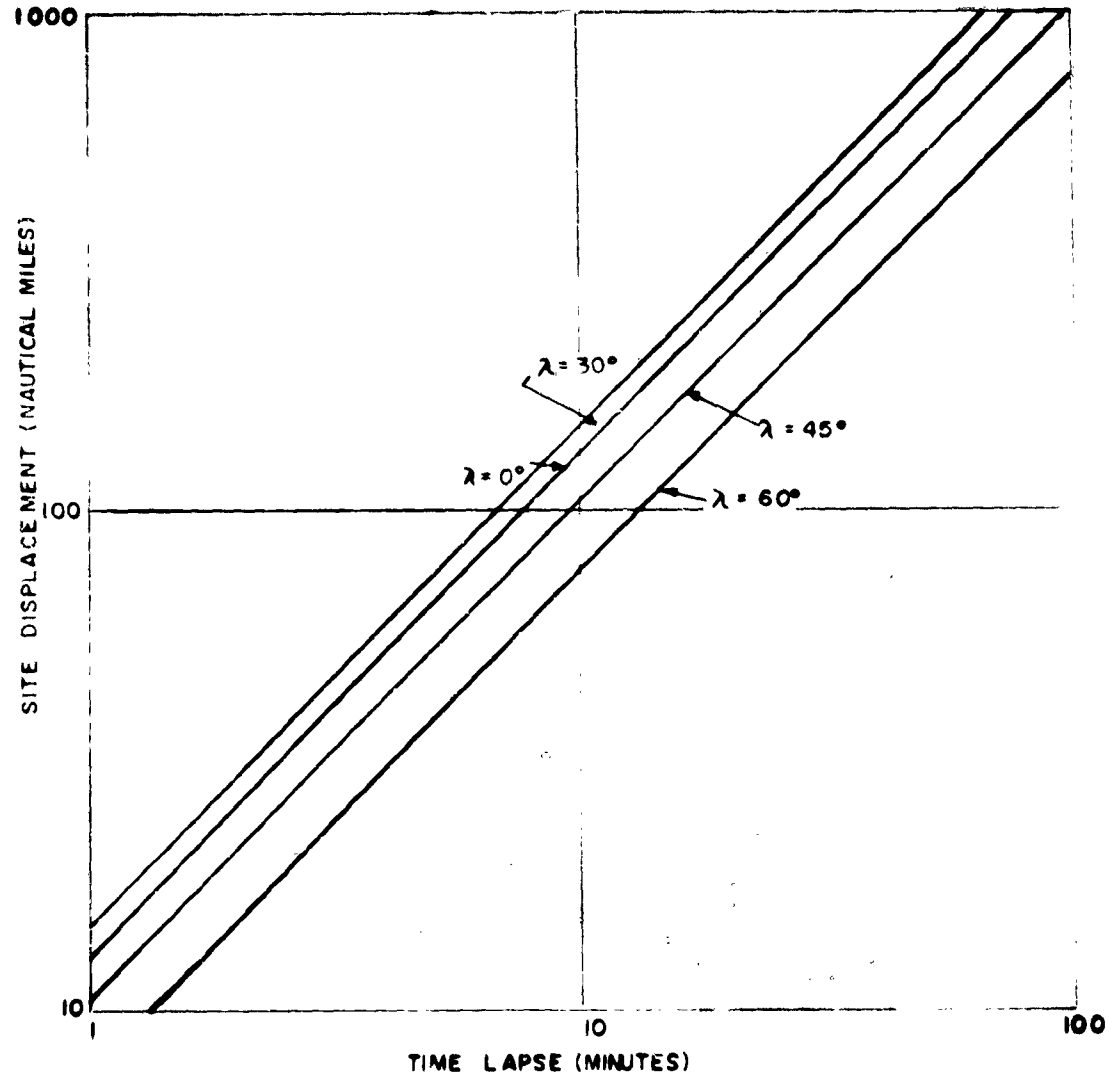


Figure IV-20B. Site Displacement Due to Earth Rotation

From Figures IV-21 and 22 it may be seen that the orbital component of the angular velocity will be greater than the rotational component for all altitudes less than about 200,000 n. miles. The exact height at which the rotational and orbital components can be equal will vary with the latitude of the observer. Above that maximum altitude, the minimum observed angular velocity can be zero.

In Figure IV-23 the minimum possible angular velocity is plotted as a function of the altitude for observers at various latitudes. These curves are obtained by taking the difference between the $\omega_{min}(E = 90^{o})$ curve of Figure IV-22 and the curves of Figure IV-21. The $\omega_{max}(E = 90^{o})$ curve of Figure IV-22 is also plotted to represent the overall maximum angular velocity which may be observed. Figure IV-23, therefore, defines the range of angular velocities which a body in space orbiting the earth may be assumed to have relative to an observer on earth.

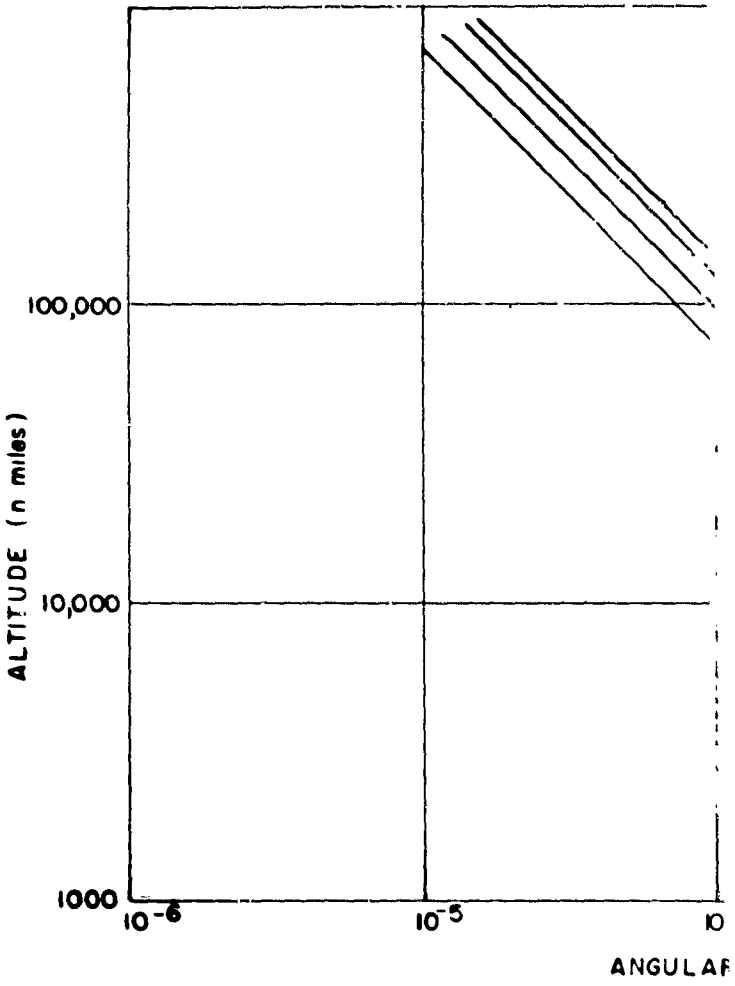
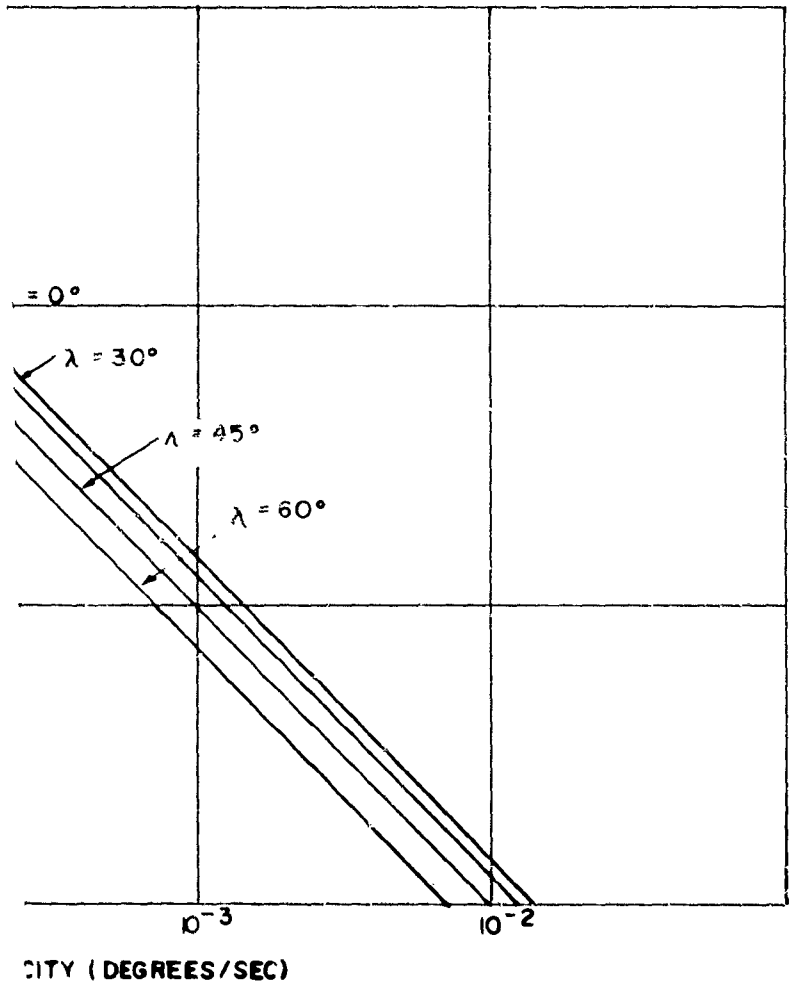


Figure IV-21. Angular Velo



to Earth Rotation Alone (Maximum)

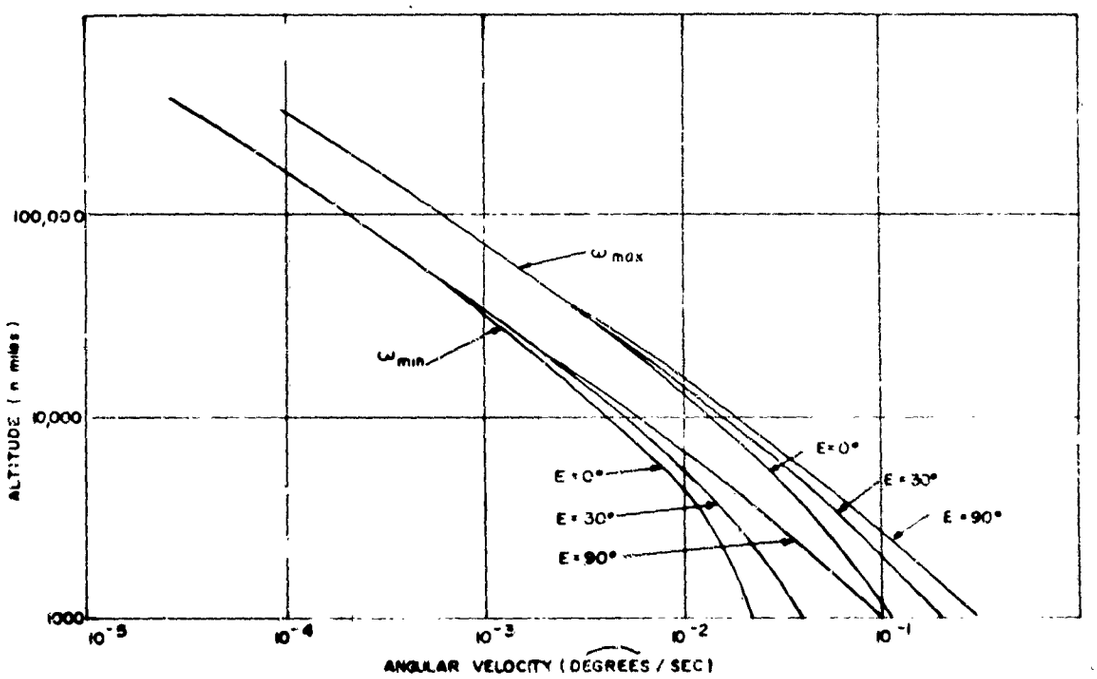


Figure IV-22. Maximum and Minimum Angular Velocity Relative to Site on Stationary Earth

The time lapse between looks necessary to insure that the apparent displacement of the body between looks exceeds the threshold displacement may be determined by dividing the threshold angular displacement by the minimum angular velocity given in Figure IV-23. The threshold time lapse is plotted in Figure IV-24 as a function of the altitude of the body and the threshold displacement, ϕ_T, assuming a site latitude of 45°.

In general, a maximum desirable displacement between views will exist, which may be determined by the necessity of correlating the successive positions of the body with each other to establish the body's motion or to track the body. If the time lapse is too large, the bodies with the larger angular velocities may be displaced so far from look to look that it may be impossible to determine whether or not it is the same body. The maximum acceptable displacement will be determined by the tracking requirements of the system, and by the target population density which the system is likely to encounter. Assuming the maximum displacement is known, the

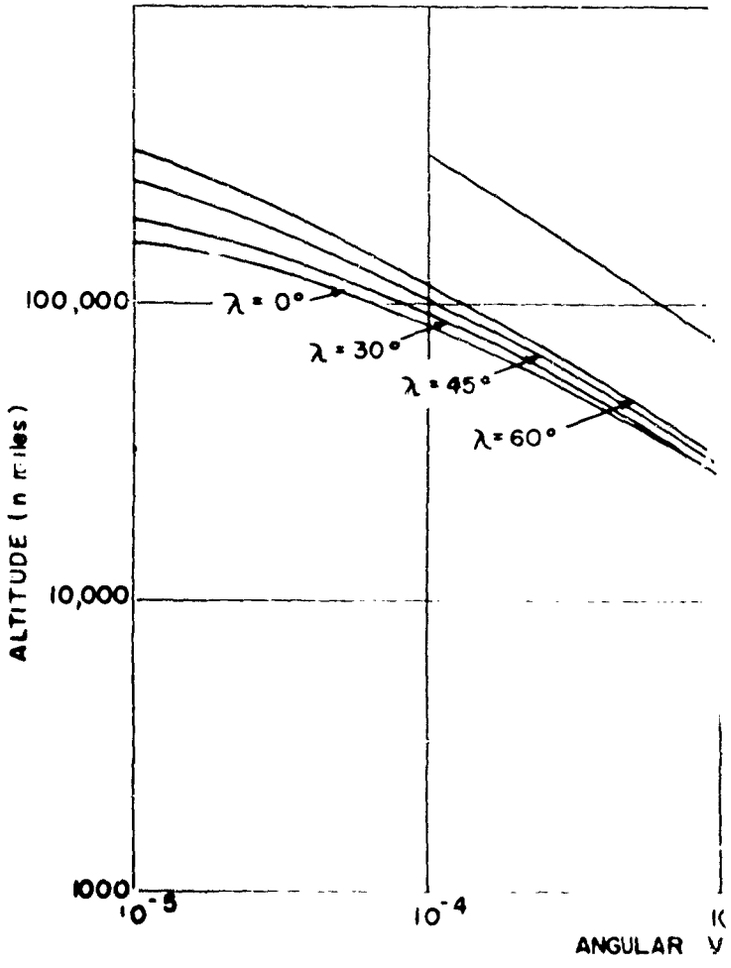
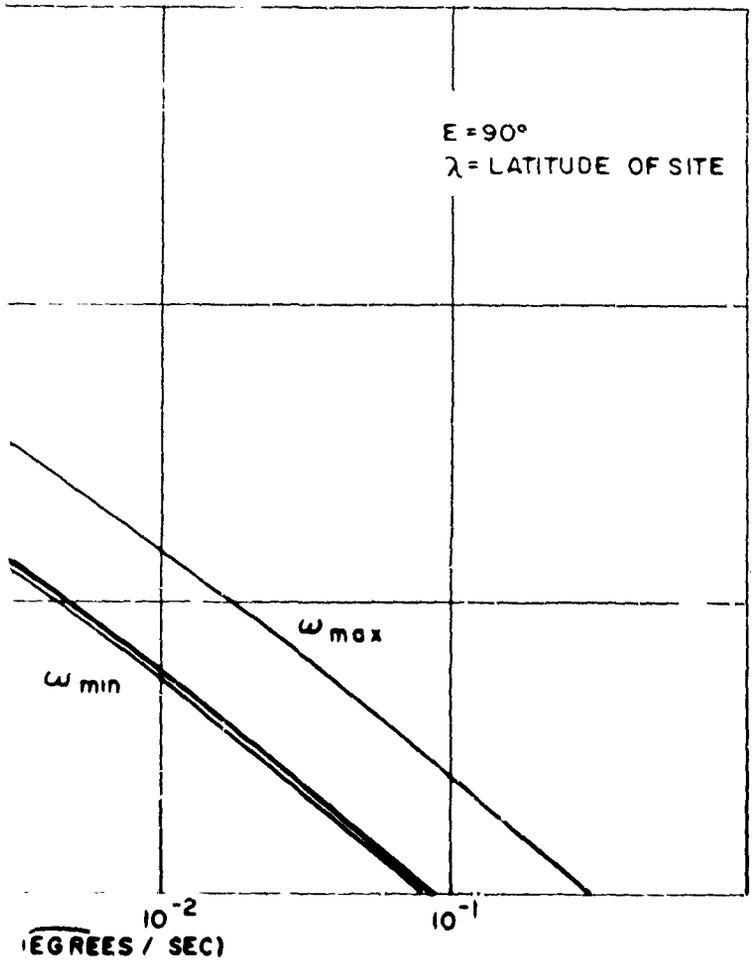
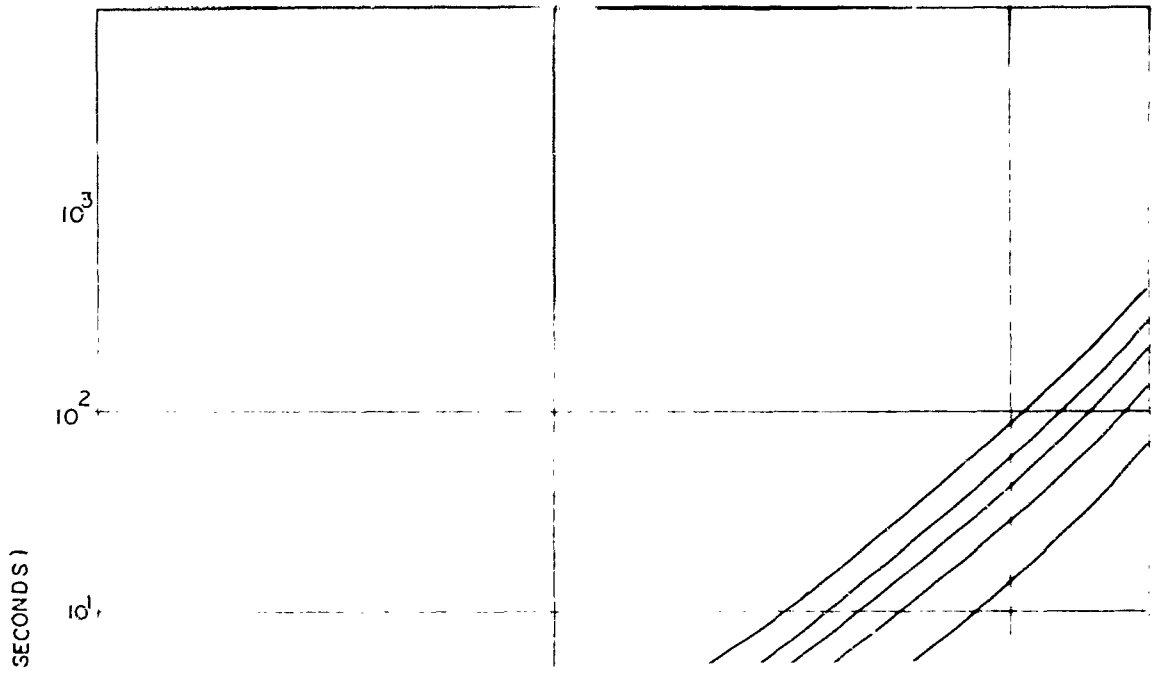


Figure IV-23. Maximum and Minimun



ular Velocity Relative to Site on Earth



t All Satellites Below a Given Altitude

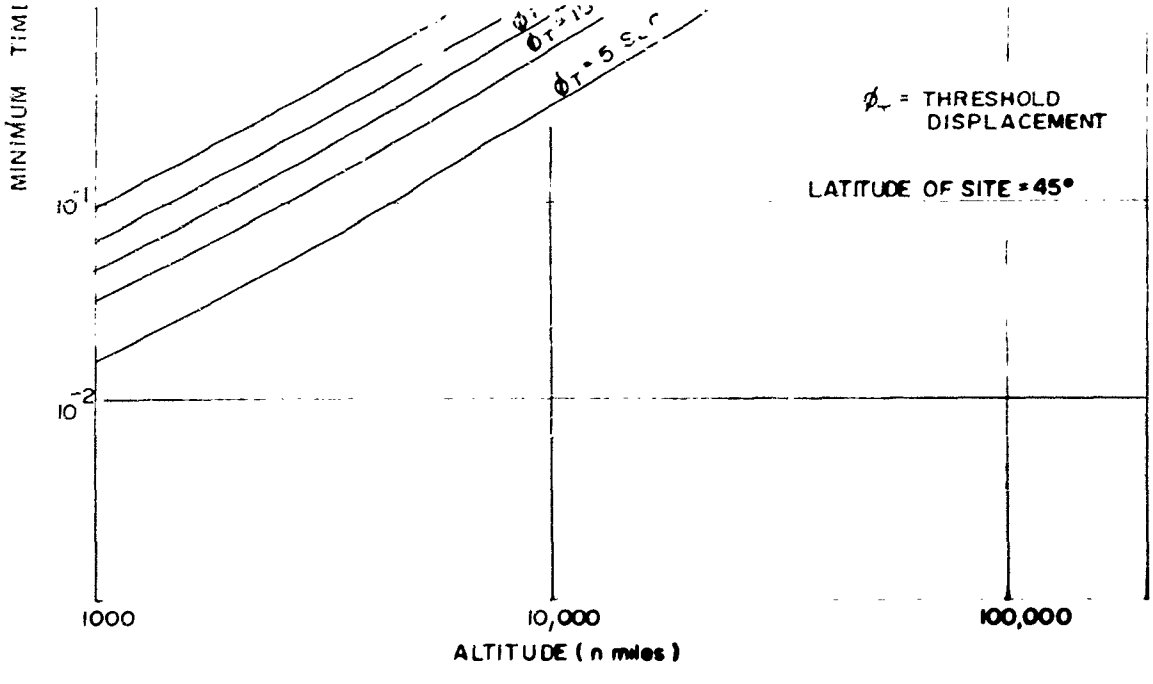


Figure IV-24. Minimum Time Lap

maximum time lapse between views may be determined for a body at given altitude by dividing that displacement by the maximum angular velocity obtained from Figure IV-23. The maximum allowable time lapse is plotted in Figure IV-25 as a function of the altitude of the body and the maximum displacement, ϕ_M.

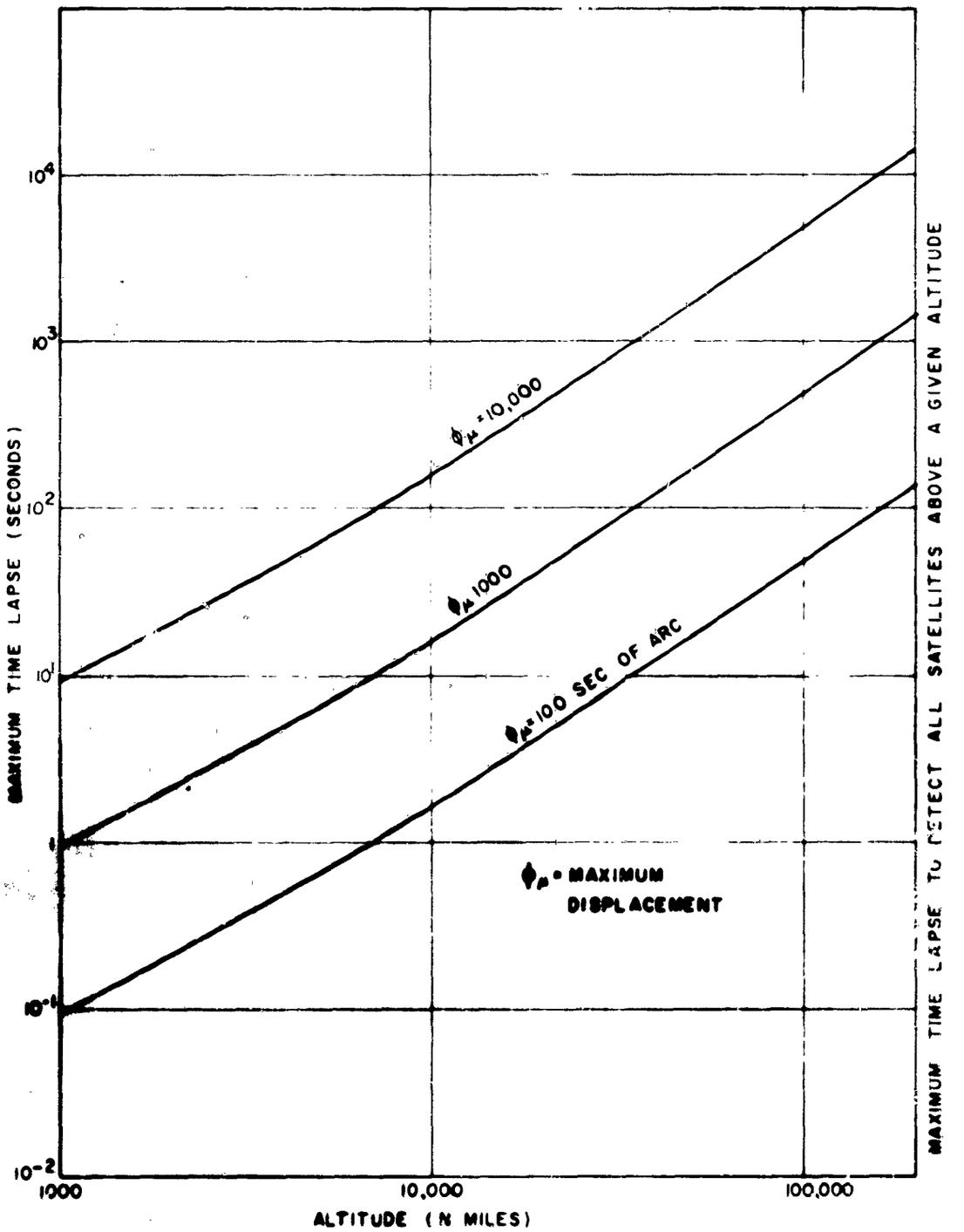


Figure IV-25. Maximum Time Lapse to Detect all Satellites Above a Given Altitude

Since both a minimum time lapse and a maximum time lapse are defined for each altitude it follows that a given time lapse will not necessarily suffice for all altitudes. In general, the height interval over which a given time lapse between looks will be adequate will be limited and, therefore, if a large height interval is to be surveyed it may be necessary to employ a number of different time lapses.

Figures IV-24 and 25 define the time lapse requirements which a single site M. T. I. space surveillance system must fulfill if a desired coverage is to be assured. As an example of their application consider the following typical system requirement:

> The system must be able to detect all bodies between 1000 n. mi and 100,000 n. mi altitude. The threshold displacement is $\phi_T = 20 \widetilde{sec}$ and the maximum displacement is $\phi_M = 1000 \widetilde{sec}$.

In order to detect targets at 100,000 n. miles a time lapse of at least 55 seconds between looks is required, as indicated by Figure IV-24. Figure IV-25 indicates that the minimum altitude which may be completely covered with a time lapse of 55 seconds is 23,500 n. miles, since below that altitude this time lapse causes an excessive angular displacement. Therefore, in order to insure coverage below 23,500 nautical miles a shorter time lapse between looks is necessary.

From Figure IV-24, the minimum time lapse required to detect all the targets at 23,500 n. miles altitude is 4.2 seconds. Figure IV-25 indicates that a time lapse of 4.2 seconds will provide coverage down to 2600 n. miles. Therefore, even with a time lapse of 55 seconds and another of 4.2 seconds the desired coverage is not obtained and a third time lapse is required.

The minimum time lapse which provides full coverage at 3600 n. miles is approximately 0.3 seconds, as seen from Figure IV-24. This time lapse will provide full coverage well below 1000 n. miles, as indicated by Figure IV-25.

Therefore, in order to obtain full coverage over the 1000 - 100,000 n. mile altitude interval with the assumed system it will be necessary to look at a particular field of view at one time, look again a few tenths of a second later, look again a few seconds later, and finally look at the same field of view about a minute later. Comparing the first look with the second look would permit detection of the low altitude targets; comparing the first look with the third look would permit detection of the intermediate altitude targets; and the comparison of the first and fourth looks would permit detection of the high altitude targets.

The above example illustrates the manner in which the curves presented above may be utilized in determining the timing requirements of the M. T. I. system if the threshold displacement and maximum displacement are known. These limiting displacements will be a function of the M. T. I. capabilities, the threat model, and the system requirements and must be specified on an individual system basis.

3. EQUIPMENT ASPECTS OF THE M. T. I. TECHNIQUE SPACE SURVEILLANCE SYSTEM

The basic scheme used to detect the apparent motion is to store a frame of the video signal output from the I. O. Sensor Electronics (camera) and then, while keeping the "looking" position fixed on the same celestial field, electronically compare successive video frames with the one stored and record the difference. As long as all objects are stationary in the field of view, the video signals from the camera

will be coincident with those from the recorder. The video comparator circuits are arranged so that no output is produced by coincident inputs and no signals are fed to monitor or output when an object, whose position has shifted between the time of recording and comparison, will generate signal which will appear on the monitor and at the output. Thus, the monitor screen will remain completely dark except when a moving target is present. Such a visual display can be incorporated into a manual acquisition system requiring a human operator, or the comparator output signal after suitable processing may be used to actuate an automatic target alarm or system as required by the application.

One of the main problems involved in such an M.T.I. concept is that of rapidly recording video information with adequate resolution, immediate availability of electrical readout and finally complete and rapid erasure at end of the cycle. To accomplish this, an electrostatic image storage tube having direct electrical readout was chosen. A storage tube, which has a single electron gun (used for both writing and reading) magnetic focus and magnetic deflection, is suited to this application if (1) it has similar resolution capability to that of the image orthicon used in the cameras, (2) readout is non-destructive thus allowing for extended comparison periods, and since (3) its single electron gun and deflection yoke mean that misregistration between writing and reading scan patterns is minimized. This last item of registration is extremely important in a system which depends upon accurate time co-incidence comparison.

Figure IV-26 shows an overall block diagram of a typical MTI delay interval system. Basically the system consists of the storage tube with its associated focus and deflection coils (omitted from the figure to save space) a mode switching unit for controlling the storage tube gun bias and storage screen bias, an image-orthicon sensor camera chain which feeds video signals and blanking to the storage tube, an output video amplifier, and a comparator unit which receives the video output from the storage tube and compares it with the camera chain output. The video output from the camera chain is delayed slightly to compensate for the delay in the storage tube output amplifier. The output of the comparator is displayed on a standard monitor screen. In order to provide for I.O. integration over several frame periods when looking for faint targets, a gating unit is included which can hold the I.O. beam off while keeping the photocathode turned on for a preselected number of frames. The I.O. beam is then turned on for one scan to produce a single frame of video output and the cycle is repeated. This gating unit is controlled by a program unit driven by the chain vertical sync. In the system bread board on a G.E. fund program for feasibility tests, the program unit also controls the storage tube mode switching unit and provides gating for the storage tube beam in synchronism with that supplied to the I.O. beam by the I.O. gating unit. The program can be set to provide for storage tube integration during the write-in mode by allowing several successive video frames to be written. Finally, the program unit also controls the duration of the readout and comparison period, that is, the number of successive video frames with the camera that are compared with the stored image on the storage tube.

Figure IV-27 is a photograph of the G.E. breadboarded laboratory model. The camera chain is on the cart at the left of the picture while the MTI equipment proper is mounted in the rack at the right. The I.O. camera is on the middle shelf of the cart and the monitor is on top with the video and sync. chassis at the left. The I.O. gating unit is the chassis just beside the camera.

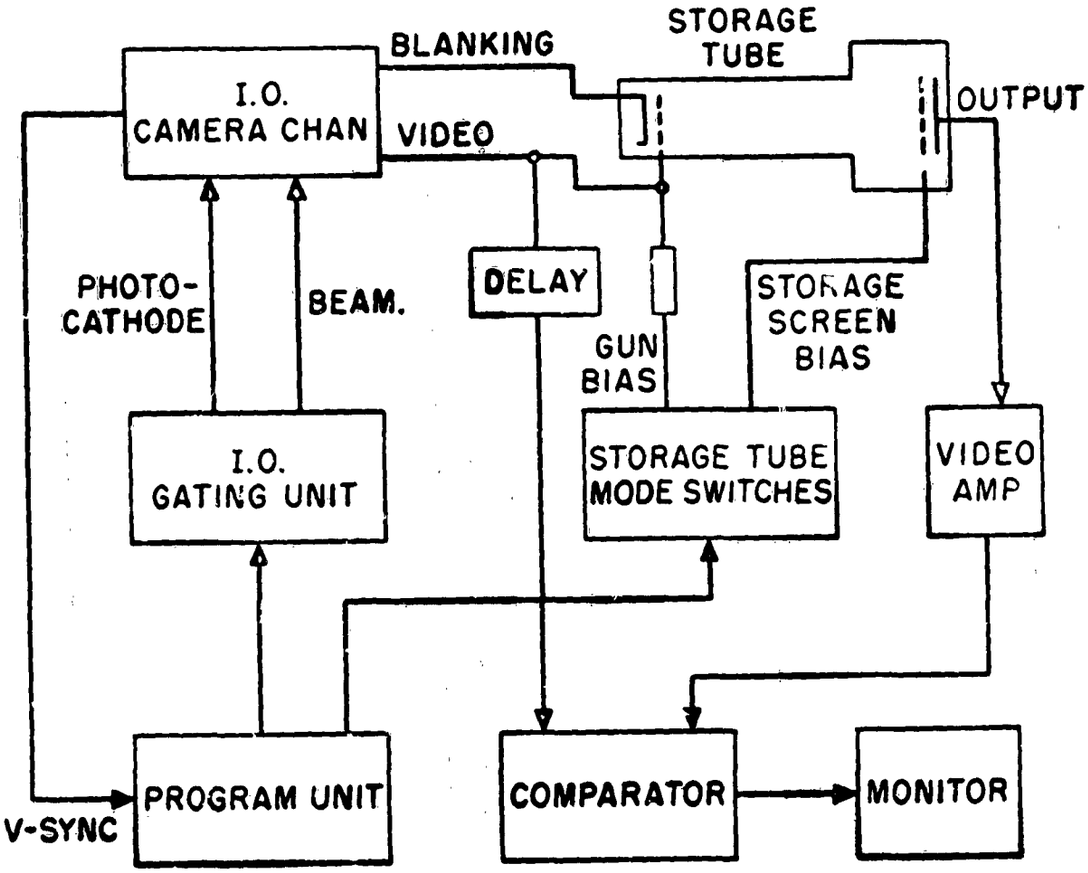


Figure IV-26. Basic MTI System

Most of the MTI rack is occupied by power supplies; the two units near the middle being the storage tube unit and the program unit. The selector switches on the front of the program unit are used to set up the desired I.O. integration period, storage tube integration period and readout period.

We have discussed the possibility of storing and comparing the output signal directly as obtained from the I.O. camera output. From our experience with the laboratory model, additional features must be incorporated in the system in order to effect a maximum degree of noise suppression and get full use of the available dynamic range of the I.O.

From our observatory tests, it has been found that a dynamic range of from 10 star magnitudes (an intensity range of 10^4) to 12-1/2 mag (10^5 intensity) will be obtained from the I.O. The absolute limiting magnitude detectable by the I.O. is dependent upon three factors:

1. The integration time allowed on the I.O. target.
2. The aperture of the optical telescope.
3. The sky background illumination.

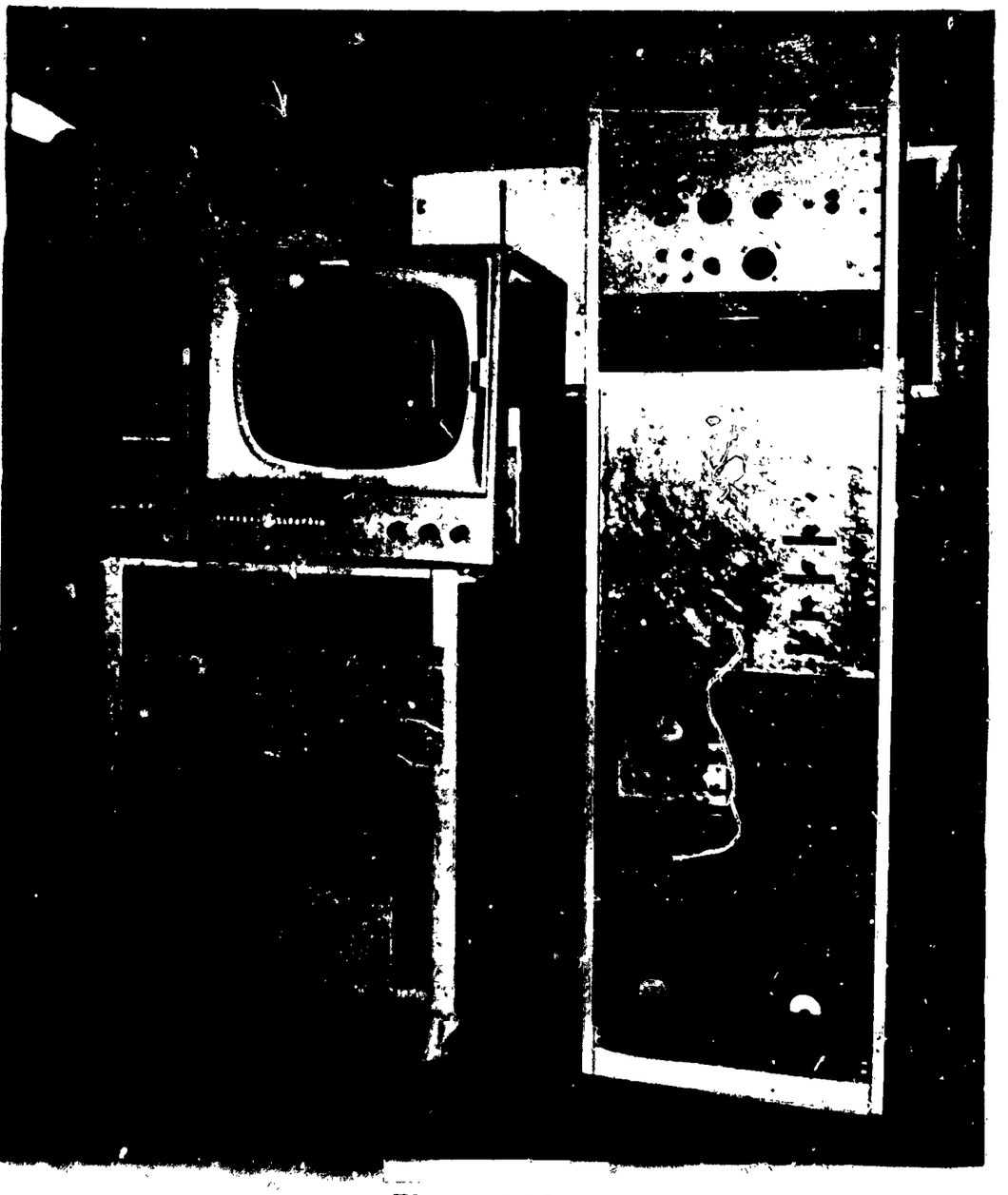


Figure IV-37.

From this limiting magnitude of detection to approximately two magnitudes below this threshold, when using medium and large f/number optics, the principal source of noise is that of the I. O. beam itself. Therefore, even under ideal conditions, noise discrimination in this range is extremely difficult. (When using small f/number optics the background noise will similarly set a limit generally about the same amount. See discussion in Section II.) At magnitudes of two or more below limiting magnitude, however, suitable processing of the video signal will give sufficient additional noise discrimination beyond that obtained by integrating a number of frames on that I. O. and on the storage tube so that accurate signal comparison can be accomplished. For example the video signal may be fed to a Schmitt trigger, so designed as to accept only a rise time typical of a star image. This gives additional discrimination against noise pulses having rise times either slower or faster than that of the desired star pulse.

In order to operate in the range of two magnitudes below the limiting magnitude, however, there may be an advantage in using two storage tubes; one recording the visual field at some time later than the other, and then comparing the two readouts. This may give a maximum of noise suppression in both comparator input channels over a single storage in-out-read system.

At the present time, the G. E. breadboard single-tube MTI system does incorporate a Schmitt trigger video processing circuit. To show the appearance of the processed video signals on the monitor screen, and to demonstrate the operation of the system in the laboratory we are using a star field simulator consisting of a group of holes punched into a piece of black cardboard and illuminated from behind. Figure IV-28 A and B shows the processed video signals, which have been recorded and read out from the storage tube, displayed on the monitor screen. The extra star in the bowl of the dipper is supposed to represent a target in the field. Actually, the background of the monitor screen can be made completely dark but we deliberately brightened it for the photograph in order to outline the monitor screen edges.

4. CONCLUSIONS

The MTI system based upon the electrostatic image storage technique has been shown to be quite feasible. While the performance tests made to date have not established the ultimate limit of the system, it has been demonstrated that complete target detection and MTI of magnitude 7 and smaller stars can be attained with a 4 inch aperture lens using a 1/30 second exposure time. Under these conditions an angular displacement between pictures of only 2.5 minutes (150 sec) angular movement or 5 scan lines is required for noncancellation using the 4-inch f/5 telescope. This is quite encouraging since the limiting magnitude for the 4-inch aperture at 1/30 second exposure is about magnitude 8.5. It would appear from this, then, that detection very close to limiting magnitude could be achieved if:

1) Noise suppression other than by simple bandwidth limiting (such as pulse width discrimination or line-to-line correlation) were used.

2) The broad, low-amplitude target signals produced by very bright objects when operating the I. O. over a very wide dynamic range were removed, by appropriate gating, from the video signal before feeding to the MTI system.

Registration should not limit the ultimate performance of a storage tube MTI, with careful scan design.

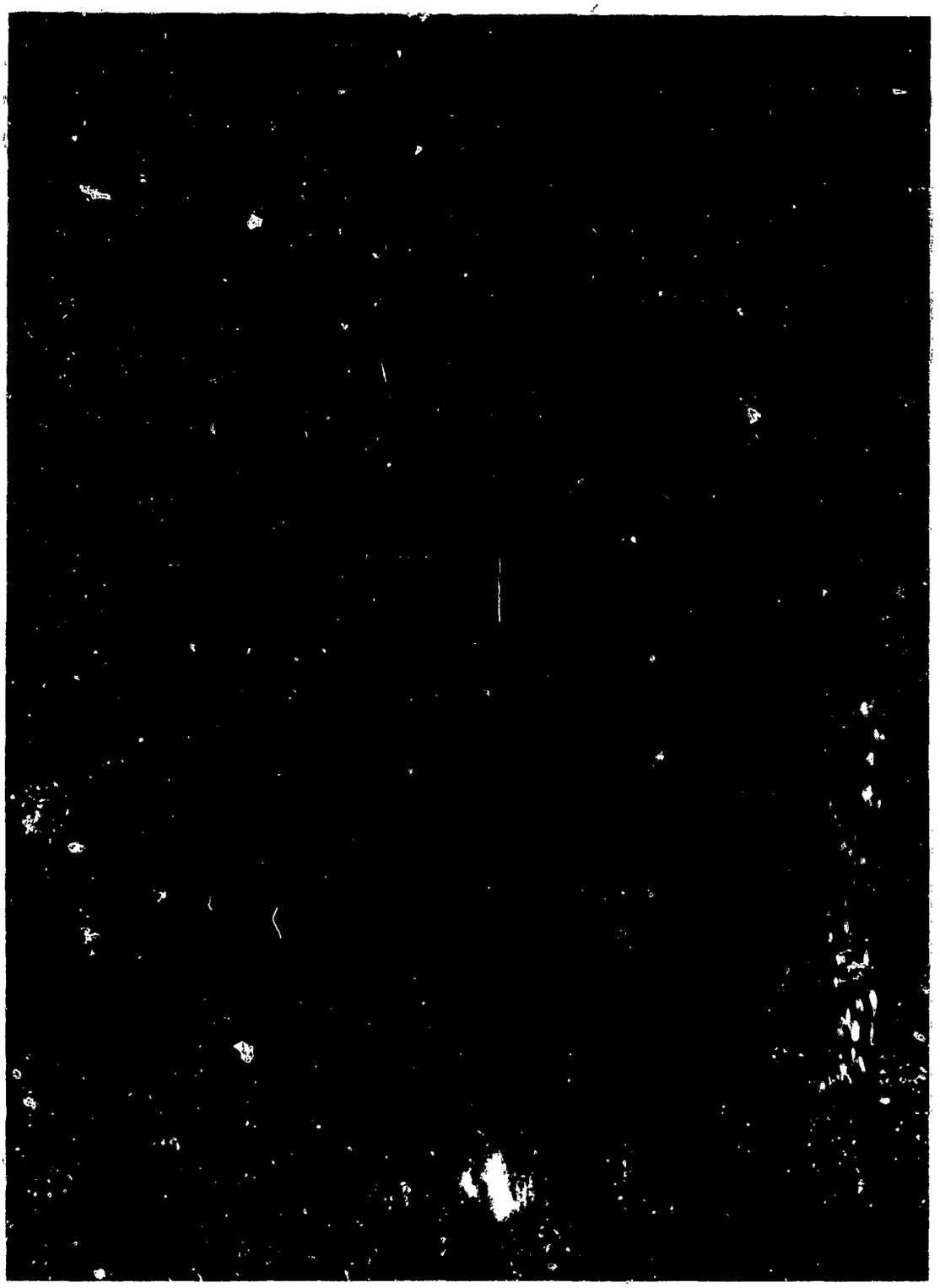


Figure IV-28A.

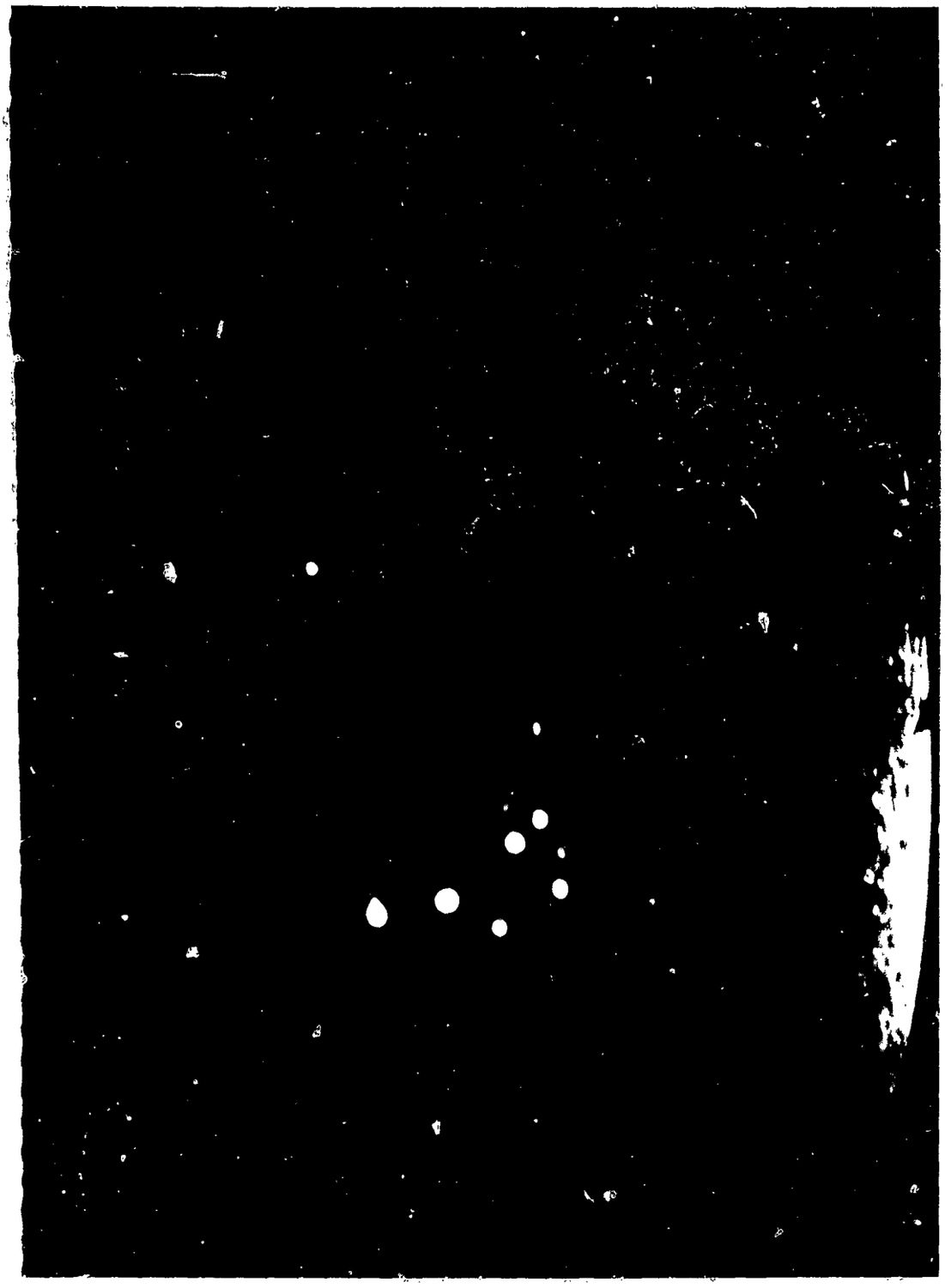


Figure IV-28B.

Any storage tube MTI system will have to consider the loss of image orthicon view time, with more than storage tube required for each image orthicon unless the orthicon is going to have a long photocathode integration time of 1/2 second or greater. The storage tube cannot store and read off more than 1 picture every second plus twice the scan period.

The storage tube with Schmitt Trigger electronic peak detection and good registration should be able to cancel all non-moving objects that the Schmitt Trigger can detect. It will also cancel most low velocity objects that move less than 1/100 of the field of view between the present and the stored view field. The electronic detection loss, compared to the eye view of the same single scan of the field, is estimated to be about 2 magnitudes. This is an intensity loss of 6.3 to 1. This means if the specific telescope and image orthicon can detect stars visually from 1 to 13 magnitudes in one scan, the storage tube will store and the electronics will cancel stars from 1 to 11 magnitudes, and the system will detect objects that move 1/100 or more of the view field between stored and compared scans, if they are 1 to 11 magnitude in intensity.

5. EQUIPMENT VARIATIONS FOR THE M.T.I. TECHNIQUE

A variation of this M.T.I. method is to use two storage tubes (or devices); one for the present and one for the delayed frame. Then compare the stored signals or videos. This method suffers in registration, because now the mis-registration or difference in write-in and readout of two storage tubes has to be considered. There are no linearities involved.

This system offers a possible advantage in some noise cancellation; however, the advantage is small if any.

Another variation is to use two I.O.'s: one exposed now but not readout until the end of delay interval when both I.O.'s are read out simultaneously and compared. In this case the registration of a pair of tubes is involved but since the sweeps are driven from a common source this is minimized to the registration of two I.O.'s (similar to color TV or 0.16%).

The advantages of the single site MTI (delay interval temporary catalog) technique are:

1) Especially suited to medium and fast moving satellites.
2) Relatively the simplest system with minimum alignment requirements.

The disadvantages of the single site M.T.I.:

1) Not readily suited to very slow moving (near sidereal rate objects).
2) Required special recording and comparison (several minutes) for slow rate objects.

E. FILM CATALOG (IMAGE CANCELLATION) SEPARATION TECHNIQUE

The film catalog image cancellation system places a film image "negative" at the image plane of the primary optics. The film has been previously exposed to the same field of view. The film density is high in image areas of low magnitude, high intensity stars. The primary lens image plane is viewed by the image orthicon

using a secondary "relay" lens. If the film density is high, with a corresponding low transmission, the corresponding star image will be attenuated and will not be detected by the image orthicon.

This image plane cancellation of star images is one method of separation. It has many problems:

1. Registration of film at image plane.
   a) Mechanical accuracy of mount and film holder.
   b) Refraction bias pointing error.
   c) Differential refraction across the field of view.
2. Film requirements.
   a) Exposure time to develop the film catalog.
   b) High density required for cancellation (may be 5 or 6).
   c) Film image size to relieve the registration problem.
   d) Small fog level to minimize detection loss of targets.

Some of the problems of a film catalog image cancellation system are analyzed in Appendix I-b: Application (Probability of Occultation) to Photographic Mask Separation. This portion of Appendix I considers the required film gamma and maximum density, to assure no loss of image detection area due to image orthicon spread. Some of the exposure time requirements are covered in Section IV-F. The summary of Separation System advantages and disadvantages Section IV-G includes the Film Catalog Image Cancellation.

F. VIDEO CATALOG CANCELLATION TECHNIQUE USING FILM NEGATIVES

The video catalog cancellation technique uses a film negative previously exposed by the primary viewing optics. The film catalog is flying spot scanned during operation, with element by element registration compared to the scanned image orthicon output. The flying spot catalog scan is converted to a video signal, and in those areas that have a catalog star video signal, the image orthicon video is cancelled. This system is similar to image catalog cancellation, with similar problems:

1) Diffractive errors across the field of view if mask was exposed at different elevation angle from the operating elevation angle.
2) Image size requirement for cancellation due to misregistration.
3) Mechanical problems of mask storage and registration alignment.

The differences between image cancellation and video cancellation include:

1) Increased image spread (occultation) using video cancellation.
2) Difference between I. O. image size and catalog image size using video cancellation. The change of image size due to intensity change of star magnitude would be different on the film catalog and image orthicon image.
3) Possibility of electronic registration and change of sweep slope on the flying spot scanner sweep, to reduce the position and differential diffraction errors of video cancellation.

The following discussion will include the topics:

F1. Differential Refraction

F2. Obtaining the Catalog

F3. Updating Catalog

F4. Registration

F5. Equipment Arrangement

F6. Image Cancellation Compared with Video Cancellation

1. DIFFERENTIAL REFRACTION

The general problem of differential refraction resembles that of astrometry, except that we are not dealing with such high precision, instead of a fraction of a second of arc we require only a few seconds of arc. There are certain inherent errors, some of which we can do away with immediately. Precession and Nutation effect the coordinate system, not the relative star positions. Thus they do not enter. Refraction and Aberration, since they affect directions, similarly do not affect us. Differential effects across a plate do, however, so we must treat them.

Differential refraction is effective only for varying zenith distances, not azimuth. If Z is the apparent zenith distance, and ζ the true zenith distance, and β is the coefficient of photographic refraction we have

$$\Delta Z = \beta \tan \zeta$$

is weakly dependent on S and also on the local temperature and pressure, and on the effective wavelength of the detector. Usually photographic is taken as 1.0155 times visual factor, but in our case, since a S-20 Image Orthicon would be used, as well as red sensitive plates the two factors would be the same, to a good approximation. At large zenith distances the sensitivity of β to ζ must be included since it will change across a plate, thus one puts

$$\beta \quad \beta_0 + \beta' \tan^2 \zeta$$

Even in the most precise astrometric work higher orders terms in this expression are negligible.

Assume a telescope is pointing at ζ, the total refraction in zenith distance will be ΔZ, as given above. The differential refraction across a plate will be

$$\Delta^2 Z(\Delta\zeta) = \beta \tan \zeta_1 - \beta \tan \zeta_2 \quad \beta(\tan \zeta_2 + \Delta\zeta - \tan \zeta_2)$$

$$\beta[\tan \Delta\zeta \quad (1 + \tan \zeta_1 \tan \zeta_2)]$$

$$\beta[\tan \Delta\zeta + \tan \Delta\zeta \tan \zeta_1 \tan \zeta_2]$$

We note that $\tan \Delta\zeta = .1$ for $5^{\circ}43'$, appreciably longer than the required field, and β is of the order of a minute. Thus, the differential refraction across a plate is roughly

$(.1 + .1 \tan^2 \zeta)$ minute, for a $5\text{-}3/4^{\circ}$ field.

It is obvious that this doubles at $\zeta = 45^{o}$, and climbs rapidly at larger zenith distances.

Thus, at zenith distances larger than 45^{o} differential refraction is a real problem.

This problem is a predictable one however, and thus can be compensated for. One simple solution is to orient the field so that the horizontal scan is orthogonal to the vertical circle through the center of the field. Thus a compensation could be made in the vertical scan circuit of the flying spot scanner.

Aberration of a differential nature must also be considered. If S is the distance of a star from the apex of the earth's motion, and k is the constant of aberration, then we have

$$\Delta S = k \sin S$$

Maximum aberration will be along this line, and so we may write,

$$\begin{aligned} \Delta^2 S \cdot (\Delta S) &= k (\sin s) - k \sin (S + \Delta S) \\ &= k (\sin s - \sin S + \Delta S) \\ &= k (\sin S - \sin S \cos \Delta S - \cos S \sin \Delta S) \end{aligned}$$

Now, $\sin \Delta S \sim .1$ at the same point as the previous tangent function, so let us again take a $5\text{-}3/4^{o}$ field. At this point $\cos \Delta S \sim .995$, or roughly 1. Thus we might write

$$\begin{aligned} \Delta^2 S &= k (\sin S - \sin S - \cos S (.1)) \\ &= k (-.1 \cos S) \end{aligned}$$

The factor k is roughly 20", this differential aberration must stay below 2" of arc, especially since all the approximations used tend to increase it. Thus we may neglect it. We have remaining one primary error that can lead to difficulties. This is caused by the misalignment of a plate. A photograph of the celestial sphere is basically a projection of the sphere on a tangent plane to the sphere. Thus any misalignment leads to two different tangent planes, with a resulting differential error. We note that the radius of this sphere is equal to the effective focal length of the optical system used.

We let the tangent point, and the origin of our coordinate system be T, the Y axis tangent to the declination circle, and X perpendicular to Y, with the unit of distance being R, the radius of the circle. Let P on the sphere have a projection P' with coordinates X and Y.

Transferring from one tangential coordinate system to another then yields equations of the form

$$\begin{aligned} X' &= X - m + Y \Delta P - (mX + nY) X \\ Y' &= Y - n - X \Delta P - (mX + nY) Y \end{aligned}$$

where m and n are simply shifts of the coordinate origin, ΔP is a rotation, and the last term is a change in the unit of length. A reasonably large error would be 10^{-4} radian. Thus a maxim m and n would be 10^{-4} R, or for a 30" focal length, 3×10^{-3}

inches. The change of scale is then (mx - nY) X~ 3.4×10^{-3} considering a 1-1/2" total plate size, this is within our limits of error.

It can readily be shown that the rotation is not bothersome either.

Thus a misalignment of 10^{-4} radian will not lead to errors that are too large.

Consider a rotational error, which would enter only because of our rotation to compensate for differential refraction. Even a coarse sensor system could hold a minute of arc, or $1/3 \times 10^{-3}$, which obviously lies below the errors in the system again. We might summarize this discussion by saying that although the effects produce bothersome errors in astrometric systems, they are just below the point where they would make our system difficult.

In a previous note it was shown that a photographic comparison system was reasonable from the time standpoint. In this note we have shown that it is reasonable from the error standpoint.

2. OBTAINING THE CATALOG

To obtain a good catalog at the capability level of a good surveillance system will require a similar optics set up especially arranged for photographic exposures. Assume, for the purposes of discussion, that we are using a 40" f.1. system with a 30" aperture, f/1.3. Such a system with ordinary plates such as 103aO, would probably have a limiting magnitude of 17.5 on a moonless clear night. Exposure times for such a system would be approximately 13.5 minutes for the limiting magnitude of 17.5, 5.5 minutes for 16.5, 1.35 minutes for 15th magnitude, and 0.135 minutes for 12.5 magnitude. Assuming that 16.5 magnitude is required, then 5.5 minutes is needed for a plate. Since we need a separate plate for each field for an image orthicon, this means 5.5 minutes are required for each $2.^{o}3 \times 2.^{o}3$ degree field, or roughly 1 minute of exposure per degree^2. The observing efficiency, including changing plates and fields, and an occasional 'goof' would probably be as about 90% with experience. The number of hours that can be spent observing varies with season and location, but could average eight hours/day over a year. At a good location it should be possible to operate 300 days per year as a minimum, so that 2400 hours are available. Discounting the bright moon nights, this would drop to about 2000 hours/year. For a 50% observing efficiency then it would be possible to cover 6×10^4 degrees^2. For an efficiency of 90%, instead of 50% coverage would be about 10^5 degrees^2 in one year. This assumes such things as automatic plate changing, and moving from one field to another adjacent one. The actual time to create a catalog would still be a year to cover the entire sky, but the problem of weather, equipment failures, and use as a back up telescope becomes much less critical. It is also apparent that full sky coverage of the system could be made available long before the year was up since the plates could be kept ahead of the sky during the year. Thus the time delay before full operation is roughly a month. We note also that this is approximately the time of the image cancellation system, since it too is capable of keeping up with the sky.

3. UP-DATING CATALOG

Since the accuracy of this catalog need not be high, four seconds of arc being more than adequate for a surveillance system, proper motion of the majority of stars will not effect it for a period of years, ten years being a safe figure, except for a few close stars of large proper motion (2 to 3 sec/yr). Thus a small proportion

of telescope time would be required after the first year to up-date the few plates that yield errors. 10% of the time spent on plates would seem reasonable, and if 20% of the operating time was spent getting new plates the catalog would be completely renewed in less than five years. Thus if an observatory was set up with two instruments, surely a minimum from the standpoint of maintenance, after the first year over 80% of the operating time of the second telescope could be spent checking for satellites, and still have a continuously revised catalog.

4. REGISTRATION

To successfully use a photographic film negative catalog, or memory, it is necessary that the photograph closely correspond to the sky. There are several effects that will affect this situation. These are as mainly,

1) Mapping error, caused by projecting of sphere on a plane photographic plate, and

2) Differential refraction, causing a scale change along one direction.

For a typical surveillance system a differential refraction error of 10 secs. across a 2-1/2 degree field is permissible, i.e., 4 secs per degree. At 0° elevation we have a differential refraction error of 10'36" approximately. At 10° this becomes 21 secs, at 30°, -3 secs, at 40°, -2 secs, at 50°, - 1.5 secs, at 60°, -1 sec, and at 70°, -1 sec. See Section I-C. Thus for elevation over 25° differential refraction is not a problem when using 2-1/2 to 3 degrees field of view.

5. EQUIPMENT ARRANGEMENT

A typical system employing a flying spot scanner to read the reference catalog for comparison with the I.O. Sensor video is blocked out in Figure IV-20.

6. IMAGE PLANE CANCELLATION VS VIDEO CANCELLATION

An image plane direct cancellation system requires better plates than video comparison system, since the film negative or plates act as a filter in the path of the light.

The light losses in a direct cancelling system (primarily in relay lens needed) is in the order of a magnitude for a well-designed system. Exposure times to reach 16.5 magnitude would be a minimum of roughly 1/3 seconds, actually in practice considering background illumination, a better S/N ratio, and a safety factor this would be of the order of 3 seconds.

The following table illustrates an estimated comparison of the three single station catalog techniques: The M.T.I. delay interval storage, the image plane direct cancelling, and the electronic or video comparison or flying spot scanner type. It should be readily noted that the mount is a critical item, and close attention should be paid to it.

	Exposure Time in Seconds	Number of Back Up Telescopes	Time to Complete Sky Coverage	Time to Coverage of Available Sky	Time to Change Field	Total Time/Field	Comments
MTI Temporary Storage Catalogue	1	1	0	0	5^s	20^s	Exposures must be long enough for appreciable motion during exposure. Slow objects a problem.
Image Plane Cancellation	3	0 (1 yr.) .5 (after 1 yr.)	1 yr.	1 mo	5^s	50^s	Memory Tube, extensive electronics. Temporary Memory only. Slow objects not a problem. Nc electronics, extensive catalogue and filing.
Electronic Cancellation	1	.5 (1 yr.) .8 (after 1 yr.)	1 yr.	1 mo.	5^s	20^s	Slow objects not a problem. Extensive catalogue and filing. Simple electronics.

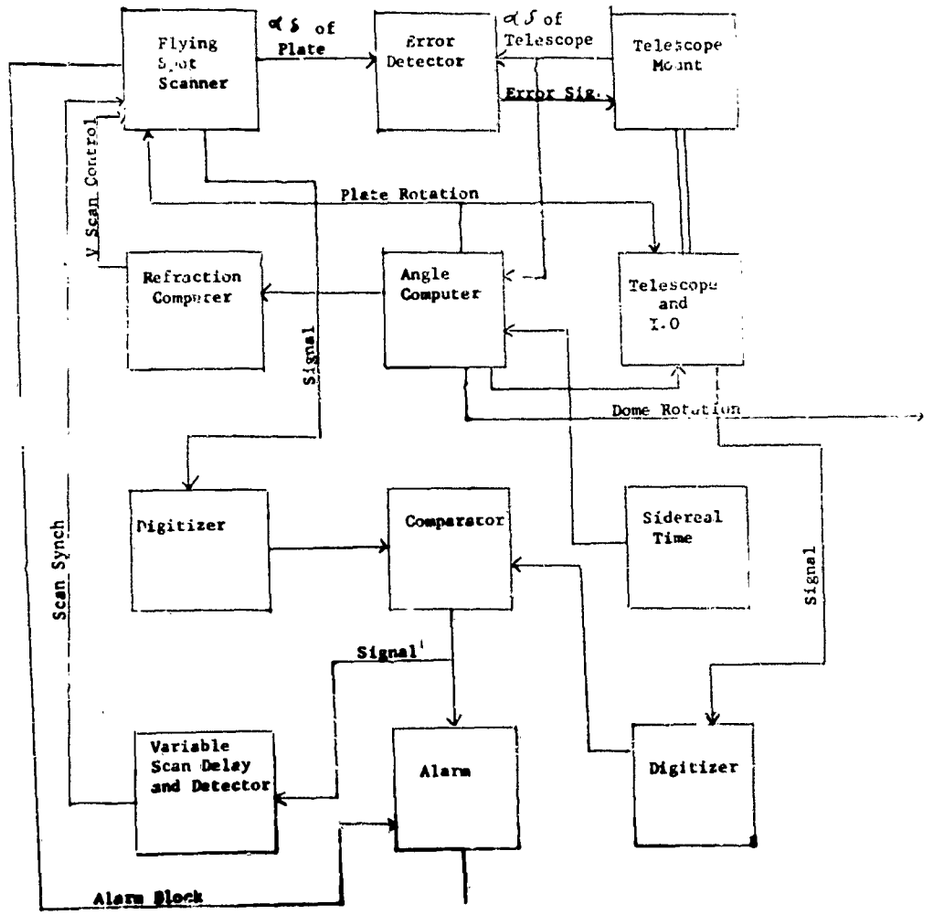


Figure IV-29.

G. SUMMARY OF SEPARATION SYSTEM ADVANTAGES AND DISADVANTAGES

The following table is a summary of advantages and disadvantages of the separation techniques discussed in Section IV.

SYSTEM	ADVANTAGES	
A) Stereo IV-C	1) No image storage requirements. 2) Additional information of a 2 image relative displacement due to one target is possible.	1) At least 2) A full T tions l 3) Progra to curv 4) Image 5) Simu
B) Storage Tube IV-D	1) Image registration should be only the write-on to read-off registration of a storage tube. (except for long storage times with the associated differential refraction and mount pointing errors.) 2) No film catalog or additional sites are required.	1) More th (if both prime t 2) Co. pl regist 3) Time d
C) Film Catalog Image Cancellation IV-E	1) Mechanical registration could be augmented by DC voltage control of flying spot scanner sweep, to servo or microposition a film catalog image. 2) By changing the sweep voltage slope of the flying spot scanner in a programmed manner, differential diffraction can be corrected.	1) Large 2) Accu image, pointing 3) Addition tial refr refrance 4) Time to 5) Image d
D) Film Catalog Video Cancellation IV-F	1) Minimum loss of detection area due to image orthicon image spread, if registration is perfect.	1) Large ca 2) Accurate image, v pointing 3) Time to 4) Differen scanner 5) Problem and imag

DISADVANTAGES
,te is required
is sync, voice channel, etc.) communica- is required.
l mount pointing (or platform survey) due
lem of 2 remoted image orthicons.
ood weather is required.
abe might be required per image orthicon torage times are required or due to erase- cycle.)
abes, and/or storage tube write-read
t can be separation-detected.
ages to store and retrieve.
ipment is required to position the film equirement of a programmed refractive .
o 30° and 30° to 20°) to correct for differen- ht be required if low (20°) elevation sur-
ost operating time.
relay lens and minimum film fogging.
ages to store and retrieve.
ipment is required to position the film equirement of a programmed refractive .
st operating time.
between film image from flying spot spread image from image orthicon.
-registration between flying spot scanner

H. SYSTEM ANGULAR MEASUREMENT ACCURACY

After Detection and Separation has been accomplished, a Space Surveillance System is expected to generate angle measurement data for later use in orbit prediction.

The purpose of this section is to study the major factors which influence the accuracy of the reported target position of an electro-optical system. Since the system under consideration is passive in that it employs the sun as the primary source of target illumination, the measured data is limited to angle only information. This information consists of angular components and their associated times. By investigating the influential factors of angular position measurement, an estimation of attainable accuracy can be made in terms of the hardware required.

The following list of angular measurement errors includes many topics that have already appeared in this report:

1. Atmosphere
2. Optics
3. Telescope Mount
4. Image Orthicon Linearity
5. Image Spread

After discussing these specific errors the conclusion will show the system angular accuracy that might result.

1. ATMOSPHERE

The atmosphere will give a refractive pointing error, and an image "dancing" error. The refractive pointing error can be programmed for standard temperative-pressure air conditions. There is a deviation from standard refractive conditions that will be considered random:

Air Temperature (-40°F to $+100^{\circ}$F) ±13%

Atmospheric Pressure (28.2 to 32.2 inches hg) ±5%

The resultant RMS percent variation is 14%. If continuous measurements of air temperature and pressure were made at the site, this RMS could be decreased to ±10%. This variation is approximately a ±2 value.

The error across the field of view due to differential refraction has been discussed in Section IV-B. The "dancing" error is also discussed in Section IV-B.

2. OPTICS

The optics errors are usually not considered random. These errors are either pincushion or barrel distortions of image position versus object angular position, and are covered in Section II-A and Section IV-B.

3. TELESCOPE MOUNT

The effect of the electro-optical positioning equipment upon the ability to measure the angular position of a body in space will now be considered.

A model illustrating the significant factors of positioning is shown in Figure IV-30. The absolute reference is taken as the celestial sphere. The problem of positioning lines of sight with respect to this absolute reference then has two practical considerations.

1) Establishment of a local reference (the local north reference at each site) with respec to the absolute reference (the celestial sphere).

2) Positioning of the local line of sight (the telescope at each site) with respect to the established local reference.

The first is a surveying and reference stability problem, the second is a hardware problem. Each will now be considered in detail.

As was indicated the local reference error has two important factors. The first is the surveying accuracy in establishing the local north reference at any given place and time. The second is the stability of this reference with respect to the celestial sphere, as a function of time.

In conjunction with design of guidance systems for ballistic missiles, the General Electric Company has recently completed an extensive study of state of the art surveying techniques. The results of this study[1] are directly applicable to the problem being considered here.

The accuracy in establishing local north as a function of time available for measurement is shown in Figure IV-31. The accuracy in establishing local latitude, longitude, and elevation above mean sea level are also included, as this information might influence the discrimination accuracy for a multi-site system. This information appears in Figures IV-32 and IV-33.

It will be assumed that the shift of the earth's crust and the concrete foundation of the mount are negligible with time. However even with this assumption the projection of the earth's geographic pole upon the celestial sphere experiences a minute but continuous translation. This motion can be interpreted as a nutation superimposed upon a constant precession.

The nutation is caused by the gyroscopic effect of the moon, sun, and other planets upon the earth. The period of this nutation is therefore composed of the harmonics of the lunar, solar, and planetary orbital periods. The maximum magnitude of this nutation is ±5.6 seconds (see reference (2)) which occurs approximately every nineteen years.

---

(1) Dopp, J. W., "Report on the State of the Art of Surveying Accuracies", G. E. TIS #R62DSD3.

(2) H. N. Russell, R. S. Dugan, and J. Q. Stewart, Astronomy, Ginn & Co., 1962.

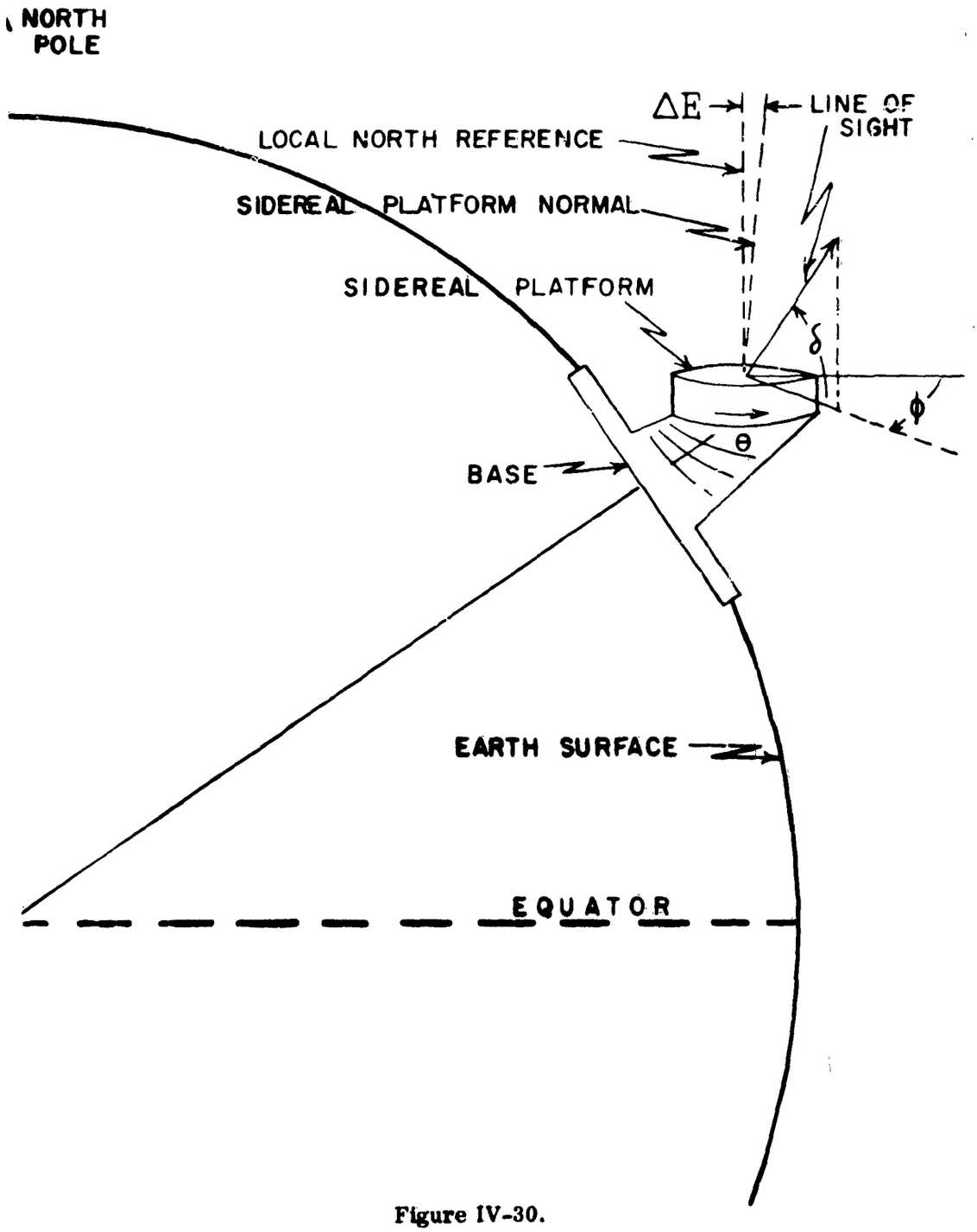

NORTH
POLE
ΔE
LINE OF
SIGHT
LOCAL NORTH REFERENCE
SIDEREAL PLATFORM NORMAL
SIDEREAL PLATFORM
δ
ϕ
θ
BASE
EARTH SURFACE
EQUATOR

Figure IV-30.

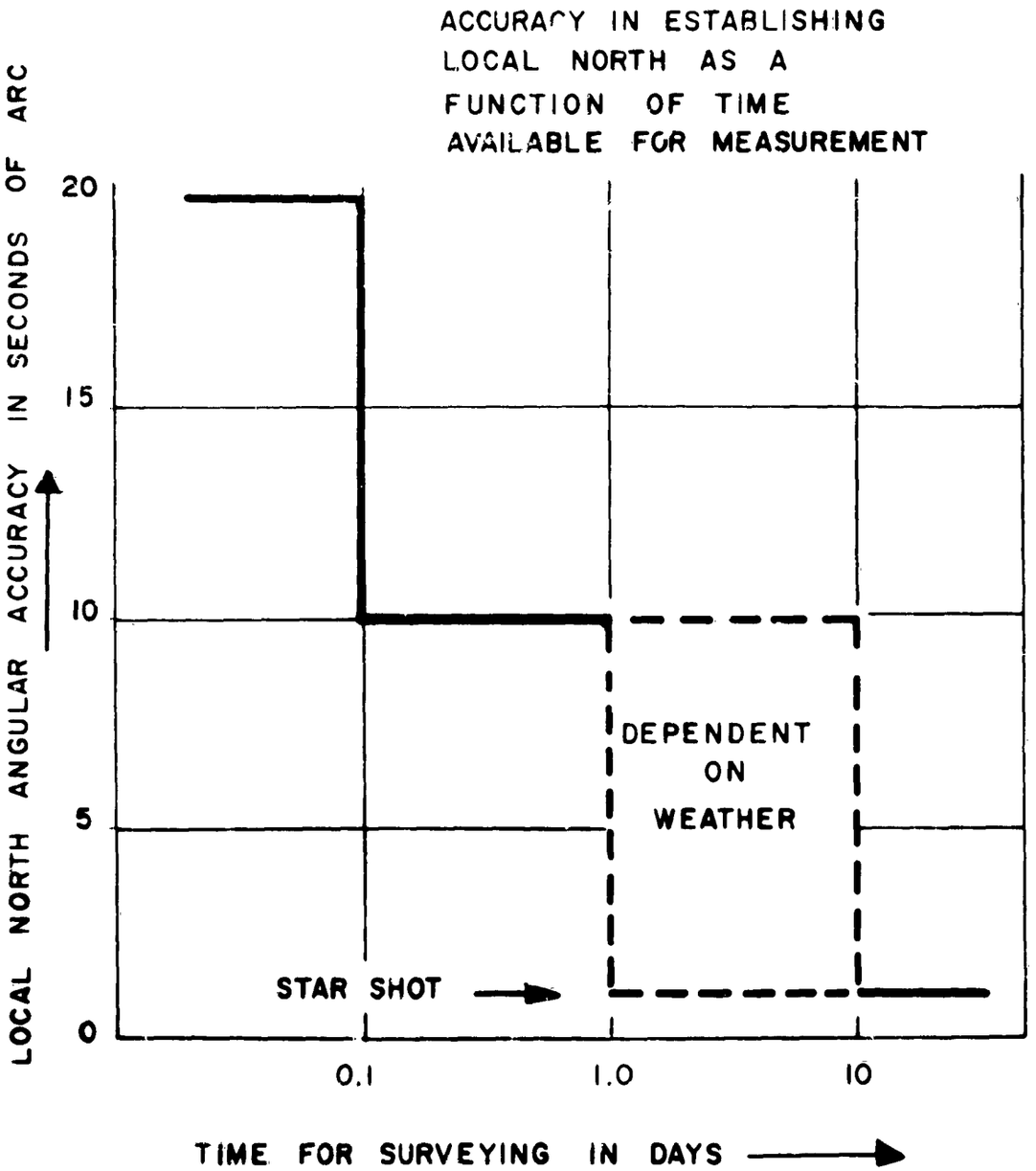


Figure IV-31. Accuracy in Establishing Local North

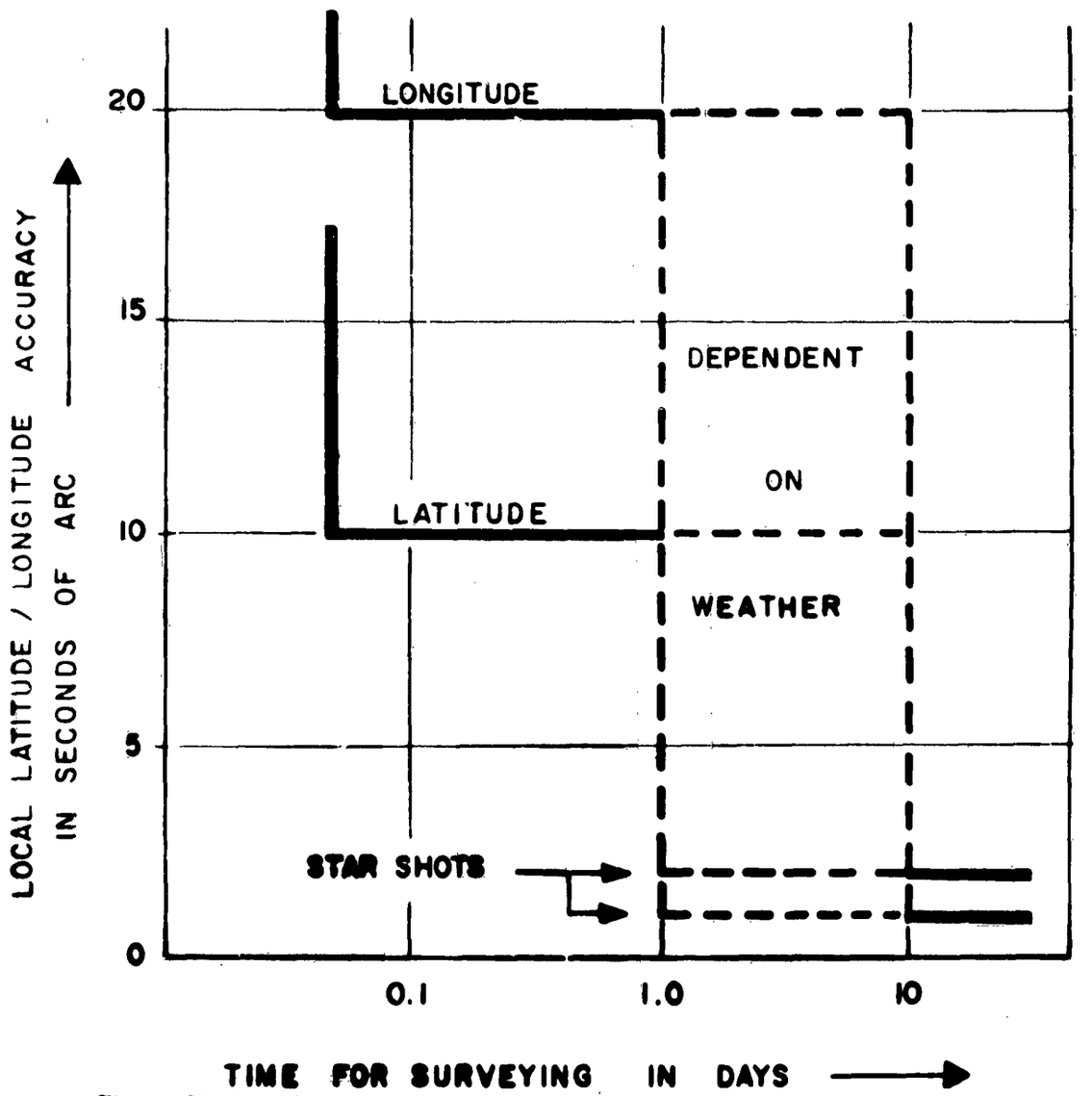


Figure IV-32. Accuracy in Establishing Local Latitude and Longitude

The precession of the earth's geographic pole is caused by the slight difference in the solar and tropic year and by the solar precession. The period of this precession is effectively 25,800 years, and the resulting magnitude is about 13 seconds per year.

ACCURACY IN ESTABLISHING LOCAL ELEVATION ABOVE MEAN SEA LEVEL AS A FUNCTION OF TIME AVAILABLE FOR SURVEYING.

IT SHOULD BE NOTED THAT ELEVATION ERROR IS AN INCREMENT ADDED TO THE RADIUS OF THE EARTH. SINCE THE RADIUS OF THE EARTH IS ON THE ORDER OF 10^7 FEET, A TEN FOOT ELEVATION ERROR IS EQUIVALENT TO ONE PART IN ONE MILLION.

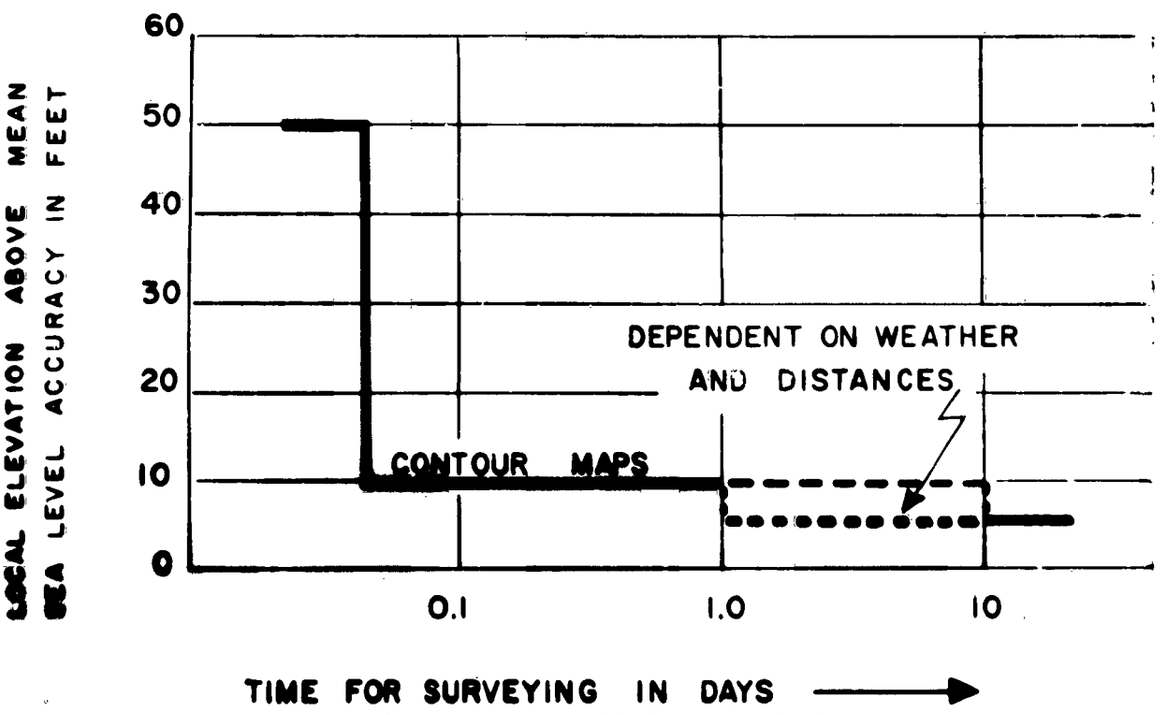


Figure IV-33. Accuracy in Establishing Local Elevation

The problem of positioning the local line of sight with respect to the local north reference is illustrated in Figure IV-30. Four major sources of error can be defined. These are:

1) Sidereal Platform Normal Error ($\Delta\epsilon$)

This is the angular accuracy in seconds that can be maintained between the local north reference and the sidereal platform normal.

2) Sidereal Angular Position Error ($\Delta\theta$)

This is the dynamic angular accuracy in seconds that can be maintained by the sidereal platform with respect to the true value of as a function of time.

3) Declination Error ($\Delta\delta$)

This is the angular accuracy in seconds to which the declination of the line of sight can be measured with respect to the sidereal platform.

4) Ascension Error ($\Delta\Phi$)

This is the angular accuracy in seconds to which the ascension of the line of sight can be measured with respect to the sidereal platform.

The practical limitations on these errors will now be considered.

By using a fairly large platform and precision bearings the sidereal platform normal error ($\Delta\epsilon$) can be reduced to a few seconds.

The errors sidereal angular position ($\Delta\theta$), declination ($\Delta\delta$), and ascension ($\Delta\Phi$) involve angular position measurements. It is assumed that an individual null seeking servo system with a suitable time constant for the required drive rate will be used to obtain each of the three angular positions. The accuracy with which this can be done is then only a function of how accurately the actual position can be measured.

There are three classical methods of accurately measuring an angle. The simplest method is to use a gear arrangement. However as the magnification increases the gear deadband eventually limits the accuracy.

A second method is the use of a direct drive precision synchro. The accuracy of this device is eventually limited by the linearity with which it can be constructed.

Both of these methods employ "precision" equipment. By using special techniques "super precision" equipment can be constructed which represents the limit of the state of the art.

Typical limiting accuracies of such equipment are shown in the table below:

Method	Best Accuracy Obtainable
Precision Gears	150 seconds
Super Precision Gears	60 seconds
Direct drive precision synchro	300 seconds
Direct drive super precision synchro	20 seconds
Direct Drive Encoder	See Figure IV-42

The third method of measuring an angle is the use of a mechanical to digital encoder. With this device the accuracy of the measurement is a logarithmic function on the number of output bits. A curve of this relationship is shown in Figure IV-34. It should be noted that the declination angle of Figure IV-30 will never exceed $\pm 90^{o}$, therefore one less bit will be required to obtain the same accuracy as for θ and Φ in Figure IV-30.

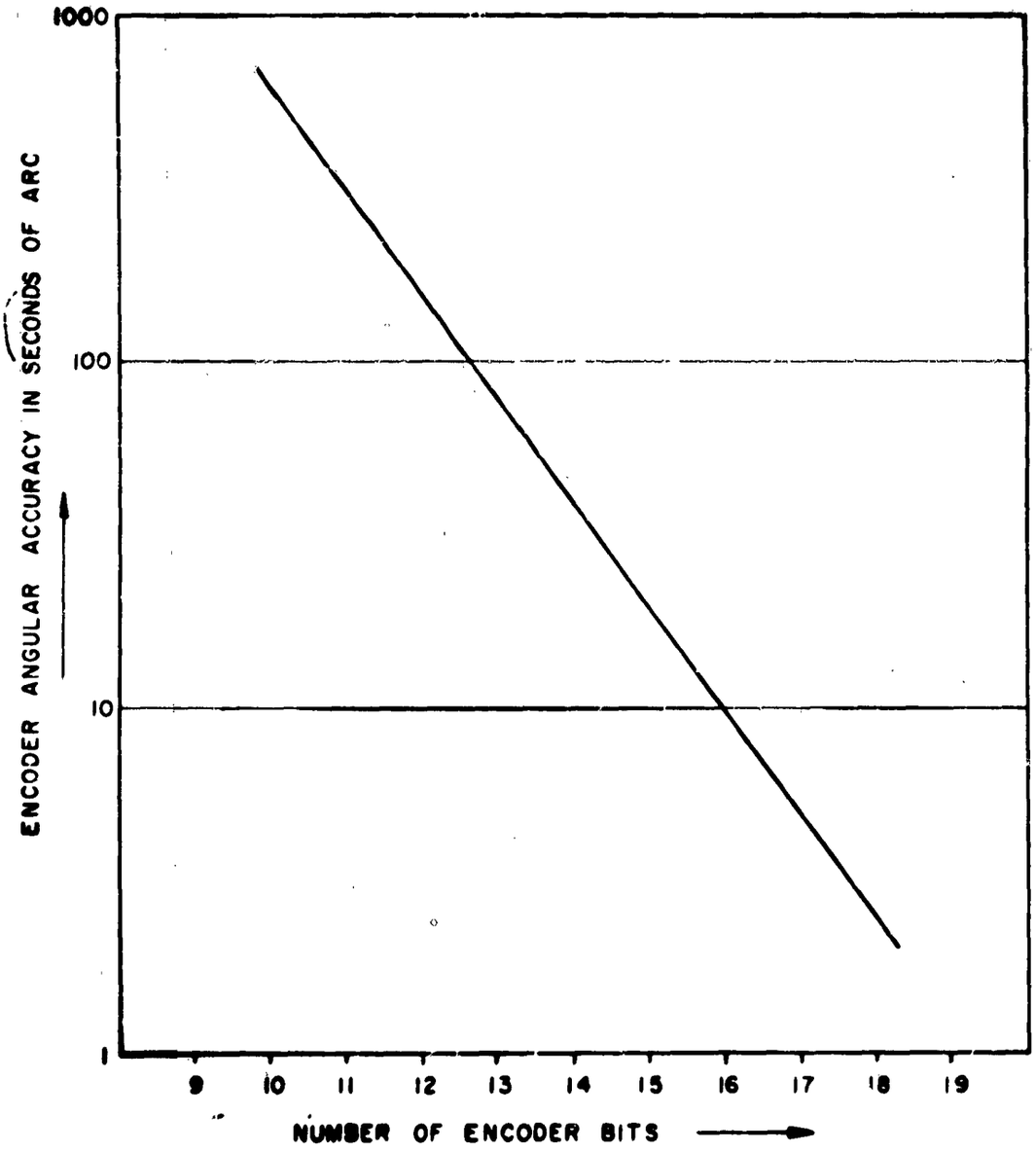


Figure IV-34. Encoder Angular Accuracy as a Function of the Number of Encoder Bits

The significant errors in electro-optical angular measurements due to the positioning equipment have been outlined and discussed above. A sidereal platform was used for an illustration of the problems involved. This scheme was chosen to facilitate target discrimination and to simplify reference coordinates. In practice a single control system might be used to obtain the resultant of θ and Φ in Figure IV-30.

It should be noted that a more simple azimuth-elevation system might also be used depending upon the target discrimination scheme chosen.

In conclusion, it can be observed that the major effect of the mount, regardless of which scheme is used, will be to limit the accuracy with which the two angular components of a target can be measured. For accuracy better than one minute of arc, a direct drive analog to digital encoder would be required. The maximum resultant angular error in measuring two-angle position will then be less than or equal to 1.414 times the individual angular component maximum error. The angular component maximum error for the direct drive encoder is given in Figure IV-34 as a function of the number of output bits.

4. IMAGE ORTHICON LINEARITY

Assuming the center of the image orthicon field of view is accurately known, the time during the scan when the target video occurs is the only method of determining the target position in the field of view. It is assumed that when this scan occurrence time of target video is converted to accurate angular position, some method is used to determine the image center. The effect of image spread on angular accuracy will be discussed later.

To accurately measure the time unit that accompanies the angular measurement, it is necessary to know the start and stop time of every image period. Then the center of each image can be equated to the time half way between the start and finish of the comparable image period. It is assumed that the accuracy of measuring the time of image formation is much more accurately known than the comparable target angle, and is not considered in this analysis.

The conversion from time during scan to position in the field of view is essentially a measurement of image orthicon linearity. The accuracy of this conversion is dependent upon the target position in the field of view. In a circle, centered in the field of view, which contains 50% of the total viewing angular area, the maximum time-position inaccuracy is ±1/4%. The maximum time-position inaccuracy at the image corners is approximately ±1/2%. These inaccuracies are approximately 2σ values.

5. IMAGE SPREAD

The image orthicon image spread may be due to relative target movement during the image period, or due to a target intensity much larger than the detection threshold intensity. Image spread due to a large target intensity is symmetrical about the true image center. This spread would be easier to convert to an image center than the "one dimensional" spread in any random direction due to relative target movement during the image period. At a 1000 nautical mile altitude, a circular orbit target could have a maximum relative velocity of 800 $\widehat{\text{sec}}$/sec. For an image period of 0.5 second, this would result in an image spread of 400 $\widehat{\text{sec}}$, 0.11 $\widehat{\text{degree}}$, or 3.6% of a 3° field of view. Due to the target intensity relationship and velocity relationship with altitude, the lower the altitude of a given satellite, the greater the intensity image spread and the greater the relative movement image spread.

6. TOTAL ANGULAR MEASUREMENT ERROR

A table will be made of the assumed 2σ angular measurement error, using "state of the art" values. The worst case values (at the corner of the field or at 20° elevation for instance) will be used.

ANGULAR MEASUREMENT ERROR

Variable	2σ Inaccuracy	2σ Error (sec) 3° Field of View
Atmospheric Refraction (20°)	±14% (150 sec)	21 sec
Field of View Differential Refraction (20°)	13 sec (3° Field)	13 sec
Atmospheric Image Dancing	6 sec	6 sec
Mount Readout Error	30 sec	30 sec
Image Orthicon Time-Position Linearity	±1/2% (3° Field 10800 sec)	54 sec

The largest error in measuring target angles for a 3 degree field of view is the image orthicon time-position linearity. This error is directly proportional to the field of view, and is the area to be improved first if greater angular accuracies are required, with 3 degree or larger field of view.

The RMS 2σ error, found by taking the square root of the sum of the squares, is 66 sec. This error assumes that processing has already solved the problems of image spread and the refractive bias pointing error.

I. HIGH RESOLUTION SYSTEMS

1. INTRODUCTION

This report is primarily concerned with Separation Techniques and their application to the Space Surveillance Task. This task necessitates maximizing the field of view and aperture at the expense of data accuracy. To illustrate this, several systems were postulated for discussion purposes, though no selection was made as to the best choice.

Where high accuracy data, or high resolution identification is included in the systems requirement, then combination systems will be needed to attain performance. Combination systems necessitate acquisition, hand over, track, and/or track while scan functions. High accuracy data and high resolution identification both need long focal length optics with corresponding small field of view.

Included here is a brief treatment of various electron optical techniques to illustrate the trades of lens and sensor parameters, video processing techniques, readout techniques and other special considerations needed for successful equipment combinations and/or systems.

For the purposes of this report we are concerned with military and/or civilian space applications. Here the emphasis should be placed on performance for maximum data and purpose, not for pretty pictures and convenient eye viewing. Therefore, the scanning format should be optimized to the application and a special effort be made to keep bandwidth down for maximum performance and minimum data handling problems.

Electro-optical equipment with an MgO tube can produce a fantastic amount of data (10 to 20 mc or higher) which may be unnecessary much of the time. Slow

scan rates can reduce bandwidth with usually the only objection being a flickering picture! A P-7 phosphor kinescope tube in the monitor with filter will reduce this for the little human monitoring necessary.

Camera recording (film and P-11 Recording Scope CR tube matched for maximum recording efficiency) is used where records are required in any event. See Section II-C.

The important considerations vary with applications, i.e., time for coverage, detection probability and discrimination are of first consideration in surveillance. False alarm, lens quality, resolution, and atmospheric perturbations are important in high resolution identification and mapping systems.

The different requirements vary the figures involved. However, the areas for making trades are:

Field of view - focal length and f/number

Resolution element size - scan lines and bandwidth

Background brightness - integration time, resolution element size - field of view

Target spreading - saturation levels, beam current control, field occupancy

Moving targets - velocity rates and directions, resolution element, time response

Video processing - electrical signal to noise, background vs signal charasteristics

Monitor recording - precision, linearities; writing rates vs film speed

2. OBJECT BRIGHTNESS

The first consideration here is in the lens selection and electronic scanning program to be used for the sensor with particular attention to background and atmospheric limitations.

If the celestial background is involved, then sky brightness and point target intensity (function of target range) will set the noise level and the contrast. Once the object is resolved into more than one resolution element with long focal length optics, the intensity of a constant resolved angular area is independent of object range. The constant angular resolved area (for example 1 $\widehat{sec}^2$) will have an earth received intensity proportional to reflectivity, but independent of range to the earth, if it is only sun illuminated and its distance to the sun remains a constant 93,000,000 miles. So 1 square $\widehat{sec}$ ($\widehat{sec}^2$) of resolved lunar surface, or 1 $\widehat{sec}^2$ of resolved Echo Balloon, result in the same Lumens/cm^2 aperture illumination, if their phase angle and reflectivity are the same.

3. RESOLUTION LIMITS

The resolution ability limit is set by the optics quality (ability to approach diffraction limit, color correction, aberration, frequency response, etc.). The number of scan lines and bandwidth (resolution element size) should be selected in keeping with optic quality. When sufficient light is available, the diffraction limit can be penetrated somewhat. The engineer is referred to Sears[4] for more extensive treatment of diffraction limits. However, it should never be necessary to place more than 2 or 3 pairs (4 at the absolute most) of scan lines (a line and spacing being a pair) for the extent of the diffraction limit.

The following table illustrates this point. Note that generally 1000 to 1200 lines represents the optimum for general high resolution work. Special treatment and study is in order before setting higher scan line requirements. The same problem is in order regarding use of film. Though a smooth and pretty picture may be attained, the information and picture content will not generally be any better than the 1000 to 1200 scanned picture since in both cases the frequency response or diffraction limit of the optics (and/or atmosphere) would be setting the performance limits.

Resolution/sensitivity on Resolved Objects for 1000 line scan (800 line effective resolution).

Optics Diameter (inches)	f/no	Focal Length (inches)	Theoretical Diffraction Limit (sec of arc)	Practical Optic Limit (sec of arc)	Resolution Element Size (800 line) Single Dimension (sec of arc)	Field of View with I.O. (sec of arc)
5	f/120	600	.9	1.	1/2	450
12	f/125	1500	.4	.6	1/4	180
24	f/100	2400	.2	.4	1/8	110
30	f/100	3000	.15	.3	.1	85
48	f/95	4500	.1	.2 to .25	.06	55

Figure IV-35A and B typifies what can be done with a 16" aperture at only 240" focal length 1029 line scan with approximately 2 sec of arc resolution element size (better than atmospheric limit on night taken).

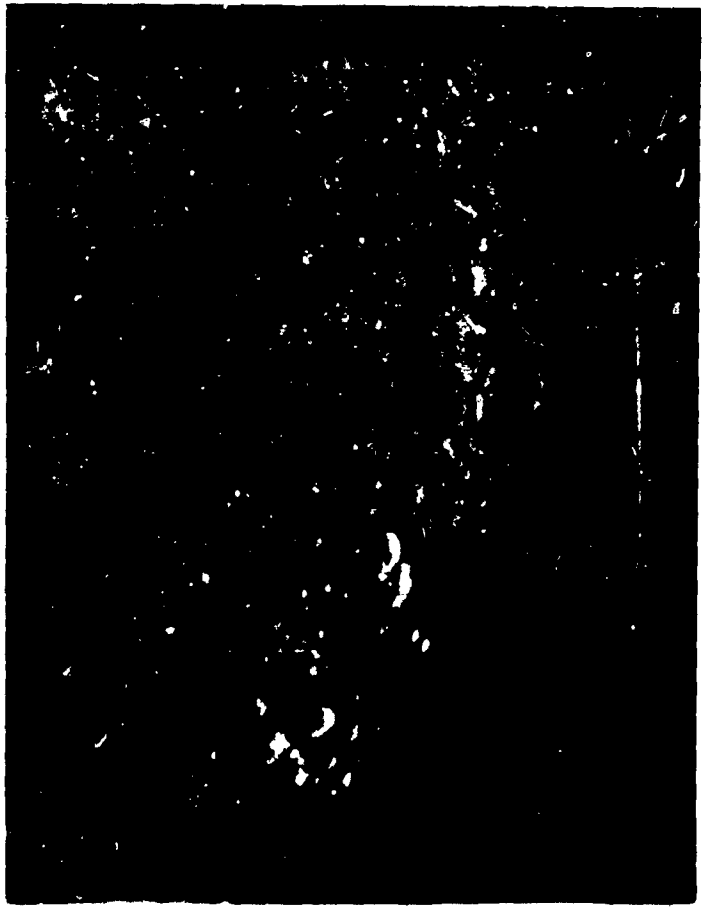
4. RESOLUTION (FAINT POINT SOURCES)

Since the smallest image detected on the MgO image orthicon is usually spread to 2 or 3 resolution elements on a side for minimum detection, the ability to separate close objects (double stars, etc.) is reduced by this factor unless special techniques are used.

Since the MgO image orthicon target itself can resolve to about 3000 lines then approximately this number of lines should be used where maximum resolution is desired, in order to reduce the point image spread area to the smallest occupation area of the I.O.'s target. At this point, optical gain (multiplier lens) should be added to the main optics until the smallest point image focus area corresponds to several lines of the 3000 line scanned area. In this way the optics, rather than the orthicon, are setting the limit and by using the maximum line resolution ability of the orthicon the optical gain is at the minimum increase for orthicon limit.

In this optimum match, the light loss and optical gain (field of view compromised least) are minimum and the resolution will be as good as film under "ideal" seeing conditions. In all practical conditions, the resolution of film will be exceeded. The combined speed (orthicon plus slower lens) is much greater than that of film, thus permitting shorter exposures (less atmospheric disturbances). For instance, for normal best speed film exposure time the atmospheric perturbations will impose a 1 to 3 sec of arc seeing limit where with the I.O. shorter exposures can attain,





Figures IV-35A and 35B. Examples of
Length RCAA Telescope and 10

ion Possible with 16-1/2", f/5 Reflector ≈ 240" Focal
Scan; 1/30 sec Rate, Continuous Scan of Moon;
ight, No Filter

theoretically, the diffraction limit of the optics system. The question may still exist, however, as to which short exposure picture presents the real picture and which includes a product of the atmosphere.

A word of caution: To read out on monitors a picture of 1000 lines (where I. O. is being scanned over 1200 lines) special monitors will be required. If one wishes to use standard high resolution monitors (1000 line ability) then additional optical gain should be used to spread the point image focus over an area of several of the 1000 line lines area which in this case will be a correspondingly larger area of the I. O. target: - Performance will still exceed film in resolution and exposure time.

5. ATMOSPHERIC "SEEING" IMPROVEMENTS

From paragraphs 3 and 4 above we have shown that for properly designed systems the optics sets the limit of equipment performance. However, for the longer focal lengths (higher resolution) the atmosphere "seeing" limits the overall system performance. In section I-C of this report a brief discussion of the atmospheric effects was given. These various effects combine to govern the practical limits on resolution and seeing. The atmospheric turbulence causes the image to blur and dance (irrespective of mount stability, etc.). The extent of the mixture of blurring and dancing depends on the number of turbulent elements (layers) between object and optics.

Small aperture telescopes have mostly dancing, whereas large apertures have mostly blurring. The total (time averaged) effect is about the same and thus the image size (of a point source) is nearly independent of aperture. Thus the seeing condition is often defined in terms of image size. Image size vs. frequency curves taken at several observatories and appear to have Poisson distribution peaking at 1-1/2 seconds at Kitt Peak and 2-1/2 sec at Mt. Palomar.

Since most observatory work is done with film, much of the established practice and discussions available are treated in this respect. Visually, it always is possible to exceed photographic resolution (with a long focal length telescope) because the dark-adapted eye time constant is about 0.2 seconds giving it the opportunity to take advantage of short instants of "good seeing".

The advantage of the greater "speed" of the image orthicon over film and human eye presents a practical way to improve resolution seeing ability by permitting shorter exposures down to a few milliseconds.

Detail design and systems engineering for this type of use of electro-optical equipment presents challenging possibilities. Hence many different schemes are being studied and some tried in various forms.

Loss of contrast caused by scattering of light by the atmosphere is another factor limiting resolution. This is important since high contrast (sharp edging, etc.) permits working below the usual resolution limits, by as much as a magnitude under some conditions.

Local site effects are important if high resolution work is to be attempted. Astronomers have learned to correct for local atmospherics, cold air vs. warm air, turbulence, air currents, dome orientation and height, ground preparation, etc., at their individual locations and all these practices should be followed in setting up sites, if good seeing is to be attained. Most schemes are based on following the

first order "dancing" effects plus manual control of optics to maintain focus as it varies. Astronomers have long been applying stabilizing schemes (move their film plates with the dancing, or exposing only when the image is at a specific point) and manually riding the optical focus as needed to get their best pictures.

With the advent of the GE thin film MgO Image Orthicon, its tremendous "speed" in relation to film presents many exciting possibilities. In addition, its image section provides an area where corrective measures can be applied so that the scanned image will already be "stabilized". Here the stabilizing signal can be from external control (photomultiplier) or by a closed loop servo around the I.O. tube itself. This technique was investigated at Dyer Observatory and is recorded in November 1959, Sky & Telescope. Refinements can be made to the methods reported to eliminate the shortcomings noted. See referenced reports.

Another technique is to use short exposure control of the I.O. image section to expose the tube at a specific condition of the target then re-expose at an instant of similar condition; repeating this until sufficient exposure time has been built up commensurate with the resolution/sensitivity desired, and then reading out. In this manner details on fast moving, rotating, etc., objects can be photographed from a monitor. This can also be used to advantage by exposing only during periods of stable mount conditions or "on target" conditions, etc., in addition to selecting exposures at times of stable atmospheric conditions.

The reverse of the above can be employed as a measuring tool for determining object stability and resolution, mount stability, tracking stability and atmospheric studies, by recording successive exposures at various intervals to obtain autocorrelation patterns of the phenomena or instability involved.

6. MAPPING TECHNIQUES

Where a distributed scene is being resolved and a high resolution picture or map is the prime requirement, advantage of the "speed" of the orthicon can be used as motion sensing element to control servoed mirrors to present a stabilized image at the film plane for photography.

An addition of an automatic shutter control to this scheme could allow photography only when the image is at best focus, and/or the instances when a selected distinguishing feature presents the smallest image ("pulsation" effect at minimum).

J. SEPARATION AND POST SEPARATION PROCESSING

Separation can be more involved than a simple cancellation of binary off-on video. To solve the problems of image spread requires handling lots of data:

1. Measure the center of symmetrically spread images, and the amount of the image spread.
2. Measure the direction and amount of relative motion during image exposure.
3. Compare the relative position displacement of each pair of image points (if there are two of them) and decide: either they are one star misregistered, or that a target is detected.

The amount of data would be large because every star in the field of view would require an image size, image center, direction and amplitude of relative motion data

storage, where the image center data could be any resolution element in the field of view.

A non-automatic feasibility system could use a scanned image of "residual" video left after video cancellation. It could use a two color display of two complete images, as an alternate. In any event, the human viewer would make the decisions about image centers, relative motion, misregistered stars or targets, and such false alarms as falling stars, the moon, or a planet that would be difficult to program for a computer. It is believed that an automatic electronic detection should proceed the viewers scanned image; because it will leave less decisions for the viewer, and also because it is necessary for a large surveillance area "automatic" system.

One problem an automatic system would have is sorting the targe to minimiz target false alarms. Some characteristics that might help decrease false alarms include:

1. Large image size; therefore large intensity lower altitude; therefore not interested unless a reasonable relative motion image spread.
2. Very large relative motion (falling stars) therefore not interested.
3. Direction of relative motion; therefore not interested in some orbits.
4. Known positions of planets, comets, asteroids, moon, etc.
5. Compare targets with known satellite orbit positions.

This brief discussion shows some of the complexities of a completely automat surveillance system, even after initial detection and separation-cancellation.

SECTION V. ORBITAL PREDICTION FROM ANGLE ONLY DATA

A. INTRODUCTION

The data obtained from electro-optical devices consists of a series of angular measurements. Any number of observations can be made with an optical sensor, each observation consisting of two angular measurements: azimuth and elevation. When predicting an orbit, this set of electro-optical data is smoothed to a set of angles, angular rates and angular accelerations at a specified reference time. The angle only orbit determination technique is then used to determine the position and velocity of the target (at the reference time) by "transforming" the smoothed angular data to target position and velocity components ($RAE\dot{R}\dot{A}\dot{E}$). After the target's position and velocity are known, the problem of orbit determination has been reduced to an equivalent radar problem and further orbit calculations can be carried out. A flow chart for the present orbit prediction scheme is shown in Figure V-1. R range; A azimuth; E elevation.

The purpose of this accuracy study is to determine the accuracies obtainable in predicting orbits from angle only data. For system design purposes it is necessary to determine the effect of data parameters (such as smoothing time, frequency of independent observations, and accuracy of angular measurements) on prediction performance. The accuracy study can be divided into two parts.

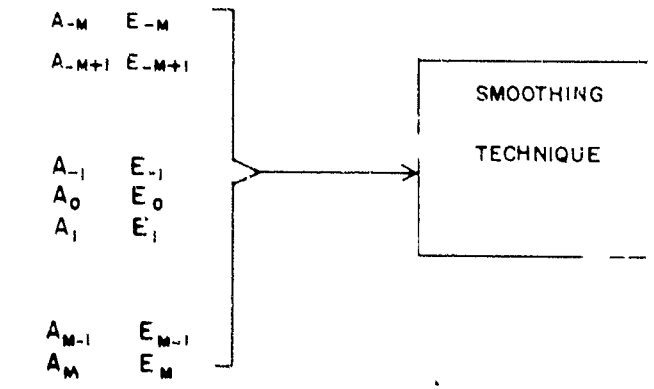
B. ACCURACY STUDY

(1) Accuracy of orbit prediction using more than three sets of angular observations.

(2) Accuracy of orbit prediction using three sets of angular observations. This portion of the study also pertains to orbit prediction from data which has been presmoothed into the "three set" form.

The purpose of the first part of the accuracy study is to estimate the efficiency (in the statistical sense) of smoothing techniques when more than three sets of optical data are smoothed. A simple quadratic fit was chosen for a model smoothing scheme (see Appendix IV). This simple fit fulfills the requirements of the accuracy study since it demonstrates typical error behavior. The simple fit was chosen in simulating orbit prediction from N observations (N > 3) so that typical errors could be generated and used to error the angular quantities A_0 $\dot{A}_0$ $\ddot{A}_0$ E_0 $\dot{E}_0$ and $\ddot{E}_0$ (see flow chart, Fig. V-12) After the previous quantities are errored it is possible to determine how observation errors propagate through the basic angle only technique. The error study was divided into two parts so that a separate investigation could be carried out on the "three observations" orbit prediction technique. This orbit prediction scheme has been programmed and checked out; it is capable of predicting an orbit exactly from three sets of unerrored optical data.

The general procedure followed in carrying out the accuracy study will first be outlined. The Monte Carlo technique was used to study propagation of measurement



WHERE:

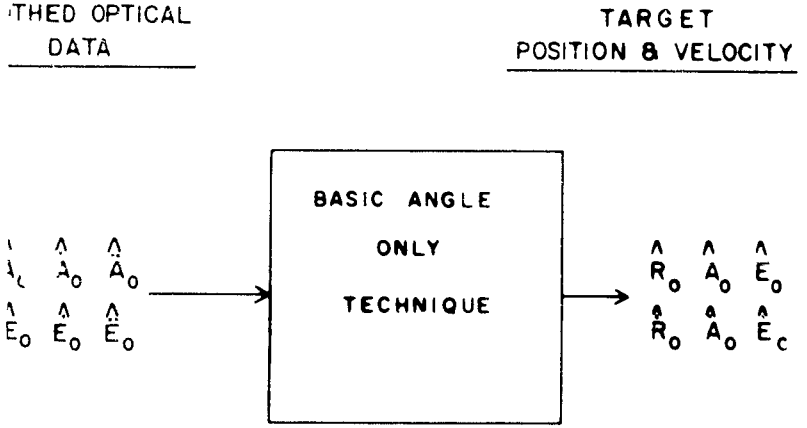
THE SUBSCRIPT "o" DENOTED REF

$M = \frac{N-1}{2}$

THE HAT(Λ) DENOTES THE BEST ES

ie $\hat{A}_o$ = THE BEST ESTIM

Figure V-1. Flow Cl



E $t = t_o$

OF AN "UNHATTED" VALUE

λ_o

bit Prediction from Optical Data

errors and to determine the standard deviations of the target's position and velocity components (σ_R, σ_A, σ_E, $\sigma_{\dot{R}}$, $\sigma_{\dot{A}}$, $\sigma_{\dot{E}}$). The Monte Carlo method is a repetitive type procedure where errored electro-optical data is simulated and then subjected to the angle only prediction technique. After the above procedure is repeated a number of times (1,000 Monte Carlo loops were used in this study), the desired standard deviations can be calculated. The randomness involved in generating the errored data gives a random quality to later errors such that no significance can be attached to any one calculation. After the position and velocity errors at the reference time were determined, a computer program was used to determine confidence volumes at future times around the orbit. The confidence volumes are regions surrounding the target's true position in space (at some specified future time) within which the target's predicted position will fall with a given degree of confidence. The size of the confidence volumes is a function of both the data parameters and the specified degree of confidence.

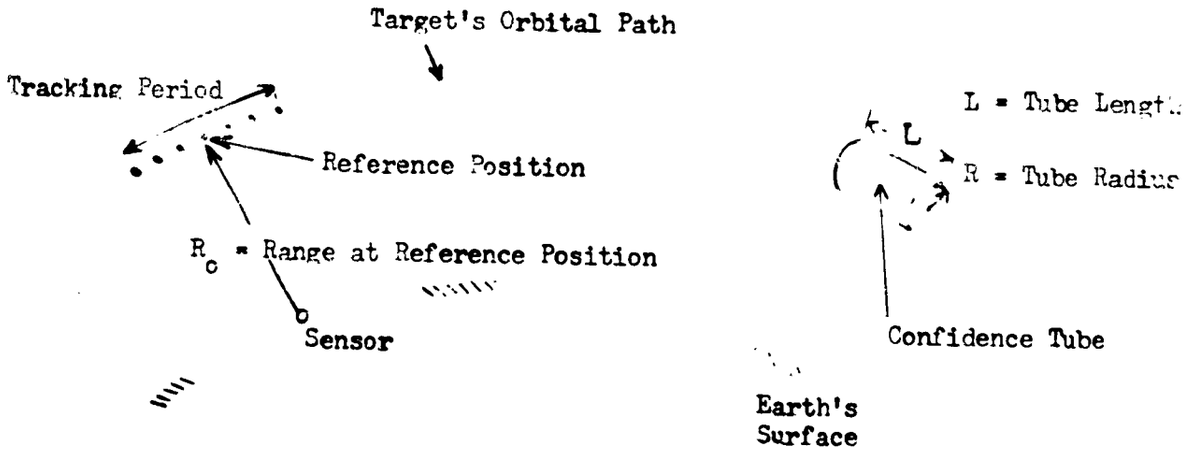
In order to simulate errored electro-optical data, it was first necessary to choose a population of orbits which sufficiently demonstrates the effects of data parameters on prediction performance. The population chosen consists of 5 elliptical satellite orbits, initially defined by their respective height of perigee, height of apogee, and inclination angle. The orbits are listed below:

ORBIT DESIGNATION	H_A (n.mi.)	H_P (n.mi.)	i (degrees)
#1	30,000	3,000	20
#2	13,000	10,000	20
#3	89,900	1,000	20
#4	1,990	1,000	20
#5	30,000	3,000	30

Various orientations of the orbits with respect to the observer (+40° latitude; -100° longitude) were considered in order to determine the effects on prediction accuracy. After the orbit was defined, a computer program (Satellite Simulator Program) was used to simulate unerrored electro-optical data. It should be mentioned that the data was simulated with a non-rotating earth. A "non rotating" prediction from data simulated with a non-rotating earth is assumed to be an excellent representation, in its errors, to a rotating prediction from live data or data simulated with a rotating earth. In the near future the angle only technique will be modified to include earth rotation. In order to simulate errored data it was necessary to generate errors to be added to the "true" data. A random number generation program which produces numbers from a normal distribution (zero mean, unity variance) was used in the first portion of the error simulation. Simple algebraic manipulations then yield errors which have the desired standard deviations and correlation. A more detailed discussion of the accuracy study will be given in one of the following sections of this report.

C. RESULTS

The more important parameters involved in this study will be defined so that the results can be more easily interpreted. A sketch should give a physical picture of the actual system.



Tracking Time - The total time interval during which optical data is obtained or the time it takes for the target to pass from one end of the tracking period to the other. Any odd number of observations can be taken during the tracking time.

Reference Position - The target's position when it is located exactly in the middle of the tracking period. An equal number of observations are taken before and after the reference position and one observation is taken when the target is located at the reference position.

Reference Range - The distance from the sensor to the target when it is located at the reference position.

Δt - The time interval between independent observations.

1. PART I - MORE THAN THREE SETS OF OBSERVATIONS

Interpretation of the Curves, Figures V-2 thru V-5.

(1) In arriving at the following results, it was assumed that azimuth and elevation angles are measured with equal accuracy. Therefore, for all the following curves the standard deviation on elevation errors (σ_E) equals the standard deviation on azimuth errors (σ_A).

(2) From the first plot, it can be seen that range errors are a linear function of observation errors. Similarly it has been shown that error volume tube radius and tube length vary linearly with observation errors (no plots have been made).

(3) All plots after No. 1 were made for the case where σ_A σ_E = 0.1°; however, results for standard deviations other than 0.1° can be obtained by a simple multiplication. To obtain a result (Range standard deviation, tube radius, tube length etc.) for observational errors other than σ_A = σ_E = 0.1°, multiply the indicated result from the graph by $10^{\circ}\sigma_{desired}$, in degrees where $\sigma_{desired}$ is the standard deviation of interest.

(4) Some of the curves have only been produced for a single orbit (Orbit #4). In these particular cases, Orbit #4 was chosen so that accuracies obtainable with electro-optical equipment could be compared with those obtainable with radar at equivalent ranges. It is realized, that electro-optical systems will be used to site targets at ranges greater than 2,000 n.mi., but Orbit #4 allows the previously mentioned comparison to be made since the target comes within radar range (minimum range = 1720 n.mi.).

(5) When predicting ahead in the orbit, a 90% confidence was used.

2. PART 2 - THREE SETS OF OBSERVATIONS

Interpretation of the curves, Figures V-9 thru V-11.

(1) In arriving at the following results, it was assumed that azimuth and elevation angles are measured with equal accuracy. Therefore, for all the following curves the standard deviation on elevation errors (σ_E) equals the standard deviation on azimuth errors (σ_A).

(2) All of the following plots were made for the case where $\sigma_A = \sigma_E = 0.01^{\circ}$. Since output errors are a linear function of input errors (see Part 1), results for standard deviations other than 0.01° can be obtained by a simple multiplication. To obtain a result (range error standard deviation, tube radius, tube length etc.) for observational errors other than $\sigma_A = \sigma_E = 0.01^{\circ}$, multiply the indicated result from the graph by $100\sigma_{desired}$, in degrees where $\sigma_{desired}$ is the standard deviation of interest.

(3) When predicting ahead in the orbit, a 90% confidence was used.

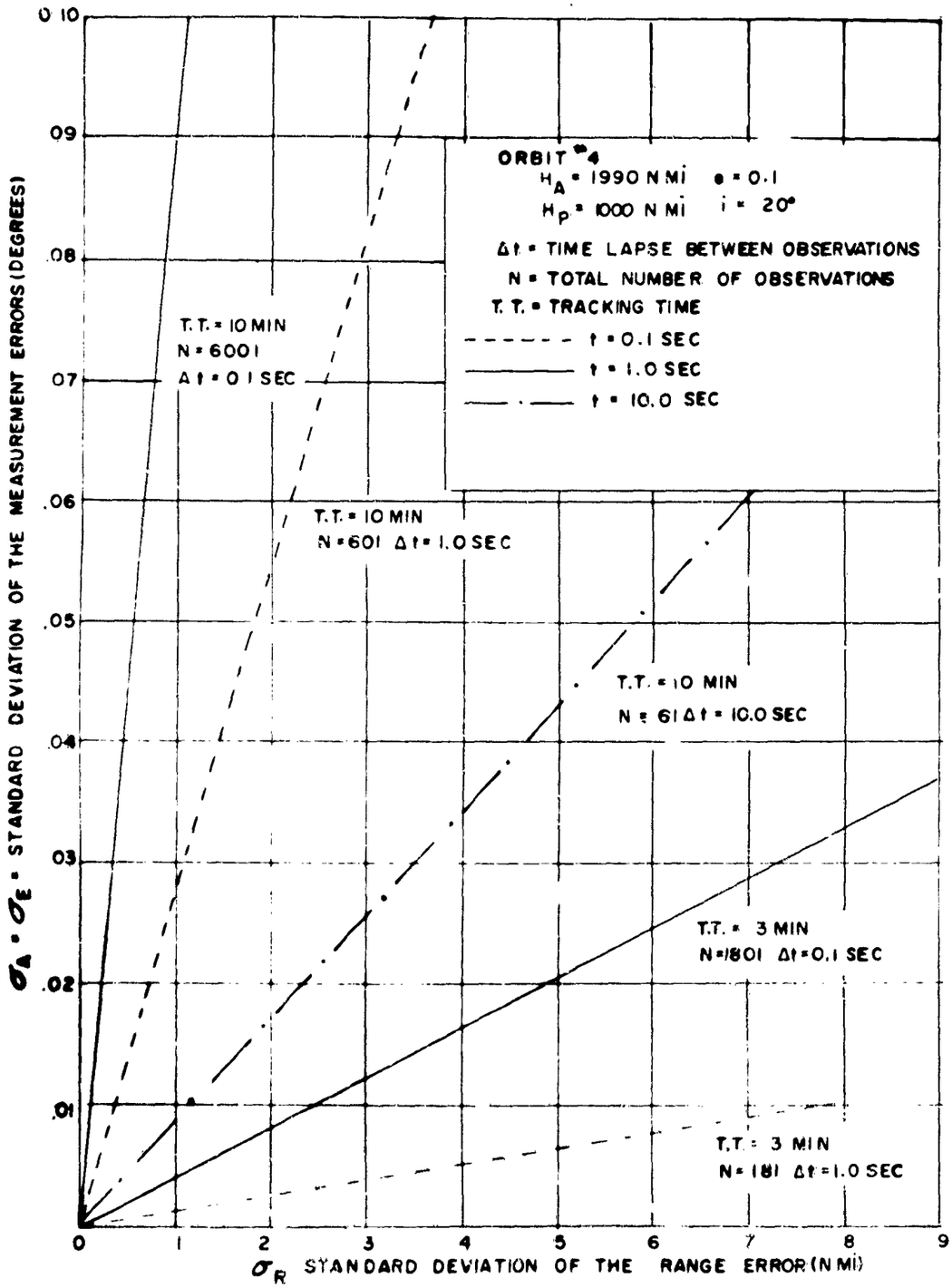


Figure V-2. Range Error at Reference Position as a Function of Measurement Errors

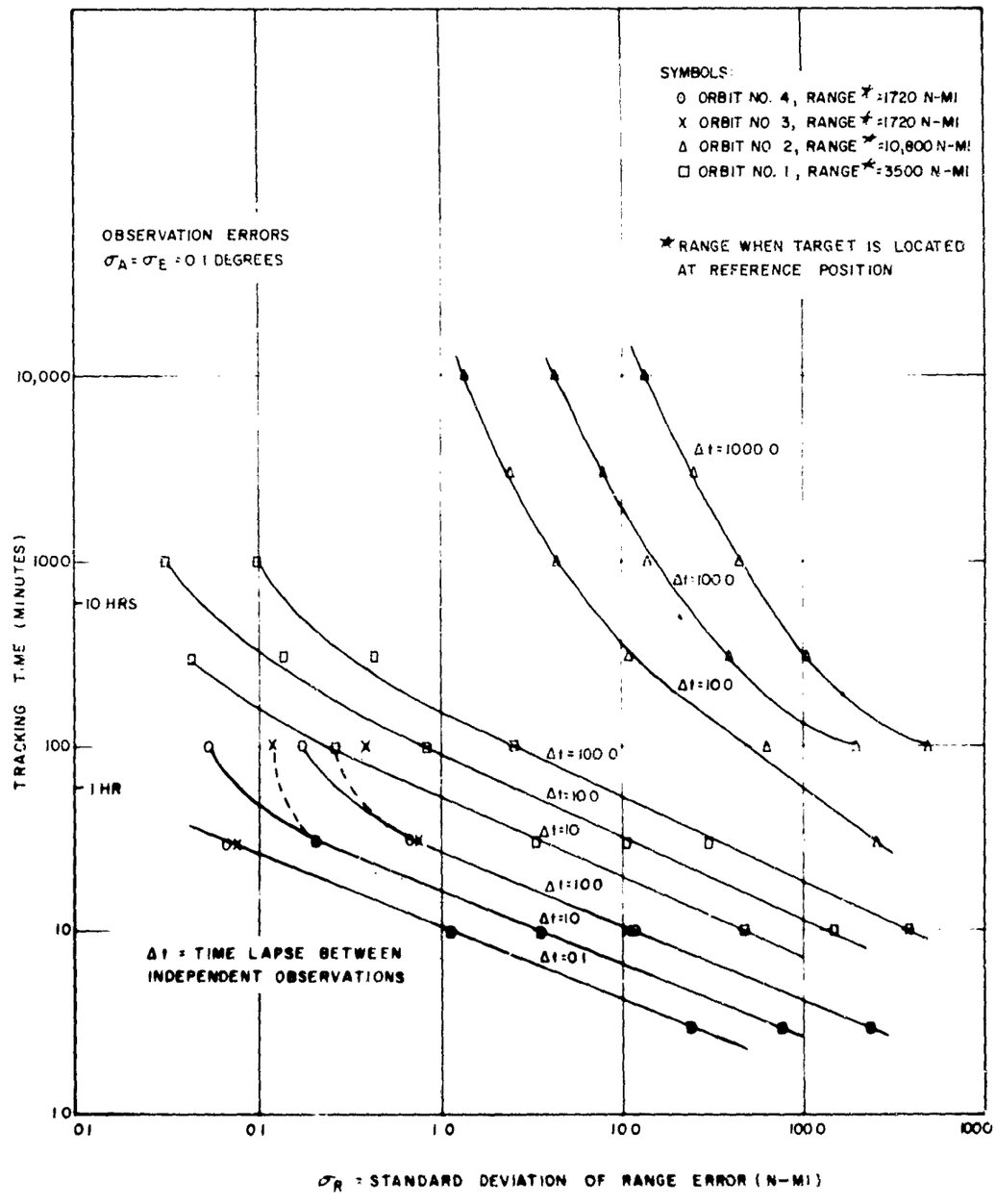


Figure V-3. Range Error at Reference Position as a Function of Tracking Time and Time Lapse Between Independent Observations

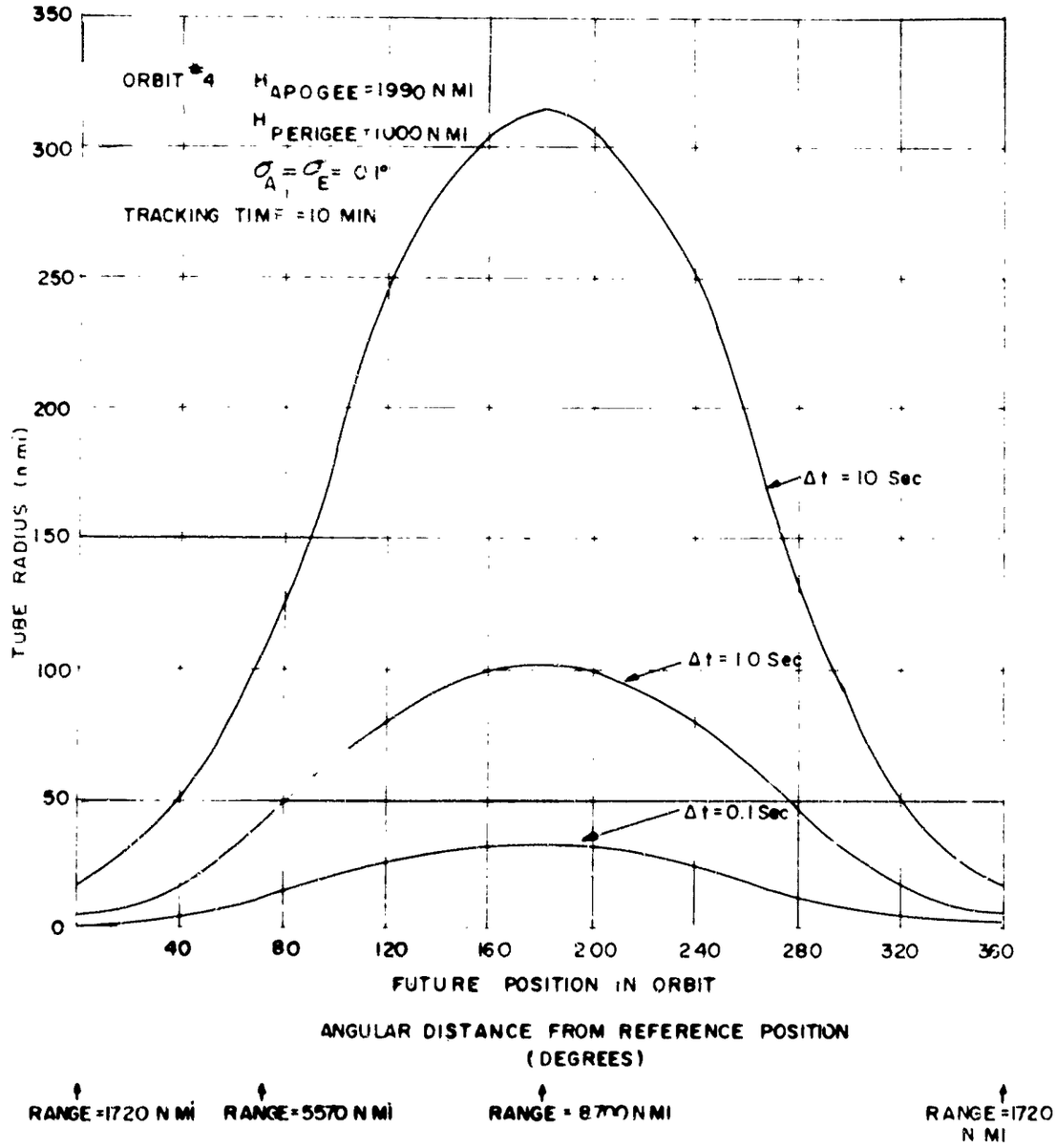


Figure V-1. Prediction Ahead - 90% Confidence Tube Radius as a Function of Angular Distance from the Reference Position

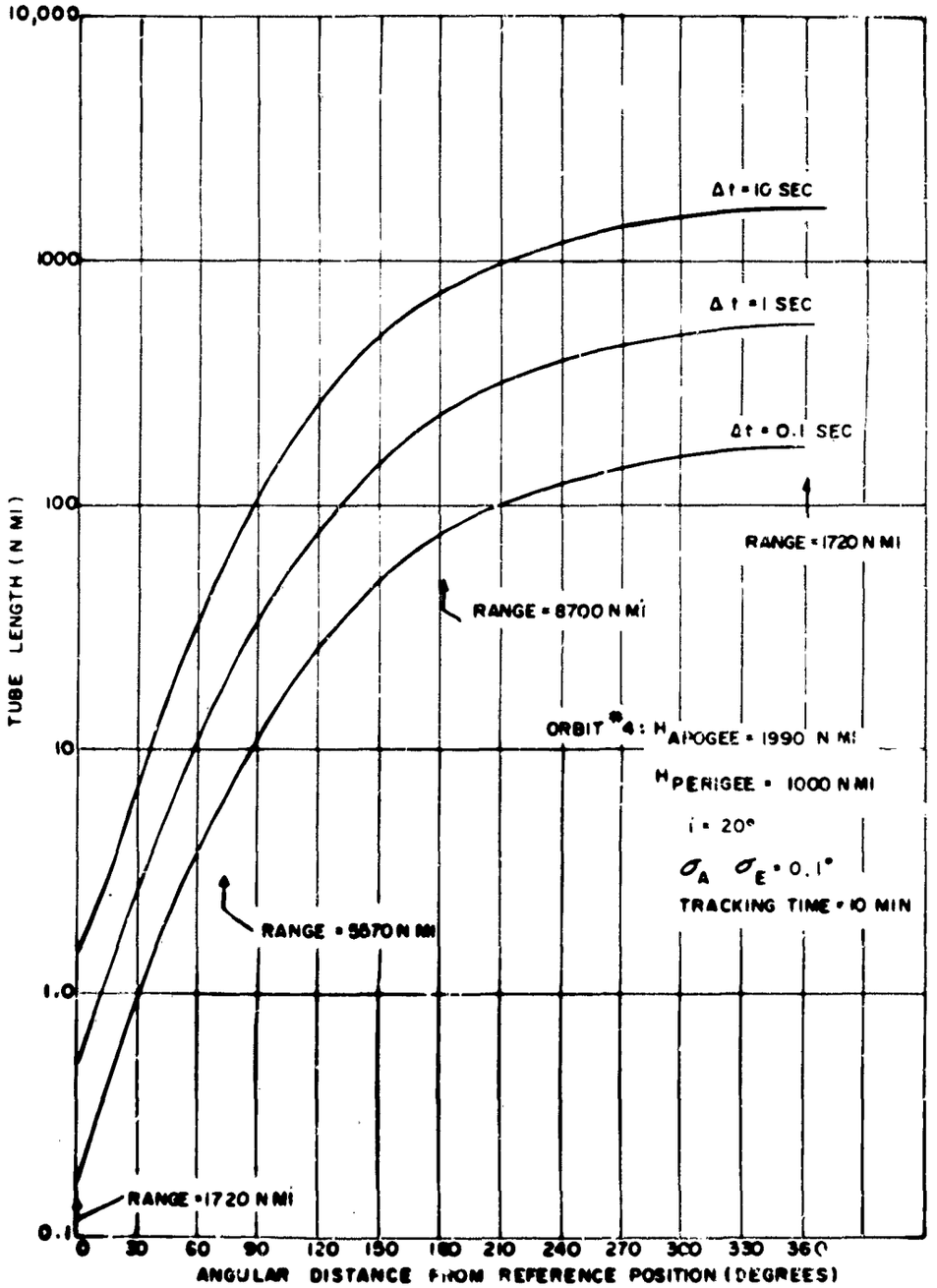


Figure V-5. Prediction Ahead - 90% Confidence Tube Length as a Function of Angular Distance from the Reference Position

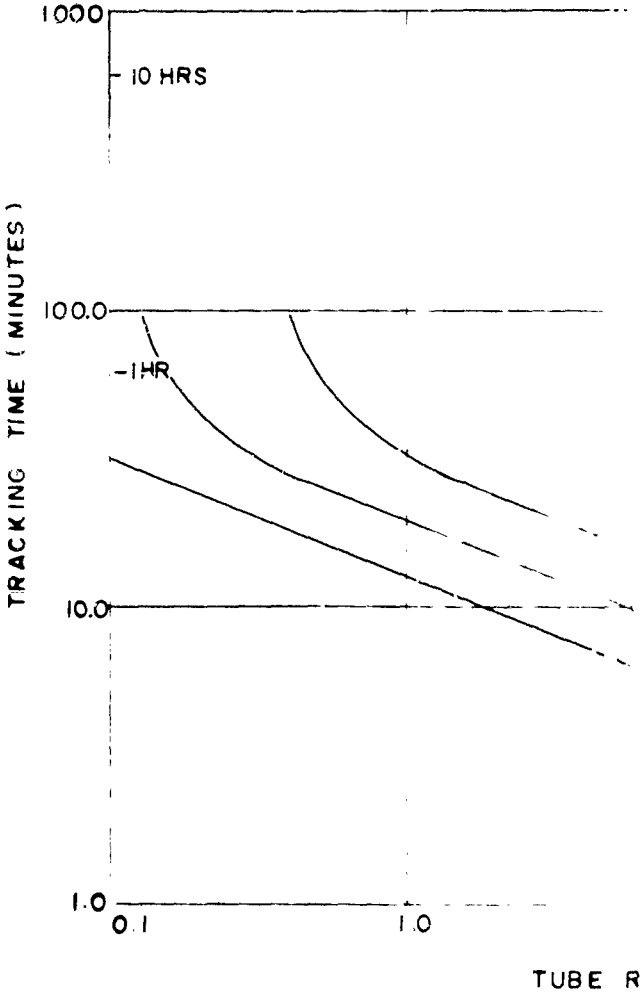
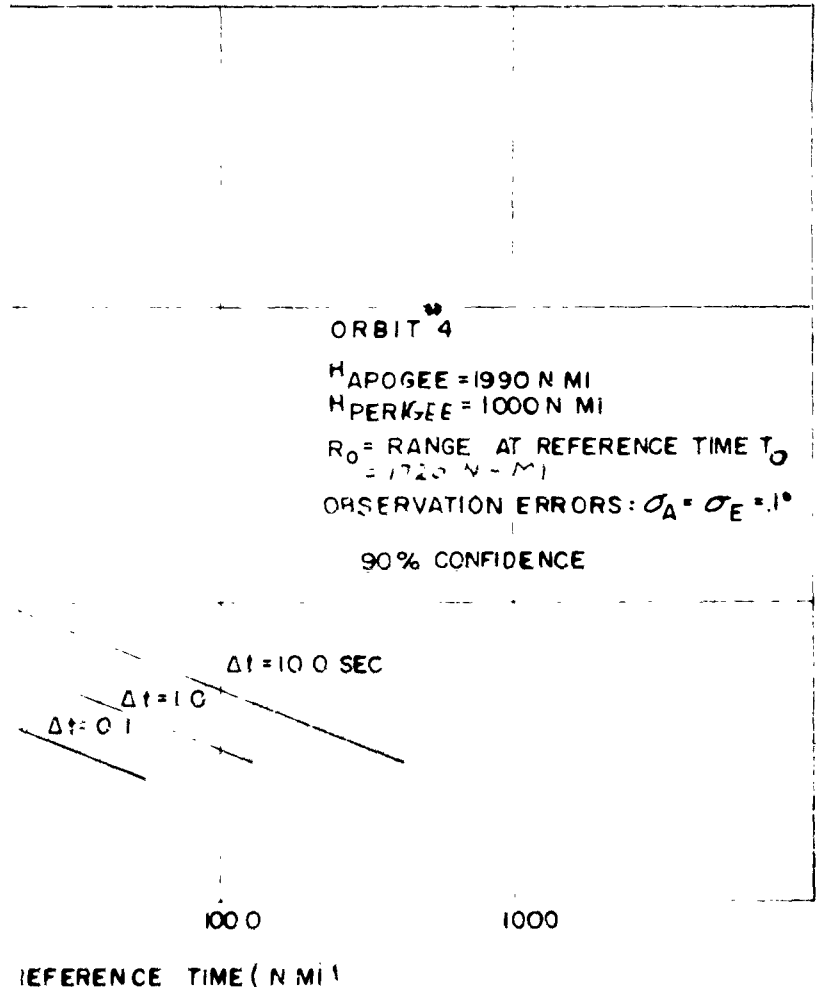


Figure V-6. Tube Radius at Reference Time as



, of Tracking Time and Time Lapse Between Observations

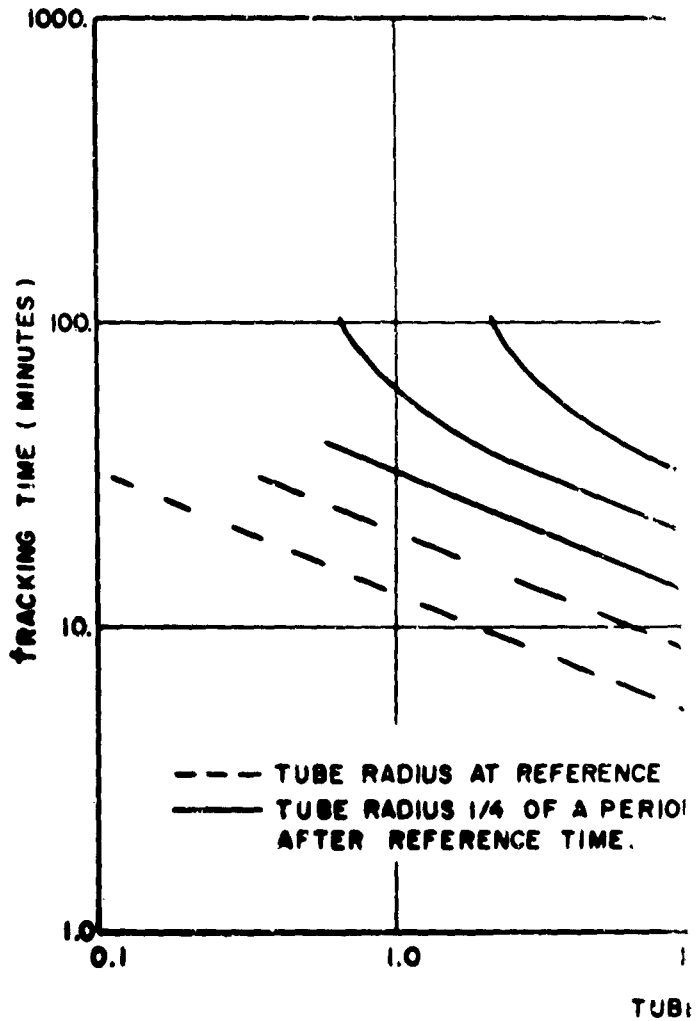
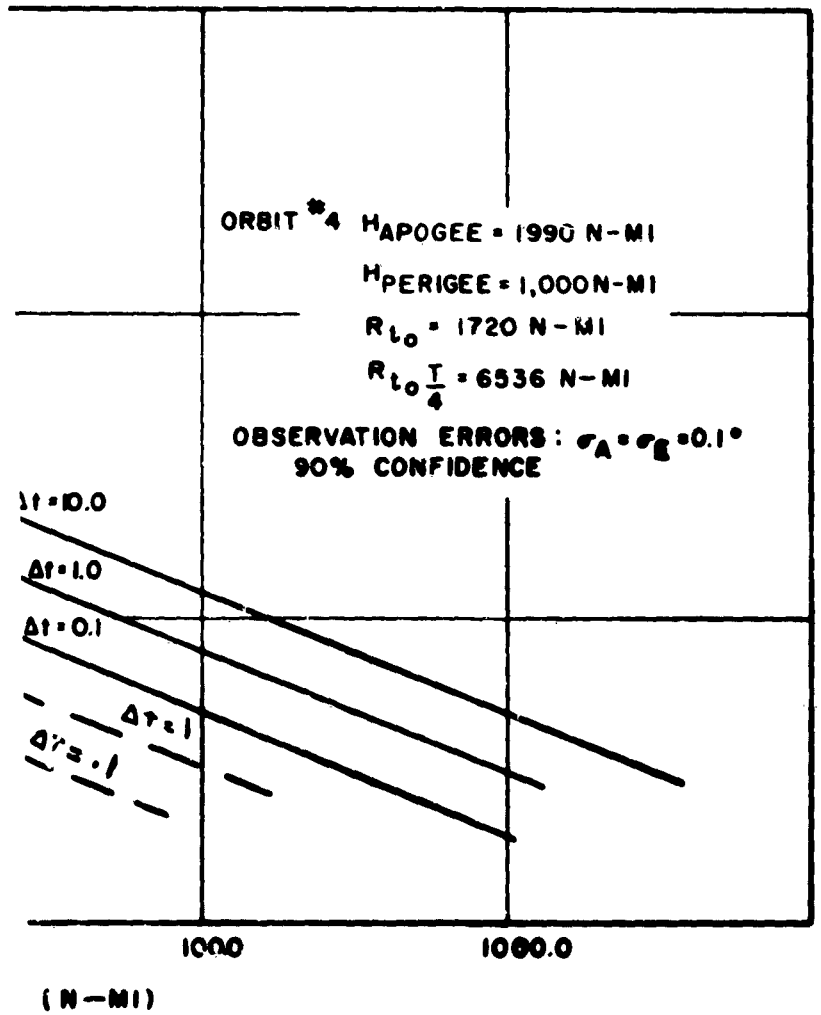


Figure V-7. Predi



ıd – Tube Radius 1/4 of a Period
'erence Time

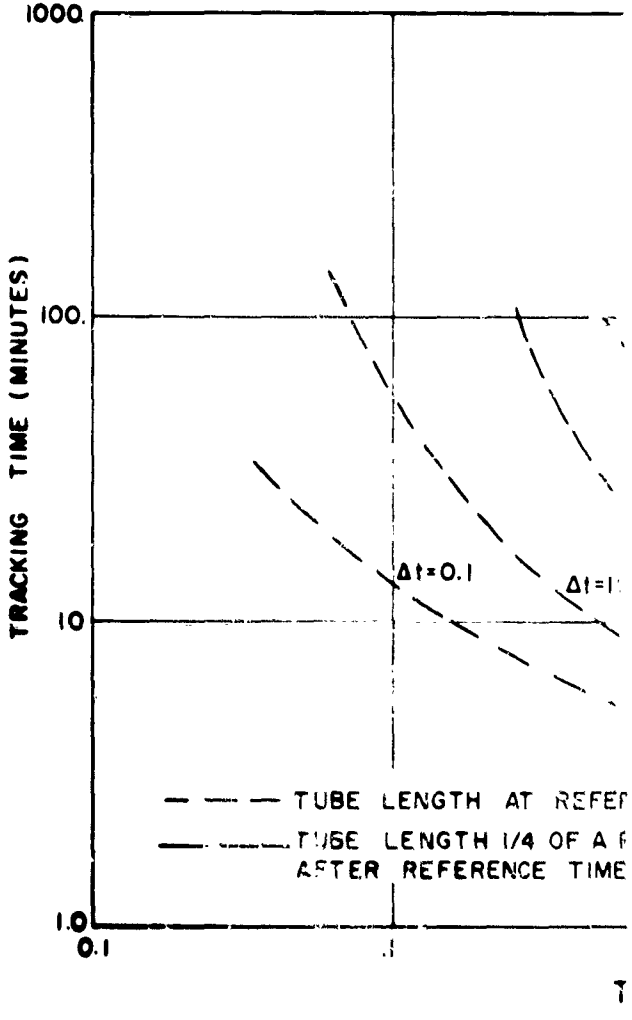
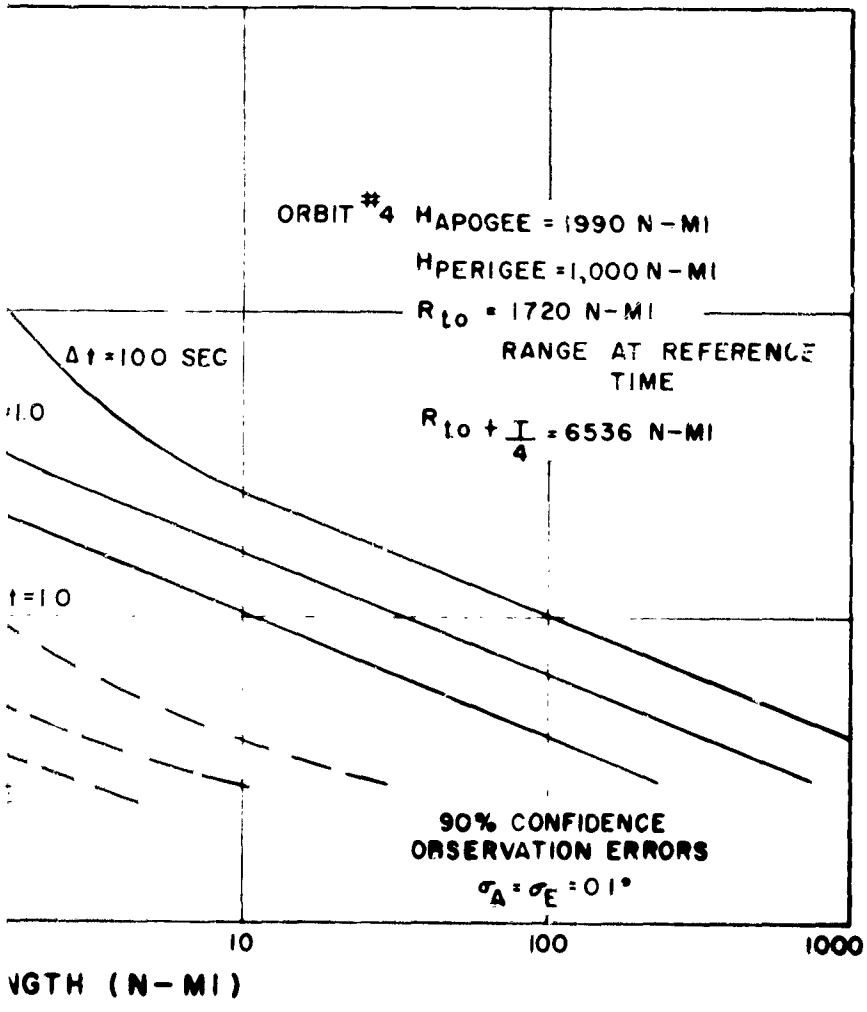


Figure V-8. Tube Length a



ce Time and 1/4 of a Period After Reference Time
tion of Tracking Time

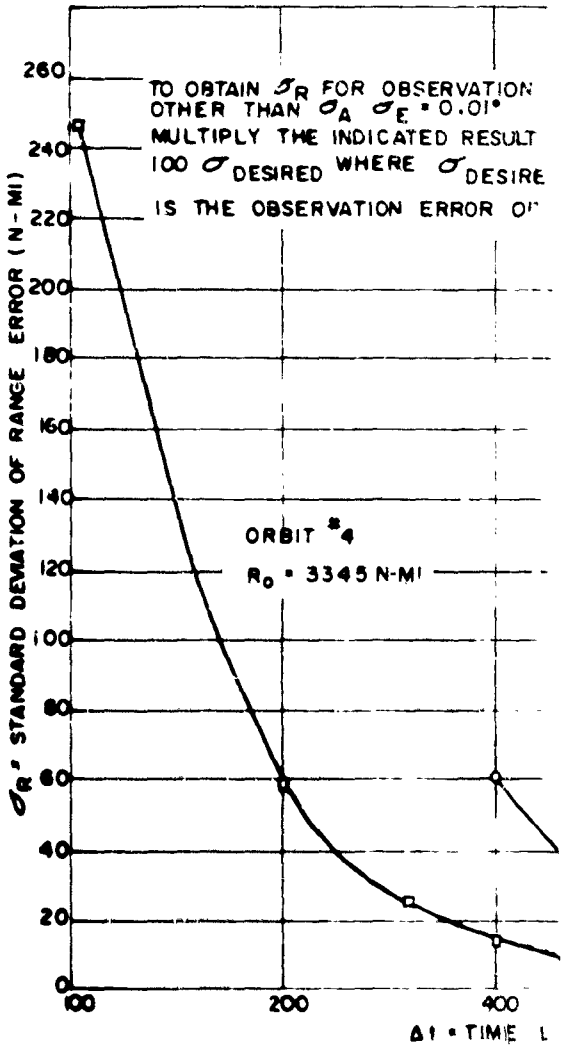
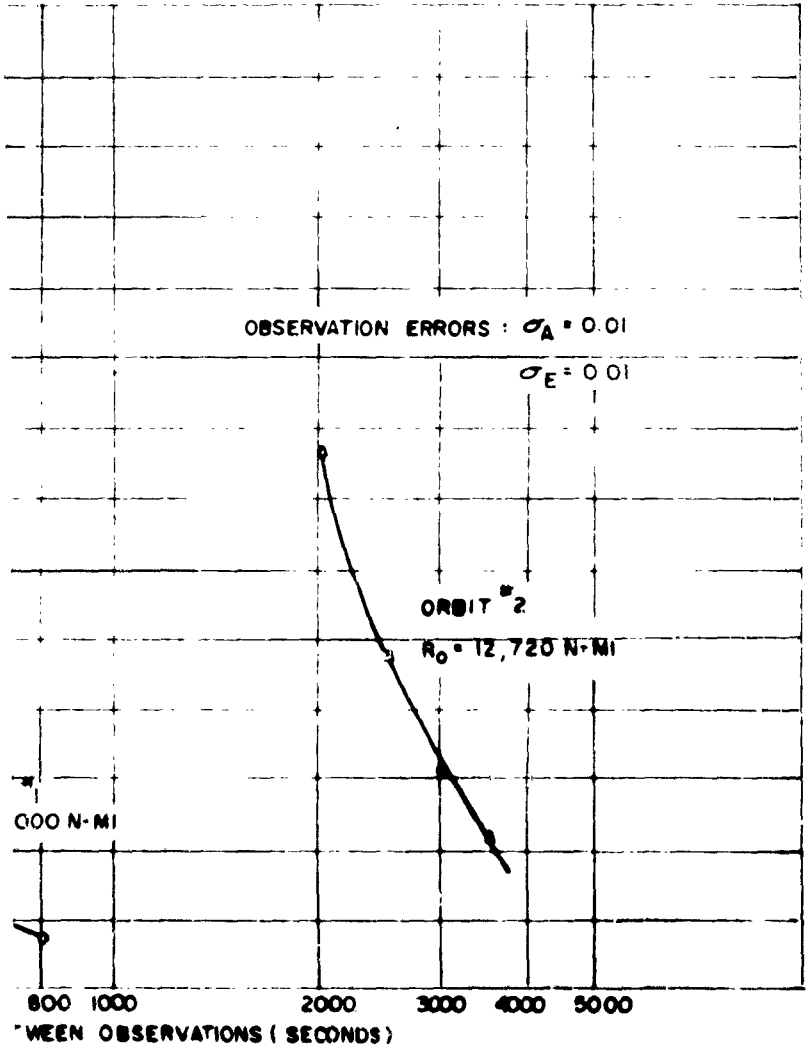


**Figure V-9. Orbit Prediction fr
Second Observation a**



**e Observations — Range Error Corresponding to the
tion of Time Lapse Between Observations**

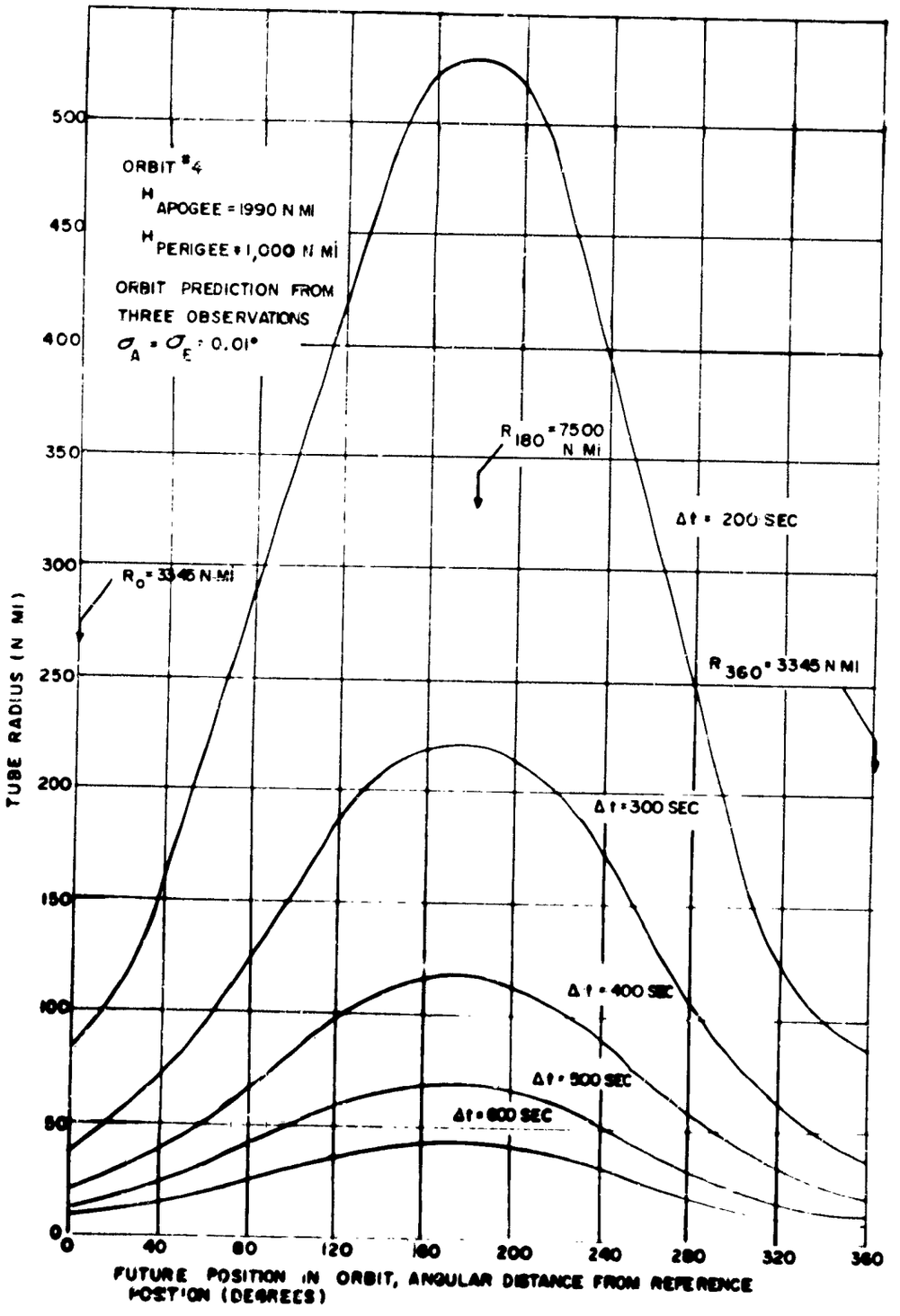


Figure V-10. Prediction Ahead — 90% Confidence Tube Radius as a Function of Angular Distance from the Reference Position

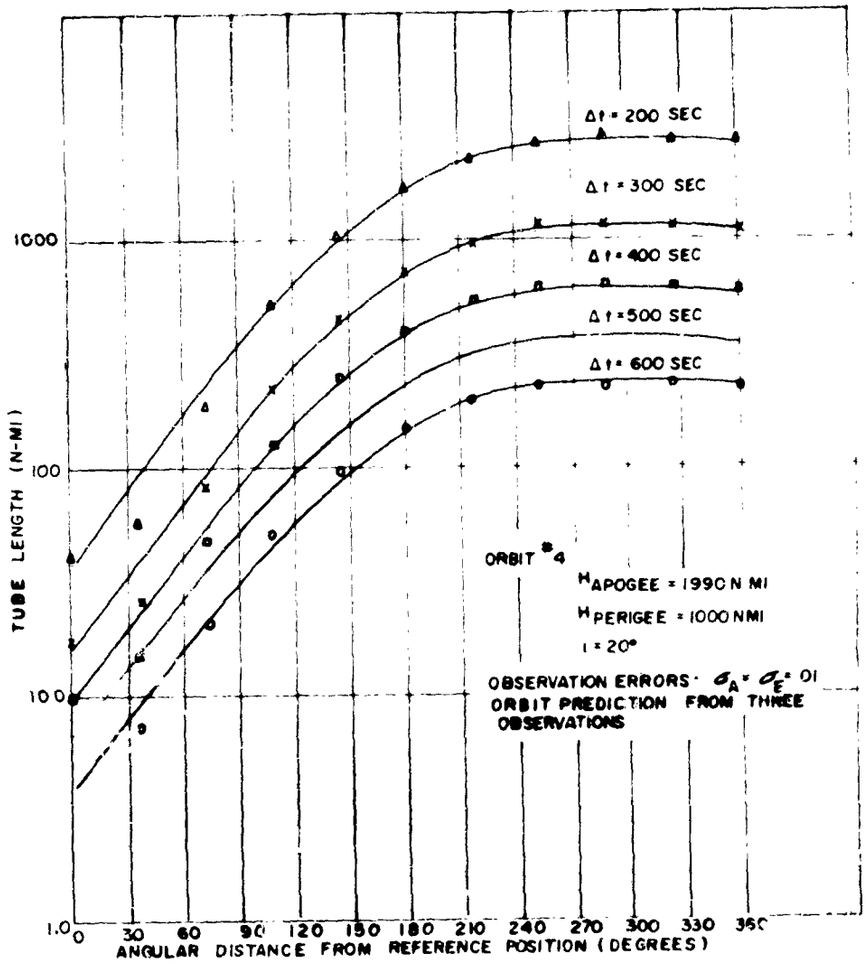


Figure V-11. Prediction Ahead — 90% Confidence Tube Length as a Function of Angular Distance from the Reference Position

3. PART 3 - MULTIPLE SITES

All of the preceding results were developed for a single site. When a multiple sensor complex is considered, it is desirable to compare the net resulting prediction accuracy to that which would be obtained from each of the sensors individually. If a target is tracked or observed simultaneously by two or more sites, with data errors independent from site to site, the optimum estimate of the orbit and thus optimum predictions of future target positions along the orbit must be based upon all of the data available. A conservative estimate of the resulting prediction accuracy is obtained from an error analysis of the slightly non-optimum orbit

estimate obtained from the weighted average of the predictions made singly from each site. Experience has shown that the error of this estimate becomes insignificant as:

- A larger and larger amount of data from each sensor is considered.
- The data itself becomes more accurate (because of the linear propagation of errors in an accurate system).
- The period of observation for each sensor is converged to the identical portion of the orbit.

For example, if target range (R) is to be estimated by considering the data available from sites 1, 2, 3, ---- N and this data, taking each site individually, generates range estimates $\hat{R}_1$, $\hat{R}_2$, $\hat{R}_3$ ---- $\hat{R}_N$ with standard deviations of $\sigma_{\hat{R}_1}$, $\sigma_{\hat{R}_2}$, $\sigma_{\hat{R}_3}$ --- $\sigma_{\hat{R}_N}$, then the grand estimate of target range is

$$\hat{R} = \frac{\dfrac{\hat{R}_1}{\sigma_{\hat{R}_1}^2} + \dfrac{\hat{R}_2}{\sigma_{\hat{R}_2}^2} + \dfrac{\hat{R}_3}{\sigma_{\hat{R}_3}^2} + \cdots \dfrac{\hat{R}_N}{\sigma_{\hat{R}_N}^2}}{\dfrac{1}{\sigma_{\hat{R}_1}^2} + \dfrac{1}{\sigma_{\hat{R}_2}^2} + \dfrac{1}{\sigma_{\hat{R}_3}^2} + \cdots \dfrac{1}{\sigma_{\hat{R}_N}^2}}$$

It can be easily shown that the standard deviation of this estimate is.

$$\sigma_{\hat{R}} = \frac{1}{\sqrt{\dfrac{1}{\sigma_{\hat{R}_1}^2} + \dfrac{1}{\sigma_{\hat{R}_2}^2} + \dfrac{1}{\sigma_{\hat{R}_3}^2} + \cdots \dfrac{1}{\sigma_{\hat{R}_N}^2}}}$$

The maximum possible value for the standard deviation of the final estimate of target range is

$$\left(\sigma_{\hat{R}}\right)_{MAX} = \sigma_{R_M}$$

The minimum possible value is

$$\left(\sigma_{\hat{R}}\right)_{MIN} = \frac{1}{\sqrt{N}} \sigma_{R_M}$$

where σ_{R_M} = the minimum standard deviation of the set $\sigma_{\hat{R}_1}$, $\sigma_{\hat{R}_2}$, $\sigma_{\hat{R}_3}$, --- $\sigma_{\hat{R}_N}$. Thus, a conservative estimate of multiple site accuracy is obtained from the relation

$$\sigma_X = K \sigma_{X_M}$$

where X = any predicted orbit parameter or future position

σX = the accuracy obtainable from N sites making near simultaneous observations

σ_{X_M} = the prediction accuracy for the best of the N sites (the minimum standard deviation)

$$\frac{1}{\sqrt{N}} \leq K \leq 1$$

If the sites are all comparable, it is standard practice to let $K = 1/\sqrt{N}$, the most optimistic value. This procedure counters the non-optimality of considering single site estimates in arriving at the final estimate, as opposed to determining the final estimate directly from all of the raw data.

D. CONCLUSIONS

1. PART 1 - MORE THAN THREE SETS OF OBSERVATIONS

The results for Part 1 show that the errors, which occur when predicting a target's position and velocity, are strongly dependent on the target's slant range. Several computer runs were made to determine how much effect parameters such as azimuth, elevation, and target velocity had on σ_R. As the second plot shows, target velocity had very little effect on range error. Changes in azimuth and elevation shifted the curves slightly but the predominant factor in all of these cases was definitely target range. If a large population of orbits were considered, they would fall into bands or families of curves and the common characteristic of any particular family would be slant range. As would be expected, prediction errors increase with increasing observation errors; in fact, prediction errors are a linear function of observation errors. The curves show that prediction errors decrease when more observations are taken during a given tracking interval. This improvement occurs because more information concerning the orbit's shape is used in prediction target position and velocity at the reference time. Once position and velocity at the reference time are determined, one can predict target position and velocity at future times, i.e., predict around the orbit. The results reveal that confidence tube radius is related to the earth central angle between the initial or reference position and the predicted position. When predicting around an orbit, the tube radius increases until the halfway point in the orbit is reached and then it decreases until the tube radius corresponding to a prediction ahead of one period equals the tube radius at time equal to zero. Tube length which is actually a time error (time error × target velocity = tube length) constantly increases as one predicts around an orbit.

2. PART 2 - THREE SETS OF OBSERVATIONS

The results for Part 2, as for Part 1, show that the errors which occur when predicting a target's position and velocity are strongly dependent on target range. The curves show that estimation errors decrease as the time interval between observations increases. The reason for this behavior is that a greater arc of the target's orbit is brought into the calculation and given observation error can produce less effect on the apparent shape of the orbit. For each particular orbit, curves are shown for a limiting range of time intervals because the angle only program does not converge for time lapses outside this range. The reasons for this behavior will now be explained. When the time lapse between observations becomes

too small, the orbit's shape approaches a straight line but it is still an arc concave toward the earth. The generated errors can cause a physically unrealizable problem by changing the shape of the orbit to a convex arc; as a result, the angle only program will not converge. When the time interval becomes too large, the quadratic equations describing azimuth and elevation yield initial estimates of angular velocities and accelerations which are so far in error that the angle only program will not converge. This trouble could be eliminated by using more exact equations which yield better initial estimates of $\dot{A}_O$, $\dot{E}_O$, $\ddot{A}_O$, and $\ddot{E}_O$. In interpreting the results, it should be realized that most of these targets are sited at very large ranges and though the absolute errors may appear large, they are actually only a small percentage of total range.

E. DISCUSSION

Included on the following pages is a detailed discussion of the methods used in the accuracy study. For both parts of the study, a flow chart is initially presented and then discussed. (Figure V-12).

The following is a discussion of those portions of the flow chart which might raise some questions. As previously mentioned, the first step in handling optical data is to smooth to a set of angles, angular rates, and angular accelerations at the reference time. For tracking periods which are small with respect to the target's period, azimuth and elevation may be represented by the following independent quadratics.

$$A_i = A_O + \dot{A}_O (t_i - t_o) + \frac{\ddot{A}_O}{2} (t_i - t_o)^2 \tag{1}$$

$$E_i = E_O + \dot{E}_O (t_i - t_o) + \frac{\ddot{E}_O}{2} (t_i - t_o)^2 \tag{2}$$

By fitting the above two independent second order polynomials to the data, it is possible to determine the best estimates of the angles, angular rates, and angular accelerations. True values can not be obtained because the data is susceptible to error. The estimates of A_O, $\dot{A}_O$, $\ddot{A}_O$ etc., will be denoted by $\hat{A}_O$, $\hat{\dot{A}}_O$, $\hat{\ddot{A}}_O$ etc. The least squares criterion was chosen to fit the above equations to the data. It specifies the second degree polynomials which minimize the sum of the squared values of the differences between the data and the polynomials at the times of observation. Using the least squares criterion, the following equations which statistically describe the best estimates of A_O $\dot{A}_O$ $\ddot{A}_O$ E_O $\dot{E}_O$ $\ddot{E}_O$ were derived (see Appendix IV). The equations are based upon a zero reference time ($t_o = 0$) and an equal number of observations before and after the reference time.

$$\sigma_{\hat{A}}^2 = \frac{2\sigma_A^2}{(\Delta t)^4 \left[\sum_{i=1}^{M} i^4 - \frac{2}{N}\left(\sum_{i=1}^{M} i^2\right)^2\right]} \tag{3}$$

$$\sigma_{\hat{\dot{A}}}^2 = \frac{\sigma_A^2}{2(\Delta t)^2 \sum_{i=1}^{M} i^2} \tag{4}$$

Figure V-12. Flow Chart — Monte Carlo for More Than Three Sets of Observations

$$\sigma_{\hat{A}}^2 = \frac{\sigma_A^2}{N - 2\left(\sum_{i=1}^{M} i^2\right)^2 \Big/ \sum_{i=1}^{M} i^4} \tag{5}$$

$$\sigma_{\hat{A}\,\hat{\dot{A}}}^2 = 0 \tag{6}$$

$$\sigma_{\hat{A}\,\hat{\ddot{A}}}^2 = \frac{-2\,\sigma_A^2 \sum_{i=1}^{M} i^2}{N(\Delta t)^2 \sum_{i=1}^{M} i^4 - 2(\Delta t)^2 \left(\sum_{i=1}^{M} i^2\right)^2} \tag{7}$$

$$\sigma_{\hat{\dot{A}}\,\hat{\ddot{A}}}^2 = 0 \tag{8}$$

In the above equations,

$$\sum_{i=1}^{M} i^2 = \frac{M(M+1)(2M+1)}{6} \tag{9}$$

$$\sum_{i=1}^{M} i^4 = \frac{M(M+1)(2M+1)(3M^2+3M-1)}{30} \tag{10}$$

The corresponding equations for elevation are identical with E's replacing A's. Equations 3 through 8 statistically define all the angular estimates ($\hat{A}$, $\hat{\dot{A}}$, $\hat{\ddot{A}}$, etc.,) and they are used to simulate the errors which exist in these estimates ($\Delta\hat{A}$, $\Delta\hat{\dot{A}}$, $\Delta\hat{\ddot{A}}$, etc).

Since $\hat{\ddot{A}}_o$ is not correlated with $\hat{A}_o$ or $\hat{\dot{A}}_o$ we can simulate $\Delta\hat{\ddot{A}}$ with a simple multiplication.

$$\Delta\hat{\ddot{A}} = \sigma_{\hat{\ddot{A}}} Z_1 \tag{11}$$

Similarly for E

$$\Delta\hat{\ddot{E}} = \sigma_{\hat{\ddot{E}}} Z_2 \tag{12}$$

where Z_1, Z_2 are two random numbers from a normal distribution, zero mean, unity variance.

Simulating $\Delta\hat{A}$ and $\Delta\hat{\dot{A}}$ is somewhat more involved, since $\hat{A}_o$ and $\hat{\dot{A}}_o$ are correlated as described by equation 7. The general equations needed to generate $\Delta\hat{A}$

and $\Delta\hat{\bar{A}}$ are derived in Appendix V. To determine $\Delta\hat{A}$ and $\Delta\hat{\bar{A}}$, calculate:

$$\theta = \frac{1}{2}\tan^{-1}\left[\frac{2\sigma_{\hat{A}_o}^{2}\,\hat{\bar{A}}_o}{\sigma_{\hat{A}_o}^{2} - \sigma_{\hat{\bar{A}}_o}^{2}}\right] \tag{13}$$

$$\sigma_{\Delta y_1}^{2} = (\sigma_{A_o}^{2}\cos^2\theta + 2\sigma_{\hat{A}_o\hat{\bar{A}}_o}^{2}\sin\theta\cos\theta + \sigma_{\hat{\bar{A}}_o}^{2}\sin^2\theta) \tag{14}$$

$$\sigma_{\Delta y_2}^{2} = (\sigma_{\hat{A}_o}^{2}\sin^2\theta - 2\sigma_{\hat{A}_o\hat{\bar{A}}_o}^{2}\sin\theta\cos\theta + \sigma_{\hat{\bar{A}}_o}^{2}\cos^2\theta) \tag{15}$$

$$\Delta Y_1 = \sigma_{\Delta Y_1} Z_3 \tag{16}$$

$$\Delta Y_2 = \sigma_{\Delta Y_2} Z_4 \tag{17}$$

$$\Delta\hat{A}_o = \Delta Y_1\cos\theta - \Delta Y_2\sin\theta \tag{18}$$

$$\Delta\hat{\bar{A}}_o = \Delta Y_1\sin\theta + \Delta Y_2\cos\theta \tag{19}$$

where Z_3 and Z_4 are random numbers from a normal population.

The equations for $\Delta\hat{E}_o$ and $\Delta\hat{\bar{E}}_o$ are similar to equations 13 through 19 with E's replacing A's and Z_3 and Z_4 replaced by Z_5 and Z_6 respectively. Equations 11 through 19 are the optical error equations referred to in the flow chart.

The only remaining portion of the flow chart which calls for explanation is the variance - covariance calculation step. After 1,000 Monte Carlo Loops the error introduced by deviations from a normal distribution was considered negligible. It then remains to determine the moment matrix which statistically describes the errors at the reference point. After 1,000 loops there are 1000 values of R, A, E, R, A and E in computer memory and each element of the moment matrix can be calculated. The following definitions were used. By definition the mean value of a variable X is:

$$\bar{X} = \frac{1}{NN}\sum_{i=1}^{NN} X_i$$

where NN = No. of Monte Carlo Loops (1,000 in this study)

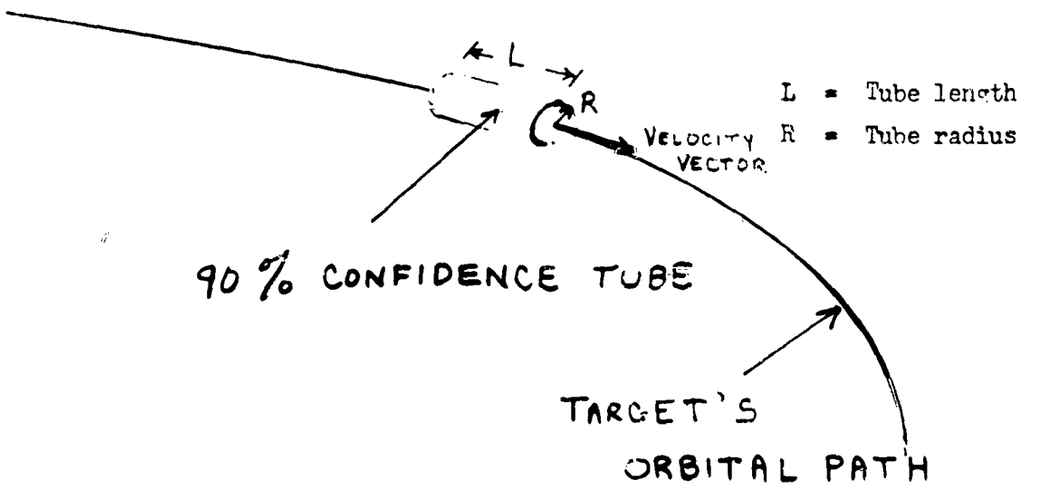
Similarly, the variance of X is defined by the following equation:

$$\sigma_X^{2} = \frac{1}{NN}\sum_{i=1}^{NN}(X_i - \bar{X})^2$$

The covariance between two variables X and Y is defined below

$$\sigma_{XY}^2 = \frac{1}{NN} \sum_{i=1}^{NN} (X_i - \bar{X}) \quad (Y_i - \bar{Y})$$

After being calculated, the mean values of R, A, E, $\dot{R}$, $\dot{A}$ and $\dot{E}$, along with the 6 × 6 moment matrix are used as the input for an in house computer program which calculates confidence volumes at specified future times in the orbit. Rather than calculate the conventional confidence ellipse an equivalent tube was determined. The confidence tube is oriented with its axis colinear with the target velocity vector. A sketch of a typical error tube is shown below.



For the case of three sets of optical data it is possible to carry out the accuracy study by using the complete angle only program which has been written and checked out. As stated in the introduction the angle only program is capable of predicting an orbit exactly from three sets of unerrored optical data. A complete flow chart for the angle only program is shown on the next page. The Monte Carlo study can be carried out by merely erroring the input to the angle only program (A_1 E_1 A_2 E_2 A_3 E_3) and calculating the moment matrix after 1,000 Monte Carlo loops.

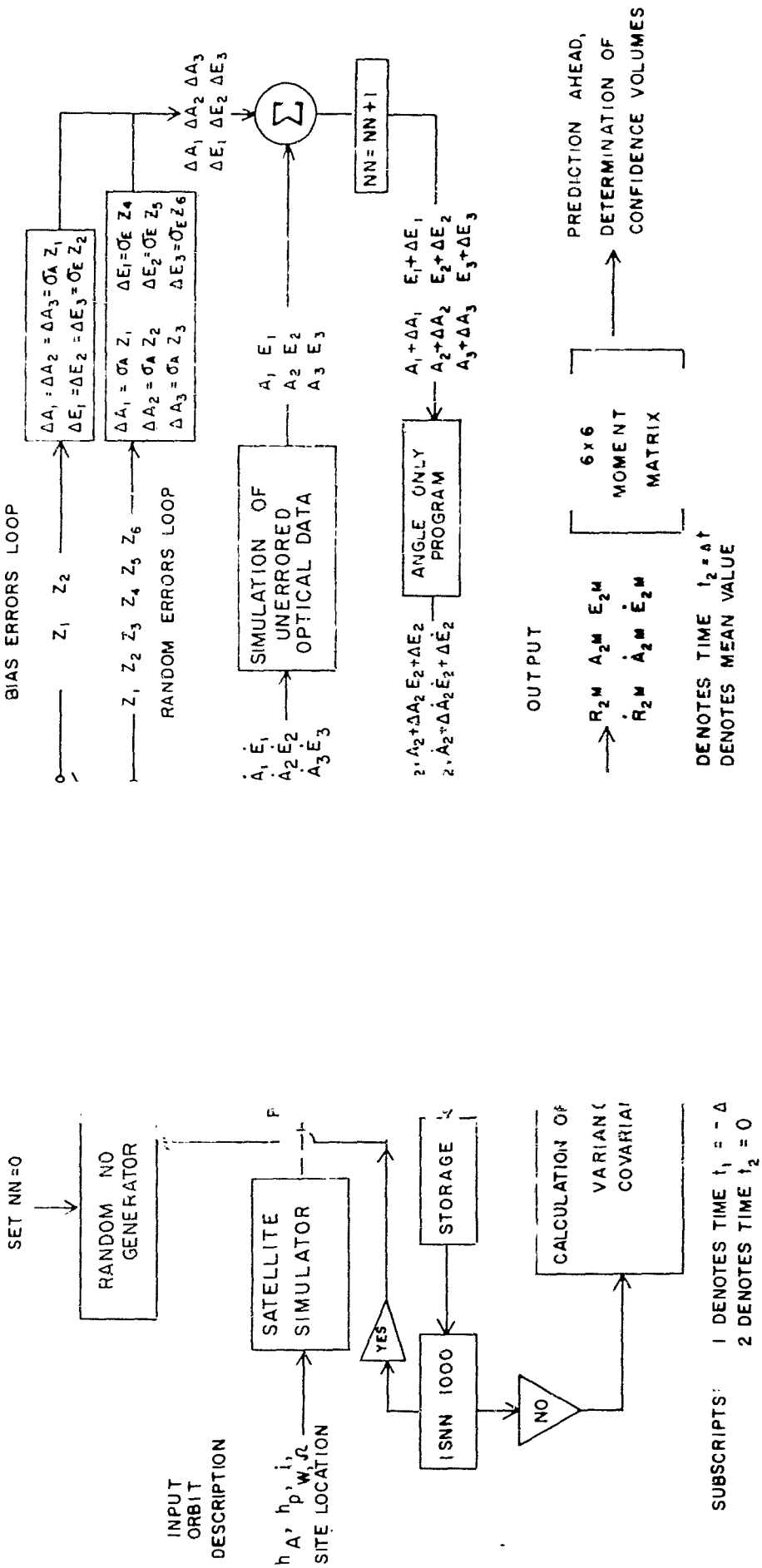


Figure V-13. Flow Chart — Monte Carlo Study for Three Sets of Observations

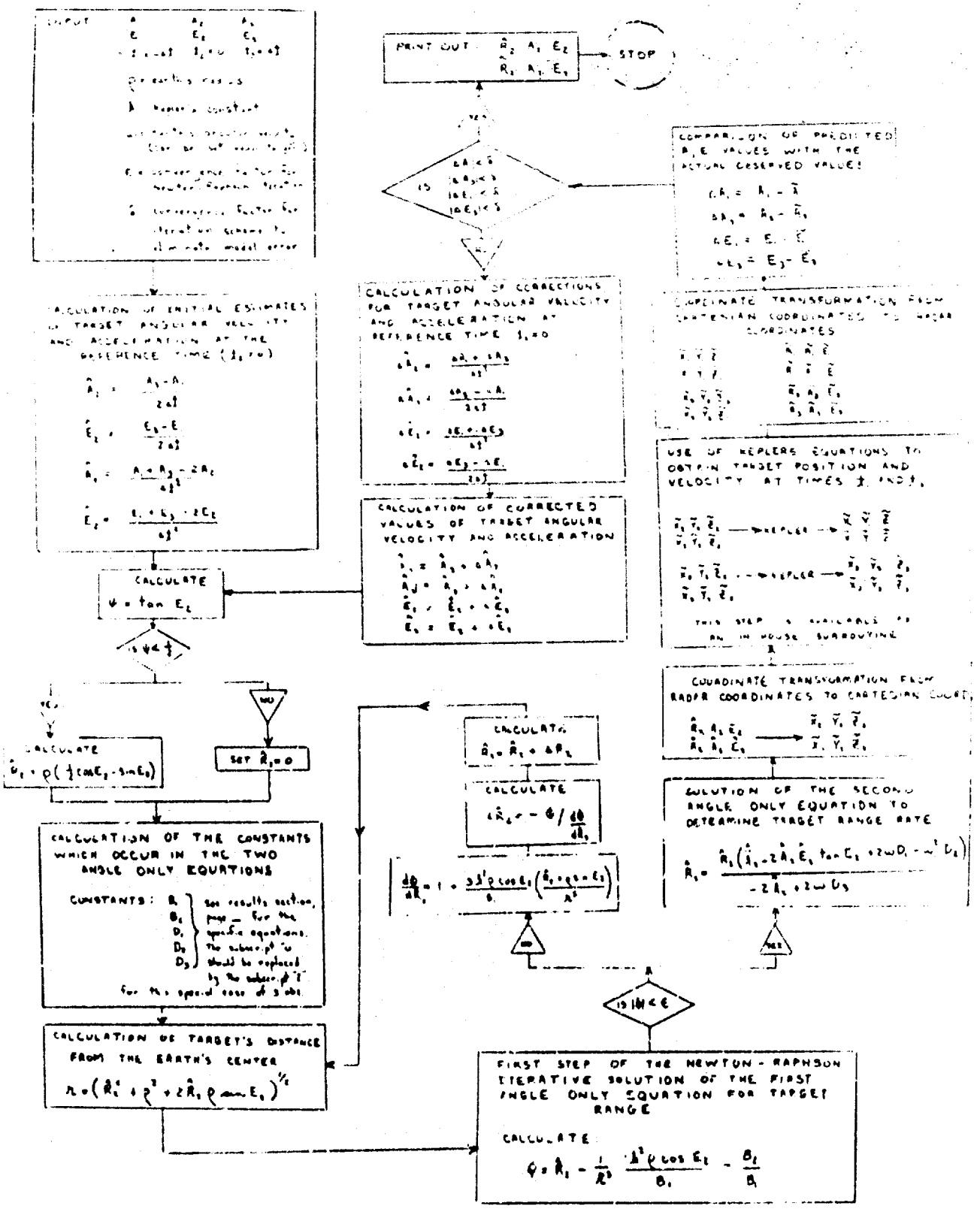


Figure V-14. Flow Chart — Orbit Estimation from Three, Equally Spaced, Sets of Optical Data

Best Available Copy

SECTION VI. RECOMMENDATIONS FOR FUTURE WORK

This report covered only techniques suitable for passive separation of orbiting objects in the night's celestial environment. Thus separation techniques not felt to offer sufficient practicality to the defined tasks were eliminated (see also Section I-A).

The study of separation by "track" direction is similar to that of time separation except particular note is taken for further alarm processing. Since alarm processing was not included in the task, this has not been discussed. The matter of a fixed mount when using a time cycle compatible to limiting star "tracks" to few resolution elements versus many for targets was compared briefly to the sidereal mount (star fixed) and found to be similar: that is, in the sidereal mount case, the stars jittered a few resolution elements due to mount or atmospheric dancing in addition to registration, thus it is a matter of whether it is more practical to have the mount jogged to respective star fields from stationary positions or from a continuing sidereal motion. Since the mount would not be clamped stationary, but held by the power drives, it requires more power to jog to the next position than in overriding a sidereal motion. Thus the latter is favored even in this case.

Allied studies not covered by this POTI task that should be considered for further study of the surveillance task include:

A. Threat Analysis

B. Hybrid Stereo - M.T.I. Storage System Study extending the effort initiated in Section III-E

C. Electronic Signal (Peak) Detection matched to frequency response band for rise time of star and/or target signals.

D. Capability and Limitations for rapid detection of distant (low intensity) objects.

E. Study of required processing (termed alarm processing) after initial separation, considering target characteristics, motions, etc., use of "a prior" knowledge of known moving targets to reduce alarm processing, etc.

F. Individual Separation Evaluation Measurements

G. Optic system specifications and measurements to insure necessary performance of large fast optics

H. Data accuracy versus orbital mechanics

I. Improving orbital predictions by track augmentation of surveillance (detection) Systems

APPENDIX I. PROBABILITY OF OCCULTATION

A. DERIVATION

Assuming a linear image growth relation, the angular image size is

$$d = a + b\,(M_t - m) \qquad m \leq M_t \qquad \text{(I-1)}$$

Where:

M_t = Threshold magnitude of the detector or the magnitude of a just detectable source.

m = Magnitude of the source.

d = Angular size of the image in seconds of arc.

a = Minimum angular size of the image or the size of a just detectable image in seconds of arc

b = Rate of image growth in seconds of arc per magnitude.

Assuming a circular image , its solid angle is

$$\omega_i\,(m) = \frac{\pi}{4}\left(\frac{\pi}{180}\right)^2 \frac{d^2}{(3600)^2} \quad \text{steradians} \qquad \text{(I-2)}$$

The solid angle of the field of view is

$$\omega_f = \phi^2 \left(\frac{\pi}{180}\right)^2 \quad \text{steradians} \qquad \text{(I-3)}$$

Where ϕ = Angular size of the square field of view in degrees.

Since the angular size of the image is proportional to the magnitude of the source, it is necessary to know the brightness distribution of the stars within the field of view. Defining

N_m = The number of stars per square degree with a brightness within the range m to m - Δ magnitudes.

The number of stars χ_m within the field of view whose brightness lies between m and m + Δ magnitudes is:

$$\chi_m = \phi^2 N_m, \qquad \text{(I-4)}$$

and the total solid angle occupied by stars within the field of view and within the brightness range m to m - Δ magnitudes is approximately:

$$\omega_m = \omega_i\,(m)\,\phi^2 N_m \qquad \text{(I-5)}$$

The total solid angle is assumed equal to the sum of the solid angles contributed from each magnitude interval Δ beginning with the threshold magnitude. Thus:

$$\omega_s = \sum_{m=M_t} \Phi^2 \omega_i (m) N_m \qquad \text{(I-6}$$

The probability of occultation Q(B) is then:

$$Q(B) = 100 \frac{\omega_s}{\omega_f} = \frac{100 \Phi^2}{\omega_f} \sum_{m=M_t} \omega_i(m) N_m \quad \text{percent} \qquad \text{(I-7}$$

Substituting equation (I-2) and equation (I-3) into equation (I-7),

$$Q(B) = \frac{100 \pi}{4(3600)^2} \sum_{m=M_t} d_m^2 N_m \qquad \text{(I-8}$$

Substituting equation (I-1) into equation (I-8),

$$Q(B) = \frac{100 \pi}{4(3600)^2} \sum N_m (a + b (M_t - m))^2$$

$$= \frac{100 \pi}{4(3600)^2} \sum N_m (a^2 + 2ab (M_t - m) + b^2 (M_t - m)^2)$$

$$= \frac{100 \pi}{4(3600)^2} \sum a^2 N_m + 2ab N_m (M_t - m) + b^2 N_m (M_t - m)^2$$

or

$$Q(B) = \frac{100 \pi a^2}{4(3600)^2} \sum N_m + \frac{100 \pi ab}{2(3600)^2} \sum N_m (M_t - m)$$

$$+ \frac{100 \pi b^2}{4(3600)^2} \sum N_m (M_t - m)^2 \qquad \text{(I-10)}$$

Now let:

$$H_1 = \frac{100 \pi}{4(3600)^2} \sum N_m (M_t - m)^2$$

$$H_2 = \frac{100 \pi}{2(3600)^2} \sum N_m (M_t - m)$$

$$H_3 = \frac{100 \pi}{4(3600)^2} \sum N_m$$

Then,

$$Q(B) = b^2 H_1 + ab H_2 + a^2 H_3 \qquad \text{percent} \qquad \text{(I-11)}$$

The probability of occultation can thus be obtained from a knowledge of the minimum size of the star image a, the slope of the image growth characteristic b, and the three constants H_1 H_2 H_3 which depend on the threshold magnitude of the detecting system and the star population in the region of the sky being examined. The probability of non-occultation P(B) is, of course:

$$P(B) = 1 - Q(B) \qquad \text{(I-12)}$$

The star population is a variable that is known only approximately. Many factors combine to make an absolute distribution very difficult to obtain. The densities that have been obtained depend to a great extent on the equipment and techniques used. Most star counts are in terms of photographic or visual magnitudes. Variations among observers is common. Neither the photographic nor the standard visual response matches the S-20 image orthicon response. Therefore it should be expected that star densities as seen by the image orthicon will differ from the other observations.

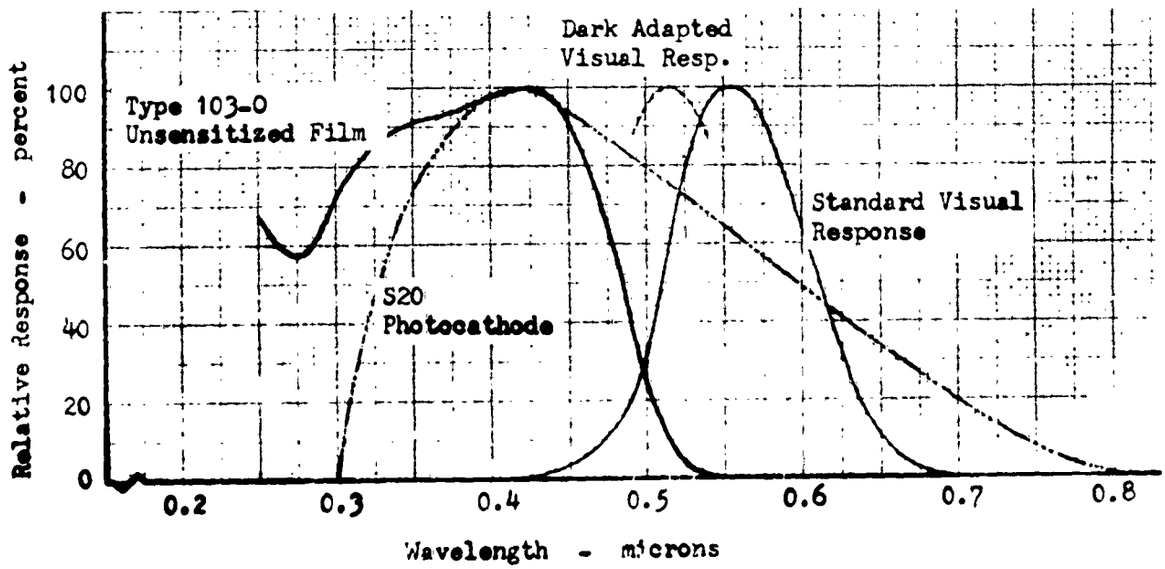


Figure AI-1. Detector Relative Response

Figure AI-1 shows the relative response of the standard eye, type 103-O unsensitized film, and the S-20 photocathode. Figure AI-2 shows the approximate distribution of the wavelength of maximum radiation and the approximate population of stars of different spectral types. Radiation from a particular class is, of course, not confined within the narrow bands shown. The bands only serve to roughly indicate the regions within which the peak radiation of that class may fall. It is seen that the S-20 response would exclude the class O and B stars that would be included in the photographic response. On the other hand, the S-20 response would include most of the class K and a few of the class M stars that would not be included in the

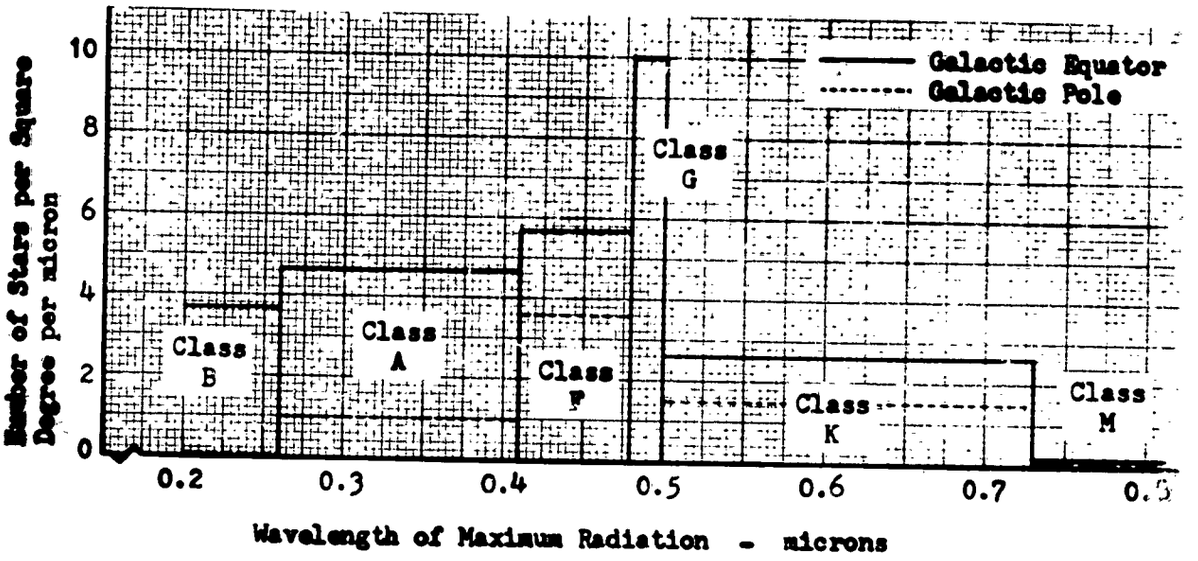


Figure AI-2. Relative Distribution of Star Classes vs Wavelength of Maximum Radiation

photographic response. At the galactic equator it would appear that stars lost at the blue end of the spectrum would not be compensated by the extra stars seen at the red end. The photographic densities would therefore be likely to be higher than the densities seen by the image orthicon at the equator. At the galactic pole it would seem that the two densities might be about equal. In the absence then of better data, the use of photographic data in image orthicon applications is probably justified as being within the range of experimental error. Visual data would probably be less accurate.

The star distributions used in this calculation are from International Critical Tables, Vol. II (McGraw Hill). Three distributions were used. These distributions are tabulated in table AI-1. The density at the galactic pole represents a minimum distribution, and that at the equator represents a maximum distribution. The 0^{o} to 90^{o} average is similar to the density between 20 and 25 degrees latitude. This represents a working average.

Using these star distributions, values of μ were computed for threshold magnitude intervals of one magnitude. These values are tabulated in table AI-2. The fractional value of the argument of table AI-2 results from the arrangement of the original data. To convert the table to integral values of threshold magnitude, table AI-2 has been interpolated to produce table AI-3. Table AI-3 presents the same information as table AI-2 except in integral values of M_t.

In order to facilitate the probability calculation, the following partial probabilities are defined:

$$F_1 = b^2 H_1$$
$$F_2 = ab H_2 \qquad \text{(I-13)}$$
$$F_3 = a^2 H_3$$

Thus: $Q(B) = F_1 + F_2 + F_3$ (I-14)

Charts have been prepared for each of these three star distributions so that equations (I-13) may be solved by entering with the values of threshold magnitude, minimum image size, image growth rate, and the product of image size and growth rate. These charts are shown in figures AI-3 through AI-11.

The use of these charts may be illustrated through an example. An image orthicon detector has a field of view of 3 degrees with a 1200 line resolution. The operating conditions are adjusted to produce a 2 line image with a threshold source.

It is required to find the non-occultation probability P(B) as a function of threshold magnitude for image growth rates of 0, 1.0, and 1.5 lines per magnitude, and for 0° and 90° galactic latitude star densities.

The number of lines are converted to equivalent angular diameters through the relation:

$$a = 3600 \frac{\Phi}{N_1} n = 3600 \frac{3 \text{ degrees}}{1200 \text{ lines}} n = 9n \quad \text{seconds} \qquad \text{(I-15)}$$

where: Φ = Field of view in degrees
N_1 = Number of lines per scan
n = Image size in lines
a = Image size in seconds of arc

Thus: a = 2 lines = 18 seconds of arc

and:

Growth Rate lines/mag.	b (sec/mag)	b^2 (sec^2/mag)	ab ($sec/mag^{1/2}$)
0	0	0	0
1.0	9	162	12.7
1.5	13.5	243	15.6

It is seen from equation (I-13) that when b = 0, then $F_1 = F_2 = 0$. Thus only F_3 need be found. For 0° latitude, enter Figure I-5 with a = 18 seconds and find $F_3 = 0.0072$ for a threshold magnitude of 9. Then:

$Q(B) = 0.0072$ percent for 0° latitude, $M_t = 9$, and b = 0

For 0° latitude and b = 1.0, enter Figure AI-3 with b 9 sec./mag. and find $F_1 = 0.00245$ for a threshold magnitude of 9. Enter Figure I-4 with ab = 12.7 and find $F_2 = 0.0052$. The value $F_3 = 0.0072$ has already been found above. Now:

$Q(B) = 0.00245 + 0.0052 + 0.0072 = 0.0149$ p · ent

Completing the process for both distributions, all image growth rates, and threshold magnitudes from 9 to 20, the results are tabulated in Table AI-4.

Table AI-1

Number of Stars per Square Degree per Half Magnitude Interval
(Derived from International Critical Tables, Vol II, McGraw Hill)

Magnitude Interval		Average Number 0^{o} Galactic Latitude	Average Number 90^{o} Galactic Latitude	Average Number 0^{o} to 90^{o} Latitude
4.0 +		.0155	.00872	.00457
4.5 to	4.0	.0108	.00608	.00303
5.0	4.5	.0184	.0104	.0056
5.5	5.0	.0313	.0175	.0087
6.0	5.5	.053	.0283	.0153
6.5	6.0	.085	.0493	.0245
7.0	6.5	.149	.0796	.0405
7.5	7.0	.241	.1316	.0678
8.0	7.5	.396	.2185	.106
8.5	8.0	.70	.364	.171
9.0	8.5	1.12	.601	.278
9.5	9.0	1.86	.945	.425
10.0	9.5	3.09	1.525	.67
10.5	10.0	4.83	2.475	1.00
11.0	10.5	8.3	4.03	1.55
11.5	11.0	13.0	6.12	2.25
12.0	11.5	21.1	9.74	3.38
12.5	12.0	36.4	15.4	4.8
13.0	12.5	53.3	24.45	6.6
13.5	13.0	89.8	36.2	9.55
14.0	13.5	137.5	56.4	13.75
14.5	14.0	218	81.2	18.5
15.0	14.5	324	123.5	24.0
15.5	15.0	499	174.5	33.0
16.0	15.5	727	257	42.0
16.5	16.0	1100	382	56.8
17.0	16.5	1560	523	70.0
17.5	17.0	2290	760	83.0
18.0	17.5	3150	1010	107
18.5	18.0	4240	1330	138
19.0	18.5	6420	1820	160
19.5	19.0	7950	2520	179
20.0	19.5	11000	3170	219
20.5	20.0	15150	3920	237
21.0	20.5	19200	5170	248

Tabulati

Average Magnitude M_t	Magnitude Interval	H_1
		0° Gal
8.75	8.5 - 9	0.0000242
9.75	9.5 - 10	0.0000694
10.75	10.5 - 11	0.000195
11.75	11.5 - 12	0.000535
12.75	12.5 - 13	0.00145
13.75	13.5 - 14	0.00388
14.75	14.5 - 15	0.0102
15.75	15.5 - 16	0.0260
16.75	16.5 - 17	0.0643
17.75	17.5 - 18	0.153
18.75	18.5 - 19	0.350
19.75	19.5 - 20	0.767
		0° to 90°
8.75	8.5 - 9	0.0000134
9.75	9.5 - 10	0.0000378
10.75	10.5 - 11	0.000104
11.75	11.5 - 12	0.000278
12.75	12.5 - 13	0.000726
13.75	13.5 - 14	0.00186
14.75	14.5 - 15	0.00465
15.75	15.5 - 16	0.0112
16.75	16.5 - 17	0.0262
17.75	17.5 - 18	0.0592
18.75	18.5 - 19	0.129
19.75	19.5 - 20	0.270

-2

H_2 and H_3

tude		90° Galactic Latitude		
	H_3	H_1	H_2	H_3
3	0.0000171	0.00000682	0.00000692	0.00000439
7	0.0000471	0.0000188	0.0000183	0.0000115
	0.000127	0.0000496	0.0000464	0.0000265
	0.000333	0.000126	0.000113	0.0000606
	0.000877	0.000307	0.000263	0.000130
	0.00225	0.000714	0.000581	0.000271
	0.00554	0.00159	0.00123	0.000528
	0.0130	0.00341	0.00249	0.000983
	0.0291	0.00697	0.00480	0.00175
	0.0621	0.0136	0.00881	0.00290
	0.127	0.0256	0.0154	0.00471
	0.241	0.0460	0.0260	0.00712
3	0.0000918			
9	0.0000241			
	0.0000636			
	0.000160			
	0.000401			
	0.000962			
	0.00220			
	0.00482			
	0.0103			
	0.0210			
	0.0401			
	0.0746			

Table AI-3

Tabulation of H_1

Magnitude	H_1 for 0^o Latitude	H_1 for 90^o Latitude	H_1 for 0^o to 90^o Latitude Average
9	0.000031	0.0000087	0.000017
10	0.000089	0.00002[illegible]	0.000048
11	0.00025	0.000062	0.000131
12	0.00068	0.000156	0.00035
13	0.0018	0.000375	0.00092
14	0.0049	0.00087	0.0023
15	0.0129	0.0019	0.0057
16	0.0322	0.0041	0.0138
17	0.080	0.0082	0.032
18	0.186	0.0160	0.071
19	0.43	0.0295	0.156
20	0.91	0.0495	0.320

Tabulation of H_2

Magnitude	H_2 for 0^o Latitude	H_2 for 90^o Latitude	H_2 for 0^o to 90^o Latitude Average
9	0.000033	0.0000088	0.0000172
10	0.000089	0.000023	0.000048
11	0.000245	0.000057	0.00013
12	0.00067	0.000140	0.00033
13	0.0018	0.000315	0.00085
14	0.0047	0.00070	0.0021
15	0.0119	0.00145	0.0051
16	0.029	0.0029	0.0117
17	0.069	0.0056	0.0265
18	0.155	0.0101	0.057
19	0.33	0.0178	0.117
20	0.68	0.029	0.23

Tabulation of H_3

Magnitude	H_3 for 0^o Latitude	H_3 for 90^o Latitude	H_3 for 0^o to 90^o Latitude Average
9	0.000022	0.0000055	0.0000119
10	0.000058	0.0000137	0.000031
11	0.000159	0.000033	0.000079
12	0.00042	0.000073	0.00020
13	0.0011	0.000152	0.00049
14	0.0028	0.00032	0.00117
15	0.0068	0.00061	0.00265
16	0.0159	0.00112	0.0058
17	0.035	0.00197	0.0122
18	0.073	0.00323	0.025
19	0.15	0.0052	0.048
20	0.28	0.0078	0.084

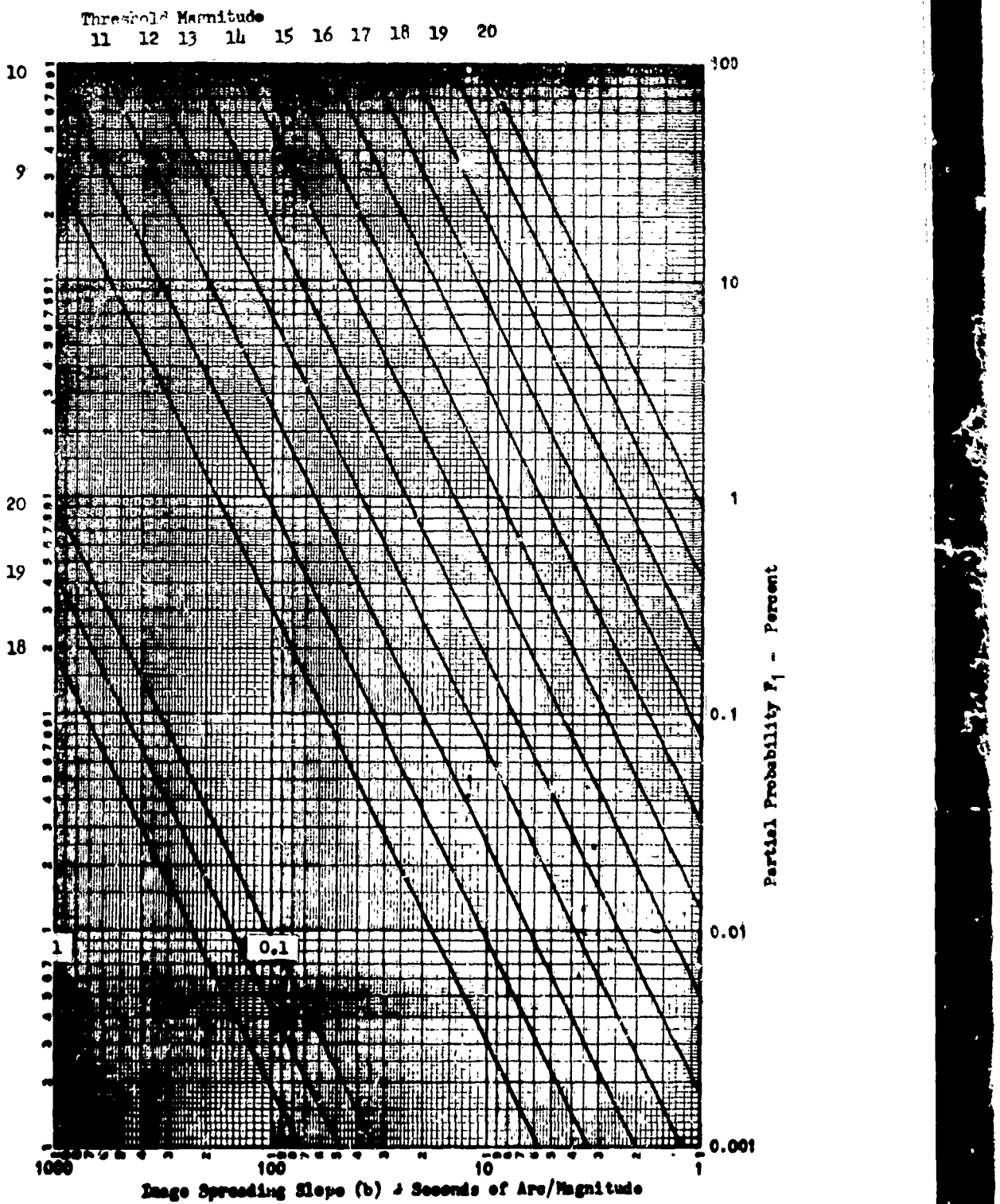


Figure AI-3. Partial Probability F_1 0^o Galactic Latitude

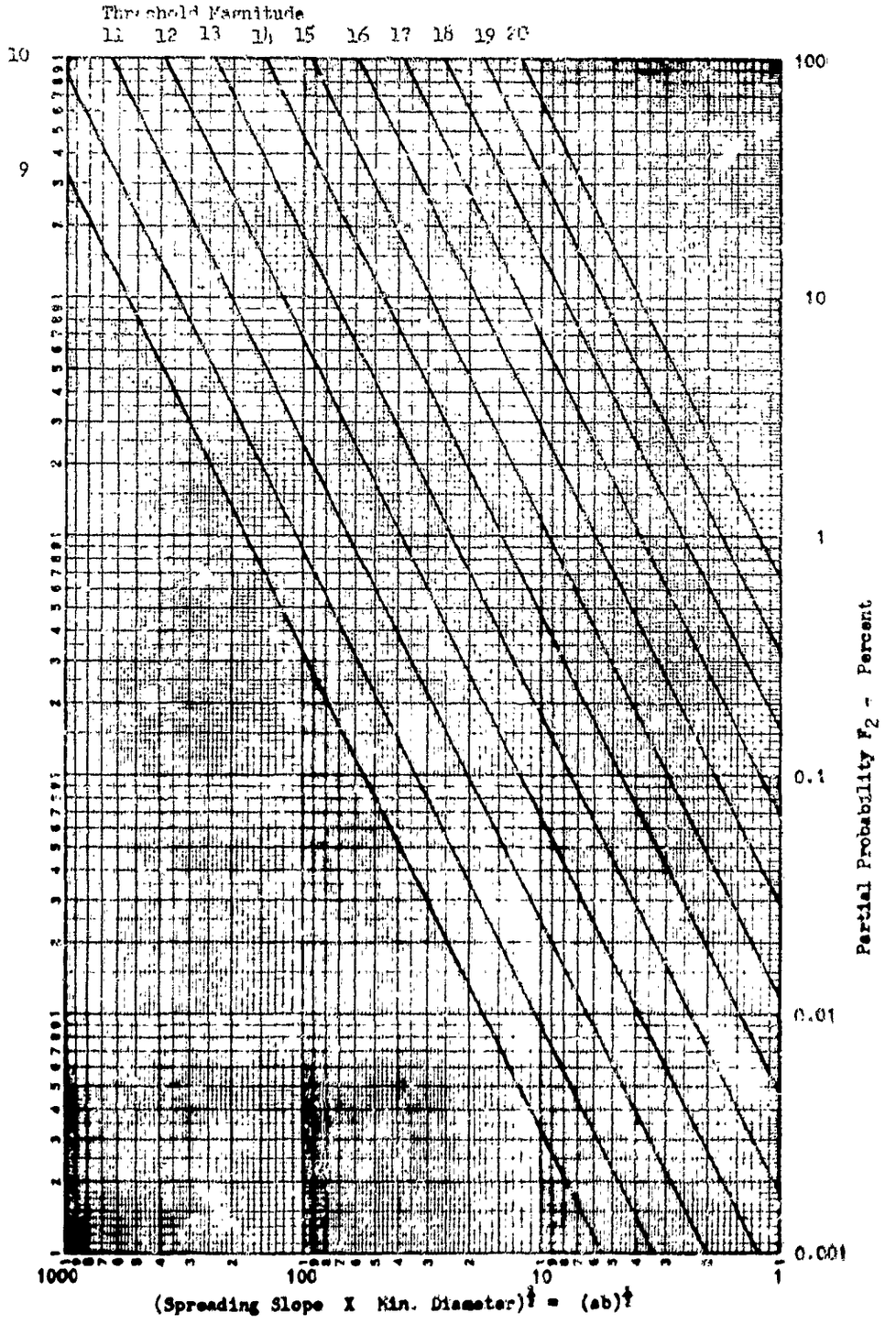


Figure AI-4. Partial Probability F_2 0° Galactic Latitude

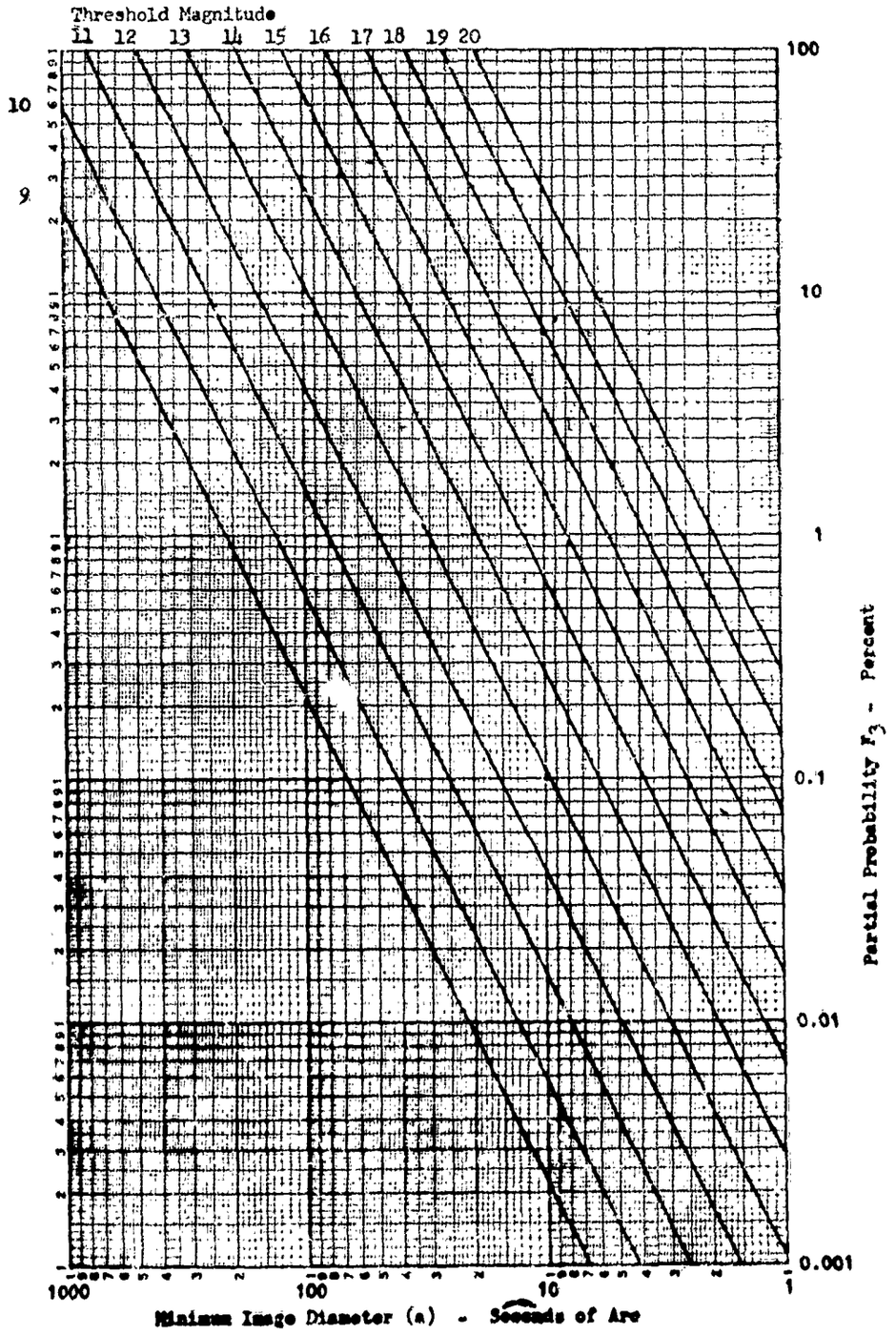


Figure AI-5. Partial Probability F_3 0^0 Galactic Latitude

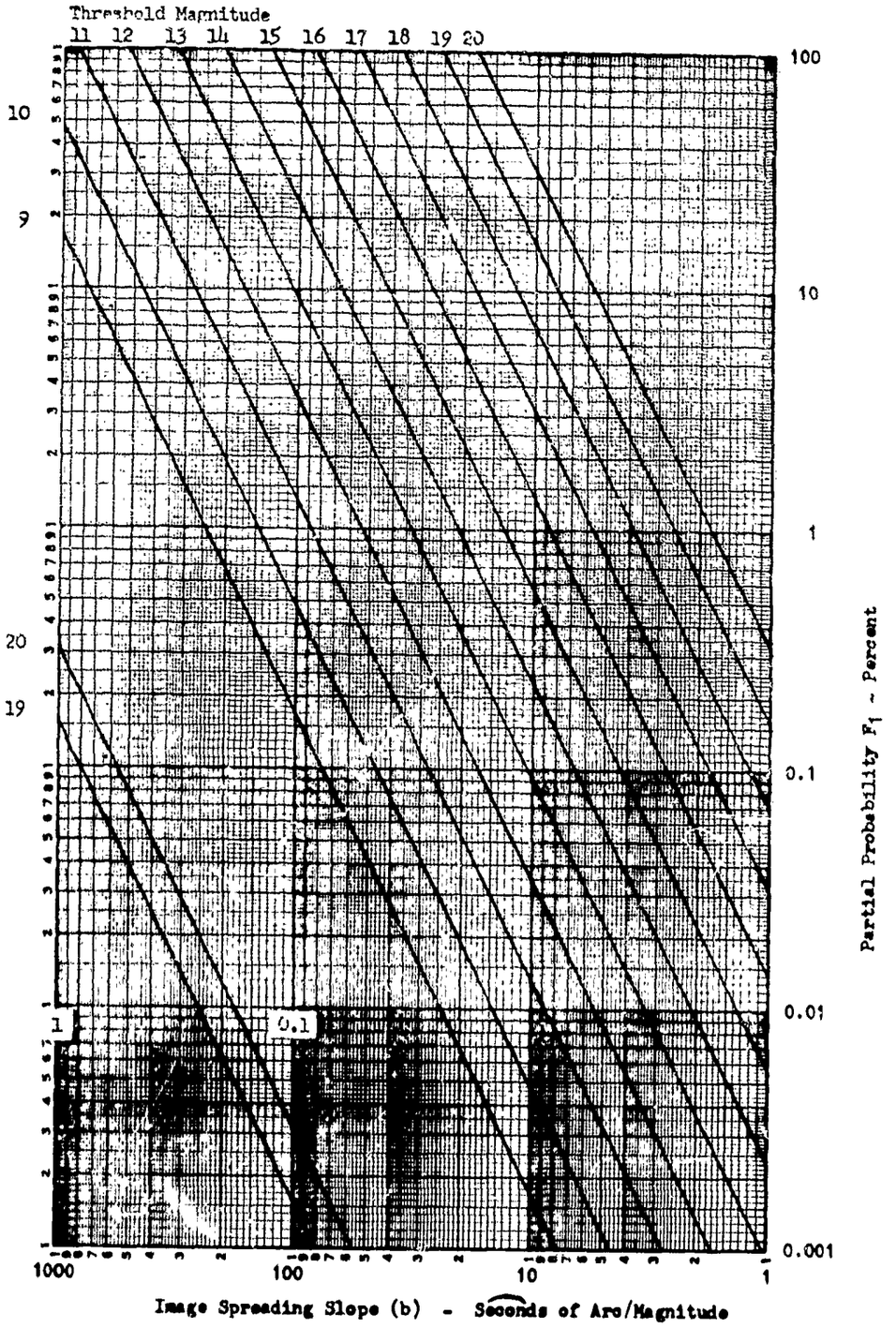


Figure AI-6. Partial Probability F_1 0^o to 90^o Average

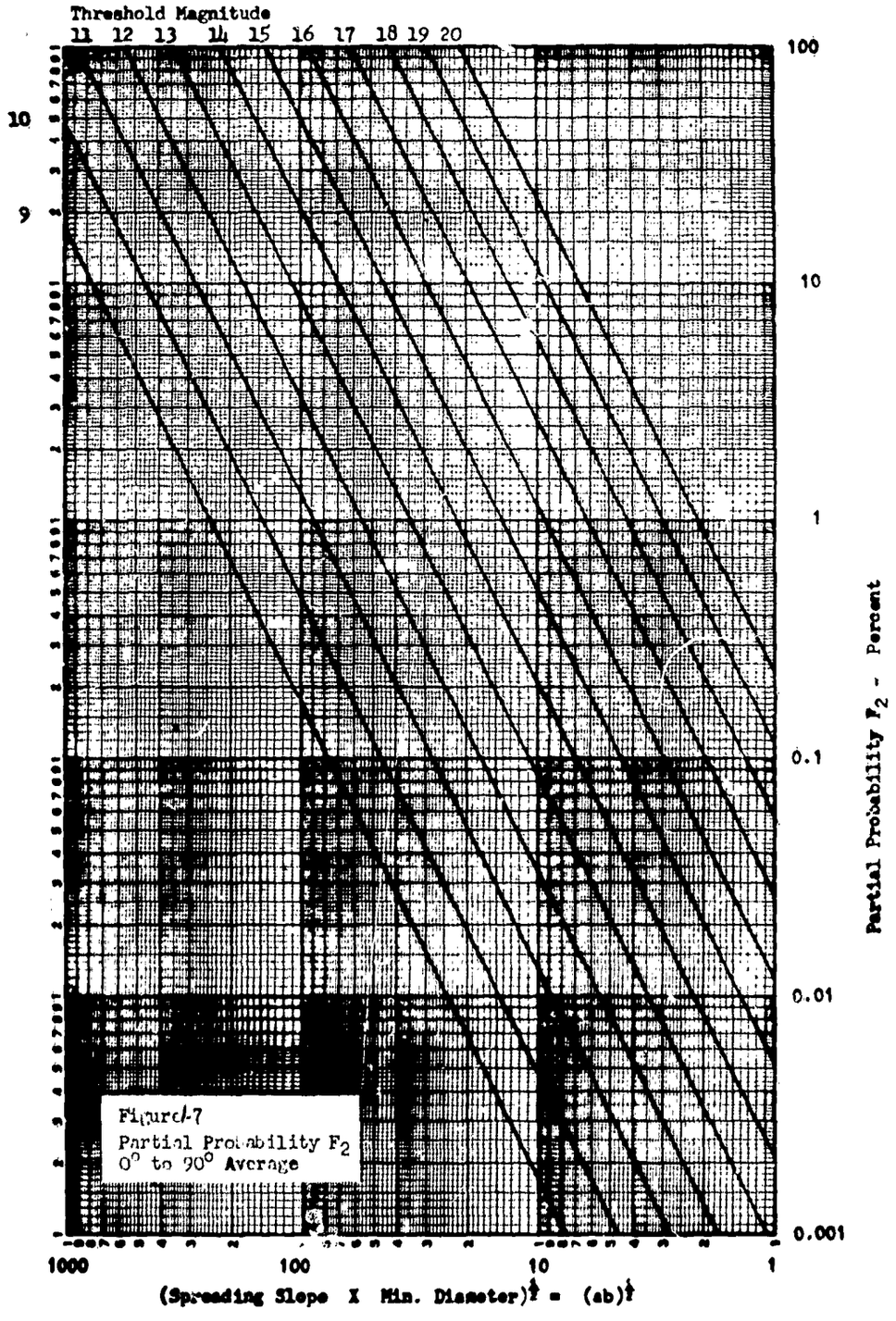


Figure AI-7. Partial Probability $F_2 0^\circ$ to 90° Average

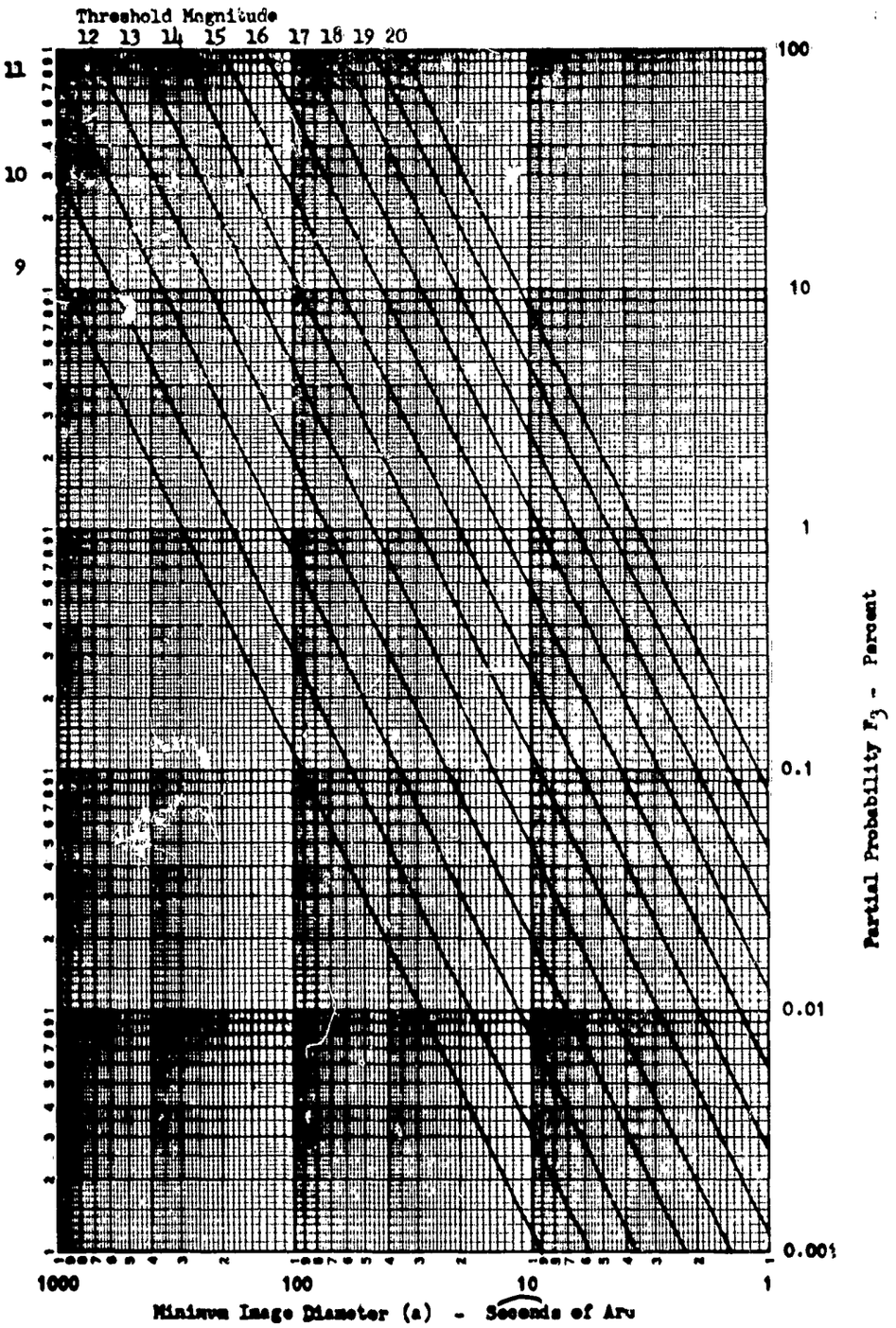


Figure AI-8. Partial Probability F_3 0^o to 90^o Average

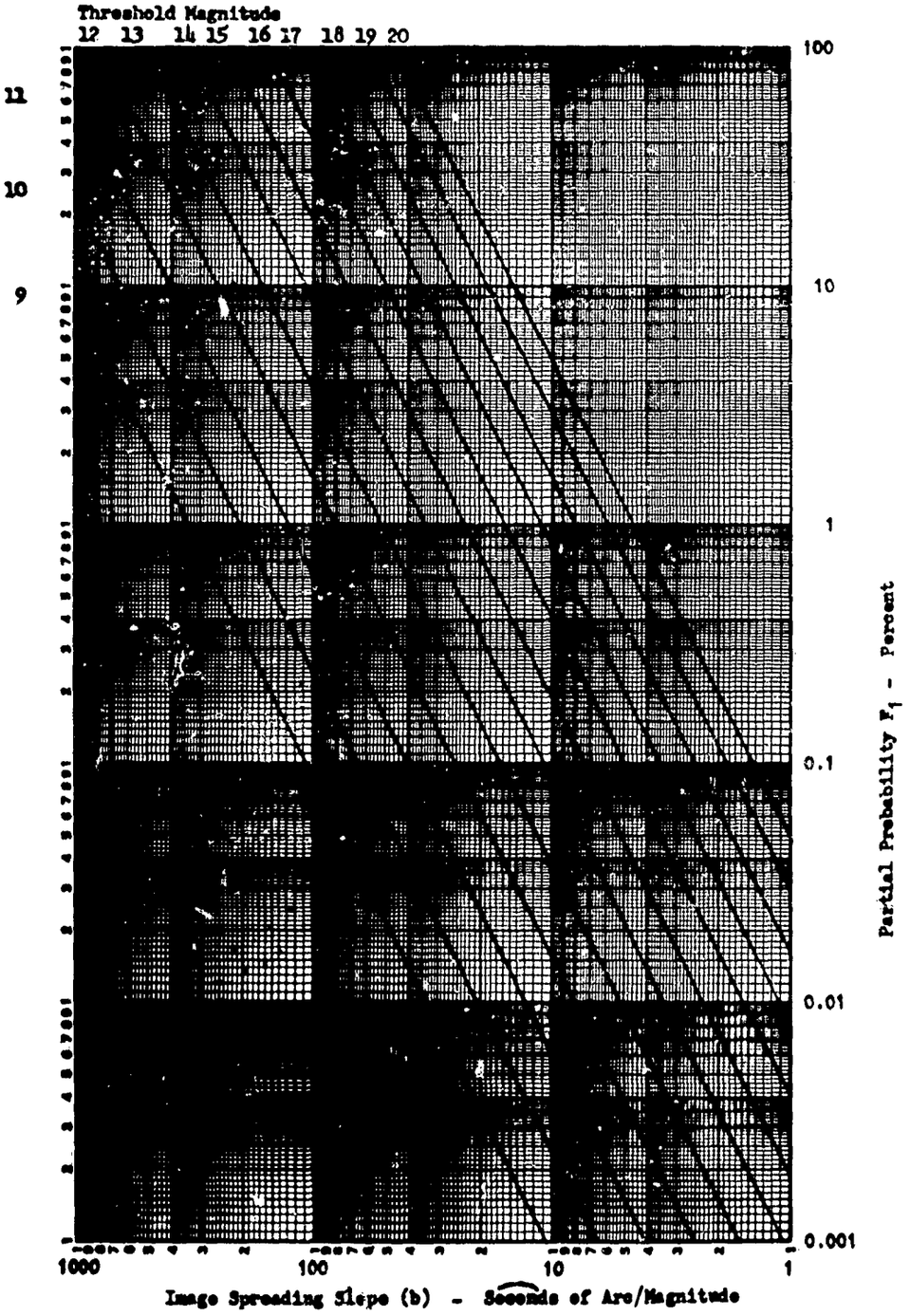


Figure AI-9. Partial Probability F_1 90° Galactic Latitude

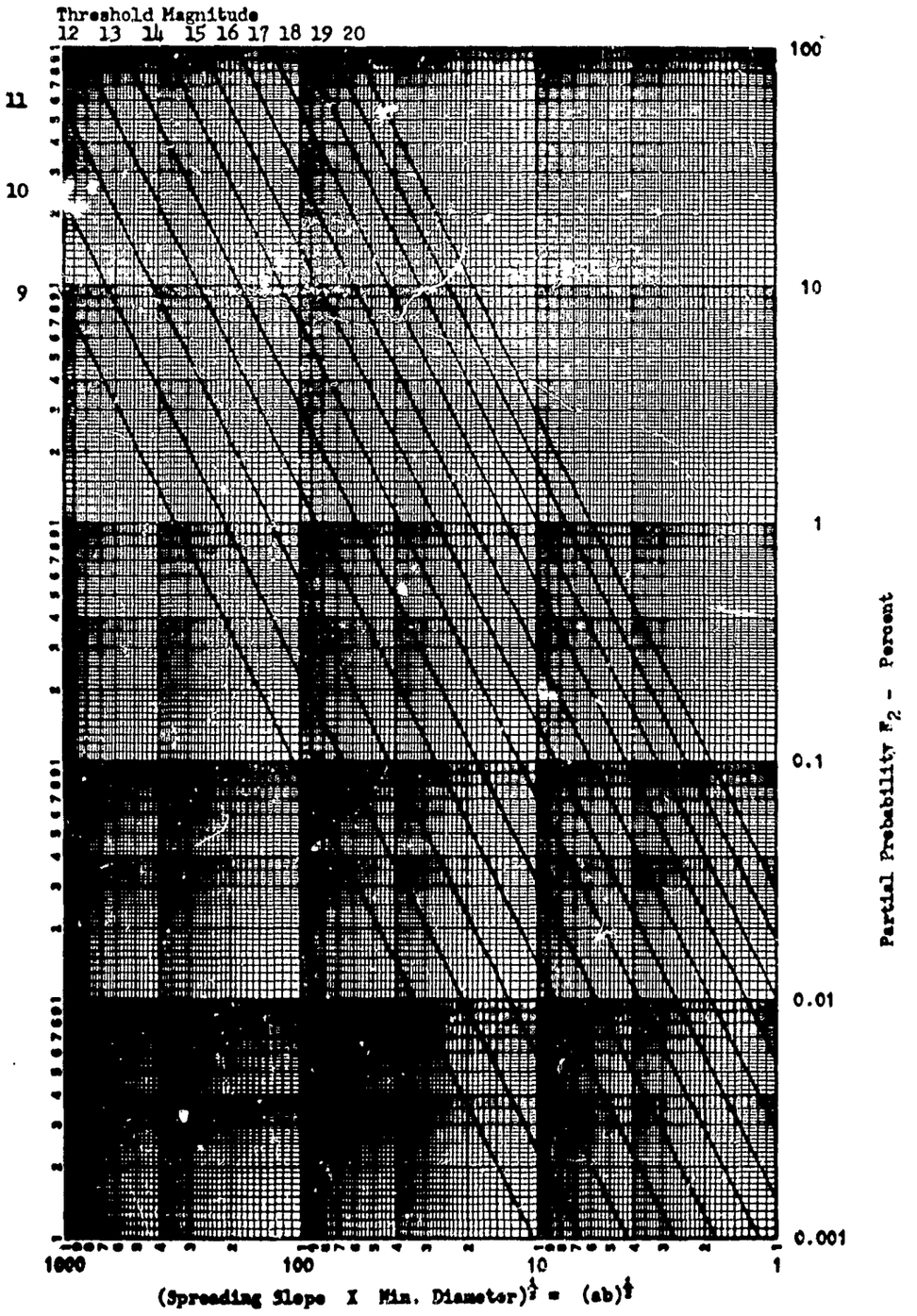


Figure AI-10. Partial Probability F_2 90^{o} Galactic Latitude

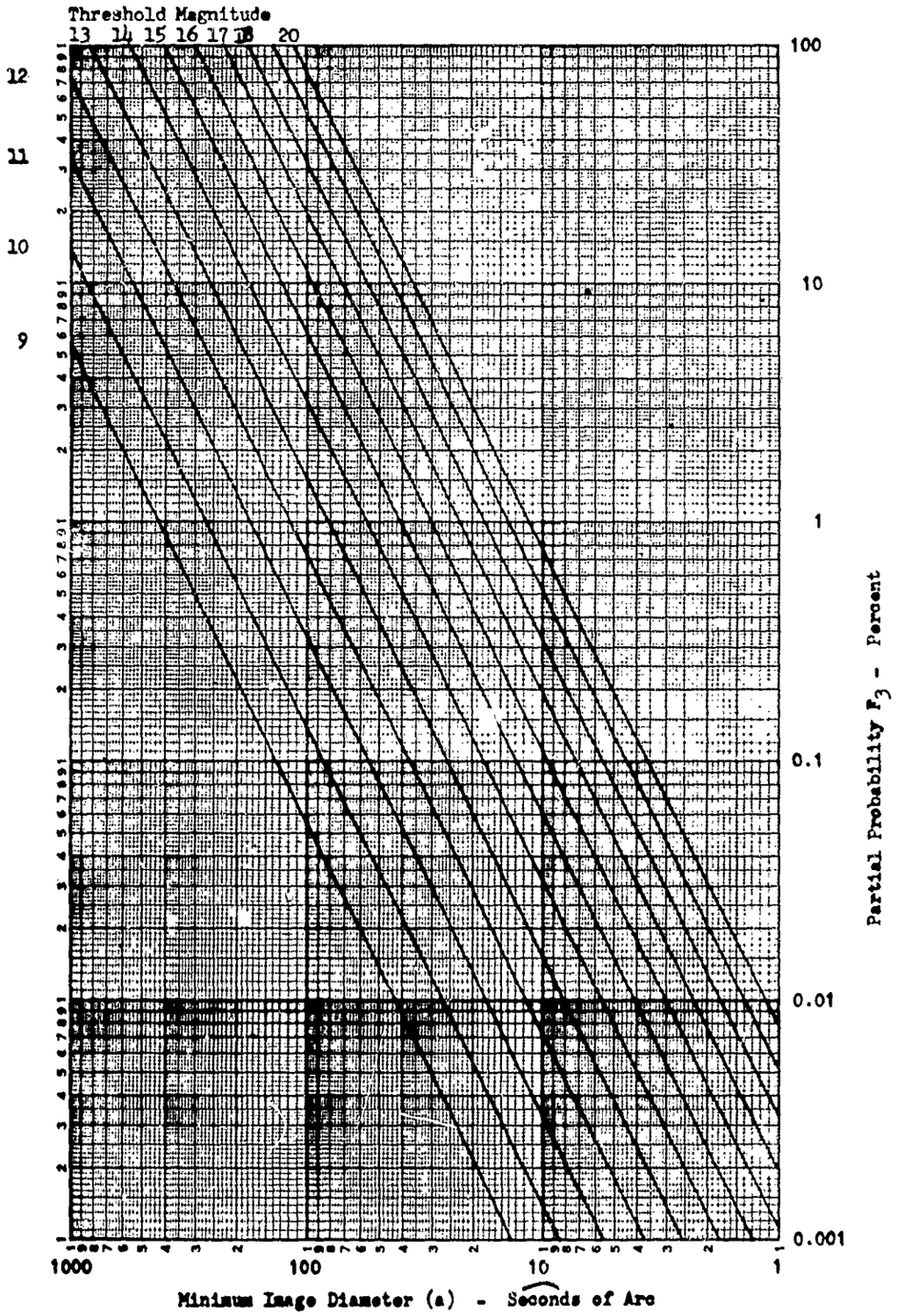


Figure AI-11. Partial Probability F_3 90° Galactic Latitude

Table AI-4

Image Orthicon Probability of Non-occultation P(B)

Number lines resolution = 1200
Field of view = 3 degrees
Minimum lines per image = 2

Threshold Magnitude	0^o Galactic Latitude P(B) b = 0	P(B) b = 1.0	P(B) b = 1.5	90^o Galactic Latitude P(B) b = 0	P(B) b = 1.0	P(B) b = 1.5
9	99.9928	99.9851	99.9794	99.99823	99.99608	99.99228
10	99.9813	99.9597	99.9433	99.9955	99.9899	99.9800
11	99.949	99.890	99.844	99.9893	99.9754	99.9507
12	99.867	99.705	99.583	99.9765	99.9414	99.879
13	99.645	99.219	98.875	99.951	99.870	99.726
14	99.10	97.94	97.06	99.898	99.714	99.384
15	97.82	94.95	92.72	99.805	99.423	98.74
16	94.9	87.7	82.1	99.64	98.85	97.43
17	88.8	71.5	57.9	99.37	97.82	94.96
18	76.3	36.3	5.8	98.97	96.05	90.7
19	51.0	-	-	98.33	93.13	83.4
20	10.0	-	-	97.5	89.0	73.2

B. APPLICATION TO PHOTOGRAPHIC MASK SEPARATION

In most separation methods, all light sources in the field of view are detected by an image tube. The output of the image tube is then used in a comparison process to reject background stars. The probability of non-occultation is primarily set by the characteristics of the image tube.

The mask separation technique employs a photographic mask in the optical system which blocks or greatly attenuates the star images while allowing the target images to proceed to an image orthicon unaffected. The result is an image detection system which is relatively insensitive to stars but which has full sensitivity for the targets of interest. The non-occultation probability in this case would be determined by the mask characteristics if the mask is constructed properly.

Figure AI-12 shows three representative density-log exposure curves for photographic material. The curves are characterized by a linear portion whose slope is represented by γ. The lower end of the curve departs from linear and approaches a slope of zero. This is the gross fog level. The upper end of the curve approaches a constant saturation density. The curves shown have the same gross fog density and the same saturation density but differ in slope.

The mask is initially exposed to produce image densities commensurate with the threshold sensitivity. In figure AI-12 the threshold magnitude is set at the exposure found by the intersection of the linear part of the curve with the gross fog density. The log exposure in this case would be -0.5. The relation between the exposure and the source magnitude is given by

$$(M_t - m) = 2.5 \log \frac{E}{E_t} \qquad \text{(I-16)}$$

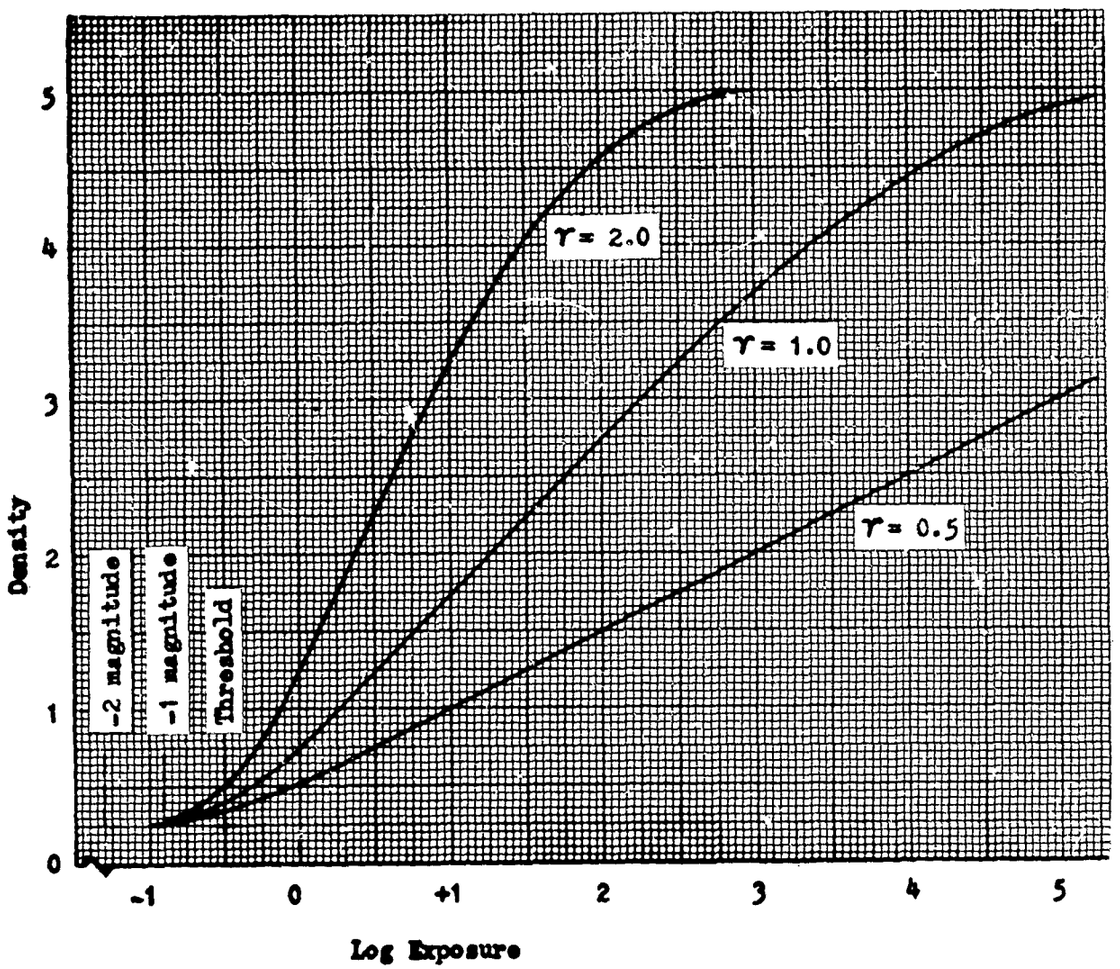


Figure AI-12. Representative Density - Log Exposure Curve

Where: M_t = Threshold magnitude

m = Magnitude of source

E = Exposure

E_t = Threshold exposure

The threshold density corresponding to the threshold exposure of -0.5 is 0.5 for the curve with $\gamma = 2$.

It is of particular interest to know the magnitude seen by the image orthicon (through the mask) in terms of the actual magnitude. This relation is obtained as follows.

$$D = \text{Log}\frac{\text{Incident Illumination}}{\text{Transmitted Illumination}} = \text{Log}\frac{\text{Illumination at Mask}}{\text{Illumination at Image Orthicon}}$$

$$D = \text{Log}\frac{E}{E_i} \tag{I-17}$$

But:

$$m - m_i = 2.5 \text{ Log } \frac{E}{E_i} = 2.5D \tag{I-18}$$

Then:

$$m_i = m + 2.5D \tag{I-19}$$

Where: m_i = Magnitude at image orthicon
m = Magnitude at mask
D = Density of mask image

The image size relation for the image orthicon, from equation (I-1), is

$$d_i = a_i + b_i (M_t - m_i) \tag{I-20}$$

Substituting equation (I-19) into equation (I-20),

$$d_i = a_i + b_i ((M_t - m) - 2.5D) \tag{I-21}$$

where $D = f(m)$ is derived from a density-log exposure curve such as figure AI-12. If the density-log exposure curve is assumed linear such that

$$D = D_t + \frac{\gamma}{2.5} (M_t - m) \tag{I-22}$$

Where: D_t = Threshold density
M_t = Threshold magnitude
γ = Slope of density-log exposure curve.

Then when equation (I-22) is substituted into equation (I-21),

$$d_i = (a_i - 2.5 b_i D_t) + (1 - \gamma) b_i (M_t - m) \tag{I-23}$$

From equation (I-23) it is seen that the slope of the new image growth curve will be the same as the original curve whenever $\gamma = 0$ such as at saturation or at the gross fog level of the mask. When γ lies between 0 and 1 the slope of the new curve will be between b_i and zero. When γ is greater than 1 the slope of the new curve is negative.

It should be remembered that the image orthicon is adjusted to produce a minimum image size a_i with a signal at the threshold level. Thus image diameters less than a_i really represent undetectable images.

Figure AI-13 shows the image size vs. magnitude characteristics of an image orthicon used with a mask having the density relations of figure AI-12. These curves were obtained by using equation (I-21) with the actual density curves. The

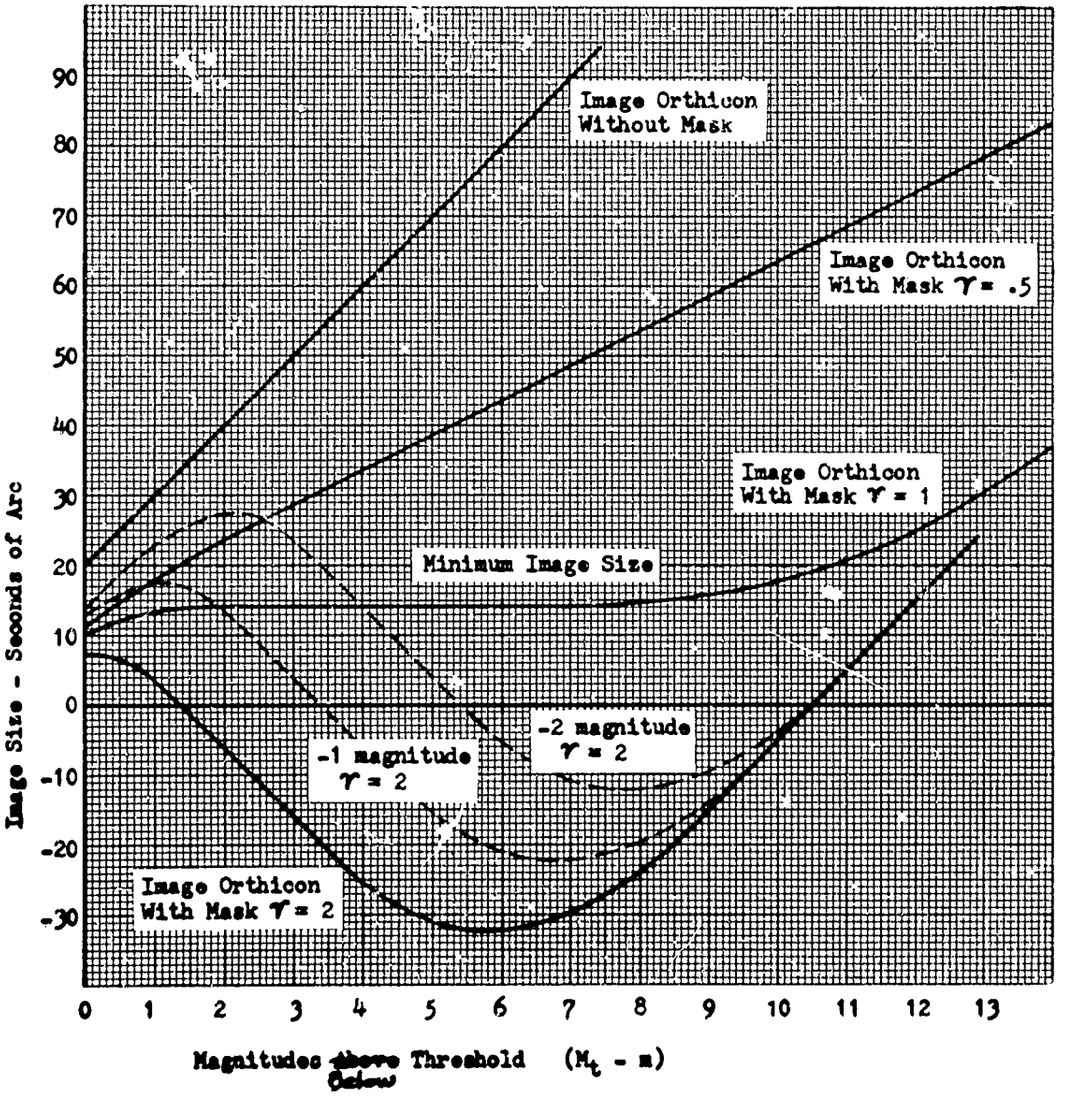


Figure AI-13. Image Growth Characteristic for an Image Orthicon Used with an Image Cancelling Mask

effects of the saturation region and the toe of the density curve can be seen. The threshold magnitude of the density curve was taken as the exposure level where the linear part of the curve intersects the gross fog level. The dashed curves in figure AI-13 show the results of setting the threshold magnitude at lower exposure levels. Note the pronounced hump of the -2 magnitude curve. The portion of the hump that lies above the image orthicon minimum image size a_i is a region where images will be detectable. If the hump were also to lie above the image size curve for the mask it would contribute to a decrease in the non-occultation probability.

One of the desirable features of a mask would be to completely block out star images. If star images were allowed to reach the image orthicon, an additional separation means would be required. The magnitude at which star images are detectable at the image orthicon is found by the intersection of the image size curve

with the minimum image size line. For the $\gamma = 2$ curve of figure AI-13 it is seen that this intersection is independent of the setting of the threshold magnitude exposure. This is a consequence of the assumption of a constant saturation density. If γ is always greater than 1 the image size curve is always negative and never intersects the minimum image size line (provided it starts at less than the mimimum image size). When a saturation limit exists where the density reaches a constant maximum, then from equation (I-23) the slope of the image size curve will be b_i, the same as it would have been without the mask. The image size curve in this region can be written as

$$d = (a_i - 2.5\, b_i\, D) + b_i\, (M_t - m) \qquad \text{(I-24)}$$

The point where this curve intersects the minimum image size line $d = a_i$ is found by setting the image size equal to the minimum.

$$a_i = (a_i - 2.5\, b_i\, D) + b_i\, (M_t - m)$$

or:

$$(M_t - m) = 2.5\, D \qquad \text{(I-25)}$$

The point at which star images are detectable is thus dependent on the saturation density. For a range of 15 magnitudes, for example, a saturation density of at least 6 would be required to prevent star images from appearing.

The discussion has brought out some of the relations necessary for insuring that the non-occultation probability would be set by the mask rather than by the image orthicon. The mask characteristics, being usually better than the image orthicon, would allow higher probabilities to be achieved. The principal improvement would result from the lower minimum image size obtainable with the mask. Neglecting for the moment alignment errors and systematic atmospheric effects, the minimum image size attainable with a photographic mask would probably be limited by atmospheric seeing conditions to something like one to three seconds of arc. The minimum image size of the image orthicon is limited by the scanning line density. At least one line is required for a detectable image and two lines are usually used. Since the total number of scanning lines is independent of the field of view, the angular size of the image will be a function of the field of view. The relations of equation (I-15) would apply.

$$a = 3600\, \frac{\Phi}{N}\, n \quad \text{seconds of arc} \qquad \text{(I-26)}$$

where Φ = Field of view in degrees
N = Number of scanning lines over the field of view
n = Image size in lines

Thus for a typical field of view of 3 degrees with 1200 scanning lines, the minimum image size would be about 18 seconds for a 2 line image. This is about 6 times greater than that obtained with a mask. Other considerations, however, will tend to narrow this difference.

APPENDIX II. BI-STATIC SPACE SURVEILLANCE SYSTEM CALCULATIONS

A. PARALLAX CALCULATIONS

In this section the equations defining the maximum and minimum parallax of a body in space relative to two separated sites on earth are derived.

The geometry of the problem is illustrated in figure AII-1. The two sites are located at points 1 and 2 and the target is at point 3. The elevation angle of the target at the first site is E_1 and A_1 is the azimuth of the target at the first sites measured counterclockwise from the great circle joining the sites. The altitude of the target is denoted by h and the great circle distance between sites by D. The parallax is deno ed by ϕ.

The spherical triangle ABC in figure AII-1 is defined on the unit sphere with the target at its center and its vertices correspond to the points where the vertical and the two lines of sight from the two sites to the target penetrate the sphere. Applying the law of cosines to this triangle,

$$\cos\phi = \cos\alpha_1, \cos\alpha_2 + \sin\alpha_1, \sin\alpha_2 \cos\Delta \qquad \text{(II-1)}$$

where α_1 is the angle between vertical and the line of sight from site 1 to the target, measured at the target; α_2 is the angle between the vertical and the line of sight from site 2 to the target, measured at the target; and Δ is the azimuthal angle between the sites, as measured at the target.

Applying the law of sines to the triangle 103, the following expression for α_1 is obtained.

$$\sin\alpha_1 = \frac{r_o}{r_o+h} \cos E_1 \qquad \text{(II-2)}$$

The law of cosines applied to the spherical triangle 124 results in the following equation

$$\cos\beta_2 = \cos\beta_1 \cos\frac{D}{r_o} + \sin\beta_1 \sin\frac{D}{r_o} \cos A_1 \qquad \text{(II-3)}$$

The angle β_1 is related to E_1 and α_1 by

$$\beta_1 = \frac{\pi}{2} - E_1 - \alpha_1 \qquad \text{(II-4)}$$

Substituting for β_1 in equation (II-3) it reduces to

$$\cos\beta_2 = \cos\frac{D}{r_o} \sin(E_1 + \alpha_1) + \sin\frac{D}{r_o} \cos(E_1 + \alpha_1) \cos A_1 \qquad \text{(II-5)}$$

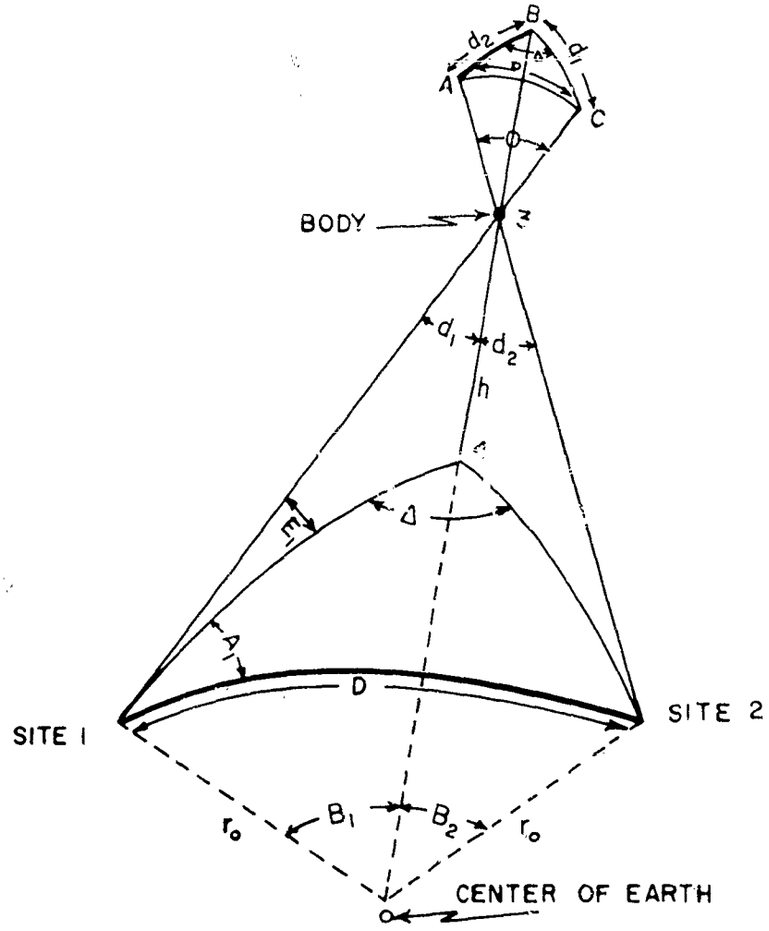


Figure AII-1. Bistatic System Geometry

The law of sines applied to triangle 203 results in the following

$$\sin \alpha_2 = \frac{r_o}{r_o+h} \sin (\alpha_2 + \beta_2) \qquad \text{(II-6)}$$

Expanding this equation and solving for α_2 the following results,

$$\tan \alpha_2 = \frac{\sin \beta_2}{\frac{r_o+h}{r_o} - \cos \beta_2} \qquad \text{(II-7)}$$

Applying the law of cosines to the spherical triangle 124,

$$\cos \frac{D}{r_o} = \cos \beta_2 \cos \beta_1 + \sin \beta_2 \sin \beta_1 \cos \Delta \qquad \text{(II-8)}$$

Substituting from equation (II-4) and solving for cos Δ,

$$\cos \Delta = \frac{\cos \frac{D}{r_o} - \sin (E_1 + \alpha_1) \cos \beta_2}{\cos (E_1 + \alpha_1) \sin \beta_2} \qquad \text{(II-9)}$$

Equations (II-1), (II-2), (II-5), (II-7), and (II-9) define the parallax in terms of E_1, h, D, and A_1.

The maximum and minimum parallax which a body at an altitude, h, will have relative to two separated sites on earth may be determined by calculating the extremal values of ϕ, from the above equations. Because of the complex nature of these equations, however, this procedure is not practical and it was necessary to actually calculate the parallax over the whole range of elevations, E_1, and azimuths, A_1, and determine the extremal values by induction. A typical result is shown in figure AII-2 where the calculated parallax is plotted as a function of the azimuth for several elevation angles, and for one height and one site separation.

From the calculations performed the following conclusions were obtained:

1. The parallax of a body at a given altitude, h, and elevation angle E_1 is minimum when the azimuth of the body is zero.

2. The parallax of a body at an altitude, h, and elevation, E_1 is maximum when the azimuth of the body is very nearly $\pi/2$ (or $3\pi/2$). Although, the maximum occurs at an angle slightly less than $\pi/2$ the discrepancy may be neglected in the present application.

3. The parallax of a body at a given altitude and azimuth varies directly with elevation, being maximum at its maximum elevation.

4. The parallax varies directly with site separation and inversely with altitude, all other parameters remaining the same.

The parametric curves presented in the chapter on the bi-static system describing the maximum parallax as a function of the site separation, altitude, and elevation angle of the body may be obtained from (II-1), (II-2), (II-5), (II-7), and (II-9) by setting the azimuth equal to $\pi/2$. Likewise the curves describing the minimum parallax may be obtained from these same equations by setting the azimuth equal to zero.

B. FIELD OF VIEW REDUCTION

In figure AII-3 the solid circle represents the field of view of one of the sites, with a diameter of θ degrees. Assume that the other site is located such that in the field of view of the second site the target will be displaced to the left by an amount equal to the parallax, ϕ. In order for the target to be in the field of view of both sites it must not be within an angle ϕ of the left boundary of the field of view of the first site. It must, therefore, appear to the right of the broken line in figure AII-3.

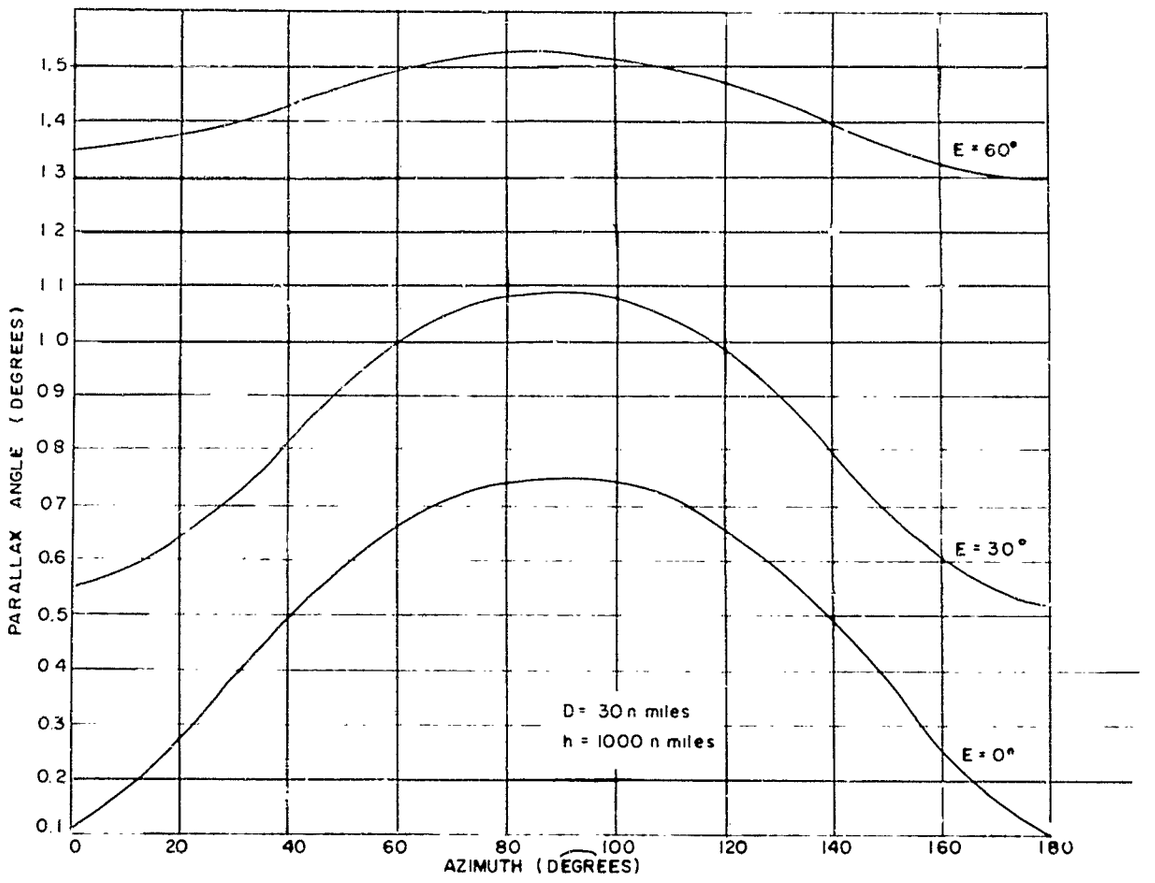


Figure AII-2. Calculated Parallax Variation with Azimuth and Elevation

The shaded region in this figure is that portion of the field of view of the first site which the target may be within and still be within the field of view of the other site. As indicated, this region is equal to the intersection of two circular beams of width θ displaced from each other a distance ϕ, equal to the parallax. The ratio of the solid angle encompassed by the shaded portion of the beam to the total solid angle of the beam is equal to the ratio of the cross-sectional area of the intersection of the two beams to the total area of one of the beams. The problem, therefore, reduces to that of calculating the area of intersection of two equal circles displaced from each other by an angle ϕ.

In figure AII-4 the coordinate geometry assumed in the calculation is shown. The area of the shaded portion of the intersection of the semi-circles is given by the integral,

$$A = \int_0^{\frac{\theta-\phi}{2}} y\,dx = \int_0^{\frac{\theta-\phi}{2}} \sqrt{\frac{\theta^2}{4} - \left(x + \frac{\phi}{2}\right)^2} \qquad \text{(II-14)}$$

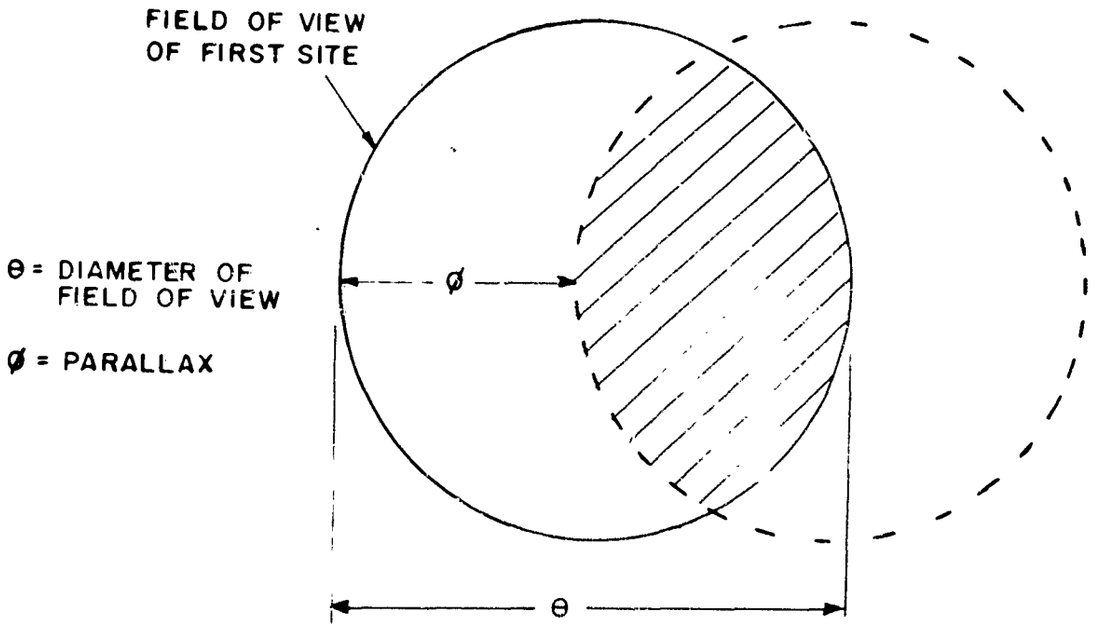


Figure AII-3. Bistatic Coordinate Geometry

Performing the integration, equation (II-14) reduces to

$$A = \frac{\pi\theta^2}{16} - \phi\sqrt{\theta^2 - \phi^2} - \frac{\theta^2}{8}\sin^{-1}\left(\frac{\phi}{\theta}\right) \qquad \text{(II-15)}$$

This corresponds to the area of one fourth of the entire shaded region in figure AII-3 and therefore, the area of this total shaded region is:

$$A_I = \frac{\pi\theta^2}{4} - \phi\sqrt{\theta^2 - \phi^2} - \frac{\theta^2}{2}\sin^{-1}\left(\frac{\phi}{\theta}\right) \qquad \text{(II-16)}$$

The area of entire circle representing the single site field of view is

$$A_S = \frac{\pi\theta^2}{4} \qquad \text{(II-17)}$$

Therefore, the ratio of the intersection area to the total area of the field of view is

$$\frac{A_I}{A_S} = 1 - \frac{2}{\pi}\frac{\phi}{\theta}\sqrt{1 - \frac{\phi^2}{\theta^2}} - \frac{2}{\pi}\sin^{-1}\left(\frac{\phi}{\theta}\right) \qquad \text{(II-18)}$$

The ratio of the solid angle coverage of the bi-static system, when it is required that the target simultaneously appear in the field of view at both sites, to the single site solid angle coverage is given by equation (II-18).

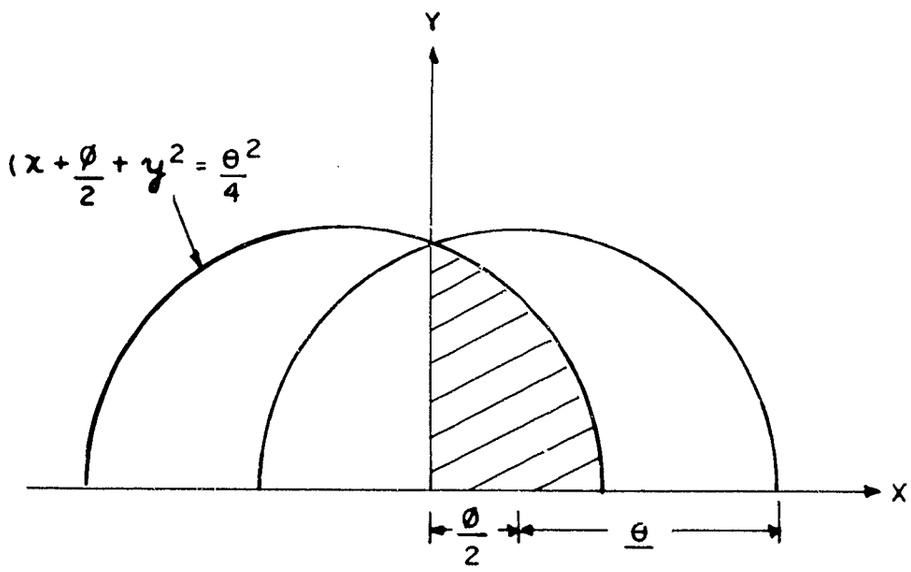


Figure AII-4. Bistatic Coordinate Geometry

APPENDIX III. SINGLE SITE M.T.I. SYSTEM CALCULATIONS

A. SITE DISPLACEMENT DUE TO EARTH ROTATION

The amount a site on the earth will be displaced with time due to earth rotation will be a function only of the site latitude. The site will move along a constant latitude circle at a constant rate. In figure AIII-1 two successive positions of the site are shown separated by a polar angle of θ degrees. The equivalent great circle distance between the site positions is denoted by D and the site latitude is denoted by λ.

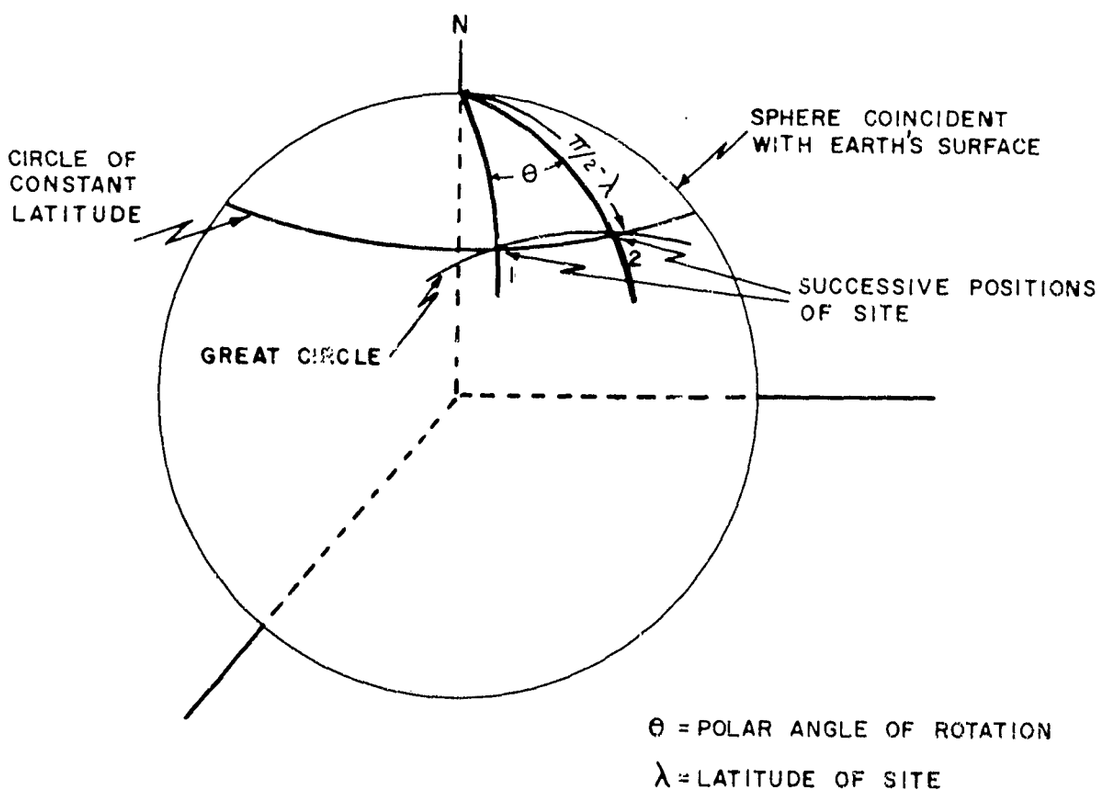


Figure AIII-1. Site Displacement Geometry

Applying the law of cosines to the spherical triangle IN2 in figure AIII-1. the following relation is obtained

$$\cos \frac{D}{r_o} = \sin^2 \lambda + \cos^2 \lambda \cos \beta \qquad \text{(III-1)}$$

The angle β may be related to the time lapse by the simple equation.

$$\beta = 15t \qquad \text{(III-2)}$$

where β is in degrees and t is in hours. This follows from the fact that the earth rotates 15° per hour.

Substituting (III-2) into (III-1),

$$\cos \frac{D}{r_o} = \sin^2 \lambda + \cos^2 \lambda \cos (15t)^o \qquad \text{(III-3)}$$

If the time is expressed in minutes, equation (III-3) becomes

$$\cos \frac{D}{r_o} = \sin^2 \lambda + \cos^2 \lambda \cos \left(\frac{t}{4}\right)^o \qquad \text{(III-4)}$$

B. SATELLITE DISPLACEMENT DUE TO ORBITAL MOTION

The general equation describing the orbit of a body in the vicinity of the earth is

$$\frac{1}{r} = \frac{g r_o^2}{(r^2 \omega)^2} (1 + e \cos \delta) \qquad \text{(III-5)}$$

where r is the distance between the center of the earth and the body, r_o is the radius of the earth, ω is the angular velocity of the body relative to the center of the earth, g is the acceleration due gravity at the earth's surface (32.2 ft/sec^2), e is the eccentricity, and δ is the angular displacement of the body from the perigee position.

Solving equation (III-5) for the angular velocity, the following equation is obtained,

$$\omega = \sqrt{\frac{g r_o^2}{r^3} (1 + e \cos \delta)} \qquad \text{(III-6)}$$

At perigee, $\delta = 0$, and (III-6) gives for the angular velocity at perigee,

$$\omega_p = \sqrt{\frac{g r_o^2}{r_p^3} (1 + e)} \qquad \text{(III-7)}$$

where r_p is the distance from the center of the earth to the body at perigee. Expressing r_p in units of r_o by

$$r_p = n r_o \qquad \text{(III-8)}$$

Equation (III-7) reduces to

$$\omega_p = \sqrt{\frac{g}{r_o}\frac{(1+e)}{n^3}} \qquad \text{(III-9)}$$

In figure AIII-2 the angular velocity relative to the center of the earth is plotted as a function of the parameter n for eccentricities of 0 and 1. The zero eccentricity corresponds to the case of a circular orbit while the e = 1 case corresponds to a parabolic orbit.

At apogee, $\delta = \pi$, and equation (III-6) reduces to

$$\omega_A = \sqrt{\frac{g}{r_o}\frac{(1-e)}{N^3}} \qquad \text{(III-10)}$$

where N is given by

$$N = \frac{r_A}{r_o} \qquad \text{(III-11)}$$

where r_A is the distance from the center of the earth to the body at apogee.

In figure AIII-3 the angular velocity at apogee relative to the center of the earth is plotted as a function of the parameter N for eccentricities of 0 and 0.8.

Figures AIII-2 and AIII-3 provide an estimate of the angular velocity of a satellite relative to the center of the earth as a function of the altitude and the eccentricity. The angular velocity relative to an observer on a stationary earth will differ from that relative to the center of the earth and the correction factor must be calculated.

For the purposes of this analysis it is sufficient to determine the maximum and minimum angular velocity which a satellite at an altitude, h, will be observed to have from a site on earth. It is assumed that the maximum angular velocity will correspond to the perigee angular velocity of a body in a parabolic orbit (eccentricity = 1.0). Although this angular velocity may be higher than that which would be observed for earth launched satellites it does represent an upper limit and, as figure AIII-3 indicates, this assumption is realistic since the perigee angular velocity is not very sensitive to eccentricity variation.

Consider the geometry in figure AIII-4 in which a target at an altitude, h, is observed from a site on earth at an elevation angle E. The orbital velocity is denoted by the vector $\vec{v}$. Since the body is assumed to be at perigee the orbital velocity, $\vec{v}$ is perpendicular to the vector, $\vec{r_1}$, from the center of the earth to the target.

The maximum angular velocity relative to the site on earth will occur when the vector $\vec{v}$ is perpendicular to the plane of $\vec{r_1}$ and $\vec{r_2}$ and will be given by:

$$\omega_{max} = \omega_p \left| \frac{r_1}{r_2} \right| \qquad \text{(III-12)}$$

Relative to Center of Earth at Perigee

Figure AIII-2. Angular

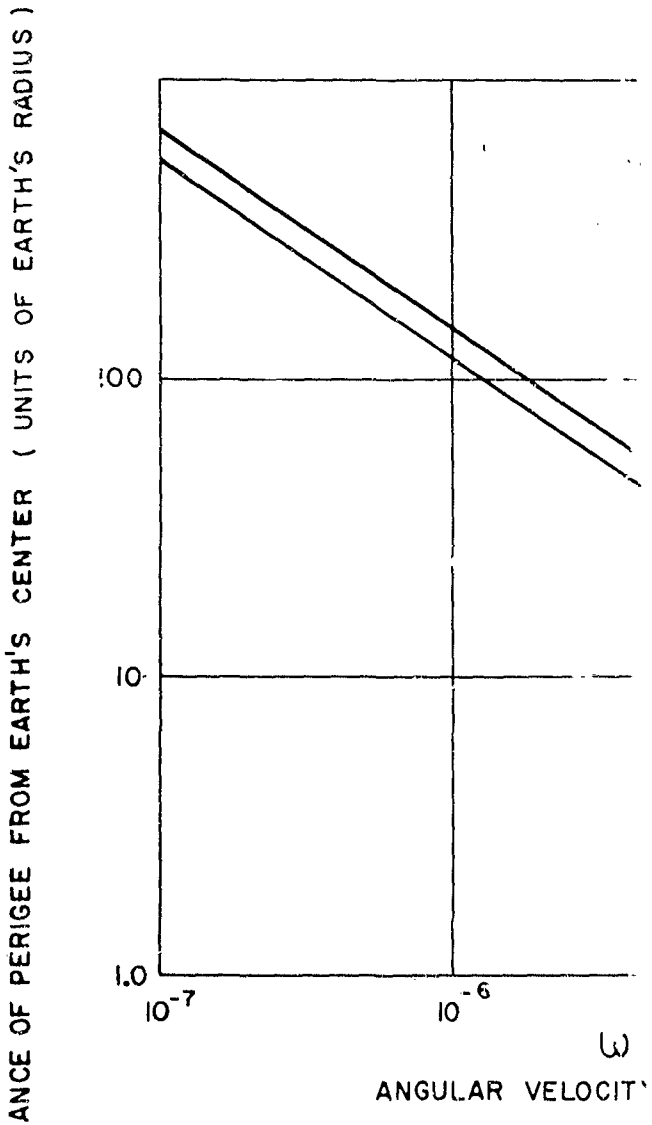
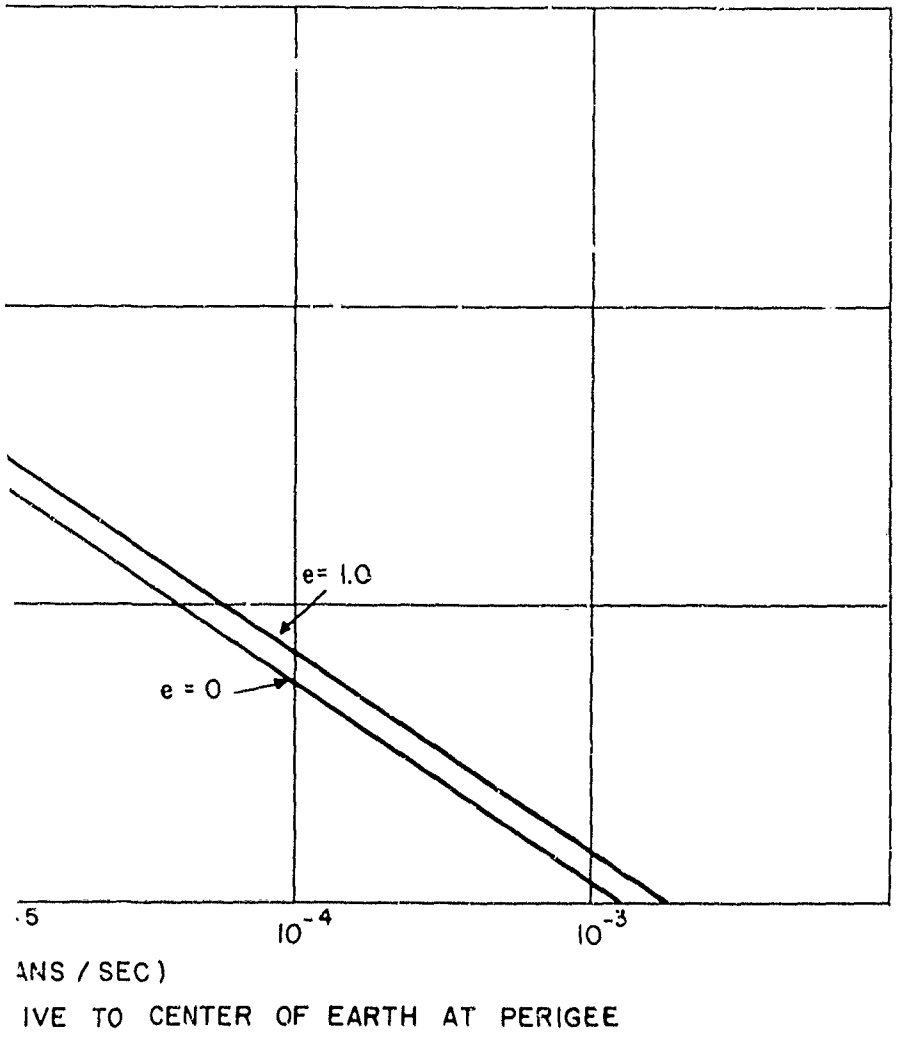


Figure AIII-3. Ang



ocity Relative to Center of Earth at Apogee

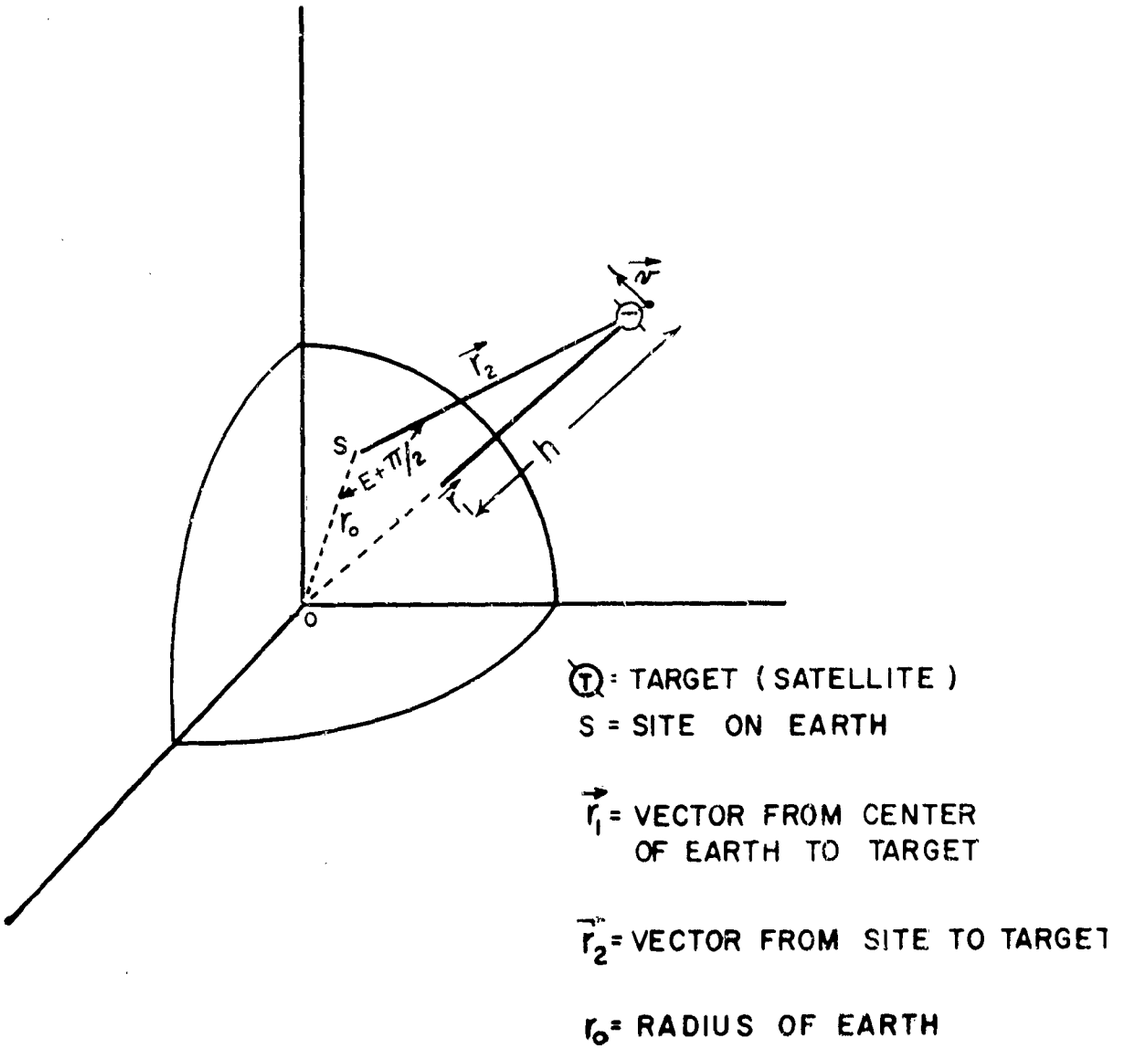


Figure AIII-4. Earth - Satellite Geometry

where ω_p is the angular velocity of the body relative to the center of the earth and is given by the e = 1 curve of figure AIII-2. The vector $\vec{r_2}$ is the vector from the site on earth to the target, as indicated in figure AIII-4.

Applying the law of sines to the triangle SOT in figure AIII-4,

$$\frac{\sin (E + \pi/2)}{(r_1)} = \frac{\sin (\pi/2 - E - \gamma)}{(r_2)} \qquad \text{(III-13)}$$

or

$$\left|\frac{r_1}{r_2}\right| = \frac{\cos E}{\cos (E + \gamma)} \tag{III-14}$$

where γ is the angle between the $\vec{r_1}$ and $\vec{r_2}$ vectors.

Substituting equation (III-14) into (III-12),

$$\omega_{max} = \frac{\omega_p \cos E}{\cos (E + \gamma)} \tag{III-15}$$

The angle γ may be evaluated by applying the law of sines to triangle in figure AIII-4. Thus

$$\sin \gamma = \frac{r_o}{r_o + h} \cos E \tag{III-16}$$

Equations (III-15) and (III-16) and figure AIII-2 define the maximum angular velocity which a body at an altitude h and at an elevation E will be observed to have relative to the site on a stationary earth.

The minimum angular velocity which a body at an altitude h will be observed to have relative to a site on a stationary earth will be assumed to correspond to the apogee angular velocity of a body in an orbit with an eccentricity of 0.8. In this case the velocity vector, $\vec{v}$, in figure AIII-4 is again perpendicular to the vector $\vec{r_1}$.

The minimum angular velocity relative to the site on earth will occur when the vector $\vec{v}$ is in the plane defined by two vectors, $\vec{r_1}$, and $\vec{r_2}$, and will be given by

$$\omega_{min} = \omega_A \left|\frac{r_1}{r_2}\right| \cos \gamma \tag{III-17}$$

where ω_A is the angular velocity of the body relative to the center of the earth and is given by the e = 0.8 curve of figure AIII-3.

Substituting from equation (III-14) into (III-17) the following equation is obtained,

$$\omega_{min} = \frac{\omega_A \cos E \cos \gamma}{\cos (E + \gamma)} \tag{III-18}$$

Equations (III-18), and (III-16) in conjunction with the e = 0.8 curve in figure AIII-3 define the minimum angular velocity which a body at an altitude h and at an elevation E relative to an observer on earth may be expected to have relative to the observer.

APPENDIX IV. SMOOTHING FOR BEST ESTIMATES

For tracking periods which are small with respect to the target's period, azimuth and elevation may be represented by the following independent quadratics.

$$A_i = A_o + \dot{A}_o (t_i - t_o) + \frac{\ddot{A}_o (t_i - t_o)^2}{2} \qquad \text{(IV-1)}$$

$$E_i = E_o + \dot{E}_o (t_i - t_o) + \frac{\ddot{E}_o (t_i - t_o)^2}{2} \qquad \text{(IV-2)}$$

(Subscript "o" denotes reference time)

The problem is to obtain the best estimates of the angular quantities at the reference time by fitting the above polynomials to the optical data. In the following analysis the estimate of a true quantity will be referred to as an estimator and denoted with a "hat" ($\wedge$).

i.e. Estimate of the true value of $A_o = \hat{A}_o$

Estimate of the true value of $\ddot{E}_o = \hat{\ddot{E}}_o$

Since the measurements are subject to errors (both random and systematic), the estimators will also be in error. The maximum likelihood criterion, which reduces to the weighted least squares criterion when measurement types are independent, specifies the estimators such that the mean square values of the errors on the estimators are smaller than the mean-square value of the errors on any other unbiased estimate. The following assumptions apply to the analysis which follows.

Assumptions:

(1) The quantities A_o, $\dot{A}_o$, $\ddot{A}_o$, E_o, $\dot{E}_o$, and $\ddot{E}_o$ will be considered functionally independent. If the actual physical constraints are introduced into the analysis, the mathematics becomes very difficult and involves the solution of 12 simultaneous equations.

(2) The reference time, t_o, will be taken as zero.

(3) Successive observations will be separated by equal time increments.

(4) An equal number of observations will be made before and after the reference time.

(5) The errors on azimuth measurements are independent of the errors on elevation measurements.

(6) The statistics are stationary or independent of time.

Assumptions (2), (3) and (4) were introduced to reduce the computational complexity involved in the smoothing technique. This will become obvious in the analysis.

Since azimuth and elevation measurements are statistically independent, the estimators which minimize the sum of the squared values of the errors between the polynomials and the measurements are the "best" estimators in the least squares or maximum likelihood sense. In equation form, the following expression must be minimized.

$$S = \sum_{i=-M}^{i=M} \frac{(A_i - \hat{A}_i)^2}{\sigma_A^2} + \frac{(E_i - \hat{E}_i)^2}{\sigma_E^2} \qquad \text{(IV-3)}$$

where:

$$\hat{A}_i = \hat{A}_o + \hat{\dot{A}}_o t_i + \hat{\ddot{A}}_o t_i^2/2$$

$$\hat{E}_i = \hat{E}_o + \hat{\dot{E}}_o t_i + \hat{\ddot{E}}_o t_i^2/2$$

σ_A^2 = Variance of the aximuth measurements

σ_E^2 = Variance of the elevation measurements

$t_o = 0$

$N = 2M + 1$ = Total number of observations

A_i, E_i } Optical measurements at time t_i

To minimize S, it is necessary to choose the estimators so that the total derivative of S equals zero.

$$dS = 0 = \frac{\partial S}{\partial \hat{A}_o} d\hat{A}_o + \frac{\partial S}{\partial \hat{\dot{A}}_o} d\hat{\dot{A}}_o + \frac{\partial S}{\partial \hat{\ddot{A}}_o} d\hat{\ddot{A}}_o + \frac{\partial S}{\partial \hat{E}_o} d\hat{E}_o + \frac{\partial S}{\partial \hat{\dot{E}}_o} d\hat{\dot{E}}_o + \frac{\partial S}{\partial \hat{\ddot{E}}_o} d\hat{\ddot{E}}_o = 0 \qquad \text{(IV-4)}$$

Since $\hat{A}_o$, $\hat{\dot{A}}_o$, $\hat{\ddot{A}}_o$, $\hat{E}_o$, $\hat{\dot{E}}_o$, and $\hat{\ddot{E}}_o$ are considered to be functionally independent, equation (IV-4) is satisfied only when:

$$\frac{\partial S}{\partial \hat{A}_o} = \frac{\partial S}{\partial \hat{\dot{A}}_o} = \frac{\partial S}{\partial \hat{\ddot{A}}_o} = \frac{\partial S}{\partial \hat{E}_o} = \frac{\partial S}{\partial \hat{\dot{E}}_o} = \frac{\partial S}{\partial \hat{\ddot{E}}_o} = 0 \qquad \text{(IV - 5)}$$

Using equation (IV-3) and carrying out the necessary partial differentiation yields:

$$\frac{\partial S}{\partial \hat{A}_o} = \sum_{i=-M}^{M} 2\left(A_i - \hat{A}_o - \hat{\dot{A}}_o t_i - \frac{\hat{\ddot{A}}_o t_i^2}{2}\right)\left(-\frac{1}{\sigma_A^2}\right) = 0 \qquad \text{(IV-6)}$$

$$\frac{\partial S}{\partial \hat{\dot{A}}_o} = \sum_{i=-M}^{M} 2\left(A_i - \hat{A}_o - \hat{\dot{A}}_o t_i - \frac{\hat{\ddot{A}}_o t_i^2}{2}\right)\left(\frac{-t_i}{\sigma_A^2}\right) = 0 \qquad \text{(IV-7)}$$

$$\frac{\partial S}{\partial \hat{\ddot{A}}_o} = \sum_{i=-M}^{M} 2\left(A_i - \hat{A}_o - \hat{\dot{A}}_o t_i - \frac{\hat{\ddot{A}}_o t_i^2}{2}\right)\left(\frac{-t_i^2}{\sigma_A^2}\right) = 0 \qquad \text{(IV-8)}$$

$$\frac{\partial S}{\partial \hat{E}_o} = \sum_{i=-M}^{M} 2\left(E_i - \hat{E}_o - \hat{\dot{E}}_o t_i - \frac{\hat{\ddot{E}}_o t_i^2}{2}\right)\left(-\frac{1}{\sigma_E^2}\right) = 0 \qquad \text{(IV-9)}$$

$$\frac{\partial S}{\partial \hat{\dot{E}}_o} = \sum_{i=-M}^{M} 2\left(E_i - \hat{E}_o - \hat{\dot{E}}_o t_i - \frac{\hat{\ddot{E}}_o t_i^2}{2}\right)\left(-\frac{t_i}{\sigma_E^2}\right) = 0 \qquad \text{(IV-10)}$$

$$\frac{\partial S}{\partial \hat{\ddot{E}}_o} = \sum_{i=-M}^{M} 2\left(E_i - \hat{E}_o - \hat{\dot{E}}_o t_i - \frac{\hat{\ddot{E}}_o t_i^2}{2}\right)\left(-\frac{t_i^2}{\sigma_E^2}\right) = 0 \qquad \text{(IV-11)}$$

The following equations are obtained by dividing the $-2/\sigma_A^2$ term out of the above equations since it is not involved in the summation.

$$\frac{\partial S}{\partial \hat{A}_o} = \sum_{i=-M}^{M}\left(A_i - \hat{A}_o - \hat{\dot{A}}_o t_i - \frac{\hat{\ddot{A}}_o t_i^2}{2}\right) = 0 \qquad \text{(IV-12)}$$

$$\frac{\partial S}{\partial \hat{\dot{A}}_o} = \sum_{i=-M}^{M}\left(A_i - \hat{A}_o - \hat{\dot{A}}_o t_i - \frac{\hat{\ddot{A}}_o t_i^2}{2}\right)\left(t_i\right) = 0 \qquad \text{(IV-13)}$$

$$\frac{\partial S}{\partial \hat{A}_o} = \sum_{i=-M}^{M} \left(A_i - \hat{A}_o - \hat{A}_o t_i - \frac{\hat{\hat{A}}_o t_i^2}{2} \right) (t_i^2) = 0 \qquad \text{(IV-14)}$$

The corresponding equations for elevation are identical to those shown above with E's replacing A's. Expanding and rearranging terms in equations (IV-12), (IV-13), and (IV-14) yields:

$$\sum A_i = \sum \hat{A}_o + \hat{A}_o \sum t_i + \frac{\hat{\hat{A}}_o}{2} \sum t_i^2 \qquad \text{(IV-15)}$$

$$\sum A_i t_i = \hat{A}_o \sum t_i + \hat{A}_o \sum t_i^2 + \frac{\hat{\hat{A}}_o}{2} \sum t_i^3 \qquad \text{(IV-16)}$$

$$\sum A_i t_i^2 = \hat{A}_o \sum t_i^2 + \hat{A}_o \sum t_i^3 + \frac{\hat{\hat{A}}_o}{2} \sum t_i^4 \qquad \text{(IV-17)}$$

where $\sum$ is used to represent $\sum_{i=-M}^{i=M}$

If it is assumed that an equal number of observations are made before and after $t_o = 0$ and that the observations are equally spaced in time, the following equations can be written.

$$\sum_{i=-M}^{i=M} \hat{A}_o = N \hat{A}_o$$

where $N = 2M + 1$ (IV-18)

N = Total no. of observations

$$\sum_{i=-M}^{i=M} t_i = 0 \qquad \text{(IV-19)}$$

$$\sum_{i=-M}^{i=M} t_i^2 = \sum_{i=-M}^{M} (i \Delta t)^2 = 2\Delta t^2 \sum_{i=0}^{M} i^2$$

$$\sum_{i=-M}^{M} t_i^2 = 2 (\Delta t)^2 \left[\frac{M (M+1) (2M+1)}{6} \right] \qquad \text{(IV-20)}$$

$$\sum_{i=-M}^{M} t_i^3 = 0 \qquad \text{(IV-21)}$$

$$\sum_{i=-M}^{M} t_i^4 = \sum_{i=-M}^{M} (i\Delta t)^4 = 2(\Delta t)^4 \sum_{i=0}^{M} i^4$$

$$= 2(\Delta t)^4 \left[\frac{M(M+1)(2M+1)(3M^2+3M-1)}{30}\right] \qquad \text{(IV-22)}$$

where Δt = time lapse between observ.

The advantage of assumptions (2) and (3) now becomes apparent, they make it possible to replace summations with closed expressions. In order to make the writing less burdensome, immediate use will not be made of all the equations (IV-18) through (IV-22). Substitution of equations (IV-18), (IV-19), and (IV-21) into equations (IV-15), (IV-16), (IV-17) yields:

$$\sum A_i = N\hat{A}_o + \frac{\hat{\hat{A}}_o}{2} \sum t_i^2 \qquad \text{(IV-23)}$$

$$\sum A_i t_i = \hat{\hat{A}}_o \sum t_i^2 \qquad \text{(IV-24)}$$

$$\sum A_i t_i^2 = \hat{A}_o \sum t_i^2 + \frac{\hat{\hat{A}}_o}{2} \sum t_i^4 \qquad \text{(IV-25)}$$

$$\left(\text{where } \sum \text{ has been used to represent } \sum_{i=-M}^{i=M}\right)$$

The expression for $\hat{A}_o$ can be obtained from equation (IV-24).

$$\hat{A}_o = \frac{\sum A_i t_i}{\sum t_i^2} \qquad \text{(IV-26)}$$

The expressions for $\hat{\hat{A}}_o$ and $\hat{A}_o$ can be obtained by solving equations (IV-23) and (IV-25) simultaneously.

From equation IV-23,

$$\hat{A}_o = \frac{\sum A_i - \frac{\hat{\hat{A}}_o}{2} \sum t_i^2}{N} \qquad \text{(IV-27)}$$

Substitution of equation (IV-27) into (IV-25) yields:

$$\sum A_i t_i^2 = \frac{\sum t_i^2 \sum A_i - \frac{\hat{\hat{A}}_o}{2} \left(\sum t_i^2\right)^2}{N} + \frac{\hat{\hat{A}}_o}{2} \sum t_i^4$$

$$\sum A_i t_i^2 = \frac{\hat{A}_o}{2}\left[\sum t_i^4 - \frac{\left(\sum t_i^2\right)^2}{N}\right] + \frac{\sum A_i \sum t_i^2}{N}$$

$$\frac{\hat{A}_o}{2} = \frac{\sum A_i t_i^2 - \frac{\sum A_i \sum t_i^2}{N}}{\sum t_i^4 - \frac{\left(\sum t_i^2\right)^2}{N}} \qquad \text{(IV-28)}$$

The explicit expression for $\hat{A}_o$ can now be obtained from equations (IV-27) and (IV-28).

$$\hat{A}_o = \frac{\sum A_i}{N} - \left[\frac{\sum A_i t_i^2 - \frac{\sum A_i \sum t_i^2}{N}}{\sum t_i^4 - \frac{\left(\sum t_i^2\right)^2}{N}}\right] \frac{\sum t_i^2}{N} \qquad \text{(IV-29)}$$

The mean values or expected values of the estimators will now be calculated in order to determine if the estimators are unbiased or not. An estimator is unbiased if its expected values (mean) is equal to the true value of the quantity being estimated. By definition then, the estimator $\hat{X}$ is unbiased if

$$E\left[\hat{X}\right] = \int_{-\infty}^{\infty} \hat{X} f(\hat{X})\, d\hat{X} = X \qquad \text{(IV-30)}$$

The expected value of a quantity which is not subject to errors is that quantity itself since an unerrored quantity is treated as a constant when using the expectation operator. For example the expected value of A_o is A_o since A_o is treated as a constant. ($\hat{A}_o$ is the estimate of the true value A_o).

The expected value of $\hat{A}_o$ can be calculated by using eauation (IV-26)

$$E\left[\hat{A}_o\right] = E\left[\frac{\sum A_i t_i}{\sum t_i^2}\right] \qquad \text{(IV-31)}$$

Since time is considered as unerrored, it can be treated as a constant.

$$E\left[\hat{A}_o\right] = \frac{\sum t_i\, E\left[A_i\right]}{\sum t_i^2} \qquad \text{(IV-32)}$$

After setting $t_o = 0$ in equation (IV-1) it is possible to write

$$E\left[A_i\right] = E\left[A_o + \dot{A}_o t_i + \frac{\ddot{A}_o}{2} t_i^2\right]$$

$$= A_o + \dot{A}_o t_i + \frac{\ddot{A}_o}{2} t_i^2 \qquad \text{(IV-33)}$$

since all the terms in the brackets are true or unerrored quantities. Substitution of equation (IV-33) into (IV-32) yields

$$E\left[\hat{A}_o\right] = \frac{A_o \sum_{0} t_i + \dot{A}_o \sum t_i^2 + \frac{\ddot{A}_o}{2} \sum_{0} t_i^3}{\sum t_i^2} \qquad \text{(IV-34)}$$

$$E\left[\hat{\dot{A}}\right] = \dot{A}_o \qquad \text{(IV-35)}$$

Therefore $\hat{A}_o$ is unbiased. The same procedure will now be used to determine the expected values of $\hat{\dot{A}}_o$ and $\hat{\ddot{A}}_o$.

$$E\left[\frac{\hat{\dot{A}}_o}{2}\right] = E\left[\frac{\sum A_i t_i^2 - \frac{\sum A_i \sum t_i^2}{N}}{\sum t_i^4 - \frac{\left(\sum t_i^2\right)^2}{N}}\right]$$

$$= \frac{\sum t_i^2 E\left[A_i\right] - \frac{\sum E\left[A_i\right] \sum t_i^2}{N}}{\sum t_i^4 - \frac{\left(\sum t_i^2\right)^2}{N}} \qquad \text{(IV-36)}$$

$$= \frac{\sum t_i^2 \left[A_o + \dot{A}_o t_i + \frac{\ddot{A}_o}{2} t_i^2\right] - \sum \left[A_o + \dot{A}_o t_i + \frac{\ddot{A}_o}{2} t_i^2\right] \frac{\sum t_i^2}{N}}{\sum t_i^4 - \frac{\left(\sum t_i^2\right)^2}{N}} \qquad \text{(IV-37)}$$

Expanding and dropping odd power terms,

$$= \frac{A_o \sum t_i^2 + \frac{\ddot{A}_o}{2} \sum t_i^4 - \frac{\sum A_o \sum t_i^2 - \frac{\ddot{A}_o}{2} \left(\sum t_i^2\right)^2}{N}}{\sum t_i^4 - \frac{\left(\sum t_i^2\right)^2}{N}} \qquad \text{(IV-38)}$$

Since $\sum A_o = A_o N$,

$$E\left[\frac{\hat{\ddot{A}}_o}{2}\right] = \frac{\frac{\ddot{A}_o}{2}\left[\sum t_i^4 - \frac{\left(\sum t_i^2\right)^2}{N}\right]}{\sum t_i^4 - \frac{\left(\sum t_i^2\right)^2}{N}} = \frac{\ddot{A}_o}{2} \qquad \text{(IV-39)}$$

By using equation (IV-27), the expected value of $\hat{A}_o$ can be found.

$$E\left[\hat{A}_o\right] = E\left[\frac{\sum A_i - \frac{\hat{\ddot{A}}_o}{2} \sum t_i^2}{N}\right] \qquad \text{(IV-40)}$$

$$= \frac{\sum E\left[A_i\right] - E\left[\frac{\hat{\ddot{A}}_o}{2}\right] \sum t_i^2}{N} \qquad \text{(IV-41)}$$

$$= \frac{\sum \left[A_o + \dot{A}_o t_i + \frac{\ddot{A}_o}{2} t_i^2\right] - \frac{\ddot{A}_o}{2} \sum t_i^2}{N} \qquad \text{(IV-41')}$$

Expansion of equation (IV-41') yields

$$E\left[\hat{A}_o\right] = \frac{N A_o + \frac{\ddot{A}_o}{2} \sum t_i^2 - \frac{\ddot{A}_o}{2} \sum t_i^2}{N} \qquad \text{(IV-42)}$$

$$E\left[\hat{A}_o\right] = A_o$$

It has now been shown that each of the estimators ($\hat{A}_o$, $\hat{\dot{A}}_o$, $\hat{\ddot{A}}_o$) is unbiased.

The next step is to determine the expressions for the variances of the estimators. The following statistical definitions will be used in the analysis. If $\bar{X}$ is the true or errorless value of X and ΔX is the error then

$$X = \bar{X} + \Delta X \qquad \text{(IV-43)}$$

If the error is random its expected value is zero and

$$E[X] = \bar{X} \tag{IV-44}$$

$$\therefore \quad X = E[X] + \Delta X \tag{IV-45}$$

$$\text{or} \quad \Delta X = X - E[X] \tag{IV-46}$$

The variance of X is defined as the expected squared value of the error ΔX.

$$\sigma_X^2 = E\left[(\Delta X)^2\right] = E\left\{\left(X - E\left[X\right]\right)^2\right\} \tag{IV-47}$$

The following relationships will also prove to be very useful throughout the analysis.

$$\sum X_i \sum Y_i = \sum_i X_i Y_i + \sum_i \sum_{\substack{j \\ i \neq j}} X_i Y_j \tag{IV-48}$$

$$\left(\sum_i X_i\right)^2 = \sum_i X_i^2 + \sum_i \sum_{\substack{j \\ i \neq j}} X_i X_j \tag{IV-49}$$

Using the previous relationships,

$$\sigma_{\hat{A}_o}^2 = E\left[\left(\hat{A}_o - E\left\{\hat{A}_o\right\}\right)^2\right] \tag{IV-50}$$

Substitution of equations (IV-26) and (IV-32) into (IV-50) yields:

$$\sigma_{\hat{A}}^2 = E\left[\left(\frac{\sum A_i t_i}{\sum t_i^2} - \frac{\sum t_i E[A_i]}{\sum t_i^2}\right)^2\right]$$

$$\sigma_{\hat{A}}^2 = E\left[\left(\frac{\sum t_i \left\{A_i - E[A_i]\right\}}{\sum t_i^2}\right)^2\right]$$

$$\sigma_{\hat{A}}^2 = E\left[\left(\frac{\sum t_i \Delta A_i}{\sum t_i^2}\right)^2\right] \tag{IV-51}$$

Making use of the relationship indicated by equation (IV-49),

$$\sigma_{\hat{A}}^2 = E\left[\frac{\sum_i t_i^2 \Delta A_i^2 + \sum_i \sum_j t_i \Delta A_i t_j \Delta A_j}{\left(\sum t_i^2\right)^2}\right]$$

$$\sigma_{\hat{A}}^2 = \frac{\sum t_i^2 E\left[\Delta A_i^2\right] + \sum \sum t_i t_j E\left[\Delta A_i \Delta A_j\right]}{\left(\sum t_i^2\right)^2} \qquad \text{(IV-52)}$$

Since it is assumed that there is nc autocorrelation or cross-correlation between angular errors at different times and that the statistics are stationary, the following equations are pertinent.

$$E\left[(\Delta A_i)^2\right] = \sigma_{A_i}^2 = \sigma_A^2 = \text{Variance of A} \qquad \text{(IV-53)}$$

$$E\left[(\Delta A_i)\ (\Delta A_j)\right] = 0 = \text{Autocorrelation of A} \qquad \text{(IV-54)}$$

Substitution of equations (IV-53) and (IV-54) into (IV-52) yields

$$\sigma_{\hat{A}}^2 = \frac{\sigma_A^2 \sum t_i^2}{\left(\sum t_i^2\right)^2}$$

$$\sigma_{\hat{A}}^2 = \frac{\sigma_A^2}{\sum t_i^2} \qquad \text{(IV-55)}$$

The variance on $\hat{\hat{A}}_o$ is defined by

$$\sigma_{\hat{\hat{A}}_o}^2 = E\left[\left(\hat{\hat{A}}_o - E\left\{\hat{\hat{A}}_o\right\}\right)^2\right] \qquad \text{(IV-56)}$$

Substituting equations (IV-28) and (IV-36) into equation (IV-56) yields

$$\sigma_{\hat{\hat{A}}_o}^2 = E\left[\left(\frac{2\sum A_i t_i^2 - \frac{2}{N}\sum A_i \sum t_i^2}{\sum t_i^4 - \frac{\left(\sum t_i^2\right)^2}{N}} - \frac{2\sum t_i^2 E[A_i] - \frac{2}{N}\sum E[A_i]}{\sum t_i^4 - \frac{\left(\sum t_i^2\right)^2}{N}}\right.\right.$$

$$= E\left[\left(\frac{2\sum t_i^2 \Delta A_i - \frac{2}{N}\sum \Delta A_i \sum t_i^2}{\sum t_i^4 - \frac{\left(\sum t_i^2\right)^2}{N}}\right)^2\right]$$

$$\sigma^2_{\hat{A}_o} = 4E \frac{\left[\left(\sum t_i^2 \Delta A_i\right)^2 - \frac{2}{N}\sum t_i^2 \Delta A_i \sum \Delta A_i \sum t_i^2 + \left(\frac{\sum \Delta A_i \sum t_i^2}{N}\right)^2\right]}{\left[\sum t_i^4 - \frac{\left(\sum t_i^2\right)^2}{N}\right]^2} \quad \text{(IV-57)}$$

The expected value of the numerator will be calculated term by term

$$E\left[\left(\sum t_i^2 \Delta A_i\right)^2\right] = E\left[\sum t_i^4 \Delta A_i^2 + \sum\sum \Delta A_i \Delta A_j t_i^2 t_j^2\right]$$

$$= \sigma_A^2 \sum t_i^4 \quad \text{(IV-58)}$$

$$E\left[-\frac{2}{N}\sum t_i^2 \Delta A_i \sum \Delta A_i \sum t_i^2\right] = -\frac{2}{N}\sum t_i^2 \; E\left[\sum t_i^2 \Delta A_i \sum \Delta A_i\right] \quad \text{(IV-59)}$$

Making use of the relationship indicated in equation (IV-48), equation (IV-59) can be written as:

$$= -\frac{2}{N}\sum t_i^2 \; E\left[\sum t_i^2 \Delta A_i^2 + \sum\sum t_i^2 \Delta A_i \Delta A_j\right]$$

$$= -\frac{2}{N}\sum t_i^2 \left[\sigma_A^2 \sum t_i^2\right]$$

$$E\left[-\frac{2}{N}\sum t_i^2 \Delta A_i \sum \Delta A_i \sum t_i^2\right] = -\frac{2}{N}\sigma_A^2 \left(\sum t_i^2\right)^2 \quad \text{(IV-60)}$$

$$E\left[\frac{1}{N^2}\left(\sum \Delta A_i \sum t_i^2\right)^2\right] = \frac{\left(\sum t_i^2\right)^2}{N^2} E\left[\left(\sum \Delta A_i\right)^2\right]$$

$$= \frac{\left(\sum t_i^2\right)^2}{N^2} E\left[\sum (\Delta A_i)^2 + \sum\sum \Delta A_i \Delta A_j\right]$$

$$= \frac{\left(\sum t_i^2\right)^2}{N^2} \quad \sum \sigma_A^2 = \frac{\left(\sum t_i^2\right)^2 \sigma_A^2 N}{N^2}$$

$$E\left[\frac{1}{N^2}\left(\sum \Delta A_i \sum t_i^2\right)^2\right] = \frac{\sigma_A^2 \left(\sum t_i^2\right)^2}{N} \qquad \text{(IV-61)}$$

Substitution of equations (IV-58), (IV-60) and (IV-61) into equation (IV-57) yields:

$$\sigma_{\hat{A}}^2 = \frac{4\left[\sigma_A^2 \sum t_i^4 - \frac{2}{N}\sigma_A^2 \left(\sum t_i^2\right)^2 + \frac{\sigma_A^2 \left(\sum t_i^2\right)^2}{N}\right]}{\left[\sum t_i^4 - \frac{\left(\sum t_i^2\right)^2}{N}\right]^2}$$

$$\sigma_{\hat{A}}^2 = \frac{4\sigma_A^2}{\sum t_i^4 - \frac{\left(\sum t_i^2\right)^2}{N}} \qquad \text{(IV-62)}$$

The variance on $\hat{A}_o$ is defined by the equation

$$\sigma_{\hat{A}_o}^2 = E\left[\left(\hat{A}_o - E\left\{\hat{A}_o\right\}\right)^2\right] \qquad \text{(IV-63)}$$

Substitution of equations (IV-27) and (IV-41) into the above equation yields:

$$\sigma_{\hat{A}_o}^2 = E\left[\left(\frac{\sum A_i - \frac{\hat{\dot{A}}_o}{2}\sum t_i^2}{N} - \frac{\sum E\left[A_i\right] - E\left[\frac{\hat{A}_o}{2}\right]\sum t_i^2}{N}\right)^2\right]$$

$$= \frac{1}{N^2} E\left[\left(\sum \Delta A_i - \left\{\frac{\hat{A}_o}{2} - \frac{\ddot{A}_o}{2}\right\} \sum t_i^2\right)^2\right]$$

$$= \frac{1}{N^2} E\left[\left(\sum \Delta A_i\right)^2 - \left\{\hat{A}_o - \ddot{A}_o\right\}\sum t_i^2 \sum \Delta A_i + \left(\frac{\hat{A}_o}{2} - \frac{\ddot{A}_o}{2}\right)^2 \left(\sum t_i^2\right)^2\right]$$

(IV-64)

The expected value of the numerator will be calculated term by term,

$$E\left[\left(\sum \Delta A_i\right)^2\right] = E\left[\sum \Delta A_i^2 + \sum_{\substack{i \\ i \neq j}} \sum_{j} \Delta A_i \Delta A_j\right] = \sum \sigma_A^2$$

$$= N \sigma_A^2 \qquad \text{where } N = 2M + 1 \tag{IV-65}$$

By using equations (IV-28), (IV-36), and (IV-39) the following relationship can be written

$$E\left[\left\{\hat{\ddot{A}}_o - \ddot{A}_o\right\} \sum t_i^2 \sum \Delta A_i\right] = E\left[2 \left\{ \frac{\sum A_i t_i^2 - \frac{\sum A_i \sum t_i^2}{N}}{\sum t_i^2 - \frac{\left(\sum t_i^2\right)^2}{N}} - \right.\right.$$

$$\left.\left. \frac{\sum t_i^2 \; E[A_i] - \frac{\sum E[A_i] \sum t_i^2}{N}}{\sum t_i^4 - \frac{\left(\sum t_i^2\right)^2}{N}} \right\} \sum t_i^2 \sum \Delta A_i \right]$$

$$= \frac{2 \sum t_i^2 \; E\left[\sum \Delta A_i t_i^2 - \frac{\sum \Delta A_i \sum t_i^2}{N}\right] \sum \Delta A_i}{\sum t_i^4 - \frac{\left(\sum t_i^2\right)^2}{N}} \tag{IV-66}$$

Making use of the relationships pointed out in equations (IV-48) and (IV-49):

$$E\left[\left\{\hat{\ddot{A}}_o - \ddot{A}_o\right\} \sum t_i^2 \sum \Delta A_i\right] -$$

$$= \frac{2 \sum t_i^2 \; E\left[\sum \Delta A_i^2 t_i^2 + \sum\sum \Delta A_i t_i^2 \Delta A_j - \frac{\sum t_i^2}{N}\left(\sum \Delta A_i^2 + \sum\sum \Delta A_i \Delta A_j\right)\right]}{\sum t_i^4 - \frac{\left(\sum t_i^2\right)^2}{N}}$$

$$= \frac{2 \sum t_i^2 \left[\sigma_A^2 \sum t_i^2 - \sum t_i^2 \sigma_A^2\right]}{\sum t_i^4 - \frac{\left(\sum t_i^2\right)^2}{N}} = 0$$

$$E\left[\left\{\frac{\hat{\ddot{A}}_o}{2} - \frac{\ddot{A}_o}{2}\right\}^2 \left(\sum t_i^2\right)^2\right] = E\left(\frac{\Delta\hat{\ddot{A}}_o}{2}\right)^2 \left(\sum t_i^2\right)^2 \quad \text{(IV-67)}$$

$$= \frac{1}{4}\sigma_{\ddot{A}_o}^2 \left(\sum t_i^2\right)^2 \quad \text{(IV-68)}$$

Substitution of equations (IV-65), IV-67), and (IV-68) into equation (IV-64) yields:

$$\sigma_{\hat{A}_o}^2 = \frac{1}{N^2}\left[N\sigma_A^2 + 0 + \frac{1}{4}\sigma_{\ddot{A}_o}^2 \left(\sum t_i^2\right)^2\right] \quad \text{(IV-69)}$$

Using equation (IV-62)

$$\sigma_{\hat{A}_o}^2 = \frac{1}{N^2}\left[N\sigma_A^2 + \frac{1}{4}\left(\frac{4\sigma_A^2}{\sum t_i^4 - \frac{\left(\sum t_i^2\right)^2}{N}}\right)\left(\sum t_i^2\right)^2\right]$$

$$= \frac{\sigma_A^2}{N} + \frac{\sigma_A^2\left(\sum t_i^2\right)^2}{N^2\left[\sum t_i^4 - \frac{\left(\sum t_i^2\right)^2}{N}\right]}$$

$$= \frac{\sigma_A^2 N\left[\sum t_i^4 - \frac{\left(\sum t_i^2\right)^2}{N}\right] + \sigma_A^2\left(\sum t_i^2\right)^2}{N^2\left[\sum t_i^4 - \frac{\left(\sum t_i^2\right)^2}{N}\right]} = \frac{\sigma_A^2 \sum t_i^4}{N\sum t_i^4 - \left(\sum t_i^2\right)^2}$$

$$\sigma_{\hat{A}_o}^2 = \frac{\sigma_A^2}{N - \frac{\left(\sum t_i^2\right)^2}{\sum t_i^4}} \quad \text{(IV-70)}$$

The last step in this portion of the analysis is to determine the covariances betwee the estimators.

The covariance between $\hat{\hat{A}}_o$ and $\dot{A}_o$ is defined by the following equation

$$\sigma^2_{\hat{\hat{A}}_o \dot{A}_o} = E\left[\left(\hat{\hat{A}}_o - E\left\{\hat{\hat{A}}_o\right\}\right)\left(\dot{A}_o - E\left\{\dot{A}_o\right\}\right)\right] \tag{IV-71}$$

Using equations (IV-28), (IV-36), (IV-26) and (IV-32) the following equation can be written

$$\sigma^2_{\hat{\hat{A}}_o \dot{A}_o} = E\left[\left(\frac{2\sum \Delta A_i t_i^2 - \frac{2}{N}\sum \Delta A_i \sum t_i^2}{\sum t_i^4 - \frac{\left(\sum t_i^2\right)^2}{N}}\right)\left(\frac{\sum \Delta A_i t_i}{\sum t_i^2}\right)\right] \tag{IV-72}$$

$$= \frac{2E\left[\sum \Delta A_i^2 t_i^3 + \sum\sum \Delta A_i t_i^2 \Delta A_j t_j - \frac{1}{N}\sum t_i^2\left(\sum \Delta A_i t_i + \sum\sum \Delta A_i \Delta A_j t_j\right)\right]}{\sum t_i^2\left[t_i^4 - \frac{\left(\sum t_i^2\right)^2}{N}\right]}$$

$$= \frac{2\sigma_A^2 \cancel{\sum t_i^3}^{\,0} - \frac{1}{N}\sum t_i^2 \sigma_A^2 \cancel{\sum t_i}^{\,0}}{\sum t_i^2\left[t_i^4 - \frac{\left(\sum t_i^2\right)^2}{N}\right]} = 0 \tag{IV-73}$$

The covariance between $\hat{\hat{A}}_o$ and $\hat{\dot{A}}$ is defined by the following equation

$$\sigma^2_{\hat{\dot{A}}_o \hat{\hat{A}}_o} = E\left[\left(\hat{\dot{A}}_o - E\left\{\hat{\dot{A}}_o\right\}\right)\left(\hat{\hat{A}}_o - E\left\{\hat{\hat{A}}_o\right\}\right)\right] \tag{IV-74}$$

Substitution of equations (IV-26), (IV-32), (IV-27) and (IV-41) into equation (IV-74) yields equation (IV-75).

$$\sigma^2_{\hat{\dot{A}}\,\hat{\hat{A}}_o} = E\left[\left(\frac{\sum \Delta A_i t_i}{\sum t_i^2}\right)\left(\frac{\sum \Delta A_i - \frac{\Delta \dot{A}_o}{2}\sum t_i^2}{N}\right)\right] \tag{IV-75}$$

$$= \frac{1}{N\sum t_i^2} E\left[\left(\sum \Delta A_i t_i\right)\left(\sum \Delta A_i\right) - \frac{\Delta \dot{A}_o}{2}\left(\sum t_i^2\right)\left(\sum \Delta A_i t_i\right)\right]$$

$$\sigma^2_{\hat{A}_o \hat{A}_o} = \frac{1}{N \sum t_i^2} E\left[\sum \Delta A_i^2 t_i + \sum\sum \Delta A_i t_i \Delta A_j\right]$$

$$- \frac{\sum t_i^2}{2} E\left[\Delta \ddot{A}_i \sum \Delta A_i t_i\right] \qquad \text{(IV-76}$$

Since $\Delta \ddot{A}_o$ is defined as $\hat{\ddot{A}}_o - E\{\hat{\ddot{A}}_o\}$ it can be seen that the second bracketed equation (IV-76) has already been proven equal to zero. See equations (IV-71) through (IV-73)

$$\sigma^2_{\hat{A}_o \hat{A}_o} = \frac{1}{N \sum t_i^2} \sigma_A^2 \sum t_i \to 0$$

$$\sigma^2_{\hat{A}_o \hat{A}} = 0 \qquad \text{(IV-77}$$

Similarly the covariance between $\hat{\ddot{A}}_o$ and $\hat{A}_o$ can be determined

$$\sigma^2_{\hat{A}_o \hat{\ddot{A}}_o} = E\left[\left(\hat{A}_o - E\{\hat{A}_o\}\right)\left(\hat{\ddot{A}}_o - E\{\hat{\ddot{A}}_o\}\right)\right] \qquad \text{(IV-78}$$

Substitution of equations (IV-27) and (IV-41) into equation (IV-78) yields:

$$\sigma^2_{\hat{A}_o \hat{\ddot{A}}_o} = E\left[\left(\frac{\sum \Delta A_i - \frac{\hat{\ddot{A}}_o}{2} \sum t_i^2}{N}\right)\left(\Delta \hat{\ddot{A}}_o\right)\right]$$

$$= \frac{1}{N} E\left[\Delta \hat{\ddot{A}}_o \sum \Delta A_i - \frac{1}{2} (\Delta \hat{\ddot{A}}_o)^2 \sum t_i^2\right]$$

$$= \frac{1}{N} E\left[\Delta \hat{\ddot{A}}_o \sum \Delta A_i\right] - \frac{1}{2N} \sum t_i^2 \sigma^2_{\hat{\ddot{A}}_o} \qquad \text{(IV-79}$$

Since $\Delta \hat{\ddot{A}}_o$ is defined as $\hat{\ddot{A}}_o - E\left[\hat{\ddot{A}}_o\right]$, the following equation can be written, usi equations (IV-36) and (IV-28)

$$E\left[\Delta \hat{\ddot{A}}_o \sum \Delta A_i\right] = E\left[\left(\frac{2 \sum \Delta A_i t_i^2 - \frac{2}{N} \sum \Delta A_j \sum t_i^2}{\sum t_i^4 - \frac{\left(\sum t_i^2\right)^2}{N}}\right) \sum \Delta A_i\right]$$

The relationships shown in equations (IV-48) and (IV-49) are again useful

$$E\left[\Delta \hat{\dot{A}}_o \sum \Delta A_i\right] =$$

$$E\left[\frac{2\sum \Delta A_i^2 t_i^2 + 2\sum\sum \Delta A_i t_i^2 \Delta A_j - \frac{2}{N}\sum \Delta A_i^2 \sum t_i^2 - \frac{2}{N}\sum t_i^2 \sum\sum \Delta A_i \Delta A_j}{\sum t_i^4 - \frac{\left(\sum t_i^2\right)^2}{N}}\right]$$

$$- \frac{2\sigma_A^2 \sum t_i^2 - \frac{2N\sigma_A^2}{N}\sum t_i^2}{\sum t_i^4 - \frac{\left(\sum t_i^2\right)^2}{N}}$$

$$E\left[\Delta\hat{\dot{A}}_o \sum \Delta A_i\right] = 0 \qquad \text{(IV-80)}$$

Equation (IV-79) can now be written as

$$\sigma_{\hat{A}_o \hat{\dot{A}}_o}^2 = \frac{\sum t_i^2 \sigma_{\hat{A}_o}^2}{2N} \qquad \text{(IV-81)}$$

Combining equations (IV-62) and (IV-81) yields:

$$\sigma_{\hat{A}_o \hat{\dot{A}}_o}^2 = -\frac{1}{2N}\sum t_i^2 \frac{4\sigma_A^2}{\sum t_i^4 - \frac{\left(\sum t_i^2\right)^2}{N}}$$

$$\sigma_{\hat{A}_o \hat{\dot{A}}_o}^2 = \frac{-\frac{2}{N}\sigma_A^2 \sum t_i^2}{\sum t_i^4 - \frac{\left(\sum t_i^2\right)^2}{N}} \qquad \text{(IV-82)}$$

All of the useful results will be repeated below and simplified using the closed expressions given by equations (IV-18) through (IV-22). In the following expressions,

$$S = \frac{M(M+1)(2M+1)}{6} = \sum_{i=0}^{M} i^2 \qquad \text{(IV-83)}$$

$$F = \frac{M\,(M+1)\,(2M+1)\,(3M^2+3M-1)}{30} = \sum_{i=0}^{M} i^4 \qquad \text{(IV-84)}$$

$M = \frac{N-1}{2}$ where N = Total number of observations

$$\sigma^2_{\hat{\hat{A}}_o} = \frac{4\sigma_A^2}{\sum_{i=-M}^{M} t_i^4 - \left(\sum_{i=-M}^{M} t_i^2\right)^2 / N}$$

$$\sigma^2_{\hat{\hat{A}}_o} = \frac{4\sigma_A^2}{2\Delta t^4 \sum_{i=0}^{M} i^4 - 4\,\Delta t^4 \left(\sum_{i=0}^{M} i^2\right)^2 / N} = \frac{2\,\sigma_A^2}{\Delta t^4 \left[\sum_{i=0}^{M} i^4 - \frac{2}{N}\left(\sum_{i=0}^{M} i^2\right)^2\right]} \qquad \text{(IV-8}$$

$$\sigma^2_{\hat{A}_o} = \frac{\sigma_A^2}{\sum_{i=-M}^{M} t_i^2} = \frac{\sigma_A^2}{2\,\Delta t^2 \sum_{i=0}^{M} i^2} \qquad \text{(IV-86)}$$

$$\sigma^2_{\hat{\hat{A}}_o} = \frac{\sigma_A^2}{N - \left(\sum_{i=-M}^{M} t_i^2\right)^2 / \sum_{i=-M}^{M} t_i^4} = \frac{\sigma_A^2}{N - 4\Delta t^4 \left(\sum_{i=0}^{M} i^2\right)^2 / 2\,\Delta t^4 \sum_{i=0}^{M} i^4}$$

$$\sigma^2_{\hat{A}_o} = \frac{\sigma_A^2}{N - \dfrac{2\left(\sum_{i=0}^{M} i^2\right)^2}{\sum_{i=0}^{M} i^4}} \qquad \text{(IV-87)}$$

$$\sigma^2_{\hat{\hat{A}}_o \hat{A}_o} = 0 \qquad \text{(IV-88)}$$

$$\sigma^2_{\hat{A}_o \hat{\hat{A}}_o} = 0 \qquad \text{(IV-89)}$$

$$\sigma^2_{\hat{A}_o \hat{\dot{A}}_o} = \frac{-\frac{2}{N}\sigma_A^2 \sum_{i=-M}^{M} t_i^2}{\sum_{i=-M}^{M} t_i^4 - \frac{\left(\sum_{i=-M}^{M} t_i^2\right)^2}{N}} = \frac{-\frac{2}{N}\sigma_A^2 \, 2\Delta t^2 \sum_{i=0}^{M} i^2}{2\Delta t^4 \sum_{i=0}^{M} i^4 - \frac{4\Delta t^4 \left(\sum_{i=0}^{M} i^2\right)^2}{N}}$$

$$\sigma_{\hat{A}_o \hat{\dot{A}}_o} = \frac{-2\sigma_A^2 \sum_{i=0}^{M} i^2}{N\Delta t^2 \sum_{i=0}^{M} i^4 - 2\Delta t^2 \left(\sum_{i=0}^{M} i^2\right)^2} \qquad \text{(IV-90)}$$

APPENDIX V. EQUATIONS FOR $\Delta \hat{A}$ AND $\Delta \hat{\hat{A}}$

During the error simulation procedure, it is desirable to take two random numbers from the random number generator (Z_1 and Z_2) and produce two gaussian variables X_1 and X_2 which have the following statistical characteristics.

$$E[X_1] = E[X_2] = 0 \qquad \text{Zero means} \qquad \text{(V-1)}$$

$$E[(X_1)^2] = \sigma_{X_1}^2 \qquad \text{(V-2)}$$

$$E[(X_2)] = \sigma_{X_2}^2 \qquad \text{(V-3)}$$

$$E[(X_1)(X_2)] = \sigma_{X_1 X_2}^2 \qquad \text{(V-4)}$$

The random number generator produces independent numbers from a zero mean, unity variance, gaussian distribution.

i.e.

$$E[Z_1] = E[Z_2] = 0 \qquad \text{(V-5)}$$

$$E[(Z_1)^2] = E[(Z_2)^2] = 1 \qquad \text{(V-6)}$$

$$E[(Z_1)(Z_2)] = 0 \qquad \text{(V-7)}$$

It is easier to solve this problem by using a little reverse thinking. Assume the X variables are known and the uncorrelated unity variance Z variables are desired. The following linear transformation proves to be convenient.

Let:

$$Y_1 = X_1 \cos\theta + X_2 \sin\theta \qquad \text{(V-8)}$$

$$Y_2 = -X_1 \sin\theta + X_2 \cos\theta \qquad \text{(V-9)}$$

where θ is a constant to be defined

Since X_1 and X_2 have zero means, Y_1 and Y_2 also have zero means. The variances on Y_1 and Y_2 will now be calculated

$$\sigma_{Y_1}^2 = E[(Y_1)^2] \quad E[X_1^2 \cos^2\theta + 2X_1X_2 \sin\theta\cos\theta + X_2^2 \sin^2\theta] \qquad \text{(V-10)}$$

Since θ is a constant, equation (V-10) reduces to

$$\sigma_{Y_1}^2 = \sigma_{X_1}^2 \cos^2\theta + 2\sigma_{X_1X_2}^2 \sin\theta\cos\theta + \sigma_{X_2}^2 \sin^2\theta \qquad \text{(V-11)}$$

$$\sigma_{Y_2}^2 \quad E[(Y_2)^2] = E[X_1^2 \sin^2\theta - 2X_1X_2 \sin\theta\cos\theta + X_2^2 \cos^2\theta]$$

$$\sigma_{Y_2}^2 = \sigma_{X_1}^2 \sin^2\theta - 2\sigma_{X_1X_2}^2 \sin\theta\cos\theta + \sigma_{X_2}^2 \cos^2\theta \qquad \text{(V-12)}$$

The covariance between Y_1 and Y_2 is defined by the following equation

$$\sigma_{Y_1Y_2}^2 = E[(Y_1)(Y_2)] - [(X_1\cos\theta + X_2\sin\theta)(-X_1\sin\theta + X_2\cos\theta)] \qquad \text{(V-13)}$$

Expansion of equation (V-13) and treatment of θ as a constant yields

$$\sigma_{Y_1Y_2}^2 = -\sigma_{X_1}^2 \sin\theta\cos\theta + \sigma_{X_1X_2}^2 (\cos^2\theta - \sin^2\theta) + \sigma_{X_2}^2 \sin\theta\cos\theta$$

$$= \sin\theta\cos\theta\,(\sigma_{X_2}^2 - \sigma_{X_1}^2) + \sigma_{X_1X_2}(\cos^2\theta - \sin^2\theta) \qquad \text{(V-14)}$$

The following trigonometric identities will simplify equation (V-14)

$$\frac{\sin 2\theta}{2} = \sin\theta\cos\theta \qquad \text{(V-15)}$$

$$\cos 2\theta = \cos^2\theta - \sin^2\theta \qquad \text{(V-16)}$$

$$\sigma_{Y_1Y_2}^2 = \frac{\sin 2\theta}{2}(\sigma_{X_2}^2 - \sigma_{X_1}^2) + \sigma_{X_1X_2}^2 \cos 2\theta \qquad \text{(V-17)}$$

By setting $\sigma_{Y_1Y_2}^2$ equal to zero, the desirable value for θ can be determined

$$\frac{\sin 2\theta}{\cos 2\theta} = \tan 2\theta = \frac{-2\sigma_{X_1X_2}^2}{\sigma_{X_2}^2 - \sigma_{X_1}^2} \qquad \text{(V-18)}$$

$$\theta = 1/2 \tan^{-1}\left[\frac{2\sigma_{X_1X_2}^2}{\sigma_{X_1}^2 - \sigma_{X_2}^2}\right] \qquad \text{(V-19)}$$

When θ takes on the value shown in equation (V-19), the Y quantities are not correlated ($\sigma_{Y_1Y_2}^2 = 0$). The following equations define Z variables which have unity variance and zero covariance.

$$Z_1 = Y_1/\sigma Y_1 \qquad \text{(V-20)}$$

$$Z_2 = Y_2/\sigma Y_2 \qquad \text{(V-21)}$$

It now remains to show that Z_1 and Z_2 have the desired characteristics

$$\sigma_{Z_1}^2 = E[(Z_1)^2] = E[(Y_1/\sigma_{Y_1})^2] = (1/\sigma_{Y_1})^2\, E[(Y_1)^2]$$

$$\sigma_{Z_1}^2 = 1 \qquad \text{(V-22)}$$

$$\sigma_{Z_2}^2 = E[(Z_2)^2] = E[(Y_2/\sigma_{Y_2})^2] \quad (1/\sigma_{Y_2})^2\, E[(Y_1)^2]$$

$$\sigma_{Z_2}^2 = 1 \qquad \text{(V-23)}$$

$$\sigma_{Z_1Z_2}{}^2 = E[(Z_1)(Z_2)] = E[(Y_1/\sigma_{Y_1})(Y_2/\sigma_{Y_2})]$$

$$= 1/\sigma_{Y_1}{}^2\sigma_{Y_2}{}^2 \; E[(Y_1)(Y_2)] = \sigma_{Y_1Y_2}{}^2/\sigma_{Y_1}{}^2\sigma_{Y_2}{}^2 \qquad \text{(V-24)}$$

$$= 0 \qquad \text{when } \theta = 1/2 \tan^{-1}[2\sigma_{X_1X_2}{}^2/\sigma_{X_1}{}^2 - \sigma_{X_2}{}^2]$$

The original problem has now been solved and it is possible to produce the correlated gaussian variables X_1 and X_2 from the uncorrelated unity variance variables Z_1 and Z_2.

In summary,

(1) Specifications:

$$E[(X_1)^2] = \sigma_{X_1}{}^2$$

$$E[(X_2)^2] = \sigma_{X_2}{}^2$$

$$E[(X_1)(X_2)] = \sigma_{X_1X_2}{}^2$$

(2) Numbers from the random number generator:

$$Z_1$$

$$Z_2$$

(3) Calculate

$$\theta = 1/2 \tan^{-1}[2\sigma_{X_1X_2}{}^2/\sigma_{X_1}{}^2 - \sigma_{X_2}{}^2]$$

$$\sigma_{Y_1}{}^2 = \sigma_{X_1}{}^2\cos^2\theta + 2\sigma_{X_1X_2}{}^2\sin\theta\cos\theta + \sigma_{X_2}{}^2\sin^2\theta$$

$$\sigma_{Y_2}{}^2 = \sigma_{X_1}{}^2\sin^2\theta - 2\sigma_{X_1X_2}{}^2\sin\theta\cos\theta + \sigma_{X_2}{}^2\cos^2\theta$$

$$Y_1 = \sigma_{Y_1}Z_1$$

$$Y_2 = \sigma_{Y_2}Z_2$$

$$X_1 = Y_1\cos\theta - Y_2\sin\theta$$

$$X_2 = Y_1\sin\theta + Y_2\cos\theta$$

The quantities X_1 and X_2 have the specified statistical characteristics.

Phone: STerling 3-4100

VOLUNTEER SATELLITE TRACKING PROGRAM
824 Connecticut Avenue
Washington 6, D. C.

PHOTOTRACK BULLETIN

30 March, 1961

SATELLITE BRIGHTNESS VALUES

One of the many properties of the stars of interest to astronomers is brightness. It is traditional among astronomers to express such brightness in terms of magnitude. The brightest of the fixed stars are said to be of first magnitude, those one hundred times fainter are said to be of fifth magnitude, and those one hundred times fainter still are said to be of tenth magnitude. Such a scale in effect classifies stars in accordance with the logarithm of the stimulus they produce. Such a scale is useful because both the human eye and photographic emulsions respond proportionally to the logarithm of the stimulus. Note that the magnitude numbers get larger as the objects get fainter. This means that it is an inverse scale, and that we must write:

$$\Delta m = -2.5(\log_{10} b/b')$$

where Δm is difference in magnitude, and b and b' are brightnesses being compared.

COMPUTING SATELLITE BRIGHTNESS

While there are many more factors that may affect satellite brightness, satisfactory values of computed magnitude (m_c) may be had by taking only four into account. They are:

m_n Nominal brightness under standard conditions;

Δm_r Brightness difference on account of range;

Δm_e Brightness difference on account of elongation (phase); and,

Δm_a Brightness difference on account of altitude above the horizon.

For standard atmospheric conditions, the following formula yields a precise value of computed magnitude in the case of a diffusely reflecting sphere whose nominal magnitude or brightness under standard viewing conditions is m_n:

$$m_c = m_n + \Delta m_r + \Delta m_e + \Delta m_a$$

obtained nevertheless agree remarkably well with values of observed magnitude (m_o).

Taking mean values of observed magnitude (m_o) for twelve satellites of different size, shape and surface, Gustav A. Bakos, Staff Astronomer at Moonwatch Headquarters has made comparisons with computed magnitude (m_c) in which he used values of nominal magnitude (m_n) that were in effect obtained as follows:

1/ Lambert's law governing the brightness of diffuse reflectors was assumed to hold;

2/ Maximum and minimum values for irregularly shaped satellites were obtained by considering two objects of standard diffuse reflectivity, one with a projected area equal to the maximum of that of the satellite, and the other equal to the minimum; and,

3/ At a range of 1000 statute miles, 180° elongation, and 90° altitude above the horizon, one square inch of projected area of standard reflectivity was assumed to have a brightness of magnitude 15.40.

The agreement between values of m_c and mean values of m_o reported by Bakos in Special Bulletin No. 53 (moonwatch) is certainly satisfactory for prediction purposes, and recommends the technique both to visual and to photographic observers.

PUBLICATION OF VALUES FOR NOMINAL BRIGHTNESS (m_n)

FUTURE MODIFIED ORBITAL ELEMENT ANNOUNCEMENT CARDS WILL CARRY MAXIMUM AND MINIMUM VALUES OF NOMINAL BRIGHTNESS (m_n) BASED UPON THE ABOVE CRITERIA.

Thus in the case of 1959 Eta-1, the expression: $m_n = 7.6/11.8$ is understood to indicate a maximum nominal brightness of magnitude 7.6 and a minimum of magnitude 11.8. Such values may be used with correction values from the graphs appearing on the back of this bulletin which were drawn by Donald C. Lokerson, or with the tables in the Moonwatch Bulletin.

DESCRIPTION OF GRAPHS AND THEIR USE

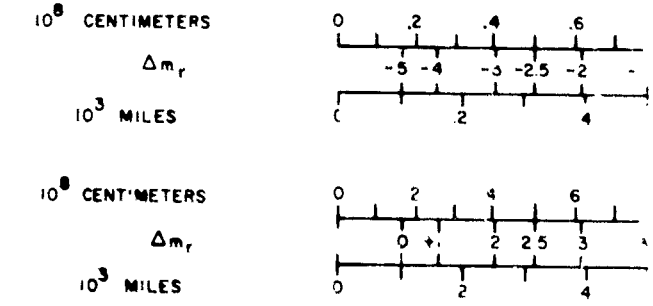
Magnitude Versus Slant Range: These graphs give corrections to values of m_n that are based upon a slant range of 1000 statute miles. They show how satellite brightness varies inversely with the square of the distance to the observer, and may be entered either in terms of statute miles or kilometers.

Magnitude Versus Elongation: Elongation is defined as the angle measured at the observer's position between a line to the source of illumination (sun) and a line to the object illuminated (satellite). In the case of a spherical diffuse reflector, the phase (portion of the visible disk that is illuminated) is equal to $(1 - \cos e)/2$. In such case, brightness varies directly with phase. The range of elongation angles normally encountered in satellite observation runs between 130° and 50°, and the average is around 90°. Computation of exact values of elongation are somewhat involved. Arrangements have been made, however, for entering the graph in terms of the equivalent phase of the moon, if it were in the same position predicted for the artificial satellite. Satisfactory estimates may be made by considering the civil time of the predicted pass, and whether it will be to the east or the west of the observer.

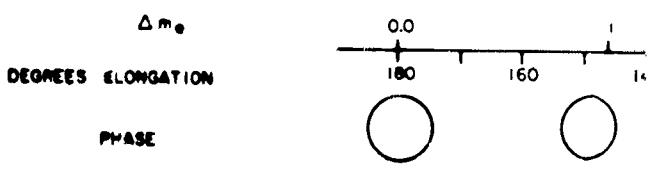
Atmospheric Extinction: The amount of atmosphere through which light from the satellite must pass in reaching an observer on the earth's surface depends upon the satellite's altitude above the observer's horizon. This table assumes that where the altitude (a) is 30°, Δm_a for photographic emulsions is + 0.3, and that the path length varies as the cosecant of a. The graph may be entered in terms of either altitude or zenith distance. Bear in mind that under poor "seeing" conditions, the deterioration in magnitude near the horizon will be much more severe than that indicated in the graph.

Best Available Copy

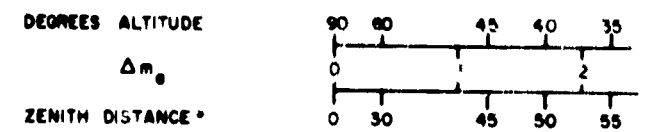
MAGNITUDE VERSUS



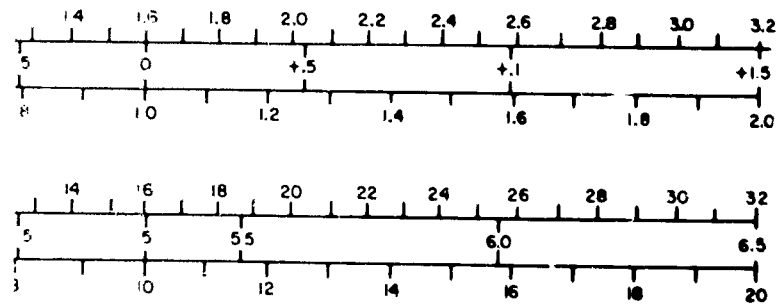
MAGNITUDE VERSUS



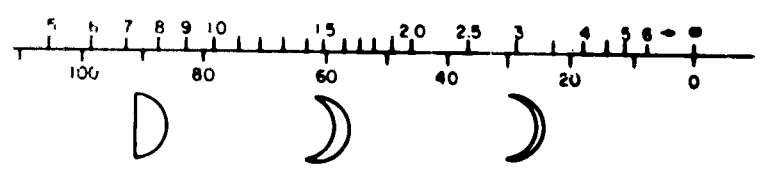
ATMOSPHERIC



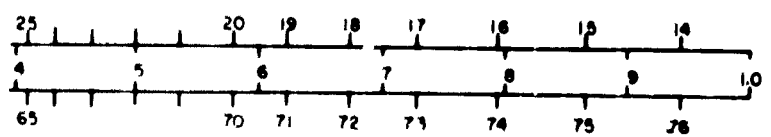
E $\Delta m_r = 5\text{LOG}(R/1000\ s/m)$
where R = slant range in s/m



N $\Delta m_\theta = -2.5\,\text{LOG}\left(\frac{1+\cos e}{2}\right)$
where e elongation



V $\Delta m_a = 0.3\ \frac{0.3}{\sin\theta}$ where θ = altitude



APPENDIX VII. CLEAR WEATHER FREQUENCY (NIGHTIME) FOR UPSTATE NEW YORK

PURPOSE: To establish a basis for estimating the percentage of clear nightime hours useable for electro-optical experiments.

ANALYSIS: The Decennial Census of U.S. Climate - Summary of hourly Observation for Syracuse and Albany for 1951-1960 issued by the U.S. Weather Bureau are used for basic data. In addition the following conditions are assumed or imposed:

1. That the 0 to .3 cloud cover represents a relative measure of "clear" weather.

2. That the "night" hours considered begin following evening twilight through to beginning of morning twilight (sun 18° below horizon) approximately 1 hour after sunset to 1 hour before sunrise.

3. That the moon phase is not a factor either as effects weather or the use of the available "clear" nights - i.e., some loss of electro-optical operating time and/or useable sky area must be considered if a "dark" clear sky is needed. On the other hand experiments involving the moon or bright sky work can be scheduled to make the most of available "clear" weather.

4. That there is assumed good correlation between hourly readings, i.e., weather doesn't change too quickly on the average.

5. That the data is basically pessimistic if we plan to use only that sky area 30° or more above horizon, i.e., the 0-30° horizon ring can be cloudy or hazy without interference to "clear night" operation, but no distinction is made in the data recorded.

DATA: The following data is extracted or processed from the referenced [redacted].

Percent (Frequency) "Clear" Weather (0 - .3 Cloud Cover)

SYRACUSE	(1) 24 hour average %	(2) Dark hour average %	(3) Approximate darkness hours	(4) Equivalent hours
January	.16	.18	10.5	1.89
February	.19	.21	9.5	2.00
March	.24	.29	8.25	2.40
April	.28	.32	6.5	2.14
May	.33	.43	5.25	2.26
June	.37	.48	4.67	2.24
July	.40	.52	4.67	2.44
August	.39	.48	6	2.88
September	.40	.49	7.5	3.68
October	.36	.41	9.0	3.69
November	.19	.23	10.25	2.36
December	.14	.17	11.25	1.91
			12 | 93.34	12 | 29.89
			7.77hours	2.5 hours
ALBANY				
January	.27	.29	10.5	3.04
February	.29	.34	9.5	3.23
March	.27	.30	8.25	2.48
April	.27	.32	6.5	2.08
May	.29	.33	5.25	2.00
June	.29	.48	4.67	2.23
July	.34	.47	4.67	2.19
August	.36	.44	6	2.62
September	.38	.46	7.5	3.44
October	.38	.44	9.0	3.95
November	.26	.31	10.25	3.18
December	.25	.29	11.25	3.26
			12 | 93.34	12 | 33.70
			7.77hours	2.80hours

DISCUSSION:

1. Column (1) gives the 24 hour monthly average percent Frequency of clear weather (0 to .3 cloud cover) direct for weather bureau data.

   Column (2) gives the dark hour average percent Frequency of clear weather (0 to .3 cloud cover) which is obtained by averaging the hourly observations for only the "dark hours" as defined in the analysis. Note the "improved" or higher percentages for dark hour "clear" weather vs the 24 hour averages.

   Column (3) gives approximate length of "dark hour" period (it is selected for the shortest period occurring in the given month, not the average for the month; thus, the relatively low yearly average (7.7 hours).

   Column (4) gives the equivalent usable hours for observation work per month that is the product of the "dark period" (3) and the percent Frequency of clear night weather (2).

2. Figures AVII-1 and AVII-2 are plots of the equivalent usable hours of clear weather by month; Column (4).

3. A practical check based on the experience at the G.E. Photoelectric Observation near Schenectady shows approximately 50% of nights from August 5 through September 15 to have been good nights. This checks well with the data as analyzed.

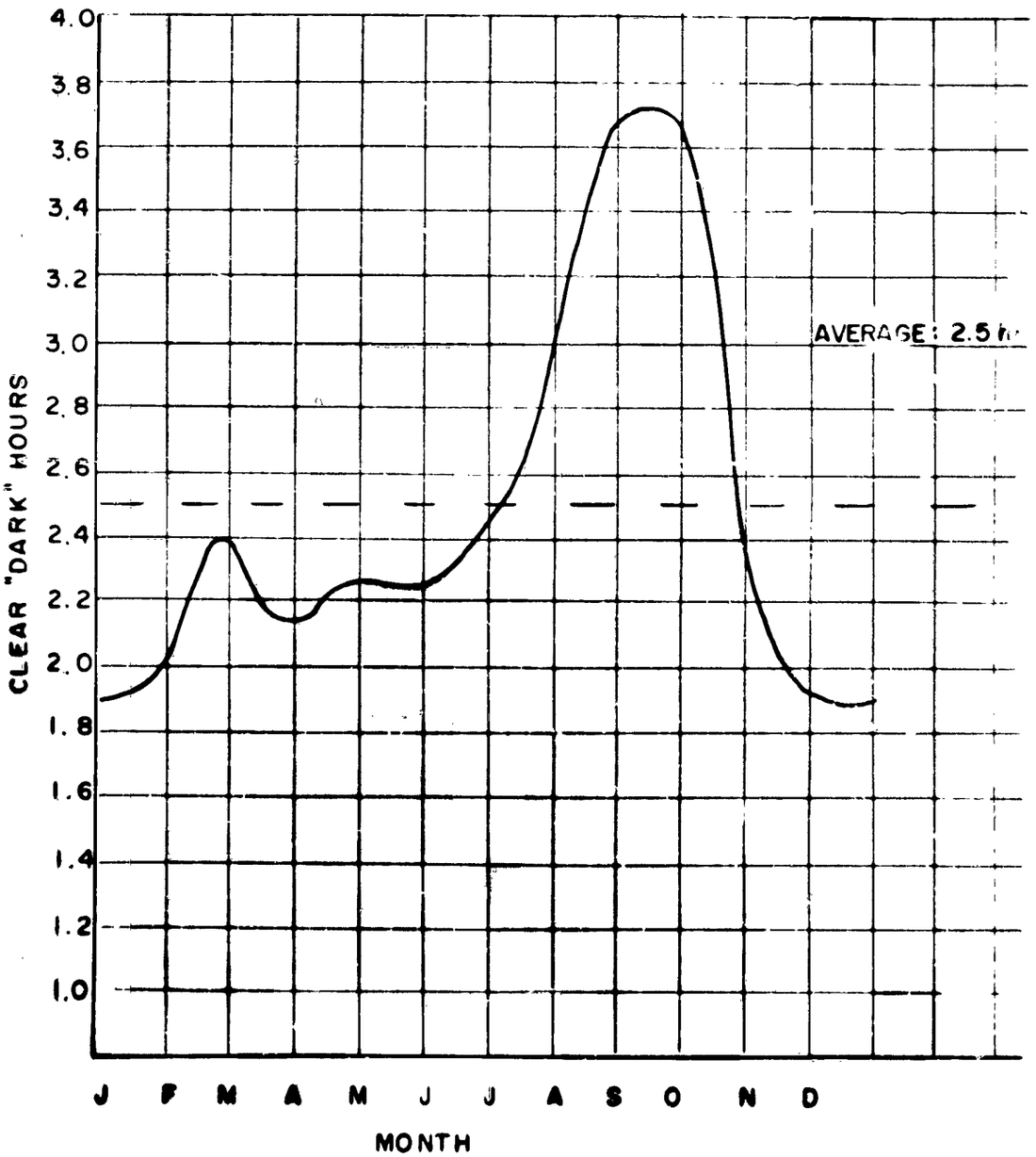


Figure VII-1. Equivalent "Dark Hours" 10 Year Average, Syracuse, N.Y.

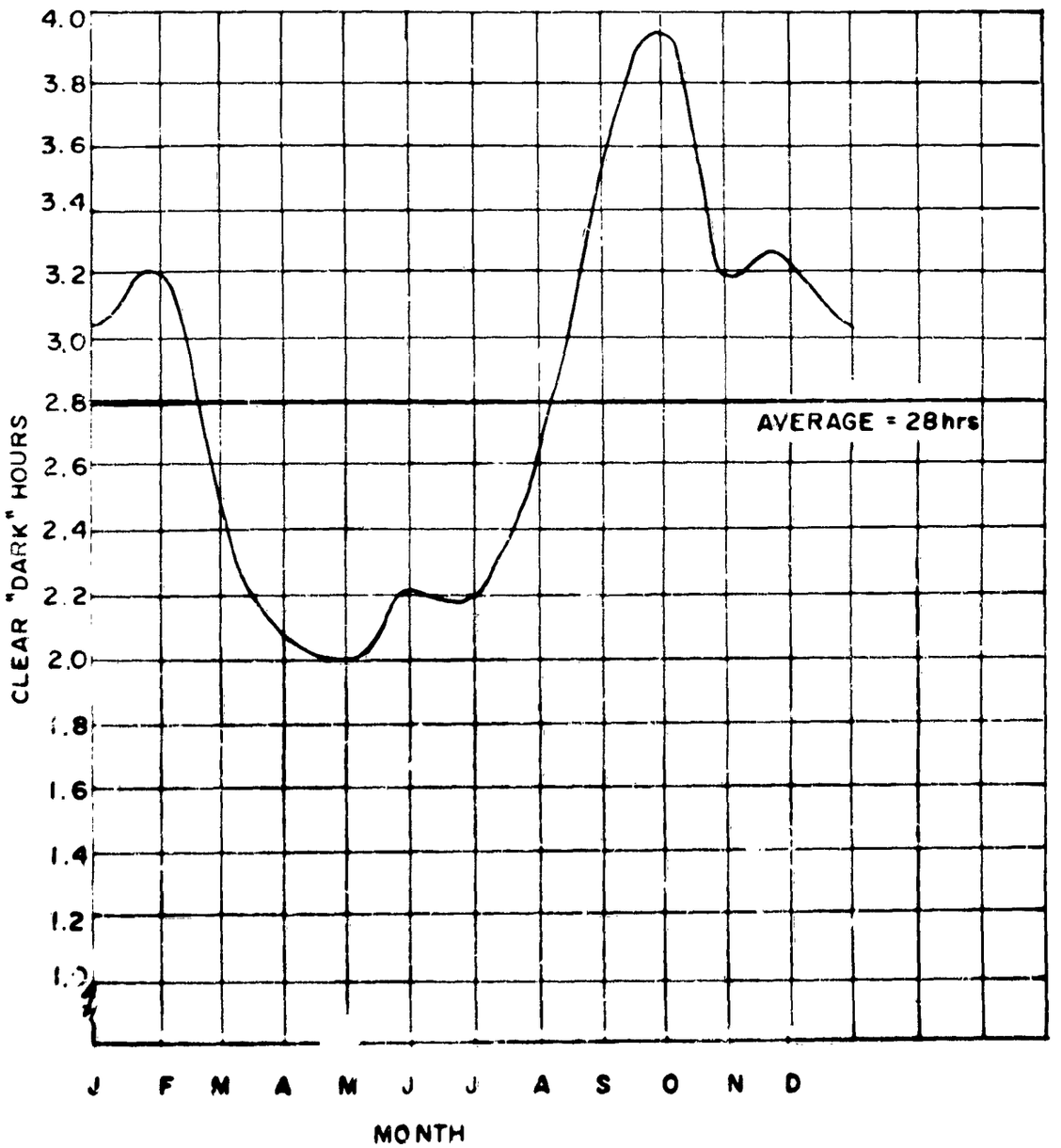


Figure VII-2. Equivalent "Dark" Hours 10 Year Average, Albany, N.Y.

GLOSSARY OF SYMBOLS, TERMS, INCLUDING CONVERSION FACTORS

SYMBOLS AND TERMS	DEFINITION	COMMON UNITS USED
Astrophysical Terms	See also Section I	
$I_{(n)}$ Intensity or Luminous Flux	The brightness or intensity of an object - subscript designating order O-1 etc -- n	magnitude (stellar), etc. candle power
$I_{(\lambda)}$ Spectral Intensity	Spectral Intensity at a given length (λ)	
m Intensity Ratio in terms of magnitude (stellar)	The ratio of Intensity sources in terms of the exponent of $5\sqrt{100}$ (stellar magnitude change) or $I_x/I_y = 10^{0.4m}$	dimensionless
m_v Visual Intensity Ratio (magnitude differences)	The stellar magnitude difference of visual sources	dimensionless
(n)m Apparent Magnitude (star, body, etc.)	The value of the object of n^{th} magnitude with reference of 0 magnitude (stellar) $0m_v = 10^6$ photons/cm^2/sec; $15m_v$=1 photon/cm^2/sec, etc.	magnitude (stellar)
(n)m_{pg} photographic magnitude (apparent)	The specific value of brightness of an n^{th} magnitude source in terms of astronomical film type 103a-O/Spectrum response - peak at 3500Å	magnitude (stellar) sometimes specific value expressed in No. of 10th magnitude stars per $\widehat{degree^2}$
(n)m_{pv} photovisual magnitude (apparent)	The specific value of brightness of an n^{th} magnitude source in terms of the eye response - peaks at 5600Å normal or at 5200Å for dark adapted	magnitude (stellar)
(n)m_{bol} bolometric magnitude (apparent)	The specific value of brightness in terms of the bolometric response curve (black body)	magnitude (stellar)

SYMBOLS AND TERMS	DEFINITION	COMMON UNITS USED
M Absolute Magnitude	Magnitude of a given star if placed at the standard distance of 10 parsecs = 32.62 light years	magnitude (stellar)
AU Mean Astronomical Unit	Means Earth-Sun distance; 93,000,000 miles = 1.4960×10^{13}cm = 499.01 light secs.	Astronomical Unit
ly light year	Distance equivalent to the propagation velocity of light integrated for a mean solar year = 9.4605×10^{17}cm = 6.324×10^{4} AU = 1/3.262 parsecs	light years
pc parsec (parallax distance)	Distance from earth at which the earth's diameter subtends an arc of one second. Thus, the distance of a star having a parallax of one second.	parsec = 3.262 ly
LO Solar Radiation	Radiation of the Sun 3.86×10^{33} ergs/sec	LO or ergs/sec
Star $M_{bol} = 0$ Star Radiation	2.72×10^{28} watts	M_{bol} (bolometric Stellar Magnitude) or watts
Celestial Equator	Extension (intersection) of a plane through the earth's equator on the heavens (celestial sphere)	
Celestial Sphere	The imaginary sphere of the heavens about the earth with the celestial equator opposite earth's equator and celestial poles at extension of earth's north and south geographic poles	
Celestial Meridian (hour circle)	Imaginary line running from pole to pole through location of an object on the celestial sphere (similar to meridian of longitude on earth)	
d, δ declination	The angle of an object above (+) or below (-) the celestial equator measured along the object's hour circle (celestial meridian of object) similar to latitude on earth	$\overset{\frown}{\text{degrees}}$ & $\overset{\frown}{\text{mins}}$.
a, RA, α Right Ascension	The angle of an object's position, (foot of hour circle) (celestial meridian of object) with respect to the first point of Aries (Vernal Equinox) in time from 0 to 24 hours. in the eastwards direction along the celestial equator	hrs. min, sec. of time at earth's rotation rate

SYMBOLS AND TERMS	DEFINITION	COMMON UNITS USED
Ecliptic	The path of the sun projected on the Celestial Sphere	
Galactic Equator	Extension (intersection) of the plane of our Galaxy (the Milky Way) on the heavens	
l Galactic longitude	The angle of an object's galactic meridian measured along the galactic equator from the galactic center. The S-N crossing of the Galactic Equator by the Celestial Equator	hour angle or degrees 1 hr. = 15°
b Galactic altitude	The angle of an object above (+) or below (-) the Galactic Equator (the plane of the Milky Way) along its Galactic Meridian Galactic Pole 191.3° RA27.7° δ Galactic Center 327.9°l - 1.3°b or 265° RA and -29° δ	
λ wavelength	The distance between two similar and successive points on an alternating wave. (m) $300{,}000/f_{(kc)}$	Angstroms, microns cm, meters
Å Angstrom	Unit of wavelength 10000Å 1 micron (μ) 1Å = 10^{-8} cm	Angstrom
Sec., min. Second, Minute	Units of time	seconds, minutes of time
$\overset{\frown}{\text{Sec.}}$, $\overset{\frown}{\text{Sec}}^2$ second(s) (2) $\overset{\frown}{\text{min.}}$, $\overset{\frown}{\text{min}}^2$ minute(s) (2)	Units of angle or arc or angle area	$\overset{\frown}{\text{seconds}}$, $\overset{\frown}{\text{minutes}}$ of arc
c/i Color Index	The difference in stellar magnitudes between photographic and photovisual magnitude $c/i = (m_{pg} - m_{pv})$	

Photometric Terms, Etc. **See also Section I**

I Intensity	Candle power of a point source of light	candle (cd) or lumens/ steradian
F Luminous Flux	Rate of flow of radiant energy	lumen (lm)
B Brightness Luminance	Luminous Intensity of a surface	candles/cm^2 (stilbs) candles/in^2 candles/ft^2 lamberts and foot lamberts

SYMBOLS AND TERMS	DEFINITION	COMMON UNITS USED
E Illuminance	Luminous flux density at a surface	lumens/ft^2 (foot candles) lumens/cm^2 (phot lumens/m^2 (lux) see p I-10
A Area	Area of a surface	in.^{2}, ft.^{2}, cm^2, m^2
r distance radius	Separation distance, radius	in., ft., miles, cm, m, km
θ Angle angle of normal from source	An angle or angle between normal and source of illumination, etc.	degrees, mins, secs.
Q Quantity of Light Luminous Energy	Integration of luminous flux (F) per time. $Q = \int F\,dt$	lumerg: Talbot lumen - sec lumen - hours
L Luminance or Luminance Emittance	Emission of light from a source; present usage combines Luminance with Brightness. Leaving L for Luminance Emittance L = F/A = B	lambert = 1/π c. dles/cm^2 ft lambert
R, ρ Reflectance	Reflectivity of a surface ratio of Brightness and Illuminance B/E = R	dimensionless
f or f/no lens, speed stop	Lens speed or ratio of Diameter to Focal Length	
D, d Diameter Lens, etc. Aperture size	Lens (aperture) diameter diameter etc.	inches cm
FL Focal Length	The location distance of primary image of a lens with object at infinity	inches, cm

For table of conversion of photometric limits see Section I

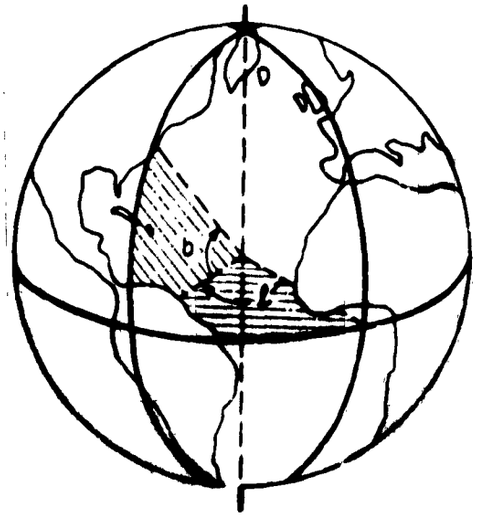
A. COORDINATE SYSTEMS

Positions of objects with respect to an observer on earth can be expressed in many coordinate systems. The selection is dependent on the parameters of the task at hand. For instance: for terrestrial positions, Latitude and Longitude are used to define locations with azimuth and elevation used to describe look angles from observer's position. For celestial objects, Right Ascension and Declination are used to define celestial position. (In astronomy galactic coordinates are also used.)

Since satellite surveillance systems are concerned with celestial motions and background, it may be convenient to orient the equipment so as to follow celestial motion rather than use the more conventional azimuth-elevation axis. Though Right Ascension and Declination position, and equatorial mounts are quite familiar to astronomers, a few descriptive diagrams may be appreciated by engineers accustomed to azimuth-elevation axis equipment.

1. COORDINATES ON THE EARTH: - LATITUDE AND LONGITUDE

By international agreement the meridian passing through Greenwich, England is the prime meridian (0°), the reference from which the Longitude or terrestrial angle to the meridian of the observer's location is measured, either east or west to 180° (to the international date line). Latitude is the angle above (N) or below (S) the equator marking the observer's location.



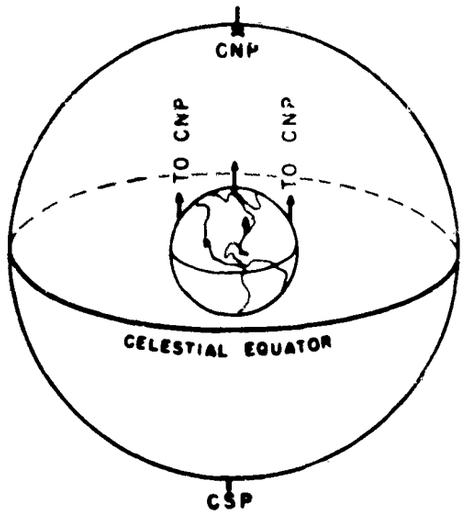
The dashed vertical line represents the rotational axis of the earth. The heavy curved line on the right side is the prime meridian passing through Greenwich Observatory. The heavy line on the left is the meridian of Washington, D.C. The horizontal curved line is the equator of the earth. The angle l is the longitude of Washington, and the angle b is its latitude.

Figure G-1. Coordinates on the Earth

2. COORDINATES FOR CELESTIAL OBJECTS

When an observer looks to the night sky, the stars appear to be located on the inner surface of a vast hollow sphere of infinite radius about the observer. Thus the natural phrase - celestial sphere.

To establish references for this celestial sphere, the terrestrial north ar poles (earth spin axis) are assume[d] extended to pierce this sphere establishin celestial north pole (CNP) and celestial south pole (CSP), respectively. Like the earth's equator projected to the celestial sphere becomes the celestial equ Thus the celestial equator is the intersection of the plane of the earth's equato the celestial sphere. See figure G-2.



CNP and represent the celestial north pole and the c south pole. The celestial equator is the tion of the plane of the earth's equator v celestial sphere.

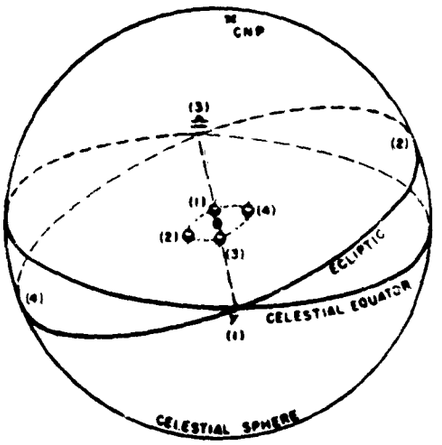
Figure G-2. The Celestial Sphere

Now then, if one stands on the earth at the north pole, the celestial north is directly overhead (Zenith); if one stands at the earth's equator, the CNP is the north horizon (since the earth's radius is small when referenced to celesti distances); if one stands in between, the CNP is elevated above the horizon by amount equal to the latitude of the observer.

Similar to the meridians of longitude on earth, "hour circles" are define the line(s) on the celestial sphere made by a plane oriented to pass through th and CSP and the object or star position. To establish a reference for measur the hour angle or Right Ascension (the angle of rotation about the CNP-CSP a the star position from the reference hour circle), the hour circle of the verna nox (often referenced as the First Point of Aries [r] is used. The vernal equ (♈) is the point where the plane of the ecliptic intersects the equator of the cel sphere going from south to north (winter to summer - northern hemisphere); 21/22.

The plane of the ecliptic represents the plane of the earth's orbit about th Since the earth's spin axis is tilted $23\text{-}1/2^{o}$ to the ecliptic, the celestial spher accordingly tilted to the ecliptic, crossing at the vernal and autumnal equinox.

This is best illustrated in figure G-3.

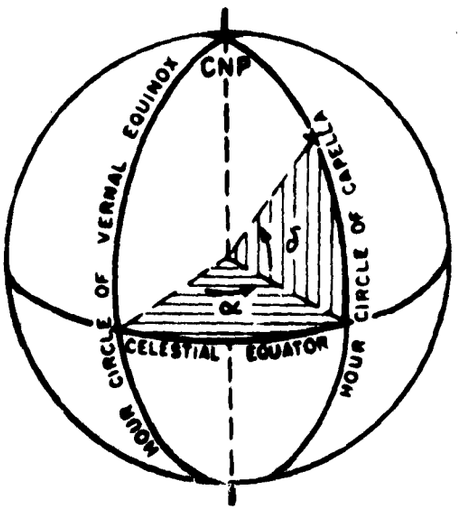


The central dot represents the sun. The location of the earth is indicated in four positions of its orbit. The intersection of the orbital plane with the celestial sphere is the ecliptic. The intersections of the ecliptic and the celestial equator are ♈, the vernal equinox, and ♎, the autumnal equinox. The rotational axis of the earth is inclined 66½° to the orbital plane, or 23½° to the normal of that plane, consequently the ecliptic makes an angle of 23½° with the celestial equator.

Figure G-3. Celestial Equator and Ecliptic

In summary, the measurement of Right Ascension is always measured eastward from the vernal equinox (♈) and is generally written in hrs., min., sec.; 24 hr 360° or 1 hr = 15° angle.

The position above (+) or below (-) the celestial equator, measured in degrees along the hour circle of the object, is termed declination, (δ). See figure G-4.



The hour circle of the vernal equinox serves as the beginning of the co-ordinate right ascension as the prime meridian on earth serves as the beginning of the co-ordinate longitude. At the intersection of this hour circle with the celestial equator is the vernal equinox. The right ascension, α, of the star Capella is measured eastward along the celestial equator, from the vernal equinox to the intersection of the hour circle of Capella with the celestial equator. The declination, δ, of Capella is measured from the celestial equator along the hour circle of the star.

Figure G-4. Coordinates on the Celestial Sphere

The rotation of the earth on its axis from west to east in a period of one sidereal day (23 hrs 56 min 4.09 sec) makes all celestial bodies (sun, moon, planets, stars) appear to turn around the earth from east to west in the same period. The solar day (24 hr) includes the 4 min ($\approx 1/365 - 1/4$) to account for the earth's revolution lost due to its orbit about the sun.

The latitude of the observer sets the elevation of the CNP above observer's horizon and likewise 90° from it, the distance from the observer's zenith to the celestial equator. If the observer moves to another latitude the elevation of the CNP will change accordingly.

An equipment mount oriented to have its prime axis pointing to the CNP (tilted to the latitude of its location) can be programmed to rotate at sidereal rate and thus stop the east-west movement of celestial bodies. Its secondary axis is oriented for measurement of declination (angle above or below the celestial equator). Such a mount is thus commonly called a "polar mount" or "equatorial mount".

3. GALACTIC COORDINATE SYSTEM

Another coordinate system of interest primarily to astronomers is based upon a great circle called the Galactic equator, considered to be in the plane of the Galaxy, about 1° north of the center of the Milky Way. Galactic latitude (b) is measured north and south from the Galactic equator. Galactic longitude (ℓ) is measured <u>eastward</u> from an intersection of the Galactic equator and the celestial equator which occurs at about 80° Sidereal Hour Angle or about 280° (18 hours, 40 minutes) Right Ascension. (SHA + RA = 360°).